AD NUMBER

AD881170

NEW LIMITATION CHANGE

TO

Approved for public release, distribution unlimited

FROM

Distribution authorized to U.S. Gov't. agencies only; test and evaluation; 1 Mar 1971. Other requests shall be referred to Attn: SMUFA-3300, U.S. Army Frankford Arsenal, Bridge and Tacony Streets, Philadelphia, Pennsylvania 19137.

AUTHORITY

F/A, D/A ltr, 9 Oct 1974

Data Systems Division · Litton Industries

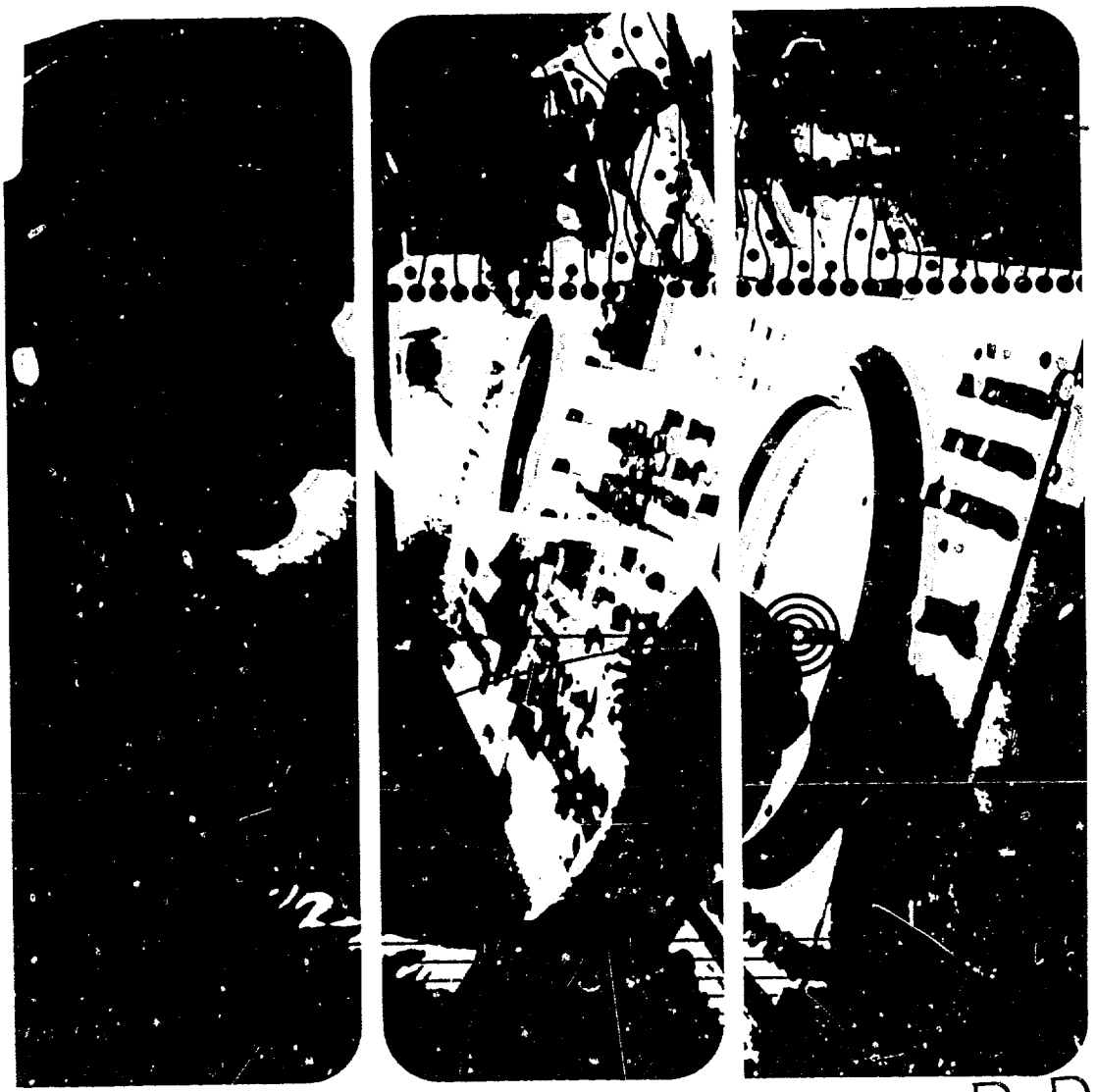

MS 00678

FINAL REPORT
A PARAMETRIC STUDY OF THE ADVANCED FORWARD AREA AIR DEFENSE WEAPON SYSTEM (AFAADS)
VOLUME I – SYSTEMS ANALYSIS

2 October 1970

U.S. Army, Frankford Arsenal
Bridge and Tacony Streets
Philadelphia, Pennsylvania 19137

Prepared by:
Data Systems Division
Litton Systems, Inc.
8000 Woodley Avenue
Van Nuys, California 91409

ACKNOWLEDGMENTS

Litton is happy to acknowledge the excellent guidance provided on this contract by Mr. Walter Ryb:, contract technical supervisor, and the substantive contributions made by Mr. Stanley Goodman and Mr. Paul Glassman of Frankford Arsenal. Mr. Stuar: Olson of Army Weapons Command provided valuable insight and advice particularly with regard to the computer simulation. The comments and encouragement of Mr. Glen Rendall of Weapons Command at the mid-course review were also very helpful. The content of these reports is, of course, the responsibility of the contractor.

FOREWORD

This report describes the research effort of the Data Systems Division of Litton Industries, Inc., under Contract No. DAAG05-70-C-0328, with the U.S. Department of the Army, Frankford Arsenal. The objective was to perform a parametric study of the fire control system to be associated with the Advanced Forward Area Air Defense (AFAADS) Weapon System.

The original RFP, to which this contractual effort is responsive, was titled 'Parametric Study, Advanced Forward Area Air Defense Weapons System (AFAADS),' and called for studies specific to an antiaircraft gun system based on a weapon having the same general characteristics as the 37mm Gatling Gun.

In the intervening time, since the 3 May 1968 date of issue of the RFP, the Army generalized the use of the acronym 'AFAADS' to include all elements of the forward area air defense of the Army, including missiles. At the present time, it appears that the effort contracted for could more properly be called 'LOFADS,' Low Altitude Forward Area Air Defense.

However, in order to maintain consistency with the wording of the contract, the term AFAADS has been used uniformly in the present report. The reader should remain aware of the fact that we are dealing here only with the antiaircraft gun system, which in turn is an element of the complete system for the forward air defense of the Army.

The report is included in two volumes. Volume I comprises the analyses and conclusions derived from an in-depth study by Mr. Herbert K. Weiss. Also provided therein are descriptions of the AFAADS System Concept as well as characteristics of AFAADS and its environment.

Volume II describes a computer simulation model used to provide the capability of predicting the performance of proposed (or existing) antiaircraft gun systems against an aircraft in a one-to-one combat situation. Results of this effort by Mr. Martin P. Ginsberg were used to derive recommended configurations and conclusions as presented in Volume I.

TABLE OF CONTENTS

Section			Page
	ACKNOWLEDGMENTS		iii
	FOREWORD		v
1	INTRODUCTION		1-1
2	SUMMARY		2-1
	2.1 CONCLUSIONS		2-1
		2.1.1 General	2-1
		2.1.2 Automation	2-1
		2.1.3 Human Operator	2-1
		2.1.4 Fire Control System	2-1
		2.1.5 System Error Budget	2-2
		2.1.6 Dynamic Calibration	2-2
		2.1.7 Artificial Dispersion	2-2
		2.1.8 Ballistic Solution	2-2
		2.1.9 Weapon and Ammunition	2-2
		2.1.10 Hardware Considerations	2-2
		2.1.11 Cost-Effectiveness Trades	2-3
		2.1.12 Improvement of Combat Effectiveness	2-3
		2.1.13 Further Applications of the Results of the Present Study	2-3
	2.2 OVERVIEW OF THE REPORT		2-3
		2.2.1 AFAADS System Concept and Characteristics	2-3
		2.2.2 Analysis of AFAADS System Requirements	2-3
		2.2.3 Simulation Results	2-4
		2.2.4 Overall System Effecti[illegible]	2-5
		2.2.5 Recommended Con[illegible]ations	2-5
		2.2.6 Recommended Pro[illegible]ns	2-5
3	AFAADS SYSTEM CONCEPT		3-1
	3.1 MISSIONS		3-1
	3.2 ORGANIZATIONS		3-1
		3.2.1 Future Trends	3-2
	3.3 FUNCTIONAL DESCRIPTION		3-2
		3.3.1 Alerting Information	3-5
		3.3.2 Surveillance, Search, Detection, and Acquisition	3-6

TABLE OF CONTENTS (Continued)

Section			Page
	3.3.3	Identification	3-6
	3.3.4	Tracking	3-7
	3.3.5	Lead Computation	3-8
	3.3.6	Firing Doctrine	3-8
4	CHARACTERISTICS OF AFAADS		4-1
	4.1	TARGET CHARACTERISTICS	4-1
	4.1.1	The Threat	4-1
	4.1.2	Threat Tactics	4-5
	4.1.3	The Flight Trajectory	4-21
	4.1.4	Target Exposure Time	4-36
	4.2	SENSOR CHARACTERISTICS	4-38
	4.2.1	Operational Considerations	4-38
	4.2.2	Types of Sensors	4-39
	4.2.3	Radar	4-41
	4.2.4	Infrared Sensors	4-47
	4.2.5	Direct Viewing Image Intensification	4-48
	4.2.6	Lasers	4-48
	4.3	OPERATOR PERFORMANCE CHARACTERISTICS	4-50
	4.3.1	Operator Dynamics in Tracking	4-50
	4.4	WEAPON CHARACTERISTICS	4-67
	4.4.1	Exterior Ballistics	4-70
	4.4.2	Terminal Ballistics	4-70
5	ANALYSIS OF AFAADS SYSTEM REQUIREMENTS		5-1
	5.1	SYSTEM CONFIGURATIONS	5-1
	5.2	COORDINATE SYSTEMS	5-6
	5.2.1	Rectangular Coordinate System	5-8
	5.2.2	Rectangular Coordinates: Rates Obtained by Gyros on the Tracking Head	5-11
	5.2.3	Polar Coordinates	5-12
	5.3	REGENERATIVE TRACKING	5-15
	5.3.1	Control Lags	5-15
	5.3.2	Complete Regenerative Tracking	5-23
	5.4	PREDICTION AND FILTERING	5-27
	5.4.1	Prediction Algorithms	5-29
	5.4.2	Filtering Algorithms	5-40

TABLE OF CONTENTS (Continued)

Section			Page
5.5	BALLISTICS		5-50
	5.5.1	3/2 Law Ballistics	5-51
	5.5.2	Projectile Gravity Drop	5-52
	5.5.3	Effect of Parameter Variations	5-52
	5.5.4	Wind	5-53
5.6	HIT AND KILL PROBABILITY		5-53
	5.6.1	Representation of the Target	5-54
	5.6.2	Single-Shot Hit Probability	5-56
	5.6.3	Probability of at Least One Hit in a Burst	5-58
5.7	ARTIFICIAL DISPERSION		5-61
	5.7.1	Polynominal Prediction Versus Noise and Artificial Dispersion	5-62
	5.7.2	Kill Probability	5-62
	5.7.3	Optimum Dispersion	5-63
	5.7.4	Criteria and Boundaries	5-64
	5.7.5	Partial Quadratic Prediction	5-64
	5.7.6	Comparison of Prediction Modes	5-65
	5.7.7	Interaction of Optimum Dispersion with Acceleration Prediction Mode in Only One Coordinate	5-66
	5.7.8	Conclusions	5-68
	5.7.9	Artificial Dispersion When Target Acceleration is Not Measured	5-68
	5.7.10	Power Required for Dither	5-73
5.8	DYNAMIC CALIBRATION OF THE AFAADS SYSTEM		5-75
5.9	MOUNT OSCILLATION AND VIBRATION ISOLATION		5-76
	5.9.1	Fire on the Move	5-77
	5.9.2	Effect of Firing the Gun	5-80
	5.9.3	Effect of Vibration on the Human Operator	5-81
	5.9.4	Conclusions	5-83
5.10	GROUND FIRE ROLE FOR AFAADS		5-84
5.11	RELIABILITY		5-85
5.12	FIRING DOCTRINE		5-87
5.13	SIMULATION RESULTS		5-88
	5.13.1	No-Noise Runs to Determine Systematic Errors Caused by Target Maneuver	5-88
	5.13.2	Simulation with Tracking Noise	5-89
	5.13.3	Simulator Results on Pass Path (Path No. 2)	5-94

TABLE OF CONTENTS (Continued)

Section				Page
		5.13.4	Simulator Results on Attack Path (Path No. 3)	5-98
		5.13.5	Simulator Results on Climbing Turn	5-110
		5.13.6	Simulator Results Against Jinking Target	5-113
		5.13.7	Simulation of Manual Tracking	5-114
		5.13.8	Conclusions	5-118
	5.14	SYSTEM EFFECTIVENESS		5-118
		5.14.1	Detection and Acquisition of Fast Targets on Low-Pass Flight Paths	5-119
		5.14.2	Detection and Acquisition of Targets on Attack Paths	5-120
		5.14.3	Comparison of Prediction, Ballistics and Tracking Options	5-121
		5.14.4	System Error Budget	5-122
		5.14.5		
6	RECOMMENDED CONFIGURATIONS			6-1
	6.1	OPTIONS FOR CONSIDERATION IN SYSTEM CONFIGURATION		6-1
		6.1.1	Relatively Low Cost, High Payoff Items	6-1
		6.1.2	Relatively Low Cost, Moderate Payoff Items	6-3
		6.1.3	Moderate Cost, High Payoff Items	6-3
		6.1.4	Moderate Cost, Moderate Payoff Items	6-4
		6.1.5	Relatively High Cost, High Payoff Items	6-4
		6.1.6	Relatively High Cost, Moderate Payoff Items	6-4
	6.2	COST CONSIDERATIONS		6-5
		6.2.1	Life Cycle Costs	6-5
	6.3	COST-EFFECTIVENESS COMPARISONS		6-9
		6.3.1	Stabilized Sight	6-10
		6.3.2	Regenerative Tracking	6-11
		6.3.3	Surveillance Radar	6-11
		6.3.4	Tracking Radar	6-11
		6.3.5	Computer	6-11
	6.4	SYSTEM CONFIGURATION		6-13
7	RECOMMENDED PROGRAMS			7-1
	7.1	AREAS FOR EXPLORATORY AND ADVANCED DEVELOPMENT EFFORT		7-1
		7.1.1	Radars	7-1

TABLE OF CONTENTS (Continued)

Section			Page
	7.1.2	Target Identification by Noncooperative Means	7-1
	7.1.3	Human Operator Performance in the Tracking Function	7-1
	7.1.4	Imaging Trackers	7-1
	7.1.5	Lasers	7-1
	7.1.6	Digital Computer	7-1
	7.1.7	Weapon	7-2
7.2	DATA COLLECTION PROGRAMS		7-2
	7.2.1	Combat Data	7-2
	7.2.2	Proving Ground Tests	7-2
	7.2.3	Noncombat Information on Target Attack Paths	7-2
7.3	RECOMMENDED AREAS FOR CONTINUATION OF THE PRESENT STUDY		7-2
	7.3.1	Simulation Improvement and Additional Simulation Studies	7-3
	7.3.2	Data Acquisition and Analysis	7-3
	7.3.3	Air Defense System Analysis and Evaluation	7-4
BIBLIOGRAPHY REFERENCE LIST			Bib-1

Appendix		Page
A	DERIVATIVES OF TARGET MOTION IN POLAR COORDINATES	A-1

LIST OF ILLUSTRATIONS

Figure		Page
1-1	Increase in Target and Gun Velocity with Time	1-2
2-1	Angle Subtended by Typical Targets at 1000-Meter Range	2-4
3-1	AFAADS System Functional Flow Diagram	3-4
3-2	AFAADS System Elements	3-4
3-3	Automatic Weapons Operational Difficulties in World War II	3-5
3-4	Flow of Command and Alerting Information to Fire Units	3-6
3-5	Visual Search, Acquisition, and Identification Functional Flow Diagram	3-7
3-6	Search/Track Functional Flow Diagram	3-7
3-7	Surveillance Radar Functional Flow Diagram	3-8
3-8	Engagement Decision by Doctrine Functional Flow Diagram	3-9
3-9	Identification Functional Flow Diagram	3-10
4-1	Comparative Speed – Altitude Envelopes	4-4
4-2	Specific Excess Power Overlays	4-5
4-3	Air-to-Surface Missile Weight versus Range	4-6
4-4	B-26 Sorties per Month During Korean War	4-7
4-5	Approximate Number of Antiaircraft Weapons in North Korea	4-8
4-6	Defense of Specific Targets	4-9
4-7	Composite Drawing Showing Over the Same Period of Time; the Percent of USAF Sorties by Night, the Number of B-26 Aircraft Lost to Antiaircraft Guns by Quarter, the Number of Red Weapons, and the Number of Fire Control Radars	4-9
4-8	Mean Probability of Seeing an Aircraft from the Ground During the Months of March, April and May	4-12
4-9	Mean Probability of Seeing an Aircraft from the Ground During the Months of June, July and August	4-13
4-10	Mean Probability of Seeing an Aircraft from the Ground During the Months of September, October and November	4-13
4-11	Mean Probability of Seeing an Aircraft from the Ground During the Months of December, January and February	4-14
4-12	Low-Altitude Approach Techniques	4-15
4-13	CH-47 Helicopter Data Showing Relationship of Airspeed to the Mean Altitude	4-16
4-14	Gravity Bomb Release Distance Graph	4-17
4-15	Straight-Line Segments of Dive/Glide Bomb Paths	4-18
4-16	Low-Altitude Bombing System	4-19
4-17	The LABS Over-the-Shoulder Delivery	4-19

LIST OF ILLUSTRATIONS (Continued)

Figure		Page
4-18	Rocket Attack Profile (Vertical Scale Expanded)	4-20
4-19	Strafing Attack Profile (Vertical Scale Expanded)	4-20
4-20	Tow-Type Missile Launch from a Helicopter	4-21
4-21	Flight Trajectory Characteristics	4-22
4-22	Comparison of Lappe and Dryden Autocovariance Functions	4-24
4-23	Relative Frequency Distributions of rms Gust Velocity from B-66 Programs	4-25
4-24	Normalized Dryden Spectrum for L=1000 Feet	4-26
4-25	Power Spectral Density of Aircraft Motion Caused by Air Turbulence	4-28
4-26	Power Spectral Densities	4-32
4-27	Power Spectral Density of Vertical Aircraft Motion in Terrain Following	4-33
4-28	Effect of Maximum Sustained Accelerations for Human Pilots	4-33
4-29	Tolerance to Vibrations Based on Various Studies After Bauer (1963) and Van Deuser (1965) as Prepared by Bekker (1969)	4-35
4-30	Relative Acceleration Capability of a High Performance Fighter/Bomber Along and Perpendicular to the Direction of Flight	4-37
4-31	Effect of Speed and Flight Path on Target Exposure Time	4-38
4-32	Initial Exposure Range	4-39
4-33	Terrain Mask Angle	4-40
4-34	Electromagnetic Spectrum Usage and Atmosphere Obstructions	4-40
4-35	Detector and Scan Combinations for IR Sensing	4-42
4-36	Sources of Angular Error in a Tracking Radar	4-44
4-37	Typical Monopulse Angle-Tracking Error Spectrum	4-44
4-38	Atmospheric Attenuation Due to Water Vapor and Oxygen Molecular Absorption	4-46
4-39	Attenuation Due to Rainfall for Various Rainfall Intensities	4-47
4-40	Cumulative Distribution Function for Rainfall Rates at Washington, D.C.	4-48
4-41	Absorption Spectrum of Water Vapor	4-49
4-42	Gas Laser Power Growth During 5 years	4-50
4-43	Gun Mount with Computing Sight Tracking Loop	4-53
4-44	Tracking Error as a Function of Time Constant	4-53
4-45	Phase Relationship of Various Types of Controls	4-54
4-46	Comparison of Response to Step-Function Manual Tracking: Three Control Laws	4-55
4-47	Effect of Control Dynamics on Tracking Error	4-56
4-48	Comparison of Open-Loop Transfer Function of Operator Plus Control for the Three Control Laws	4-58

LIST OF ILLUSTRATIONS (Continued)

Figure		Page
4-49	Amplitude and Phase of Operator's Describing Function for the Three Control Laws	4-58
4-50	Error Comparison: Linear Portion of Human Operator's Response	4-60
4-51	Comparison of Closed Loop Response, Manual Tracking	4-61
4-52	Spectral Density of Azimuth Velocity	4-62
4-53	Spectral Density of Angular Velocity of Control Motion	4-63
4-54	Comparison of Relative Error with Observed Error versus Display Gain	4-65
4-55	Variation of Tracking Error with Magnification	4-66
4-56	Variation of Detection and Recognition Range with Magnification	4-67
4-57	Variation of Fixed Optical Field with Magnification	4-67
4-58	Cumulative Probability of Target Detection versus Range	4-68
4-59	Cumulative Probability of Target Identification versus Range	4-68
4-60	Contours of Mean Detection and Identification Range	4-69
4-61	Mean Detection Range versus Angular Sector Scanned	4-69
4-62	Velocity versus Range Ballistics of the Vigilante T324E22 and Three-Proposed Improved Rounds	4-73
4-63	Time of Flight versus Range Ballistics of the Vigilante T324E22 and Three-Proposed Improved Rounds	4-73
4-64	Graph of Side Area versus Aircraft Weight	4-74
4-65	Graph of Frontal Area versus Aircraft Weight	4-74
4-66	Graph of Fuselage Length versus Aircraft Weight	4-75
4-67	Hypothetical Target Vulnerability	4-75
5-1	Elements of a Basic Tracking Loop	5-2
5-2	Elements of System with Sensors and Gun Independently Mounted on Same Vehicle	5-2
5-3	Trailer-Mounted Version of the Vigilante Antiaircraft Weapon System	5-3
5-4	Matador Antiaircraft System	5-4
5-5	Layout of the 5PFZ-B Antiaircraft Tank	5-4
5-6	Layout of the 5PFZ-C Antiaircraft Tank	5-5
5-7	Elements of an On-Carriage, Disturbed Reticle Lead-Computing Sight System	5-5
5-8	Elements of a System Whereby the Sensors are Mounted on Gun with Lead Subtruction	5-7
5-9	Elements of a System Utilizing Inertial Stabilization of Sight Line	5-7
5-10	Elements of Tracking Loop with Stabilized Sight	5-8
5-11	Elements of System with Stabilized Sight, Unstabilized Gun and Correction for Tilt	5-8

LIST OF ILLUSTRATIONS (Continued)

Figure		Page
5-12	Typical Coordinate Systems	5-9
5-13	Geometric Representation of Rectangular Coordinate System	5-10
5-14	Flow Diagram of Rectangular Coordinate System	5-10
5-15	Geometric Representation of Polar Coordinate System	5-13
5-16	Polar Coordinate Projection in Slant Plane	5-13
5-17	Spherical Triangles Showing Lead-Angle Derivation	5-13
5-18	Flow Diagram of Regeneration in Polar Coordinates	5-14
5-19	Angular Miss Caused by Sensor Servo Lag	5-18
5-20	Linear Miss Caused by Sensor Servo Lag	5-19
5-21	Angular Miss Caused by Sensor and Gun Servo Lags Combined	5-19
5-22	Linear Miss Caused by Sensor and Gun Servo Lags Combined	5-20
5-23	Elements of Lag Compensating System	5-20
5-24	Settling Time of a Lag Correcting Circuit	5-21
5-25	Undesired Ripple in a Lag Correcting Circuit	5-22
5-26	Elements of a Regenerative Unit with Servo Lag Correction	5-23
5-27	Velocity Regeneration in the Rectangular Coordinate System	5-25
5-28	Position Regeneration in the Rectangular Coordinate System	5-25
5-29	Elements of a Range Regeneration System	5-26
5-30	Elements of a Range Regeneration System with Doppler Rate Input	5-26
5-31	Elements of a Range Regeneration from Angular Velocity System	5-28
5-32	Radius of Turn as a Function of Aircraft Speed	5-29
5-33	Time to Turn 90 Degrees as a Function of Aircraft Speed	5-30
5-34	Elements of a Polynomial Predictor	5-31
5-35	Probability of Using Linear versus Quadratic Prediction Mode	5-33
5-36	Relative Values of Prediction Mode	5-33
5-37	Geometric Drawing of Attack on Known Point	5-37
5-38	Flow Diagram of Decision Algorithm for Defense Against Attack of Known Point	5-39
5-39	Comparison of a System with Least-Square Prediction (a) and a System with Errorless Constraint for a Number of Deterministic Signals (b)	5-41
5-40	Comparison of Variance Reduction for Three Velocity-Smoothing Algorithms	5-46
5-41	Comparison of Variance Reduction for Three Acceleration-Smoothing Algorithms	5-46
5-42	Velocity Variance Reduction	5-47

LIST OF ILLUSTRATIONS (Continued)

Figure		Page
5-43	Acceleration Variation Reduction	5-47
5-44	Effect of Number of Data Points on Variance Reduction for Velocity Smoothing	5-49
5-45	Prediction Variance as a Function of Smoothing Algorithm	5-49
5-46	Ballistic Parameters Affecting Miss Distance	5-51
5-47	Heavy Antiaircraft Rounds Per Aircraft Kill from 1915 to 1918	5-54
5-48	Heavy and Light Antiaircraft Rounds Per Aircraft Kill from 1939 to 1945	5-55
5-49	Eighth Air Force Aircraft Hit by Antiaircraft versus Altitude	5-56
5-50	Probability that a Hit Destroys an Aircraft as a Function of Projectile Weight[41]	5-56
5-51	Noise Amplification on Quadratic and Linear Prediction	5-63
5-52	Contours of Constant-Hit Probability with Linear Prediction	5-66
5-53	Region for Employing Increased Dispersion	5-67
5-54	Linear versus Quadratic Prediction Modes	5-68
5-55	Optimum Prediction Modes	5-69
5-56	Partial Quadratic Prediction	5-70
5-57	Linear Prediction versus 'Best' 3-Point Predictor	5-71
5-58	Probability Contours versus Time of Flight Using Linear Prediction	5-72
5-59	Probability Contours versus Time of Flight Using Optional Partial-Quadratic Prediction	5-73
5-60	Probability Contours versus Time of Flight Using Linear and Quadratic Prediction	5-74
5-61	Comparison of Quadratic Prediction in One versus Two Coordinates	5-76
5-62	View Through Sight Showing Out-of-Adjustment Condition of System	5-77
5-63	Power Spectral Density of Various Terrains	5-78
5-64	Computer Simulation of the M-56 Vehicle Suspension System	5-80
5-65	Vehicle Pitch Response	5-81
5-66	Vehicle Response as a Function of Terrain and Vehicle Speed	5-82
5-67	The Nord/Vosper Specially Designed Aiming Turret	5-83
5-68	Simulation Flight – Path No. 1	5-89
5-69	Time of Flight Ballistics Used on Simulation	5-90
5-70	Remaining Velocity Ballistics Used on Simulation	5-90
5-71	Comparison of Prediction Modes of Vigilante Ballistics No. 1	5-91
5-72	Flow Diagram Depicting Use of Simulation to Optimize System	5-93
5-73	Typical Summary Print Out	5-94

LIST OF ILLUSTRATIONS (Continued)

Figure		Page
5-74	Effect of Smoothing Time on Distribution of Miss Distances for Ballistics No. 1	5-96
5-75	Horizontal Projection of Simulation Flight Path No. 3	5-100
5-76	Altitude versus Time Projection of Simulation Flight Path No. 3	5-101
5-77	Target Velocity Along Flight Path versus Time for Simulation Flight Path No. 3	5-101
5-78	Distribution of Miss Distances for Path No. 3	5-103
5-79	Effect of Dispersion on Number of Bursts with K < 0.20 Measure with Quadratic plus Energy Prediction and Based on: 2 Replications, Smoothing No. 2 and Ballistics No. 3	5-103
5-80	Effect of Dispersion on Kill-Sec Measure with Quadratic plus Energy Prediction and Based on: 2 Replications, Smoothing No. 2, and Ballistic No. 3	5-104
5-81	Effect of Dispersion on Number of Bursts with K < 0.20 Measure with Linear plus Energy Prediction and Based on: 2 Replications, Smoothing No. 2 and Ballistics No. 3	5-104
5-82	Effect of Dispersion on Kill-Sec Measure with Linear plus Energy Prediction and Based on: 2 Replications, Smoothing No. 2, and Ballistics No. 3	5-105
5-83	Effect of Varying Range Noise Variance	5-105
5-84	Effect of Varying Elevation Noise Variance	5-106
5-85	Effect of Dispersion on Path No. 3 Based on the Single-Shot Kill Probability versus Time	5-108
5-86	Effect of Rate of Fire and Ammunition Load	5-109
5-87	Effect of Rate of Fire on Target Survivability as a Function of Time	5-110
5-88	Effect of Azimuth Boresight Error on Kill-Sec Measure with Linear plus Energy Prediction and Based on: 2 Replications, Smoothing No. 2 and Ballistics No. 3	5-111
5-89	Effect of Azimuth Boresight Error on Number of Bursts with K < 0.20 Measure with Linear plus Energy Prediction and Based on: 2 Replications, Smoothing No. 2 and Ballistics No. 3	5-111
5-90	Distribution of Miss Distances as a Function of Boresight Error	5-112
5-91	Distribution of Miss Distances on a Climbing Turn	5-112
5-92	Deviation with Time on Jinking Path Normal to Mean Flight Path	5-114
5-93	Effect of Threshold Setting in Automatic Prediction Selection Algorithm for 'Kill-Sec' Measure	5-116
5-94	Effect of Threshold Setting in Automatic Prediction Selection Algorithm for Number of Bursts with K > 0.20' Measure	5-116

LIST OF ILLUSTRATIONS (Continued)

Figure		Page
5-95	Effect of Gun Dispersion on Effectiveness of Rate-Aided Manual Tracking for the 'Kill-Sec' Measurement	5-118
5-96	Effect of Gun Dispersion on Effectiveness of Rate-Aided Manual Tracking for the 'Number of Bursts with $K > K_0$' Measure	5-118
5-97	Effect of Target Acquisition Mode on Firing Envelope	5-119
6-1	Factors Contributing to Total Cost of Ownership	6-6
6-2	Comparison of Overall System Cost and Effectiveness	6-15

LIST OF TABLES

Table		Page
I-1	Aircraft Losses to Flak and Fighters	1-1
III-1	Assignment of ADA Battalions Within Field Army	3-3
III-2	Battalion Communications Network	3-3
III-3	Consideration in Selecting Firing Doctrine	3-10
IV-1	Tactics for Munition Delivery	4-3
IV-2	A Comparison of the Thrust/Weight Ratio of Various Aircraft	4-4
IV-3	Estimates of the Probability of Seeing the Ground from an Aircraft During the Months of March, April and May	4-10
IV-4	Estimates of the Probability of Seeing the Ground from an Aircraft During the Months of June, July and August	4-11
IV-5	Estimates of the Probability of Seeing the Ground from an Aircraft During the Months of September, October and November	4-11
IV-6	Estimates of the Probability of Seeing the Ground from an Aircraft During the Months of December, January and February	4-12
IV-7	Typical Air-to-Surface Munitions Circular Probable Errors	4-22
IV-8	Typical Values of T_a	4-28
IV-9	Terrain Standard Deviation and Characteristic Length Data	4-31
IV-10	Comparison of Terrain Roughness Factors	4-31
IV-11	Effect of Short Duration 'Eyeballs in' Acceleration	4-35
IV-12	Maneuver Capability of Airplane with T/W 0.85 at Sea Level	4-36
IV-13	Sensor Categories	4-42
IV-14	Comparative Mean-Square Tracking Errors for Compensatory Tracking	4-57
IV-15	Error Variances for Various Control Laws	4-59
IV-16	Transfer Functions of Control Motion Referenced to Input	4-61
IV-17	Characteristics of the Vigilante, T250 Gatling Gun	4-71
IV-18	Characteristics of the Vulcan, XM-163 Gatling Gun	4-72
V-1	Typical Radar-Sensor Servo Lag Coefficients and Lag Components	5-17
V-2	Position Smoothing Algorithms	5-43
V-3	Velocity Smoothing Algorithms	5-44
V-4	Acceleration Smoothing Algorithms	5-45
V-5	Expected Number of Hits with 100 Rounds	5-75
V-6	Summary of the Time the Systematic Error was Less than 15 Meters	5-92
V-7	Comparison of Smoothing Times and Ballistics by 'Kill-Seconds' Measure	5-95
V-8	Comparison of Smoothing Times and Ballistics by 'Number of Samples Within 2 Meters' Measure	5-95
V-9	Comparison of Smoothing Times and Ballistics by 'Number of Bursts with $K > 0.20$' Measure	5-96

LIST OF TABLES (Continued)

Table		Page
V-10	Variance Ratios for Optimum Smoothing of Position, Velocity, and Acceleration	5-97
V-11	Effect of Dispersion Based on: 2 Replications, Smoothing No. 2 (1.8 sec) and Ballistics No. 1	5-97
V-12	Effect of Lag and Regeneration Based on: 9 Replications, Smoothing No. 2 (1.8 sec) and Ballistics No. 3	5-98
V-13	Comparison of Linear and Quadratic Prediction Based on: 9 Replications and Smoothing No. 2	5-99
V-14	Effect of Improved Tracking Based on: Smoothing No. 1 (1.8 sec) and a Gun Dispersion of 4 mils	5-99
V-15	Comparison of Prediction Algorithms and Ballistics Based on: 9 Replications, Path No. 3, and Smoothing No. 2	5-102
V-16	Effect of Noise Variance Using Linear plus Energy Prediction Based on: 2 Replications Each, Smoothing No. 2 and Ballistics No. 3	5-106
V-17	Comparison of Smoothing Times plus Noise Using Linear plus Energy Prediction and Based on: 9 Replications, Ballistics No. 3 and Path No. 3	5-107
V-18	Comparison of Effect of Lags Using Linear plus Energy Prediction and Based on: 9 Replications, Ballistics No. 3 and Smoothing No. 2	5-108
V-19	Comparison of Prediction Algorithms on a Climbing Turn	5-113
V-20	Course Content of the 0.5g Jinking Maneuver	5-113
V-21	Course Content of the 2 - 3g Jinking Maneuver	5-113
V-22	Comparison of Prediction Modes on Jinking Path by 'Kill-Sec' Measure	5-113
V-23	Comparison of Prediction Modes on Jinking Path by 'Number of Bursts with $K > 0.20$' Measure	5-115
V-24	Comparison of Prediction Modes on Jinking Path by 'Number of Samples with Miss $<$ 5 Meters' Measure	5-115
V-25	Comparison of Prediction Modes on Jinking Path Plus Straight-Line Segments	5-115
V-26	Effect of Threshold Setting on Jinking Path Plus Straight-Line Segment	5-115
V-27	Simulation Parameters for Manual-Tracking Mode	5-117
V-28	Comparative Effectiveness of the Various Tracking Modes	5-117
VI-1	Options for System Components and Functions	6-2
VI-2	Very Rough Fire-Unit Procurement Cost Estimates of Air Defense Gun Systems	6-6
VI-3	Estimated Life Cycle Costs of 32 AFAADS Fire Units	6-7
VI-4	Cost of Ownship and Operational Measures	6-8
VI-5	Breakdown of Cost of Ownership	6-8
VI-6	Hypothetical Comparison of Configuration Having Various Capabilities (2 Sheets)	6-14

LIST OF TABLES (Continued)

Table		Page
A-I	Derivatives of Azimuth Angle	A-1
A-II	Derivatives of Elevation Angle	A-2
A-III	Derivatives of Slant Range	A-2

SECTION 1
INTRODUCTION

In spite of the advent of surface to air missiles, the antiaircraft gun has maintained an important position in air defense operations.

In Korea the U.S. Air Force lost 550 aircraft to enemy antiaircraft guns and only 140 to enemy aircraft. In Vietnam, according to newspaper reports,[1] by August 1970 the United States had lost 1736 helicopters to enemy action while in flight, and 1388 fixed-wing aircraft were brought down by enemy action while in flight. Only a very small number of these losses was to enemy surface to air missiles and aircraft.

The helicopter, because of the nature of its operations, is often exposed to enemy small arms fire, and many of the helicopter losses were probably to small arms. The fixed-wing aircraft, however, were shot down by enemy automatic weapons and antiaircraft guns, in spite of their high speeds and probable use of countermeasures.

Looking at the record of antiaircraft guns and automatic weapons since 1915, as shown in Table I-1, the remarkable way in which the guns have kept pace with aircraft development will be noted. The table does not show the tremendous repair burden imposed by antiaircraft, since for every aircraft destroyed by fragmenting projectiles about 20 were damaged and for every aircraft destroyed by an impacting projectile, 3 to 5 were seriously damaged.

Since the gun must aim ahead of the aircraft at a predicted position, the competition between gun and aircraft can be displayed in simplified form as a competition between aircraft speed and projectile velocity. The growth in aircraft speed at sea level, and of gun velocity with time is shown in Figure 1-1. The ratio of the two velocities represents the lead angle which must be generated by the fire control computer, and this has in fact increased steadily with time, but much more slowly than the increase in target velocity at sea level.

In spite of the demonstrated effectiveness of antiaircraft guns, and the continued improvement and potential of antiaircraft gun systems, their development suffered a hiatus in the United States with the advent of the surface to air guided missile. The usual limited funds, coupled with the apparent very high potential of missile systems, caused the development of improved gun systems to be almost dormant for the period from 1950 to 1970.

During this period, development of gun systems continued in France, Russia, Sweden, Switzerland, and West Germany. This development resulted from an early appreciation of the problems the missile systems would have against very low flying aircraft, and the likelihood that effective SAMs would drive aircraft to

Table I-1. Aircraft Losses to Flak and Fighters

Date	Losses by	Losses to				Number of Defending			
		A/C	Flak	Joint	Opns	AA	L/MAA	AAMG	Fighters
1915-16	Zeppelins	7	3			← 70 →			110
1917-18	Gothas	10	11	9	33	← 480 →			384
1915-18	German A/F	2000	400						1340
1916-18	Allied A/F	4842	1590			← 2576 →		900	1530
1940	Luftwaffe	986	357		390	1,280	695	2,930	700
1944-45	V-1	1847	1878		3004	800	1800		300
1942-45	USAAF E, MTO	6800	7821		3797	12,170	4680	14,710	2000
1944-45	B-29	58	48	29	79	1,250			550
1950-53	USAF	140	550	68	810	750	1500		1100

00678-101

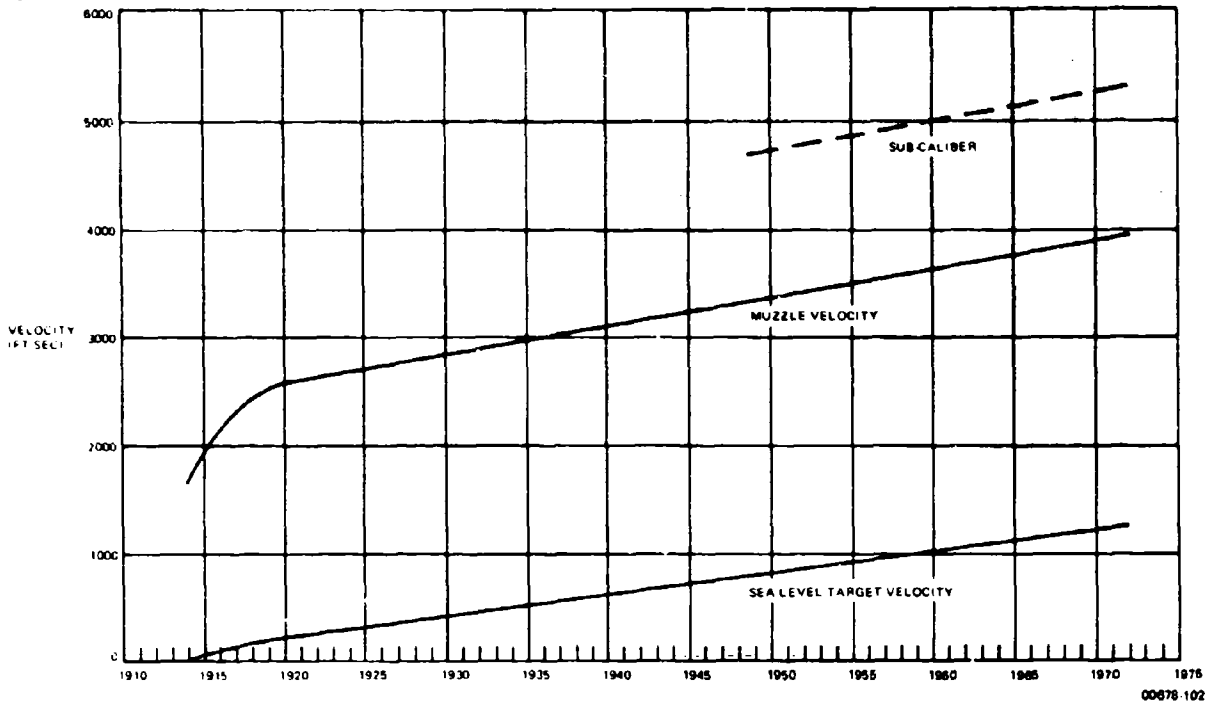

Figure 1-1. Increase in Target and Gun Velocity with Time

very low altitudes. Although missile systems can be built to meet the low altitude threat, terrain limitations require very large numbers of fire units to cover the Army's forward area, and the required proliferation of missile systems can be more costly than gun systems, yet provide no better coverage of a zone where the gun is effective.

The Army's recognition of the renewed potential of the guns compared with low altitude missile defense, once the medium and high altitude missile defense has driven aircraft to very low altitudes, led to the AFAADS program, and in particular, to the present contract, the objective of which is 'to make a preliminary determination of the parametric characteristics of the fire control system to be associated with . . . an Advanced Forward Area Air Defense (AFAADS) Weapon System.'

The present effort, emphasizing the fire control system aspects of AFAADS, supports a much larger program of the Army Weapons Command, in which a large number of candidate gun systems were compared on an overall cost-effectiveness basis. Contractual support on the overall model was provided by the University of Michigan. The sensor, weapons, and cost characteristics developed in the Weapons Command program were not made available to Litton. However, a description of the University of Michigan air defense simulation was made available, and many of the concepts developed in it were adapted for the simulation used in the present contract.

The present study explores the design options and parameters of the fire control system in greater detail than was possible in the AFAADS top level, system comparisons. Although the weapon used for reference in the present study was the 37mm Vigilante Gatling Gun, the analysis, methodology, and the computer simulation are completely general, and can be applied to any predicted fire weapon.

WHAT'S NEW?

Before presenting the findings of this study, a few of the principal changes in the antiaircraft problem and the technology for its solution that have occurred over the past 20 years will establish a context. Some of these are listed as follows:

Target	Faster Aircraft
	Helicopters
	Terrain Following
	Stand-Off ASMs
	'Free-Maneuver' Bombsights
AAA Systems	Depressing SAM Cover
	Sensors
	Computer Capability
	Gun Performance

Targets are faster, the helicopter has become operational in large numbers, aircraft can follow the contours of the terrain at night and in bad weather, air to ground guided munitions exist, and air to ground fire control systems have been reported which do not require the aircraft to fly a straight line path segment.

Favoring the antiaircraft gun is the appearance of surface to air missiles, which drive targets to low altitude within range of the gun, better sensors, and the extremely versatile digital computer. Sensors include K-band radars which are small, compact, and emit narrow beams with small reflectors; and by using frequency agility, track more accurately and to lower angles and are resistant to ECM. Night tracking in fair weather can be accomplished by conventional 'hot-spot' infrared trackers, and by modern imaging trackers in both the optical and infrared bands. Automatic tracking is possible with all of these devices. The laser provides accurate range under all conditions and has applications to imaging trackers as well.

The greatest breakthrough has been in the development of military-qualified digital computers which can provide a computing capability in very small volume that is so great that is is not an exaggeration to say that any prediction algorithm that can be conceived and demonstrated to be desirable, can be implemented in a digital computer, within available space limitations on the gun mount. This capability is associated with reliability expressed as several thousands of hours between failures, and mean times to repair of the order of minutes.

Servomechanisms for positioning sensors and gun have improved steadily in response time, and high precision 'gearless drives' are operational.

The rate of fire achievable with the Gatling Gun has always been high, and weapon performance benefits from the progressive improvement associated with increasing muzzle velocity.

The only component of the system that has not improved with time has been the man, who still has the same visual acuity and response time that he had in World War I antiaircraft operations. Consequently, a principal concern in realizing the advantages of improved technology in an air defense system is the design of the system so that it is not constrained by the limitations of the man.

SECTION 2
SUMMARY

The report contains a large number of conclusions and recommendations, associated with each topic treated. In particular some 44 options with regard to fire control algorithms, tracking modes, and hardware design trade-offs are presented and discussed in Section 6, Recommended Configurations.

In the present section we summarize some of the principal conclusions and provide a brief overview of the contents of the report. The conclusions are stated in absolute form, for clarity, rather than hedging them with conditions. Their basis, and appropriate reservations will be found in the report.

2.1 CONCLUSIONS

A summary of the principal conclusions are presented in the following paragraphs.

2.1.1 General

a. Modern antiaircraft guns have the potential of delivering highly effective fire against low flying targets which is relatively unexploited by existing fire control systems.

b. This potential can be realized in guns of Vigilante caliber only by providing satisfactory target detection and acquisition means, accurate tracking and ranging information, a precise solution to the prediction problem, and by effective system calibration and alignment in the field. The AFAADS system should be designed to deliver precision fire, rather than as a shot gun.

2.1.2 Automation

The principal effect of increased target speed is to reduce target exposure time. This requires that the time, from target detection to firing, be reduced to a degree only attainable by automation. Once the target has been detected, the tracking sensors should be put on target automatically.

2.1.3 Human Operator

a. The man cannot perform effectively in the tracking function unless he is assisted by regenerative tracking. With optical magnification in his sight he has the potential, still to be demonstrated, of tracking as well as the best automatic tracking sensors.

b. The man cannot adequately perform the initial detection and target acquisition function, even with improved RAID information.

c. The man cannot identify targets visually until they have approached to such a close range that most of the effective firing envelope of the Vigilante gun is lost.

d. Ideally, the human operator would have only decision functions, consisting of veto power on the automatic operation of the system.

2.1.4 Fire Control System

a. A number of alternate prediction options have been identified, each of which is preferred for a particular category of target flight path.

b. The ability of a computer to automatically select a preferred algorithm and deliver appropriate gun orders without requiring additional settling time has been demonstrated. This algorithmic switching may take place several times during a target pass.

c. Among the new prediction algorithms which have been developed and demonstrated on the simulation are:

(1) Correction for target acceleration in a dive based on a 'constant total energy' concept.

(2) Algorithm for defense of a known point, in which the prediction makes use of the known position of a small, vital ground target that is being defended.

d. The ability of the computer to use an algorithm correcting for target rate of turn, without degrading performance against non-turning targets, has been demonstrated.

e. The ability of the computer to switch automatically between quadratic and linear prediction against a target path composed of both jinking and straight line segments has been demonstrated, with resulting effectiveness greater than with either mode used alone.

f. The feasibility, stability, and effectiveness of a regenerative tracking algorithm has been demonstrated.

g. Highly effective performance over a wide range of assumed tracking errors was demonstrated with 1.8 second data smoothing time. With the best radar tracking considered to be reasonably attainable, effective performance was demonstrated with 0.4 second smoothing.

h. Smoothing time should preferably be a function of time of flight. This is probably most easily achieved by a recursive algorithm.

i. Design of the regenerative tracking circuits and the filters for the prediction function should be

carried out as an integrated operation. The resulting optimum weights applied for regeneration and prediction may, however, not be identical.

j. The regeneration algorithms should provide the capability of maintaining a continuous solution based on intermittent, irregular, inputs of actual or estimated range. Algorithms to do this are described in the report.

k. A rectangular coordinate system appears to provide the smallest total number of required coordinate transformations in implementing the array of prediction algorithms considered to be desirable.

2.1.5 System Error Budget

The dynamic instrumental errors of the AFAADS system should not exceed root mean square values of 2 meters out to 2000 meters slant range, nor 2 mils beyond 2000 meters start range. Dynamic instrumental errors are defined as overall errors against a 600-knot unaccelerated target, with zero tracking errors, and excluding gun and ammunition dispersion.

2.1.6 Dynamic Calibration

To achieve the maximum operational effectiveness, the system must have integral means for both static and dynamic calibration in the field by methods simple enough so that the system can be checked out by its crew without special equipment. A method for dynamic calibration is described in the report.

2.1.7 Artificial Dispersion

With the instrumental errors indicated above, and dynamic calibration, 'optimum' dispersion under normal operating conditions will be only 2 or 3 mils. For those infrequent cases where increased dispersion is desired, such as operation in a degraded system mode, it should be produced by dithering the gun servos.

2.1.8 Ballistic Solution

a. A correction for the effect of wind on the trajectory should be incorporated.

b. Time of flight should be computed to 0.005 second.

c. The allowable systematic error in muzzle velocity is 1.5 meters per second. It may be necessary to provide automatic muzzle velocity measurement on the mount, if this tolerance cannot be held by ammunition quality control.

2.1.9 Weapon and Ammunition

a. The 37mm Vigilante Gatling Gun should incorporate an additional, intermediate rate of fire capability between 3000 rpm and 120 rpm. 1200 rpm appears appropriate.

b. Muzzle velocity should be increased and projectile drag coefficient reduced. Continued improvement in effectiveness is anticipated as these values are improved above the best values considered in this study. The interaction with projectile terminal effectiveness must be considered.

c. With improved muzzle velocity and ballistics, it will be possible to deliver effective fire against air targets beyond 4000 meters range.

2.1.10 Hardware Considerations

a. The desired flexibility in utilization of prediction options can be attained with current state of the art in digital computers. The high reliability and low maintenance costs of a digital computer are expected to result in lower life cycle costs and higher availability than an analog solution of equal capability.

b. The problems of the effects of gun shock and vibration on the tracking process while the mount is stationary, and the effects of rolling and pitching of the mount and vehicle when firing on the move, can be solved by a stabilized line of sight. Complete stabilization of the system, including the guns, is probably not necessary.

c. Radar tracking is required for all-weather operation. Considerations of dish size and beam width indicate a K-band radar. The provision of frequency agility will reduce the angle and range tracking errors caused by glint and multipath effects and increase resistance to countermeasures.[1]

d. If radars are used on the AFAADS mount, they may have the shortest mean time between failures, longest times to repair, and highest support costs of all the system hardware components, in part because of the severe vibration and shock environment, unless they are designed to overcome the environmental problems. Radar developments for AFAADS should include special funding for high reliability, low maintenance design.

e. For non-radar tracking, imaging sights with automatic tracking should be investigated as offering the potential of more accurate tracking under fair weather, day/night conditions than can be achieved with manual tracking.

f. The tactical usefulness of employing the laser range finder both as a range finder against aerial targets, and as a target designator for the delivery of remotely fired homing missiles against ground targets, should be considered as a means for augmenting the ground support capability of AFAADS at small incremental cost.

2.1.11 Cost-Effectiveness Trades

Given a reference design configuration, a design option that adds 10 percent to overall system effectiveness is cost effective if it adds no more than 300,000 dollars to the total 10-year life cycle cost of a fire unit, considering all direct and overhead costs allocated against the fire unit on a battalion basis.

2.1.12 Improvement of Combat Effectiveness

All historical records show a very rapid improvement of the effectiveness of antiaircraft gun systems during the course of a conflict. AFAADS should incorporate an element for recording the attack paths of enemy aircraft as they are encountered so that prediction modes can be modified, decision thresholds changed, and the overall system capability periodically modified in the field to best match the changing tactics of enemy aircraft.

2.1.13 Further Applications of the Results of the Present Study

In the course of this study a computer simulation of the predicted-fire air defense problem has been developed which is of great generality and has applicability to all predicted-fire weapon systems. It is modular in construction, so that the program modules defining the prediction algorithms, for example, can be changed as desired without rewriting the complete program. The same flexibility exists in the target path program, the tracking program, the ballistics program, the terminal effects program, and the program for analyzing and printing out detailed point by point analyses of individual runs, or statistical summaries of large numbers of replications. This is a tool that can be applied effectively in all future analysis and development activity concerned with predicted-fire air defense systems.

2.2 OVERVIEW OF THE REPORT

This section discusses briefly the content of the major section of the report.

2.2.1 AFAADS System Concept and Characteristics

The AFAADS concept is initially defined by its mission, the organizational structure in which it will function, and the targets against which it must operate. The fire control system emphasized in the present study is additionally constrained by the characteristics of the sensors and the capability of human operators, and by the performance of the weapon. These topics are taken up in Sections 3 and 4.

The environmental context in which AFAADS will operate is developed in Section 3. This section defines missions, typical organizations, information flow, and functions performed by AFAADS at the top level of system definition. It provides a basis for assessing the quality of alerting information that will be provided AFAADS from external sources. The organizational structures provide a basis for later estimates of overall system cost for use in cost-effectiveness trades.

The characteristics of targets and target flight paths are developed in Section 4.1. This section serves as a basis for selection of typical flight paths for analysis, and for the selection of prediction algorithms. It includes an evaluation of the maneuver capabilities of targets, typical attack paths, flight paths in terrain following, and the effects of air turbulence in producing 'flight roughness.' Estimates are made of the range at which targets will first be exposed to AFAADS as a function of altitude, and of the total exposure time.

A brief survey of sensor characteristics with emphasis on the magnitude and power spectral densities of tracking errors is provided in Section 4.2. The essence of the tracking problem is indicated by Figure 2-1 which shows the angle subtended by typical targets[2] at 1000 meters. Unless the sensor can track to a small fraction of the angle subtended by the target, wander of the tracking point over the target area will cause large errors in predicted position. With accurate tracking the large subtended angle makes the target easier to hit.

The characteristics and capabilities of the human operator are summarized in Section 4.3 as they apply to the AFAADS problem. The human operator is deficient in ability to detect targets at satisfactory ranges and in the tracking function has, at best, a 1 Hz equivalent bandwidth.

Gun and ammunition characteristics are summarized in Section 4.4. Some rough estimates are made of terminal ballistics, including target vulnerability to 37mm projectives for use in subsequent system effectiveness computations.

2.2.2 Analysis of AFAADS System Requirements

Within the constraints of mission, target, organizational employment, sensor, and weapon capabilities, a comprehensive analysis by both analytical means and computer simulation is carried out to define the fire control system. Since the fire control system cannot be considered properly without considering its interaction with all other system elements, the approach is that of an overall systems analysis.

Sections 5.1 through 5.5 are specifically concerned with defining the coordinate system and prediction, as well as the smoothing and regeneration algorithms of the fire control system.

System configurations for uncoupling the sight from the gun motion are described. Coordinate systems are compared and typical prediction algorithms in polar and rectangular coordinates are compared.

Methods for accomplishing regenerative tracking in both rectangular and polar coordinate systems are presented, and the additional use of the regenerated

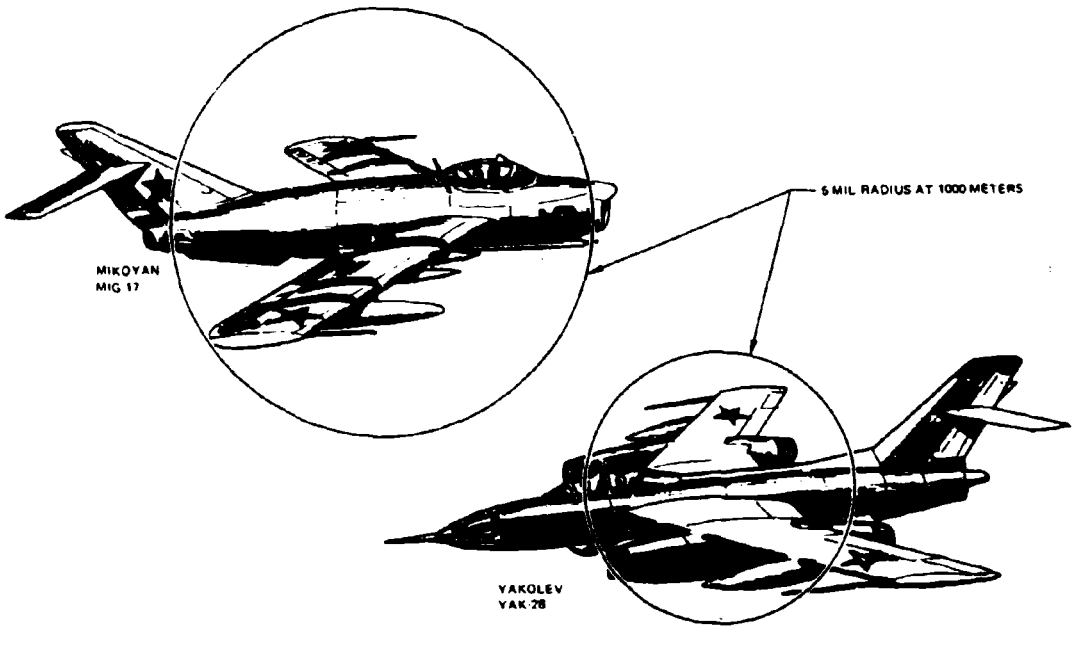

Figure 2-1. Angle Subtended by Typical Targets at 1000-Meter Range

information to reduce servomechanism lags at the sensor and gun is described. Algorithms for degraded mode operation are presented.

A number of prediction algorithms are developed, *including at least two which are new.* An analysis of weighting functions for smoothing measured target data is presented.

A brief analysis is presented of the effect of inaccuracies in the ballistic solution on system performance, and the effects of variations in muzzle velocity, drag coefficient and other parameters are derived. The deflection of the trajectory by wind is estimated.

Having developed a number of candidate solutions to the fire control problem, the study continues with the development of the methodology for obtaining hit and kill probabilities. This includes a consideration of aim wander and a method for resolving it into systematic and random components. Analytical evaluations of the interactions among prediction mode, tracking noise, target maneuver and artificial dispersion are carried out as a prelude to more realistic evaluation of these effects on the simulation. An analysis of the expected characteristics of operation of a switching algorithm to choose automatically between linear and quadratic prediction is described. Its purpose is to anticipate performance of similar algorithms on the simulation and estimate the probable effects of tracking noise on desirable threshold settings.

Additional supporting studies reported in this section include a description of a method of dynamic calibration of the system, an analysis of the effects of firing on the system and its operator, fire on the move, ground fire, and firing doctrine. There is a discussion of the methodology for incorporating system reliability into overall configuration analysis.

2.2.3 Simulation Results

Perhaps the most important, and certainly the most interesting, material in this section is the report of simulation results in Section 5.13. This section reports the results of comparisons of six basic prediction algorithms, three sets of ballistics, and three smoothing times, with simulated radar and manual tracking against a half dozen different target path types. Not all combinations of system options were run against all target path types, but a progressive resolution of preferred options was accomplished using three indices of effectiveness. The effectiveness of the automatic prediction mode selection was demonstrated. Among the system characteristics explored, in addition to those named above, were the effects of varying gun dispersion, sensitivity to noise variance in each of the input parameters, effect of boresight error, effects of lag in

the sensor and gun servos, and the stability and effectiveness of regeneration algorithms. Additional conclusions regarding firing doctrine and rate of fire of the gun were drawn from analytical manipulation of some of the simulation outputs.

2.2.4 Overall System Effectiveness

The section concludes with a review and summary of all of the material reported in this section from the point of view of overall system effectiveness in both normal and degraded operating modes. The candidate prediction options and modes are ranked in order of preference, and a tentative instrumental error objective for system development is proposed.

2.2.5 Recommended Configurations

About 44 algorithmic, hardware, and configuration options identified in the course of the study are presented in Section 6.0 and grouped according to expected contribution to system effectiveness, and cost. Each is discussed.

In order to provide a basis for selecting among options on the basis of both effectiveness and cost, some estimates are made of AFAADS life cycle costs. It is shown that a useful guide for system element selection can be derived in spite of large uncertainties in complete system life cycle costs. Because of the long service life of air defense gun systems, the importance of low maintenance costs is emphasized.

Finally, to put the whole effort in perspective, three complete system configurations are described: (1) for day/fair weather, (2) day and night/fair weather, and (3) all-weather. An example is given of how these can be compared on an overall cost-effectiveness basis.

2.2.6 Recommended Programs

The final section of the report presents and discusses areas in which exploratory and advanced development effort in hardware, data collection and experimentation, and analysis will significantly advance the capabilities of future predicted-fire air defense systems. Included is an identification of those areas of recommended activity that represent natural continuations of the effort completed under the present contract.

SECTION 3
AFAADS SYSTEM CONCEPT

In order to place AFAADS in an appropriate systems context, it is assumed that this gun system will fit into the complete air defense system in a manner which is an extension of, but roughly comparable with, that currently defined for Vulcan and Chaparral, and within a generally similar organizational structure. Within this structure, the following paragraphs discuss mission, organization, and the implications of these factors on the operational concept.

3.1 MISSIONS

The overall air defense mission is to destroy hostile aircraft and missiles, or to nullify or reduce their effectiveness. In forward area air defense, the air defense forces have the objective of limiting the effectiveness of enemy air efforts to a level permitting freedom of action of friendly forces of all types. The overall air defense system is composed of a mix of manned interceptors and ground-based air defense artillery (ADA) weapons, including surface-to-air missiles, to permit the advantages of one type of weapon to offset the limitations of the other, and to ensure a defense in depth. The ground-based ADA weapons add depth to the defense and offset weakness in the defense provided by the interceptors.

A typical field army ADA defense is a composite of several weapon system types. Area coverage over all or most of the field army area is provided by Nike Hercules type missiles. This is complemented by Hawk type missiles for medium and low altitude defense. The effectiveness of these missile systems is presumed great enough to force enemy aircraft to very low altitudes to penetrate below their coverage volume, taking advantage of terrain. The self-propelled Hawk, automatic weapons, and the Chaparral are positioned forward to complement the coverage provided by the longer range weapons, and protect the high-value forward area targets and subareas against low altitude air attack.

Currently, Chaparral and Vulcan provide only a fair-weather capability. It may be expected that any enemy using modern tactical aircraft will be able to operate, acquire ground targets, and attack them under all-weather conditions at low altitude.

Automatic weapons (including AFAADS) allocated to a field army, corps, or division, would normally be used to provide a low altitude defense for: priority nuclear delivery means, march columns, assembly areas, critical base installations, and selected units. Their deployment would be influenced by the coverage offered by the longer-range area defense ADA weapons. Currently, automatic-weapons fire units are normally allocated and deployed in increments of two fire units, with four weapons constituting a minimum defense.

In addition to air defense, automatic weapons may perform a secondary mission of ground support.

The missions of air defense automatic weapons are further detailed as follows:

a. *Limited area defense.* The extended area coverage of AFAADS, as compared with the present Vulcan, allows it to be considered for a limited, weighted-area defense within the division area as now contemplated for Chaparral.

b. *Vital area defense.* This would be the normal use of AFAADS in a non-mobile role. It would complement the area defense provided by the longer range missiles; or when this coverage is not available, or limited, protect the vital areas to a degree appropriate to their value.

c. *Small unit defense.* A local-area defense capability is provided responsive to the requirements of a small unit. This might include a column on the move. If the route of the march column is secure from ground attack, a leap-frogging deployment of the air defense is preferred to permit better siting of the fire unit. Otherwise the ADA units would move with the column. Whether AFAADS would stop to meet an air attack, or fire on the move, would depend on its capability to deliver accurate fire while moving. In this role, AFAADS might augment the ground security fires of the defended unit in addition to providing air defense.

d. *Ground support.* When ADA automatic weapons are specifically employed for ground support, fire support plans are expanded to include ADA automatic weapons fires. Weapon positions are selected by the supported unit commander. The high-velocity, flat trajectory of antiaircraft automatic weapons fire makes direct fire the usual mode of operation; although indirect fire may be called for infrequently.

3.2 ORGANIZATIONS

The organizational structure of the Army, like that of industry, is continually changing. The organizations currently described may, however, be used as guides to the way that the AFAADS gun system could be integrated into the Army.

Air defense fire units would normally be organized into air defense battalions. The composition of the battalion would depend on its assignment; i.e., whether

it was to be organic to a division, with mobility consistent with that of the division; or allocated at corps or brigade level. Fire units might include: AFAADS gun systems, Chaparral or a later follow-on, and in some configurations, Hawk, or a later surface-to-air missile. Hypothetical organizations incorporating AFAADS include the following:

a. Air Defense Artillery Battalion (Self-Propelled).

(1) Organic to armored, infantry, and mechanized infantry divisions.

b. Air Defense Artillery Battalion (Towed), allocated to:

(1) Corps Air Defense Artillery Groups.

(2) Field Army Air Defense Artillery Brigades.

(3) Communications Zone Air Defense Artillery Organizations.

c. Air Defense Artillery Battalion (STRABAD) (Towed).

(1) Allocated to U.S. Strike Command for worldwide deployment on a contingency basis.

The principal differences across organizational types are: (1) those associated with mobility requirements of the Air Defense Artillery Battalion (ADAB) which are organic to divisions. This assignment favors self-propelled fire units, (2) the lesser mobility requirement of ADABs assigned at higher levels which allows less expensive towed mounts, and (3) those with emphasis on minimum weight for ADABs for rapid worldwide deployment by air (STRABAD).

Considering the composition of a self-propelled ADAB, one might find the organizational structure and numbers of fire units to be as follows:

Personnel: 760 per Battalion

Two Batteries per Battalion

Two Firing Platoons per Battery

Two Firing Sections per Platoon

Four Fire Units per Firing Section

One AFAADS per Fire Unit (SQUAD)

---

32 AFAADS Fire Units per Air Defense Battalion

576 AFAADS Fire Units per Field Army

The organization of a current air defense artillery battalion includes a Forward Area Acquisition Radar Platoon (FAAR) with 12 radars per battalion. Information acquired by these radars is disseminated throughout the battalion by digital data link, and is displayed on Rapid Alerting Identification Display devices (RAID) which are allocated one per ADA Platoon plus one per squad. The use of RAID information by AFAADS is discussed later.

The aggregate numbers are based on the assumption of a field army with 3 corps and 4 divisions per corps. Assignment of ADA Battalions at the various levels of the field army, and typical areas covered by each organization, are indicated in Table III-1.

Communication nets in which the air defense battalion may typically operate or monitor, are shown in Table III-2. These are considered in a following section with regard to their effect on alerting and early warning information received at the AFAADS fire unit.

In configuring a battalion organization to include AFAADS, various changes from the current Vulcan/Chaparral organization may be anticipated. If AFAADS mounts a surveillance radar (one per fire unit, or one per platoon), the information it acquires will supplement and may replace that gathered by the present FAARs. Furthermore, it may be desirable to inject this information into the forward area defense command and communications net in the same manner as employed for the FAAR information.

The balance between AFAADS and Chaparral, or its successor in terms of numbers of fire units, may be modified depending on the AFAADS effectiveness and all weather coverage.

3.2.1 Future Trends

The integrated air defense system for the field army will change from the current practice as just described, with the advent of improved digital communications, integration with the Army's air traffic regulation system, realization of an Army-wide aircraft position and reporting system, and the acquisition of TOS and AN/TSQ-73. The aircraft position determination and reporting system, in particular, will simplify the IFF problem. A forward area command post (FACP) may be implemented to collect, correlate, display, and disseminate information collected by the FAARs and other sources. The FACP may be located intermediate to the AN/TSQ-73 and AFAADS/Chaparral/Redeye Battalions or Batteries. Battery Entry Track and Storage Equipment (BETSE) may provide more accurate and comprehensive information on enemy air activity at the battery level and below, than is presented by RAID.

None of these developments will relieve the fundamental requirement for autonomous operation of AFAADS. However, while the overall system is functioning, the information it provides can substantially improve AFAADS effectiveness.

3.3 FUNCTIONAL DESCRIPTION

The functional flow of activities on the AFAADS system is shown at the top level in Figure 3-1. The principal system elements are shown in Figure 3-2.

Table III-1. Assignment of ADA Battalions Within Field Army

Organizational Level	Area (sq mi)	Front (mi)	Battalions of ADA Assigned (Total Field Army)			
			Hercules Type	SP Hawk Type	Towed Hawk Type	AFAADS/ Chaparral Type
Field Army	20,000	125	6	-	4	3
Corps (3)	2200 (ea)	40	-	9	3	3
Division (12)	60-240 (ea)	6-12	-	-	-	12
		Total number of battalions	6	9	7	18
		Total number of batteries*	24	27	28	72
		Total number of fire units*	24	81	56	576 Chaparral 576 AFAADS

*Computed from data presented in Army Field Manual, FM 44-1

00678-310

Table III-2. Battalion Communications Networks

External Radio Nets

Division Command Net (FM)

Division Warning Broadcast Net (AM-VOICE) ..... AFAADS Batteries Monitor:
- Air Alerts
- CBR Warnings
- Nuclear Events

Division Operations/Intelligence Net (RATT Net No. 1)

Division General Purpose Net (RATT Net No. 3)

Supported Unit's Command Net (FM) ..... AFAADS Batteries Operate In and Monitor.

Internal Radio Nets

Battalion Command Net (FM) ..... AFAADS Battery Commanders Operate In.

Air Defense Liaison Net (SSB-VOICE)

Operations/Intelligence Net (SSB-VOICE) ..... AFAADS Battery Monitors:
Early Warning, Operations, Intelligence Information Between Battalion HQ and FAAR Teams

Battery Command Net (FM) ..... AFAADS Battery Commander and Platoon Leaders

Platoon Operational Command Net (FM) ..... AFAADS Platoon Leader, Platoon Sergeant and Fire Units Operate In.

Rapid Alerting Identification Display (RAID) Data Link ..... Platoon Radar Teams (FAAR) to AFAADS Sections and Fire Units:
One-Way Digital Data Link
- Coarse Direction
- Tentative Identification
- Early Warning

00678-311

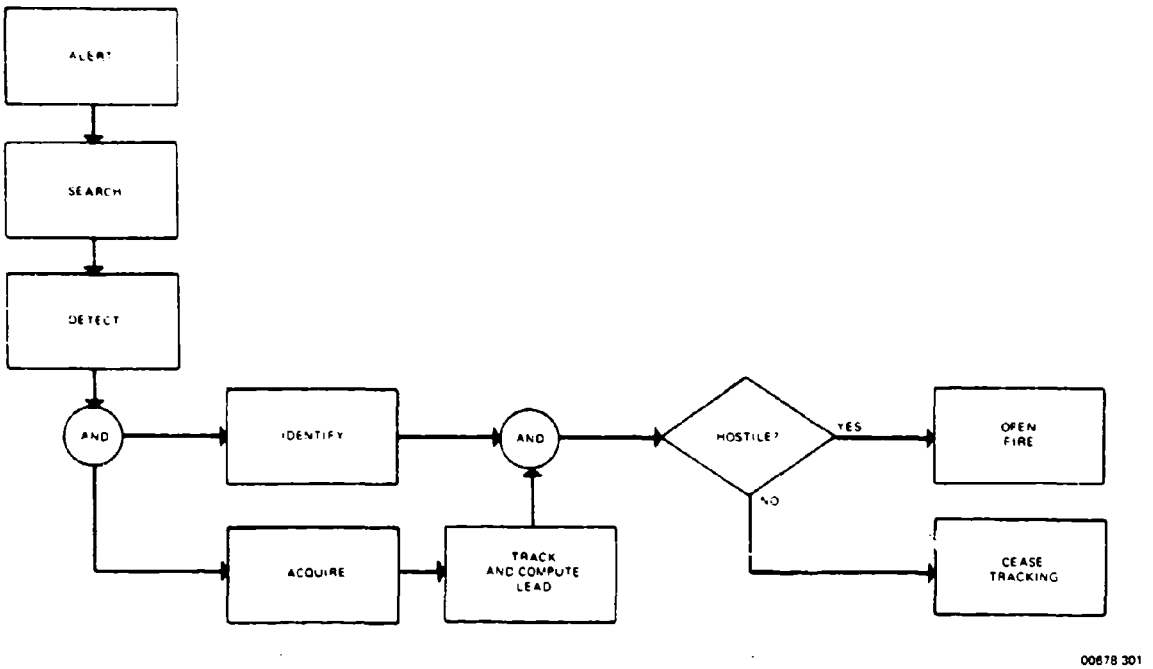

Figure 3-1. AFAADS System Functional Flow Diagram

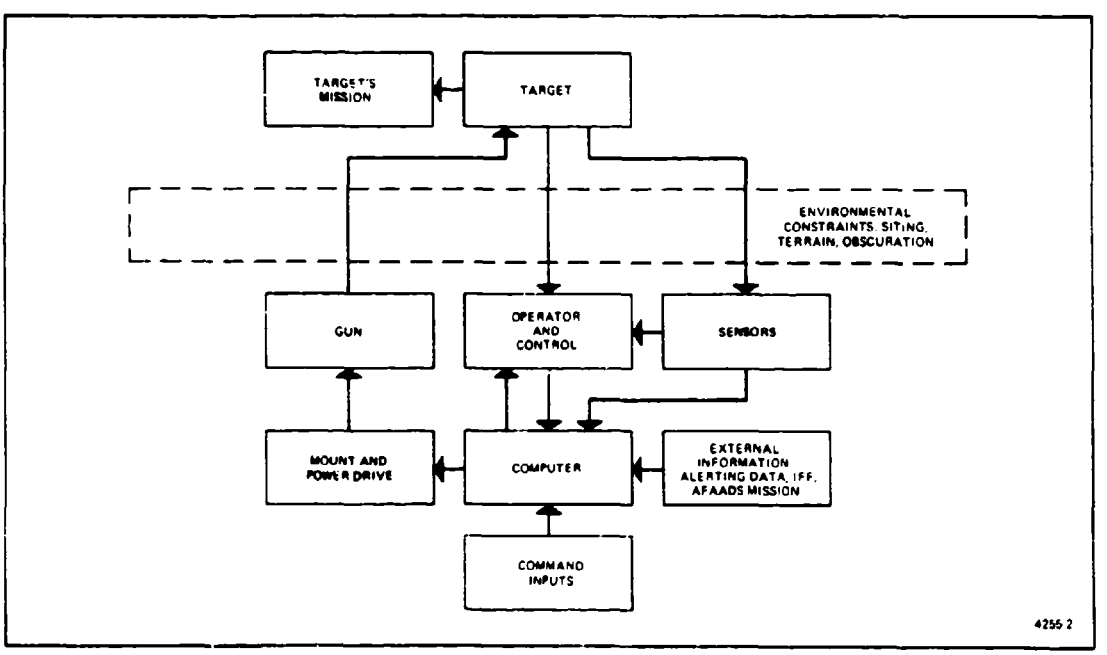

Figure 3-2. AFAADS System Elements

The functions will now be discussed in the context of mission and organization as developed in the two sections preceding.

U.S. antiaircraft weapons have not been employed in warfare since World War II. In many ways, the AFAADS operational problems are similar to those of WW II automatic weapons for air defense. Figure 3-3 shows the results of a survey of the operational problems of automatic weapons in WW II.

The findings of Figure 3-3 were based on a survey of 1925 targets, of which it was found that only 27 percent were engaged fully and without difficulty, and 35 percent were not engaged at all. Clearance problems were the major causes of not firing at all, and acquisition problems were the major causes of not firing for the maximum available time.

Acquisition can be improved by providing AFAADS with early warning and target position data from the battalion surveillance system, and by the use of on-carriage surveillance devices. Clearance problems may be reduced by improved target identification devices, and doctrine.

3.3.1 Alerting Information

The fire unit operates in the Platoon Operational Command Net (Voice, FM), and receives coarse direction, tentative identification, and early warning of alert from the Forward Area Acquisition Radar Platoon (FAAR) via digital data link. The latter information is displayed on the Rapid Alerting Identification Display Device (RAID). In addition, the platoon leader may operate in the command net of any divisional unit supported by the platoon. The flow of information to the fire unit is shown in Figure 3-4.

The RAID device is a box 12 in. by 9-3/4 in. by 5-1/2 in. with a 7 in. by 7 in. display containing 49 squares, each transparent, backed by light bulbs, and representing 4 km per side of each square. Color of the light indicates hostile, friendly, or unknown. Depending on the range from the fire unit at which a target is first displayed on RAID, the required search angle may be as large as 90 degrees, but probably averages less than 45 degrees.

Since information is transmitted digitally, the information now displayed by RAID might be introduced to and shown on the display of an on-carriage surveillance device, if one is incorporated in AFAADS. Data allowing higher resolution and essentially continuous track could be accepted. The possibility also exists of passing information back from AFAADS in digital form to a Forward Area Air Defense Command Post for integration with FAAR and other data to build up a complete air defense situation display.

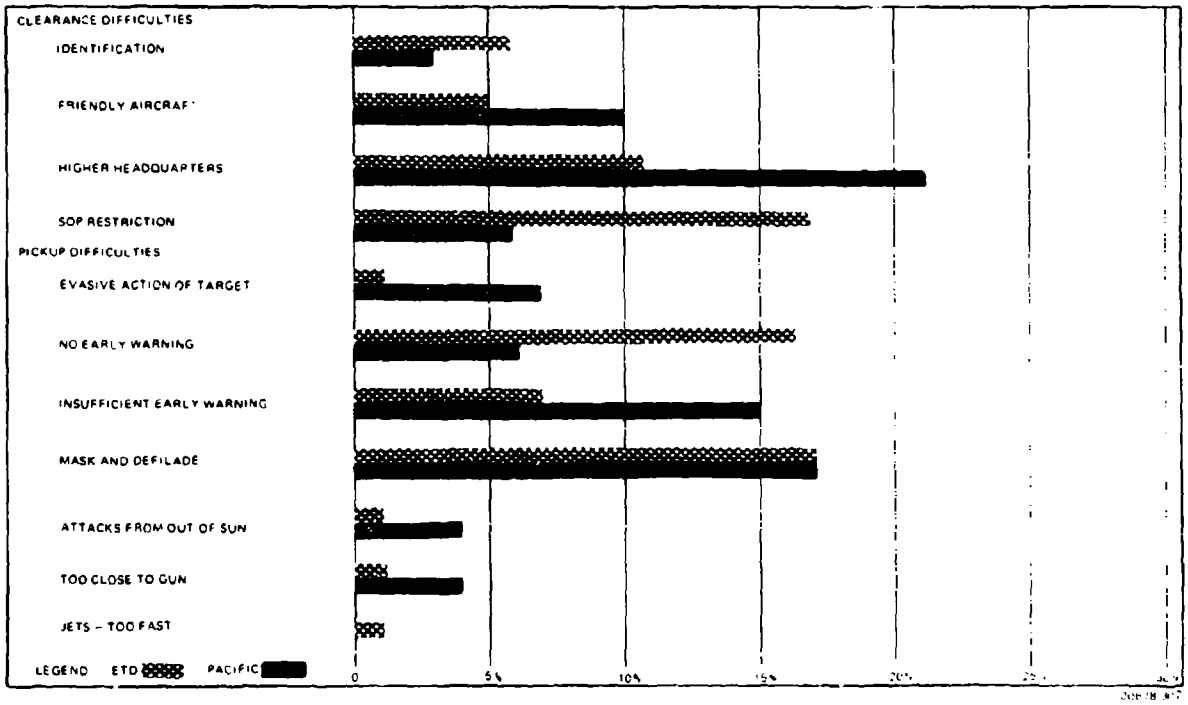

Figure 3-3. Automatic Weapons Operational Difficulties in World War II

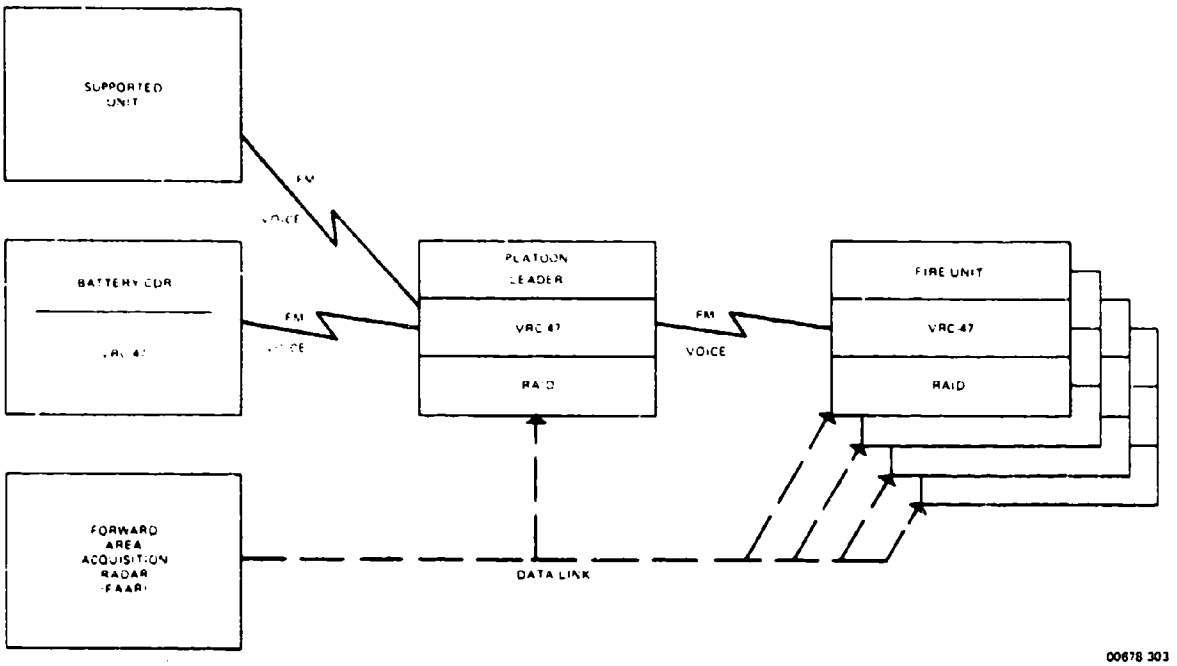

Figure 3-4. Flow of Command and Alerting Information to Fire Units

3.3.2 Surveillance, Search, Detection, and Acquisition

Normally the fire unit would perform surveillance consistent with the situation status. Depending on alert and RAID information, search would be narrowed to a more restricted region. Once detected, a target would be tracked while the identification process was accomplished in order to minimize reaction time.

The details of this process could be as simple as visual search, detection, acquisition, and identification by the gunner, if no surveillance system were available on the mount; it could include use of a nonvisual tracking sensor in a search mode; or it could include surveillance by one sensor and transfer of information to another for tracking.

Figure 3-5 shows the simplest mode in which all operations are performed visually by the gunner.

Figure 3-6 shows the functional flow of activities when search is performed by a radar or IR tracker which converts to a track mode when a target has been detected

Figure 3-7 shows a more versatile system in which surveillance and tracking are performed by separate sensors (as in the European formula). Figure 3-7 has been developed to show a multitarget mode in which a surveillance radar may operate continuously so that new targets appearing while the tracker is engaged may be monitored until the tracker has disposed of its current target. A capability is also suggested for the surveillance radar of Track-While-Scan (TWS) track keeping and generating preliminary rate measurements which may be transferred to the computer with a new target assignment to reduce solution time.

Such a system might have two operators. Data transfer to the tracking sensors would preferably be automatic, with nonautomatic secondary modes as shown in the figure.

The surveillance system might be installed on one AFAADS vehicle out of four, and serve all four. This is consistent with deployment distances between fire units in antiaircraft gun defenses.

3.3.3 Identification

A target may be identified to the AFAADS fire unit by command communications link, by the RAID display, or by local identification at the fire unit.

Identification at the fire unit may be by positive IFF return if AFAADS utilizes a surveillance and/or tracking radar. It may be by visual identification, which requires that the target be allowed to approach much closer than detection range before opening fire. It may be by established doctrine, which bases the decision to engage on the state of alert and a set of rules which

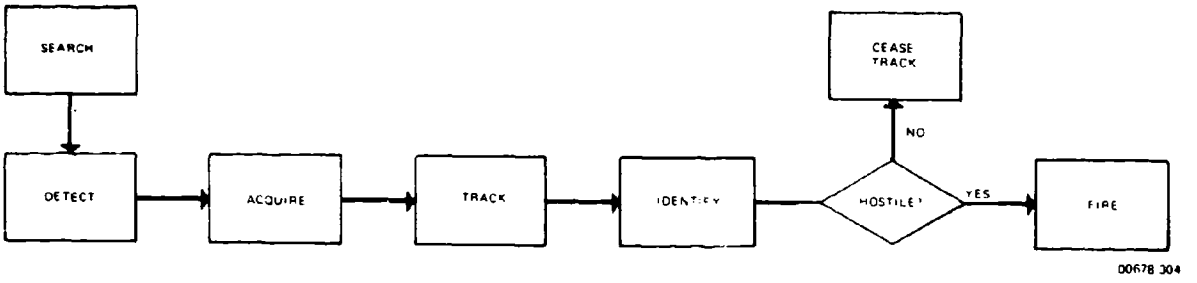

Figure 3-5. Visual Search, Acquisition, and Identification Functional Flow Diagram

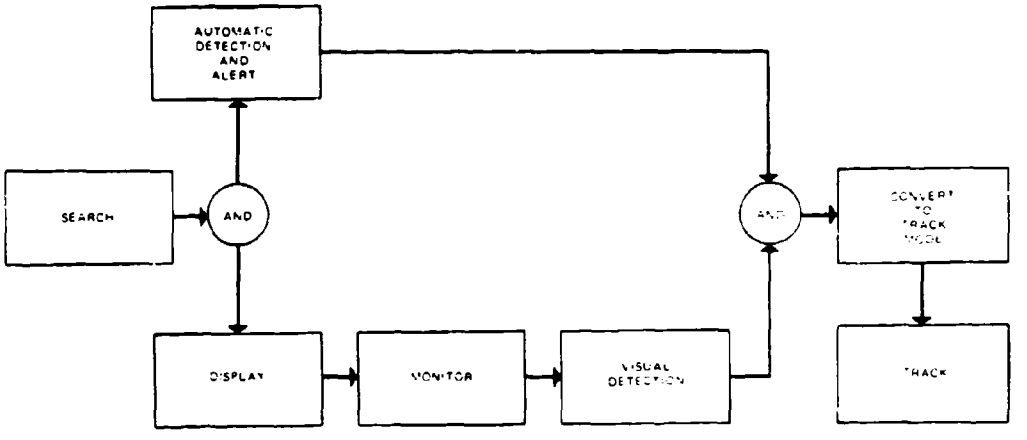

Figure 3-6. Search/Track Functional Flow Diagram

consider departures from established air corridors, altitude, speed, and hostile action. A flow diagram for engagement decision by doctrine is shown in Figure 3-8.

Future identification methods may, depending on the success of research, be based on signature analysis of the reflected radar or laser signal from the target, or by infra-red or acoustic signature analysis. Acoustic signature analysis would be too slow (except possibly for helicopter targets) if performed at the fire unit for the fire unit, however, the large number of acoustic sensors contemplated in the Integrated Battlefield Command System concept suggests that their sensings may be utilizable on a battlefield-wide basis.

The above alternatives for identification at the fire unit are shown in Figure 3-9.

3.3.4 Tracking

The options for tracking modes will be covered in Section 4.2, Sensor Characteristics. We note at this point, however, that consideration must be given to operation in various degraded modes as well as operation with all components function. Modes include:

a. Normal operation, 3-D inputs.

b. Range information denied, angular information available, computer operational.

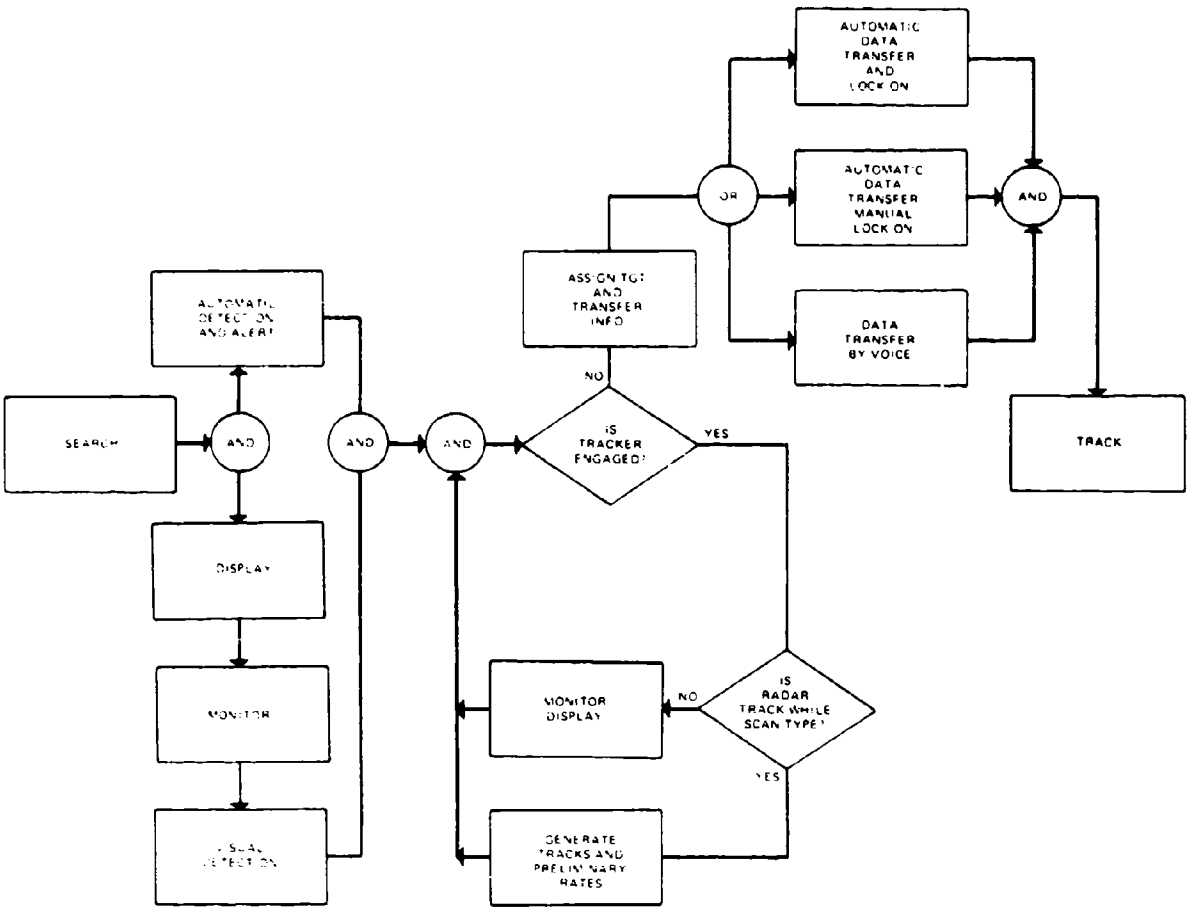

00678 306

Figure 3-7. Surveillance Radar Functional Flow Diagram

c. Range and angle information available, computer inoperative.

d. Angle information only, computer inoperative.

3.3.5 Lead Computation

Determination of preferred algorithms for lead computation is a central task of this study effort, and is dealt with in depth in Section 5, Analysis of AFAADS System Requirements.

3.3.6 Firing Doctrine

With a finite ammunition load on the mount, and the very high rate of fire of the Vigilante, it is not possible to fire continuously for more than a few seconds without exhausting the ammunition and requiring reloading. Some of the considerations in establishing a firing doctrine are presented in Table III-3.

Any useful doctrine must be very simple. Some of the decision elements, such as: whether the computer has settled; whether the target is within effective range; how long it will be within range; and others, can be evaluated by the computer to give the gunner at least an open fire, and cease fire indication. Much more can undoubtedly be done in automating the firing doctrine, and this is a subject for analysis.

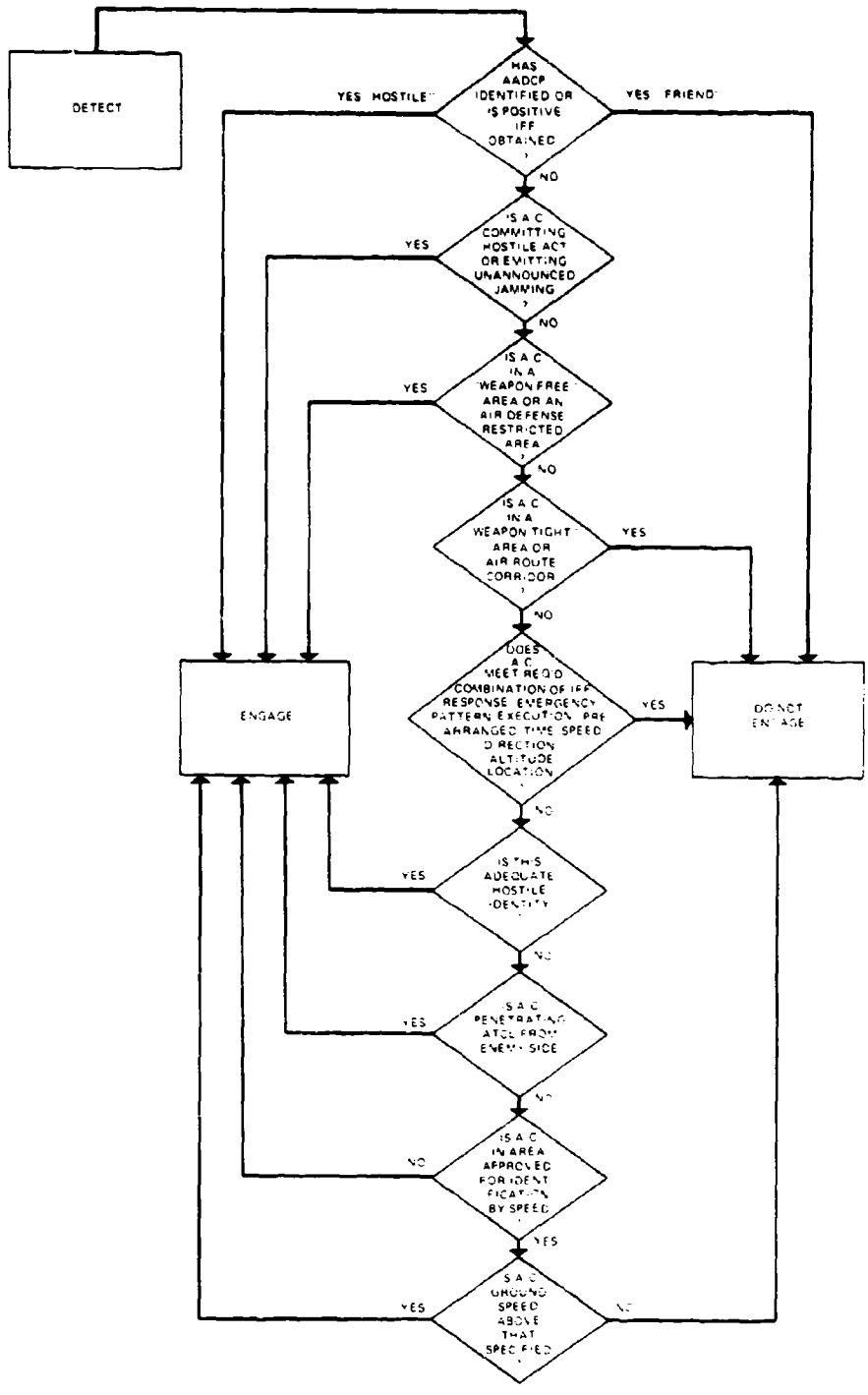

Figure 3-8. Engagement Decision by Doctrine Functional Flow Diagram

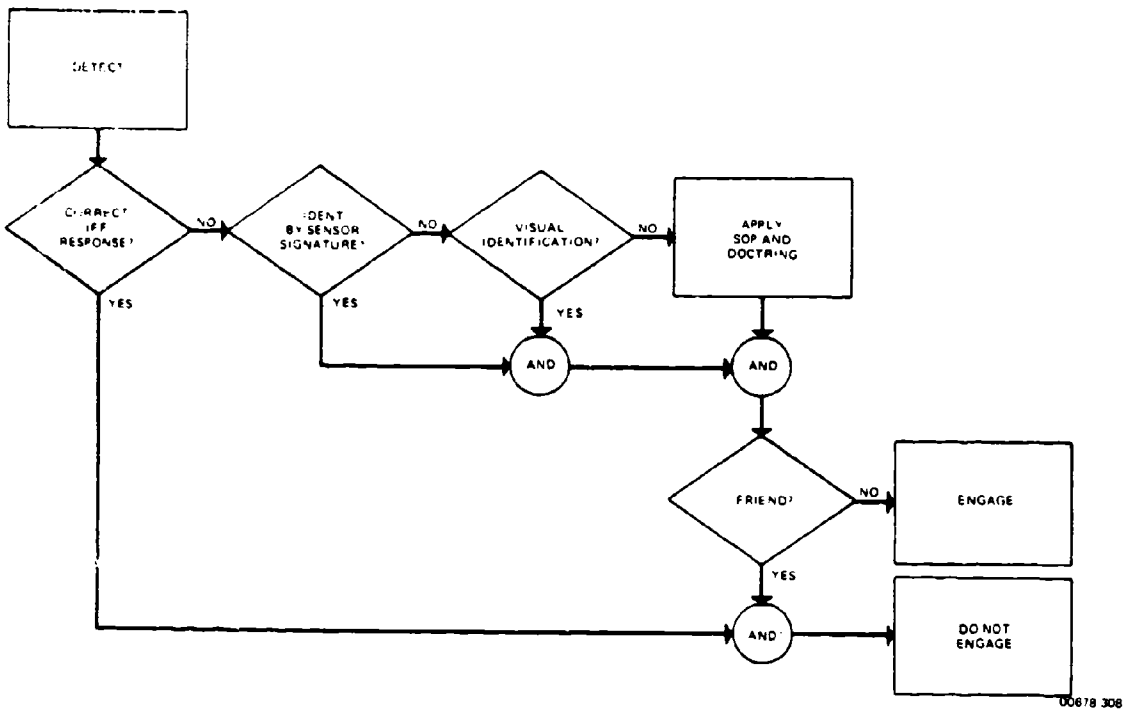

Figure 3-9. Identification Functional Flow Diagram

Table III-3. Consideration in Selecting Firing Doctrine

Firing Doctrine Options	AFAADS System Considerations	Tracking Modes	Target Types	Target Path
Rate of Fire	Ammunition Load	Automatic	Helicopter	Direction
Rounds per Burst	Solution Time	Visual Angle/Auto. Range	Slow Piston Engine A/C	Range
Open Fire Range	Prediction Options		Fast Piston Engine A/C	Altitude
Interval Between Bursts	Dispersion	System Degraded (Range and/or	Jets	Speed
Cease Fire Range		Lead Computation Inoperative)	Ground Targets	Mission

00678-309

SECTION 4
CHARACTERISTICS OF AFAADS

4.1 TARGET CHARACTERISTICS

The purpose of this section is to define the characteristics of the air targets against which AFAADS may be used and to emphasize those parameters which will affect the performance of the AFAADS System most critically. Since AFAADS will be operational in the future when many of its targets may consist of air vehicle types not yet operational, the identification and projection of target parameters, most likely to affect AFAADS capabilities, are considered to be of much greater interest than the precise description of details of existing potential enemy threat vehicles. Present vehicles and forces do, however, serve as base points to assist projection.

AFAADS is concerned with a very restricted region of operation of threat vehicles, namely that lying from about 10,000 ft altitude to ground level. A moderately higher altitude band is of interest in defining the acquisition ranges desired of AFAADS sensors.

Flight at low altitudes may involve terrain following, in which case an irregular flight trajectory will be generated which causes problems in prediction. Maximum speed of multiple-Mach aircraft at low altitude is not likely to be much in excess of Mach 1. As a result, the maximum speed to be handled by AFAADS is somewhat limited, but the interaction of the flight path with terrain, both in sighting and prediction phases of an engagement, is critical.

As a short range weapon, AFAADS will often be used in the close defense of an important point or small area targets. It will thus be engaging enemy threat vehicles during the terminal phase of their attack on ground targets. It is necessary to understand the constraints placed on the attacking aircraft by its own fire control system and munitions load in order to understand what kinds of target trajectories AFAADS must attempt to predict. Currently the attack paths of aircraft delivering iron bombs, rocket fire, and gunfire on small targets include short straight segments on which predicted fire may be highly effective. Aircraft fire control systems under development may cause such straight segments to be of negligible length in the future.

Air-to-surface missiles allow the attacking aircraft to release its weapons at greater distances from the ground target, thereby reducing its exposure to local defenses, while providing greater accuracy in warhead delivery. However they weigh more and cost more than the simpler weapons they replace and, depending on their effectiveness, may impose an additional cost on the enemy which, in itself, justifies AFAADS.

The following paragraphs develop the preceding considerations in greater detail.

The following base line operational limits for AFAADS have been provided by the Army for air targets.

a. Target speed 0-600 knots (1013 f/s).

b. Maximum altitude 3000 meters (9840 ft).

c. Maximum slant range 3000 meters (9840 ft).

d. Maximum target acceleration 5g.

As will be shown later, the defense envelope defined above is relatively small when compared with the release ranges of many of the likely air-to-surface munitions. In the analysis, therefore, it will not be considered an absolute barrier, but rather, the variation in system effectiveness with maximum range will be developed.

4.1.1 The Threat

The development of tactical air capability by all of the major powers is proceeding along roughly comparable lines. The following brief description of Soviet air, with emphasis on tactical and logistic aircraft and helicopters, provides a general background on Soviet current force structure as well as an indication of the support that can be provided by the Soviets to small countries aligned with the communist bloc.

Soviet air forces include the following five main categories: (1) the Long Range Air Force (long- and medium-range strategic bombers); (2) the Tactical (or front-line) Air Force, which includes fighters and light bombers; (3) the air element of the Air Defense Command (fighter-interceptors); (4) the Naval Air Force; and (5) the Air Transport Force (including an independent force for the airborne divisions). There are about 9,800 combat aircraft in all, and the total personnel strength of the five categories listed above is about 505,000.

Tactical Air Force. The strength of the Soviet Tactical Air Force has remained fairly constant for the last nine years. Altogether there are nearly 4,000 aircraft. These include light bombers, ground-attack and interceptor fighters, transport aircraft, helicopters and reconnaissance units.

The aircraft in service still contain a significant proportion of obsolescent types such as the MiG-17 *Fresco*, MiG-19 *Farmer*, and the Il-28 *Beagle*. The most notable high performance aircraft in service are the fighter-interceptor *Fishbed* (MiG-21), the ground-attack *Fitter* (Su-7), the supersonic light bomber *Brewer* (Yak-28) which is gradually replacing the *Beagle*, and

the twin-engined reconnaissance aircraft *Mandrake*. Ground-attack aircraft may now be equipped with tactical air-to-surface missiles, similar to NATO's *Bullpup* and *Martel*. Of several new fighter and fighter-bomber types, including a variable-geometry aircraft resembling the American F-111, displayed at the Moscow Air Show in July 1967, the supersonic strike version of the *Foxbat* is reported to be coming into service.

Air Transport Force. About 1500 short- and medium-range transport aircraft, including twin-engined Il-14s *(Crate)* and An-24s *(Coke)*, some 600 four-engined An-12s *(Cub)* and Il-18s *(Coot)*. A few An-22 *(Cock)* heavy transports are now also in service. There are in addition civil airliners belonging to Aeroflot, some of which could be adapted to military use in time of war; these include about 150 long-range aircraft of the Tu-104 *(Camel)*, Tu-114 *(Cleat)*, Tu-124 *(Cookpot)*, and Tu-134 *(Crusty)* classes.

Helicopters in use with the ground forces include the troop-carrying *Hook* (Mi-6) and *Hip* (Mi-8), the heavy load-carrier *Harke* (Mi-10), and the smaller *Hare* (Mi-3) and *Hound* (Mi-4). The *Homer* (Mi-12), a very heavy load-carrier may shortly be entering service. The total helicopter inventory is probably around 1,500.

Observations of Soviet tactical air operations in field exercises in East Germany have indicated tactics similar to those of the United States and other Western countries; i.e., low altitude approach to the vicinity of a target, pop up to acquire the target, and then an attack pass appropriate to the munition type being delivered. Like most other countries, the Soviets have been observed experimenting with helicopter-launched missiles for the attack of ground targets.

Missiles. Tactical missiles in use by the ground forces include those of the *Frog* and *Scud* series, which are carried on modified tank chassis and wheeled launchers, and have ranges of up to 150 miles according to model and the type of warhead carried (high-explosive, chemical or nuclear). There are also two larger cruise missiles - *Shaddock*, with a range of up to 250 miles, and the shorter range *Salish*. A new missile system associated with *Scaleboard*, first seen in November 1967, may have a range of 450 miles.

These missiles and follow-on designs are unlikely to be profitable targets for AFAADS. If, however, SAM defenses drive the cruise missiles to very low altitudes and with the incorporation of terrain following equipment, the missiles may penetrate the defensive envelope of AFAADS.

4.1.1.1 Categories of Targets, Munitions, and Tactics

In this section categories are established for target vehicles, their munitions, and tactics for approach to the target and weapons delivery. Later paragraphs develop relevant characteristics in greater detail.

Target Vehicles. The target vehicles, that were considered for this report, include:

a. Fighters in ground support.

b. Fighter/Bombers.

c. Bombers.

d. Helicopters.

e. V/STOL Aircraft.

f. Logistic Aircraft.

g. Cruise Missiles.

The distinction among fighters, fighter/bombers, and bombers for AFAADS may be expanded according to:

a. Size (detection, tracking accuracy, hit probability, payload).

b. Speed.

c. G-limit (evasive action, terrain following capability).

d. Tactics resulting from the preceding characteristics.

Helicopters may be further subcategorized according to type and mission such as:

a. Reconnaissance.

b. Gunship.

c. Logistic.

V/STOL aircraft are operational. The British VTOL Harrier fighter is being procured by the U.S. Marine Corps and tactics for its use are being developed.

Logistic aircraft will be targets for AFAADS principally in defense against an air assault operation. They are unlikely to impose any requirements additional to those established by the more maneuverable attack aircraft and helicopters.

The existence of cruise missiles, and the possibility that effective SAM defenses will drive them to altitudes penetrating the AFAADS defense envelope suggests that they should be considered in a complete threat evaluation.

Air to Surface Munitions. These include:

a. Guns.

b. Unguided Rockets.

c. Iron Bombs

d. Guided Bombs.

e. Air to Surface Missiles.

Air to Surface Weapon Guidance. A partial categorization of air to surface guided weapons by type of guidance is as follows:

a. Visual control all the way (SS-11).

b. Automatic following of manually controlled sight line (TOW).

c. TV head with control from launch aircraft.

d. Semi-active homing: Radar homing: Laser Target designation.

e. Passive homing: Optical contrast: Infrared.

Tactics. Approach-to-the-target and attack-of-the-target are the two consecutive phases of an attack on a ground target, and are discussed in detail later. Tactics for attack of a ground target depend on the type of munition being delivered and the type of fire control system, or missile guidance system used by the attacking aircraft. The following table subcategorizes attack tactics.

4.1.1.2 Aircraft Characteristics

A convenient way of summarizing military aircraft performance capabilities is by means of altitude-speed envelopes, with 'excess-power' overlays. Figure 4-1 shows such envelopes for the F-104G, F-4 and MiG-23 aircraft. These envelopes bound the region within which the aircraft can maintain steady flight. Note that the maximum Mach number at sea level is much lower than that at altitude for the aircraft shown. The contours are for the aircraft in 'clean' configuration.

Table IV-1. Tactics for Munition Delivery

Munition	Type of Attack
Guns	Strafe
Unguided Rockets	
Iron Bombs	Level Glide Dive Dive-toss LABS LABS (over the shoulder) Laydown Standoff
Guided Munitions	Guided all the way Launch and leave Pop-up

00678-401

As thrust/weight ratios increase with time, maximum speed at sea level will increase slowly. However external stores drastically reduce maximum speed. The Dassault Milan, for example, has a capability of Mach 1.2 at sea level, clean, but only Mach 0.87 with full external stores of 14 bombs. Its high altitude speed is given as Mach 1.8. Even in the clean configuration, maximum Mach is achieved only in non-maneuvering flight (dives excluded). An aircraft which has delivered its munitions will be of lesser interest to AFAADS than one which is on its way to target. The thrust/weight ratio of light bombers is much less than that of fighter-bombers with a corresponding reduction in the performance envelope. This is illustrated by the following table.

Within the performance envelope of Figure 4-1, contours can be drawn to show the excess power available to the pilot by applying maximum throttle or afterburner. Figure 4-2 shows such contours for the F-104G and a proposed Lockheed design (CL-981). Specific excess power (P_s) is defined as the excess of maximum thrust over drag, multiplied by speed, per pound or aircraft weight, i.e.,

$$P_s = (T-D)v/W$$

It may be interpreted as the maximum steady rate of climb which can be sustained at each point within the performance envelope, or divided by (v), as the maximum horizontal acceleration (in g) which can be generated at that point in level flight.

From Figure 4-2 one can determine that the F-104G flying at Mach 0.6 at sea level can develop an acceleration along the flight path of 0.8g.

This acceleration is small compared with that which the airplane can generate by turning, pull-up, or push-over. The maximum acceleration which the airplane can generate is limited only by structural or pilot g-tolerance limits. Limits are higher for fighter than for bomber aircraft, and for positive (eyeball-in) than negative (eyeball-out) accelerations. For this reason, tactical maneuvers involving a series of high-g arcs to place the aircraft in an attack position are likely to involve aircraft rolls so that the pilot experiences only eyeball-in acceleration.

As a point of reference, the Dassault Milan is stated to have the following capability of sustained acceleration in a stabilized turn at low altitude.

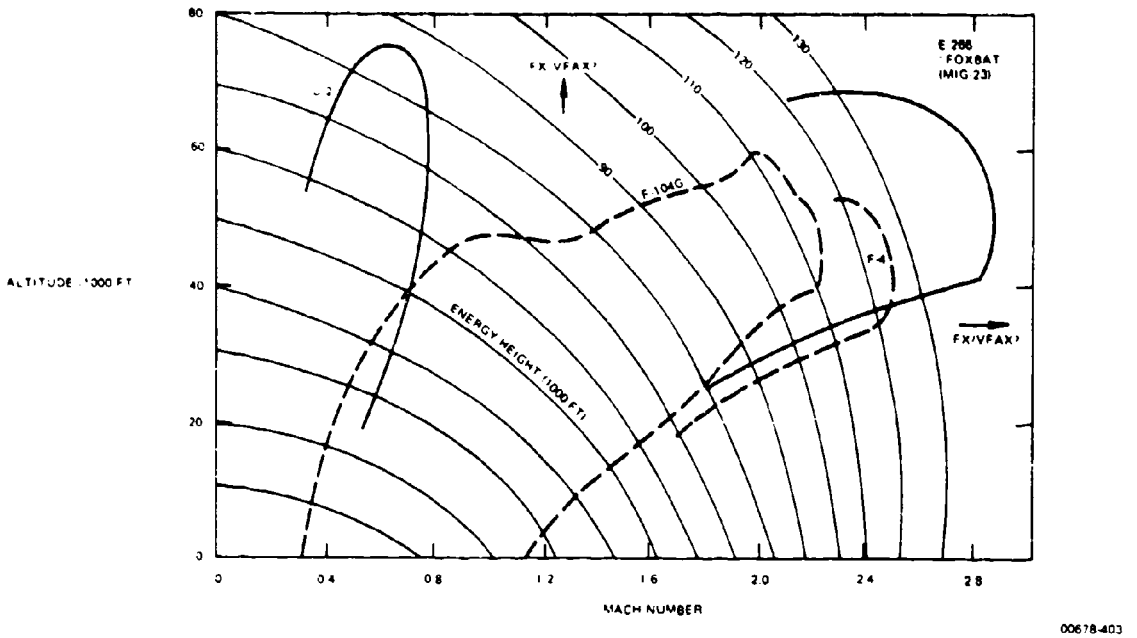

Figure 4-1. Comparative Speed - Altitude Envelopes

Speed	Acceleration	Turning Radius
510 mph	?g	2500 ft
340 mph	4.?g	1720 ft

Table IV-2. A Comparison of the Thrust/Weight Ratio of Various Aircraft

Aircraft Type	Thrust Weight Ratio
F-104G (clean)	0.85
Dassault Milan (clean)	0.74
Dassault Milan (max stores)	0.53
IL-28 (Beagle)	0.27
TU-16 (Badger)	0.22

00678-402

Lateral accelerations required to degrade a predicted fire system by jinking are relatively small, compared with the maximum acceleration capability of any of the target aircraft, and are set by tactics rather than by aircraft performance maxima.

When maneuvering flight is sustained for extended periods of time, as in terrain following, the maximum accelerations are set principally by pilot tolerance for continuous 'g' fluctuations, rather than by aircraft limits. Terrain following is discussed at length in a following section.

The information presented above has been taken from unclassified sources. Energy-maneuverability charts for a large number of current U.S. and foreign military aircraft can be found in classified literature.

4.1.1.3 Helicopter Characteristics

Helicopters may have lower maximum g-structural limits than fixed wing aircraft. From the point of view of AFAADS, however, their principal difference is in their capability to fly slow and to conform very closely to terrain contours in 'nape-of-the-earth' flying. They may, in addition, 'pop-up' briefly from behind a hill, release their weapons, and then drop out of sight with very short exposure time.

4.1.1.4 Air-to-Surface Guided Weapon Characteristics

While the characteristics of a large number of current Free World air to surface guided weapons is known, little information is available in the open literature on small Soviet tactical air-to-surface missiles. There is, however, no reason to believe that the

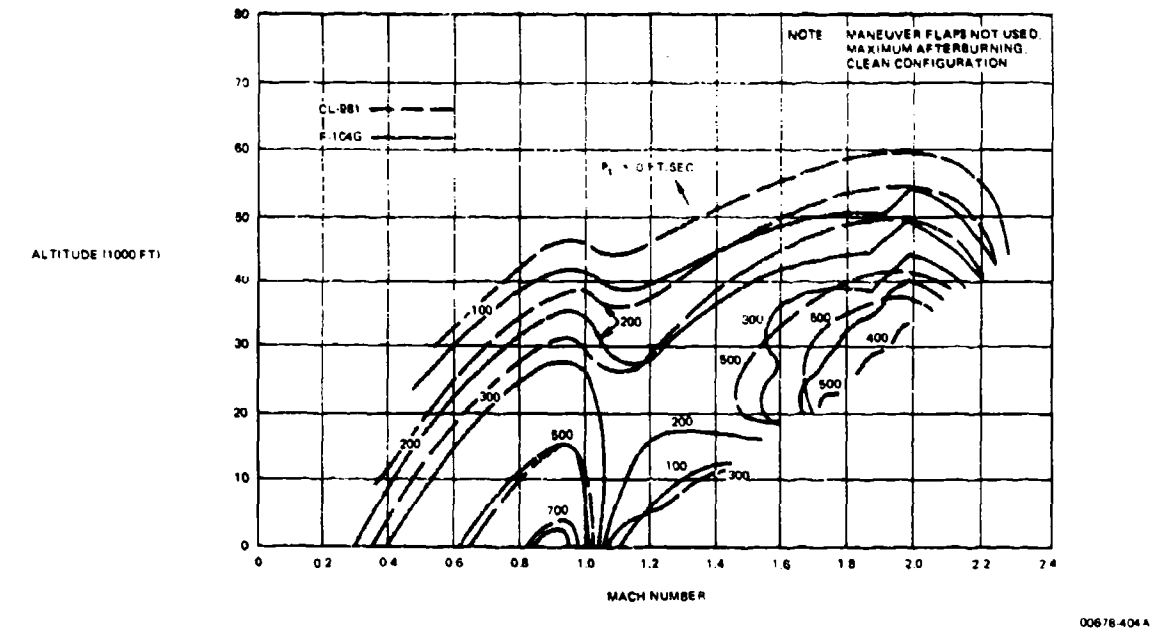

Figure 4-2. Specific Excess Power Overlays

Soviets will follow different lines of development of small tactical missiles from those of the Free World.

As an indication of the price that an aircraft pays in terms of weight for carrying missiles, Figure 4-3 summarizes the missile launch weight versus range. Also shown, where available, are the warhead weight in parenthesis and the guidance type. Note that weight increases approximately as the range squared, up to the ten nmi range.

Wire guided missiles have a maximum range of 2 mi, and in almost all cases are intended for launch from helicopters. Increased range requires that the wire be replaced by radio or other link. The most primitive systems require the operator to steer the missile to the target by observing both the target and a flare in the tail of the missile. More advanced systems track the flare automatically and slave the missile to a sight line directed by the operator. Sight stabilization assists the operator in keeping his sight on target while the launch aircraft takes evasive action.

More advanced systems for longer range utilize TV homing, with the picture transmitted back to the operator who controls the missile. This system may be combined with optical contrast homing, which allows the missile to home on a target designated by the operator via the TV link. Once locked on, the missile homes, and the launch aircraft can leave the area. IR homing may also be used. There are several antiradiation missiles. These systems and inertial guidance increase launch range, allow the carrier aircraft to leave after launch, and minimize exposure of the aircraft to defensive fire.

A current hybrid system with promising reports involves missile homing on a laser spot placed on target by a ground observer, or by an observer in another aircraft.

4.1.2 Threat Tactics

As previously stated, it is necessary to understand the constraints placed on the attacking aircraft by its own fire control system and munitions load in order to understand what kinds of target trajectories AFAADS must attempt to predict. In addition, the ability of the enemy to attack at night or in inclement weather is important to the choice of sensors for AFAADS.

In the following paragraphs night operations are reviewed from a historical point of view, then some problems associated with weather are discussed, and, finally tactics are described in detail.

4.1.2.1 Night Capabilities

An important consideration of AFAADS design is the need for the capability of acquiring targets at night. A good example of the tactics employed in the acquisition of targets at night in the past is provided

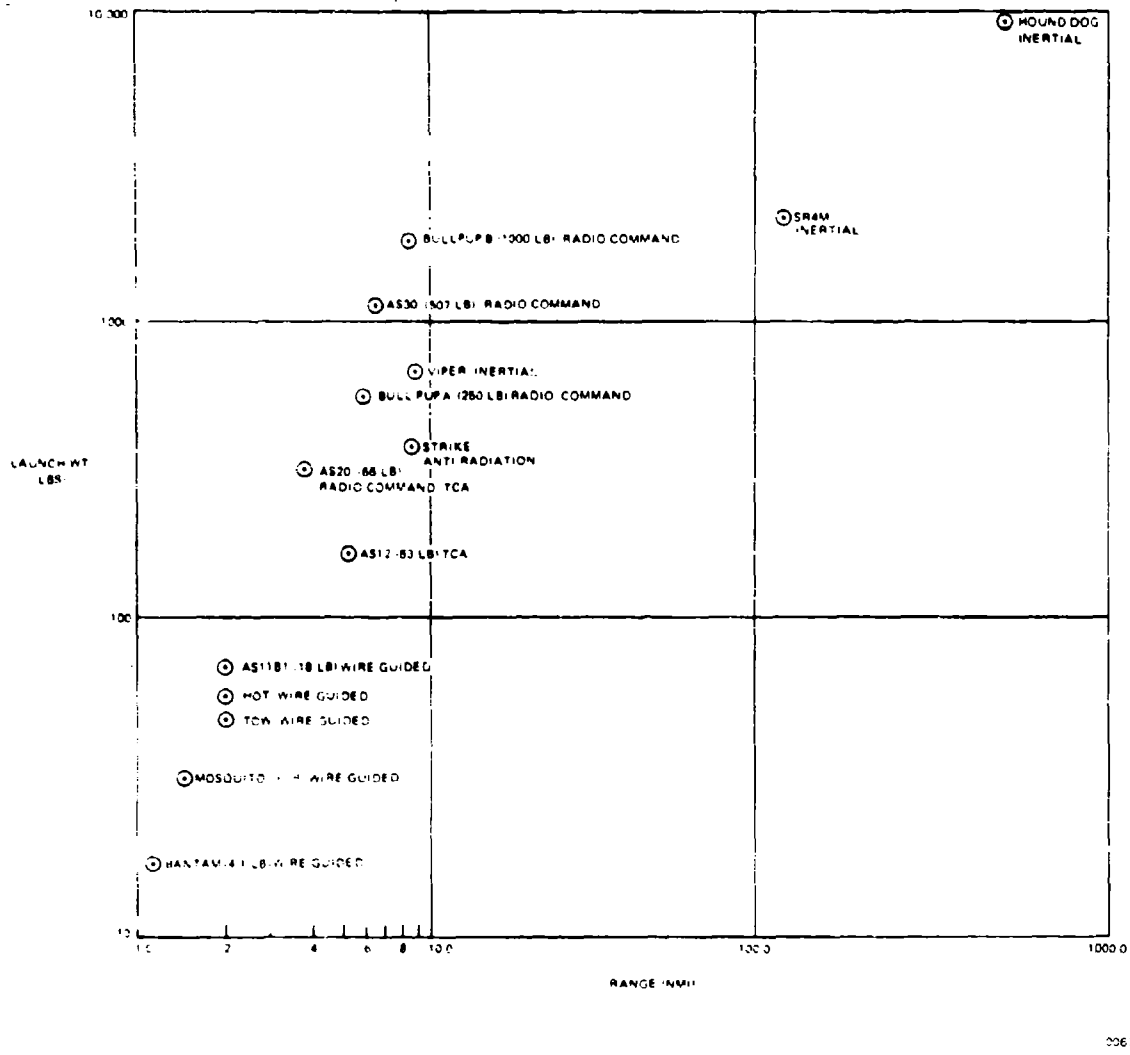

Figure 4-3. Air-to-Surface Missile Weight versus Range

by Korean War operations. Once the USAF gained air superiority in Korea, the enemy took immediate countermeasures by moving supplies and men at night. Since the Air Force had few planes capable of night attack against moving targets, it became a matter of developing special tactics to cope with the problem. Since the B-26 was the principal tactical bomber of the USAF in Korea, the tactics employed were influenced by (1) the capabilities of these aircraft, (2) the rough and mountainous terrain of North Korea, (3) changes in weather which made positive identification of landmarks difficult, and (4) the availability of natural or artificial illumination. In the early stages of night operations, acquisition of the target during moonlit nights was made by flying low. On the darker nights the search for targets was made at altitudes of about 2000 feet above the terrain which meant that the searches were conducted at from 3000 to 4000 feet in the western half of Korea and from 5000 to 6000 feet in the mountainous regions of eastern Korea. From these altitudes, pilots seldom had difficulty spotting enemy convoys by virtue of their illuminated headlights. Once the convoy was spotted, the B-26 would drop a flare at about 3500 feet upwind of the target and begin strafing passes with figure-eight turns down as low as 200 feet in order to make two or three passes before the flare burned out.

In western Korea, pilots began firing from altitudes of 2000 to 1500 feet; and in eastern Korea, pilots started their strafing passes from 6000 to 5000 feet

and pulled up at a height of from 2000 to 1500 feet. Because of the hazardous terrain and uncertainty of the aerial charts, the B-26 crews usually pulled up from strafing attacks at altitudes of not less than 1000 feet higher than the highest published height of terrain features in the vicinity of a target. While bombing attacks were used against enemy convoys, it was felt that low-level strafing runs were more damaging to the enemy. However, as the war progressed and better tactics were devised, the evidence indicated that bombing was much more effective than strafing over a period of time and under all conditions. It was found that bombing tactics worked best on the darkest nights, when the crews scouted for lights of enemy convoys. Upon locating an enemy convoy, they analyzed the convoy's size and direction of movement. Once the analysis was completed, the bomber's crew took an attack heading, usually one which paralleled the road or intersected it at a slight angle. When the aircraft was committed to the attack, the bombardier synchronized on either the first available light or the portion of the road containing the largest number of vehicles. Bombing from 7000 feet, a crew achieved success which varied with its successful analysis of the bombing problem.

Figure 4-4 plots B-26 sorties per month over the duration of the war. After mid-1951 almost all sorties were at night.

Another tactic employed was one in which the pilot cruised with reduced power at about 15,000 feet until he spotted a string of truck lights. He then entered a shallow glide and released his bombs from 6000 to 4000 feet. Because the aircraft approached suddenly and quietly, Red convoys usually did not have time to extinguish their lights before the B-26 laid his bombs on them. As a result the B-26 seldom drew any ground fire.

During the periods of inclement weather which normally grounded most air attacks, the USAF used MPQ-2 and MSQ-1 bombing director radars to place close-support bombs against deeply entrenched enemy troops, supply dumps, and artillery. During a three-month period, over 3000 bomb runs were made, and over 5000 tons of bombs that were dropped, using three tactical air-direction posts to control the aircraft. An Air Force evaluation had indicated that the circular probable error of ground-radar directed B-26s was 1177 feet.

To provide local defense of their installations in North Korea, the Communists increased their flak order of battle to reach peak totals of approximately 786 antiaircraft artillery guns and 1672 automatic weapons in the winter of 1952-53 (see Figure 4-5). The principal heavy gun was the Soviet 85mm M-1939 piece, the effective ceiling of which was about 25,000 feet. The principal automatic weapon was the Soviet 37mm M-1939, which could fire approximately 160

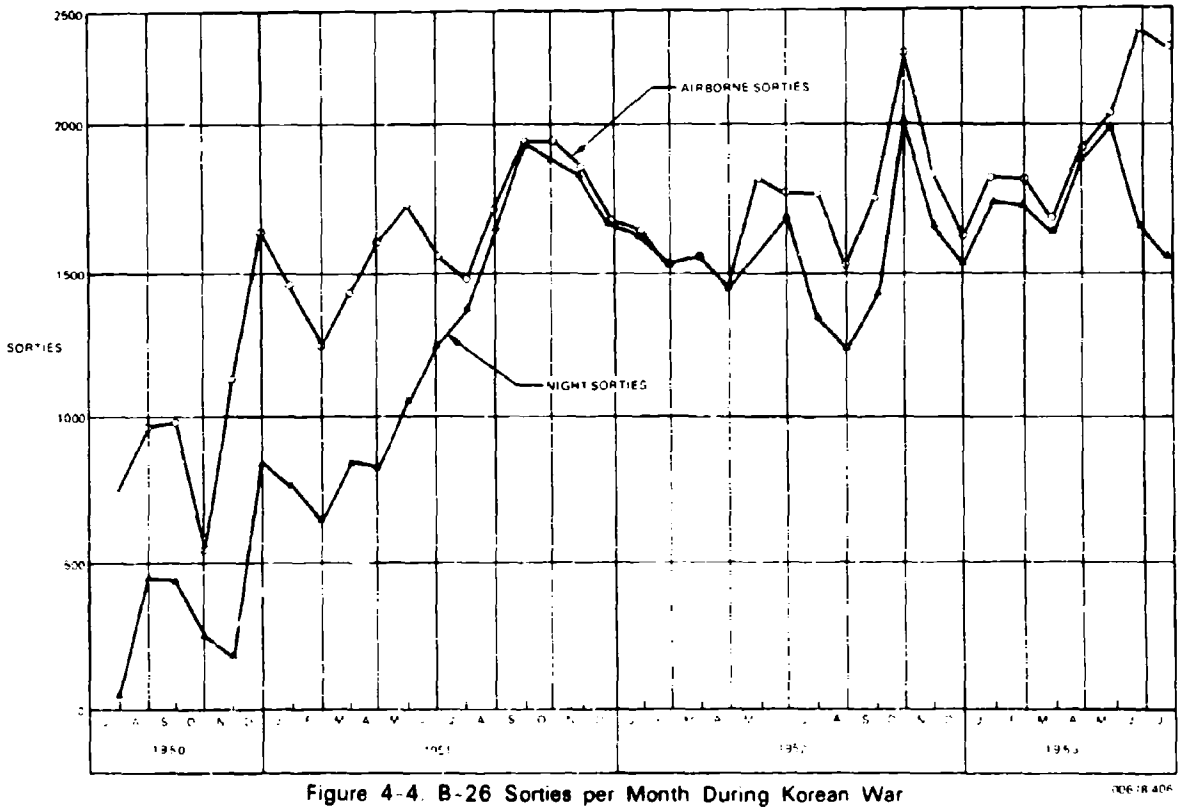

Figure 4-4. B-26 Sorties per Month During Korean War

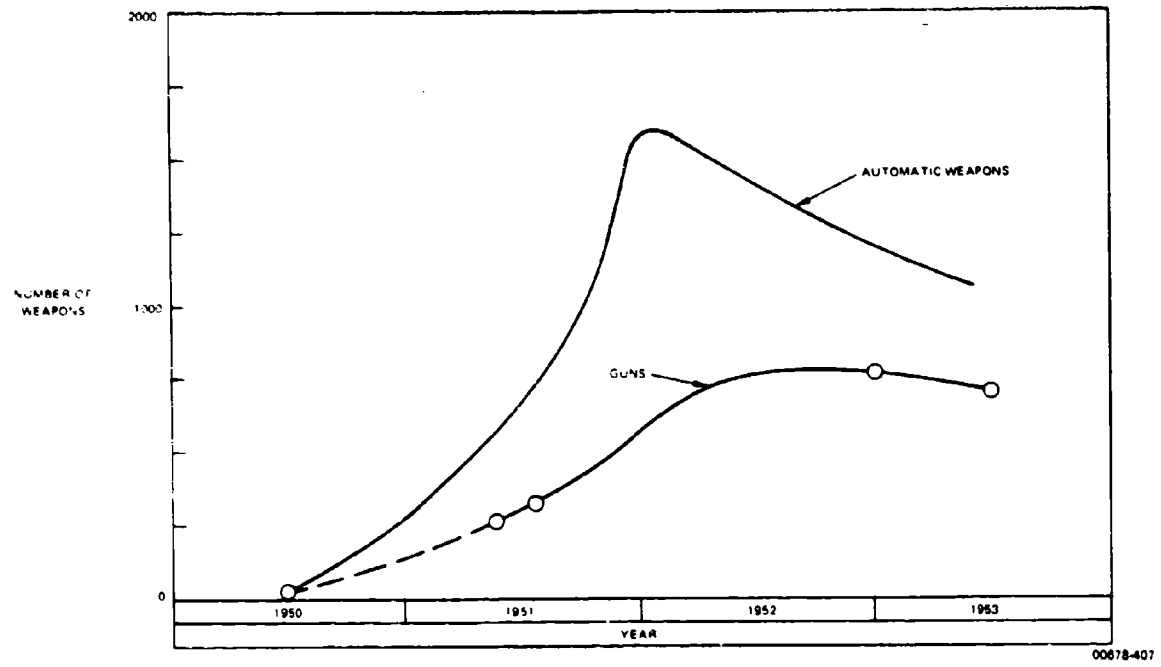

Figure 4-5. Approximate Number of Antiaircraft Weapons in North Korea

rounds a minute up to an effective ceiling of about 4500 feet. Concurrent with the increased availability of Red guns was the increased defense of specific targets as shown in Figure 4-6. Lacking enough gun-laying radars and forced to use day-fighters in a night-fighter role, the Reds made extensive use of searchlights. On clear nights the searchlight beams ranged up to 30,000 feet, and those which were paired with radars or sound control mechanisms could locate and track an aircraft until other visually directed lights could switch on and provide additional illumination of the plane.

Figure 4-7 is a composite drawing showing over the same period of time: (1) the percent of USAF sorties by night, (2) the number of B-26 aircraft lost to antiaircraft guns by quarter, (3) the number of Red weapons, and (4) the number of fire control radars.

Conclusion. It is evident from Figure 4-4 that radar control at night of all North Korean weapons could have made the B-26 strikes sustain unacceptable losses. (The maximum number of B-26s in the theater was 232, and the production line had been stopped several years previously.)

4.1.2.2 All-Weather Capabilities

Since one of the considerations in AFAADS is the need for all-weather sensors, a brief survey has been made of the probability that an aircraft may be obscured from the ground by clouds in good weather.

The probabilities of a clear line-of-sight, based on real observations covering much of the Northern Hemisphere, as limited by cloud cover, are described in a report[1] by L. A. Bertoni. The author states that these estimates should be considered as a first approximation since: (1) the observations were taken in a subjective manner, (2) the estimates were based only on about one year of data, and (3) cloud variability may be quite large within some of the 10° sectors sampled. In order to reduce the subjectivity of the observer and because a great many of the observers would probably lack meteorological training, the type of observation was limited to a 'Yes' or 'No' (check-off) answer.

A check of statistics of clear days, as summarized from standard surface observations, reveals that they provide a much more optimistic picture than that provided by observations of the ground by an aircraft observer as indicated by the 72,000 observations on which the report was based. It appears that what is defined as a clear day by a ground observer is not a clear day to an airborne observer.

However, although this discussion is based on airborne observations, it has been assumed that if the airplane can't see the ground, then it cannot be seen from the ground. Two angles were selected for discussion. They are -90° and -30° from the horizon as

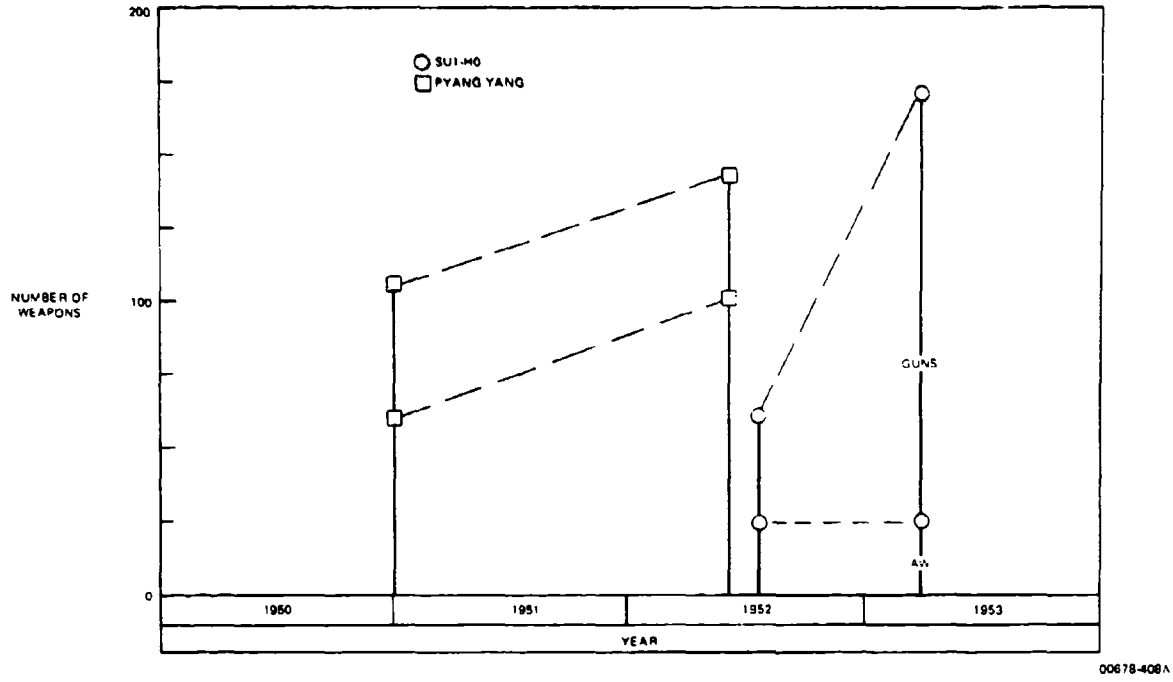

Figure 4-6. Defense of Specific Targets

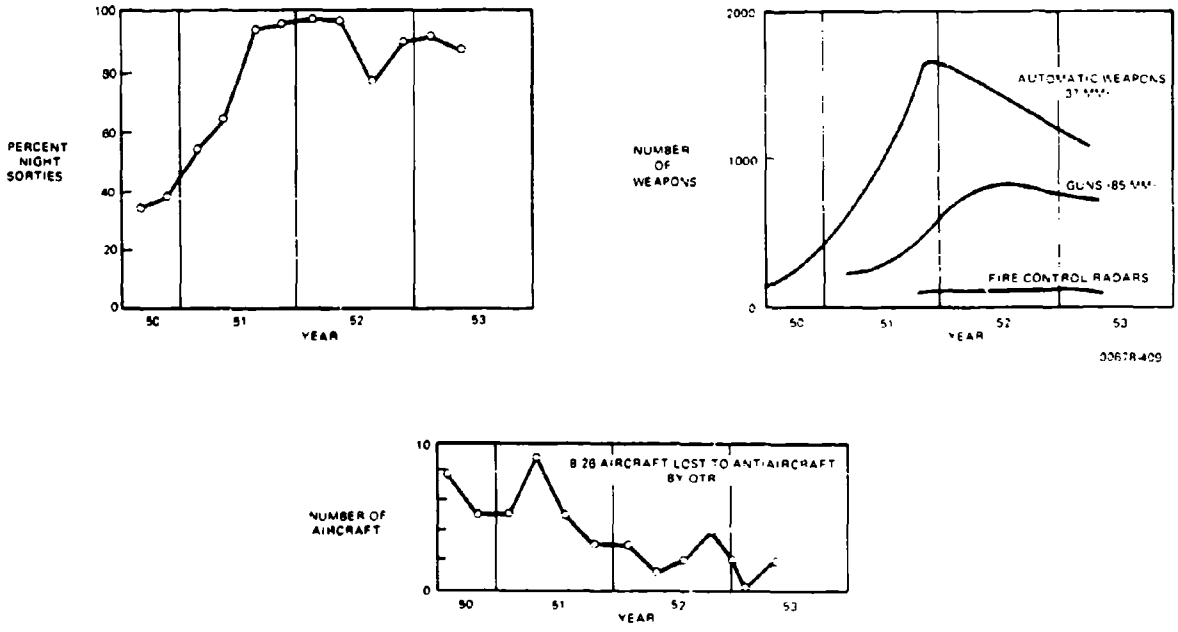

Figure 4-7. Composite Drawing Showing Over the Same Period of Time; the Percent of USAF Sorties by Night, the Number of B-26 Aircraft Lost to Antiaircraft Guns by Quarter, the Number of Red Weapons, and the Number of Fire Control Radars

recorded by an airborne observer flying at the following altitudes: below 1800 ft, 1801 to 3600 ft, 3601 to 7400 ft, 7401 to 14,999 ft, 15,000 to 24,999 ft, 25,000 to 34,999 ft, 35,000 to 44,999 ft, and above 45,000 ft. Although observations were recorded as high as 45,000 ft, AFAADS is only concerned with those observations below 15,000 feet. The observations were further grouped into seasons: the winter season being December, January, and February; the spring season being March, April and May; the summer season being June, July, and August; and the fall season consisting of September, October, and November.

Tables IV-3 through IV-6, representing the four seasons, tabulate the probability of seeing an aircraft from the ground. The probability is designated as low, mean, or high. The low probability represents the lowest estimate of probability of seeing an aircraft for all sectors considered at a particular altitude and a particular season; the high probability represents the highest estimate of probability of seeing an aircraft for all sectors considered at a particular altitude and a particular season. The mean probability is the mean of all these estimated probabilities. It should be noted that each probability in any particular sector is based on no less than ten observations. These figures were derived from a random sampling of observations obtained all over the Northern Hemisphere from 20°E westward through 0° to 110°E longitude and from the equator to 80°N latitude. Graphs of the tables are shown in Figures 4-8 through 4-11. It is interesting to note that in all four graphs the aircraft can be seen a greater percentage of the time at higher altitudes at -30° than directly overhead. On the average there is about a 50 percent probability that an aircraft at 5000-ft altitude will not be obscured by clouds.

A comparison was made in the report between aircraft observations and surface cloud and sunshine observations by McCabe.[2] The differences were substantial. Some of this difference may be explained by Lund[3] who states: "Since the sunshine recorder does not detect 'thin' clouds, the probability of a clear line-of-sight, as defined in this paper, exceeds the probability of a cloud-free line-of-sight by an amount equal to the probability of 'thin' clouds, roughly 6 to 20 percent at the stations under study." More may be explained by the fact that smoke, haze, and ground fog are not detected by the sunshine recorder, yet their presence can be a serious obstruction to seeing the aircraft from the ground.

If the small sample of aircraft observations is representative of the true relationship between probabilities deduced from standard surface weather observations and the actual probability that air crews can see the ground, estimates of clear lines-of-sight from the air, based upon standard surface weather observations, are very greatly inflated. Moreover, these observations disclose that the aircraft can be seen less than 62 percent of the time.

Table IV-3. Estimates of the Probability of Seeing the Ground from an Aircraft During the Months of March, April and May

Time of Year	Angle of Sight from Horizontal	Altitude (feet)	Probability of Sight (percent)			No. of Observations
			low	mean	high	
Spring	-90	1,800	29	76	100	393
Spring	-30	1,800	0	71	100	393
Spring	-90	1,801 - 3,600	40	85	100	373
Spring	-30	1,801 - 3,600	40	77	100	373
Spring	-90	3,601 - 7,400	0	70	100	373
Spring	-30	3,601 - 7,400	0	64	100	373
Spring	-90	7,401 - 15,000	17	51	89	2,509
Spring	-30	7,401 - 15,000	9	45	100	2,509

00678-410

Table IV-4. Estimates of the Probability of Seeing the Ground from an Aircraft During the Months of June, July and August

Time of Year	Angle of Sight from Horizontal	Altitude (feet)	Probability of Sight (percent)			No. of Observations
			lowest sector	mean over N.Item	highest sector	
Summer	-90	1,800	50	78	100	720
Summer	-30	1,800	25	71	100	720
Summer	-90	1,801 - 3,600	0	59	100	768
Summer	-30	1,801 - 3,600	0	52	100	768
Summer	-90	3,601 - 7,400	0	49	96	1,180
Summer	-30	3,601 - 7,400	0	41	96	1,180
Summer	-90	7,401 - 15,000	13	46	100	2,255
Summer	-30	7,401 - 15,000	0	40	100	2,255

00678-411

Table IV-5. Estimates of the Probability of Seeing the Ground from an Aircraft During the Months of September, October and November

Time of Year	Angle of Sight from Horizontal	Altitude (feet)	Probability of Sight (percent)			No. of Observations
			low	mean	high	
Fall	-90	1,800	30	81	100	1,107
Fall	-30	1,800	30	76	100	1,107
Fall	-90	1,801 - 3,600	25	73	100	920
Fall	-30	1,801 - 3,600	38	72	100	920
Fall	-90	3,601 - 7,400	13	56	94	1,338
Fall	-30	3,601 - 7,400	13	52	100	1,348
Fall	-90	7,401 - 15,000	13	44	95	3,378
Fall	-30	7,401 - 15,000	0	37	84	

00678-412

Table IV-6. Estimates of the Probability of Seeing the Ground from an Aircraft During the Months of December, January and February

Time of Year	Angle of Sight from Horizontal	Altitude (feet)	Probability of Sight (percent)			No. of Observations
			low	mean	high	
Winter	-90	1,800	58	93	100	1,358
Winter	-30	1,800	45	82	100	1,358
Winter	-90	1,801 - 3,600	0	65	89	1,190
Winter	-30	1,801 - 3,600	27	65	89	1,190
Winter	-90	3,601 - 7,400	20	50	80	2,330
Winter	-30	3,601 - 7,400	14	46	80	2,330
Winter	-90	7,401 - 15,000	0	39	100	7,719
Winter	-30	7,401 - 15,000	0	42	100	7,719

00678-413

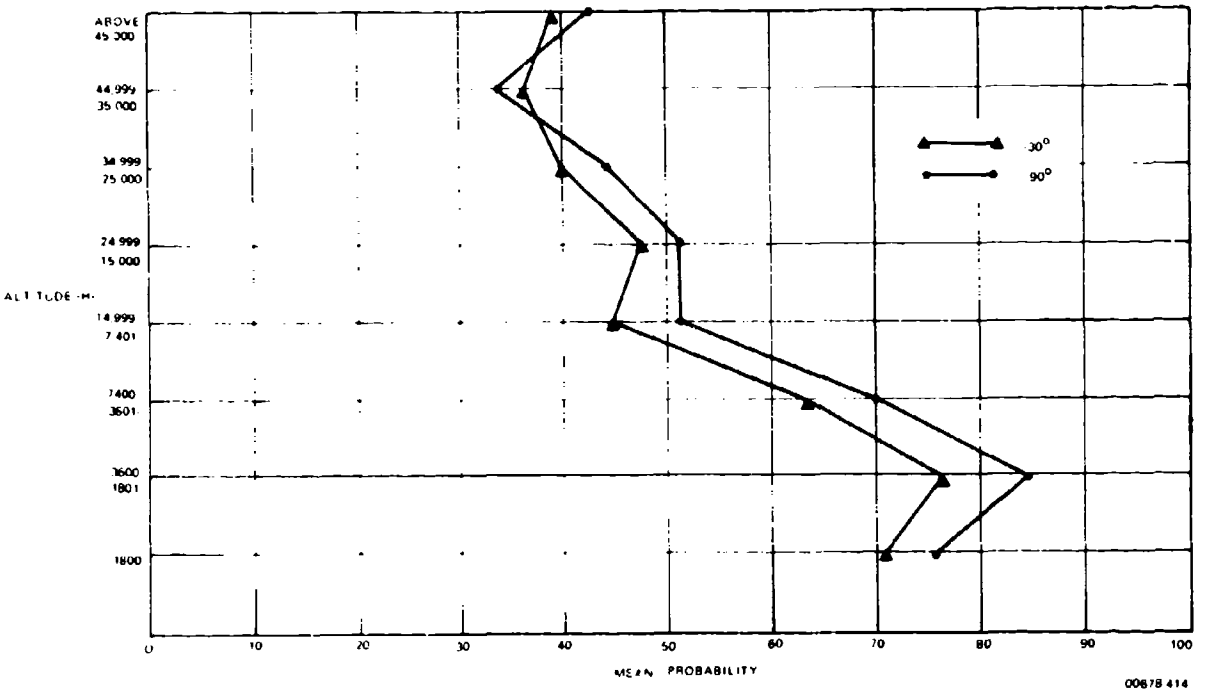

Figure 4-8. Mean Probability of Seeing an Aircraft from the Ground During the Months of March, April and May

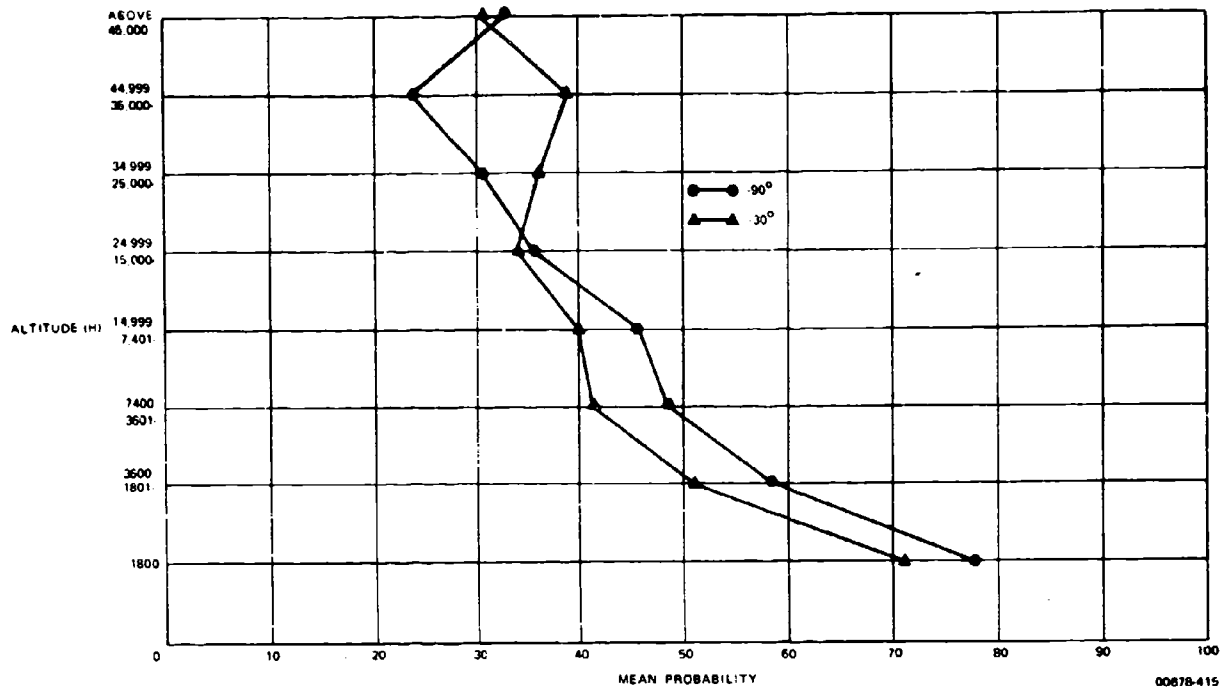

Figure 4-9. Mean Probability of Seeing an Aircraft from the Ground During the Months of June, July and August

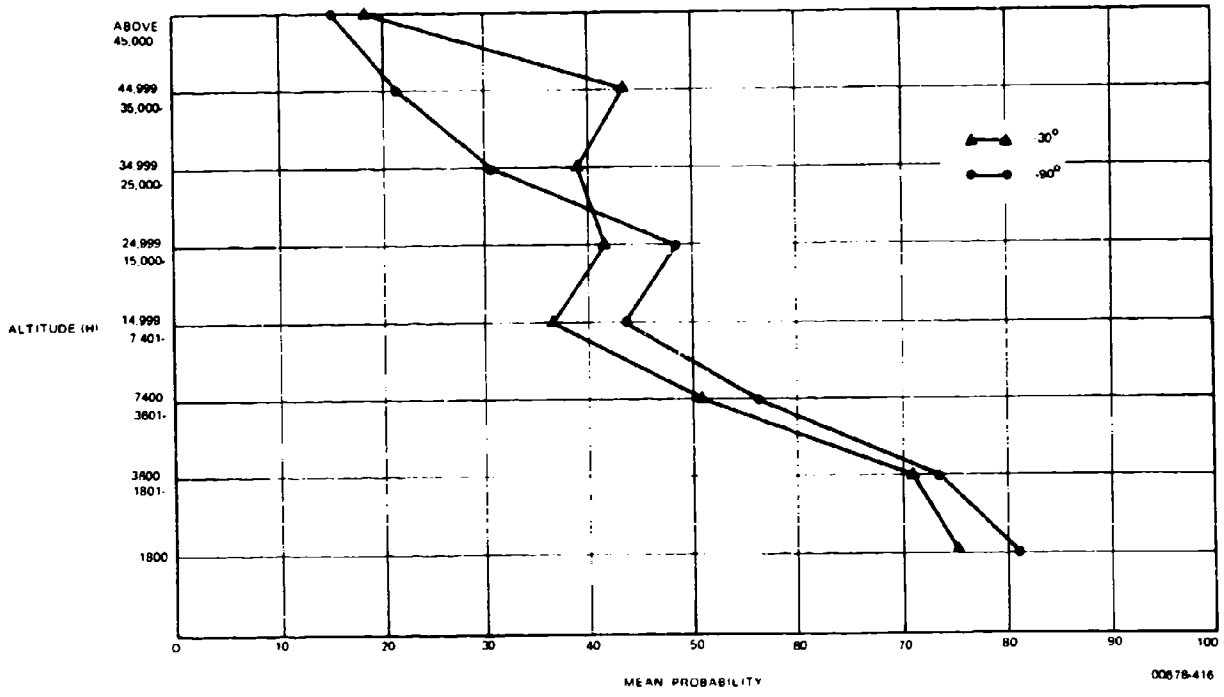

Figure 4-10. Mean Probability of Seeing an Aircraft from the Ground During the Months of September, October and November

This position is further substantiated by an assessment of the visual tracking problem in the weather environment of West Germany[4], which is as follows: 'Visual control requires clear optical target sighting and tracking, in which obviously the meteorological visibility factor will have a definite influence. In West Germany, for example, the meteorological visibility in only 50 percent of all cases is 6 miles or more, in about 25 percent of all cases it is 4-6 miles and in about 15 percent, under 4 miles. The optical ground-to-air sighting probability is even less and without prior warning by forward observers is a maximum of 50 percent of the meteorological visibility, and with prior warning it can reach 70 percent. The absolute limit of optical perception of aircraft with the naked eye is physically limited and in the optimum case is about 8 miles. These factors therefore influence the capabilities and limitations of AA systems using visual tracking.'

4.1.2.3 Multiple Aircraft Attack

Although this study is primarily concerned with the 'one-on-one' problem, multiple aircraft attacks are a consideration in overall system design, especially in the surveillance and target assignment activities.

One way of degrading a defense is to saturate it. The more aircraft that are within the defense boundary at a given time, the higher the probability that at least one will succeed in destroying the defended target. Fighter bombers may attack simultaneously (or nearly so) from different directions. Some aircraft may deliver suppressive fire while others attack a defended vital area. Attack helicopters may be likewise used in an organized attack in which gun ships lay down suppressive fire on the antiaircraft units, while others launch missiles.

AFAADS can only shoot at one target at a time. However, rapidly switching from one target to another, as the first is destroyed or passes its weapon release point, will improve overall AFAADS system effectiveness.

At the fire unit level, this is accomplished by the fire unit commander's decision to engage a new target, and its effectiveness is governed by the speed with which he can cause the weapon to acquire the newly designated target. He might do this by observing the plan position indicator of the AFAADS surveillance radar, if one is provided. Another option is to give the surveillance radar a multiple track maintenance capability, so that when a new target is designated by the commander, it can immediately provide the fire control computer with initial position and rates, thereby drastically reducing the time to generate firing data against the new target.

4.1.2.4 Approach to the Target

If the target aircraft has been driven to low altitude by the possibility of encountering a SAM defense, the

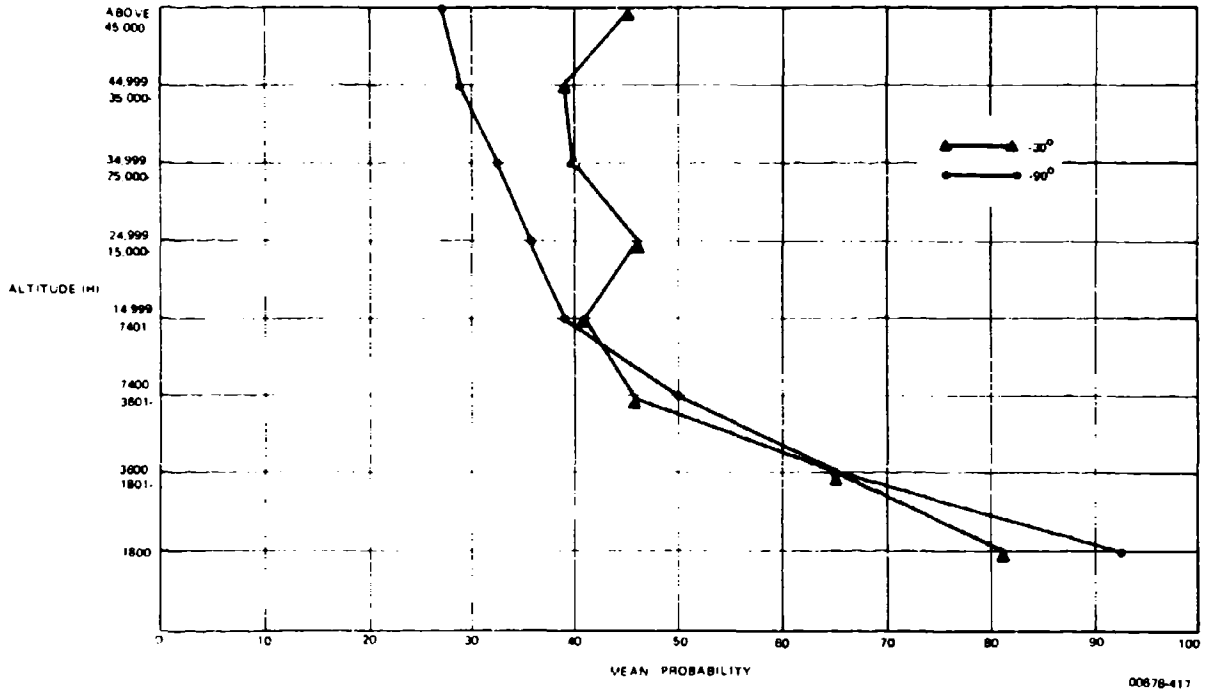

Figure 4-11. Mean Probability of Seeing an Aircraft from the Ground During the Months of December, January and February

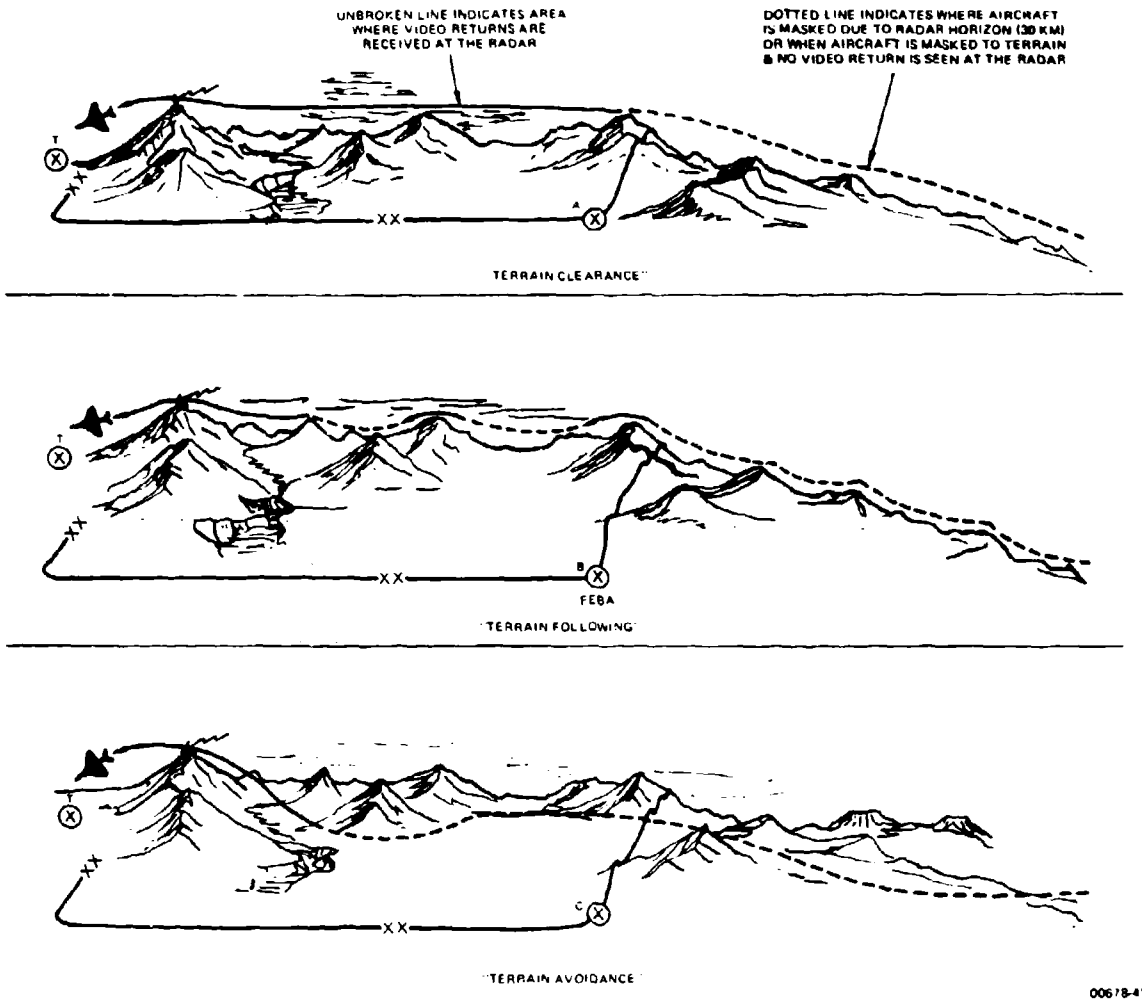

Figure 4-12. Low-Altitude Approach Techniques

height above ground level that can be maintained depends on the terrain following equipment carried, the speed of the aircraft, and the ground roughness. Ground 'roughness' can be characterized by the standard deviation of terrain variations from a mean value, and the power spectral density (or slope changes per mile, etc.) which describes how rapidly terrain height varies.

The slower the airplane flies, the more exactly it is able to conform to terrain variations. At very high speeds it is limited by the pilot (human or automatic) plus airplane response, and the g-tolerance of the pilot and crew.

Figure 4-12 shows three types of low level approach. At very high speeds the aircraft path is distorted only by major terrain prominences. At intermediate speeds closer conformity to terrain is possible. At very slow speeds terrain can be followed very closely, and in addition the aircraft can move freely in a horizontal plane to take advantage of terrain cover.

A very simple model presented later in the report suggests that the mean height of an aircraft attempting to follow terrain contours can be estimated by the expression:

$$\underline{h} \cong 3(G\nu T)^{1/2} \qquad (4.0)$$

where:

G is a number (dimensions in feet) characterizing the terrain

v is aircraft speed in ft/sec

T is the aircraft/pilot response time in seconds

h is expressed in feet.

Typical values of (G) may be as follows:

DTerrain	G
Smooth	0-2.5 ft
Moderate	2.5-10 ft
Rough	10-25 ft
Very rough	25 ft

(T) may be in the range 0.5 to 1.0 second. Helicopter data from Fort Ord shows that the $v^{1/2}$ relation is actually found by experiment (see Figure 4-13). A more accurate expression for very high speeds is given later in the report.

4.1.2.5 Pop-up Maneuver

When approaching the target at very low altitude, at some predetermined distance from the target area, the pilot may climb in preparation for his terminal attack maneuver. Typically, this may involve a pull-up at moderate acceleration (2g), with a climb attitude of 30°, and then a slow pushover into level flight as speed drops. A more violent and abrupt pop-up might consist of a (3-5g) climb and roll, and then an inverted pushover at the top, also at a high-g acceleration.

In any case, the throttle may be advanced in the climb, to augment the kinetic energy traded for potential energy. The end points of such a maneuver are related by the equation:

$$h_2 - h_1 = (v_1^2 - v_2^2)/(2g) + \int_{t_1}^{t_2} P_s \, dt \qquad (4.1)$$

where:

h = altitude

v = velocity

P_s = specific excess energy.

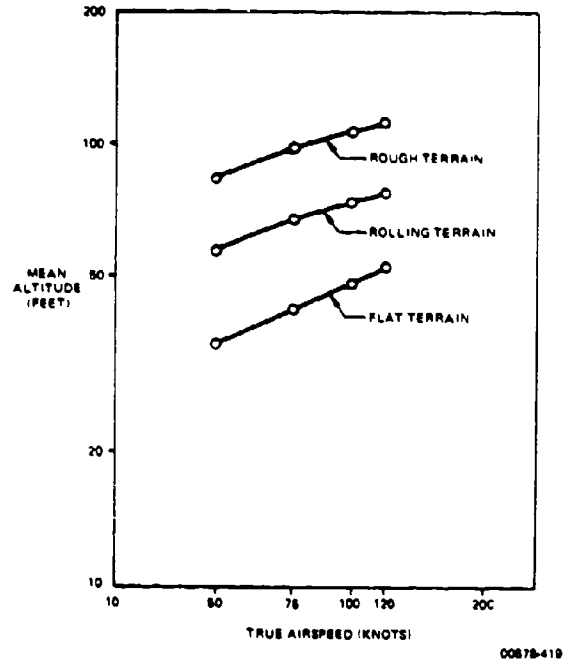

Figure 4-13. CH-47 Helicopter Data Showing Relationship of Airspeed to the Mean Altitude

4.1.2.6 Bombing Tactics

The following bombing tactics are representative of the tactics against which AFAADS must defend.

4.1.2.6.1 Horizontal Bombing

The loci of bomb release points for level bombing at various altitudes and speeds is shown in Figure 4-14. A simple empirical expression which fits the curves of the figure is:

$$R_b = c_1 h^{1/2}(v + c_2) \qquad (4.2)$$

It is readily seen from the figure, where the 10,000-ft range envelope of AFAADS is sketched in, that if AFAADS is at the defended point, the target can be attacked by level bombing without the necessity of the bomber penetrating the AFAADS envelope. Disposition of AFAADS in an area defense makes this more difficult. However it is presumed that SAM defenses have driven the bomber to under 3000 meters.

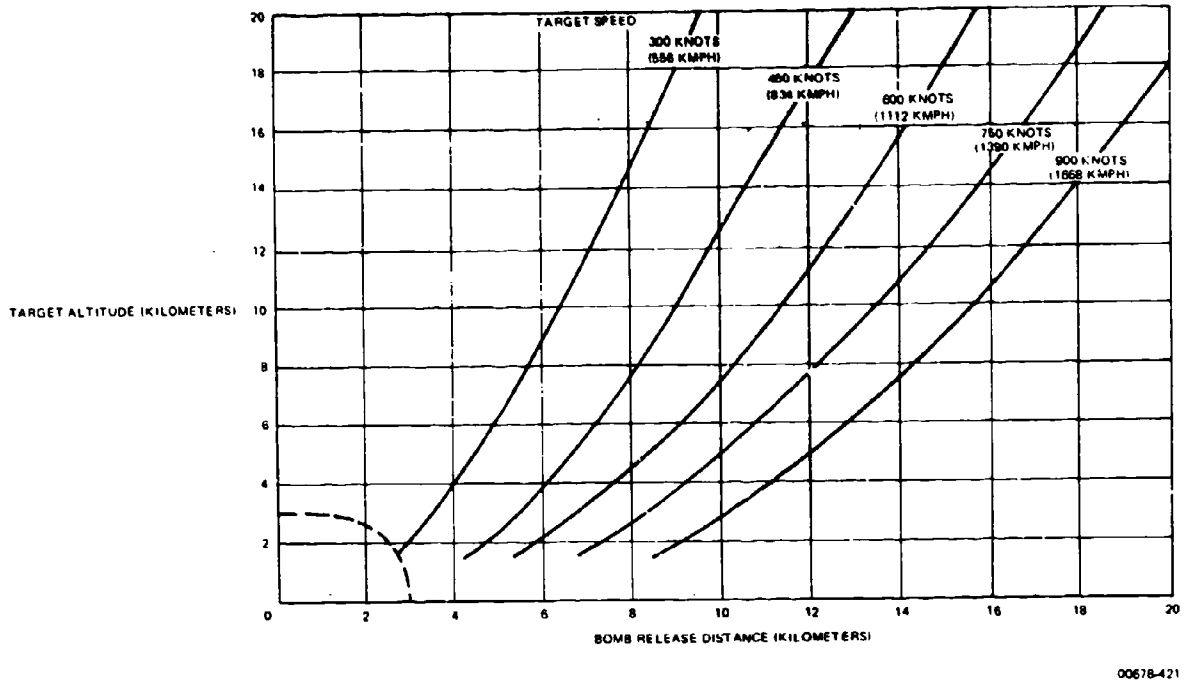

Figure 4-14. Gravity Bomb Release Distance Graph

Subject to target acquisition problems, bombs can be delivered in level flight at very low altitude by 'lay-down' techniques. Flights may be as low as 300 ft at speeds of 400 to 900 knots. Fall of the bomb is then retarded by drogue chutes or retarding fins to allow the aircraft to escape its own bomb pattern.

When the target position is accurately known, it may be attacked by level bombing with the aircraft under the control of equipment such as the AN/TPQ-10. This relieves the pilot of the target acquisition problem, allows attack at night or in bad weather; and depending on terrain characteristics, allows low level run-in.

4.1.2.6.2 Glide and Dive Bombing

The distinction between using a glide or dive bombing approach, depends on whether the attack path is less than or greater than 45°. Typically an approach may be at very low altitude to the vicinity of the target, then a pop-up manuver could be executed (possibly in a climbing turn if the target is first sighted at low altitude), then circling out of range of the target defenses keeping the target in sight, then rolling in and diving along a straight attack segment, and finally, breaking away at maximum 'g' after bomb release.

A possible sheaf of attack segments is shown in Figure 4-15. The length of a segment depends on the time the pilot requires to set up his bomb computer and establish a stable sight line. The bomb release points can be moved radially away from the target to reduce aircraft vulnerability, but at the expense of bomb circular probable error (CEP). The segments shown in the figure represent time intervals of about 15 seconds, of which less than half is within the sketched AFAADS defensive envelope.

Speed is not constant along the segment, since the airplane accelerates depending on the throttle setting and the angle of dive. For an 0.5g acceleration, a linear predictor would, if directly to the side of the dive plane, develop an along-course error, depending on smoothing time, of at least:

19 ft at 1.5 sec time of flight

76 ft at 3.0 sec time of flight

If the bomb is released at slant range (D_r) and dive angle (θ), the slant range of the closest approach to the target by the attacking aircraft, assuming a constant-g pullup of radius (ρ), is:

$$D_{min} = \left(\rho^2 + D_r^2\right)^{1/2} - \rho \qquad (4.3)$$

and if the airplane must pullup with a minimum ground clearance (H_m), then:

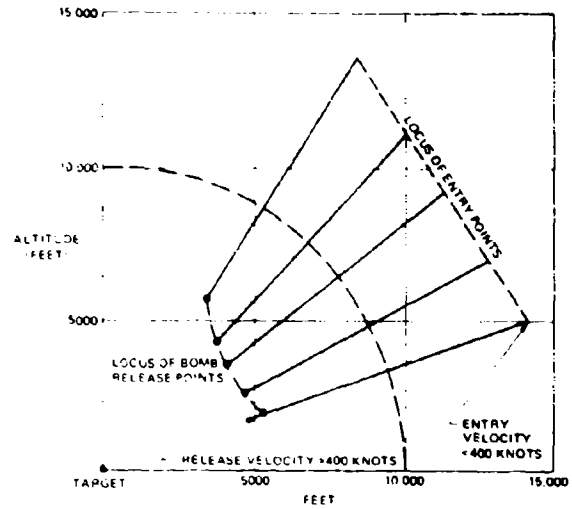

00878-422

Figure 4-15. Straight-Line Segments of Dive/Glide Bomb Paths

$$H_m = H_r - \rho(1 - \cos\theta)$$

$$= D_r \sin\theta - \rho(1 - \cos\theta) \qquad (4.4)$$

(H_m) and (ρ) thus fix release range (D_r) as a function of angle of dive (θ) for the minimum feasible (D_r). As noted earlier, larger (D_r) may be required because of aircraft vulnerability. The expressions are only approximate, since the bomb trajectory is not straight, and the airplane's trajectory deviates slightly from a straight line because of the sight angle to correct for bomb ballistics.

4.1.2.6.3 Use of Advanced Bombsight

The straight line path segment described above may be drastically shortened with future air-to-ground avionics. An unclassified description of the bombsight installed in the A-7 aircraft states:

'The bombing techniques possible with the A-7 include the dive toss, used to train pilots, and others such as level, loft and over-the-shoulder. Steep angle bombing is viewed as the primary means and is the one practiced most frequently.

In bombing, strafing and firing rockets, pilots use the attack symbology on the head-up display for aiming and tracking while in the dive. The pilot first places the aiming reticle on the target and depresses the designate button. He then is free to maneuver in the dive, although at the release point he must have the target in line with a bombfall line (a vertically oriented line of predicted impact points) displayed on the head-up display. Symbology also indicates when to pull out of the dive. During the dive, sensors feed the computer information on dive, angle, airspeed, wind drift, altitude and range to the target and the computer calculates the right time for release based on previously entered weapons ballistics.

The central computer is assisted in its job of keeping track of ordnance information by an armament station control unit located in the left side of the fuselage and accessible to ground crewmen. This unit helps to economize the computer workload and provides a convenient location for the ordnance crews to enter information about the stores carried.

The A-7E, like the early A-7 models, has the same airframe and carries a variety of weapons including the Texas Instruments Shrike anti-radiation missile, the Walleye television glide bomb, Rockeye, Sadeye, Weteye, Snakeye and Sidewinder missiles for defense.

There are no plans at present to use the A-7 for carrying Condor, Navy's large TV-guided standoff missile.

Latest electronic countermeasures gear, both passive and active are built into the A-7E to assist in penetrating areas protected by radar networks, surface to air missiles and anti-aircraft guns.'

4.1.2.6.4 Low Altitude Bombing System (LABS)

As the aircraft approaches the target at low altitude, the pilot chooses his path to fly over a pred termined check point. He flies a prespecified distance beyond this point directly at the target, and then pulls up at about 45 degrees. After the bomb is automatically released, the pilot continues his pullup through a loop and reversal of direction of flight.

A rough idea of the distance of approach of the aircraft to the target can be obtained by considering a vacuum trajectory for the bomb. The ground distance travelled by the bomb from release to impact is approximately:

$$R \approx (v^2/g) + h_r \qquad (4.5)$$

where:

R = ground distance

v = release velocity

h_r = release altitude (small)

The radius of curvature of the aircraft in the loop is:

$$\rho = v^2/ng \qquad (4.6)$$

where: ng is the radial acceleration.

If n = 5, then the closest approach of the airplane to the target is about 0.8R. For a release velocity of 400 knots, (R) is over 10,000 ft, and thus it is seen that the exposure of the aircraft to local defenses at the target is minimal.

A variation of the LABS delivery termed, 'over-the-shoulder,' can be used when the pilot does not acquire the target until he passes over it. He may then loop with the bomb released automatically at 90-120 degrees. The aircraft rolls and leaves before the bomb completes its fall.

These maneuvers are illustrated in Figures 4-16 and 4-17.

Large unguided rockets may also be lofted by this method. In a typical pass, the airplane may pull up from about 200 feet, release at 800 feet, and continue through its loop, while the rocket travels 36,000 feet to target.

4.1.2.7 Direct Fire Weapons Tactics

The following tactics are descriptive of the type of tactics that may be encountered in the AFAADS environment.

4.1.2.7.1 Unguided Rocket Run

The tactical elements discussed for use in glide and dive bombing apply in general to the delivery of unguided rockets. Rocket dispersion is a function of aircraft velocity at release (decrease with increasing velocity), but may be of the order of 10 mils.

Figure 4-18 shows an attack profile including an approach at low level; pop-up to 5000-7000 feet; pushover to a 30-degree dive; straight run to rocket release at 5000 feet slant range from target, and pullout. For a 5000-foot release, rocket CEP will be about 50 feet.

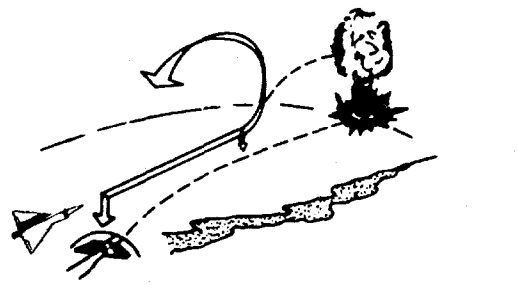

00678-423

Figure 4-16. Low-Altitude Bombing System

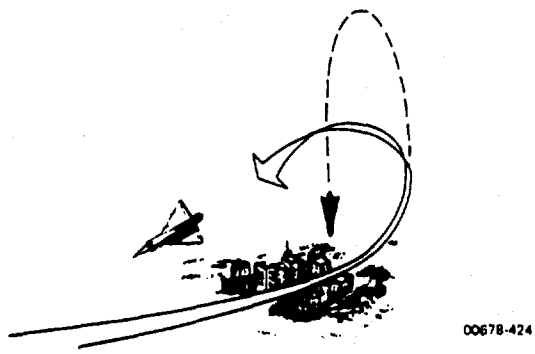

00678-424

Figure 4-17. The LABS Over-the-Shoulder Delivery

4.1.2.7.2 Strafing (Guns)

Strafing may be conducted at rather shallow glide angles of 5-6 degrees (about 100 mils). If the firing segment begins at an altitude of 500-800 feet, the initial range to target will be 5000-8000 feet, and with a constant throttle setting, acceleration along the flight path will be only about 0.10g. Figure 4-19 shows a possible attack profile.

In strafing a troop column, the pattern shown could be initiated aiming first at the nearest end of the column. A slow pullup, initiated early would cause the bullets to strafe the whole column.

An entirely different attack pattern could be followed by an aircraft with guns depressed for ground strafing. Attack on a column could then be made by a level pass as low as 50 feet, firing continuously. A strafing attack might be made at supersonic speed, limited only by the pilot's ability to see the target.

4.1.2.7.3 Air to Surface Missile (Guided All the Way)

In the case of short range missiles (up to 2 nautical miles) the launch vehicle (helicopter) may come within range of AFAADS. Figure 4-20 illustrates a possible 'pop-up' maneuver whereby the helicopter rises above a terrain prominence, acquires its target, launches its

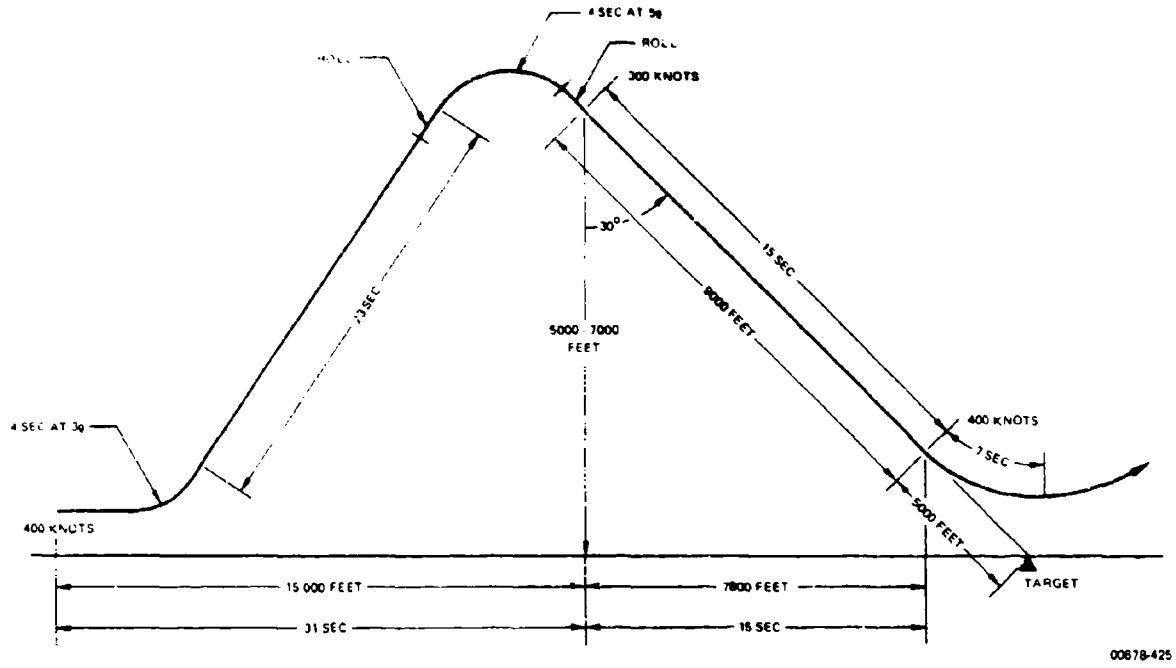

Figure 4-18. Rocket Attack Profiie (Vertical Scale Expanded)

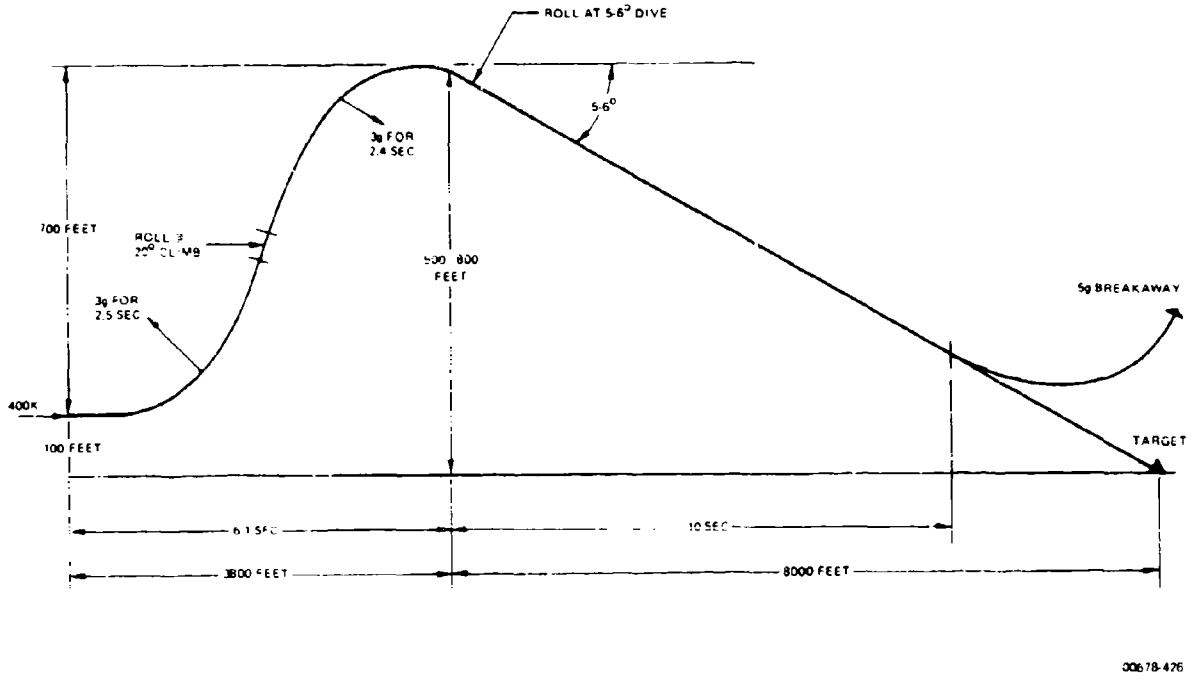

Figure 4-19. Strafing Attack Profile (Vertical Scale Expanded)

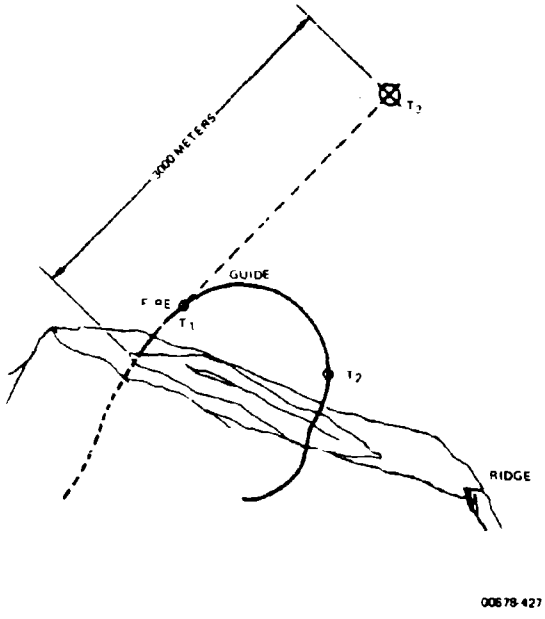

Figure 4-20. Tow-Type Missile Launch from a Helicopter

missile, and remains in sight while maneuvering, but holding a line of sight to target until missile impact. Exposure time would not exceed: time to acquire the target plus flight time of the missile.

4.1.2.8 Threat Effectiveness

As a rough indication of the effectiveness of aircraft with some of the weapons discussed, circular probable errors (CEP) mentioned in unclassified literature have been collected in Table IV-7. No check of validity of these values has been made.

4.1.3 The Flight Trajectory

In this section the characteristics of the target aircraft's flight trajectory are developed for use later in the tracking, filtering, and prediction phases of the study. It is convenient to develop the trajectory characteristics under the general headings of turbulence, terrain following, free maneuver, and attack on ground targets, as indicated in Figure 4-21.

The influence of air turbulence on the aircraft motion is best described statistically. It causes flight path deviations from the mean which may be sufficiently large to require consideration in both the tracking and prediction problem. It also causes aircraft accelerations at low altitude which limit the ability of the pilot to do close terrain following.

Terrain following aircraft will be important targets for the AFAADS system. The object of terrain following is to delay detection by ground radars and observers, and to remain, if possible, under the low altitude coverage limits of SAMS. This brings the aircraft within the altitude limits of AFAADS. However, terrain following complicates the gun prediction problem, since the airplane follows an irregular flight path conforming to some degree to ground contours. The flight path of terrain following aircraft has both deterministic and stochastic elements. If the fire control computer stored local terrain data, this could be used in improving prediction. On the other hand, the actual flight path, although driven by the terrain contour, varies depending on the dynamics of the terrain following control (automatic or human), the errors of the control system, and random deviations from the desired path produced by air turbulence.

The category of free maneuver includes evasive action commanded by the pilot which is constrained only by the dynamics of the aircraft and the pilot's desire to minimize exposure time to fire. Rather than fly straight and level over defended areas en route to target, the pilot may, if he is not contour flying, make small course and altitude changes at frequent intervals. Since relatively small accelerations can produce prediction errors much larger than gun dispersion, such 'jinking' will degrade the fire control system and must be evaluated.

The most important phase of the target aircraft's trajectory from the point of view of AFAADS is the 'end game,' i.e., the attack on a ground target. Most U.S. aircraft losses in Korea and Vietnam to ground fire are believed to have occurred in this phase. Depending on the type of weapon carried by the aircraft and the characteristics of its fire control system, the aircraft's freedom to maneuver, during weapon delivery, is restricted and therefore accurate weapon delivery may require that the aircraft fly a straight line path for 5-10 seconds or longer. Maneuvers prior to this flight segment may also be limited by the pilot's need to acquire the target and keep it in sight while he positions himself for his attack run. After weapon release, the pilot may pull maximum 'g' in breakaway but his attack path may have brought him to within very close range of the AFAADS defending the target.

4.1.3.1 Air Turbulence

In the analysis of fire control systems for heavy antiaircraft during World War II and shortly thereafter, it was recognized that a principal component of prediction error resulted from what was called 'roughness of flight.' Since projectile times of flight were as long as 30 seconds, the deviation of the airplane from

Table IV-7 Typical Air-to-Surface Munitions Circular Probable Errors*

Attack Path	Altitude	CEP	Comments	Bibliography * Reference
Level bombing	7000 ft	350 ft	Korea	16
Glide bombing	1000-1500 ft (30°)	140 ft	Korea	16
"Conventional bombing"		300-350 ft	Current	6
Laser homing bomb		10-12 ft	Current	6
2.75" FFAR (helicopter launch)		10 mils dispersion		13
Glide bomb (A-4 aircraft)	30° dive	95-100 ft	Non-combat	14
(A7A/B aircraft)		70-75 ft		
(A-7E aircraft)		60 ft		

*Unclassified sources

00678-428

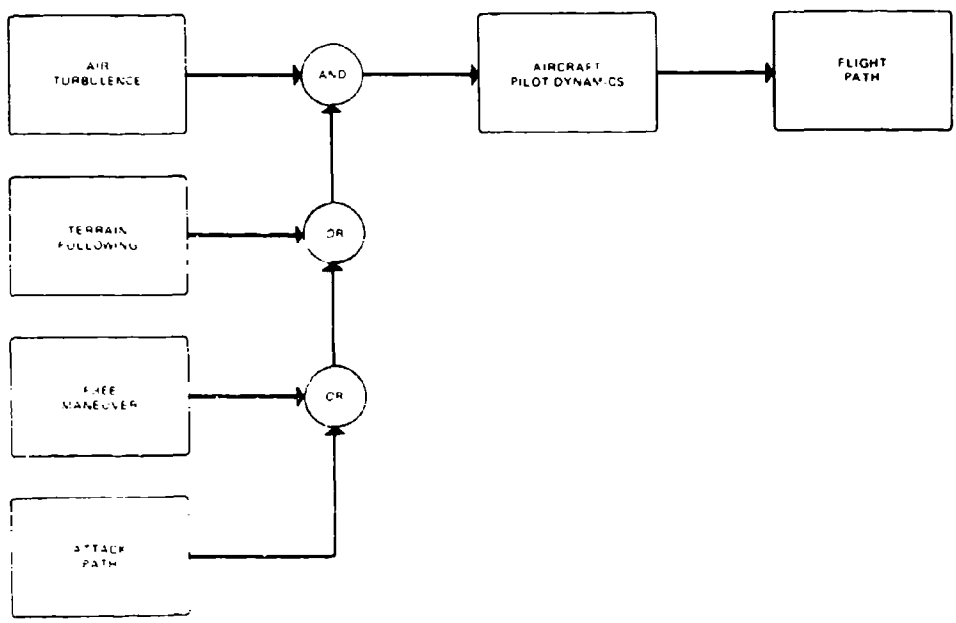

00678-463

Figure 4-21. Flight Trajectory Characteristics

a straight line, caused simply by air turbulence, could amount to a component equal to the other errors of the system, even when the aircraft was not deliverately evading.

The effect is expected to be much less for the short times of flight of AFAADS, however, to determine this, a brief review of the effect of air turbulence on the aircraft is appropriate.

Air turbulence may affect AFAADS system performance in the following ways:

a. It prevents the aircraft from flying an unaccelerated course, even though the pilot may be trying to fly 'straight and level.'

b. The resulting aircraft perturbations will affect the tracking process, and to the degree that they are unpredictable, they will contribute to the prediction error.

c. The angular aircraft motions resulting from turbulence will affect the 'glint' component of radar tracking error.

d. The accelerations produced by turbulent air will limit the capability of the target to do terrain contour flying in rough air.

4.1.3.1.1 Characteristics of Turbulence

Air turbulence may be accurately represented over very long flight segments as a stationary random process. It is remarkable that the form of the power spectral density function is essentially constant for all altitudes and meteorological conditions, and moreover, corresponds to that determined originally by von Karman from theoretical considerations.

Turbulence may be considered in three orthogonal components, one along the flight path (longitudinal), one vertical, and the horizontal perpendicular to both (lateral).

Measurements confirm that the lateral and vertical power spectral density functions are essentially identical, and that they differ from that for the longitudinal component. The longitudinal component has the least effect on aircraft displacements and will not be considered here.

4.1.3.1.2 Spectral Density Functions

We first define the characteristics of atmospheric turbulence independently of the aircraft, then introduce the dynamics of the aircraft.

Define:

$\Phi_{|}(\Omega)$ = spectral density function of vertical or lateral turbulence (ft^3 rad-sec^2)

Ω = frequency, rad/ft

$\Phi(\Omega)$ = normalized spectral density function (rad/ft)$^{-1}$

$\sigma_{u,v}$ = rms gust velocity along vertical, lateral axis

R(s) = normalized autocovariance

s = lag (ft)

L = "Scale" of Turbulence (ft)

The normalization is taken to result in:

$$\Phi_{|}(\Omega) = \sigma^2\Phi(\Omega) \tag{4.7}$$

$$\int_0^\infty \Phi(\Omega)d\Omega = 1.0 \tag{4.8}$$

The power spectral density and the autocovariance are related by:

$$R(s) = \int_0^\infty \Phi(\Omega)\cos \Omega s\, d\Omega \tag{4.9}$$

$$\Phi(\Omega) = \frac{2}{\pi}\int_0^\infty R(s)\cos \Omega s\, ds \tag{4.10}$$

Some of the closely equivalent forms which have been used to describe the power spectral density, and, in the simpler cases, their corresponding autocovariances are as follows:

a. Von Karman: $$\Phi(\Omega) = \frac{L}{\pi}\frac{1+(8/3)(1.339L\Omega)^2}{[1+(1.339L\Omega)^2]^{11/6}} \tag{4.11}$$

b. Dryden: $$\Phi(\Omega) = \frac{L}{\pi}\frac{1+3\Omega^2L^2}{(1+\Omega^2L^2)^2} \tag{4.12}$$

$$R(s) = \left(1-\frac{s}{2L}\right)e^{-s/L} \tag{4.13}$$

c. Lappe: $$\Phi(\Omega) = \frac{L}{(1+\Omega L)^3} \tag{4.14}$$

$$R(s) = 1-\frac{s}{L}\left[Ci\left(\frac{s}{L}\right)\sin\left(\frac{s}{L}\right) - \left[si\left(\frac{s}{L}\right)-\frac{\pi}{2}\right]\cos\left(\frac{s}{L}\right)\right] \tag{4.15}$$

d. Modified Lappe:

$$\Phi(\Omega) = \frac{2}{\pi}\left[\frac{aL_1}{1 + L_1^2\Omega^2} + \frac{(1-a)L_2}{1+L_2^2\Omega^2}\right] \quad (4.16)$$

$$R(s) = ae^{-s/L_1} + (1 - a)e^{-s/L_2} \quad (4.17)$$

In all cases except the von Karman function, (ϕ) drops off as Ω^2 for a large Ω. For the von Karman function, the asymptote is $\Omega^{-11/6}$. As instrumentation has improved, the 11/6 power has been determined to be a better representation. The difference is negligible for present purposes and so we use the simpler forms.

At the low frequency end of the spectrum, the Dryden and von Karman functions are asymptotically equal, but the Lappe function has an asymptote almost three times as large. Lappe proposed his function based entirely on experimental data, including that taken in low level flight with the B-66. A recent analysis of additional experimental data disagrees with Lappe's finding, and the question of which form is best for low frequencies seems to be still unresolved.

The relevance to the present problem is that the low frequency end of the spectrum contributes most to airplane displacement, which is our central concern. Comparison of the autocovariance functions illustrates a further reason for interest. The Dryden autocovariance has a positive and negative segment, as shown in Figure 4-22; so that its value is close to zero beyond S/L = 2.0. The Lappe function, on the other hand, decays much more slowly and suggests that the resulting displacements of the airplane may be substantially higher than if the Dryden function held.

The disagreeable form of the Lappe autocovariance, involving sine and cosine integrals, can be avoided, by approximating R(s) as the sum of two exponentials. This creates what we call the Modified Lappe function. It is equivalent to the Lappe and more tractable for analysis.

Figure 4-23 shows typical ranges of (σ_u) experienced in B-66 tests.

4.1.3.1.3 Parameters

Once the mathematical form has been chosen, the power spectral density is completely defined by two parameters; the rms gust velocity, and the scale of turbulence (L).

Both the rms gust velocity and scale length (L) depend on surface roughness (terrain type), height above the surface, wind conditions (both velocity and shear), and atmospheric stability.

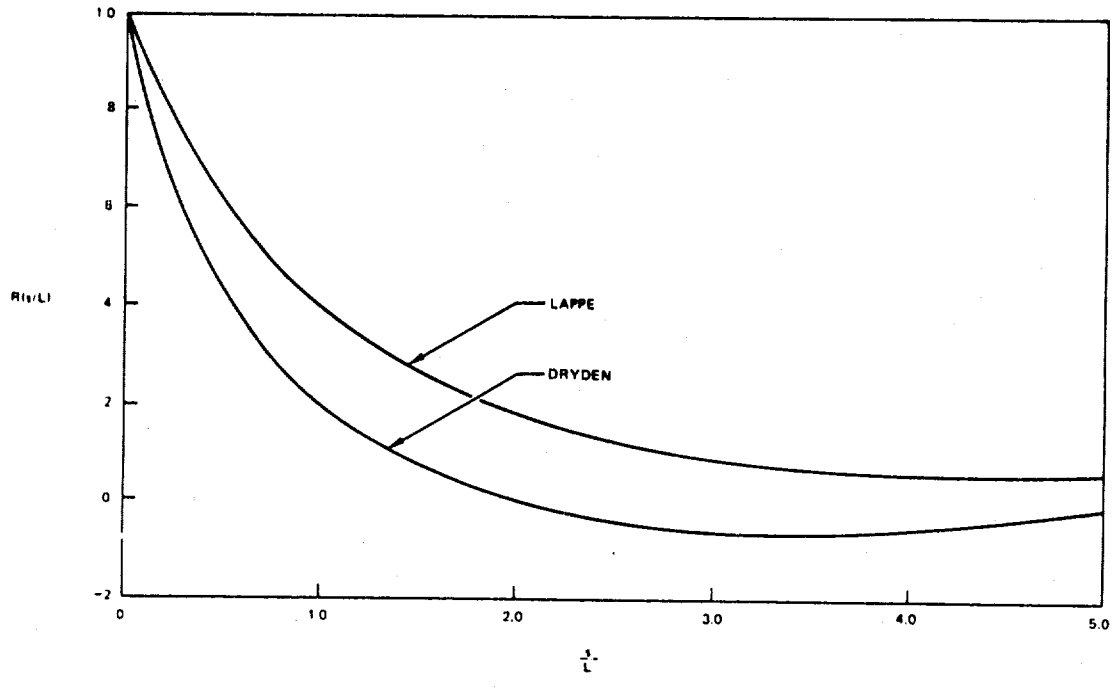

Figure 4-22. Comparison of Lappe and Dryden Autocovariance Functions

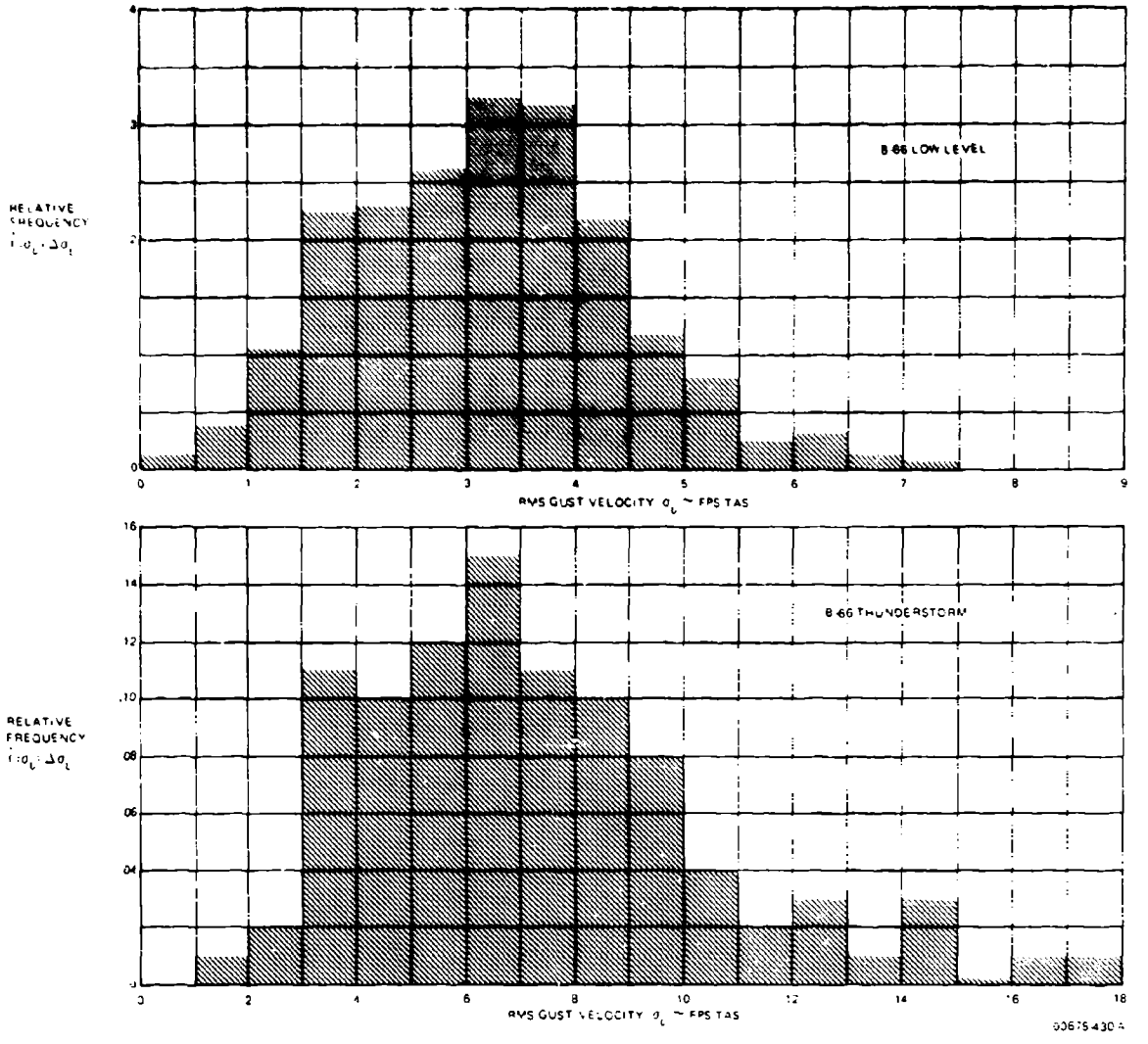

Figure 4-23. Relative Frequency Distributions of rms Gust Velocity from B-66 Programs.

Bases for estimating (σ) and (L) for particular sets of terrain-altitude-meteorological conditions are given in the reference literature.[17,18,19,20] In this program we are interested primarily in low altitude turbulence, where the terrain effect is important.

In general, the rougher the terrain (mountains compared with farmland), the larger the value of (L). (L) increases rapidly with altitude to about 1000 feet and more slowly thereafter. At all altitudes, (L) increases with increasing instability of the atmosphere. It seems reasonable to consider (L) in the range 500-1500 feet in the present analysis.

The rms gust velocity increases with mean wind velocity at flight altitude, with terrain roughness, and with atmospheric instability. Since the ratio of mean wind velocity at altitude to surface wind increases with altitude because of boundary layer effect, rms gust velocity for a given surface wind velocity increases with altitude. Values in the range of 3-7 feet/second seem reasonable for present purposes.

Convective storm turbulence is much more severe than non-storm turbulence and will not be considered here.

4.1.3.1.4 Sampling of the Gust Spectrum by the Airplane

The power spectral density functions have been defined in terms of linear extent. As the airplane flies through the gust structure, the power spectral density of gust magnitudes, which it experiences, scales with the velocity. The forcing function on the airplane is then:

$$\Phi(\omega) = \frac{1}{V}\Phi\left(\frac{\omega}{V}\right) \qquad (4.18)$$

where $\omega = \Omega/V$

Figure 4-24 shows the normalized Dryden spectrum for L = 1000 feet as experienced by airplanes at three different velocities. The abscissa is shown in cylces per second, (f), where:

$$f = \omega/2\pi$$

Consequently, the faster the airplane the larger the high frequency content of the gust spectrum which it experiences.

4.1.3.1.5 Vertical Response of the Airplane

The vertical displacement of the airplane caused by gusts may be discussed in terms of the low, medium, and high portions of the gust spectrum. At the low frequency end, the pilot (either human or autopilot) will act to prevent excessive deviations from the desired altitude. In the mid-portion of the spectrum, the disturbance is too rapid for the pilot's response, and the airplane moves in accordance with relative angle of attack changes caused by the gust velocity. At the very high end of the spectrum, lift changes (which require aircraft travel of about 6-10 chord lengths to reach a steady state) cannot follow the gust fluctuations, and there is additionally reduced airplane displacement.

Consider the mid-range first. Assuming that the airplane remains level its vertical displacement in response to a gust is given by:

$$T_a\ddot{z} + \dot{z} = u \qquad (4.19)$$

where:

z = vertical displacement

u = gust velocity

$$T_a = \frac{W/S}{g\rho/2\,VC_{La}} \qquad (4.20)$$

W/S = wing loading

g = acceleration of gravity

ρ = air density (slugs/ft^3)

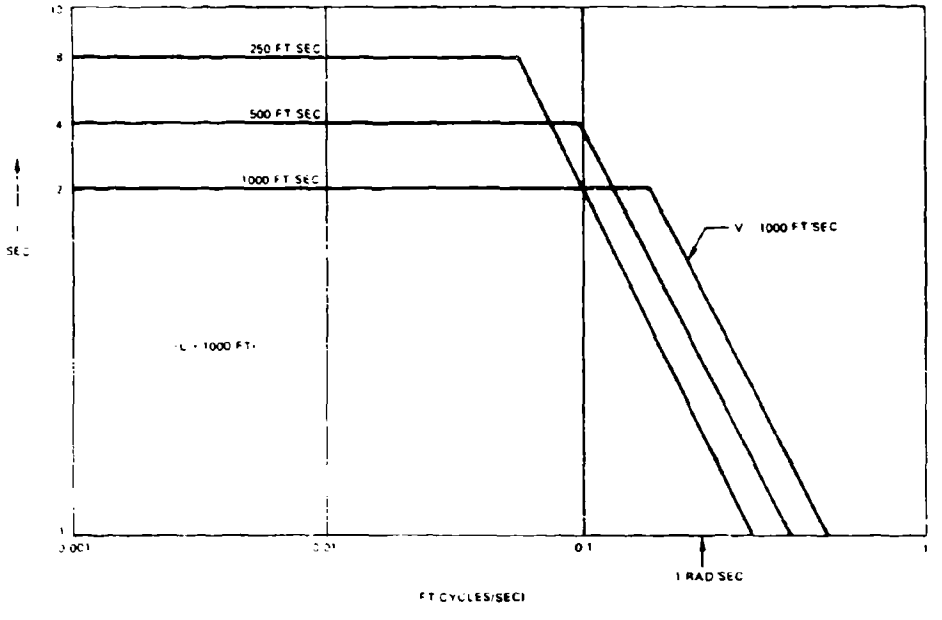

00678 431

Figure 4-24. Normalized Dryden Spectrum for L 1000 feet

V = aircraft velocity

$C_{L\alpha}$ = slope of the lift curve (rad^{-1})

If the transfer function of the response of the airplane, (M_j), (displacement, velocity, or acceleration, etc.) to gust velocity (u) is $T_j(i\omega)$, then the mean square value of the airplane's response to the gust spectrum is:

$$|M_j|^2 = \sigma_u^2 \int_0^\infty \Phi(\Omega)\, |T_j(i\Omega V)|^2\, d\Omega \qquad (4.21)$$

where: $\omega = \Omega V$

The values of $T(i\omega)^2$ corresponding to (4.19) are:

Displacement: $$\left|\frac{z}{u}\right|^2 = \frac{1}{\omega^2\left(1+\omega^2 T_a^2\right)} \qquad (4.22)$$

Velocity: $$\left|\frac{\dot{z}}{u}\right|^2 = \frac{1}{\left(1+\omega^2 T_a^2\right)} \qquad (4.23)$$

Acceleration: $$\left|\frac{\ddot{z}}{u}\right|^2 = \frac{\omega^2}{\left(1+\omega^2 T_a^2\right)} \qquad (4.24)$$

We see at once that we cannot use (4.22) over the whole gust spectrum since the integral is unbounded. Of more direct interest, however, is the mean square deviation of the airplane from an observed position in some time (t_o). If the deviation is (Δ), the transfer function is:

$$\Delta/u = \frac{e^{pt_o}-1}{p\left(1+pT_a\right)} \quad ; \quad p = d/dt \qquad (4.25)$$

and:

$$\left|\frac{\Delta}{u}\right|^2 = \frac{2-2\cos\omega t_o}{\omega^2\left(1+\omega^2 T_a^2\right)} \qquad (4.26)$$

For the Dryden spectrum:

$$\left(\frac{\sigma_\Delta}{\sigma_u}\right)^2 = \frac{2}{\pi}\left(\frac{L}{V}\right)^2 \int_0^\infty \frac{(1+3x^2)(1-\cos bx)}{x^2(1+x^2)^2(1+\lambda^2x^2)}\, dx \qquad (4.27)$$

where:

$x = L\Omega$

$b = \frac{Vt_o}{L}$

$\lambda = \frac{VT_a}{L}$

$\omega = V\Omega$

and for the modified Lappe spectrum:

$$\left(\frac{\sigma_\Delta}{\sigma_u}\right)^2 = \frac{4}{\pi}\left(\frac{L}{V}\right)^2 \int_0^\infty \left[\frac{\alpha\beta_1}{1+\beta_1^2x^2} + \frac{(1-\alpha)\beta_2}{1+\beta_2^2x^2}\right] \frac{1-\cos bx}{x^2(1+\lambda^2x^2)}\, dx \qquad (4.28)$$

Although these expressions can be easily integrated, we note simply that for small (b),

For the Dryden spectrum:

$$\left(\frac{\sigma_\Delta}{\sigma_u}\right)^2 \cong t_o^2\left[\frac{2+\lambda}{\lambda(1+\lambda)^2}\right] \qquad (4.29)$$

and for the modified Lappe spectrum:

$$\left(\frac{\sigma_\Delta}{\sigma_u}\right)^2 \cong t_o^2\left[\frac{\alpha\beta_1}{\lambda+\beta_1} + \frac{(1-\alpha)\beta_2}{\lambda+\beta_2}\right] \qquad (4.30)$$

Some typical values of (T_a) for a variety of aircraft are shown in Table IV-8.

Using the Dryden spectrum for an example, we note that for a turbulence scale length of 1000 feet, an airplane flying 1000 feet/second with a (T_a) of 0.38 second will have a rms displacement, caused by a 3 feet/second gust structure, of about 5.5 feet in 3 seconds. Since λ is independent of airplane velocity, we would not expect the deviation to change with velocity.

The very small value of 5.5 feet suggests that, to the degree the above assessment is correct, we need not consider turbulence as a significant error source for AFAADS.

The assumption of a level airplane is probably not sufficient, however, to explain the effects of turbulence on vertical motion, for reasons discussed in the following paragraphs.

4.1.3.1.6 Comparison with Experimental Data

One of the best experimental and anlytical studies of the 'roughness of flight' of aircraft was carried out by Dr. Glanville Harries.[23] He obtained power spectral densities (PSD) of the lateral and vertical motion which are replotted in Figure 4-25.

These PSDs peak at about 0.020 and 0.032 cps, corresponding to lightly damped oscillations with periods of about 50 and 30 seconds. It is suggested that the gust spectrum, which is uniform over this frequency range, is exciting the phugoid plus pilot mode in

Table IV-8. Typical Values of T_a

	Aircraft	Velocity (Kts)	Velocity Mach	Altitude (10^3 ft)	T_a (sec)
Low Altitude High Speed	F-106B	1004	0.90	0	0.38
	F-94C	960	0.86	0	0.34
	B-52	675	0.60	0	0.91
High Altitude Cruise	F-106B	1936	2.0	40	1.27
	F-94C	715	0.73	35	1.34
	B-52	747	0.77	56	5.50
Low Altitude Landing Approach	F-6A(F4D-1)	202	0.18	0	1.12
	F-106B	222	0.20	0	1.27
	F-94C	235	0.21	0	1.45
	RA-5C	211	0.19	0	1.75
	B-52	333	0.30	2	2.18

00678-432

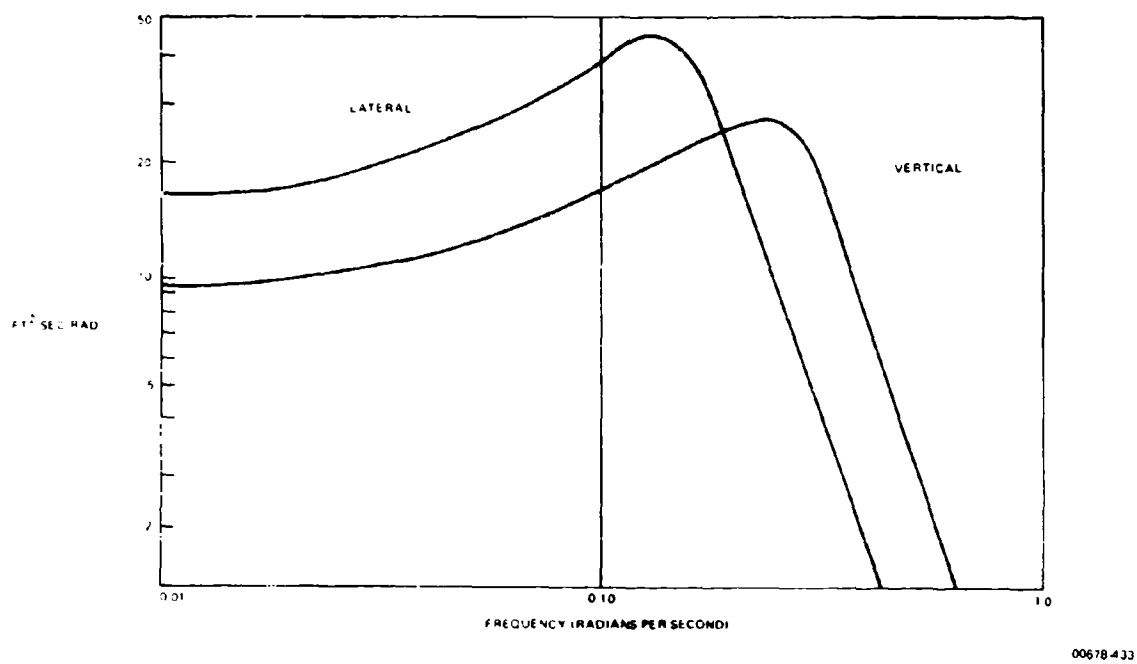

00678-433

Figure 4-25. Power Spectral Density of Aircraft Motion Caused by Air Turbulence

vertical motion, and the Dutch-roll plus pilot mode in lateral motion. The major source of damping of these modes is provided (for airplanes without yaw dampers or more complex autopilots) by aerodynamic drag. Since this source is proportionately less for high speed airplanes, this may explain why Harries' data show an increase in the 'flight roughness' effect across airplane types of increasing design speeds. We remain unconvinced that the flight roughness magnitude will increase for a given airplane as its speed is increased.

It is of course easy to determine that accelerations experienced in a given gust structure increase rapidly as airplane speed is increased.

Harries found, for the Vampire aircraft (350 mph), that a 5-second smoothing time with least squares linear extrapolation, gave a flight roughness prediction error of about 6 feet in each coordinate normal to the flight direction, per second of prediction. This is a rather larger value than the estimate obtained assuming a level airplane, and consequently indicates that the level airplane model is insufficient. Harries also showed, for vertical motion, a direct correlation of this factor with the quantity we have called T_s'.

Further investigation of the correlation between the gust structure and the displacement of the airplane would be of considerable interest. For the present study, we use values based on Harries' experimental results.

We also note that the autocorrelations obtained by Harries were:

$$\text{Vertical } R(s) = e^{0.1s} \cos 0.2s$$

$$\text{Lateral } R(s) = e^{0.06s} \cos 0.12s$$

The exponential terms decay so slowly that the effect of flight roughness falls into that category of disturbances which are essentially constant in magnitude during the prediction period, and randomly distributed across widely separated intervals.

Although Harries does not give the variances associated with the above autocorrelations, some rough calculation indicates that a standard deviation of 20 feet, associated with the autocorrelation functions, would give a prediction error of 6 feet per second of time of flight between 5 and 10 seconds (t_p), for 5 second smoothing.

The fact that aircraft deviations from a mean flight path is caused by air turbulence are rather small is indicated by a study of altitude deviations in general aviation which indicate, for example, that an F-27 aircraft flying at below 5000 feet showed a 56-feet standard deviation from reference altitude under manual control, and 13.0 feet under autopilot. Above 5000 feet for the same aircraft, the deviations was 18 feet for autopilot; but the sample for manual control was too small for fair comparison. The general observation was made that an autopilot with altitude hold maintained the deviations to about half the value achieved by the man, and an autopilot without altitude hold was intermediate between the two.

4.1.3.1.7 Summary

Flight roughness will have only a small effect on AFAADS effectiveness when the target is not deliberately evading. The slow decay of the autocorrelation with time requires that the effect be considered as essentially constant during a one-second firing sequence, but randomly distributed across widely spaced sequences. A better analytical model relating flight roughness, the airplane plus pilot dynamics, and the gust structure would be very helpful.

4.1.3.2 Terrain Following

To place 'terrain following' in a historical perspective, we can hardly do better than to quote from the autobiography[26] of Major James McCudden, British Ace of WWI:

'Xmas, 1913 came, and with it cold and frosty weather and also a good deal of flying. On Boxing Day ... we got the old Bleriot No. 292 out and went 'contour chasing' over the Plain... . For the benefit of the uninitiated one may explain that 'contour chasing' means flying close to the ground, following its contours down into valleys and up hill-sides. It is a dangerous form of sport as there is no chance of picking a landing place if the engine stops, but it is quite amusing, and it is a form of flying worth practicing because of its value in war.'

The reasons for 'contour chasing' have not changed, i.e., to deny the enemy early warning, and avoid ground fire. McCudden's memoirs also contain detailed descriptions, absent in most pilot reminiscences, of the effectiveness of ground fire of all calibers against military aviation even in the earliest days of the use of aircraft in warfare.

In addition to creating problems in detection and acquisition, an airplane attempting to fly as low as possible by following terrain contours generates an irregular flight path which may create problems in flight path prediction for AFAADS. In this section, some of the resulting flight path characteristics are described and the effect of this input variation on the prediction problem is assessed.

While recognizing that helicopters and 'slow' aircraft will weave in direction around terrain prominences, of greater inportance are altitude variations,

and the path changes in a horizontal plane that principally affect exposure time. As will be seen, altitude variations in themselves pose a major prediction problem.

First note that AFAADS might consider terrain effects in two ways. One is to put local terrain explicitly into the computer. There may be some advantage (and there is certainly increased system cost) in this approach since any local terrain configuration will probably differ substantially from the average terrain characteristics of the general region surrounding the site. This approach may be cut to feasible dimensions by recognizing that only a gross representation would be necessary to adequately describe the local terrain restrictions on low altitude flight.

The second approach, and one which is used in this section to size the problem is to consider a statistical description of terrain, and to determine how large the flight path deviations are likely to be for an airplane doing terrain following.

Terrain can be described in statistical terms similar to those used to discuss the effects of air turbulence. A number of measurements have been made of the power spectral densities (PSD) of terrain irregularities. From measurements of ground elevation from a horizontal straight line, power spectral densities can be computed, and these, together with the rms variation of elevation from the mean terrain height over the measured segment, provide similar inputs for analysis to those which were used for air turbulence. It is interesting that the distribution of such deviations has been determined in several analyses to be adequately represented by a normal distribution.

One of the problems in using the PSDs, available in the literature, is the usual one of estimating the PSD of a process from records of limited length. Persons interested in terrain microstructure(e.g., for cross-country vehicle movements) tend to consider large terrain variations as trends to be subtracted out before computing PSD. On the other hand, computations of PSD for macrostructure including hills and mountains, properly omit the fine detail of short wavelength. The result is that the measured variances tend to be sensitive to the objective of the analysis, and in the case of macrostructure PSD, the slope of the PSD for high frequencies is steeper than would be compatable with that obtained in microstructure PSDs.

In the following analysis, we choose to represent the terrain PSD by the function:

$$\Phi_1(\Omega) = \sigma_t^2 \frac{2}{\pi} \frac{L d\Omega}{1 + \Omega^2 L^2} \qquad (4.31)$$

Figure 4-26 shows some PSDs used in an Air Force paper[28], and apparently those were derived from a Cornell paper[31] which pioneered this type of analysis. Another useful study by Ling Temco Vought[27] is compatible over the frequency range of interest to us, but shows a second break frequency at wavelengths shorter than about 600 feet which appears to be inconsistent with the PSDs computed for microstructure and charted in Bekker's compendium.[33]

The above relationship allows us to describe a terrain sample by the standard deviation (σ_t) and a characteristic length L. Table IV-9 collects some samples of these parameters from several references which appear compatible with our present objectives.

4.1.3.2.1 Upper Limit to Flight Path Deviation

To obtain an upper limit on flight path deviation caused by terrain following, assume that the airplane follows the terrain contour perfectly at some constant height above the terrain. This is, of course, not possible and will be later modified. However, it does give a first approximation to the desired result. Assume that the airplane is observed at (t) and determine its mean square deviation from the observed height at time ($t + t_o$). This is obtained as:

$$\left(\frac{\sigma_\Delta}{\sigma_t}\right)^2 = \frac{4}{\pi}\int_0^\infty \frac{(1 - \cos bx)dx}{1 + x^2}$$

$$= 2(1 - e^{-b}) \; ; \; b = vt_o/L \qquad (4.32)$$

For small b:

$$(\sigma_\Delta/\sigma_t)^2 \cong 2\,(vt_o/L) \qquad (4.33)$$

$$\sigma_\Delta^2 \cong G_t\,(2vt_o) \qquad (4.34)$$

(G_t) is defined as the terrain roughness measure. It collects in one term, the two descriptive parameters (σ_t) and (L). It corresponds to the terrain roughness factor (F) used by LTV[27] but has the simple dimension of feet. The correspondence is shown in Table IV-10.

For a moderate terrain roughness (G_t = 9 feet) and a time of flight of 3.0 seconds, we find σ = 230 ft for a 1000 f/s aircraft, and 160 feet for a 500 f/s aircraft. Clearly the potential effect on AFAADS prediction error is very large.

Table IV-9. Terrain Standard Deviation and Characteristic Length Data

Area	Source	Standard Deviation σ (ft)	Characteristic Length L (ft)
Tunguska Plateau, USSR (Moderate)	LTV[27] Pg. 8	341	12,500
Korea Highlands, Korea (Rough)	LTV[27] Pg. 8	683	9,990
Lawrence, Kansas	Hayre and Moore[29] (Para. 8.2)	5.63	8,400
Tees Nos, Arizona	Hayre and Moore[29] (Para. 8.2)	49	750
Turtle Mountain, North Dakota	Hayre and Moore[29] (Para. 8.2)	8.2	1,420
Gila River, Arizona	Hayre and Moore[29] (Para. 8.2)	13.6	1,080
White River, Arizona	Hayre and Moore[29] (Para. 8.2)	5.18	740
Mountain Park, New Mexico	Hayre and Moore[29] (Para. 8.2)	1,030	3,650
Sandia Park, New Mexico	Hayre and Moore[29] (Para. 8.2)	250	1,010
Meadow Springs Canyon (Fairly Smooth)	Erickson[30] (Para. 8.3)	290	9,350
Meadow Springs Canyon (Moderately Rough)	Erickson[30] (Para. 8.3)	230	1,870
Meadow Spring Canyon (Rough)	Erickson[30] (Para. 8.3)	250	1,340
Meadow Springs Canyon (Very Rough)	Erickson[30] (Para. 8.3)	310	1,560

00678-435

Table IV-10. Comparison of Terrain Roughness Factors

Terrain Type	Terrain Roughness Factors	
	F (LTV)	G_t
Smooth	0-50	0-2.5
Moderate	50-100	2.5-10
Rough	100-150	10-23
Very Rough	> 150	> 23

00678-436

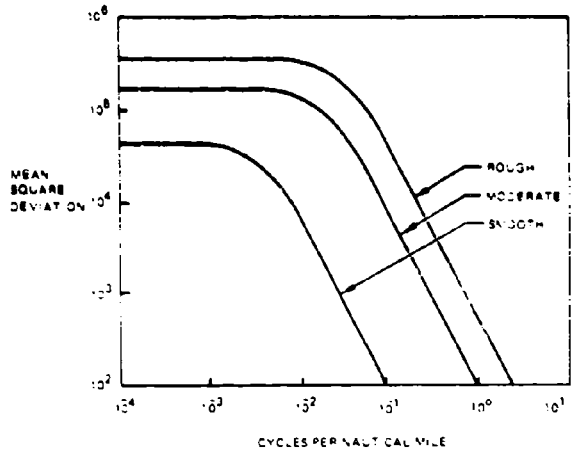

Figure 4-26. Power Spectral Densities

4.1.3.2.2 Contour Chasing Ability of Aircraft

The exact description of what goes on when an airplane attempts to fly as low as possible for extended periods of time is complex and involves not only the characteristics of the terrain, but the airplane sensors and control system, pilot response, etc. We develop here a very simple aggregated type of model, which is consistent with a limited amount of experimental data, and allows us to interpret terrain PSDs in terms of inputs to AFAADS.

Assume that the pilot is attempting to maintain a constant height (h_o) above the terrain surface and define the following quantities on a vertical axis through the airplane at time (t):

h_t = terrain height above its mean

h = aircraft height above the terrain mean

E = aircraft deviation from the h_o desired by the pilot

Then:

$$E = h - h_o - h_t \tag{4.35}$$

Now make the simplest possible assumption regarding the control law, namely that the rate of change of aircraft altitude is proportional to the error:

$$dh/dt = -E/T_c \tag{4.36}$$

where: T_c = a time constant aggregating pilot (human or automatic) and aircraft characteristics.

Then:

$$E/h_t = sT_c/(1 + sT_c) \; ; \; s = d/dt \tag{4.37}$$

and:

$$(\sigma_e/\sigma_t)^2 = \frac{2}{\pi}\int_0^\infty \frac{(L/V)\,d\omega}{1+(\frac{L}{V}\omega)^2} \quad \frac{(\omega T_c)^2}{1+(\omega T_c)^2} \tag{4.38}$$

$$= \lambda/(1+\lambda) \; ; \; \lambda = VT_c/L$$

If we now assume that the pilot will tend to set (h_o) of sufficient magnitude that the probability of a deviation ($-E> h_o$) is very small, for example: $h_o = 3\sigma_t$ we find:

for $\lambda << 1.0$; $\sigma_e^2 \sim G_t v T_c$

$$h_o \sim 3\left(G_t V T_c\right)^{1/2} \tag{4.39}$$

and we expect mean height above terrain to increase as the square root of aircraft speed.

The data, presented previously in Figure 4-13 for CH-47 helicopters, confirm this trend. The data are consistent with a value of $(T_c) \cong 0.5$ sec.

Using the above relationships to determine the variance of the aircraft deviation from a straight line path (σ_s^2), we find:

$$\left(\sigma_s/\sigma_t\right)^2 = (1+\lambda)^{-1} \tag{4.40}$$

and if $(\lambda) << 1.0$, the variance is very nearly equal to the variance of the terrain itself.

With $(T_c) \cong 0.5$ sec, the break frequency of the control loop is at 2 rad/sec. This is generally higher than the break frequency of the terrain PSD when sampled at aircraft speeds up to sonic.

We therefore conclude that we can approximate the PSD of aircraft vertical deviations in terrain following by using the PSD of the terrain, converted to a function of rad/sec by introducing aircraft velocity. This approximation is in the form:

$$\frac{2}{\pi} \frac{(L/v)\,d\omega}{1+(L\omega/V)^2} \tag{4.41}$$

Typical PSDs in this form are shown in Figure 4-27.

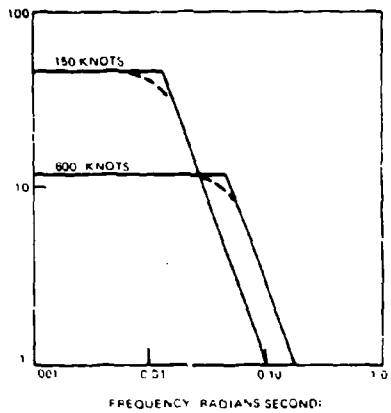

00678-437

Figure 4-27. Power Spectral Density of Vertical Aircraft Motion in Terrain Following

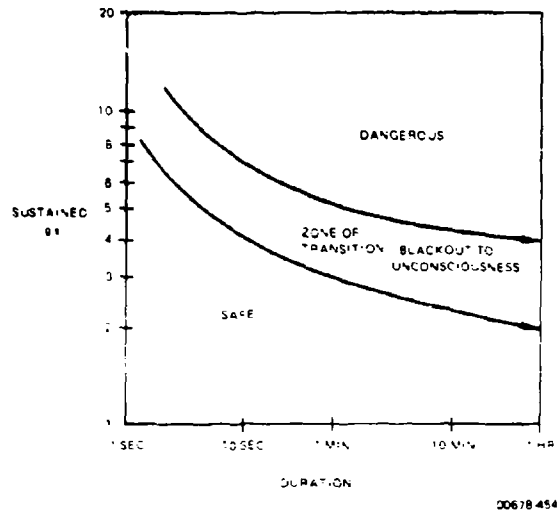

00678-454

Figure 4-28. Effect of Maximum Sustained Accelerations for Human Pilots

4.1.3.2.3 Aircraft Acceleration

The simple model developed thus far may be extended to determine the implications in terms of the mean square acceleration experienced by the aircraft in terrain following. To obtain convergence of the integral it would be necessary to include at least one more high-frequency attenuation term in the control model. This has not yet been worked through.

For reference, Figure 4-28 shows the maximum sustained accelerations which have been indicated for human pilots[34], with effects as listed in Table IV-11.

For random vertical accelerations, of the sort experienced in contour flying, a reference for frequencies below 1 Hz has not yet been located, but Figure 4-29 from Bekker[33] summarizes some findings for frequencies above 1 Hz. It seems unlikely that the pilot would willingly experience a sustained rms acceleration of random nature of more than 0.3 to 0.5g. Increasing aircraft speed might therefore be associated with larger effective (T_e) for a given terrain profile.

As input functions the PSDs (shown in Figure 4-28) have the following characteristics::

a. The break frequency is well below that of the AFAADS tracker (man or automatic), so that the tracking system should be able to track the motion.

b. The PSD corresponds to an autocovariance function of the form ($e^{-\tau}$). It is well known that the best prediction function for a stochastic variable of this form is an interpolation between the most recent measurement and the mean of past measurements.

c. The mean square deviation of the airplane from the most recent measurement during a 3-second time of flight can be 100 feet or more.

d. A prediction algorithm using altitude rate will be relatively ineffective and may generate a prediction error substantially greater than 100 feet.

It is therefore concluded that 'contour chasing' represents a unique problem for the development of altitude prediction algorithms. The report section on prediction will examine this problem in greater detail. It may be that the best solution is to make no altitude prediction below some minimum altitude, i.e., assume that 'future' altitude equals 'present' altitude.

4.1.3.3 Energy Concept of Maneuverability

The total energy of an aircraft at any time is the sum of its potential and kinetic energies. It can add to this sum by advancing the throttle, or lighting the afterburner, or it can subtract from the total by dropping drag flaps, or retarding the throttle and allowing energy to be dissipated as drag. Increasing or decreasing total energy is, however, a slow process compared with the facility with which potential can be traded for kinetic and vice versa, by manipulation of the controls. It was observed many years ago, when a large number of evasive aircraft paths was analyzed[35], that rather large changes in altitude and speed could take place with very small associated changes in the sum of kinetic and potential energies.

Recently, the 'energy concept of maneuverability' has been applied to the evaluation of fighter aircraft by Major Boyd, and a great deal of basic information

has been accumulated on the rate at which aircraft can change total energy.

Since we are interested in relatively short prediction times (a few seconds) for AFAADS, we are interested in determining whether it is feasible to capitalize on the relative invariance of total energy in the prediction algorithms. The most likely application is to apply a correction to the prediction vector along the flight path to correct for acceleration in a dive, or deceleration in a turn. Since the first order correction is derivable from velocity measurements only, no additional noise is introduced in the prediction process. The appropriate algorithms are developed later in this report.

The following paragraphs review briefly the energy relationships, when energy is increasing or decreasing, to indicate the rates of change which can be attained.

4.1.3.3.1 Rate of Change of Energy

The total energy of an airplane at altitude (h) and speed (v) is:

$$E = mhg + 1/2\, mv^2 \qquad (4.42)$$

where: $m = W/g$, W = airplane weight.

The specific energy is defined as energy per pound, and is:

$$E_s = E/W = h + (v^2/2g) \qquad (4.43)$$

The rate of change of specific energy is:

$$dE_s/dt = dh/dt + (v/g)\, dv/dt \qquad (4.44)$$

and is denoted by the symbol (P_s):

$$P_s = dE_s/dt \qquad (4.45)$$

P_s can also be derived from the thrust-drag balance of the airplane:

$$m\, dv/dt = T - D - W \sin\theta \qquad (4.46)$$

where: T = thrust, D = Drag, and θ = angle of climb. This expression can be written in the form:

$$(T - D)\, v/W = dh/dt + (v/g)\, dv/dt \qquad (4.47)$$

from which:

$$P_s = (T - D)\, v/W \qquad (4.48)$$

This quantity can be computed in the v-h plane for a particular aircraft design in steady flight.*

The contour $P_s = 0$ bounds the region in which the aircraft can maintain steady flight. At a particular point in the region, the corresponding value of (P_s) indicates the range of dh/dt and dv/dt which are accessible to the aircraft. For example, if dh/dt = 0, then:

$$\left[(dv/dt)/g\right]_{max} = P_s/v \qquad (4.49)$$

and if dv/dt = 0,

$$(dh/dt)_{max} = P_s \qquad (4.50)$$

For the F104G aircraft whose (P_s) contours were shown in Figure 4.2 as solid lines and reading the contours at sea level, values were obtained for maximum horizontal acceleration in 'g' (by lighting the afterburner) and maximum rate of climb in feet/seconds as shown in Table IV-12. The F104G has a maximum T/W of about 0.85.

Note in the table that at about Mach 0.7 the maximum acceleration approaches T/W. Fighter-bombers and light bombers will have lower T/W and their maximum positive acceleration along the flight path will be less. These accelerations are, in any case, small compared with that perpendicular to the flight path which are limited only by the pilot's 'g' tolerance and the aircraft structural strength.

The maximum dh/dt indicated corresponds to a climb angle of about 40 degrees. The time to change path angle by (θ), at speed (v) and radial acceleration (ng) is:

$$t = \theta v/ng \qquad (4.51)$$

A 5g pullup, initiated at 1000 f/s, would require about 5 seconds to reach a 40-degree climb angle.

If we conclude that the maximum acceleration along the flight path which can be expected from a high performance fighter in the clean configuration is about 0.8g (resulting from thrust alone), and that fighter-bombers with stores and light tactical bombers may develop a maximum of perhaps 0.4g, then we infer that a correction to the prediction algorithm, based on the gravity acceleration of flight path inclination, alone will give us a useful improvement in prediction. This is

*P_s contours change when the aircraft is not in steady flight, for example during a pull-up. Similar contours can be computed for a steady 5g turn, etc.

Table IV-11. Effect of Short Duration 'Eyeballs in' Acceleration

g's	Effects
2.5-7.0	Visual symptoms appear
3.5-8.0	Blackout
4.0-8.5	Confusion, loss of consciousness
18-23	Structural damage, especially to spine

00678-436

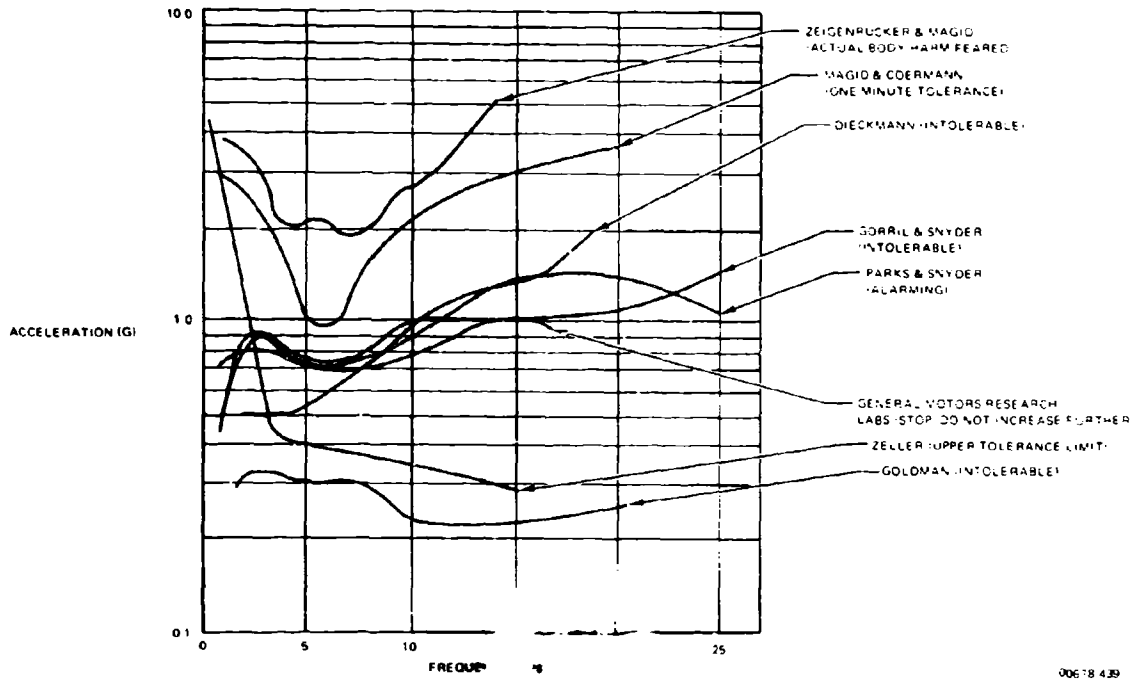

Figure 4-29. Tolerance to Vibrations based on [illegible] after Bauer (1963) and Van Deuser (1965) as prepar[illegible] 969)

equivalent to assuming constant total energy, and implemented simply by computing rate of change of velocity (v) along the flight path as:

$$dv/dt = -g \sin\theta = -g(dh/dt)/v \qquad (4.52)$$

4.1.3.4 Target Deceleration in Turn

As we have noted in the preceding section, the principal means a pilot has for accelerating his airplane is to pull back the stick. He can generate as high as 8g that way; more if he doesn't worry about losing his wings or blacking out. By lighting his afterburner, or conversely, cutting the engine and opening drag flaps he can generate less than 1g along the flight path, to which he can add or subtract up to 1g in a climb or dive. This suggests that accelerations greater than 1-2g along the flight path are unlikely, as compared with 8g perpendicular to the flight path.

On second thought, however, one realizes that the 8g lift doesn't come free. Lift causes 'induced' drag, and very large induced drag is produced by high lift coefficients. We estimate this effect below.

Table IV-12. Maneuver Capability of Airplane with T/W 0.85 at Sea Level

V (FPS)	M	P_s (FPS)	$\dot{v}/g$	$\dot{h}$	$\dot{h}/v$
450	0.4	300	0.7	300	0.67
675	0.6	500	0.8	500	0.74
960	0.85	700	0.8	700	0.73
1120	1.0	500	0.5	500	0.44
1230	1.1	100	0.1	100	0.08

00628-440

Drag coefficient (C_D) is for all airplanes fairly well approximated:

$$C_D = C_{Do} + k C_L^2 \qquad (4.53)$$

where: C_{Do} is the minimum drag coefficient for zero lift

k is a constant depending among other things on wing aspect ratio.

In cruising flight, an airplane has maximum range (and nearly minimum endurance) for minimum C_D/C_L, which we find upon differentiating (4.53) to occur at:

$$k\left(C_L^*\right)^2 = C_{Do} \qquad (4.54)$$

Suppose the airplane is flying at this cruise speed in level flight and the pilot pulls back on the stick thereby generating lift (C_L), then the ratio:

$$C_L/C_L^* = n \qquad (4.55)$$

is the number of g's of acceleration generated.

The drag ratio is:

$$D/D^* = \frac{C_{DO} + kn^2 C_L^{*2}}{C_{DO} + k C_L^{*2}} \qquad (4.56)$$

$$= (1 + n^2)/2, \text{ on substituting (2)} \qquad (4.57)$$

The engine was providing ($T = D^*$) and for a lift drag ratio of about 12/1 at cruise, $D^*/W = 0.08$. The acceleration along the flight path is then:

$$(D^* - D)/W = 0.08(1 - n^2)/2 = (1 - n^2)/24$$

If the pilot pulls 8g normal to the flight path, he will decelerate along the flight path at-2.7g.

For an afterburner capability of T/W = 1.0, he still slows down at -1.7g on full afterburner.

By using maneuver flaps he can obtain a better relationship between (C_a) and (C_L) than that indicated by (1). It is noted that the Mirage is reported to have a steady 7g turn capability with a T/W of 0.74.

There is, however, the probability that large decelerations along the flight path can be developed in high-g turns.

We summa .e the acceleration capability of the target very roughly in Figure 4-30, indicating that, in general, the capability of producing acceleration perpendicular to the flight path is much greater than the capability of accelerating along the flight path.

4.1.4 Target Exposure Time

As a target approaches AFAADS, we are interested in estimating the range at which AFAADS first has an unobstructed line of sight to the target, and the time that the target remains exposed. Low flying aircraft and, in particular, helicopters may appear, pass behind an obstacle, appear again, and etc. In general, the faster the aircraft, the less likely the flight path is to be thus segmented within the AFAADS volume of interest. On the other hand, it it probable that helicopters will be particularly adept at using local terrain for concealment to close in on a target before briefly exposing themselves to release their armament.

This section provides only an introductory review of the problem to obtain rough estimates of the ranges and exposure times within which AFAADS must successfully operate.

4.1.4.1 Nape of the Earth Flying

Experiments with CH-47 helicopters performed at Fort Ord have been referred to in prior sections of this report. The trends, indicated by that data, have been freely extrapolated to higher speeds, and are shown in terms of target exposure time and initial exposure range in Figures 4-31 and 4-32. These trends are

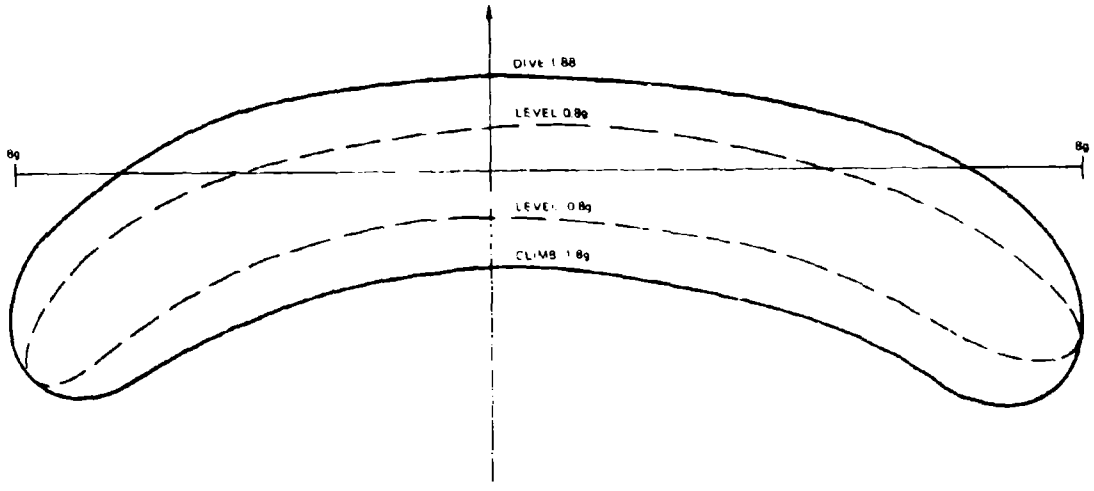

00578-441

Figure 4-30. Relative Acceleration Capability of a High Performance Fighter/Bomber Along and Perpendicular to the Direction of Flight

represented by the curves marked 'nape of the earth flying.'

The curves of exposure time are for aircraft flying essentially straight lines past the gun. It will be realized that the curves are very rough averages and actual times and initial ranges will vary widely with particular situations. Where possible, the gun will be located to have the widest possible field of view.

The curves do indicate that a very slow-flying helicopter can approach very close to the gun (which is presumed located close to the defended target) before exposing itself. Once exposed, however, its slow speed in a fly-by gives the gun ample time to acquire and fire, thereby suggesting that this is an unlikely aircraft tactic.

As speed becomes very low, the initial exposure range curves become asymptotic to those of a vehicle moving on the surface of the terrain, and are therefore directly related to the power spectral density (PSD) of the terrain.

It should be noted that both experimentation with helicopters flying the nape of the earth, and the development of tactics are being pursued energetically. It is expected that extensive data will be available shortly which will allow more detailed analysis of this mode of flight as it interacts with the air defense system.

One would expect that 'rough' terrain would be associated with a shorter initial exposure range than 'flat' terrain. In the limited experimental data reviewed, the converse appeared to be the case: apparently because in the small terrain sample available the CH-47 could fly lower at a specified speed over 'flat terrain' than over rough terrain, and thus delay exposure. The differences, as indicated by the narrowness of the band shown, may not be significant in view of the small sample.

4.1.4.2 Terrain Mask

The concept of a 'terrain mask' is a convenient one for estimating initial exposure range and time for aircraft flying essentially level. The terrain mask angle is that angle of elevation at a specified range which has a clear line of sight from the observing point to the specified range. Figure 4-33 shows typical mask angles[36] versus range (for some terrain in Pennsylvania). Mask angles for a wide variety of terrain samples are given in Cornell reports.[37]

Initial exposure ranges and exposure times for fly-by targets are shown in Figures 4-31 and 4-32 for 500 and 1000 meter altitudes and 6 degree terrain masks. Six degrees was chosen as a 'worst case'.

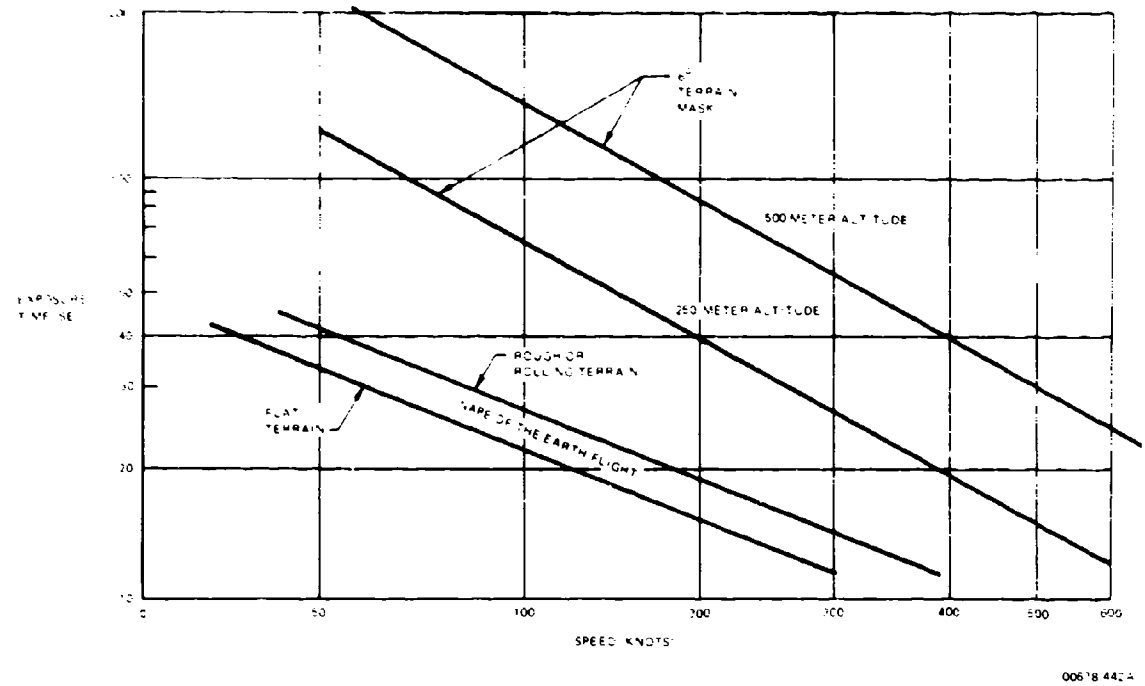

Figure 4-31. Effect of Speed and Flight Path on Target Exposure Time

The principal observation is that at all speeds, terrain following aircraft are more difficult targets than aircraft flying level.

4.1.4.3 Pop-up plus Weapon Delivery Time

The appropriate tactic for a helicopter to use to capitalize on the short initial exposure range in the nape of the earth flying at low speed is to approach its target to within air-to-surface munition range under concealment of terrain, rise just enough to obtain a free line of sight to its ground target, fire its armament, and then retreat behind terrain cover. This would reduce its exposure time to the time to acquire its ground target, aim, and fire; and in the case of guided-all-the-way weapons such as TOW, to guide the weapon in. Exposure time could thus be as short as 5-20 seconds. The target path, even during weapon guidance, may be quite irregular.

4.2 SENSOR CHARACTERISTICS

This section discusses the characteristics of candidate sensors which may be used to obtain tracking and surveillance information for AFAADS. Emphasis is on providing a basis for estimates of inputs to the prediction function, rather than on the design of the sensor, which is beyond the scope of this study. This section does not consider the man as a sensor. Human operator performance characteristics are developed in Section 4.3.

4.2.1 Operational Considerations

The combination of sensors to be installed on AFAADS depends on two decisions, each of which is only partially amenable to the analytical solution. These are as follows:

a. The capability desired for AFAADS at night and/or in inclement weather.

b. The autonomous surveillance and target acquisition capability desired for AFAADS. This in turn depends on the quality and timeliness of the alerting information transmitted to the fire unit from the FAAR radars and other sources of early warning information.

If AFAADS is highly effective by day but limited in effectiveness at night or in bad weather, the enemy will shift the weight of his attacks, to the degree that his equipment permits, to these times of reduced AFAADS capability. The capabilities of both the U.S. Air Force and Army aircraft to operate, locate targets, and successfully attack them regardless of night or weather, are increasing very rapidly. There is no reason to believe that a technologically sophisticated enemy will confine his attacks to clear-daytime operations. This is precisely the enemy against whom AFAADS will be required to defend, since it is unlikely that a technologically unsophisticated enemy will be able to maintain

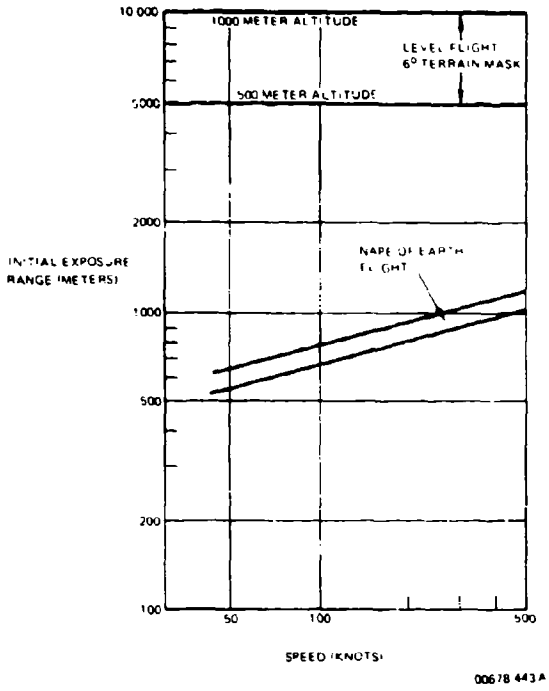

Figure 4-32. Initial Exposure Range

any significant air strike capability against U.S. air power.

If AFAADS is only effective under clear-day conditions, it will force the enemy to employ more costly all-weather strike aircraft even though these will be unopposed by AFAADS except in clear-day operations. However, if AFAADS has an all weather capability, it will degrade enemy effectiveness under all conditions, but at an increased expense of equipment to both sides. We return to this subject in discussing cost-effectiveness in a later section of this report. It is clear that the decision requires good military judgement as well as analysis.

In the following paragraphs a wide spectrum of sensors is reviewed. At the possible expense of convincing detail, only unclassified information is presented.

The most important sensor, man, is discussed in Section 4.3, Human Operator Characteristics.

4.2.2 Types of Sensors

The numbers of types and ranges of characteristics of potential sensors for AFAADS are extremely large, and increasing with continued research. As a point of departure for organizing a discussion of sensors, Figure 4-34 illustrates the usage of the electromagnetic spectrum, the nomenclature, and the atmospheric obstructions to radiation as a function of frequency.[56]

The atmosphere is relatively opaque to ultraviolet radiation. The bands of interest for AFAADS include the following:

a. Visual: 0.3 to 0.85 micron.

b. Near Infrared: 0.85 to 2.0 microns.

c. Far Infrared: 2.0 to 1000 microns.

d. Microwaves: above 1000 microns.

Sensor systems may be categorized as active or passive. Active sensor systems illuminate the target and detect the reflected radiation. The source may be continuous or intermittent, and its emitted radiation may be coded to improve discrimination of the reflected signal from background noise. Passive systems detect radiation emitted by the target (such as infrared) or radiation from the general background reflected by or interrupted by the target (such as in the case of ordinary visual observation).

To detect the target, its signature must lie in a band transmittable through the atmosphere, and a detector sensitive to the wavelength transmitted must be available.

At the tracker, the received signal may be tracked either as a point source, or as a formed image. For AFAADS, available radars will probably not allow image generation; consequently, the target will be tracked as a complex source with the attendant error characteristics as discussed in a following paragraph. The simplest forms (and least expensive) of IR trackers are non-imaging trackers.

The first use of infrared for antiaircraft fire control was based on tracking the target as a point source. The U.S. Army Signal Corps originally contemplated using the SCR-268 Radar as a device to put a more accurate infrared tracker on target. Rapid radar advances lessened Allied interest in IR trackers. However, German equipment, employed in WWII for tracking aircraft by near IR trackers, was capable of tracking piston engined bombers, passively, to 5000 meters.

Point source tracking may be done by scanning or by monopulse methods. Scanning may be mechanical or electronic. Since a scanning device compares signals received at slightly different times and compares amplitudes, fluctuations in signal strength, not associated with scanner axis position, cause tracking errors.

Image forming systems may produce an image directly, by electronic scanning, or by mechanical scanning. The eye forms an image directly. An imaging tube can provide an image in the visible range by a cathode, which emits electrons in proportion to the amount of visible or infrared radiation from the original images projected on its surface by the optics, and a phosphor screen which is then stimulated by the emitted electrons to recreate the image in the visual range. The first tube of this type by RCA in the 1930s

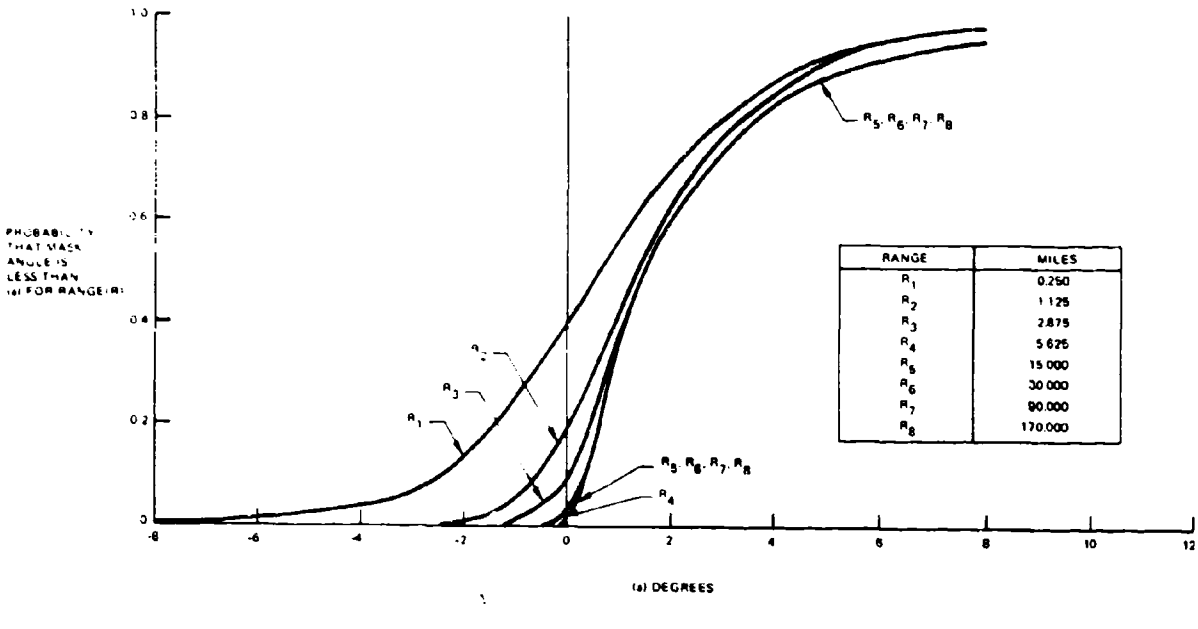

Figure 4-33. Terrain Mask Angle

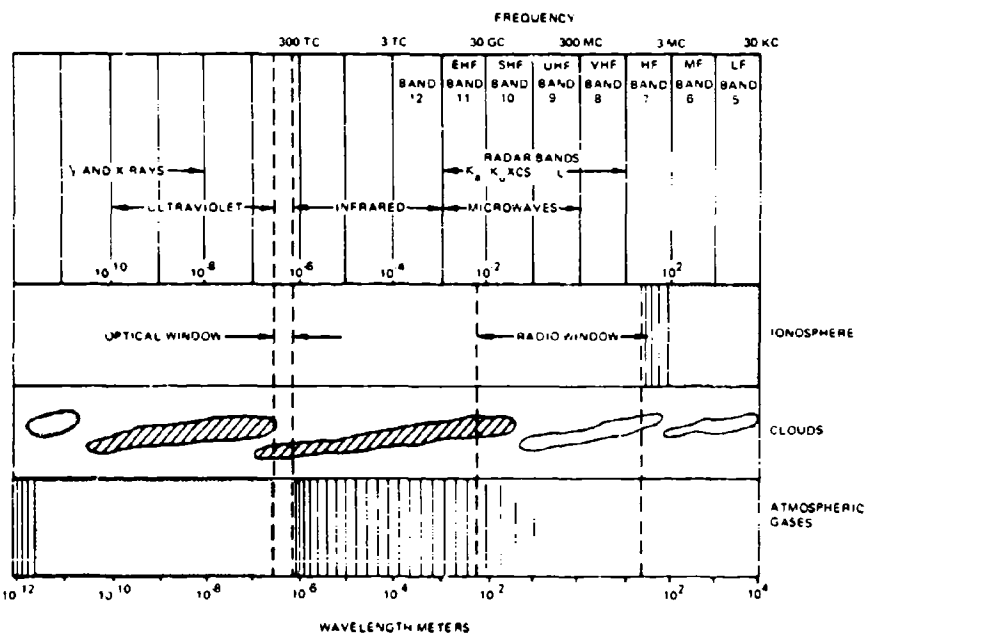

Figure 4-34. Electromagnetic Spectrum Usage and Atmosphere Obstructions

stimulated German and Japanese developments which led to their WWII systems. While modern direct viewing image intensification systems are far more efficient, the concept of forming a complete image without scanning is similar.

Electronic scanning is based on modulation of a scanning electron beam by an image projected on a suitable surface whose resistance at each point is proportional to the intensity of the IR image at that point. The modified scanning beam then goes on to illuminate a fluorescent screen, thereby recreating the IR image in the visual range.

Mechanical scanning may employ very large numbers of small detectors to build up an image on a viewing screen.

The very large number of ways of producing an image from an IR detection device is illustrated by Figure 4-35 (adapted from Reference 60).

Once an image has been formed, it may be tracked manually or automatically. Automatic tracking depends on image contrast. However, since the image will normally have a good contrast against its background, the tracker can average between edges (for example, by closing gates on the image to enclose it in a rectangular box) and thereby track the center of the box. Consequently, an image tracker should be less sensitive to signal strength fluctuations than a point source tracker.

Clearly, an identical process could be performed without the intermediate stage of forming an image. However, since the image can be examined by the human operator, some recognition may be possible of target type; or if more than one target appears, the operator may select one. In ground fire, the image will be necessary for target recognition, selection, and aiming.

Acoustic sensors represent an additional category. The speed of sound is too low to make these of much interest as trackers. However, experiments indicate that helicopters flying low will often be heard before they are seen. Consequently, there may be a place for antiaircraft acoustic sensors in the battlefield surveillance system, if not in AFAADS fire control.

Table IV-13 summarizes the sensors considered to be of principal interest for AFAADS and the information obtainable from them.

4.2.3 Radar

In the following paragraphs, radar is discussed to a degree appropriate to estimating the characteristics of the data which radar sensors may provide to AFAADS. Because AFAADS must track low altitude targets, and since precision tracking is necessary, we consider principally monopulse doppler radar. As points of reference, the AFAADS surveillance radar may be considered to be S-band with; CSC^2 antenna, two stacked beams, or possibly with frequency diversity. The tracking radar might be K_u-band with frequency diversity.

The discussion of errors follows Barton closely, using expressions given in his texts.[41,42]

The two principal problems in obtaining precise radar tracking for AFAADS appear to be associated with 'glint' at all elevation angles, and 'multipath' at very low angles only. Glint refers to variations in the apparent angle of arrival of reflected signals from the target caused by interference phenomena among reflecting elements of the target. Multipath returns at low angles present the tracker with multiple targets, from which it has difficulty in resolving the true target.

The standard deviation of the angular deviations in apparent target direction caused by glint is approximately proportional to the angle subtended by the target. How much of the power spectral density of glint appears as tracker error depends on the bandwidth of the tracking servos. A wide servo bandwidth is desirable at short ranges to hold acceleration lag within acceptable values. The bandwidth of glint increases very roughly with the rate of angular rotation of the target relative to the tracking line, and, hence, with angular velocity of tracking. These two interacting characteristics determine the fraction of the glint spectrum which appears in the radar output.

Research is underway on techniques to reduce the effects of both glint and multipath on radar tracking accuracy, and these are discussed in later paragraphs.

4.2.3.1 Radar Angular Accuracy

Radar angular error may be discussed (following Barton) in the following categories:

a. Thermal noise.

b. Clutter and interference.

c. Multipath reflections.

d. Target glint and scintillation.

e. Quantization and array error.

f. Dynamic Lag.

g. Atmospheric propagation.

h. Monopulse network error.

i. Servo and mechanical error.

Figure 4-36 is a well known representation of the combined effects of sources a, d, e, g, h, and i on angular tracking accuracy as a function of range.[39]

The curve for a monopulse radar may be considered

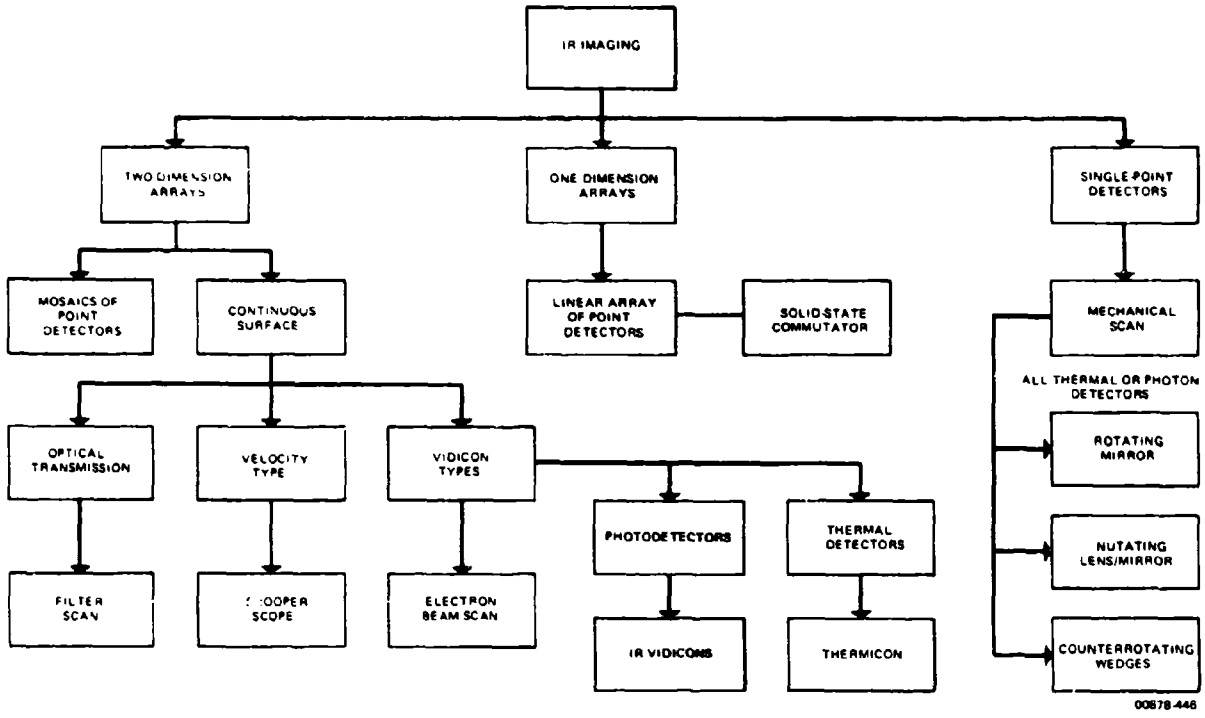

Figure 4-35. Detector and Scan Combinations for IR Sensing

Table IV-13. Sensor Categories

	Type	Measured Information			Environmental Use		
		Angle	Range	Range Rate (Doppler)	Clear Day	Clear Night	All Weather
Passive Systems	Optical Sight	X			X		
	Direct-Viewing Image Intensification (0.3 - 2.9 μ)	X				X	
	Low Light Level TV	X				X	
	Far Infrared (2 - 1000 μ)						
	Non-Imaging	X				X	
	Imaging	X				X	
	ECM Noise Source Tracker	X			X	X	X
Active Systems	Radar	X	X	X	X	X	X
	Near Infrared (0.85 - 2.0 μ)						
	Imaging	X				X	
	Laser						
	Range Pulse Only		X	X	X	X	
	"Optical Radar"	X	X	X	X	X	
	Imaging	X	X	X	X	X	

00678-447

to be the square root of the sum of the squares of three components:

a. Thermal noise:

$$\sigma_t = \frac{\theta}{[(2S/N)(f_r/\beta_n)]^{1/2}} \text{ Radians for } S/N > 1 \quad (4.58)$$

b. 'Instrumental Accuracy': an aggregate of sources e, h, and i, which are expressed as:

$$\sigma_i \cong \text{constant} \sim 0.10 \text{ mils} \quad (4.59)$$

If source g is included, this value may be about doubled.

c. Target glint (assuming no reduction in servo system):

$$\sigma_g \cong 0.35\, L_t/D \text{ Radians} \quad (4.60)$$

The coefficient '0.35' depends on the distribution of scatterers assumed for a theoretical model, and if possible, it should be obtained experimentally.

where:

θ	= radar beamwidth (radians)
S/N	= signal to noise power ratio
f_r	= repetition rate (pps)
β_n	= servo bandwidth (cps)
L_t	= target dimension (meters)
D	= target range (meters)

Figure 4-37 shows a typical power spectral density function for monopulse tracking error in angle.

The bias component will be discussed separately in terms of dynamic lags in target following. Thermal noise extends uniformly over the whole spectrum. The figure illustrates short range operation (normal AFAADS operating range), where the glint component is large because of the large angle subtended by the target. At very long ranges, glint is submerged in the thermal noise, and performance is dominated by the ratio of signal power to noise.

Equation (4.60) assumed that the sensor servo bandwidth was wide enough to pass the full glint spectrum. When this is not the case, the estimate may be modified as in the following paragraph.

4.2.3.1.1 Power Spectral Density of Glint

Very few measurements of the characteristics of glint have appeared in the open literature.[45] In the absence of experimental data under the radar-target-flight path conditions of interest, it is conventional to represent the glint power spectral density as:

$$\phi(f) = \frac{\sigma_G^2}{\pi f_0} \frac{1}{1 + (f/f_0)^2} \quad (4.61)$$

where:

f = frequency (Hz) and (f_0) is given by:

$$f_0 = 2\omega_s L/\lambda \quad (4.62)$$

where:

ω_s = the	angular velocity of rotation of the target relative to the line of sight.
L = the	target dimension
λ = wave	length

Barton's examples[42] are for cases where the sensor servo passes the complete glint spectrum. However, the object of frequency diversity is to spread the glint spectrum so that part is outside the servo bandpass. Barton's examples are also for rather slow targets; since ω_s is proportional to target speed, we would expect the glint spectrum to widen for fast targets at close ranges.

To the degree that Equation (4.61) is acceptable, we can write the variance of tracking error after the glint spectrum has been modified by the servo as approximately:

$$\sigma_1^2 = \int_{-\infty}^{\infty} \phi(f) \frac{df}{1 + (f/\beta_n)^2} = \sigma_G^2 \frac{\beta_n}{\beta_n + f_0} \quad (4.63)$$

Servo bandpass may be made a function of range for reasons cited earlier; such as, low bandpass at long ranges to improve signal to noise, and wide bandpass at short ranges to keep lag within bounds. Since angular lag is approximately:

$$\text{Lag} \sim \omega_s \beta_n^2 \quad (4.63a)$$

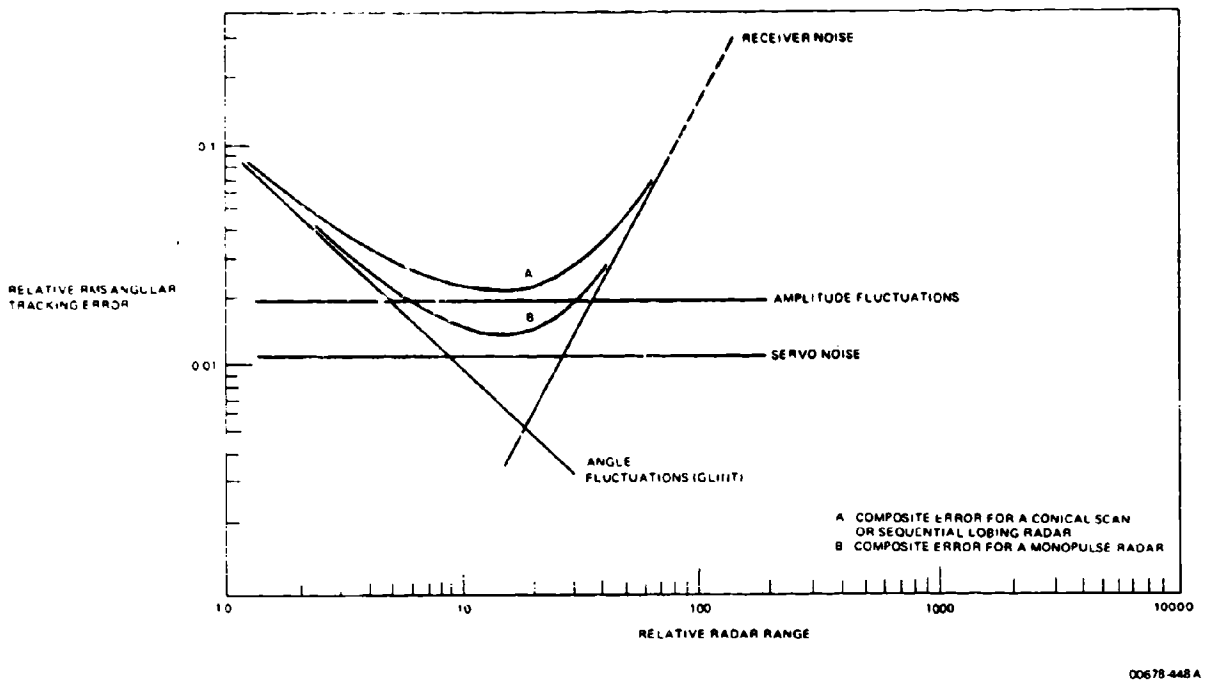

Figure 4-36 Sources of Angular Error in a Tracking Radar

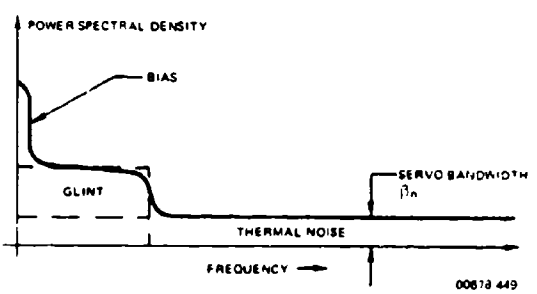

Figure 4-37. Typical Monopulse Angle-Tracking Error Spectrum

and

$$\dot{\omega}_a \sim (v/D)^2 \qquad (4.63b)$$

where: D = range v = target speed, β_n might reasonably be made inversely proportional to D within some maximum and minimum limits).

Since:

$$\omega_a \sim v/D \qquad (4.64)$$

then:

$$\sigma_t^2 = \frac{\sigma_G^2}{1 + (kvL/\lambda)} \qquad (4.65)$$

where k is a constant. We expect, as before, that the variance of tracking error caused by glint will have a constant linear, as opposed to angular, value with range, also that its value will be reduced by short wavelength and high target speed.

The points to be made from the above discussion are that for high target speeds, the glint spectrum may extend outside the servo passband. Frequency diversity is intended to increase the fraction outside. Servo gain should be a function of range. To place all of these elements in proper context for system evaluation, experimental data on the glint spectrum is necessary.

It is worth reiterating that if 'instrumental' error can be held to 0.1 - 0.2 mil, a target with dimensions 3 meters in elevation and 15 meters in length might be expected to generate a glint-caused angular error of 1.0 mil in elevation and 5 mils in azimuth. It is hoped to do much better than this for AFAADS and so considerable effort to finding out *how* is desirable.

4.2.3.1.2 Lag Errors

Dynamic lag (error source f), resulting from tracking servo characteristics, will be considered explicitly

in the evaluation, to maintain the distinction between slowly varying errors (lag), and rapidly varying errors (effect of glint). Lag is given conventionally by the expression:

$$L = (dA/dt)/K_v + (d^2A/dt^2)/K_a + \ldots; \quad (4.66)$$

where: A is angle and K_a, the acceleration lag constant, is related approximately to tracking servo bandwidth by:

$$K_a \sim 2.5\,\beta_n^2 \quad (4.67)$$

The above expression holds only when no regenerative aid is provided to the sensor servos. Regeneration is discussed in a later section. It offers some promise in permitting reduced β_n (equivalent), thus reducing glint-caused errors, yet not incurring undesirable lags.

One of the practical problems associated with wide servo bandwidths in positioning devices with significant inertia is the torques generated in the system at high frequencies. Since torque is proportional to the product of inertia and angular acceleration, high frequencies in the system will be associated with large torques, gear wear, and power dissipation in following noise.

4.2.3.1.3 Use of Frequency Diversity

One method of reducing angular errors caused by glint is the use of frequency agility or diversity.[38,4] Since the apparent direction of signal arrival from the target is a function of frequency, frequency agility increases the effective number of independent measurements of target position in a given time.

In addition, frequency agility increases the ECM resistance of the radar by denying the enemy the possibility of concentrating all of his jamming power at a single carrier frequency (spot jamming).

Some theoretical computations of potential improvement in tracking accuracy with frequency diversity suggest a potential improvement of a factor of 2.5.

Another approach to increasing the information rate to reduce the effect of glint is polarization agility.[39] Polarization agility is being investigated as a part of the Army MICOM, Phase Return Error Program. The MICOM program is reported to include:

a. Polarization agility.

b. Frequency agility.

c. Combined polarization and frequency agility.

d. Adaptive signal processing.

A factor of 2 improvement in angular accuracy with a pulse doppler conical scan radar has been noted by polarization agility alone and the program is to include monopulse doppler.

In view of the active research and development program directed to reducing the effect of glint on tracking error, it seems likely that by the time AFAADS enters engineering development it will be possible to include techniques which will allow a standard deviation of tracking error considerably less than the 0.35 of target linear extent indicated for currently operational state of the art.

4.2.3.1.4 Multipath Errors

The angular error introduced by multipath returns is of major importance to AFAADS because of its emphasis on nape of the earth flying targets. The standard deviation of elevation error σ_m (radians) from this source may be estimated from:

$$\sigma_m = (\theta\rho)\,(8A_s)^{1/2} \text{ radians} \quad (4.68)$$

where:

θ = radar beamwidth (radians)

ρ = ground reflectivity (voltage ratio)

A_s = sidelobe attenuation power ratio

This has a maximum at an elevation of about 0.8 times the half power beamwidth, and is negligible at about four times this value. The important point is that the effect is minimized by a narrow beam, thereby emphasizing the desirability of short wavelength radar such as K_u. A 1.8 cm radar with a 1-meter dish should have a beamwidth of about 1 degree.

As in the case of glint, research is under way to reduce multipath errors. An approach[40] which has demonstrated potential is signal processing based on the recognition that the problem is one of discriminating between two targets (the real and the multipath image).

No record has been found of experiments to reduce the effects of multipath by physically constraining the servo so that it cannot track an 'underground' target. This might be done with relatively coarse local terrain data stored in the computer.

Azimuth multipath is a lesser problem than elevation, and multipath introduces negligible errors in range measurements.

4.2.3.2 Radar Range Tracking Accuracy

As in the case of angular tracking, the error in measuring range may be considered in three categories; 'instrumental,' glint, and thermal. The standard deviation of the glint spectrum may be approximated as:

$$\sigma_g = 0.35L \qquad (4.69)$$

where: L is target range dimension.

Range following and readout may be by mechanical servo, or completely electronic. The power spectral density of range glint is estimated as having the same form as that of angular glint. It is probably preferable to have a tight servo and perform range and range rate smoothing (if the latter is not obtained from doppler) in the computer.

When range rate is obtained by doppler measurement, glint again is a major error source. Its magnitude is estimated as:

$$\sigma_f = 0.35(2L\omega_a/\lambda)\,\text{Hz} \qquad (4.70)$$

converting to meters/second:

$$\sigma_v(\text{m/sec}) = \sigma_f(\text{Hz})(\lambda/2) \qquad (4.71)$$

$$\sigma_v = 0.35\,(\omega_a L)\ \text{m/sec} \qquad (4.72)$$

At crossover where ω_a may be 1 rad/sec, σ_v can be quite large. However, the remarks, made previously about the bandwidth of glint and the possibility of improving the data rate of uncorrelated signal samples by frequency and polarization diversity, apply to the above estimates. The remarks, about the desirability of obtaining comprehensive measurements of the glint spectrum, also apply.

4.2.3.2.1 Choice of Frequency

For reasons discussed previously, a short wavelength is desirable for the tracking radar; subject to the availability of transmitting equipment generating satisfactory power, and the atmospheric and weather attenuation. Figure 4-38 shows atmospheric attenuation of microwaves from the S-band down into the millimeter range.[62] The K_a- and K_u-bands are in the windows to the left and right of the 1.5 cm, H_2O-absorption band.

Attenuation due to rainfall is shown in Figure 4-39 as a function of frequency.[62] Although drawn as continuous lines, the curves should be considered to apply only in the windows of Figure 4-38.

A complete radar selection study would include an evaluation of the frequency and duration of rainfall of varying magnitude in operational areas worldwide. At this point we show only a rainfall density function for Washington D.C.,[62] (Figure 4-40), which indicates that light rain (attenuation in K_a-band for 0.2 dB/km) is exceeded only 97 hours per year, or 1.1 percent of the time.

There appears to be no problem in obtaining equipment of adequate power to utilize K_u for AFAADS tracking. The whole field of millimeter microwave

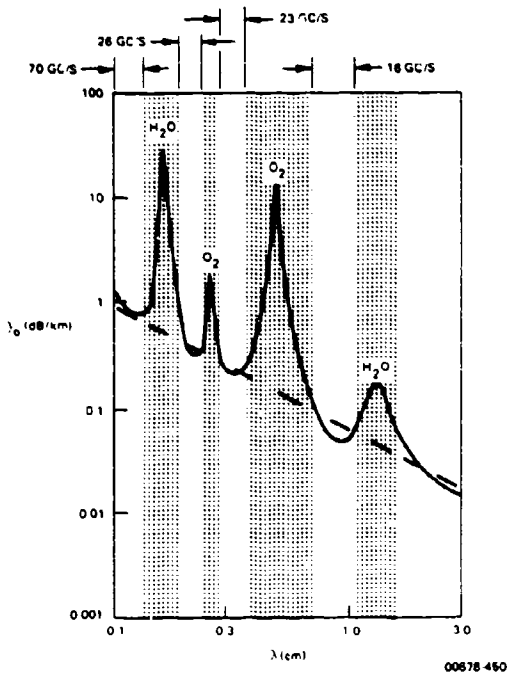

Figure 4-38. Atmospheric Attenuation Due to Water Vapor and Oxygen Molecular Absorption

equipment is advancing rapidly, but a comprehensive evaluation would be required to determine the potential and feasibility of still shorter wavelengths for AFAADS.

4.2.3.3 ECM

We consider briefly some of the considerations in possible noise jamming of the AFAADS radars.[46,47,48,49] The target aircraft may carry noise jamming equipment which, beyond burnthrough range, would deny AFAADS range information. A monopulse radar could track very accurately on the noise source, and by sharing angular information, several AFAADS fire units could obtain target position by triangulation. This would be a relatively simple computation for the computer.

However, a stand-off jammer (SOJ) would experience a number of difficulties caused by the geometry of the problem. To be effective at long range it must inject its signal into the main beam of the tracking radar, which is only 1 degree or less. As the radar tracks the close-in target, its beam has a high angular velocity; and since the SOJ aircraft must also remain in this beam, an extremely difficult problem of coordination between the two aircraft is presented when angular velocities are low and an impossible one when they are high. If the target aircraft flies straight in at

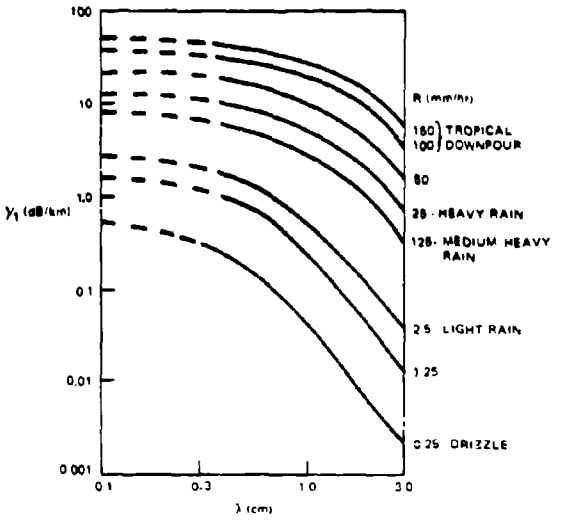

Figure 4-39. Attenuation Due to Rainfall for Various Rainfall Intensities

the radar so that angular velocity is zero, the SOJ aircraft may follow it; but by tracking the SOJ source, the radar will be within a degree of the incoming target, and on such a course, range information is not essential for prediction. Coordination of paths between SOJ and attack aircraft further deprives the attacker of freedom to maneuver, which may be unacceptable in the terminal phase.

To summarize, the SOJ aircraft has the advantages of high emitted power, high antenna gain if a steerable antenna is provided, and one-way transmission. The AFAADS radar has the advantage that the target is closer than the SOJ aircraft. ECCM techniques such as sidelobe reduction and cancellation may make noise jamming ineffective except when injected into the main beam, and a narrow beam creates the coordination problems for the SOJ aircraft as noted previously. The use of frequency agility widens the band over which noise must be transmitted to be effective.

One additional difficulty for the jammer is created by terrain. If the attacking aircraft flies high, the tracking radar beam has a rapid sweep rate in elevation. If the attacker flies nape of the earth, it will be extremely difficult for both SOJ and attacker to stay in the tracking radar main beam because of intervening terrain obstructions.

4.2.4 Infrared Sensors

Passive infrared sensors have the advantage over active sensors that the target is not aware that he is being tracked until he is fired upon. The signal strength decreases only as the square of range, instead of the fourth power as with active systems. The power and weight of the IR system can be low compared with radar. Because of the very short wavelength, IR has the potential of very high resolution with a small collector diameter. There are no side lobes, and no low angle tracking problems.

Passive systems are difficult to jam, countermeasure, and decoy. They have the capability (shared by visual spectrum light intensification sensors) of night operation.

Infrared, like visual techniques however, has the disadvantage of being unable to penetrate fog and clouds, although it has a slight superiority in haze penetration over the visual spectrum.

Figure 4-41 shows the atmospheric windows for infrared.[50]

4.2.4.1 Target Emitted Radiation

IR signatures of aircraft targets can be found in classified literature. Here we cite only an unclassified reference.[58] Detection depends on the emission from the heated skin, hot engine parts and by the radiation from the plume of hot gases from the engine. For aircraft detection, the radiation from the heated parts of the skin is more important than that from the plume, except at frequencies where the plume has high emissivity. The emitted radiation is proportional to both the emissivity and the blackbody radiance of a part.

The parts near the engines are heated by them and are strong sources of radiation. The hot nacelles and air intakes give a strong contribution to the total radiation from the front aspect. From the rear the tail pipe dominates the radiation. However, at 4.3μ the plume radiation is stronger than that from the tail pipe because of the greater area of the plume and the emission from hot CO_2 molecules in the plume. At supersonic speeds the skin may become so hot that it dominates the radiation.

4.2.4.2 Non-Imaging Trackers

Non-imaging infrared trackers have reached an advanced state of development for antiaircraft missile homing heads. They are small, lightweight, and of relatively low cost. For a ground installation it might be expected that, over AFAADS ranges, the tracking error would depend on the distribution and relative intensities of heated areas on the airplane, and the way in which these vary with aspect. Depending on whether the tracker scans, or compares direction of signal source by a multiple detector arrangement, the

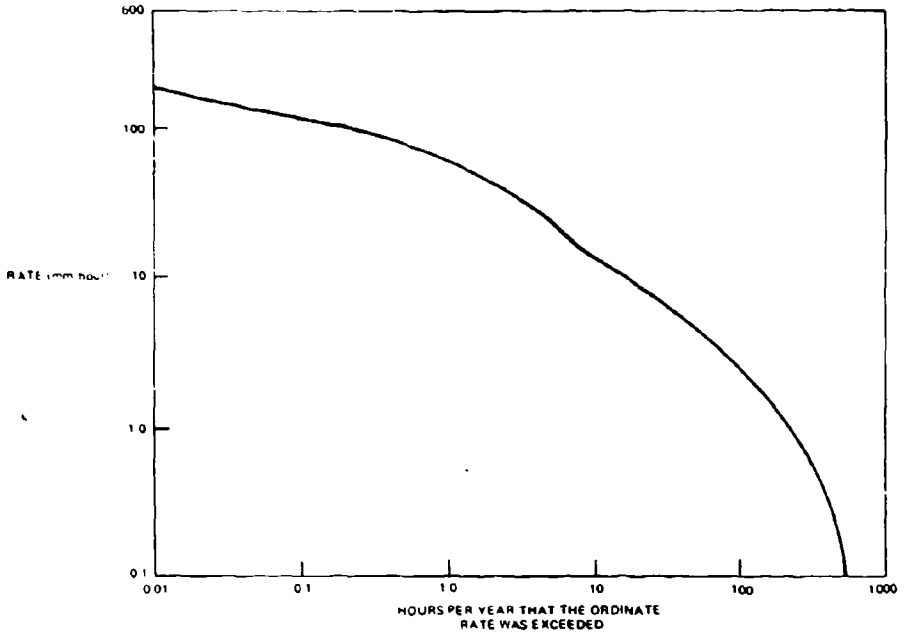

Figure 4-40. Cumulative Distribution Function for Rainfall Rates at Washington, D.C.

effect on tracking error would be similar to that of glint and scintillation on radar tracking. However, since phase interference is not involved, the wander of the point tracked by the ground sensor should stay on the surface of the target (assuming that the plume is excluded by optical filtering), and therefore, tracking accuracy should be better than that obtainable with a radar.

A non-imaging device also has the potential of operating in a surveillance mode. After a target is detected, the field of view could be closed in for precise tracking, or the target turned over to a tracking sensor.

4.2.4.3 Imaging Trackers

Figure 4-35 indicated the wide variety of techniques that are conceivable for infrared image production.

An air-to-ground passive-imaging device, operating in the 8- to 13-micron window, has been reported under development for the UH-1 helicopter AAQ-5 armament and control system. The system is described as having 375 mercury-doped germanium detectors that are sequentially sampled for vertical scan, with mechanical/optical horizontal scan. The resulting picture has 375 lines.

A ground-based version of this system is conceivable. It would have the advantage of providing the AFAADS gunner with excellent fair weather, and ground-to-ground capability in addition to the capability of seeing air targets at night.

4.2.5 Direct Viewing Image Intensification

The Army has currently available for use a family of night-vision sights including the starlight scope, a crew-served weapons sight, and a night observation device. They use image-intensification in the visual range, i.e., using light reflected by objects from starlight, starglow, etc. A device of this family could be mounted on AFAADS for surface fire at night in good weather. Cost is relatively low, and it is anticipated that similar sights will be mounted on the majority of Army ground-to-ground weapons.

4.2.6 Lasers

Capabilities and applications of lasers are developing so rapidly that an assessment of current capability will be out of date by the time this report is printed, and any rationally based forecast is likely to be conservative because of the rate of appearance of new information.

Lasers are currently available to operate within the visible spectrum, the near infrared, and the far infrared. In particular, an He-Ne gas laser is available to operate at 3.39 microns in the 3-5 micron atmospheric window, as well as a CO_2-N_2-He gas laser which is available to operate at 10.6 microns in the 7-14 micron

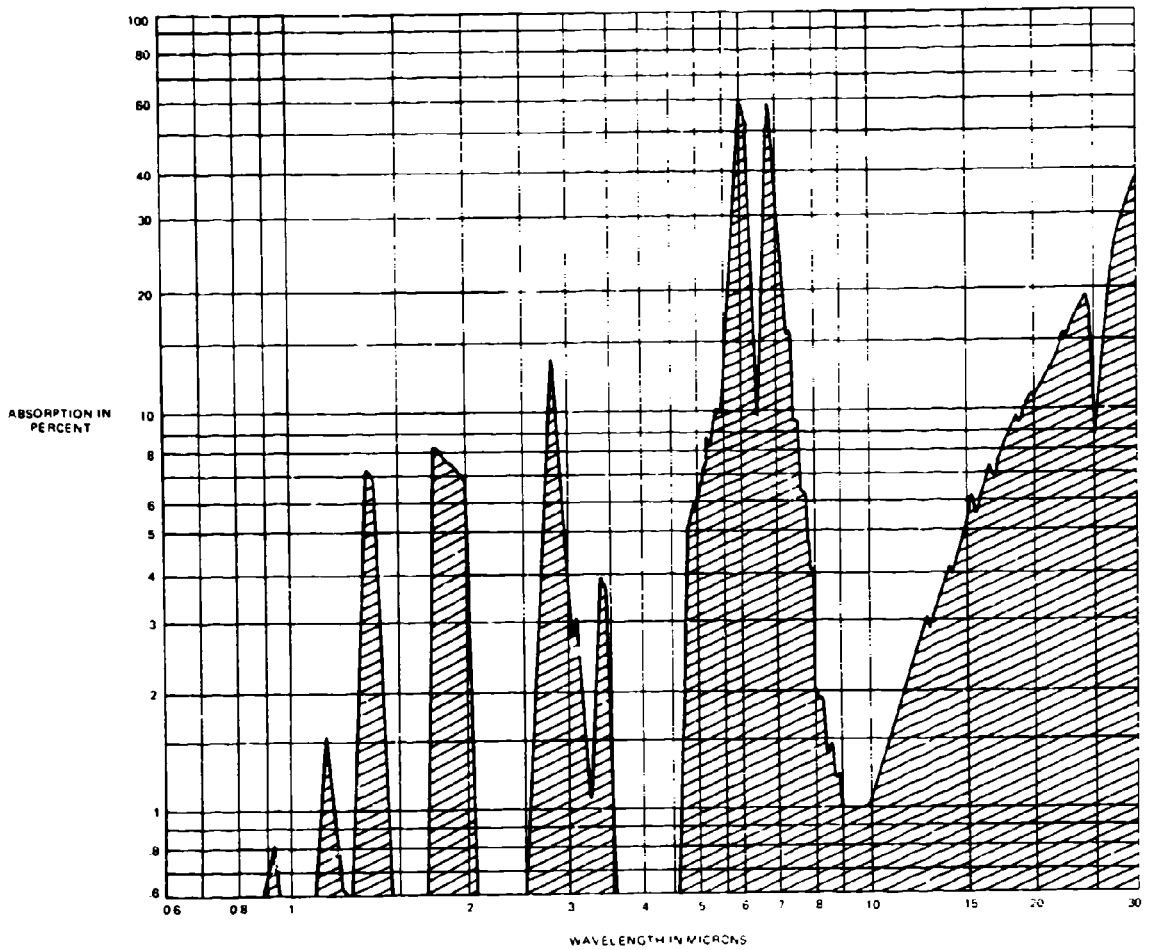

Figure 4-41. Absorption Spectrum of Water Vapor

window. For both these windows, detectors have been available for a long time.

A Ruby laser at 6943 A^{O} is on the upper edge of the visible spectrum, and a solid-state Nd-glass laser is available to operate in the near infrared at 1.06 microns.

The first generation of laser range finders is operational, with the low pulse rate considered adequate for use against ground targets. Pulse rates, consistent with ranging requirements in the antiaircraft problem, are state of the art.

A problem with laser ranging on an aircraft target is the narrowness of the laser beam required to obtain satisfactory range within available power. The precision required of tracking with present laser beams and powers is incompatible with the accuracy of radar tracking.

There are three solutions: One is to increase laser power and use a wider beam. Figure 4-42, which shows how rapidly the available power of gas lasers has increased over a 5-year period,[63] suggests that this solution is only a matter of time. The second solution is to build a laser tracker.[65,66,67] This would allow precision angular tracking consistent with a very narrow laser beam. Such 'optical radars' are under development and some equipment is operational in experimental installations. The third solution is to increase detection sensitivity.

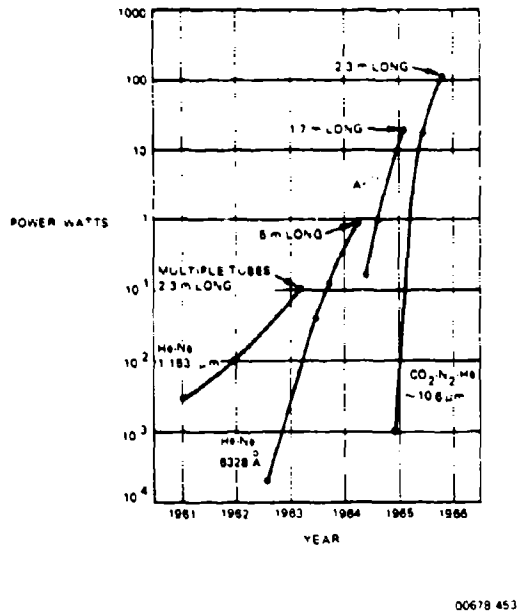

Figure 4-42. Gas Laser Power Growth During 5 Years

Methods of performance analysis comparable to those used for microwave radar are in the literature,[61] including estimates of the spectrum of target 'scintillation,' as well as methods for computing probability of detection, etc.

As noted earlier, since a laser can be chosen to operate in an infrared region which is also desirable for passive viewing, the option of having a tracker with optional active or passive tracking modes exists. This would allow, in either case, the option of automatic tracking in angle, under operator surveillance, with greater precision than that which could be achieved by direct manual control, or by radar. It would be subject to the usual weather limitations, but would be a day or night system.

The cost of a laser range finder alone will probably be relatively low. The cost of an imaging system and automatic tracking loop will probably approximate that of a radar.

4.2.6.1 Lasers for Target Designation

A whole family of guided weapons for air and ground launch is being developed with the capability of homing on a target designated by a laser spot. AFAADS should probably have this capability in its ground role so that the capability of its gun in direct fire can be augmented by supporting fire delivered from aircraft or surface launchers to its rear. An AFAADS concept, somewhat beyond the scope of the present study, might contemplate an optical radar for tracking and illuminating an aerial target, so that firepower could be delivered by man-portable missiles homing on the illuminated target, and thereby supplement the gunfire.

4.3 OPERATOR PERFORMANCE CHARACTERISTICS

In this section we consider the capabilities of the human operator as a component of the AFAADS system. The operator's abilities to detect targets visually, to identify them, and to track them are reviewed.

In all three categories, it is found that the man's capabilities are marginal when compared with AFAADS operational requirements. It is concluded that he must have assistance in initial target acquisition, to narrow his field of search. Optical magnification will assist him in extending his range of visual target identification, but positive IFF would eliminate a serious delay in opening fire. In the tracking function he requires assistance (regenerative tracking) to narrow the bandwidth of the signal he is attempting to follow. As a servomechanism, the man has an effective bandwidth of only about 1 Hz which is too narrow for conventional tracking controls. His precision of tracking is also limited by his visual acuity, so that moderate (3X) magnification seems desirable for tracking.

Whether all three activities are performed by one man depends on the design configuration and trade-off analyses.

There may be more than one man on the AFAADS fire unit. For example, on a self-propelled version there may be a fire unit commander, a driver, and a gunner. A normal distribution of responsibility would be: for the commander to assume the surveillance, identification, and target designation function, for the driver to support the commander in monitoring the radio net, and for the gunner to acquire and track the target, and fire the guns. Reloading could be done by the gunner and the driver.

On the most austere version, such as a one-man mount, all of these functions would be performed by the gunner.

From the point of view of assessing AFAADS effectiveness, the most difficult operation to evaluate is the performance of the human operator in tracking, and this function is therefore treated in some depth. It is the first subject taken up in the following paragraphs. Target detection and identification are reviewed in the last paragraphs of the section.

4.3.1 Operator Dynamics in Tracking

A great deal of work has been done in the development of analytical describing functions for the human

operator performing a tracking function. Most of this work since World War II has been based on operator performance in tracking stochastic, as opposed to deterministic inputs. As the bandwidth of the stochastic input is narrowed, however, the signal begins to have characteristics resembling those appropriate for the angular tracking of an airplane which will always have some perturbations superimposed on the analytic component of motion as a result of flight roughness and maneuver. The principal difference is the extremely large excursions in angular velocity and acceleration in the aircraft tracking problem, when the target is at short range. Keeping in mind the differences and similarities, we are able to draw what we consider to be significant conclusions from the available experimental data.

We will find that from a frequency response point of view, the man is not a very good servo. However, human tracking is important because this mode also has the potential of more precise tracking than automatic radar tracking; since at the shorter ranges, where the target subtends a large angle compared with the desired precision of tracking, the operator can attempt to track a designated point on the target. For example, the operator can attempt to track the junction of the wing and fuselage; whereas a radar may wander over the presented area of the target (or an even larger area).

To realize this precision of tracking, however, extreme care must be given to the matching of the operator's control dynamics to the operator's characteristics. The most precise tracking might be achieved by having two operators; one to track in azimuth, and one in elevation. This introduces the problem of getting both men on target initially, and the short engagement time. Limitations on space in the mount probably preclude this approach. One man tracking in both coordinates may not track as precisely as two men, each with a single coordinate, but he probably will acquire the target sooner.

However, the principal problem in tracking high speed, close-in targets is that associated with the high angular accelerations required to stay on target. The operator is busy in both coordinates at just the time when the target is closest, and most likely to be hit if tracking is good. This problem may be ameliorated if regenerative tracking is provided and if the dynamics of the regenerating control loop can be designed to assist on courses which are capable of being regenerated, and not interfere on courses which cannot be regenerated. More specifically, if the target flies an unaccelerated course, the regenerative loop should allow the operator to zero his control in a few seconds, and thereafter make only small corrections. If the target weaves or turns, the regenerative loop should still aid, by compensating for the mean target motion, but not degrade the operator's ability to track the residual target motion.

One of the arguments for imaging sights (TV, IR, etc.), with automatic tracking, under conditions when an operator could track the target, is that the servo lag can be less than the lag of a human operator. (The man is a 1 Hz servo in a 6 Hz world.) Tracking accuracy with a gated edge tracker may be equal to or better than that of the man, and tolerances on the automatic tracking system can be established in production, whereas human operators come in a wide range of capabilities and motivations.

However, from a cost point of view it is advisable to determine the system characteristics that best utilize operator capabilities. Visual human tracking may be a principal operating mode; even in an automatic system, it will be a back-up mode.

Unfortunately for the development of precise tracking devices operated by human operators, man is a highly adaptive controller. He has been put in control of systems that would never have been considered, had a servo been required to close the tracking loop. And, unfortunately, controllability and precise tracking are not necessarily the same thing.

All of the experimental data on tracking devices indicate that a man performs the tracking function best when his job is extremely simple. He does the most precise tracking with a system in which there is no phase lag between the control motion (or application of force to a force controller) and the motion of the sight. Some of the more pertinent experimental results are summarized in later paragraphs. It is significant to note at this point, however, that the rate control, almost universally used in tracking systems, has been shown to be inferior to a position control; and early 'classical' experiments showing apparently contrary results have recently been shown to be in error by Poulton.[103]

To drive a mount, however, one needs a rate component. A better solution is aided tracking, in which the operator's adjustment of the control adjusts position (a correction he sees immediately) and rate (a correction which has a 90-degree phase lag). Against a constant angular velocity target this method works very well. If the time constant, defining the rapidity with which the rate component builds up, is large enough, the tracking unit feels to the man as if it were a simple position control.

Aided tracking worked extremely well against the low angular velocity and acceleration targets of WWII. AFAADS has a more difficult problem because of the high peaks in acceleration and higher derivatives. As discussed in the radar section, this problem is not unique to the man; a conventional servo using only angular information has the same problem.

The object of 'unburdening' the man thus leads us to the requirement for regenerative tracking, in which we take advantage of the fact that we can generate the required accelerations and higher derivatives from the principal component of target motion, i.e., constant linear velocity, and use these regenerated components to assist the tracker. The derivatives of angular motion associated with the process of tracking an unaccelerated target may be considered an artifact of the tracking process. By changing the tracking process, we eliminate them (after a short setting time) from the operator's job, and consequently leave him only with the task of coping with actual target accelerations.

With this objective in mind, we list briefly the characteristics of the target motion.

Once the operator has acquired the target and manipulated the controls to get the cross hairs on the target, the subsequent activity required of him and his resulting errors, depend on the discrepancy between the rates generated by his tracking system, and the rates generated by target motion.

The target motion, considered as a forcing function on the tracking system, may be considered in the following categories of components:

a. *Deterministic*. The target flies a straight line, an arc, or some other theoretically predictable curve for an extended period of time. Even when the target is unaccelerated, the angular rates and accelerations required of the tracking device are difficult to cope with at close passing ranges.

b. *Stochastic*. The target path is disturbed by rough air. The irregular flight path caused by terrain following may be considered as a stochastic component for analysis of the tracking process.

c. *Quasi-stochastic*. The pilot deliberately produces an irregular flight path by manipulating the controls. The resulting path may consist of a series of straight segments joined by arcs, a sinusoidal weave, etc. The frequency content is likely to be lower than in case b.

In order to develop a quantitative assessment of the operator's capabilities in tracking, we summarize what is known about his performance and interaction with control and target dynamics in the following paragraphs.

The elements of a tracking loop are shown in Figure 4-43. An operator manipulates a control which governs the motion of a mount. The operator looks through a sight fastened to the mount and operates his control to keep the cross hairs centered on the target. The inputs shown as 'noise' represent disturbances mostly uncorrelated with the target motion such as the operator's inability to sense error and error rates perfectly, his muscular tremors in operating the control, and the effects on the tracking process of the shock and vibration caused by a gun firing and being carried on the mount.

In this section the mount is considered to be simply a tracking mount with a fixed sight. The more complex case of a lead-computing sight on a gun mount is not considered appropriate as an AFAADS solution. The effect of shock and vibration of the operator is treated in Section 5.

It is necessary at this point to digress briefly to define the range of options of control dynamics that are pertinent to AFAADS.

The simplest type of control is one in which the displacement of the controlled member 'C' is directly proportional to the displacement of the operator's control 'P'; this is sometimes called 'direct' tracking or 'position control' and is described by:

$$C = \lambda P \; ; \; Y_c = \lambda \tag{4.73}$$

In another frequently used type of control, the rate of the controlled member is proportional to the displacement of the control. 'Rate control' is described by:

$$\dot{C} = \mu P \; ; \; Y_c = \frac{\mu}{s} \tag{4.74}$$

It was found during World War II that tracking accuracy of antiaircraft tracking devices was improved over both (4.73) (4.74) when control laws were combined; this was called 'rate-aided' tracking.

where:

$$\dot{C} = \mu P + \lambda \dot{P} \; ; \; Y_c = \frac{\mu + \lambda s}{s} \tag{4.75}$$

$$\dot{C} = \mu (P + \tau \dot{P}) \; ; \; \tau = \lambda / \mu \tag{4.76}$$

and τ had a value in the range of 0.2 to 1.0 second. Figure 4-44 shows how average tracking error of a particular device varied with time constant τ for a particular class of inputs.[95]

As a basis for comparing control dynamics by inspection, they may be represented by their traces in the phase plane, i.e.,

$$Y_c = \left| A(\omega) \right| e^{i\phi(\omega)} \tag{4.77}$$

These phase portraits for the simple controls just discussed are shown in Figure 4-45.

For position control the controlled member has, of course, zero phase difference from the control.

For rate control the controlled member lags the control by 90 degrees. Rapid control movements (high ω) have little immediate effect on the controlled member.

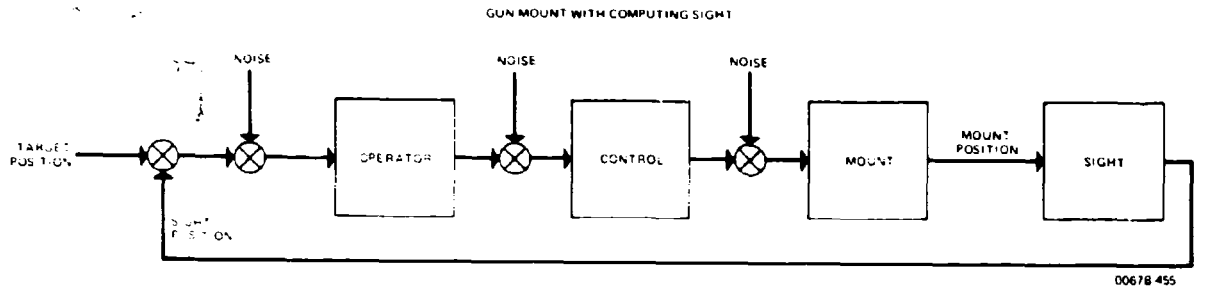

Figure 4-43. Gun Mount with Computing Sight Tracking Loop

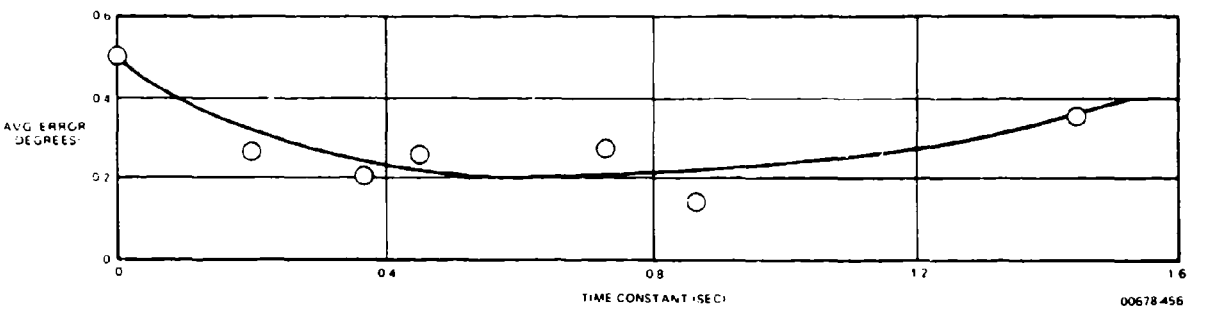

Figure 4-44. Tracking Error as a Function of Time Constant

For rate-aided control the controlled member lags the control by less than 90 degrees, and the higher the frequency, the less the lag. In simpler terms, the operator sees the effect of an abrupt control movement immediately.

Figure 4-45 also shows a phase portrait for an acceleration control for which there is a 180-degree lag at all frequencies:

$$\ddot{C} = \eta P \; ; \; Y_P = \frac{\eta}{s^2} \tag{4.78}$$

The French SS-10 wire-guided missile responds as an acceleration controlled device; it is known to be controllable, but only after considerable operator training. A way of improving acceleration control is to combine it with rate and position, i.e.,

$$\ddot{C} = \eta P + \mu \dot{P} + \lambda \ddot{P} \; ; \; Y_p = \frac{\eta + \mu s + \lambda s^2}{s^2} \tag{4.79}$$

thereby yielding the final phase portrait as shown in Figure 4-45. A good deal of experimentation with this type of control was done at the MIT Radiation Laboratory during World War II. The data are not currently at hand, but the acceleration component in the Radiation Laboratory tests is believed to have degraded tracking accuracy somewhat over simple rate-plus-position.

It was concluded from these early experiments that a desirable control introduced no more than a 90-degree phase lag between operator and controlled element, that a zero phase lag for high ω was desirable, and that large phase lags should be allowed to occur only at low ω, if at all.

The improvement in tracking, possible by modifying rate tracking with a phase lead network thereby obtaining the equivalent of rate-aided tracking, was demonstrated in 1962 by Frost[11] in a rather spectacular experiment. His optimum transfer function was:

$$Y_c = (\mu s)(1 + sT_1)^2 \; (1 + sT_2) \tag{4.80}$$

Of particular interest are the questions of whether these early findings have been substantiated by the experimental work performed since WWII and whether further quantification of the operator performance is possible. We find that a positive answer can be given to both questions as developed in the following paragraphs.

As noted, most of the post-WWII work has been

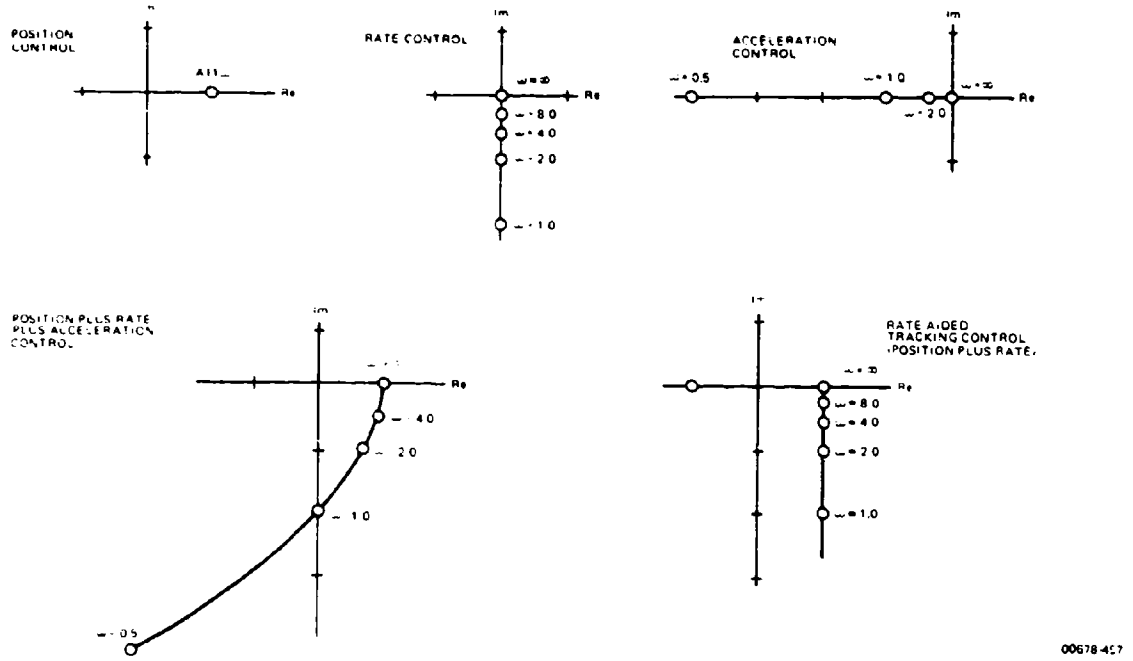

Figure 4-45. Phase Relationship of Various Types of Controls

done on non-deterministic input functions. Since originally the object was to prevent the operator from learning the course, the input functions were composed of several randomly phased sine waves. It was then discovered that with a larger number of these sine waves (such as ten), the analytical process of deriving a quasi-linear describing function for the operator's response was greatly simplified. Most work has been done with this kind of input, as pioneered by Tustin, Elkind, McRuer, and Krendel.

A good deal is now known about how to represent the man as an equivalent linear system in the tracking function. For the types of inputs described previously, it has been found that when the input has little high frequency content and the control is either of the position or rate types, almost all of the operator's response can be described by a linear describing function. The portion of his response which is not linearly correlated with the input, or 'remnant' (a term introduced by Tustin), is very small.

The operator's response can be further rationalized in servomechanism terminology. He must cope with an inherent time lag of about 0.2 second. He can adjust his response as if he had an internal compensatory lead-lag network with adjustable parameters. He adjusts his gain to maintain loop stability. In this terminology, the man can function as a non-linear adaptive servomechanism as the nature of the input signal changes. However, and fortunately for most of the currently available analytical tools, most of the man's adaptive setting of his operational parameters is related to the dynamic characteristics of the system he is controlling and these settings are less sensitive to the characteristics of the input function.

A direct attack was made on the non-linear aspect of the man's performance in the antiaircraft tracking problem by Rosenberg and Siegel.

It is unfortunate that their study was constrained by limited funding from reaching the definitive results that would have been directly applicable to the AFAADS problem.

4.3.1.1 Interaction of Man and Control

The most illuminating exposition of the difference among the three basic control types, position, rate, and acceleration, is furnished by showing how an operator responds to a step input with each type.[94] This is shown in Figure 4-46.

The operator's delay of about 0.2 second is apparent in all cases. The position control provides the most rapid response. The acceleration control is not only slow, but oscillatory.

Fisher[94] was able to reproduce the results of Figure 4-46 with a computer simulation of the man, using the

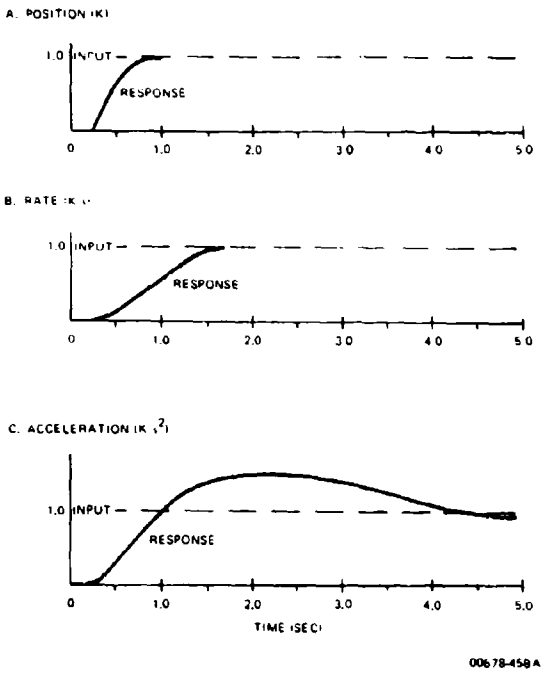

Figure 4-46. Comparison of Response to Step-Function Manual Tracking; Three Control Laws

describing functions obtained by stochastic input experimentation. A similar finding for a ramp input is reported by Young.[107] This is the basis for the prior statement that the operator's describing function depends more strongly on the control than on the input.

The quasi-linear describing functions obtained with stochastic inputs, together with the performance of the operator against such inputs with a wide variety of control types, are shown in Figure 4-47 as phase portraits, some of which include almost a 270-degree phase lag in the control.[74,76,92,93]

The input could be described by a rectangular spectrum defined by its cut-off frequency, supplemented by a shelf of much lower amplitude. The shelf is extended to higher frequencies to facilitate computation of the operator's describing function at higher frequencies than those represented in the conspicuous portion of the input.

This type of input has some relevance to the antiaircraft tracking problem because of the stochastic components of airplane motion noted in earlier paragraphs. In the experiments with the control dynamics shown in Figure 4-47, the operator manipulated a small control stick and observed a CRT display. The experiment was designed to compare 'pursuit' tracking (where the operator pursued a moving target over the face of the CRT with a moving reticle) with 'compensatory' tracking (where he attempted to zero a simple spot). Differences between these modes were, in general, small compared with the effect of control dynamics.

For the same input spectrum (the function that the operator attempted to follow or zero-out) the numbers in the boxes in Figure 4-47 show comparative mean square tracking errors, for compensatory tracking, which corresponds to the antiaircraft tracking problem.

Control dynamics were as shown in Table IV-14.[74]

The World War II generalization that 'the greater the phase lag in a control, the poorer the tracking' is confirmed. For phase lags approaching 270 degrees, the error variance is eighteen times as large as for position tracking, thereby corresponding to a standard deviation of error over four times as large.

To see how the operator response adjusts to the dynamics of the control he is operating, we now look at the operator describing functions derived from these experiments.[74,76,92,93] Since we are only interested in low phase-lag controls for AFAADS, we confine our attention to position, rate, and acceleration controls.

Following servomechanism practice, it is now conventional to depict the describing function in terms of the open-loop gain and phase. Since it has been determined by experiment that the operator tends to adjust his own gain in inverse proportion to the gain of the control, so that the product is constant, most gain-phase (Bode) plots present the operator describing function Y_p combined with the control transfer function Y_c, as Y_pY_c.

Characteristic forms of Y_pY_c are shown in Figure 4-48 in terms of absolute amplitude and phase as functions of frequency. The input function from which these functions were derived had a rectangular spectrum with cut-off frequency at 2.5 rad/sec. The forms are shown for the three basic control types: 'pure' position, rate, and acceleration controls.

According to conventional feedback control theory, system stability requires positive phase margin at gain 'crossover,' i.e., where $YY_c = 1.0$. It can be seen by inspection that this is true in Figure 4-48. However, phase margin at crossover is least for the acceleration control.

In Figure 4-49 the control characteristics have been removed to show operator phase and amplitude. Here the fact that the operator provides phase lead in the case of acceleration control is obvious.

To a very close first approximation, it has been found that, above a threshold of display gain, operator rms errors are proportional to rms input and therefore, performance can be normalized by taking the ratio of

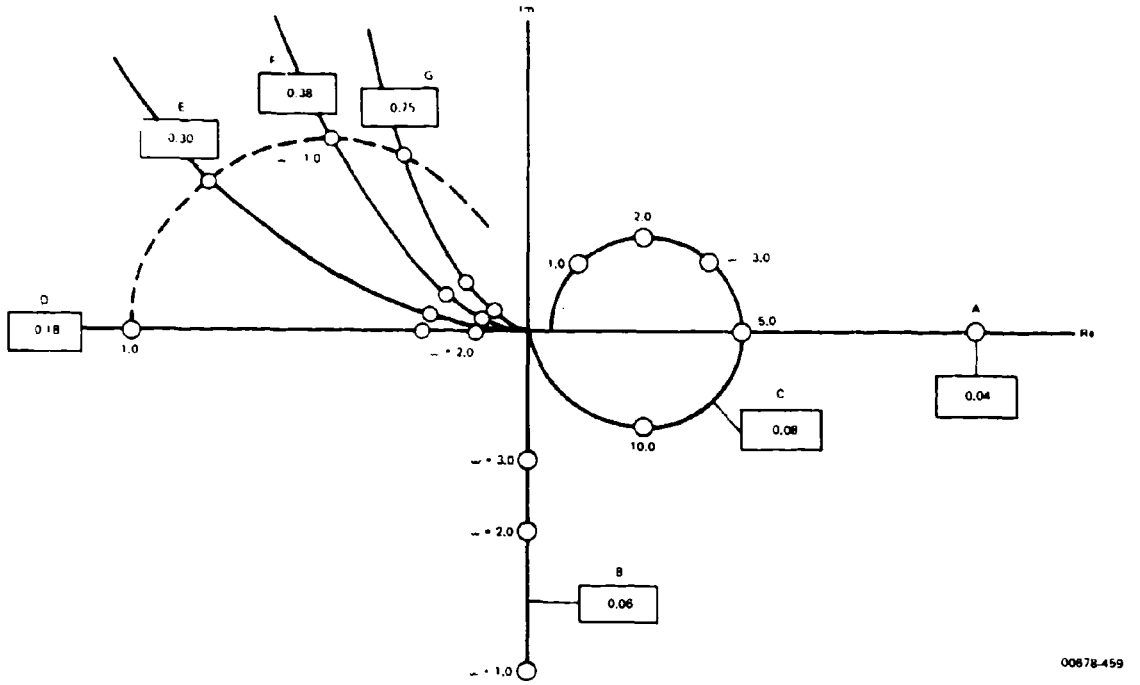

Figure 4-47. Effect of Control Dynamics on Tracking Error

rms errors to rms input. Table IV-15 shows the normalized overall mean square errors (σ^2_e/σ^2_i), the component associated with the linear portion of the operator's response (σ^2_o/σ^2_i), and the remaining component or 'remnant' (σ^2_n/σ^2_i). These values[74] are for rectangular input spectra with cut-off frequencies as noted, and for four sets of control dynamics. The rapid increase in error with high frequency component of input, as defined by the cut-off frequency of the rectangular input spectrum ω_c, is evident. The most accurate tracking in Table IV-15 corresponds to 0.10 inch on the tube, or a 3.4 miliradian angle subtended at the operator's eye. This is not good enough for AFAADS, and will be discussed later under 'Display Gain.'

Now, what does all this mean in terms of the man's performance in the tracking loop. Again following servomechanism practice, we can convert the open loop describing function to the closed loop response and show output/input ^{2} and error/input ^{2} as a function of frequency.[108] This has been done for Figures 4-50 and 4-51.

It can be observed at once that position tracking has a wider bandwidth (as expected), but rate and acceleration tracking do a better job of reducing error at low frequencies (as also expected). To attempt to obtain the best of both worlds conclude that we should use the equivalent of rate-aided tracking in the expectation that such a control will perform like a position control at high frequencies and like a rate control at low frequencies. Unfortunately only limited modern Bode data on rate-aided tracking controls is available.[83]

One more conclusion can be drawn from Figures 4-48 through 4-51; the widest bandwidth that can be attributed to the man functioning as a servomechanism is only slightly over 1 Hz (2π radians/second). We know from our prior examination of angular tracking lags in the case of radar (Section 5.3.1) that even 6 Hz is marginal for this problem. And so we again come back to the need to narrow the bandwidth of the operator's problem by providing regenerative tracking.

Why is the man limited to 1 Hz? The upper limit of rapidity of his response is set by his biological delay time of about 0.2 second. One might draw an analogy with a mechanical servomechanism, whose upper limit of frequency response is determined by the torque/inertia value of the motor; a limit that can be approached but not exceeded by compensating networks in the control.

The effective gain that the man can use depends on the requirement to keep the tracking loop stable. If he is following an input signal with wide bandwidth, he attempts to minimize the lag in his response (above the irreducible minimum), but this limits the maximum gain he can use and keep the loop stable. For a low input bandwidth he can respond less rapidly, but use

Table IV-14. Comparative Mean-Square Tracking Errors for Compensatory Tracking

Configuration	Y_c	$(\text{rms Error})^2$ ω = 1.5 Rad Sec	Type
A	K_c	0.04	Position tracking
B	K_c/s	0.055	Rate tracking
C	$K_c(s+0.25)/(s+5)^2$	0.08	
D	$K_c s^2$	0.18	Acceleration tracking
E	$K_c s(s-0.5)$	0.30	
F	$K_c/s(s-1.0)$	0.38	
G	$K_c/s(s-1.5)$	0.75	

00678-460

higher gain; and the higher gain results in reduced error.

Elkind showed that with position tracking[79,80] the operator's describing function could be represented as:

$$Y_p = K_p e^{-\tau s}(1 + sT_I) \qquad (4.81)$$

where τ 0.2 second. As input bandwidth was decreased, the operator increased gain K_p, and lag T_I to maintain loop stability in such a way that the ratio:

$$K_p/T_I \sim \text{constant} = 9 \text{ rad/sec.}$$

K_p in turn increased about inversely as the square of the effective bandwidth of input. In the limit, the man functions as a rate controller operating on a position control. This explains the apparent anomaly of how an operator with the given transfer function can eliminate a steady state position error after a step input, as we know he does in practice.

For rule-of-thumb estimates of the lag of the operator as related to input velocity and acceleration, we can use the slope methods of estimating K_v and K_a from the open loop transfer function. For example, in Figure 4-48 we observe that the $Y_c Y_p$ curve for a rate control has a uniform slope of 20 db/octave and intersects the zero db axis at about 4.5 rad/sec, corresponding to $K_v = 4.5$ sec^{-1}. McRuer has determined that the crossover frequency is almost independent of forcing function bandwidth (Reference 75, Figure 75), which is a helpful generalization for our problem. By a similar graphical procedure one can obtain both K_v and K_a for rate-aided tracking from Russell's experimental data (Reference 75, p. 121) for which we find:

Aiding ratio Time constant	K_v	K_a
1 sec	10 sec^{-1}	9 sec^{-2}
0.5 sec	10 sec^{-1}	9 sec^{-2}

Considering the stability in crossover frequency noted by McRuer over wide changes in input bandwidth, we are inclined to feel that the above values will give us good estimates of the operator lag in the AFAADS tracking problem, for the nonregenerative tracking mode.

We have one final observation to make about the AFAADS tracking problem, and that is based on a display of its frequency content. Suppose that we obtain the power spectral density of a pass course, and multiply it by the transfer function of the control, so that we obtain the power spectral density required of

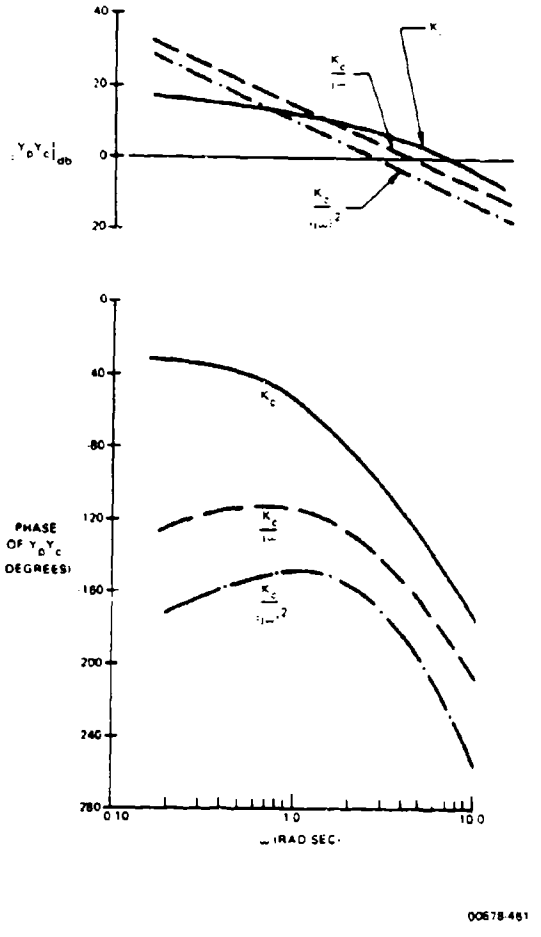

00678-461

Figure 4-48. Comparison of Open-Loop Transfer Function of Operator Plus Control for the Three Control Laws

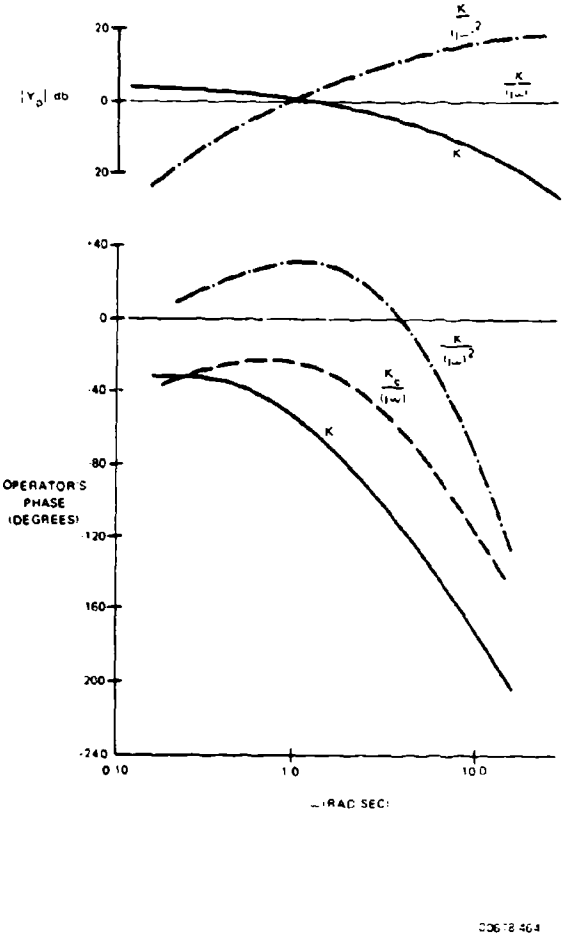

00678-464

Figure 4-49. Amplitude and Phase of Operator's Describing Function for the Three Control Laws

the operator's control motion, if he is to track perfectly. A measure of the difficulty of the problem will be the fraction of the PSD that falls above about 1 radian/second. We can obtain this as follows:

If a specified function of time f(t) is converted to a frequency function $G(j\omega)$ by the Fourier transform:

$$G(j\omega) = \int_{-\infty}^{\infty} e^{-j\omega t} f(t)\, dt \qquad (4.82)$$

and the input is applied to a linear system with transfer function $Y(j\omega)$, the frequency function describing the system output is:

$$G_0(j\omega) = G(j\omega)\, Y(j\omega) \qquad (4.83)$$

and the distribution of power across frequency is given by:

$$|G_0(j\omega)|^2 = |G(j\omega)|^2 |Y(j\omega)|^2 \qquad (4.84)$$

Note that this has *not* been normalized by dividing by time.

Azimuth Tracking. Angular velocity in azimuth as a function of time from the point of closest approach to the tracking unit (unaccelerated target), is given by:

Table IV-15. Error Variances for Various Control Laws

Y_c	ω_i Rad/Sec	σ_c^2/σ_i^2	σ_p^2/σ_i^2	$\sigma_n^2\sigma_i^2$
K_c	1.5	0.04	0.03	0.01
	2.5	0.05	0.044	0.006
	4.0	0.12	0.09	0.03
$\frac{K_c}{S}$	1.5	0.055	0.035	0.020
	2.5	0.08	0.06	0.02
	4.0	0.25	0.16	0.04
$\frac{K_c}{S^2}$	1.5	0.18	0.08	0.10
	2.5	0.23	0.16	0.07
	4.0	0.80	0.58	0.22
$\frac{K_c(S+0.25)}{(S+5)^2}$	1.5	0.08	0.05	0.03
	2.5	0.10	0.05	0.05
	4.0	0.13	0.11	0.02

NOTES:
a. Stick Control, 30-degree Range.
b. σ_i = 1/2-inch.
c. Eye to Scope Distance = 29 inches.
d. 0.10 inch ≅ 3.4 mils.

00678-465

$$\dot{a}_t = \frac{vR_m}{R_m^2 + v^2t^2} \qquad (4.85)$$

$$= \frac{\lambda}{1+\lambda^2t^2} \; ; \; \lambda = \frac{v}{R_m} \qquad (4.86)$$

The tracker is unlikely to track beyond some maximum range. Let the probability of tracking at a range R be:

$$\frac{1}{1+(R/R_c)^2} \; ; \; R^2 = R_m^2 + v^2t^2 \qquad (4.87)$$

Then the Fourier transform of the time function of azimuth rate is:

$$G(j\omega) = \int_{-\infty}^{\infty} e^{-j\omega t} \frac{1}{1+\left(\frac{R_m}{R_c}\right)^2+\left(\frac{R_m}{R_c}\right)^2\lambda^2t^2} \frac{\lambda\, dt}{1+\lambda^2t^2} \qquad (4.88)$$

$$= \pi\left[e^{-\left|\frac{R_m\omega}{v}\right|} - \frac{1}{\mu} e^{-\mu\left|\frac{R_m\omega}{v}\right|}\right] \qquad (4.89)$$

where:

$$\mu^2 = 1 + \left(\frac{R_o}{R_m}\right)^2 \qquad (4.90)$$

We are interested principally in cases for which $\mu >> 1.0$, hence:

$$G(j\omega) \cong \pi e^{-\left|\frac{R_m\omega}{v}\right|} \qquad (4.91)$$

and:

$$|G(j\omega)|^2 = \pi^2 e^{-\left|\frac{2R_m\omega}{v}\right|} \qquad (4.92)$$

Control position 'C' is related to azimuth angle α_t of the tracking device by

$$\alpha_t = Y_c C \qquad (4.93)$$

Table IV-16 gives Y_c and $1/Y_c$ for a number of control laws. The latter function, multiplied by $G(j\omega)^2$ gives the relative power in the spectral density of control rate as a function of frequency.

The spectral content of azimuth velocity for two pass courses is shown in Figure 4-52. The value R_m/v = 2/3 sec corresponds to the most difficult AFAADS course. By comparing the frequency content against Figures 4-50 and 4-51, we note that substantial

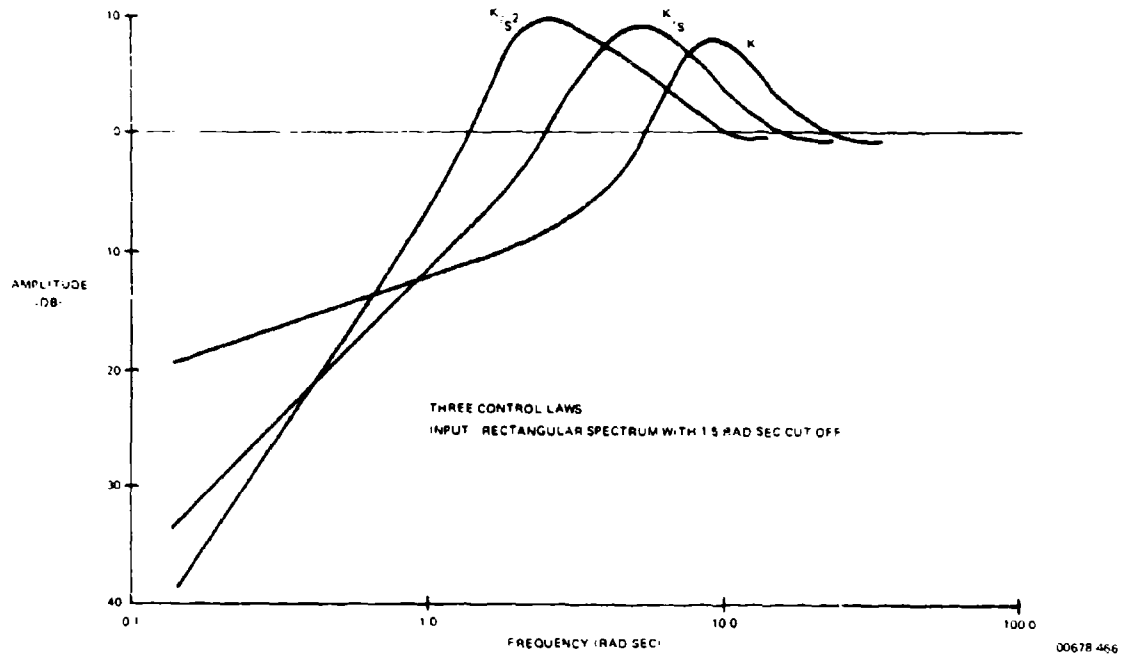

Figure 4-50. Error Comparison. Linear Portion of Human Operator's Response

power is present at those frequencies where the human performance is expected to deteriorate. Applying the transfer functions for rate tracking, position tracking, and aided tracking (Figure 4-53), we note that in terms of the frequency content of the control motions required of the operator, rate tracking intensifies the high frequency content. Both rate and rate-aided tracking eliminate the low frequency content, but that is the easy end of the spectrum for the operator.

Again, we conclude that a direct attack must be made on reducing the high frequency content of the input function and this leads again to regenerative tracking.

Discussions thus far, have been principally concerned with the portion of the operator's response that can be linearly related to the input function by a linear describing function. We have noted the experimental findings that when the input is not too difficult and the control is docile, the component of error *not* described by this linear relationship is very small compared with total error.

However, if we succeed in almost completely unburdening the operator in the limit, this 'remnant' may be the dominating determinant of our system performance. The following paragraphs review what is known about it.

A recent study of remnant[104,105] relates it to the total variance of tracking error in the system as seen by the operator. For position tracking, remnant is reliably represented as white noise out to at least 20 rad/sec, down 20 dB in density from the error variance (i.e., the remnant PSD divided by σ^2 is 0.01 per rad/sec). For rate tracking, the PSD starts at a slightly higher level, but breaks at about 3.3 rad/sec, so that:

$$\phi_{rem}/\sigma_e^2 = 0.035/(1 + .09\omega^2) \qquad (4.94)$$

The model argues that the source of remnant is in the operator's perception of error and error rate, rather than in his hand movements in operating the control. Noise in neuromuscular dynamics is subsumed in these error processes, and so the effect of control scale factor, for example, does not appear explicitly.

Earlier experiments with less precise experimental measuring equipment[78], as well as WWII experiments, however, indicated that when tracking can be done accurately, the scale factor of the control should be as low as possible (i.e., large movement for given correction) to minimize errors resulting from sources in the neuromuscular dynamic component. The effect appears as a reduction in the fraction of operator response, which is explainable by the linear model, as control sensitivity is increased. It has been noted that the operator controls his own gain, so that the product (operator gain) times (control gain) equal constant.

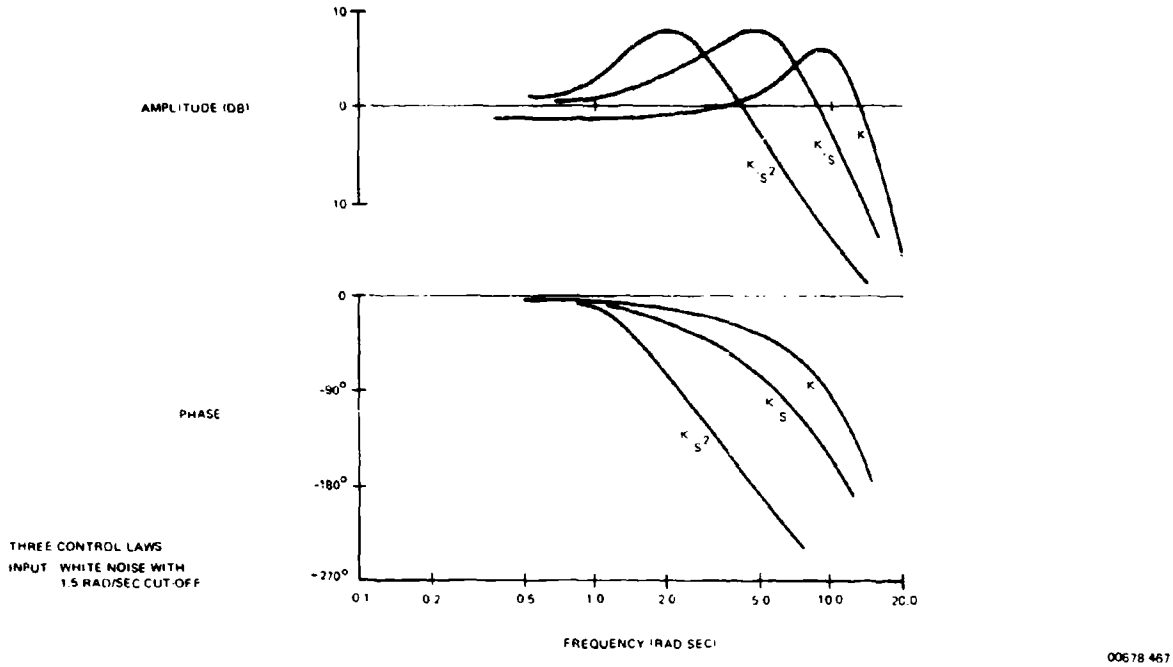

Figure 4-51. Comparison of Closed Loop Response, Manual Tracking

Table IV-16. Transfer Functions of Control Motion Referenced to Input

Control Type	Y_c	$\left\|\frac{1}{Y_c}\right\|^2$	ω for Peak Power
Position	K_c	$1/K_c^2$	0
Rate	K_c/S	$\omega^2 K_c^2$	λ
Acceleration	K_c/S^2	$\omega^4 K_c^2$	2λ
Rate-Aided	$K_c\left\|1+\frac{1}{ST}\right\|$	$\frac{1}{K_c^2}\left\|\frac{\omega^2T^2}{1+\omega^2T^2}\right\|$	$\lambda\left[1+\lambda^2T^2+\right.$!

00678-468

The result is that the operator describing function is hardly changed by control gain increase, but the remnant is increased. (About as $K_c^{2/3}$; from some rough estimates of the published data).

As tracking becomes more precise, it is also probable that remnant approaches an asymptotic minimum rather than retaining a constant proportionality to total error, so that control scale factor is increasingly important as tracking becomes more precise.

An apparently contradictory finding has been presented by Beare and Kahn[109] who show error increasing with rate of control motion. However in their experiments, control changes in input amplitude and velocity changes are of much larger variation; so that the single effect of control sensitivity appears only in their analysis of variance, and not explicitly in their figures.

If we can succeed in providing a precise tracking instrument for AFAADS, with minimal bandwidth of input, the tracking error may be expected to result principally from the visual acuity of the operator, and

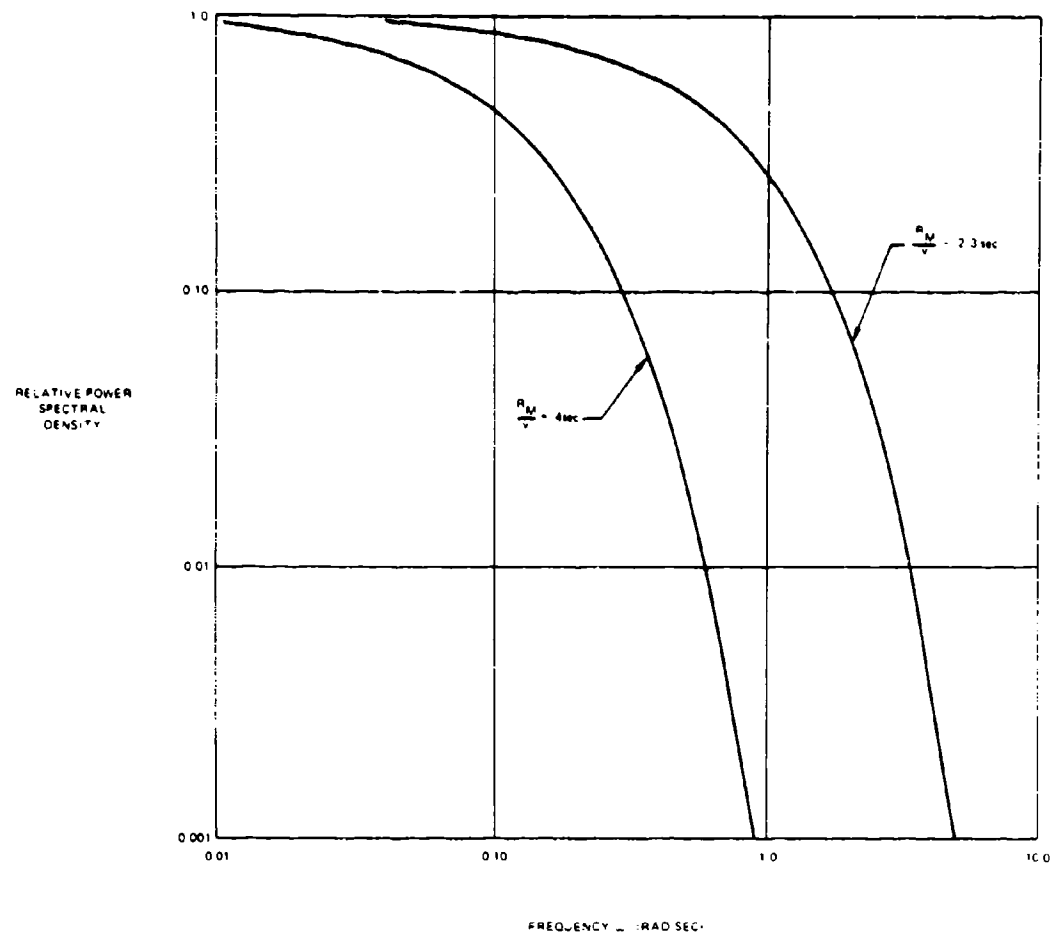

Figure 4-52. Spectral Density of Azimuth Velocity

the characteristics of his manipulator (scale factor, spring centering, displacement versus force type, etc.) as reflected in neuromuscular 'noise.'

In following sections, the characteristics of manipulators are reviewed as well as the effects of visual acuity and magnification on the tracking process. However, before turning to these topics, we review briefly some experimentally determined expressions, for manual tracking error, based on data acquired by tracking aircraft targets in real life, and comment on them in the light of our review of operator characteristics to this point.

4.3.1.2 Experimentally Determined Visual Tracking Errors

The following three expressions have been given for manual tracking errors (Lockheed/Eglin)[102]; where θ = angular velocity in mils/second.

a. Local Director, optical sight, low inertia mount ($7.0 + 0.10\theta$ mils)

b. Gun tracked with two handwheels, (2 man) ($3.5 + 0.025\theta$ mils)

c. Remote control director with optical tracking ($0.5 + 0.025\theta$ mils)

The data base and conditions of experiment have

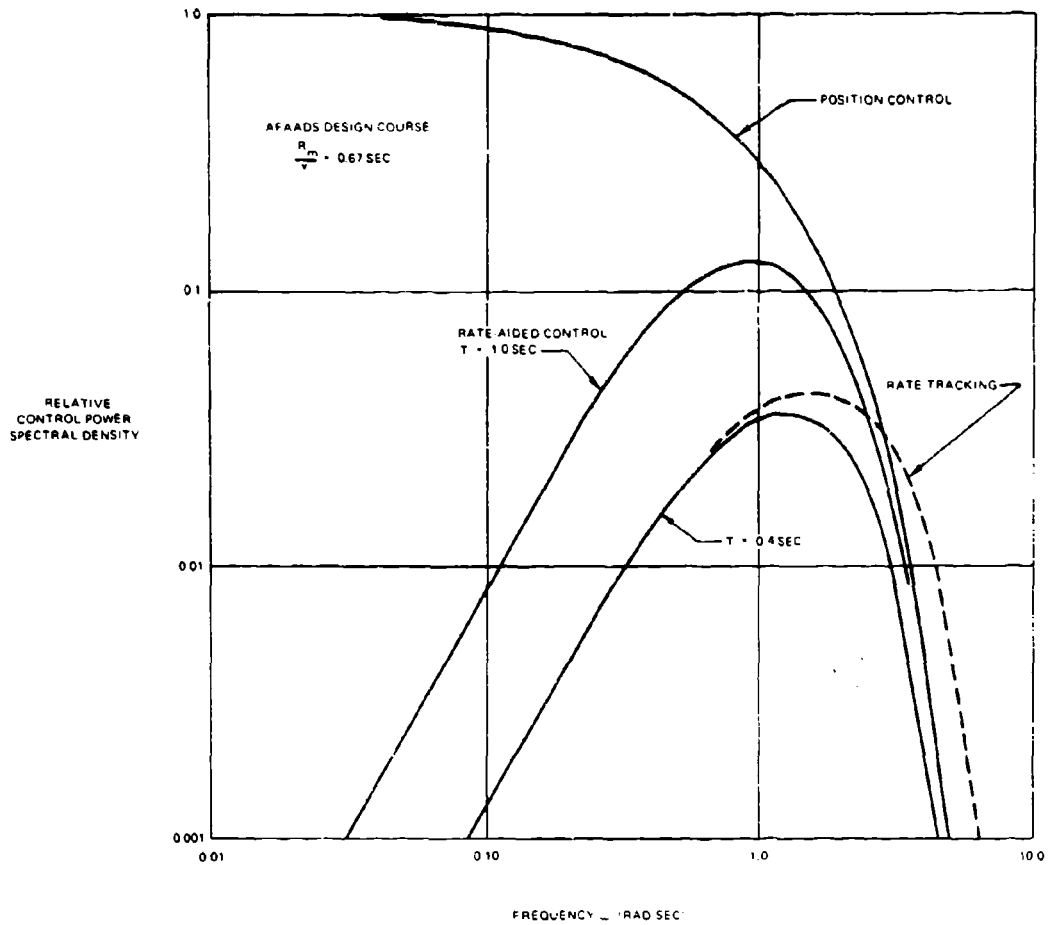

Figure 4-53. Spectral Density of Angular Velocity of Control Motion

not been obtained, and so the explanation of the functions can be only conjectural at this stage.

We suggest three hypotheses which should be examined when data are available:

a. The quasi-linear model of the man is satisfactory with constant K_v, K_a, etc. This is consistent with the coefficient of θ equal to 0.10; but not with the smaller values, unless the man introduces a lead component in his tracking function.

b. The man is able to eliminate velocity lag by introducing lead in his response, but he cannot eliminate acceleration lag. Since high acceleration and high angular velocity occur in about the same tracking region, the effect shown as velocity might be an acceleration effect.

c. The man sets his tolerance on tracking precision by the apparent target size; i.e., as long as the tracking cross hair is on the fuselage he feels that he is tracking satisfactorily. We examine the consequences of this assumption in the following paragraphs.

Assume that angular tracking error has a standard deviation proportional to target dimension in the relevant coordinate. Let the effective value of this dimension be L, and consider azimuth tracking. The standard deviation of the error is, in angular units:

$$\sigma_{mils} = 1000 (L/D) \sec e_o \qquad (4.95)$$

Thus if L = 5 meters, and Dcos e_o = 200 meters, then σ_{mils} = 25 mils.

We may also consider that L, the longitudinal dimension of the target, should be projected into the plane perpendicular of the tracking line, in which case:

$$\sigma_{mils} = 1000 (L/D) \sin a_o \cos e_o \qquad (4.96)$$

Now consider the expression for rate of change of azimuth angle, which is:

$$\dot{a}_o = da_o/dt = (v/D) \sin a_o \cos e_o ;$$

$$v = \text{target speed} \qquad (4.97)$$

Combining (4.96) and 4.97) we obtain:

$$\sigma_{mils} = (L/v) \dot{a}_o \text{ , where } \dot{a}_o \text{ is in mils/second} \qquad (4.98)$$

If L = 5 meters, and v = 200 meters/sec, then:

$$\sigma_{mils} = 0.025 \dot{a}_o \qquad (4.99)$$

This is the same coefficient obtained from the second and third expressions for visual tracking data.

4.3.1.3 Manipulator Types

The types of manipulators available for a human operator tracking in two coordinates include: Handlebar, Stick, and Ball.

The former two may be free-moving, spring-restrained, or a 'force' type. The 'force' type generates an output signal proportional to the force or pressure exerted on it.

As noted earlier for movable controls, the experimental evidence supports the objective of having the largest possible manipulator deflection for a given response signal. Since the total travel of a stick or handlebar is limited, non-linear relationships between motion and response are often used. This allows precise tracking at low velocities at the expense of high velocities. However, high angular velocities occur less frequently. When the mount is slewed at maximum velocity to get on target initially, no precision is required.

The ball control (invented by Frankford Arsenal) can have any desired scale factor. Furthermore, it has the distinct advantage in a two-dimensional tracking problem that it reduces the problem to one in a single dimension from the point of view of the operator so that he simply moves the surface of the ball in the direction he desires to make a correction. The Frankford Arsenal 'Duster' fire control was intended to have a stick control for initial target acquisition and a ball for precision tracking.

Experiments [93,115] indicate that the force control provides at least equally accurate tracking to that of a movable stick or handlebar, which is fortunate since its desirability from an engineering point of view makes it a design engineer's choice. The operator's describing function is nearly the same if the control output is expressed in terms of pressure on the control for a force controller; as compared with control movement for a movable control manipulator.

4.3.1.4 Effect of Magnification in the Optical System on Tracking Error

This section addresses the effect of magnification in the optics of the visual sight on operator tracking accuracy. Tracking errors may be considered to arise from two sources: the dynamics of the target motion and the control, and the ability of the operator to resolve small tracking errors. The latter is related to visual acuity.

Many experiments in tracking an oscilloscope display indicate that display gain, which corresponds to optical power, has a threshold type of effect on error. Once gain is raised above some value, further increases do not reduce tracking error. For high display gain and stochastic inputs, variance of error is very closely proportional to variance of the input signal.

Errors which arise from system dynamics are considered in prior sections. This section considers the component of error which varies with magnification.

Relevant experiments vary widely in instrumentation and method. Some of the more significant are summarized. It appears that for optical tracking one may write for the standard deviation of tracking error:

$$\sigma_e = (0.60/M) + \sigma_d \text{ mils} \qquad (4.100)$$

where σ_d is the standard deviation of error resulting from dynamics.

If the system objective for tracking accuracy is of the order of 0.50 mil, therefore, some magnification is desirable in the optics. M = 3.0 appears to be a reasonable value. The interaction between magnification and mount vibration needs to be investigated, since vibration may prevent the indicated gain from being realized.

If σ_e is the order of several mils, there is no point in using any magnification other than M = 1.0; from the point of view of tracking accuracy.

Oscilloscope tracking experiments indicate that magnification, measured in terms of linear displacement on the tube face per unit of input, affects the tracking process as a threshold effect. Above the threshold, error depends on the function being tracked and the control, but not magnification. Below the threshold, the standard deviation of error approaches a constant linear

value on the display, and hence is inversely proportional to magnification when referenced to the input.

In an investigation by Seidenstin and Birmingham[88] of the effect of display gain on accuracy of oscilloscope tracking, both electronic gain (on the display) and optical gain (by changing the distance of the operator's eye from the tube) were studied. It was found that both gains had the same effect, and that the data could be aggregated in terms of their products. The improvement in accuracy was less than the inverse gain. A replot of the results indicates that the error could be expressed as:

$$\sigma = a + b/G \qquad (4.101)$$

where a,b are constants and G is gain.

A more recent experiment in which display gain was varied is that of Baty.[113] In this experiment a stochastic input was used and referenced as a signal to noise ratio (S/N) with respect to the assumption that visual noise corresponds to visual acuity with a standard deviation of 1 minute of arc (0.3 mil). Tracking was accomplished with a rate control, and the scope was 50 cm (19.6 inches) from the operator's eye. Figure 4-54 shows Baty's results replotted for three bandwidths of the forcing function. We note first that in Baty's experiment, the asymptotic minimum error on the tube face was only 0.008 in. and secondly that magnification reduced error until the signal had a 10 mil input excursion at the operator's eye, corresponding to a S/N ratio of about 33.

If we suggest that the standard deviation of error can be expressed as:

$$\sigma_e^2 = \sigma_o^2 + K\sigma_i^2 \qquad (4.102)$$

or:

$$\sigma_e = \sigma_o + K\sigma_i \qquad (4.103)$$

we find that the latter expression fits Baty's data better, and yields:

$$\sigma_e(\text{mils}) = 0.37 + 0.094\,\sigma_i(\text{mils}) \qquad (4.104)$$

Consequently, we find an absolute minimum error at the operator's eye of about 0.40 mil; about the same as the value usually given for visual acuity.

A WWII report[116] on tracking, through optical systems of magnifications 1, 6, and 20 for which the target type is not at hand, gave the results shown in Figure 4-55. These results indicate that error can be expressed as:

$$E(\text{mils}) = (0.62/M) + 0.20 \text{ mils} \qquad (4.105)$$

A recent Aberdeen experiment, [117] intended to develop maximum precision tracking for laser experiments, used a 248-inch focal length optical system for

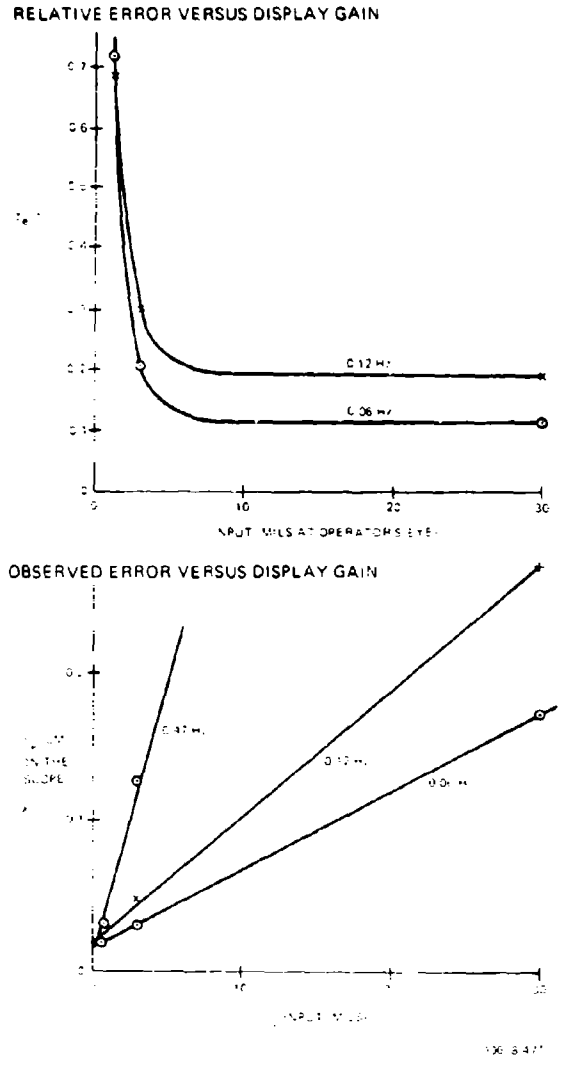

Figure 4-54. Comparison of Relative Error with Observed Error versus Display Gain

tracking a 100-120 mph target at ranges at which azimuth rate was about 0.50 degree/second. A target painted on the side of the aircraft was tracked. Boresight errors were a major problem, and systematic errors over a run varied, between runs, from near zero to as much as 0.29 mil. Standard deviations about these means were in the range of 0.07 to 0.25 mil; indicating that precision angular tracking can be obtained operationally.

If we are seeking fractional-mil tracking accuracy and succeed in 'unburdening' the operator by provision of a *good* regenerative tracking system, the limiting accuracy seems likely to be a value which is closely related to the visual acuity of the operator. It seems

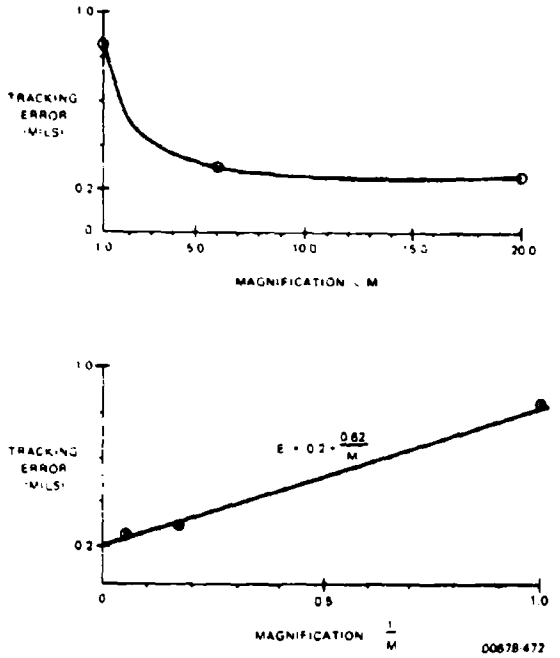

Figure 4-55. Variation of Tracking Error with Magnification

likely that some magnification will be required in the system to reduce this error to a magnitude consistent with the overall error budget. A magnification of about 3.0 seems consistent with this objective. The effect of vibration as a function of magnification needs to be investigated.

4.3.1.5 Detection and Identification

Another aspect of magnification is the range at which targets can be detected and identified. Many factors affect these ranges, and the present discussion will be limited to very good viewing conditions, which should provide upper limits. Figure 4-56 shows the ranges of detection and identification of an F-86 aircraft flying at 250 knots and an altitude of 3000 ft at Yuma Test Station, Arizona. The monocular viewing devices were fixed, and the observers field of search was the field of the fixed optical device. This is shown in Figure 4-57. One would expect the range of both identification and detection to increase as the square root of magnification under these conditions. This expectation is confirmed by Figure 4-57, with the expection of the 3X optic, which was much better than expected. No explanation for this was found.

Visual acuity was indicated to be a critical parameter in the discussion of the effect of magnification on tracking accuracy and display gain. An experiment with the optics described previously determined the angular thresholds for seeing small black matte targets against terrain background and against an empty- field background. This experiment provided the following results:

Optical System	Terrain Background	Empty Field Background
2½ and 3 power	0.12 – 0.18 mil	0.11 – 0.13 mil
1 power optics	0.47 mil	0.45 mil
Bare eyes (binocular vision)	0.26 mil	0.22 mil

In a comparison of 6 x 30 binoculars with the unaided eye in the observation of a variety of aircraft types including both prop and jet aircraft, it was found that mean detection ranges (under optimum Texas sighting conditions) were from 8600 to 13,000 meters, and that the detection ranges with binoculars were not consistently different from those with the unaided eye. In this experiment, the observers had about 5 minutes warning and knew the approximate direction of approach to within about ±15 degrees. Tentative recognition was at 4 to 6000 meters with the unaided eye, and 5 to 8000 meters with binoculars. Positive recognition was at 2 to 3000 meters with the unaided eye, and 3 to 5000 meters with binoculars.

When the sector assigned to the observer was further widened, both detection and identification ranges decreased drastically for the unaided eye. Other experiments were conducted over very flat terrain (near Gila Bend, Arizona) under conditions of excellent (15 mile) meteorological visibility. T-33, F-86, and F-100 aircraft were run in at 400 knots, and ranges of detection and identification (regardless of whether right or wrong) were recorded. The sector assigned to an observer for scanning was a parameter, and varied from 45 degrees to 360 degrees. Airplane altitudes were either 500 or 1500 feet.

Figure 4-58 shows the cumulative distribution of detection probability as a function of range, and Figure 4-59 shows the same information for identification. Narrowing the sector scanned improved both probabilities, but note that only about one-third of the detections had occurred by the time the airplane closed to 3000 yards, and that the 50 percent point on identifications is well under 2000 yards.

The T-33 (straight wings) was correctly identified 97 percent of the time, but the F-86 and F-100 (swept wings) only about 75 percent of the time.

Since the report gives some information on the effect of minimum crossing distance, Figure 4-60 has been provided to show the mean detection and recognition contours in the horizontal plane. This figure suggests that an airplane coming straight in at the observer may

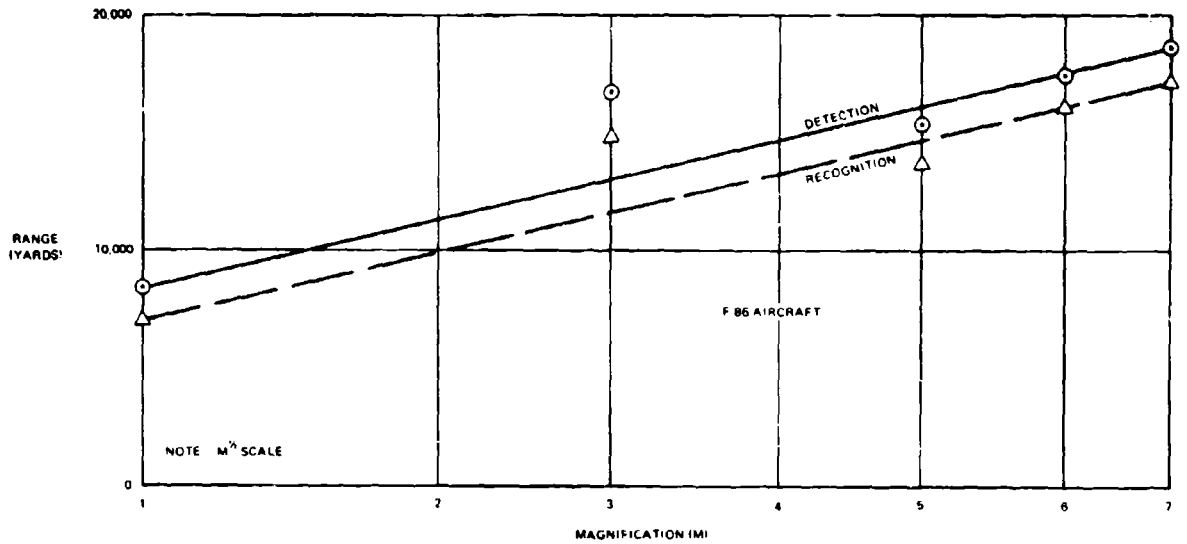

Figure 4-56. Variation of Detection and Recognition Range with Magnification

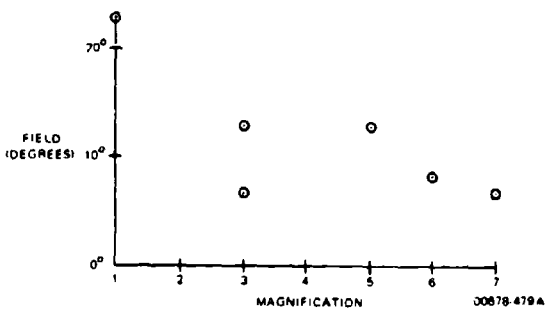

Figure 4-57. Variation of Fixed Optical Field with Magnification

be very difficult to detect and identify. But this effect was negligible when the direction of approach was known more closely in advance[119]. Figure 4-61 shows mean detection range as a function of sector scanned. Since the RAID device reduces the scanning area to about 45 degrees, it should provide an improvement of about 50 percent in average detection range under optimum conditions.

The results suggest very strongly, however, that visual target detection and identification will impose very severe limitations on AFAADS effectiveness. It has not been possible to make a thorough search for experimental data in this field, and such a study should be performed, to supplement the results noted above.

4.4 WEAPON CHARACTERISTICS

The weapon, the characteristics of which have been used for reference in this AFAADS study, is the T250 Gatling-type gun designated as the Vigilante. In retrospect, Dr. Gatling's gun has had a long and distinguished career. The United States Navy and Army adopted the original Gatling gun in 1862 and 1866 respectively.[122] By 1880 Gatling was demonstrating a rate of fire of 1200 rounds per minute, and before the turn of the century 3000 rounds per minute had been attained with a gun driven by an electric motor. Gatling guns of that era were built in calibers from 0.50 to 0.75 inches in 6- and 10-barrel models with muzzle velocities of less than 1500 fps. The Union Army bought 12 Gatling guns, complete with 12,000 rounds of ammunition for 12,000 dollars. These guns were used in the siege of Petersburg, Virginia. Costs have increased somewhat since that time.

The following paragraphs present the modern gun characteristics, some of the ammunition options under consideration, and a brief discussion of target vulnerability.

Characteristics of the modern T250 Gatling gun are

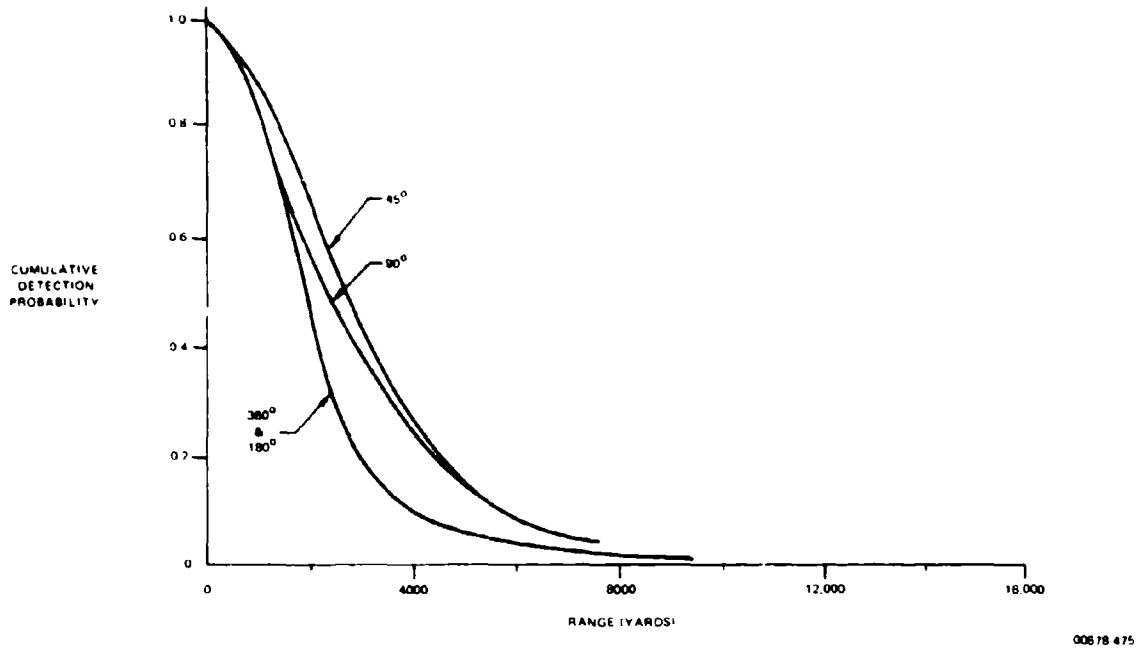

Figure 4-58. Cumulative Probability of Target Detection versus Range

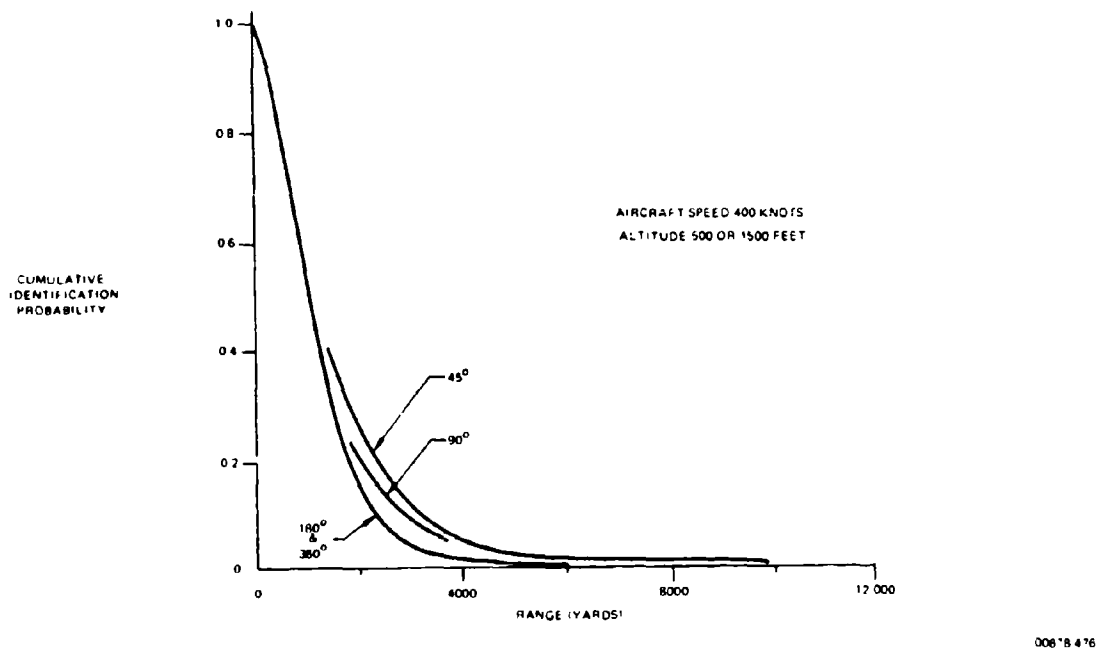

Figure 4-59 Cumulative Probability of Target Identification versus Range

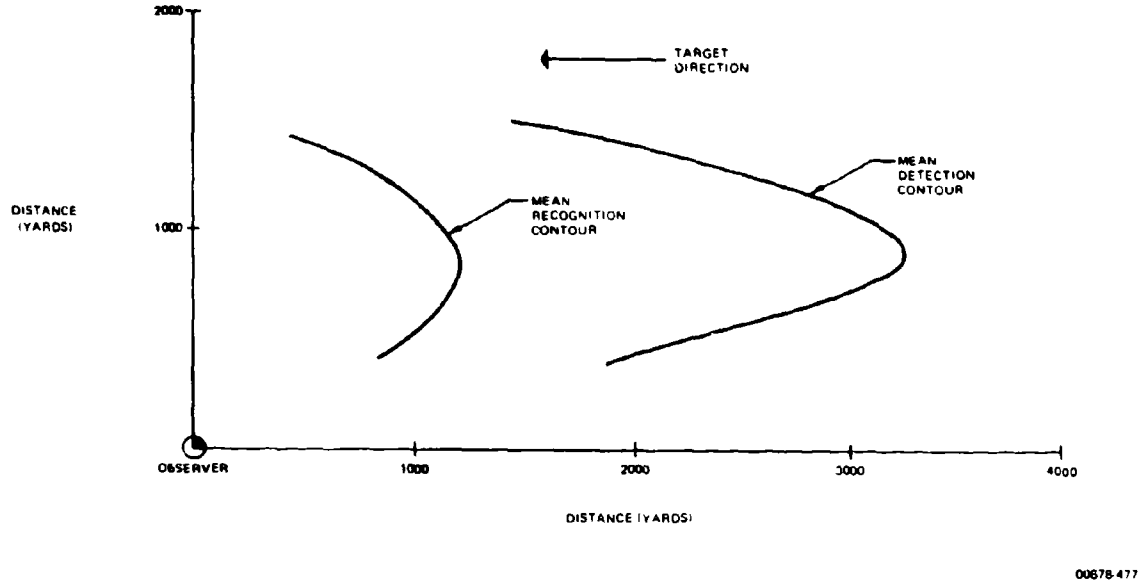

Figure 4-60. Contours of Mean Detection and Identification Range

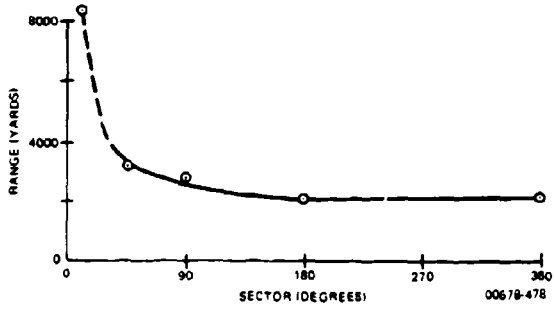

Figure 4-61. Mean Detection Range versus Angular Sector Scanned

shown in Table IV-17. For comparison, the characteristics of the 20-mm version used in the Vulcan air defense system are shown in Table IV-18.

4.4.1 Exterior Ballistics

Both Figure 4-62 showing remaining velocity versus range and Figure 4-63 showing time of flight versus range, include the 'present' Vigilante round (T324E22) and three proposed improved rounds. The rounds plotted on these two figures have the following characteristics:

a. Designates the T324E22 at 3000 fps muzzle velocity.

b. Designates the T324E22 round without rotating band, at 3600 fps and weighing 1.6 lb.

c. Designates a boat-tailed round with rotating band at 3600 fps muzzle velocity.

d. Designates the preceding round without rotating band.

The ballistics are believed to have been computed for 10° Quadrant Elevation. Case (4) represents ballistics about the same as those attributed to the Swiss-made 35mm Oerlikon.

4.4.2 Terminal Ballistics

Data were not available on the effectiveness of the 37mm round against aircraft targets. However, since estimates of target vulnerable area were desired for the kill computations reported later in this study, some very rough estimates were made. These are described below.

First, estimates of typical target sizes and their presented areas were desired. From the open literature, dimensions of current fighters, fighter-bombers, and tactical bombers, were abstracted. Approximate computations of aircraft side area, frontal area, and wing area were then made from the published outline drawings.

Figure 4-64 shows side area (including the fin) plotted against normal takeoff weight. Figure 4-65 shows frontal area plotted against normal takeoff weight for a fixed wing aircraft. Wing area if plotted on the side-area chart would follow the same trend by remaining within the same scatter pattern of points. Figure 4-66 shows the aircraft length versus normal takeoff weight.

Although the frontal area of the aircraft is related to the pilot's dimensions for small aircraft, as the aircraft size increases, the engine intake area increases in size. This relationship accounts in part for the trend with gross weight.

Similar trends were obtained for helicopters.

It was concluded that to within a factor of 2.0 the following approximate expressions could be used:

a. Frontal Area = 0.10 Side Area.

b. Wing Area = Side Area.

c. Side Area $\propto$ Weight.

d. Fuselage Length $\propto$ $(\text{Weight})^{1/2}$.

Some very gross estimates were made of the probability that a hit would produce a target kill as a function of aircraft gross weight. Considerably more work is required in this area, and only the Ballistic Research Laboratories have the facilities to produce an authoritative relationship. Critical considerations include: whether the pilot and copilot (if any) are protected by armor, what kind of protection is provided against fuel fires, duplication of vulnerable components, etc. Interpretation of the kill probabilities in terms of mission kills requires consideration of the degree to which the aircraft is depending on automatic equipment, its vulnerability, and where the target is on its flight path.

Figure 4-67 has therefore been designated 'hypothetical' kill probabilities in hope that it will stimulate the experts in the field to replace it by a better representation. It does give a very rough idea of how much of the presented area of the target should be reduced in the kill computations.

It is believed that the trend of kill probability with the weight of the high explosive carried by the projectile in the 37mm range is valid. The M54 37mm projectile carried only 0.10 pound of high explosive, the T-37 was designed for 0.25 pound, and the German 'Mine' family of 30mm and 55mm projectiles carried 28 percent of their weight in high explosive. For a 37mm projectile weighing 1.6 pounds, a 28 percent load would be 0.46 pound of high explosive. However, since the German projectiles were designed for a 2000 fps muzzle velocity, there is a tradeoff for the system designer between high explosive content and muzzle velocity.

The curves of Figure 4-67 are consistent with German combat data against the B-17 and so they are not entirely hypothetical.[123] [124] For a constant high explosive content, they have been drawn so that over the linear range, probability is inversely proportional to aircraft weight. This makes vulnerable area independent of aircraft weight in this region. For a much more conservative estimate of target vulnerability, refer to Dr. Brandli's estimate, reproduced in Section 5.6.

Table IV-17. Characteristics of the Vigilante, T250 Gatling Gun

Caliber	37 MM
Number of Tubes	6
Diameter of Gun Cluster	10.0 inches
Rate of Fire	High 3000 RPM
	Low 120 RPM
Burst Size	48 rounds
Bursts per Load	Normal: 3 (144 Rounds)
	Optional: 4 (192 Rounds)
Round Weight	3.4 lbs
Projectile Weight	1.65 lbs
Muzzle Velocity	T4231E22 3000 fps
	Improved 3600 fps
Tube Cant	45 minutes of arc
Dispersion	Adjustable by Changing Tube Cant
Time of Recharge	
Drum Between Bursts	2 sec
Magazine Reload Time	2.5 minutes
Elevation Limits	-5 degrees to > 85 degrees
Moments of Inertia	
of Armament Package	Azimuth: 6280 in-lb-sec^2
	Elevation: 5060 in-lb-sec^2
Power Requirements	For Acceleration: 108 HP
	For steady state 42 HP

00678-480

Table IV-18 Characteristics of the Vulcan, XM-163 Gatling Gun

Caliber	20 MM
Number of Tubes	6
Rate of Fire	High (for Bursts): 3000 RPM
	Continuous: 1000 RPM
Burst Size Options	10 Rounds per Burst
	30 Rounds per Burst
	60 Rounds per Burst
	100 Rounds per Burst
Load	1100 Rounds (linkless feed)
	300 Rounds (linked feed)
Elevation Limits	-5 degrees to 80 degrees
Max Azimuth Rate	60 degrees/sec
Max Elevation Rate	45 degrees/sec
Max Acceleration	
(Az, El)	160 degrees/sec^2
Maximum Lead Angle	25 degrees
Tube Life	2500 Rounds/bbl
Weight	Towed 3000 lb
	Self-propelled 26,000 lb

00678-481

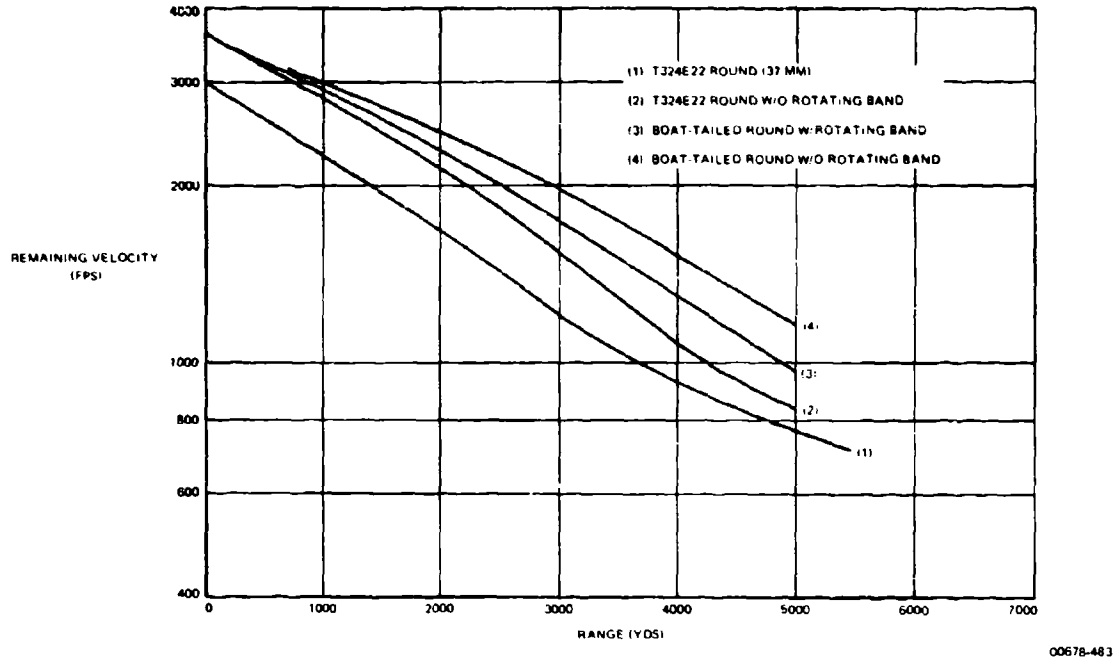

Figure 4-62. Velocity versus Range Ballistics of the Vigilante T324E22 and Three-Proposed Improved Rounds

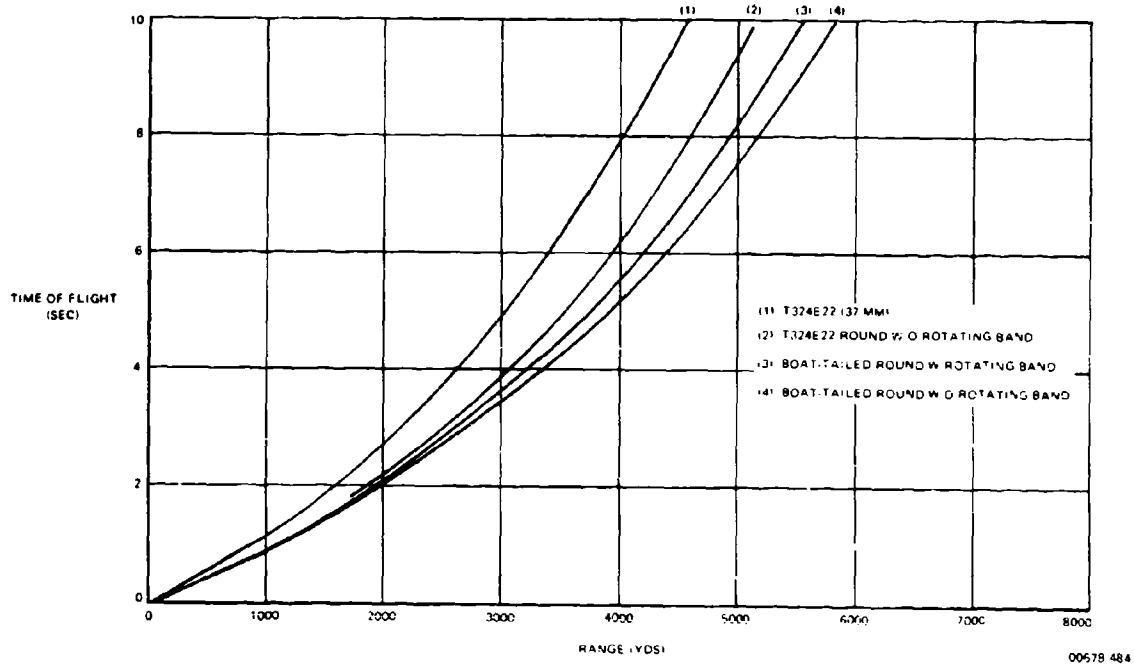

Figure 4-63. Time of Flight versus Range Ballistics of the Vigilante T324E22 and Three-Proposed Improved Rounds

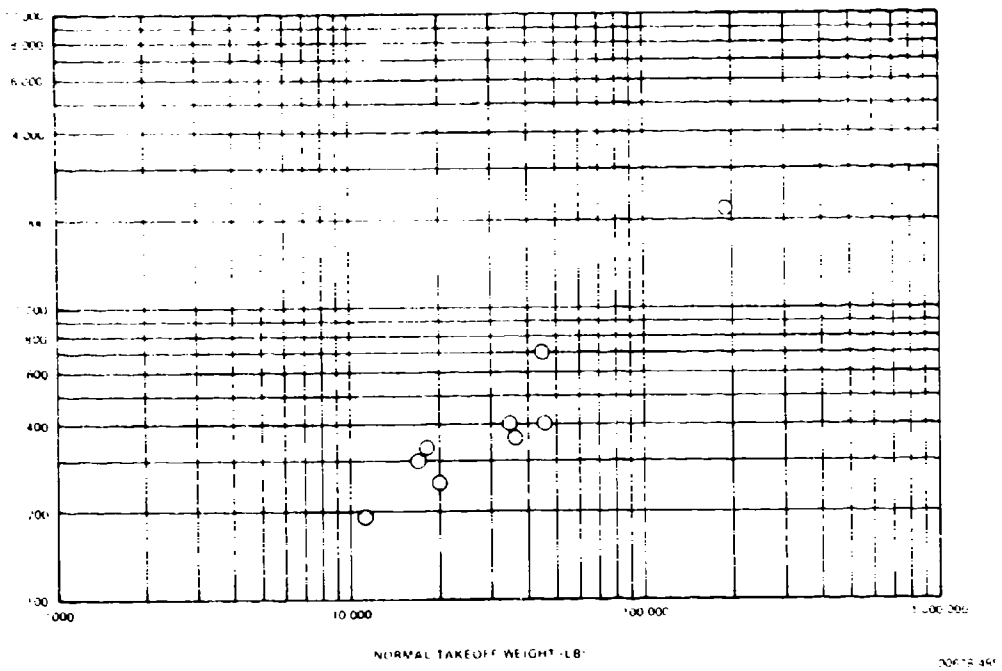

Figure 4-64. Graph of Side Area versus Aircraft Weight

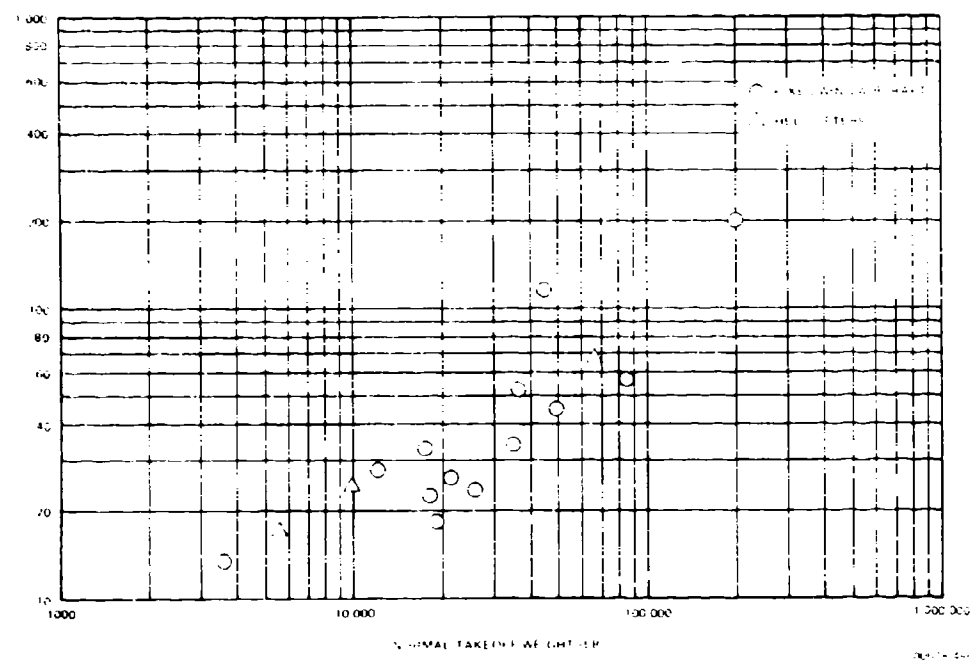

Figure 4-65. Graph of Frontal Area versus Aircraft Weight

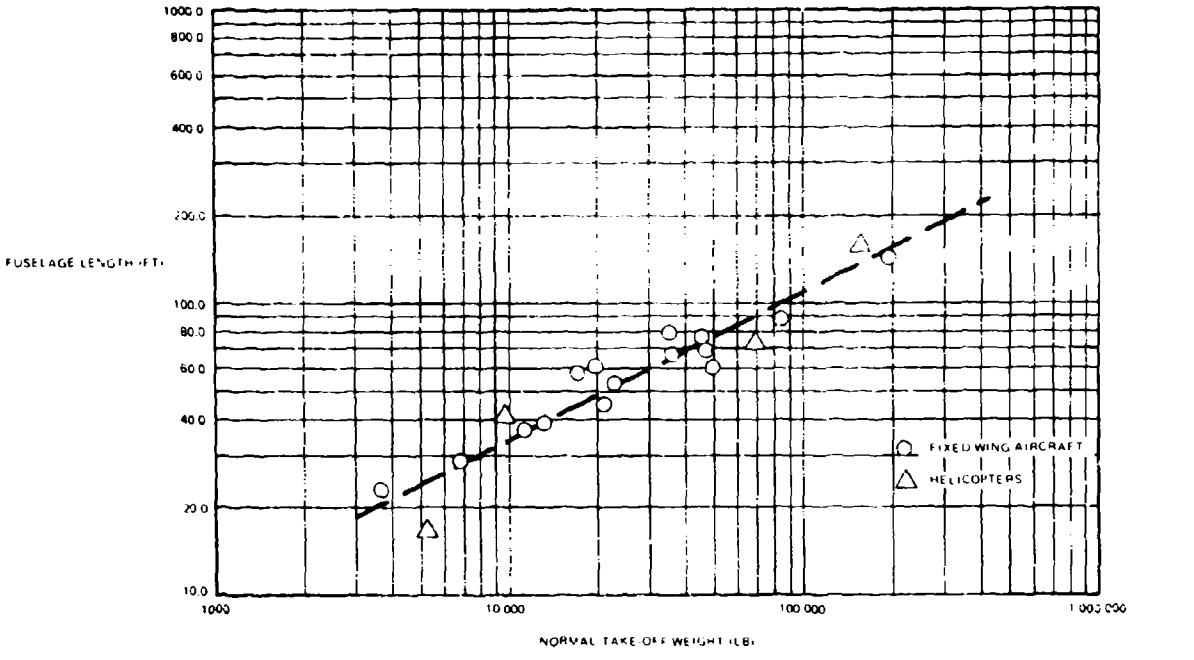

Figure 4-66. Graph of Fuselage Length versus Aircraft Weight

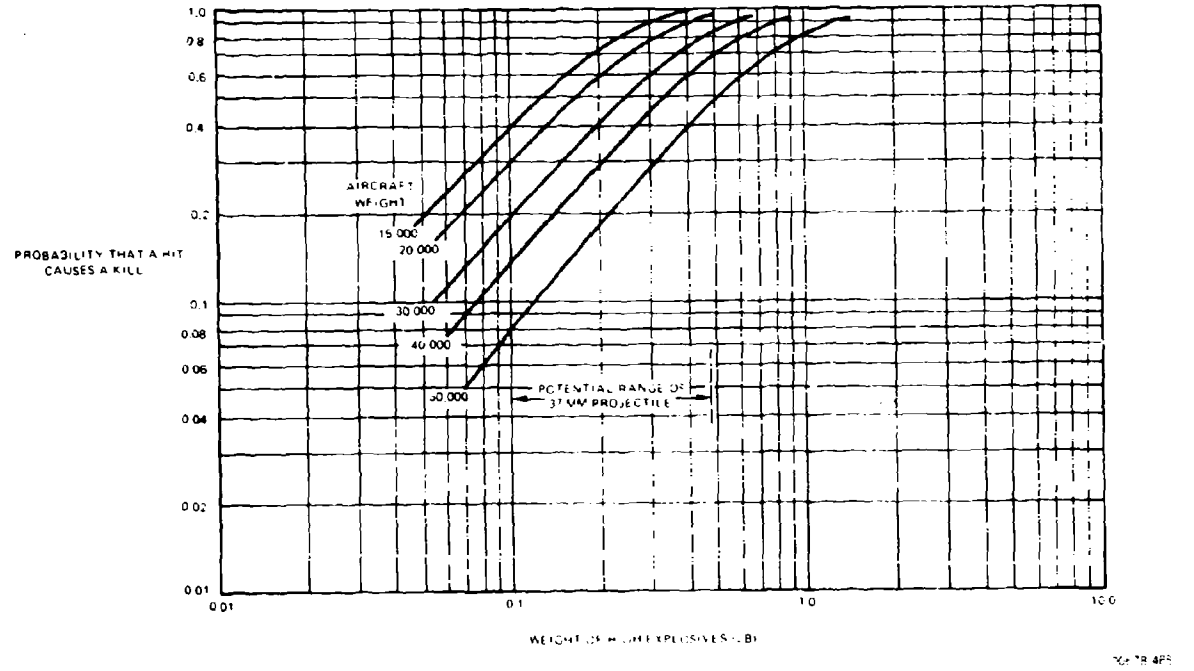

Figure 4-67. Hypothetical Target Vulnerability

SECTION 5
ANALYSIS OF AFAADS SYSTEM REQUIREMENTS

5.1 SYSTEM CONFIGURATIONS

The three basic components of the AFAADS weapon system are the sensors, the computer, and the weapon. The sensor acquires target present position data, the computer predicts future position, and the weapon fires at the predicted position. The process is, for our purposes, continuous. Air defense systems have been built to fire only a single salvo at each target, however, our interest is in a gun system that may fire continuously, or in a series of bursts.

An objective is to have all components of the AFAADS system mounted on the same vehicle (or mount for a towed version). The following paragraphs discuss some of the resulting options in arrangements, in view of this objective.

An additional objective is that AFAADS have a fire on the move capability. The implications of this will be discussed.

Figure 5-1 shows the elements of the tracking loop for angular tracking of the target. The discussion of range tracking would be similar but simpler (since vehicle motion does not affect range measurements significantly), and so range tracking will not be discussed explicitly.

In Figure 5-1 and the following figures, D represents a unit vector aligned as indicated by the following subscripts:

t: along the tracker-target line.

s: along the axis of the sensor.

v: along an axis fixed in the vehicle or mount.

g: along the axis of the gun tube (we ignore trajectory curvature in this discussion).

D_ϵ represents an error vector.

As indicated by Figure 5-1, the sensor (which may be a man) observes the difference between sight and target orientation, and generates a corrective signal which is applied to a control and/or servo, which in turn drives the sight relative to the vehicle to reduce the observed error. Since the whole apparatus is on the vehicle, vehicle motion is an extraneous input which must be corrected out in the tracking function.

If both sensor and gun are mounted on the same vehicle, but independently of each other, the addition of the computer and gun to the system is straightforward (Figure 5-2). This may be difficult to accomplish from a design point of view. To achieve a compact design it would be desirable to mount the sensors on the lower carriage of the gun (i.e., the portion of the carriage that traverses in azimuth) Figures 5-3 through 5-6 show typical configurations of this type.[1,2,3] It is conceivable that the sensor complex might be mounted on a ring concentric with and internal to the training circle of the gun's lower carriage with a separate drive from the vehicle. While this would effectively uncouple the sensor and gun motions, it would require some design ingenuity as well as more powerful servos to drive the sensor complex than some of the alternate options discussed below.

A simple solution, from a design point of view and an often undesirable one from an operational point of view, is to mount the sensor unit on the gun; compute leads from appropriately delayed gun rates, and set the sensor back from gun position by the lead angle. Vulcan employs this approach. Figure 5-7 shows the elements of this disturbed reticle lead-computing sight solution. As shown, the operator controls the gun movement directly, but observes the consequences of his adjustment of the control only after it has filtered through the gun servos and the computing sight. This system can be made to work satisfactorily (within the limits of accuracy of whatever lead computation is provided) provided that certain precautions are taken in the design of the control. These precautions are: that the control have a significant position component, and that the lag in the gun servos be very small. This type of system has been unpopular when put on a mount with rate control. The rate control introduces a 90-degree phase lag in the loop from operator's hand back to his eye, the sight adds another 45 degrees, and the gun servos add additional lag. As discussed in the section of human operator performance, phase lag in the operator's control loop of whatever magnitude is undesirable and degrades tracking accuracy. The Navy has been successful with disturbed reticle sights because they have been mounted on units that are pointed directly by the operator, without rate drives. The Mark 63 director, for example, consists of a pointing unit with a lead computing sight but without power drive. The operator, by tracking, aims his director at the desired predicted position, which is transferred by servos to an adjacent 40mm or 3 inch/50 gun mount.

It is possible, by putting phase advance components in the control unit of the system shown in Figure 5-7 and by using very high performance gun servos, to build a system that will be as easy to control as a tracking system without a. However, the problem of manual tracking in high acceleration regions remains. The concept should not be discarded as a candidate for minimum cost systems because of experiences with some unfortunately proportioned past designs.

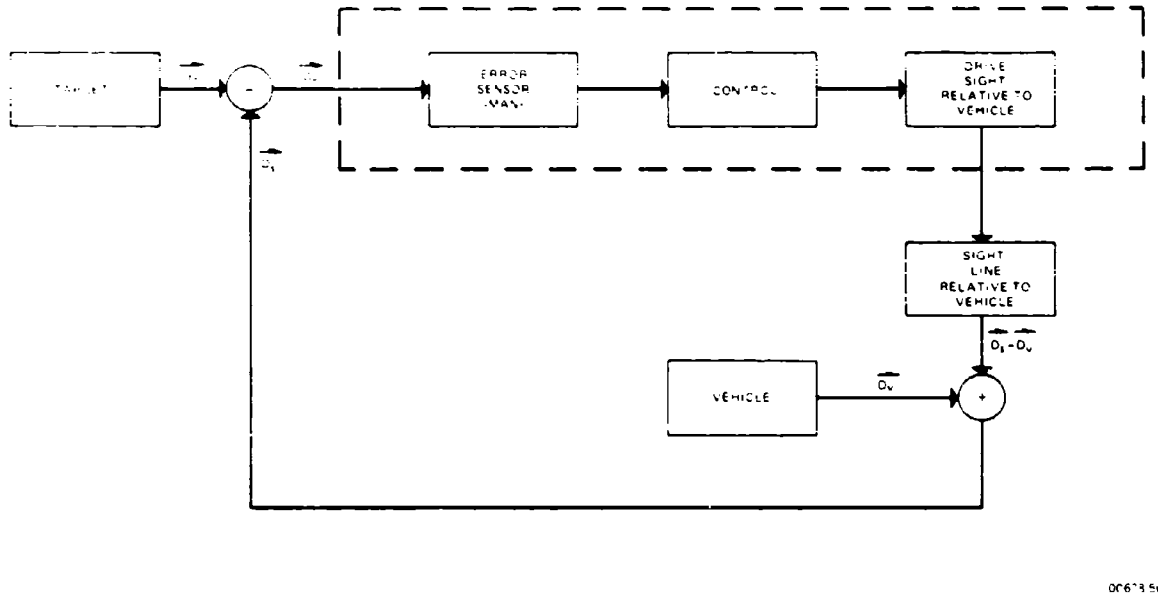

Figure 5.1. Elements of a Basic Tracking Loop

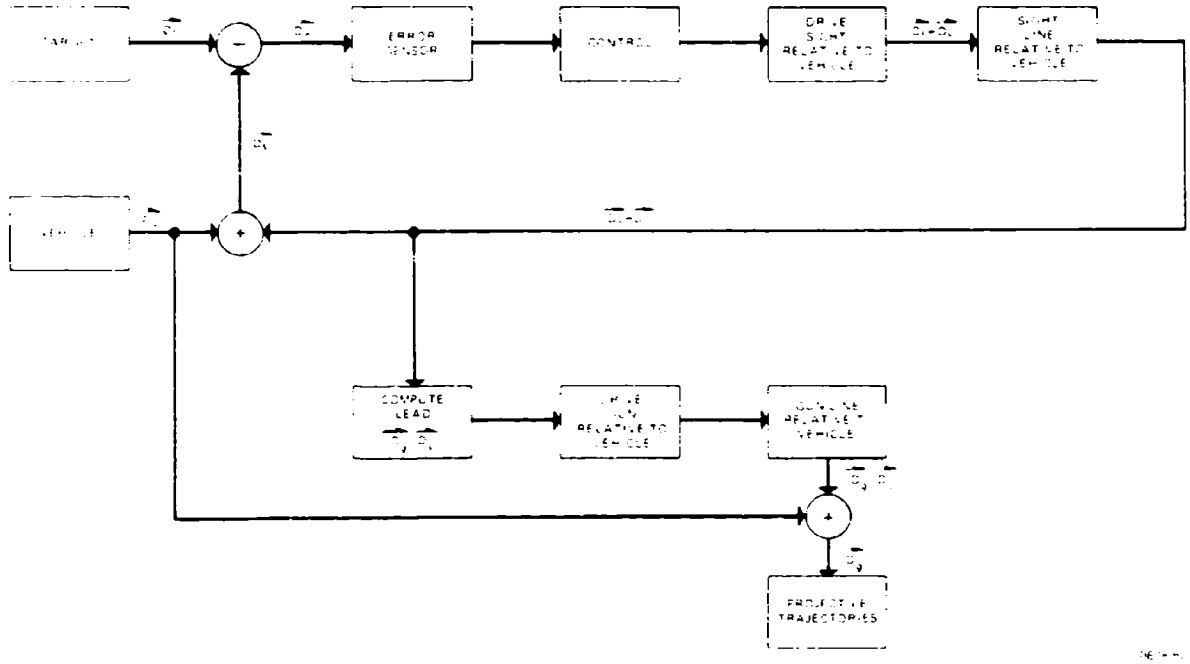

Figure 5-2 Elements of System with Sensors and Gun Independently Mounted on Same Vehicle

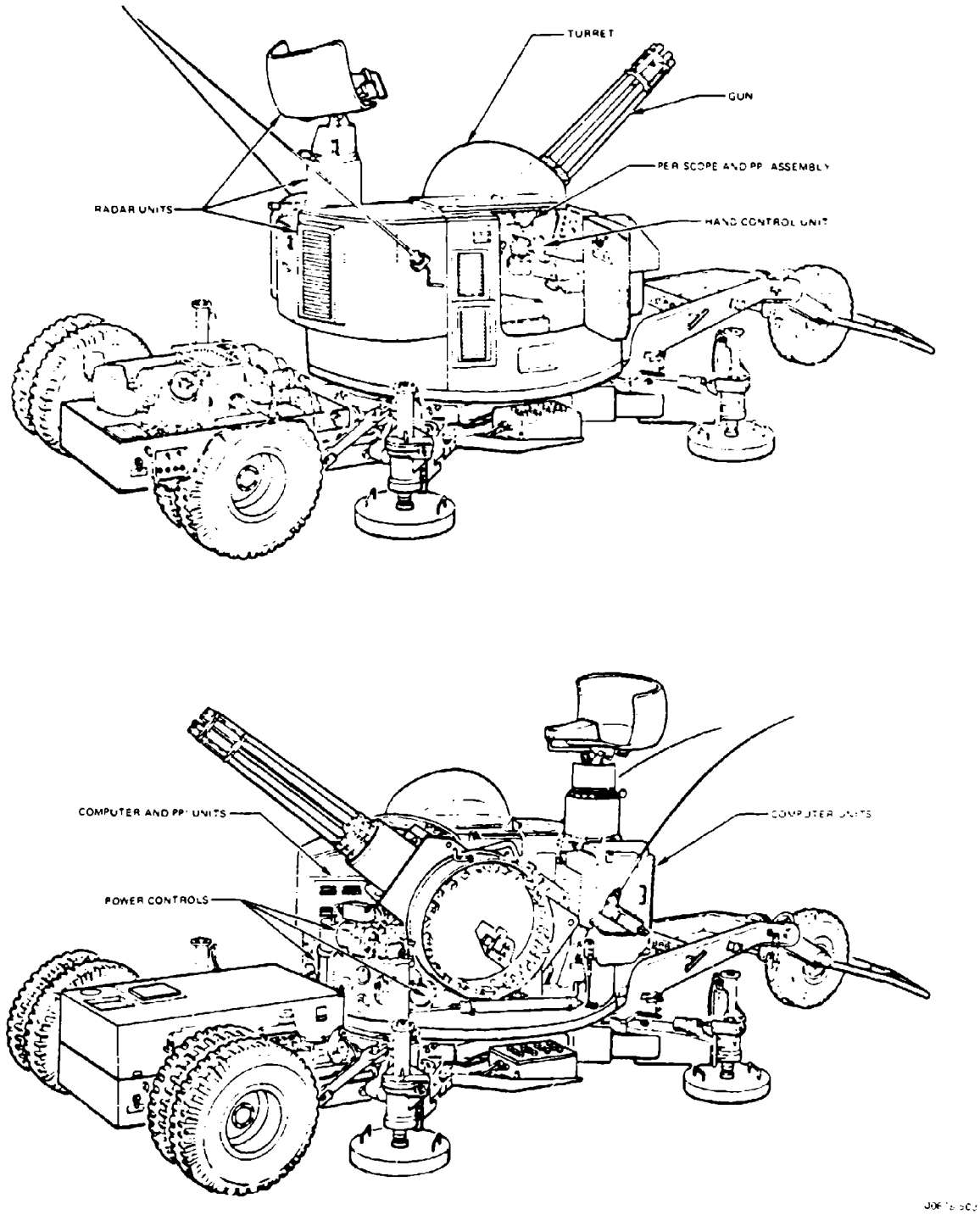

Figure 5-3. Trailer-Mounted Version of the Vigilante Antiaircraft Weapon System

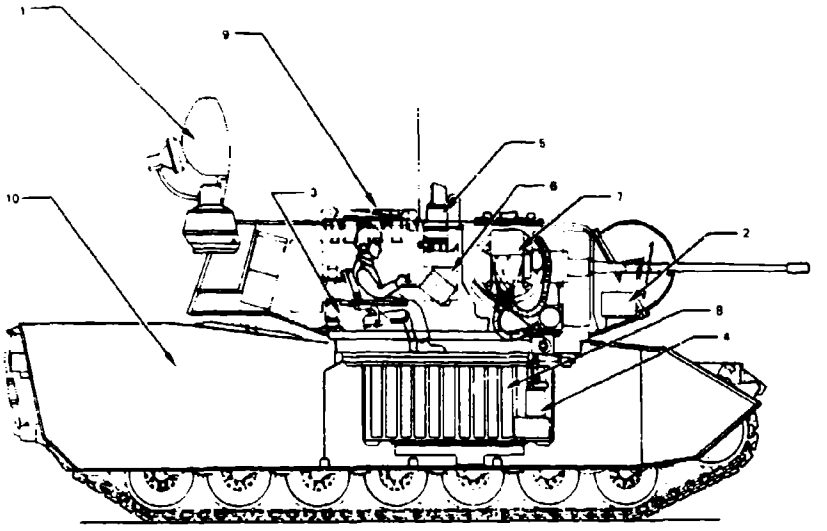

KEY

1 SURVEILLANCE RADAR (SIEMENS)
2 FIRE CONTROL RADAR (AEG TELEFUNKEN)
3 MAIN COMPUTER (AEG TELEFUNKEN)
4 SUBSIDIARY COMPUTER (RHEINMETALL)
5 SURVEILLANCE OPTICS (RHEINMETALL)
6 OPERATING CONSOLE
7 WEAPONS INSTALLATION (RHEINMETALL)
8 MAGAZINE
9 TURRET WITH HATCHES (RHEINMETALL)
10 CHASSIS (PORSCHE KRAUSS MAFFEI)

9894-1A

Figure 5-4. Matador Antiaircraft System

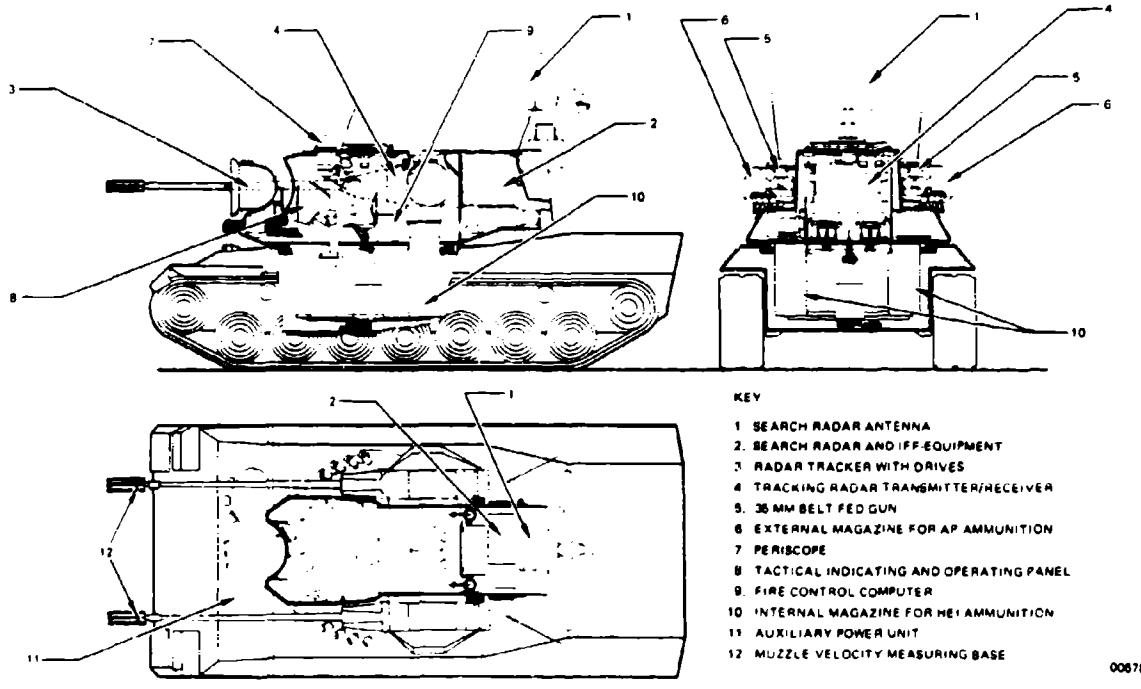

KEY

1 SEARCH RADAR ANTENNA
2 SEARCH RADAR AND IFF-EQUIPMENT
3 RADAR TRACKER WITH DRIVES
4 TRACKING RADAR TRANSMITTER/RECEIVER
5 35 MM BELT FED GUN
6 EXTERNAL MAGAZINE FOR AP AMMUNITION
7 PERISCOPE
8 TACTICAL INDICATING AND OPERATING PANEL
9 FIRE CONTROL COMPUTER
10 INTERNAL MAGAZINE FOR HE AMMUNITION
11 AUXILIARY POWER UNIT
12 MUZZLE VELOCITY MEASURING BASE

00678-804

Figure 5-5. Layout of the 5PFZ-B Antiaircraft Tank

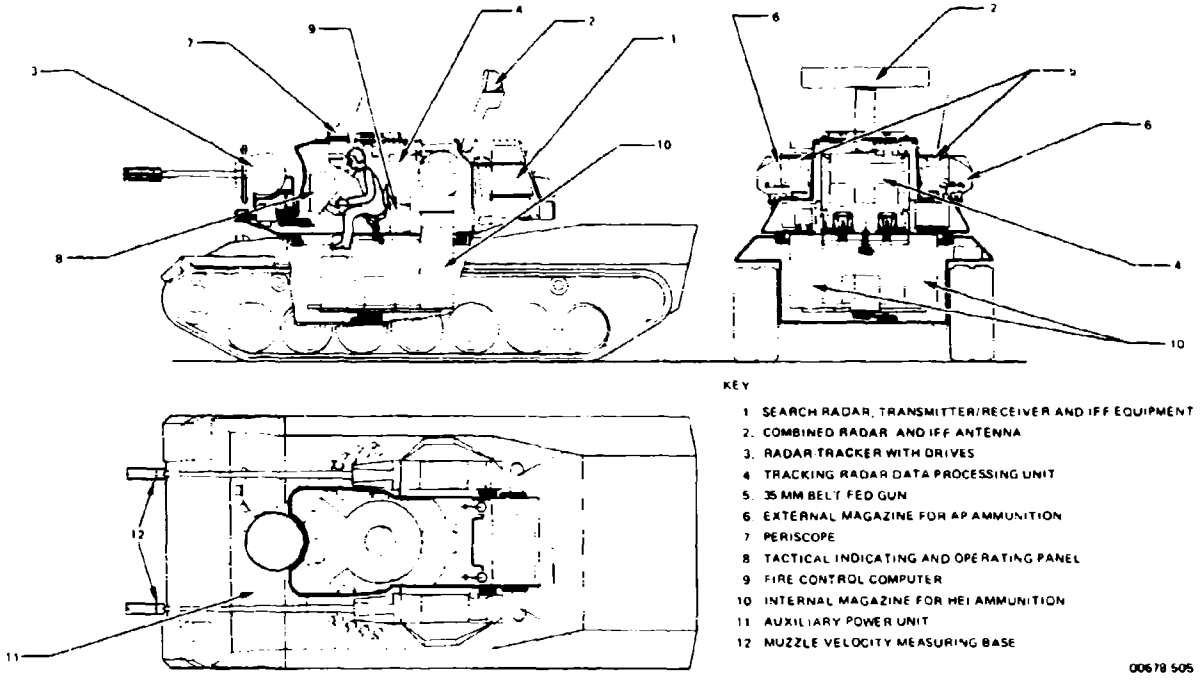

Figure 5-6. Layout of the 5PFZ-C Antiaircraft Tank

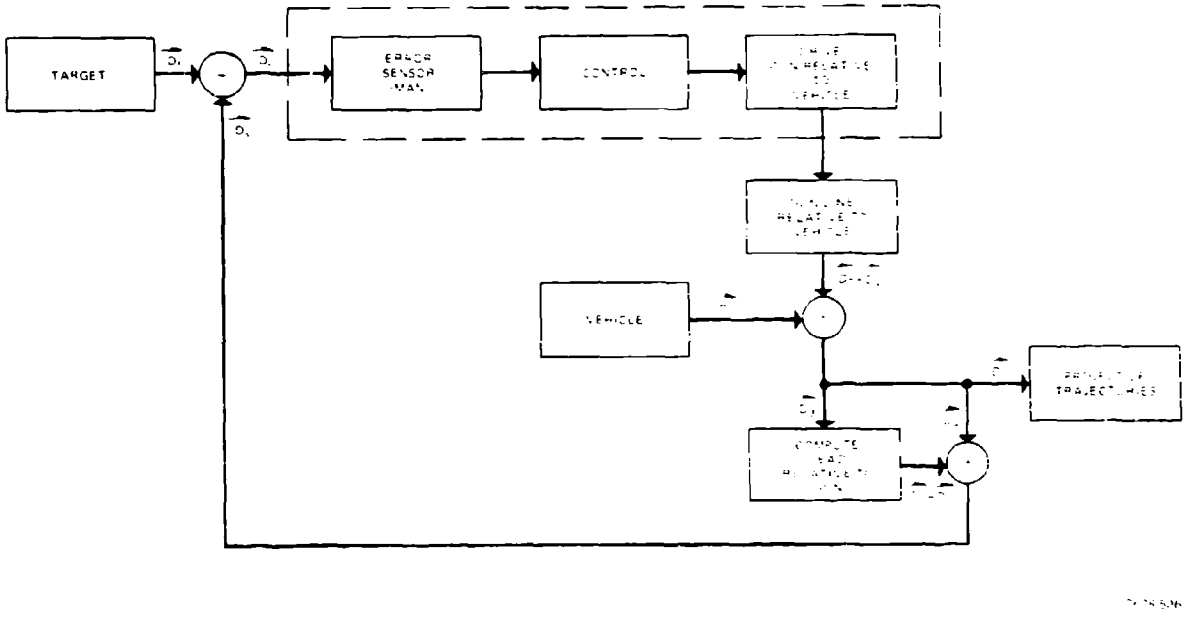

Figure 5-7. Elements of an On-Carriage, Disturbed Reticle Lead-Computing Sight System

The circulation of tracking errors through the complete lead computation and gun positioning loop can be essentially eliminated by the arrangement shown in Figure 5-8. Here the sensor is mounted on the gun lower carriage, as in the configurations shown in Figures 5-3 through 5-6. However, the same servo that drives the gun in azimuth relative to the mount, rotates the sensor pedestal in the opposite direction by an equal angle. Thus the gun traverse has no effect on sensor traverse (within the resilience and backlash tolerances of the respective drives). The sensor elevates independently of the gun on its own pedestal.

This seems to be the most straightforward and economical solution for AFAADS.

The elements of sight stabilization against vehicle motion are indicated in Figure 5-9. An inertial reference is provided in the sight head, and servos maintain the sight line in a prescribed relation to the reference in spite of vehicle motion. The sight line is caused to move in space, as indicated in Figure 5-10, by applying a precessing torque to the gyros constituting the inertial reference.

The complete system is shown in Figure 5-11. Angular velocities of the target in the inertial reference system are obtained from the precessing torques in the sight head. These, together with azimuth and elevation relative to the vehicle, are transmitted to the computer which generates gun orders. A separate vertical reference unit may provide corrections for vehicle tilt if these are considered of significant magnitude. Since the rates are obtained in inertial space, the orientation of the lead vector is independent of vehicle angular motion except to the degree that the motion is introduced to the smoothing function through the angles. This needs to be analyzed, but is considered to be a small effect. This solution is considered preferable to a stable element on the vehicle to which all measurements are related, because it avoids errors in data transmission. Stabilization of the sight line against the effects of gun fire even when the vehicle is not moving is considered highly desirable, and this should be achieved. The system as shown does not lend itself easily to acceleration predictions in the computer algorithms, but these can certainly be omitted for fire on the move.

5.2 COORDINATE SYSTEMS

A ground station tracking an aircraft target most naturally measures target azimuth in a horizontal plane with respect to a reference direction such as North, elevation angle with respect to the horizontal, and slant range to the target. Such a tracking unit has two axes; it rotates in azimuth about a vertical axis, and elevates about a horizontal axis. Azimuth angle, elevation angle, and slant range are the basic measurements, however, a doppler radar allows the direct measurement of rate-of-change of range as well.

Depending on the application, other coordinate systems have been used, particularly in cases where it is desired to stabilize the tracking mount against motion of the vehicle carrying it. Figure 5-12, reproduced from Ewing[4], shows nine types of tracking mounts.

An advantage of a three-axis mount, such as (g) in the figure, is that the train and elevation axes can be positioned so that the cross-elevation axis is perpendicular to the slant plane containing the tracking station and the target velocity vector. When this position has been achieved, tracking of an unaccelerated target is reduced to a one-dimensional problem. The target, moreover, may be tracked continuously without excessive angular velocities required of the mount, even though it may pass directly overhead. A German tracking unit of this sort was built during WWII. Three-axis mounts have been suggested for U.S. Army tracking equipment from time to time.[5]

For AFAADS we will consider only the type of 2-axis mount shown in Figure 5-12(b). This limits tracking above some elevation angle (such as 85 degrees), and this limit must be considered in conjunction with the maximum angular velocity and acceleration capabilities provided for the mount. A small conical 'dead zone' above a fixed tracker is acceptable because of the small volume of space it defines. On a rolling and pitching vehicle, such as a destroyer, the influence of such a dead zone extends over a much larger volume because of vehicle motion, and this is a reason for considering mounts with more than two axes for Naval applications.

To go from measurements of target present position to estimates of target future position, it is necessary to make some assumptions about the target path. In particular, in order to filter tracking errors from the measured target position data, it is desirable to convert the position data to functions whose derivatives vary slowly with time in order to use an effective smoothing interval.

The second and higher derivatives of the target position measurements in the original polar coordinates are too large in certain regions of interest to allow effective smoothing without introducing input errors caused by the delayed rates which must be corrected later in the computational process.

The most natural parameters on which to do data smoothing are those describing target motion in target centered coordinates. These are the magnitude and direction of the target velocity vector, and possibly the rates of change of these quantities.

If the prediction assumption is simply that the target

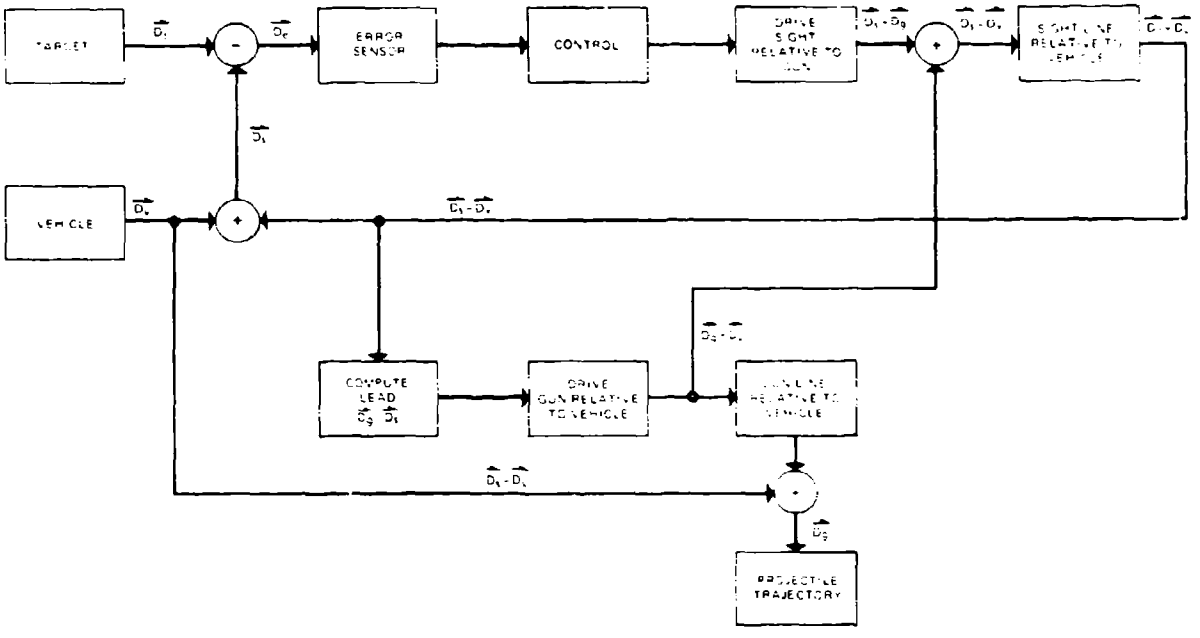

Figure 5-8. Elements of a System Whereby the Sensors are Mounted on Gun with Lead Subtruction

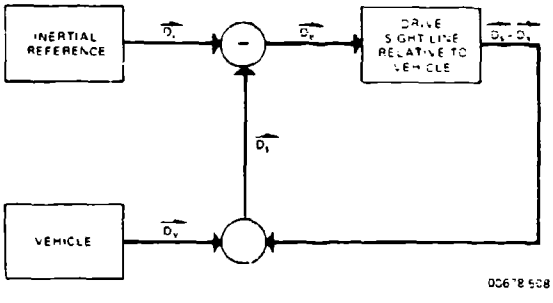

Figure 5-9. Elements of a System Utilizing Inertial Stabilization of Sight Line

is unaccelerated, then invariant functions can be computed to use in smoothing. These functions can be imbedded in rectangular, polar, or mixed coordinate systems. In rectangular coordinates the invariants are simply the linear target velocity components along each coordinate axis.

If one wishes to admit the assumption of a turning target, or one that accelerates along its flight path when it dives, the algorithms are considerably more straightforward in a rectangular coordinate system.

The early antiaircraft fire control systems, and many World War II systems based their lead computations simply on the product of azimuth and elevation angular velocity by time of flight, without any attempt to smooth the angular velocity measurements (except by instructing the human trackers to track smoothly and accurately).

More sophisticated systems, based on angular tracking velocities, applied the appropriate trigonometric corrections so that the solution had no geometric errors when the target path was unaccelerated.

The functional transformations involved in several typical fire control solutions are outlined in the following paragraphs to illustrate the effect of coordinate system.

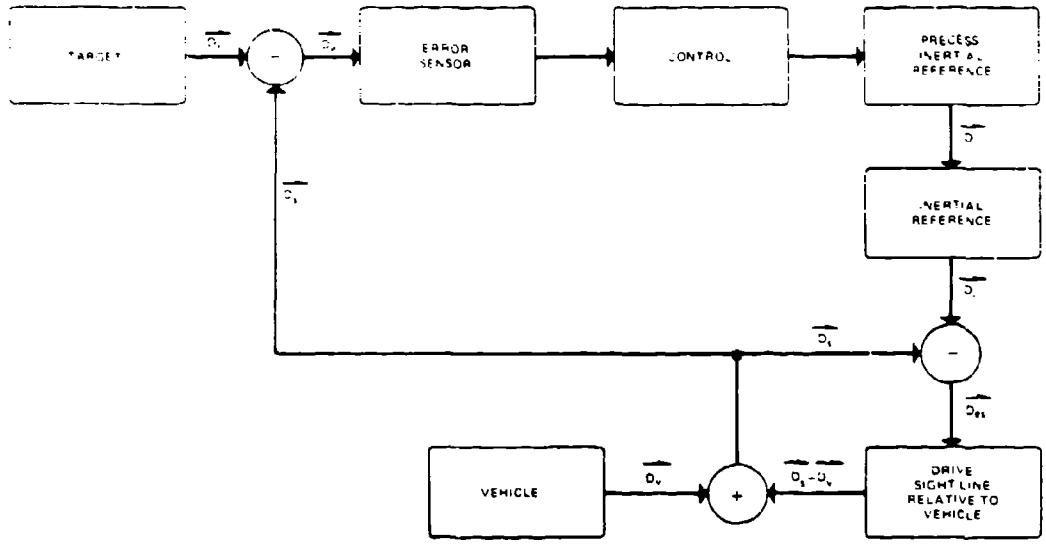

Figure 5-10. Elements of Tracking Loop with Stabilized Sight

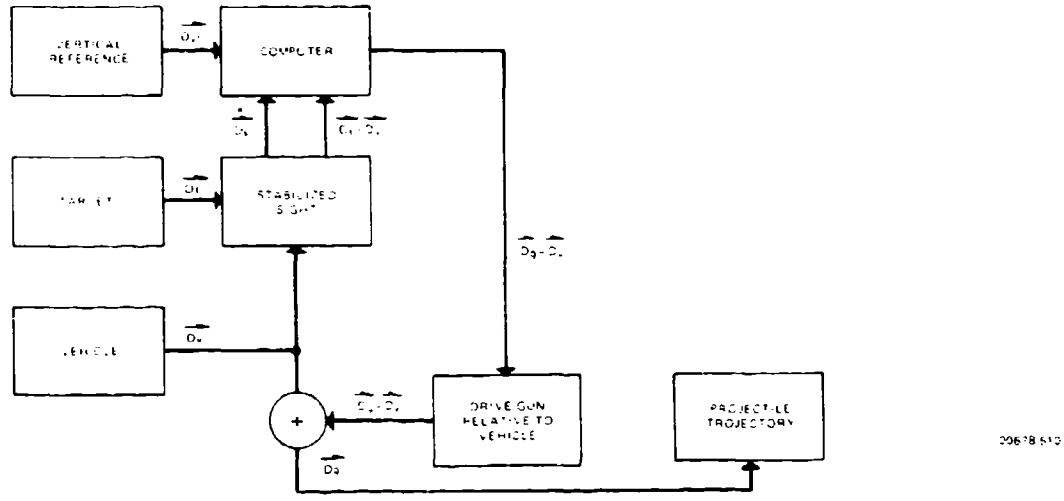

Figure 5-11. Elements of System with Stabilized Sight, Unstabilized Gun and Correction for Tilt

5.2.1 Rectangular Coordinate System

This coordinate system was used in the U.S. Army/Sperry M-2,3,4 directors and the Bell Telephone Laboratory's M-9, except that the first three types used altitude rather than slant range as an input.

A geometric representation of the rectangular coordinate system is shown in Figure 5-13. A flow diagram of this system is shown in Figure 5-14.

The tracking unit provides:

D_o = slant range

e_o = elevation angle

A_o = azimuth angle in the horizontal plane from an arbitrary reference (such as North)

The first coordinate conversion obtains target position in a rectangular coordinate system, in which:

$$X_o = D_o \cos e_o \sin A_o \qquad (5.1)$$

$$Y_o = D_o \cos e_o \cos A_o \qquad (5.2)$$

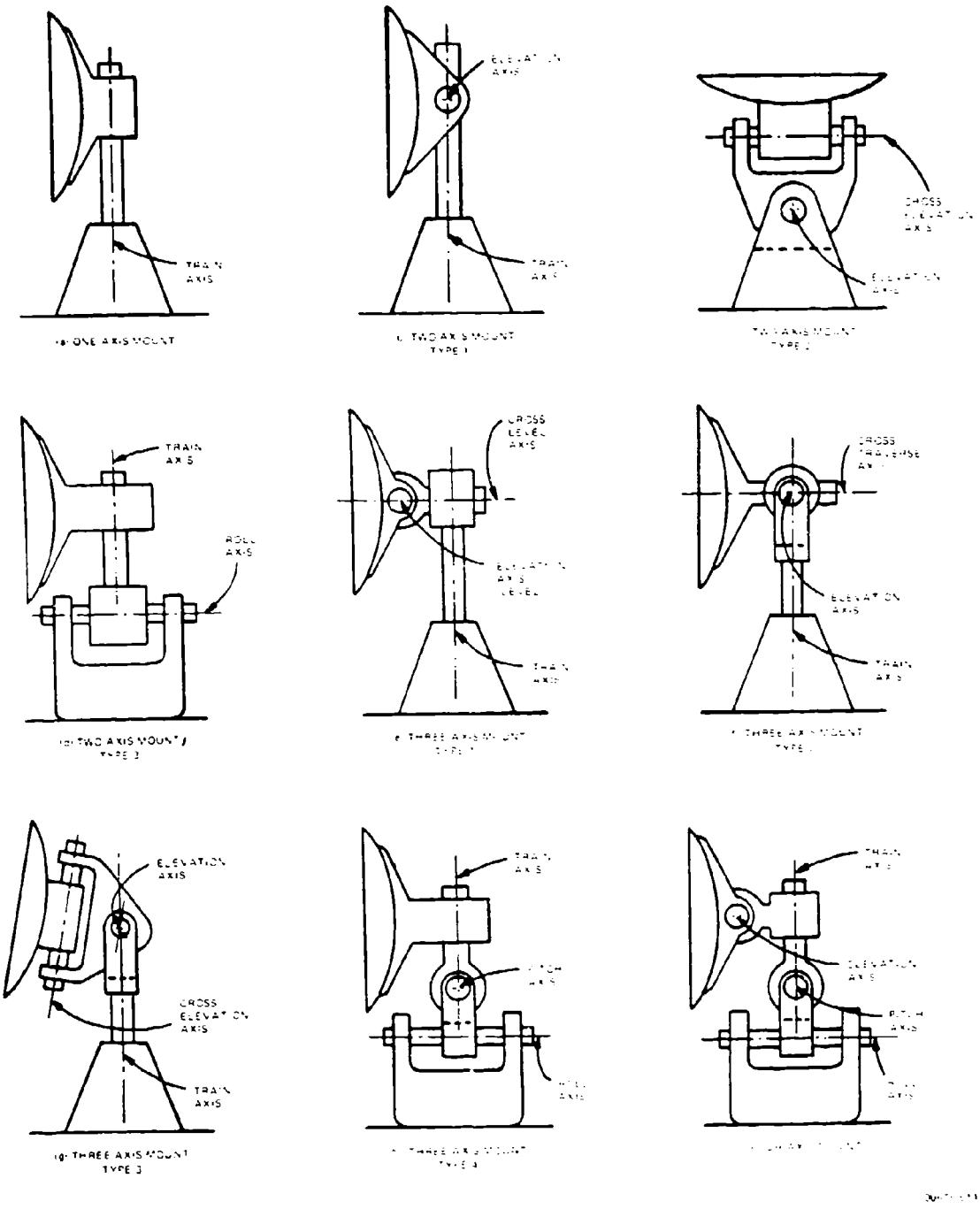

Figure 5-12. Typical Coordinate Systems

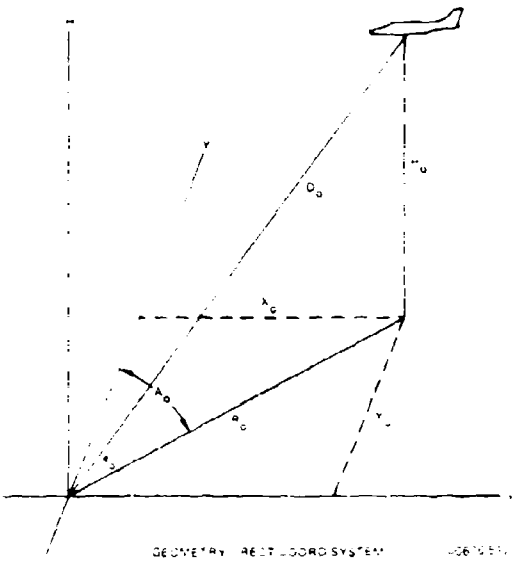

Figure 5-13. Geometric Representation of Rectangular Coordinate System

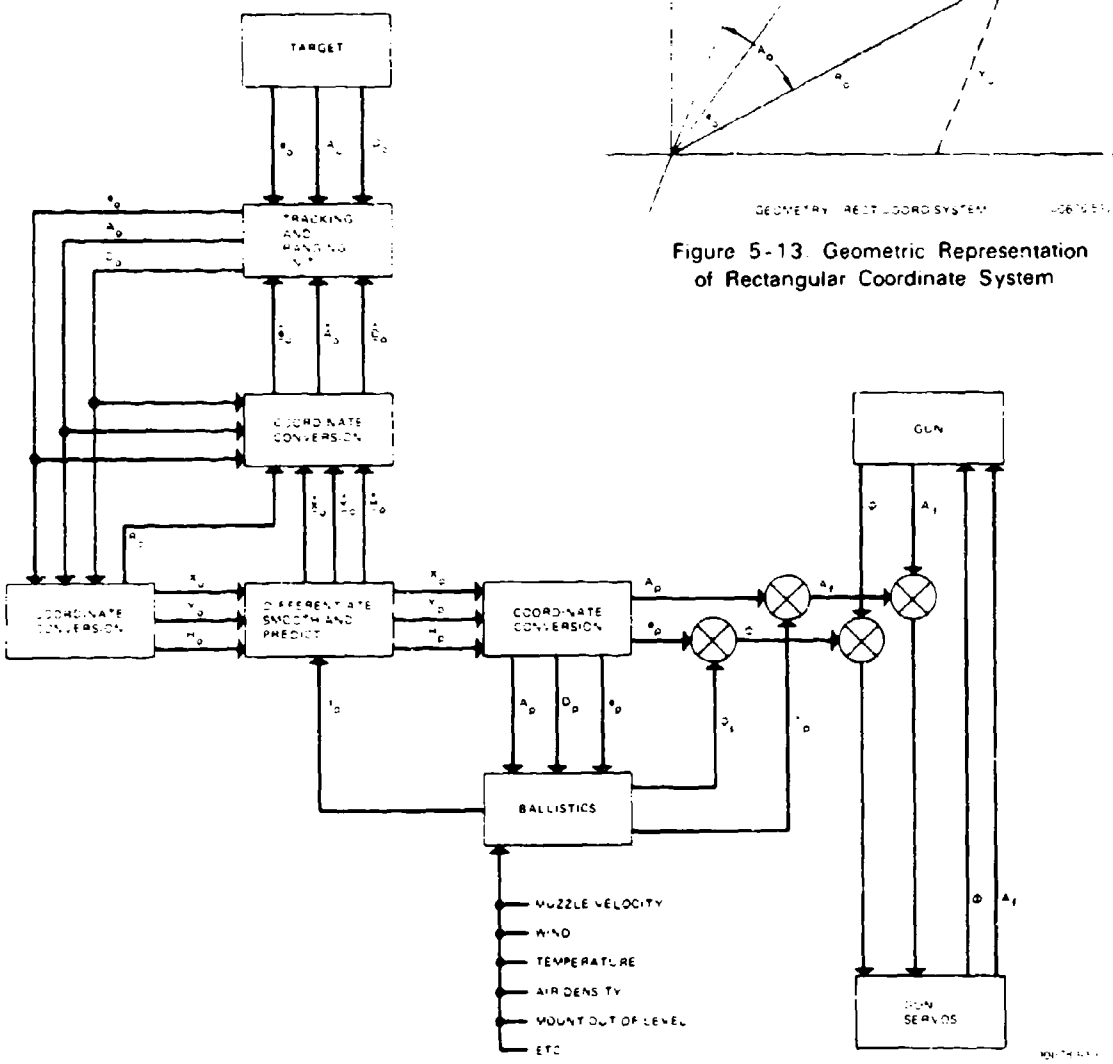

Figure 5-14 Flow Diagram of Rectangular Coordinate System

$$H_o = D_o \sin e_o \tag{5.3}$$

and it also derives range to target in the horizontal plane as:

$$R_o = D_o \cos e_o \tag{5.4}$$

The differentiating, smoothing, and predicting unit obtains smoothed measure of rates (and possibly accelerations) in each of the rectangular coordinates. For simplicity at this stage, assume that only rates are measured, and designate a smoothed rate such as that in the X coordinate as $\dot{X}_o$.

A digital computer would obtain this quantity as

$$\dot{\underline{X}}_o(t) = \sum_{j=o}^{n} a_j X_o(t - j\Delta) \tag{5.5}$$

and an analog computer would obtain it as:

$$\dot{\underline{X}}_o(t) = \int_o^{\infty} W(\tau)\, X_o(t - \tau)\, d\tau \tag{5.6}$$

From the smoothed rates, rates in the polar coordinate system are regenerated and fed back to the tracker according to the relations:

$$\dot{D}_{or} = \dot{\underline{X}}_o \sin A_o \cos e_o + \dot{\underline{Y}}_o \cos A_o \cos e_o + \dot{\underline{H}}_o \sin e_o \tag{5.7}$$

$$\dot{e}_{or} D_o = -\dot{\underline{X}}_o \sin A_o \sin e_o - \dot{\underline{Y}}_o \cos A_o \sin e_o + \dot{\underline{H}}_o \cos e_o \tag{5.8}$$

$$\dot{A}_{or} R_o = \dot{\underline{X}}_o \cos A_o - \dot{\underline{Y}}_o \sin A_o \tag{5.9}$$

Predicted values of the rectangular coordinates for time of flight t_p are computed as:

$$X_p = X_o + \dot{\underline{X}}_o\, t_p \tag{5.10}$$

$$Y_p = Y_o + \dot{\underline{Y}}_o\, t_p \tag{5.11}$$

$$H_p = H_o + \dot{\underline{H}}_o\, t_p \tag{5.12}$$

A coordinate conversion unit converts these to polar coordinates according to the relations:

$$D_p = H_p \sin e_p + X_p \sin A_p \cos e_p + Y_p \cos A_p \cos e_p \tag{5.13}$$

$$e_p = \tan^{-1}[H_p / (X_p \sin A_p + Y_p \cos A_p)] \tag{5.14}$$

$$A_p = \tan^{-1}(X_p / Y_p) \tag{5.15}$$

The quantities D_p, e_p enter the ballistic unit, which generates:

$$t_p = t_p(D_p, e_p, \lambda_1, \lambda_2, \ldots) = \text{time of flight} \tag{5.16}$$

$$\phi_s = \phi_s(D_p, e_p, \lambda_1, \lambda_2, \ldots)$$

= superelevation (gravity drop, vertical jump, ...) (5.17)

$$\delta_s = \delta_s(D_p, e_p, A_p, \lambda_1, \ldots)$$

= azimuth correction for drift, jump, wind, etc. (5.18)

and λ are parameters common to all trajectories such as gun muzzle velocity, air density, wind, ammunition lot, temperature, etc.

Time of flight is fed back to the prediction unit. The elevation and azimuth corrections are added to A_p, e_p to produce gun firing orders A, ϕ. The gun servos drive the gun to null gun position against A, ϕ.

5.2.2 Rectangular Coordinates: Rates Obtained by Gyros on the Tracking Head

Suppose that the system has a stabilized line of sight (possibly based on three gyros with orthogonal spin axes; one in the vertical plane and perpendicular to the line of sight, one in the horizontal plane and perpendicular to the line of sight, and one along the line of sight). Tracking is accomplished by torqueing the gyros, whence the precessional moment is a measure of angular velocity and is available for use in the computation. It is also assumed that rate of change of slant range is obtained from a doppler radar. The three angular rates obtained are:

$\dot{e}_o$ = elevation rate

$\dot{\tau}_o$ = traverse rate = $\dot{A}_o \cos e_o$

$\dot{\omega}_o$ = rate of rotation about the line of sight = $\dot{A}_o \sin e_o$

XSU_{Bo}, YSU_{Bo}, H_s are obtained as before, but the rates in rectangular coordinates (unsmoothed) may now be obtained as:

$$\dot{X}_o = (\dot{D}_o \cos e_o - e_o D_o \sin e_o) \sin A_o + \dot{\tau}_o D_o \cos A_o \tag{5.19}$$

$$\dot{Y}_o = (\dot{D}_o \cos e_o - \dot{e}_o D_o \sin e_o) \cos A_o - \dot{\tau}_o D_o \sin A_o \quad (5.20)$$

$$\dot{H}_o = \dot{D}_o \sin e_o + \dot{e}_o D_o \cos e_o \quad (5.21)$$

These rates may now be smoothed, and regenerated rates fed back to the tracker after being derived from the following relationships:

$$\dot{D}_{or} = (\dot{X}_o \sin A_o + \dot{Y}_o \cos A_o) \cos e_o + \dot{H}_o \sin e_o \quad (5.22)$$

$$\dot{e}_{or} D_o = -(\dot{X}_o \sin A_o + \dot{Y}_o \cos A_o) \sin e_o + \dot{H}_o \cos e_o \quad (5.23)$$

$$\dot{\tau}_{or} D_o = \dot{X}_o \cos A_o - \dot{Y}_o \sin A_o \quad (5.24)$$

The advantage of using rates obtained from a stabilized sight is that they are independent of vehicle roll and pitch. Further analysis may show that no additional corrections are needed for fire from a moving vehicle, since the corrections for the very small rotations of the coordinate system caused by vehicle roll and pitch, when moving on a fairly smooth road, will be very small compared with the corrections which would have to be introduced to compensate for the corresponding rolling and pitching rates.

The ψ_z rate has not been used in the above relations. This can be essential when rate regeneration and possibly prediction are done in polar, rather than rectangular, coordinates.

5.2.3 Polar Coordinates

The first 'exact' solution in polar coordinates was developed by Vickers in England. It had no geometric error against a target flying a constant speed, constant altitude, straight line. The Vickers solution is generalized below to include diving targets. The notation is identical with that used in the prior examples of rectangular coordinates with the following additional symbols:

- α = the angle in the horizontal plane between the target velocity vector and the range vector. ($\dot{\alpha}_o = -\dot{A}_o$)
- R = horizontal range
- θ = angle of climb of the target
- δ = lead angle in the horizontal plane
- $\sigma = e_p - e_o$

Geometric representations of the polar coordinates are shown in Figures 5-15 through 5-17.

We note first that the azimuth, elevation, and slant range rates are:

$$\dot{\alpha} = \frac{v \sin \sigma_o \cos \theta}{R_o} \quad (5.25)$$

$$\dot{e} = \frac{v \sin \theta \cos e_o + v \cos \theta \sin e_o \cos \alpha_o}{D_o} \quad (5.26)$$

$$\dot{D} = -v \cos \theta \cos \alpha_o \cos e_o + v \sin \theta \sin e_o \quad (5.27)$$

From Figures 5-15 through 5-17 and preceding relations:

$$R_p \cos \delta = R_o - v \cos \theta \, t_p \cos \alpha_o = R_o - \dot{R} t_p \quad (5.28)$$

$$R_p \sin \delta = v \cos \theta \, t_p \sin \dot{\alpha}_o = R_o \dot{\alpha} t_p \quad (5.29)$$

$$\sin \delta = \dot{\alpha} t_p \frac{D_o}{D_p} \frac{\cos e_o}{\cos e_p} \quad (5.30)$$

$$\sigma = e_p - e_o \quad (5.31)$$

$$\sin \sigma = \sin e_p \cos e_o - \cos e_p \sin e_o \quad (5.32)$$

$$= \frac{H_p R_o - R_p H_o}{D_o D_p} \quad (5.33)$$

$$H_p = H_o + v t_p \sin \theta \quad (5.34)$$

$$R_p = R_p(1 - \cos \delta) + R_o - v t_p \cos \alpha_o \cos \theta \quad (5.35)$$

$$\sin \sigma = \frac{t_p}{D_p} [v \sin \theta \cos e_o + v \cos \theta \cos \alpha_o \sin e_o]$$

$$\sin e_o \cos e_p (1 - \cos \delta) \quad (5.36)$$

$$\sin \sigma = \dot{e} D_o \frac{t_p}{D_p} - \sin e_o \cos e_p (1 - \cos \delta) \quad (5.37)$$

In the slant plane defined by D_o and the target path then:

$$D_p \cos \Delta = D_o + \dot{D} t_p \quad (5.38)$$

where Δ is lead angle in the slant plane. We wish to

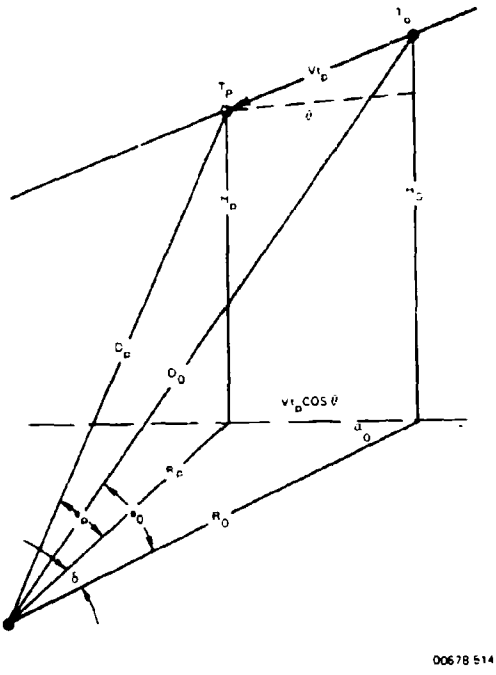

Figure 5-15. Geometric Representation of Polar Coordinate System

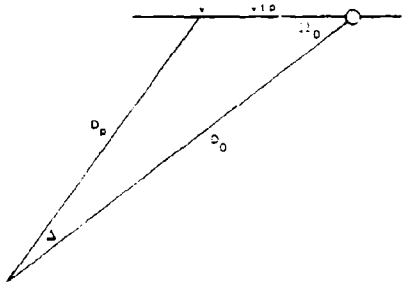

Figure 5-16. Polar Coordinate Projection in Slant Plane

express ▲ in terms of δ and σ. From the spherical triangle of Figure 5-17:

$$\cos \Delta = \cos \sigma \cos \delta_T + \sin \sigma \sin \delta_T \cos E \quad (5.39)$$

and from the spherical triangle of Figure 5-17:

$$\sin e_o = \cos \delta_T \sin e_o + \sin \delta_T \cos e_o \cos E \quad (5.40)$$

$$\cos \delta_T = \sin^2 e_o + \cos^2 e_o \cos \delta \quad (5.41)$$

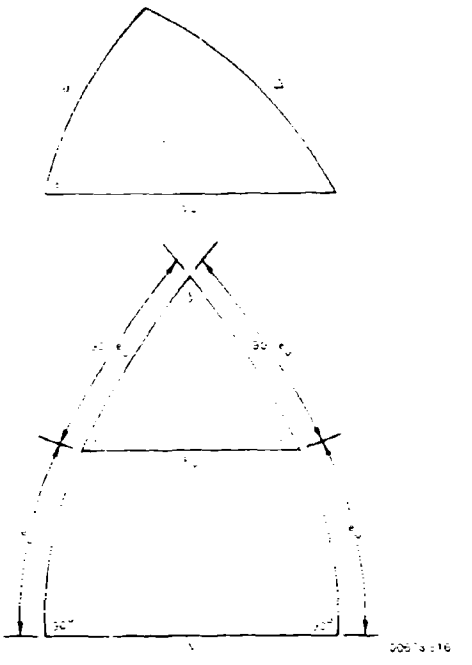

Figure 5-17. Spherical Triangles Showing Lead-Angle Derivation

Eliminating δ, and E from the above three expressions;

$$\cos \Delta = \cos \sigma - (1 - \cos \delta) \cos e_o \cos e_p \quad (5.42)$$

hence:

$$D_p = \frac{D_o + \dot{D} t_p}{\cos \sigma - (1 - \cos \delta) \cos e_o \cos e_p} \quad (5.43)$$

On examining Equations (5.30), (5.37), and (5.43), it is clear that the trigonometry is not simplified by using polar coordinates. Even for this simple case of a target flying a constant-speed straight line, many sine, cosine functions must be generated and manipulated. We are still left with the problem of smoothing the input rates, since any attempt to smooth A, e and D directly will impair the accuracy of the solution.

For full predictor solutions, polar coordinates had the advantage in the days of mechanical predictors that the scale factors of the instrument could be adjusted to handle only the lead angles, which for targets of that vintage were not large. Rectangular coordinate solutions, on the other hand, required some elements that had a range equal to the maximum target range expected to be encountered. Hence it was believed that instrumental errors could be minimized best by the

polar coordinate (or one-plus) type of solution. This argument probably does not hold for modern computers.

One method of smoothing the data is to smooth the polar coordinate velocities directly, and correct for the input lag errors (introduced by this process) by applying additional correction terms in the solution. Another is to smooth the computed lead angles δ and σ, since they vary less rapidly than the input angular velocities, and then apply corrections to the solution. This was done in an ingenious design by Frankford Arsenal during WWII.

It is also possible to smooth the input rates, without steady-state lag, by a regenerative unit operating in polar coordinates, along the following lines:

Define the three orthogonal angular velocities measured at the sight head by: $\dot{r}_o$, $\dot{e}_o$, $\dot{\psi}_o$.

These are interrelated by the expression:

$$\dot{r}_o = \dot{a}_o \cos e_o \tag{5.44}$$

$$\dot{r}_o = \dot{\Omega}_o \cos \psi_o \tag{5.45}$$

$$\dot{e}_o = \dot{\Omega}_o \sin \psi_o \tag{5.46}$$

$$\dot{\psi}_o = \dot{a}_o \sin e_o \tag{5.47}$$

$$\dot{\psi}_o = \dot{r}_o \tan e_o \tag{5.48}$$

$$\dot{\Omega}_o D_o = v \sin \Omega_o \tag{5.49}$$

$$\dot{D}_o = -v \cos \Omega_o \tag{5.50}$$

A flow diagram of the process of smoothing and regeneration, using the above relations, is shown in Figure 5-18. The complete solution of the prediction process is not diagrammed, since it can be inferred from the expressions given earlier.

Although the rectangular coordinate system, as previously defined, is easiest to discuss, it is not necessarily the best choice for the final AFAADS design. What design is chosen depends on the prediction algorithms the designer chooses to mechanize, and the hardware he has available. Design analysis might indicate, for example, that if a stabilized sight head with internal gyros is used, rate regeneration and smoothing might most efficiently be done in polar coordinates within the sight head, to minimize error accumulation in data transfer. Having good, smoothed rates, one might then prefer to predict in polar coordinates. Corrections for target acceleration could be developed in polar coordinates and applied within the computer. The elements of the problem, of course, do not change with the coordinate system.

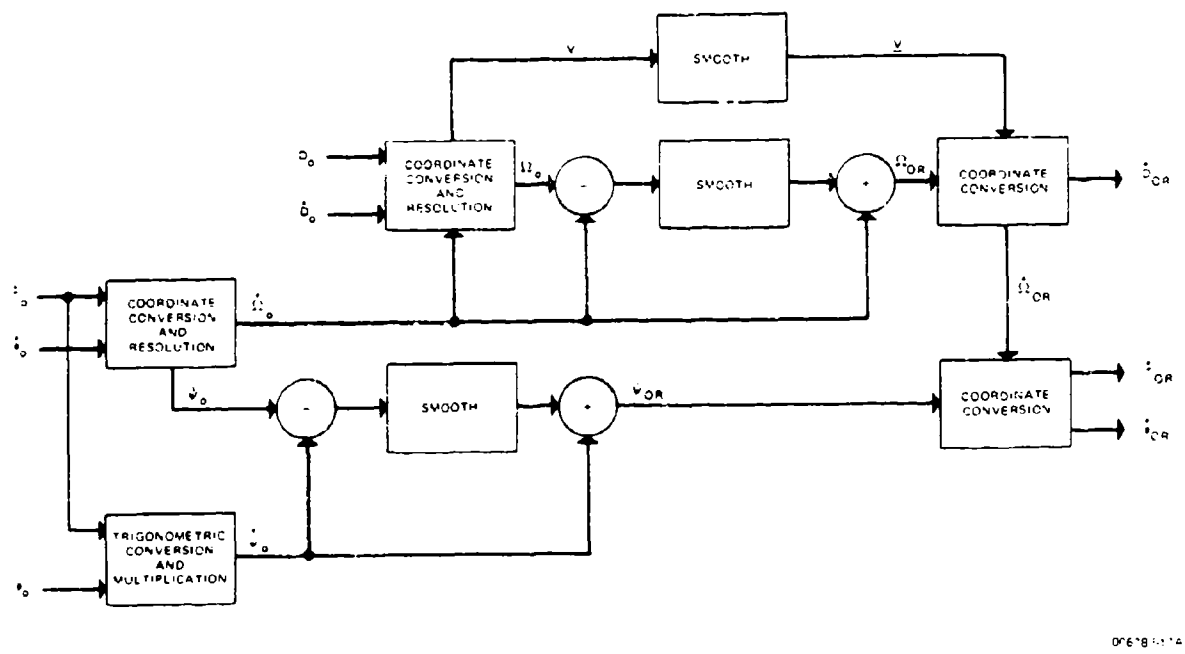

Figure 5-18. Flow Diagram of Regeneration in Polar Coordinates

5.3 REGENERATIVE TRACKING

As previously developed in Sections 4.2, Sensor Characteristics, and 4.3, Operator Performance Characteristics, the angular velocities and accelerations, developed by high velocity targets passing close to AFAADS, and to a lesser degree, the slant range acceleration, create problems in providing control loops which are tight enough to avoid undesirable lags. The human operator performance is most seriously impaired, if only a conventional rate, or a rate-aided tracking control is provided him. This impairment results from the 1 Hz bandwidth equivalent of the man performing a servomechanism function. In the case of radar, although a tight servo will reduce lag, it also passes the whole glint spectrum which results in a standard deviation of tracking error of comparable magnitude to the linear dimensions of the airplane. The ability of the gun to follow high angular velocities and accelerations may also be limited by the torque-inertia parameters feasible in the design.

In a sense, the high accelerations required of the tracking unit to follow an unaccelerated target are an artifact of the coordinate system. Regenerative tracking is based on the assumption that some parameters of the target path are constant, or vary slowly, so that these can be measured and used to regenerate tracking information. The regenerated data can then be fed back to the tracker. The elements of the process are identical with the lead prediction problem in aiming the gun, which also assumes that some parameters of target motion are constant during projectile time of flight.

In addition to assisting the sensors, and if necessary the gun in normal operation of the system, regenerative tracking can assist the system in tracking through intervals where the target is obscured from the sensors. Such obscuration may be caused by smoke at the gun mount, or by terrain obstacles between the tracker and the target. In the case of sensors which occasionally miss a data point (such as current laser range finders), the regenerative process allows the solution to carry through the missing data.

In the early days of radar, when targets were slow, it was possible to track for brief intervals of lost signal by simply freezing the angular tracking rates at their last values. This is not possible for most of the AFAADS operational region because target angular velocity measured at the tracker is usually changing rapidly.

Some operational objectives for regenerative aiding are as follows:

a. The tracking dynamics must be conservative, i.e., the regenerative aid must provide a substantial improvement in tracking accuracy against an unaccelerated target, but it must also provide tracking at least as good as conventional tracking against an accelerated target.

b. When a human operator is in the tracking loop, the system must provide him with consistent and unambiguous response, i.e., any specified control movement must always result in the same dynamic response of the sight reticle. When the man is tracking in two coordinates (elevation-traverse), this consistency is especially important. An elevation adjustment must appear only as an elevation movement of the sight, etc.

c. It is desirable to have regeneration function as a normal element of the tracking loop, rather than cutting it in after tracking has begun. This requires careful design of the regeneration loop with regard to stability and settling time.

d. The system must degrade gracefully. It should function with incomplete inputs; for example, without range, and loss of the range input during a course should not cause loss of target.

e. The system should continue to generate gun orders and regenerated-sensor position based on last measured rates even when all data from the target is lost for a short interval, as when the target passes behind a terrain obstruction or the operator's vision is obscured by smoke.

f. Whether regeneration should be done, using rates determined from the prediction process or separately in a component specifically for this purpose (possibly in the tracking head), is a design trade-off to be resolved from overall system considerations. The optimum rate smoothing function for regenerative tracking is not necessarily the optimum smoothing function for lead prediction, and the compromises involved in merging the functions require an in-depth analysis.

The general concept of regenerating tracking rates was sketched briefly in the prior section on coordinate systems. In the present section we review briefly the magnitude of the lags introduced by conventional tracking loops, and then develop in greater detail the characteristics of regenerative tracking systems.

5.3.1 Control Lags

In this paragraph we consider first servomechanism lags, and then estimate the lags likely to be produced by the human operator.

The AFAADS system will incorporate a number of servo units to drive the sensors, the gun, and some of the computer components. Because of the high angular velocities and accelerations developed in tracking fast close-in targets, servo lag is an important consideration. The principal problems are expected to be associ-

ated with the sensor and gun servos. Servos internal to the system are not expected to be a problem because of the very low inertia of the components they drive.

In the following discussion it should be remembered, however, that the state of the art of servomechanism and associated drive design is sufficiently advanced so that, with the exception of loops including the man functioning as a servo, both the sensor and gun loops can be designed to have small and acceptable lags without regeneration, even against AFAADS courses.

The price paid is in higher maximum torque/inertia capability of the drive, and more stringent design requirements on gear backlash, shafting resilience, and general structural rigidity. In the case of the radar, a wide-band servo will pass more of the glint spectrum, especially with frequency diversity. For AFAADS, however, there is a system optimization trade-off between data smoothing in the radar servo loop and data smoothing in the prediction function. The sensor servo bandwidth would normally be made an inverse function of range to reduce the contaminating effect of thermal noise on the signal to noise ratio at long ranges. At short ranges, it may be better to pass the whole glint spectrum and filter the error caused by glint in the prediction unit.

Gearless drives have been developed for high performance trackers.

The U.S. Navy Mk 74 Gun and Guided Missile Fire Control System, for example, employs a gearless drive motor, built by General Electric. The Mk 73 Director component of this system is driven by an amplidyne - controlled, direct-drive motor. The power drive is a combination of a direct-drive dc motor and an advanced servo control. The stator of the train motor is a part of the structure of the director base, and the rotor is an integral part of the rotating column. A similar arrangement is used in elevation. This system eliminates gear trains in the drive[7].

The error signal is fed through an amplifier, into the control field of an amplidyne generator. The output of the amplidyne generator is connected to the armature of the direct-drive motor which positions the director rotor. All structural members of the equipment have resonances in excess of 20 Hz. This equipment has been in service since 1960.

To estimate the magnitude of servo lag error as a function of servo parameters, consider the conventional method for estimating servo lag, as expressed by the formula:

$$L = (d\theta/dt)K_v + (d^2\theta/dt^2)K_a + (d^3\theta/dt^3)K_3 + \ldots \quad (5.51)$$

where: θ is the function which the servo is trying to match, L is lag, and the K_i are coefficients determined by analysis of the servo transfer function.

It is assumed that the servo is linear in the range being considered.

The 'Design Point' course for AFAADS, which stresses the target following ability most severely, is described by:

Target speed: 600 knots

Minimum horizontal crossing range: 200 meters

Altitude: 200 meters

For a specified minimum horizontal range, maximum elevation acceleration against a level target is experienced when altitude equals minimum horizontal range. Maximum elevation angular velocity is experienced against a slightly higher path, but the maximum differs in magnitude by only 4 percent.

For the given parameters the following maximum derivatives of input functions are obtained:

	Azimuth	Elevation	Slant Range
Velocity	88 deg/sec	21 deg/sec	308 meters/sec
Acceleration	88 deg/sec^2	68 deg/sec^2	472 meters/sec^2

The angle loops are assumed to be closed by first order servos with zero-position lag on constant-position input.

The following table (V-1) lists the values of K_v and K_a, which have been indicated to have been used in various radar tracking servos in the past. Also included are the associated lags on the preceding course.

In all cases, acceleration lag dominates. It should be noted that K_a for the modern conical scan radar was set to reduce the effects of scintillation, and the set is for long range tracking. A much larger K_a would reduce lag, but at the expense of scintillation-caused error.

The value of K_v, under the radar marked 'X', was estimated from results of some extensive field analyses of the performance of a WWII type conical scan pulse radar without MTI against very low flying targets.

At the point on the target path where acceleration peaks, the 1-degree lag corresponds to a linear distance of only 4 meters at the target. However, with a 1-degree beam, a lag of several degrees would cause the radar to lose the target.

Even with large K_a, the higher derivatives might cause problems and would need to be investigated by a complete servo analysis.

Table V-1. Typical Radar-Sensor Servo Lag Coefficients and Lag Components

System	SCR-584	Airborne Radar	Modern Monopulse	Modern Conical Scan	X
Coefficient					
K_v	200 sec^{-1}	125 sec^{-1}	500 sec^{-1}	500 sec^{-1}	12 sec^{-1}
K_a	16 sec^{-2}	13 sec^{-2}	90 sec^{-2}	0.63 sec^{-2}	Unknown
Azimuth Lag					
Velocity	0.04 deg	.07 deg	0.02 deg	0.02 deg	7.3 deg
Acceleration	5.5 deg	6.8 deg	1.0 deg	140 deg	Unknown
Elevation Lag					
Velocity	0.01 deg	0.02 deg	0.004 deg	0.004 deg	1.7 deg
Acceleration	4.2 deg	5.2 deg	0.8 deg	108 deg	Unknown

Note: 1 degree = 17.7 mils

00678-519

For an instrumentation servo, values of K_v = 500 sec^{-1} and K_a = 3330 sec^{-2} have been reported. These values should allow adequate following of the angular information within the computer. Lags in the range servo and the range-rate servos (in the case of doppler range-rate measurements) are not considered to represent a problem because of the very light loads on the servos. In addition, a range error affects prediction error principally through the computed average shell velocity which is a second order effect. One estimate for a range servo indicates K_v = 2000 sec^{-1} and K_a = 90 sec^{-2}. In all-electronic ranging systems, servos are not required.

5.3.1.1 Simulation Runs

To indicate the effect of sensor lag, when the errors propagate through the complete prediction function, the Ginsberg simulation was run with zero noise input and lag inserted by Equation 5.51 to two terms. For all three coordinates, K_v = 500 sec^{-1} and K_a = 90 sec^{-2} were used, overemphasizing the probable range error. Figures 5-19 and 5-20 show the results in terms of the errors at the closest approach of shell to target using Vigilante ballistics. The computation was printed out at one second intervals of present time.

The magnitudes shown in the figures indicate that errors at the target, caused by sensor lag are of comparable magnitude to those estimated from Equation (5.51). The error caused by azimuth lag changes sign at midpoint, where the contributions of elevation and range lag are maximum. The root mean square angular miss curve and the curve of linear miss (distance of closest approach of projectile to the target) may in fact have cusps at the peak for this reason, but the one-second printout of the data chosen for these runs is not sufficiently fine-grained to show this detail.

The simulation runs were then repeated with gun lag in addition to sensor lag. Coefficients for the gun servos were set at K_v = 250 sec^{-1} and K_a = 50 sec^{-2}. Results are shown in Figures 5-21 and 5-22. The errors with the previously noted coefficients are all unacceptably large.

5.3.1.2 Estimated Lags Introduced by Human Operator

As developed in Section 4.3 there is a limited basis for approximating the lag of a human operator employing rate-aided tracking in terms of the coefficients K_v = 10 sec^{-1} and K_a = 9 sec^{-2}. More extensive data on position tracking suggests that in this case one might estimate K_a as high as 30 and K_v as high as 20 (Systems Technology, Inc.) or 40 (Elkind). For rate tracking alone, extensive data indicates a maximum value of K_v of only about 5 sec^{-1}. In view of the miss distance developed on the simulation with much higher performance servomechanisms in the tracking loop, a human operator would not be expected to perform satisfactorily on the chosen course without regenerative aid. How badly the man *can* perform is indicated by the experimental manual tracking data obtained in the tracking experiment for which the radar coefficients were designated 'X'. For manual tracking, the effective K_v was 1/2 sec^{-1}.

5.3.1.3 Reduction in Servo Lag

A servo loop with K_v > 3000 sec^{-1}, K_a > 500 sec^{-2}, and appropriately higher coefficients will develop no lag problems. It is believed that these values are within the state of the art, even for gun servos. If these values

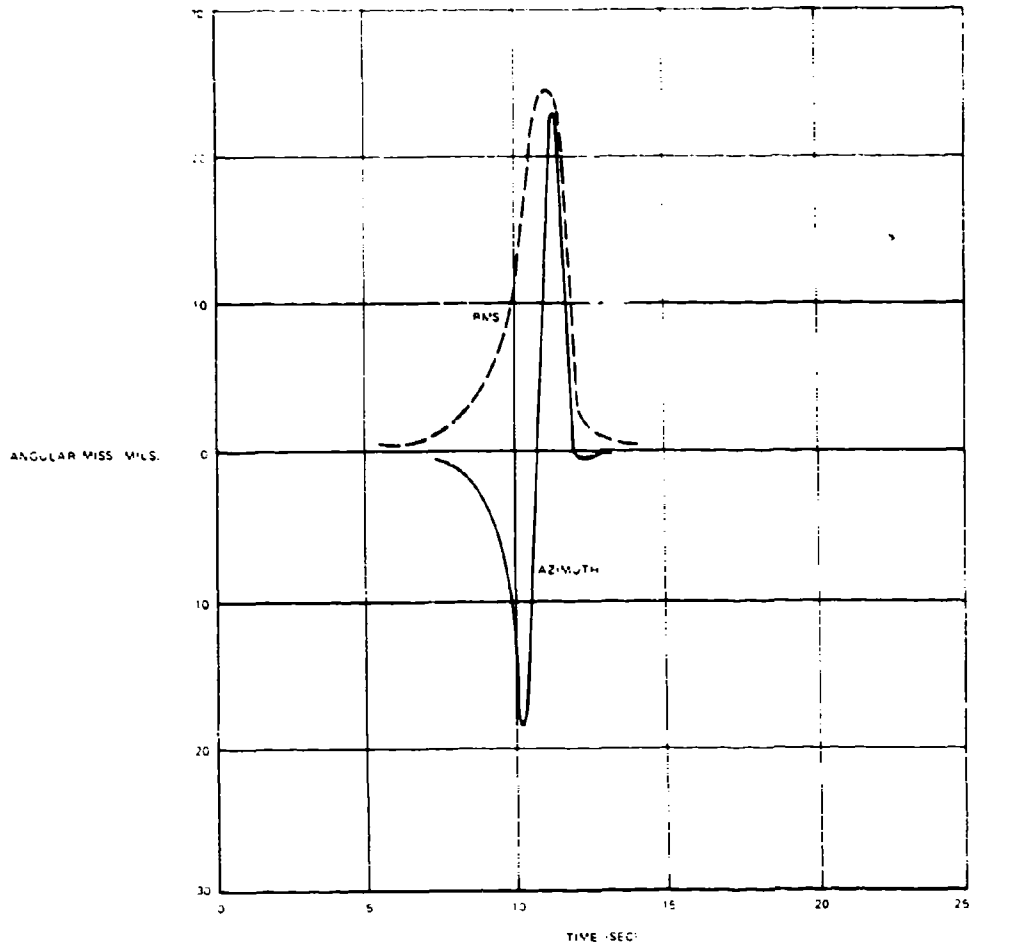

Figure 5-19. Angular Miss Caused by Sensor Servo Lag

are not attainable because of limited available torque/inertia capability, or for other reasons, various other methods of lag compensation are possible. One method, which has had some operational use, is to correct the sensor output signal electronically by adding the error signal measured in the servo loop. This does not reduce the physical pointing error of the sensor, but it improves the accuracy of the output data. Another method is to compute the expected sensor lag from the smoothed rates in the computer, and then inject a lag correction between the sensor output and the computer input. This method depends on the constancy of servo performance parameters and will fail if the servo is out of adjustment. However, since it is easy to test on the present level of simulation detail, a few simulator runs, described in the following paragraphs, were made of this mode to test stability. The method also does not reduce actual sensor pointing error.

Sensor pointing error can also be reduced by injecting a compensating signal into the sensor error measurements, which in effect, 'boosts' the servo by giving it advance warning of high velocity and acceleration requirements. This is probably the preferred solution.

The latter two methods are described below. Although they use some of the elements of a regenerative tracking function, their objective is limited to reducing sensor lag in continuous tracking.

System elements are shown in Figure 5-23, which

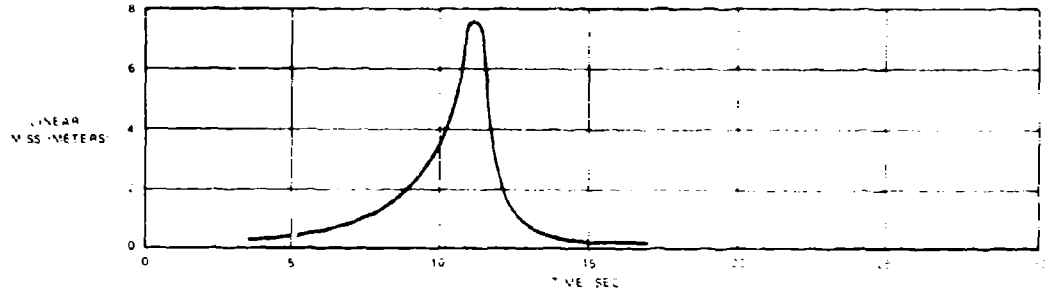

Figure 5-20. Linear Miss Caused by Sensor Servo Lag

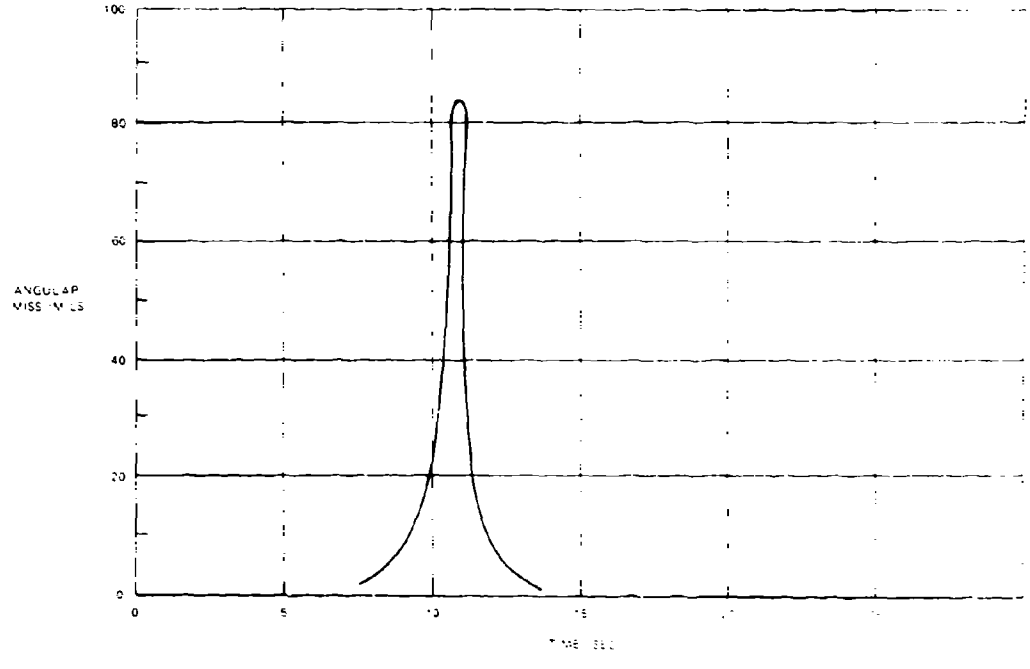

Figure 5-21. Angular Miss Caused by Sensor and Gun Servo Lags Combined

defines the notation. In terms of the transfer function Y_s, Y_r:

$$\theta_o/\theta_i = \left[1 + Y_s^{-1} - Y_r\right]^{-1} \qquad (5.52)$$

where Y_r is the feed-forward transfer function for lag compensation. K_v, K_a can be identified for the uncompensated servo by expanding this ratio in general as a series in s, so that:

$$\theta_o/\theta_i = 1 - \left(s/K_v\right) - \left(s^2 K_a\right) - \ldots \qquad (5.53)$$

and solving for Y_s^{-1}:

$$Y_s^{-1} = \left(s\,K_v\right) + s^2\left(K_v^{-1} - K_v^{-2}\right) + \ldots \qquad (5.54)$$

The servomechanism will have no velocity or acceleration lag if, to terms in s^2:

$$Y_r = Y_s^{-1} \qquad (5.55)$$

We therefore desire a feed-forward signal to inject in the servo error input which is:

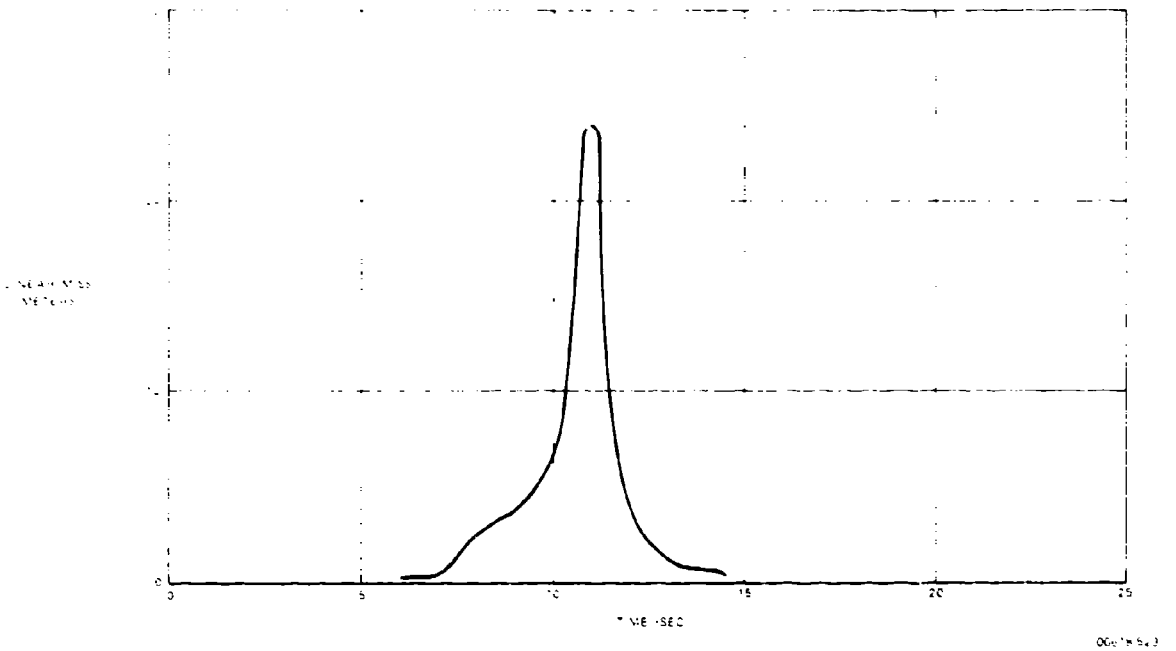

Figure 5-22. Linear Miss Caused by Sensor and Gun Servo Lags Combined

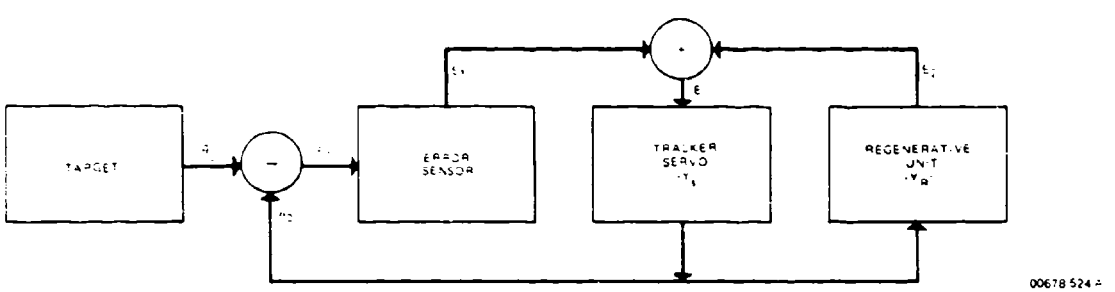

Figure 5-23. Elements of Lag Compensating System

$$E_2 = \theta_r K_v^{-1} + \theta_r \left(K_a^{-1} - K_v^{-2} \right) \qquad (5.56)$$

where the subscript 'r' designates 'regenerated' velocity and acceleration computed from the smoothed, and hence delayed, velocities developed in the smoothing unit.

Since even smoothed measurements of acceleration are expected to be unacceptably noisy, it is considered preferable to assume that the target is flying an unaccelerated course, and compute the geometric accelerations from velocities on this assumption. This is an acceptable assumption even when the target is accelerated, as is shown in a later paragraph.

The particular algorithms used will depend on the coordinate system employed in regeneration. As an example, algorithms are developed on the assumption that a rectangular coordinate system is used, with target velocities smoothed in rectangular coordinates.

From the rectangular coordinate system shown previously in Figure 5-14 with the notation there defined, the polar coordinate rates are easily determined in terms of the rectangular components of target velocity

V_x, V_y, and V_z (symbol Z is used for H in the interest of uniformity of notation) as:

$$R^2\dot{A} = YV_x - XV_y \quad (5.57)$$

$$D^2\dot{e} = RV_z - Z\dot{R} \quad (5.58)$$

$$R\dot{R} = YV_y + XV_x \quad (5.59)$$

$$D\dot{D} = R\dot{R} + ZV_z = XV_x + YV_y + ZV_z \quad (5.60)$$

Next, on the assumption that the target path is unaccelerated, the polar coordinate accelerations are determined from the preceding relations as:

$$R\ddot{A} = -2\dot{R}\dot{A} \quad (5.61)$$

$$\ddot{R} = R(\dot{A})^2 \quad (5.62)$$

$$D^2\ddot{e} = -2D\dot{D}\dot{e} - R(\dot{A})^2Z \quad (5.63)$$

$$D\ddot{D} = (D\dot{e})^2 + (R\dot{A})^2 \quad (5.64)$$

This is sufficient information to develop the desired feed-forward lag correction signal.

Because of the way that accelerations are computed, the system is inherently non-linear. An in-depth analysis of response time and stability needs to be made to ensure satisfactory performance.

It was possible to make a quick determination of the probability of system stability by considering the recirculation of the corrective signal through the regenerative loop on the simulator. This is equivalent to imposing the lag correction at the servo output.

Because of insufficient time, no attempt was made to optimize the combination of smoothing function and feed-forward function. In the available velocity smoothing element of the simulation, velocities were smoothed by least-squares weighting over a 0.4 sec 5-point memory. The initial transient was extremely large. The system response consisted of a rapidly damped component, and a very lightly damped ripple, the latter of which is a characteristic of improperly compensated sampling feedback systems. However, the system was stable. Figure 5-24 shows that the principal error decayed in about 0.8 sec. Figure 5-25 shows that the ripple persisted for 5 seconds. Both characteristics are unsatisfactory, but correctable by better design.

When the feed-forward signal injection was delayed until the rate measurements had settled (0.4 sec) neither the initial transient nor the ripple appeared, and the simulation generated the proper lag correction over the remainder of the course.

Since stability of this non-linear 3-dimensional system has been demonstrated, it seems probable that

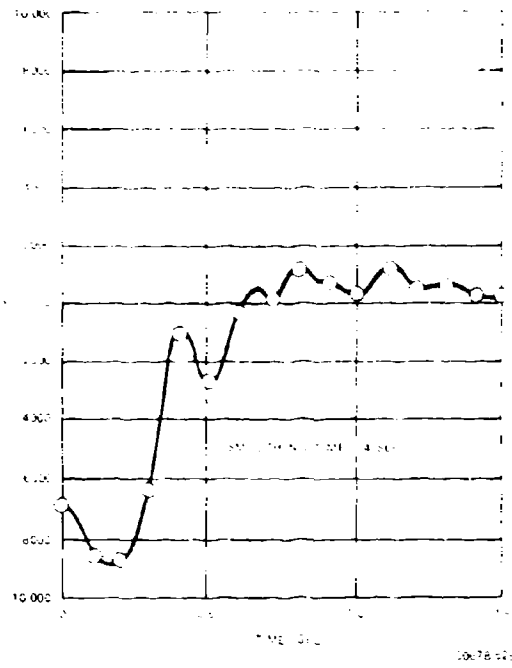

Figure 5-24. Settling Time of a Lag Correcting Circuit.

further analysis, by applying conventional techniques for designing sampled servo systems, will eliminate ripple and allow substantial reduction and shortening of the initial transient. However, the intimate interaction with the velocity weighting function should be noted.

5.3.1.4 Lag Compensation for Gun Servos

The method of injecting an anticipatory signal into the error signal of the servo loop can be used to reduce the lag of the gun servos, if they do not have sufficiently large K_v, K_a . . . The gun can be considered to be pointing (except for minor ballistic corrections) at a point which leads the real target by: target velocity x time of flight. If V is target velocity, this point has a velocity of V $(1 + t_p)$. Gun angular velocities and accelerations can be computed using the equations developed earlier for the sensor, but using the velocity of the predicted point.

Injection of this correction in the gun servo loop is more straightforward, since the gun motion does not feed back into the velocity measurements.

The necessary expressions are developed in the following paragraphs.

The gun points at a target moving at a velocity V $(1 + t_p)$. Then a method of computing velocities in

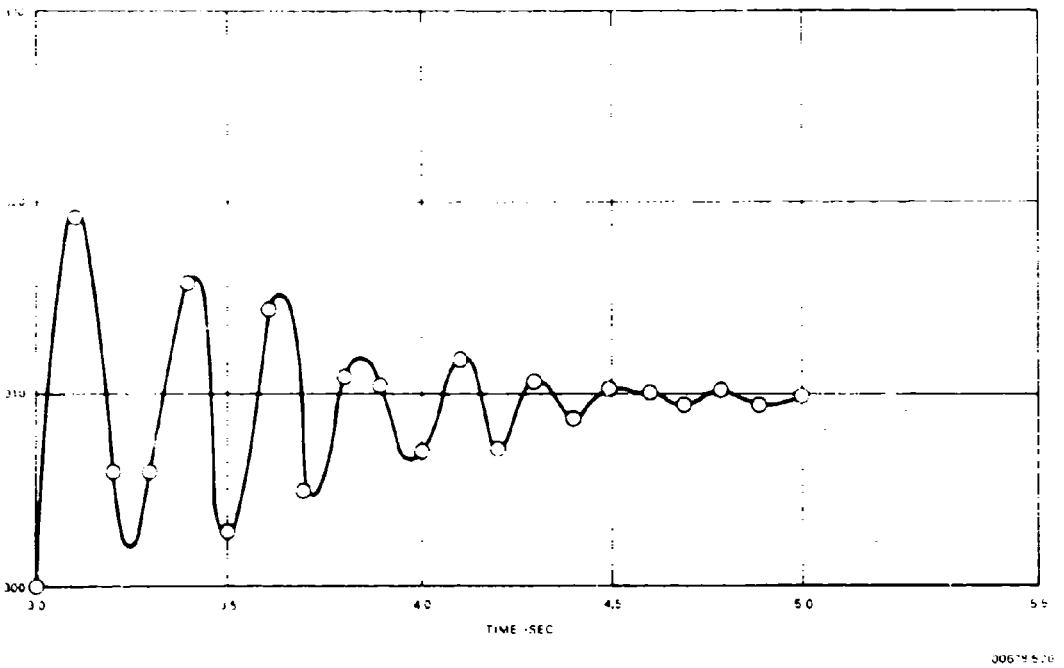

Figure 5-25. Undesired Ripple in a Lag Correcting Circuit

gun coordinates is to use the expressions given as Equations (5.57) through (5.60) but multiplied by $(1 + \dot{t}_p)$, i.e.:

$$\dot{A}_p = \dot{A}_{p1}(1 + \dot{t}_p) \qquad (5.65)$$

$$\dot{e}_p = \dot{e}_{p1}(1 + \dot{t}_p) \qquad (5.66)$$

$$\dot{R}_p = \dot{R}_{p1}(1 + \dot{t}_p) \qquad (5.67)$$

$$\dot{D}_p = \dot{D}_{p1}(1 + \dot{t}_p) \qquad (5.68)$$

where the subscript '1' indicates the values computed without correction for rate of change of time of flight.

To obtain $\dot{t}_p$, consider the expression for D_p:

$$\dot{D}_p = \dot{D}_{p1}(1 + \dot{t}_p) \qquad (5.69)$$

and since

$$dD_p/dt = (dD_p/dt_p)(dt_p/dt), \qquad (5.70)$$

then

$$\dot{D}_p = \dot{t}_p v_r \qquad (5.71)$$

where:

$$v_r = dD_p/dt_p = \text{projectile remaining velocity at } D_p \qquad (5.72)$$

$$\dot{t}_p = \dot{D}_{p1}/(v_r - \dot{D}_{p1}) \qquad (5.73)$$

At midpoint where the lag correction is needed most, t_p is very small, and hence can probably be taken as zero.

To obtain accelerations, note that we can write:

$$\ddot{D}_p = v_r \ddot{t}_p + a_r(\dot{t}_p)^2 \qquad (5.74)$$

where:

$$a_r = d^2D_p/dt_p^2 \qquad (5.75)$$

The term a_r is simply the deceleration of the shell along its trajectory, and can be approximated as:

$$d^2D_p/dt_p^2 = -kv_r^{a_1} \qquad (5.76)$$

where k, σ_1 are projectile characteristics.
then:

$$\ddot{A}_p = \ddot{A}_{p1}(1+\dot{t}_p)^2 + \dot{A}_{p1}\ddot{t}_p \qquad (5.77)$$

$$\ddot{e}_p = \ddot{e}_{p1}\left(1 + \dot{i}_p\right)^2 + \dot{e}_{p1}\,\ddot{i}_p \qquad (5.78)$$

$$\ddot{D}_p = \ddot{D}_{p1}\left(1 + \dot{i}_p\right)^2 + \dot{D}_{p1}\,\ddot{i}_p \qquad (5.79)$$

$$\ddot{i}_p = \left[\ddot{D}_{p1}\,v_r^2 - \left(\dot{D}_{p1}\right)^2 a_r\right] \cdot \left(v_r - \dot{D}_{p1}\right)^3 \qquad (5.80)$$

If D_p and hence i_p are very small, so that their contribution to the rate computation can be neglected, then:

$$\ddot{i}_p \sim \ddot{D}_{p1}/v_r \sim V^2/(v_r D_p) \qquad (5.81)$$

5.3.2 Complete Regenerative Tracking

The tracking system with complete regenerative tracking is shown schematically in Figure 5-26. For completeness, the lag correction signal is shown explicitly, although it might not be needed, depending on the servo characteristics. In normal operation the tracker servo reproduces the regenerated target position, but superimposes on the regenerated data the corrections responsive to the tracking error which is measured directly by the sensor. If the target is obscured, this error input is interrupted and the tracker operates on regenerated rates only. Also shown is the input from an outside source such as the surveillance radar which allows the tracking sensors to be put on target automatically.

Implementation of the regenerative function is straightforward when the loop is closed by a servomechanism and follows the flow diagrams shown in Section 5.2. When the error sensor in Figure 5-26 is a man and angular tracking is considered, there is a further consideration having to do with the objective of providing a position component in the man's control.

As discussed in Section 4.3, one would like the movement of the operator's sight to be related to the movement of his control, in spite of intervening dynamics, according to the aided tracking relation:

$$\theta_{cl} = K\theta_c\left[1 + (sT)^{-1}\right] \qquad (5.82)$$

This could be done in the circuit of Figure 5-26 by making the error signal E (shown as emitting from the sensor) proportional to the movement of the man's control. If his control is a Frankford Arsenal 'ball' there is no problem, because the ball has unlimited rotation. However, with a handlebar or joystick control, the accumulated errors in integrating the regenerated rates would eventually require a position error correction beyond the limits of movement of the control. This can be prevented by making the operator's control movement simultaneously a position input and an input to the regenerated rate integrator. His control

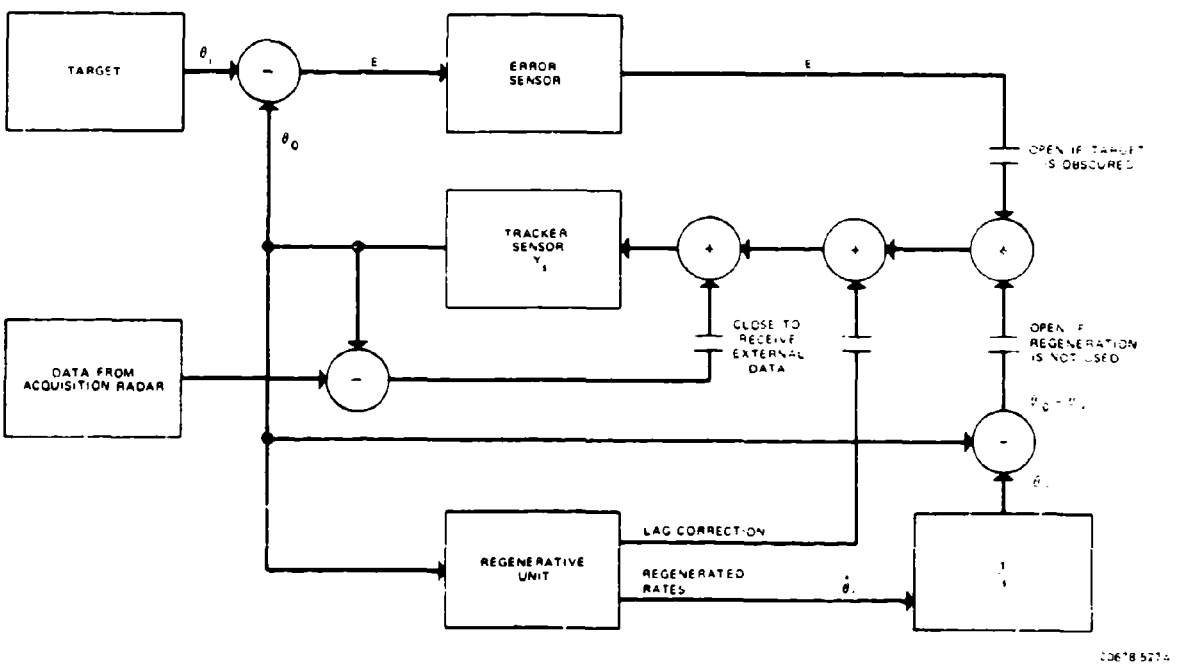

Figure 5-26. Elements of a Regenerative Unit with Servo Lag Correction

will then respond (except for delays in the tracker servo response) as:

$$\theta_o = K\theta_c \left[1 + (sT_1)^{-1} + (sT_2)^{-2}\right] \quad (5.83)$$

This response, although less desirable than Equation (5.82), should permit more precise tracking than that possible with a simple rate control, even when the latter has a regenerative aid.

It appears that the regenerative tracking system provided on the present Vigilante system corresponds to the operator control law:

$$\theta_o = (K\theta_c s)[1 + (sT)^{-1}] \quad (5.84)$$

i.e., lagged rate tracking.

If the circuit has been correctly understood, there is no position component. It might be expected therefore to provide tracking accuracy superior to rate tracking without regeneration, but less precise than the same system with a direct position component.

The elements of the regenerative unit with manual control are shown in Figure 5-27. Only the horizontal plane solution is shown for simplicity. An alternate configuration, in which the regenerative unit develops regenerated present position rather than velocities, is shown in Figure 5-28. The smoothed values of X and Y must be updated to present time by using smoothed velocities, hence the overall dynamics should be identical. However, the system of Figure 5-27 has the advantage that it can operate as conventional aided tracking if the regeneration elements fail.

5.3.2.1 Effect of Target Acceleration

It is desired that regenerative tracking assist the operator (man or machine) principally when the target is unaccelerated and that it not degrade tracking performance by providing conflicting information when the target accelerates. It is easily shown that the requirements on the tracker to follow the polar components of target motion caused by target acceleration are relatively light; so that regenerative tracking will help in this case also.

Consider azimuth tracking. If the target is turning in a horizontal plane at a rate of turn ω_a, there will be two components of azimuth motion not provided by the regeneration. One is caused by the target acceleration directly. The second is caused by the fact that the regenerated rates are developed from smoothed (hence lagging) target velocities, so that the regenerated rates will correspond to the target direction at the midpoint of the smoothing interval.

A target rate of turn ω_a causes an azimuth acceleration, from this source alone, of:

$$\ddot{\alpha} = V\omega_a \cos\alpha / R_t \quad (5.85)$$

and:

$$\ddot{\alpha} = ng\cos\alpha / R_t \quad (5.86)$$

where n is number of g's acceleration.

This is at maximum when the target is headed directly at the tracker. For example, a 5g turn at 200 meters represents an azimuth acceleration of 250 mils/sec^2. This 'worst case' value is substantially less than the maximum value of geometric acceleration.

During a time $T_s/2$, where T_s is smoothing time, target heading changes by $\omega_a T_s/2$, corresponding to a change in angular rate of:

$$\Delta\dot{\alpha} = (V/R_m)\sin\alpha\cos\alpha\,\omega_a T_s \quad (5.87)$$

$$= (\omega_a T_s/R_m)\sin\alpha\cos\alpha \quad (5.88)$$

For 2-sec smoothing, a 5g turn, and R_m = 200 meters, the angular velocity deficiency in the regenerative tracking circuit will be 250 mils/sec. Again, this value is substantially less than the maximum value of the geometric component.

It is concluded that the assumption of an unaccelerated target for the regenerative tracking system is satisfactory, and that such a system will provide substantial assistance, even against accelerated targets. In azimuth, the unregenerated angular velocity and acceleration components have maximum values only about one-sixth of the respective total values.

5.3.2.2 Regeneration with Partial Information

The algorithms, described in the preceding section, have been based on the simultaneous use of range-, azimuth-, and elevation-input information. A few algorithms employing information in fewer than three coordinates are described in the following paragraphs.

Range can be regenerated from range information only. This is possible because the second derivative of the square of range is constant, when the target is unaccelerated. This may be seen from the following relationship:

$$D^2 = D_m^2 + x^2 \quad (5.89)$$

where:

D_m = minimum horizontal range

x = distance along the target path from the target to the point of minimum range

then:

$$d\,dt(D^2) = -2Vx \quad (5.90)$$

where:

V = target velocity

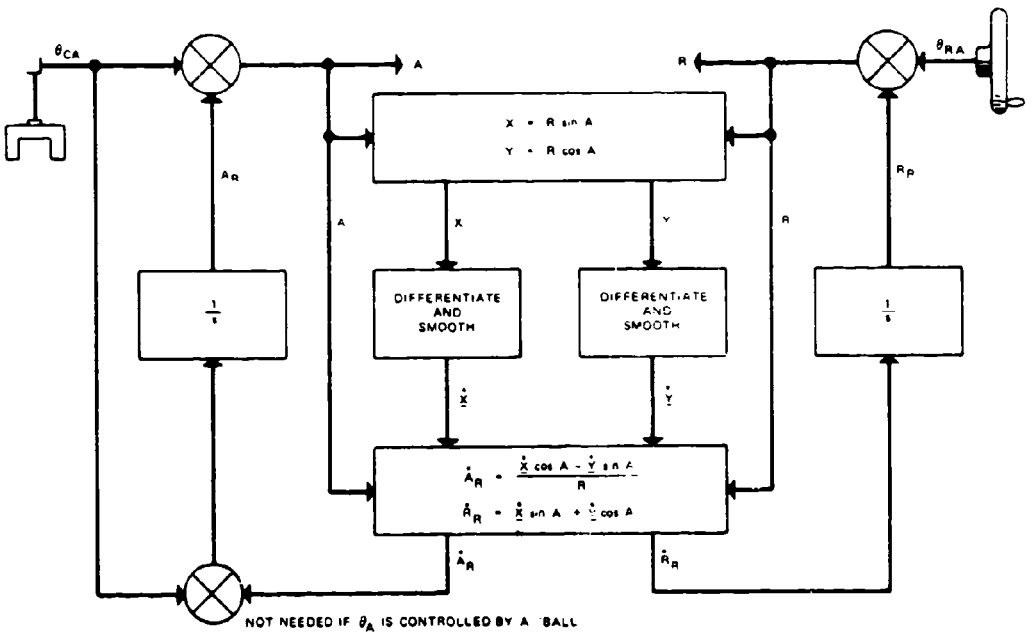

Figure 5-27. Velocity Regeneration in the Rectangular Coordinate System

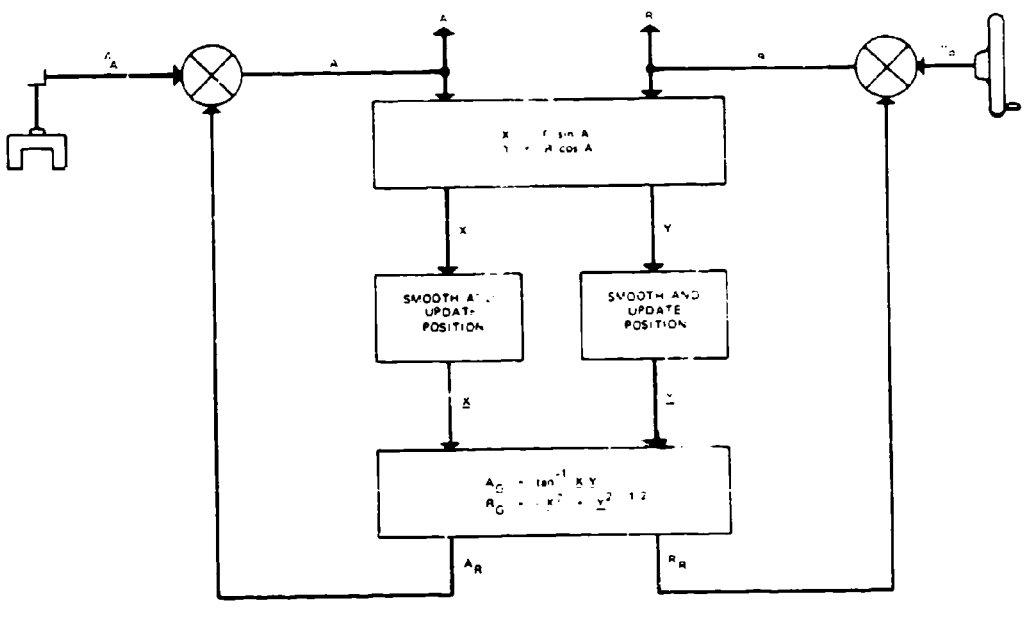

Figure 5-28. Position Regeneration in the Rectangular Coordinate System

and finally:

$$d^2/dt^2(D^2) = 2V^2 = \text{constant} \qquad (5.91)$$

Figure 5-29 shows a regenerative unit when range-only is available. Figure 5-30 shows a regenerative unit for use when both range and range rate (from a doppler radar or laser) are available.

The former loop can be closed by a man instead of a servo. The integration of acceleration can be given a relatively long time constant to minimize the effect of the phase lag on the man.

Doppler rates are sufficiently precise so that the system shown in Figure 5-30 may have relatively short time constants. It should be useful in assisting the doppler radar to track continuously through nulls in the doppler signal.

It is interesting to note that both systems allow time of flight to be computed with no additional information, according to the relations:

$$D_p^2 = D_o^2 + t_p\left[d/dt\left(D_o^2\right)\right] + (1/2)\,t_p^2\left[d^2/dt^2\left(D_o^2\right)\right] \qquad (5.92)$$

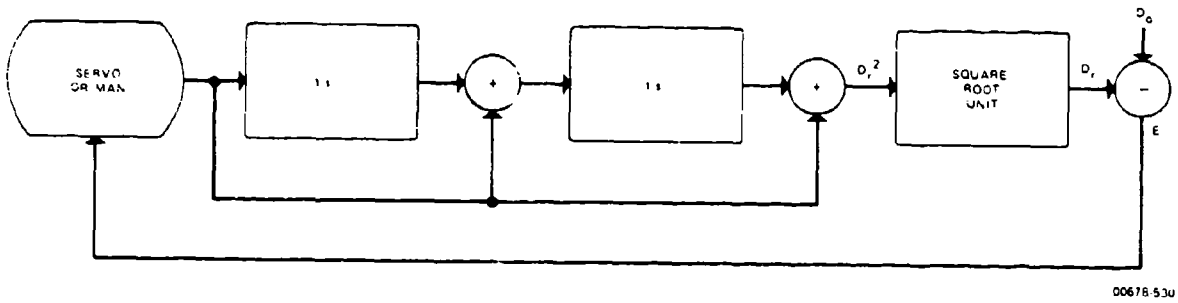

Figure 5-29. Elements of a Range Regeneration System

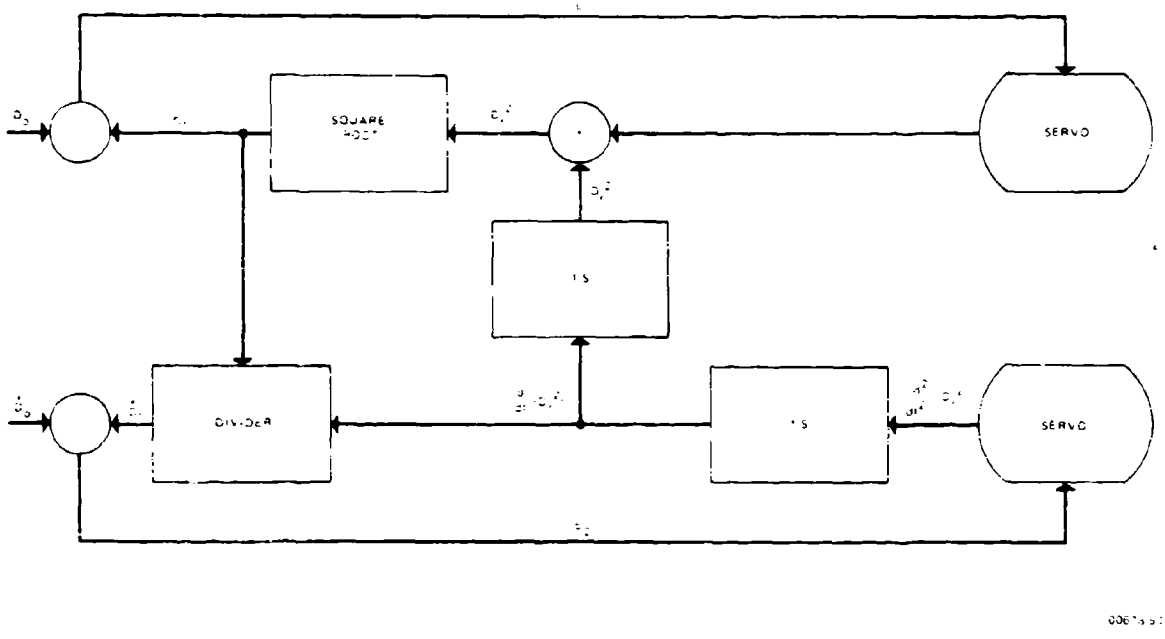

Figure 5-30. Elements of a Range Regeneration System with Doppler Rate Input

$$t_p = t_p(D_p) \qquad (5.93)$$

The effect of noise on the computation needs to be investigated. However, it is probable that the system incorporating Doppler rates would be entirely satisfactory.

Both systems should be helpful in the laser servo loop to assist in carrying through missed measurements.

5.3.2.3 Azimuth Regeneration

It should be possible to regenerate azimuth on a similar basis, using no more than two integrators. This follows from the relations:

$$\cot \alpha = x/R_m \qquad (5.94)$$

$$d/dt(\cot \alpha) = V/R_m = \text{constant} \qquad (5.95)$$

$$d^2/dt^2(\cot \alpha) = 0 \qquad (5.96)$$

Both α and the parameter V/R_m are initially unknown. The rate of change of α is known as:

$$d\alpha/dt = -dA_0/dt \qquad (5.97)$$

where: A_0 is the azimuth angle from an arbitrary reference.

However, it has not been possible to develop an appropriate regenerative circuit using azimuth alone in the available time. For the reader who wishes to do this we note two additional relations that may be helpful:

$$2\ddot{A}\dot{A} = 3(\ddot{A})^2 - 4(\dot{A})^4 \qquad (5.98)$$

which can be put into the form:

$$d^2/dt^2[(\dot{A})^{-1/2}] = (\dot{A})^{3/2} \qquad (5.99)$$

5.3.2.4 Solution with Estimated or Intermittent Range Inputs

A possible degraded mode of operation of the AFAADS system is one in which range information is denied (ECM or range finder inoperative), or intermittent (widely spaced laser returns). In either case we would like the regeneration and prediction functions to operate smoothly and as accurately as possible between measured or estimated range inputs.

An applicable relation is:

$$|\dot{\Omega}_0|D_0^2 = V D_m \qquad (5.100)$$

where Ω_0 is angular velocity of the sight line in the slant plane and:

$$\dot{\Omega}_0^2 = \dot{e}_0^2 + (\dot{A}_0 \cos e_0)^2 \qquad (5.101)$$

These relations may be used as shown in Figure 5-31. From the normal angular tracking process, Ω_0 is generated. An estimated value of the parameter VD_m is set in and a resolving unit computes and displays D_0. The operator need not know the value of VD_m but simply adjusts its input until the D_0 reading agrees with his estimate of range. On a one-man mount this is a busy operation for the operator. However, once set, D_0 will change smoothly and can be fed to the computer.

If intermittent range measurements are obtained from a laser, a servo can close the loop and refine the setting of VD_m with each measurement so that the generated D_0 matches the measured point.

In this scheme, range will be as noisy as the angular velocities and the system requires further analysis in detail supported by computer simulation

5.4 PREDICTION AND FILTERING

The most critical element of input data for the design of an optimum AFAADS system is the quantitative description of target paths. One would like to know the relative frequency of occurrence, duration, and relative importance of path segments of various types. This information is lacking. It can be argued that since the flight path is, to a considerable degree, a matter of choice of the pilot, such a compendium could not be produced. However, the pilot does not have complete freedom of choice, since he has a mission to accomplish within constraints imposed by aircraft maneuverability, weapon type, and weapon fire control system.

The purpose of the extended discussion of Target Characteristics in Section 4.1 was to attempt to identify and quantify the types of target paths with which AFAADS must cope. However, it is clear that to maximize the effectiveness of its antiaircraft effort in the long run, the Army should maintain a continuous effort to accumulate and analyze, on a systematic statistical basis, records of real aircraft on actual military missions within the range of antiaircraft fire.

From the current examination of target characteristics, the following elements have been abstracted as a basis for considering what kinds of prediction modes should be considered for AFAADS.

The range of speed should be from zero to about Mach 1.5. Although most attacks on ground targets will be conducted at subsonic speeds, strafing attacks at supersonic speeds are possible. It is believed that target velocity will normally increase in a dive, and decrease in a climb or high-g turn.

The largest values of target acceleration will occur in a direction normal to the flight path.

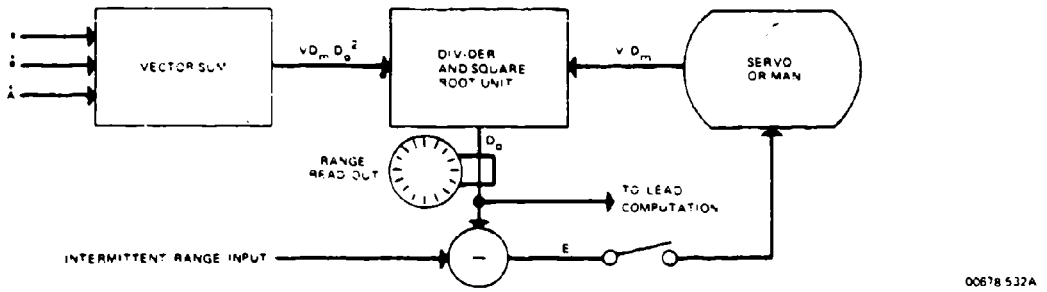

Figure 5-31. Elements of a Range Regeneration from Angular Velocity System

Current airborne fire control systems require that the aircraft fly a line segment that is approximately straight for a short period of time prior to the release of iron bombs. Advanced fire control systems may eliminate the straight segment, but their accuracy remains to be proven. A strafing attack will normally have a straight line trace in the ground plane.

The most 'normal' maneuver for an aircraft is a constant rate of turn, which can be maintained with the controls approximately centered. This includes a straight line as a special case. A pilot who has reached the target area and is visually searching for his target may hold a relatively constant rate of turn as he searches.

Since the time to turn through a given angle is:

$$T = V\theta/(ng) \qquad (5.102)$$

where θ = angle, V = aircraft speed, and n is the number of 'g' of radial acceleration, the time to turn can be relatively long at high speeds. Thus, a pilot turning for a second pass on a target and flying at 250 meters/second will require 40 seconds to turn 180 degrees at 2g and 16 seconds at 5g. At 75 knots, a helicopter turning at 2g would require 4.8 seconds. The turn, if performed totally within the AFAADS envelope or even in part, would thus persist for longer than the projectile time of flight, thus the aircraft might be engaged with a curvilinear prediction. The radius of turn of the helicopter would be only 280 meters; however for an aircraft at 5g, it would be 1300 meters. Figure 5-32 depicts the radius of a turn for an aircraft flying at various speeds. Figure 5-33 graphically represents the time of an aircraft to turn 90 degrees for a given speed.

The effect of flight roughness caused by air turbulence has a small effect on prediction error as compared with other causes of error. However, the irregularity of flight path produced by terrain following creates a serious problem in prediction, and must be dealt with explicitly.

Deliberate 'jinking' by pilot on a passing, but not terrain-following path, can substantially degrade a prediction scheme. A similar problem is created by the evasive maneuvers of a helicopter after it has released its air-to-ground armament.

We conclude, therefore, that it is necessary to examine a number of prediction options on plausible courses. As long as the target aircraft has a straight line segment in its repertoire of attack paths, this should be the basic element of the AFAADS prediction option, since the payoff in target kills is highest when it occurs.

Additional options have the highest priority if they widen the variety of attack paths that can be engaged successfully without degrading the effectiveness against a low-acceleration target. An option such as curved flight prediction must be used with discretion because of the time involved in switching back to straight line prediction when the target stops turning. Even though the predictor may make the transition in negligible time, the effect at the target will be delayed by projectile time of flight.

Whether option changes should be at the discretion of the operator or the computer is to be determined. It is probable that the computer should make decisions, among those allowed it a priori by the operator with operator override control.

The number of options to be included depends on the cost in terms of computer complexity and their effectiveness. Comparative effectiveness will be presented later from simulation runs.

The effectiveness of prediction depends on the quality of the input data as well as the prediction algorithm, hence prediction and data filtering are complementary parts of the same problem. In the following paragraphs, prediction algorithms are discussed on the assumption that data smoothing is done properly. In a later section, methods of data smoothing are discussed.

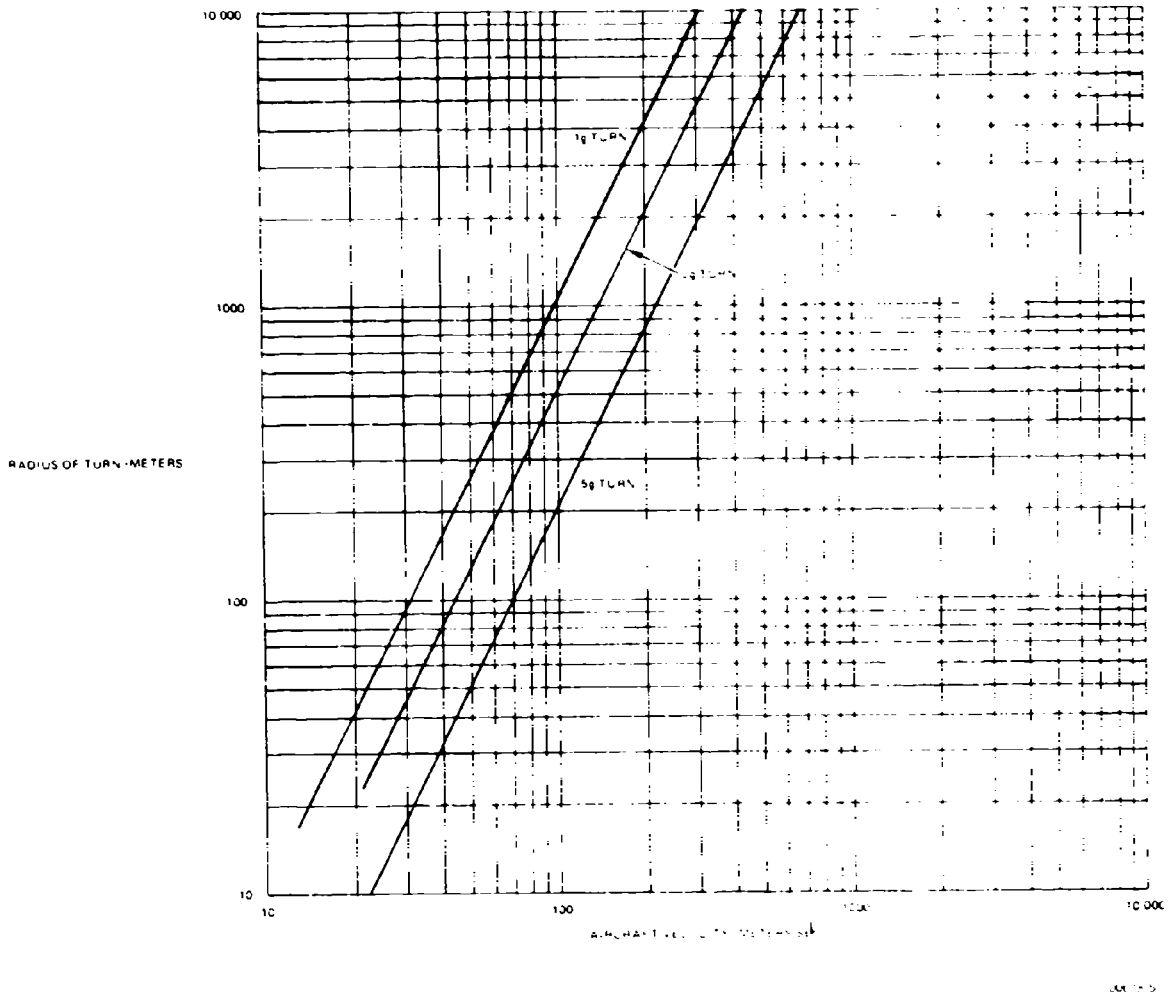

Figure 5-32. Radius of Turn e - Function of Aircraft Speed

5.4.1 Prediction Algorithms

The following discussion begins with the conventional polynomial predictors and then continues to more exotic types. This discussion will be phrased in terms of a rectangular coordinate system, although it will be recognized, as previously discussed in the section on coordinate systems, that similar operations can be performed in other coordinate systems, usually at the expense of considerable additional trigonometry.

Beginning with the assumption that target present position has been transformed to rectangular coordinates, it is desired to compute a predicted position. Following Blackwell, the elements of a polynomial predictor (up to and including acceleration) are shown in Figure 5-34 in Blackwell's notation.

s are weighting functions applied to posi- ments. The outputs of the three weighting erations are, respectively, smoothed posi- y, and acceleration. Both coefficients k_1, k_2 output of the filter above it for lag caused moothing time (they update the smoothed estimate to present time), and extrapolate the smoothed polynomial for time of flight α.

Typical values of k_1 and k_2, for the same equivalent smoothing times T_s in each derivative, are:

$$k_1 = \alpha + (T_s 2) \qquad (5.103)$$

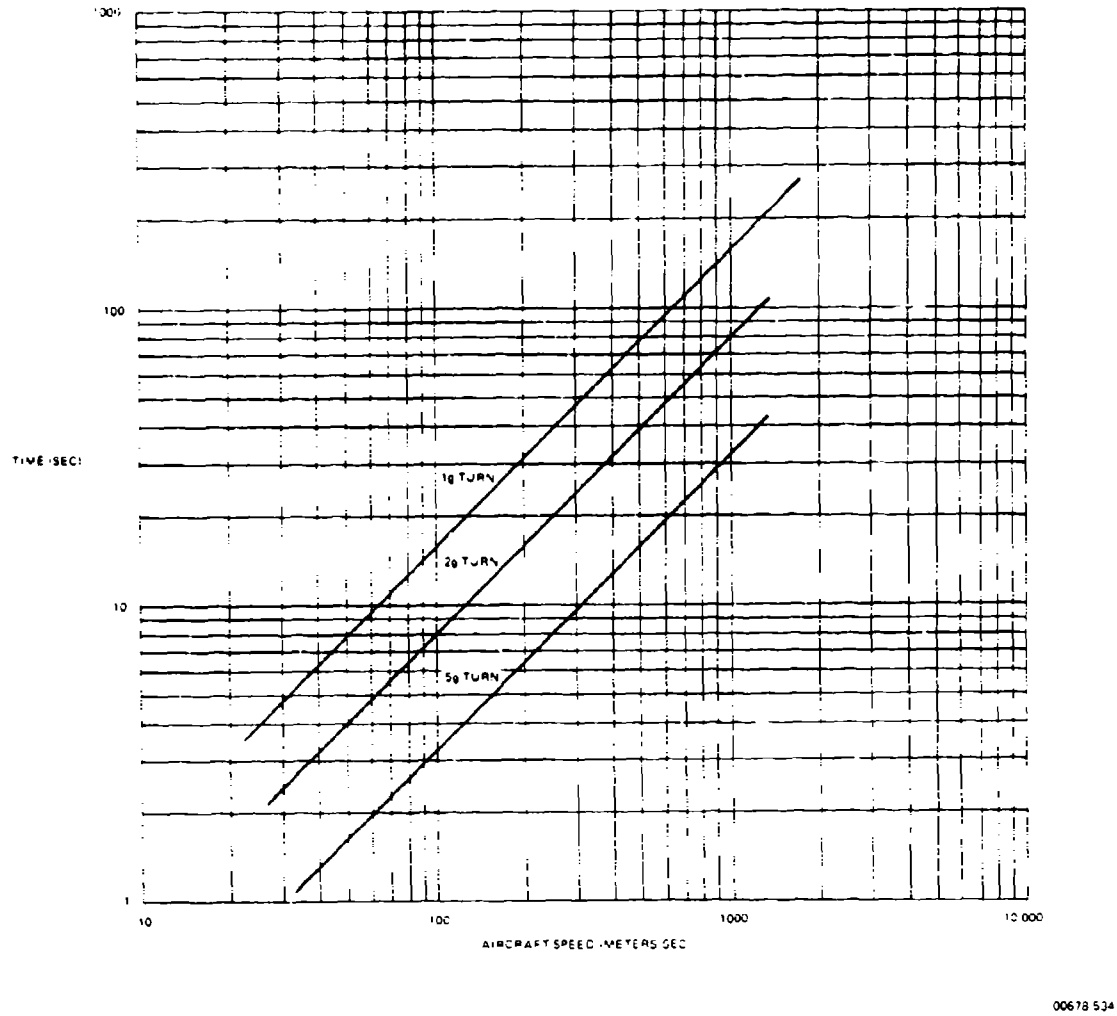

Figure 5-33. Time to Turn 90 Degrees as a Function of Aircraft Speed

$$k_2 = (1\ 2)\left|\alpha^2 + \alpha T_S + \left(T_S^2 \cdot 6\right)\right| \quad (5.104)$$

The filters may be discrete or continuous.

5.4.1.1 Prediction for Unaccelerated and for Turning Flight

For reasons developed below, we prefer not to use the acceleration measurement for AFAADS in the same form as shown in Figure 5-32. However, the principle of maintaining separate computations of position, velocity, and acceleration allows flexibility in constructing alternate prediction options on demand within the computer, without incurring additional filter settling times. Filters with different smoothing times can also be run simultaneously (subject to computer capacity limits) if desirable, to allow the option of changing smoothing time without introducing transients in individual filters.

The simplest predictor utilizes only the upper two elements of Figure 5-34. However, the curved flight algorithm considered for AFAADS is based on the following considerations. It is believed that the only turns of sufficient constancy and duration to qualify as predictable path segments will be those in a horizontal plane. They can be superimposed on vertical motion of the aircraft, such as climbing or descending turns, but vertical acceleration is unlikely to be large for extended periods of time, while a 3g turn may continue for over 25 seconds in the case of a high performance aircraft.

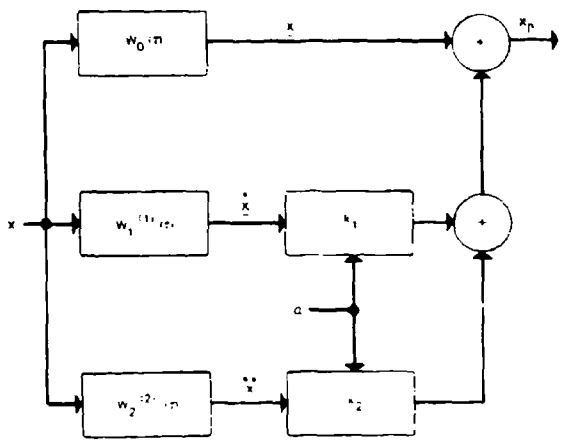

00678 535

Figure 5-34. Elements of a Polynomial Predictor

The use of an acceleration measurement in prediction amplifies the effect of tracking noise. If an acceleration algorithm is used in all three coordinates, the amplified noise will be present in each, whether there is a target acceleration in that coordinate or not. By using an acceleration element in only one dimension, namely perpendicular to the flight direction and in a horizontal plane, we minimize the effect of tracking noise.

The algorithms are as follows:

Let the target velocity projected in the horizontal plane be V_h, and its heading relative to the Y-axis be θ.

Then: $\dot{X} = V_h \sin\theta$ (5.105)

$$\dot{Y} = V_h \cos\theta \quad (5.106)$$

$$\ddot{X} = V_h \cos\theta\omega_a = \omega_a\dot{Y} \quad (5.107)$$

$$\ddot{Y} = -V_h \sin\theta\omega_a = -\omega_a\dot{X} \quad (5.108)$$

where: ω_a = rate of turn of the aircraft.

Solving for ω_a:

$$\omega_a = (\ddot{X}\dot{Y} - \ddot{Y}\dot{X})/(\dot{X}^2 + \dot{Y}^2)$$

We compute ω_a, by the preceding algorithm, from the smoothed rectangular coordinate rates and accelerations in X and Y. For short arcs typical of AFAADS prediction and the same smoothing time of all the filters, we can then predict X and Y according to the relations:

$$X_p = \underline{X} + \underline{\dot{X}}[\alpha + (T_s/2)] + (1/2)\underline{\dot{Y}}\omega_a\left[\alpha^2 + \alpha T_s + \left(T_s^2/6\right)\right] \quad (5.109)$$

$$Y_p = \underline{Y} + \underline{\dot{Y}}[\alpha + (T_s/2)] - (1/2)\underline{\dot{X}}\omega_a\left[\alpha^2 + \alpha T_s + \left(T_s^2/6\right)\right] \quad (5.110)$$

where α = time of flight, and the bars represent values smoothed over T_s.

Prediction over large fractions of a circle would require inclusion of trigonometric terms, but the above approximations have been verified on the simulation as satisfactory for AFAADS.

To compromise between the effect of noise on the curvature correction and the bias in aim point caused by the turn, it may be desirable to use some fraction less than 1.0 of the curvature correction. This can best be determined on the simulation.

The question of how to decide when to use the rate of turn correction arises. It is clear that:

a. It should not be used unless the target is turning, because of the amplification of tracking noise in measuring accelerations.

b. Because of this added noise in quadratic prediction, the linear prediction will probably be better against very slight turn rates.

Implicit in the decision to use quadratic prediction is the assumption that the target will hold a constant turn rate long enough for AFAADS to predict and fire a few rounds. There is also a penalty in switching back to the linear mode; since, even if both are carried in the computer, so that there is no delay in making the linear prediction, a segment of the new linear path equal in length to time of flight will be fired with quadratic prediction.

Since target acceleration will never be measured perfectly, we want to bias our choice of mode in the direction of linearity when measured accelerations are small. We can do this by the threshold criterion just mentioned, or we can use a more sophisticated and

probably more efficient gradient criterion. The two criteria (where A_m is measured target acceleration) are:

a. Threshold

(1) If $|A_m| \le C$ then use Linear Mode.

(2) If $|A_m| > C$ then use Quadratic Mode.

b. Gradient

(1) If $|A_m| \le C_0$ then use Linear Mode.

(2) If $C_0 < |A_m| \le C_1$ then use a fraction $(|A_m| - C_0)/(C_1 - C_0)$ of the quadratic correction.

(3) If $C_1 < |A_m|$ then use the full quadratic correction.

The gradient criterion is most easily tested on the simulator. We can do some analysis of the threshold criterion, however, and the following paragraphs attempt this.

5.4.1.2 Linear versus Quadratic Switching Criterion

In this section we discuss the process of deciding which algorithm to use, i.e., whether to use the linear or quadratic prediction when the absolute value of the measured acceleration exceeds some specified value C.

Since target position measurements are contaminated with noise the measured value of acceleration A_m will differ from the true value A_t, and the probability density function of the difference is assumed to be:

$$f(A_m|A_t)dA_m = \frac{1}{\sqrt{2\pi}\sigma_A} e^{-\frac{(A_m - A_t)^2}{2\sigma_A^2}} dA_m \qquad (5.111)$$

where estimates of the variance in the error in measuring A_t are obtained from the filter analysis.

Let $P(Q|A_t)$ be the probability that we use the quadratic prediction when true acceleration is A_t, and $P(L|A_t)$ be the probability that we use the linear algorithm when true acceleration is A_t.

Then:

$$P(Q|A_t) = \int_c^{\infty} f(A_m|A_t)\,dA_m + \int_{-\infty}^{-c} f(A_m|A_t)\,dA_m \qquad (5.112)$$

$$P(L|A_t) = \int_{-c}^{c} f(A_m|A_t)\,dA_m = 1 - P(Q|A_t) \qquad (5.113)$$

$$P(L|A_t) = \frac{1}{\sqrt{2\pi}\sigma_A} \int_{-c}^{c} e^{-\frac{(A_m - A_t)^2}{2\sigma_A^2}} dA_m \qquad (5.114)$$

When target acceleration is zero we want a very high probability of using linear prediction.

$$P(L|0) = \frac{1}{\sqrt{2\pi}\sigma_A} \int_{-c}^{c} e^{-\frac{A_m^2}{2\sigma_A^2}} dA_m \qquad (5.115)$$

This value can be obtained from tables. However a convenient approximation to the integral is the Polya-Williams approximation:

$$\frac{1}{\sqrt{2\pi}} \int_{-x}^{x} e^{-\frac{t^2}{2}} dt \le \left[1 - e^{-\frac{2x^2}{\pi}}\right]^{1/2}$$

with an error that never exceeds 0.0075 (5.116)

If $P(L|0) = 1.0 - \Delta$, where Δ is small then:

$$P(L|0) = \left[1 - e^{-\frac{2}{\pi}\left(\frac{C}{\sigma_A}\right)^2}\right]^{1/2} \sim 1 - \frac{1}{2} e^{-\frac{2}{\pi}\left(\frac{C}{\sigma_A}\right)^2} \qquad (5.117)$$

$$C = \sigma_A \left[-\frac{\pi}{2} \log_e (2\Delta)\right]^{1/2} \qquad (5.118)$$

Then the probability of using linear or quadratic prediction as a function of true target acceleration A_t is as shown in Figure 5-35

Obviously, the smaller the value of σ_A, the smaller the value of C that we can set.

The function shown in the figure is:

$$P(Q|A_t) = 1 - P(L|A_t) \qquad (5.119)$$

where:

$$P(L|A_t) = \frac{1}{\sqrt{2\pi}\sigma_A} \int_{-C-A_t}^{C-A_t} e^{-\frac{y^2}{2\sigma_A^2}} dy \qquad (5.120)$$

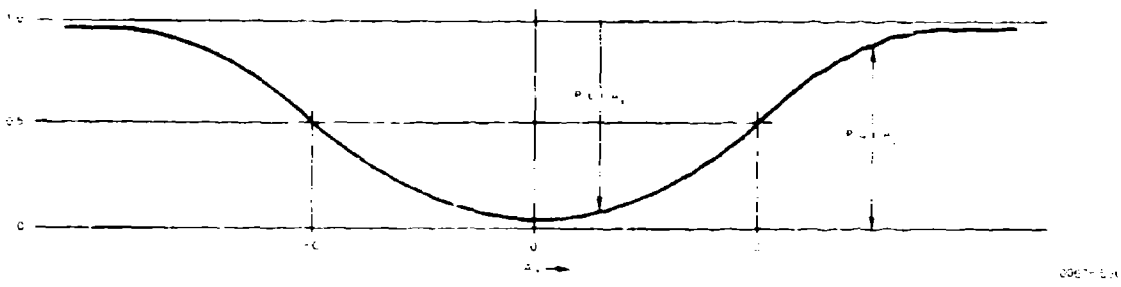

Figure 5-35. Probability of Using Linear versus Quadratic Prediction Mode

For $A_t \geq 0$:

$$P(L|A_t) \cong \frac{1}{2}\left\{\left[1 - e^{-\frac{2(C + A_t)^2}{\pi\sigma A^2}}\right]^{1/2} \pm \left[1 - e^{-\frac{2(C - A_t)^2}{\pi\sigma A^2}}\right]^{1/2}\right\} \quad (5.121)$$

where: the (+) sign is used for $A_t < C$, $\pi\sigma A^2$

and (-) sign is used for $A_t > C$

also:

$$P(L|A_t) \sim \frac{1}{2}\left\{1 \pm \left[1 - e^{-\frac{2(C - A_t)^2}{\pi\sigma A^2}}\right]^{1/2}\right\} \quad (5.122)$$

To decide where to set C, and in fact whether to use quadratic prediction at all, we must consider:

a. If the target does not accelerate, how much better is linear than quadratic prediction (since the latter is more strongly degraded by noise).

b. What is the probability that the target will fly an accelerated leg.

We can formalize the guesses involved in 'b', and to a lesser extent in 'a' as follows:

For linear prediction against an accelerated target, we write a value function (the kill probability could be used):

$$V_L(A_t) \quad (5.123)$$

A reasonable form is:

$$V_L = V_0\, e^{-A_t^2/(2s^2)} \quad (5.124)$$

where V_0 and s can be related to terms in the kill probability formula. For quadratic prediction against a target of any A_t:

$$V_Q = V_1 = \text{constant}. \quad (5.125)$$

These value functions are compared in Figure 5-36.

Now we need to guess the relative frequency with which we will encounter accelerations A_t (this guess is already implicit in our choice of V_0 and V_1). Since this is pure conjecture at this point, we write the probability density function in a form which will facilitate integration:

$$P(A_t)dA_t = \frac{1}{\sqrt{2\pi}\,\sigma_t}\, e^{-\frac{A_t^2}{2\sigma_t^2}}\, dA_t \quad (5.126)$$

The value of our system, with the switching option is, then

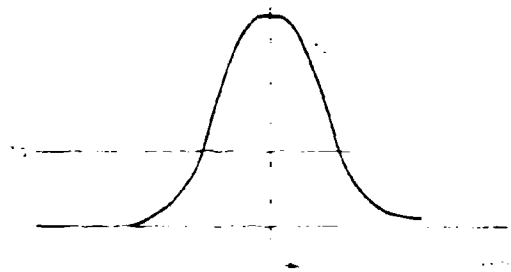

Figure 5-36. Relative Values of Prediction Mode

$$V = \int_{-\infty}^{\infty} p(A_t) \left[P(L, A_t) V_L(A_t) + P(Q, A_t) V_q \right] dA_t \qquad (5.127)$$

Rather than integrating at this point, differentiate with respect to C to obtain optimum C. The only terms containing C are P(L, A_t) and P(Q, A_t)

After some rather tedious algebra we find that the optimum value of C is given by:

$$C^2 = \frac{\sigma_A^4}{S^2} \left(\frac{1+\mu}{\mu^2} \right) \left[\log_e \left(\frac{V_0}{V_q} \right) - \frac{1}{\mu} \log_e (1+\mu) \right] \qquad (5.128)$$

One more expression is of interest. Once we have determined C, the probability of using the linear option is:

$$P(L) \cong \left[1 - e^{-\frac{2}{\pi} \left(\frac{C^2}{\sigma_A^2 + \sigma_t^2} \right)} \right]^{1/2} \qquad (5.129)$$

The above expressions are relatively opaque. The following two cases are simple examples to illustrate the rationale for determining the probability of using the linear option:

Let:

$$s = 0.20g \quad \sigma_t = 1.0g$$

The first expression states that an acceleration of $2^{1/2}(0.2) = 0.37g$ reduces the effectiveness of the linear algorithm to 37 percent of its zero 'g' value. The second expression indicates that we expect almost all target accelerations to fall within $3 \times 1.0 = 3g$.

Assume that $V_0/V_q = 100$. This represents a very high noise content of the quadratic mode.

Case I: Let $\sigma_A = 0$

This assumes that we can measure accelerations perfectly. For this case:

$$C^2 = s^2 \log_e (V_0 / V_q) \quad ;$$

$$C/s = 2.1, \quad C = 0.40g \qquad (5.130)$$

then: P(L) = 0.34

We then use the linear prediction with a probability of 0.34

Case II: Let $\sigma_A = 1.0g$

This is rather poor acceleration measurement. Working through the numbers we find that:

$$c = 1.5g$$

then:

$$P(L) = 0.74$$

Since the quadratic algorithm is so rarely used for this set of parameters, we would probably not choose to build it into the computer. Note that the low P(L) results from the large error in measuring acceleration σ_A.

A consideration in using the threshold criterion is how rapidly the decision algorithm changes modes, depending on noise. Some rough estimates, based on zero crossing theory, indicate that when target acceleration is at the threshold, option changes will occur at about one per second. This 'chattering' is undesirable, and can be subdued by requiring several samples to exceed C within a specified time to switch to the quadratic option. The linear mode can be favored at this point by requiring fewer confirmatory samples to go from quadratic to linear than from linear to quadratic.

It is likely, however, that exploration of the decision algorithm on the computer will indicate that the gradient criterion is the preferred basis for computer selection of this prediction mode.

If it turns out that the prediction for target rate of turn is both superior to linear prediction against turning targets, and above some acceptable threshold of effectiveness as well, and that constant rate of turn arcs are likely to be experienced in real life often enough to maintain interest in this algorithm, further thought can be given to refining the decision algorithm. In addition to the gradient criterion, one might also include consideration of the direction of approach of the target. If it is turning preparatory to attack, one might prefer not to use the turn prediction at all to avoid degradation of the probable subsequent straight line segment. However once the target has passed the gun, the computer might be allowed the option of including a turn, if detected, to catch the turning phase of a reattack.

World War II experience with curved flight predictors indicated that for very long times of flight they were not superior to straight line predictors. However the question is still open for AFAADS. As shown later, simulation results indicate that the quadratic mode is, in fact, useful at short times of flight.

5.4.1.3 Constant Energy Prediction

A prediction mode which corrects for target acceleration in a dive, or deceleration in a climb, can be implemented without a penalty for noise amplification. It is based on the following considerations:

The sum of kinetic and potential energy of an airplane at a specified time can be written:

$$V^2 + 2g\,Z = E \qquad (5.131)$$

where V = velocity, Z = altitude, E = energy

Differentiating:

$$Va + g\,V_Z = (dE/dt)/2$$

where: a = acceleration along the flight path.

The pilot can thus, with zero change in E, trade kinetic for potential energy, or vice versa. He can also generate a positive dE/dt by advancing his throttle, or a negative dE/dt by retarding it.

Clearly, what we would like to have are records of dE/dt over a variety of flight maneuvers, with associated V, Z to determine reasonable ranges of dE/dt as a function of situation. We may note, however, that the maximum horizontal acceleration which the pilot can generate by throttle is somewhat less than 1.0g. If we are interested in short times of flight, we may derive most of the benefit from the above relationship by considering dE/dt to be zero over the prediction time.

This means that we will always associate an acceleration with a vertical velocity. This has the advantage that we need not perform an acceleration measurement to get an acceleration correction. It has the disadvantage that we will get an acceleration prediction after the airplane has settled to a steady-state sink rate. To determine which is the more important consideration requires that real flight paths be analyzed.

Two alternate approaches that do require an acceleration measurement are (a) to treat vertical acceleration as motion along an arc, and measure pitch rate in a manner analogous to turn rate in the curved horizontal flight algorit (2) in a more sophisticated manner measure dE/ ...d predict on that basis. These alternatives should be kept in mind when real data becomes available.

For the present we assume a straight line segment, and a rectangular coordinate system. Then:

$$A_V = -g\frac{V_Z}{V} \qquad (5.132)$$

$$A_Z = A_V\frac{V_Z}{V} = -g\left(\frac{V_Z}{V}\right)^2 \qquad (5.133)$$

$$A_h = A_V\frac{V_h}{V} = -g\left(\frac{V_Z V_h}{V^2}\right) \qquad (5.134)$$

$$A_X = A_h\frac{V_X}{V_h} = -g\left(\frac{V_Z V_X}{V^2}\right) \qquad (5.135)$$

$$A_Y = A_h\frac{V_Y}{V_h} = -g\left(\frac{V_Z V_Y}{V^2}\right) \qquad (5.136)$$

where: V_x, V_y, V_z are the smoothed velocities in rectangular coordinates, and the a_i are corresponding accelerations. Also:

$$V_h^2 = V_X^2 + V_Y^2 \qquad (5.137)$$

$$V^2 = V_h^2 + V_Z^2 \qquad (5.138)$$

The prediction algorithms, including the updating of position and velocity for the lag incurred in smoothing are:

$$X_p = X + V_X\left[a + (T_S/2)\right] - (g/2)(V_X V_Z/V^2)\left[a^2 + aT_S + (T_S^2/6)\right] \qquad (5.139)$$

$$Y_p = Y + V_Y\left[a + (T_S/2)\right] - (g/2)(V_Y V_Z/V^2)\left[a^2 + aT_S + (T_S^2/6)\right] \qquad (5.140)$$

$$Z_p = Z + V_Z\left[a + (T_S/2)\right] - (g/2)(V_Z/V)^2\left[a^2 + aT_S + (T_S^2/6)\right] \qquad (5.141)$$

where α = time of flight.

This concept is similar to one proposed by H.W. Bode many years ago. Unfortunately, Bode's implementation was imbedded in a curved flight predictor, and was never tested separately. Bode also included a limiter for long dives, so that diving velocity eventually reached a constant value.

5.4.1.4 Prediction Algorithm for Defense Against Attack on a Known Point

For a long time it has been conjectured that it might be possible to make use of the known position of a defended point (such as a bridge) in antiaircraft gun prediction. Naval interceptor aircraft, for example, routinely use interception tactics which keep them between the defended ships and approaching bombers, in spite of evasive app aches by the bombers. Dr. Tappert and his associates at Frankford Arsenal worked on this problem before the availability of digital computers, but the computing mechanisms then available did not appear to allow a feasible solution.

In the current study a feasible algorithm has been demonstrated on the simulation. Its description follows:

For free fall weapons, as in level and dive bombing, the launch aircraft must fly a track, the projected horizontal trace of which must at some point pass through the target being bombed (except for wind corrections, which can be included, but are not discussed here for simplicity). In dive bombing, the aircraft path, when extrapolated, at some point passes through the ground target (except for minor deviation caused by sight angle).

Only sophisticated bombsights allow the launch aircraft freedom of maneuver except for the instant of weapon release. Most systems require that the launch aircraft fly a straight-line course for as long as ten seconds before bomb release. This is prime time for antiaircraft fire.

Similar comments apply to air-to-surface missiles, if the missile is considered as a possible target; although some consideration must be given to whether the missile is free fall, lift supported, or powered.

The following development is in terms of a dive bomb attack. For level bombing the method is similar and differs only in detail.

The target is tracked, and its heading H computed with respect to the line connecting target position and the point on the ground suspected of being a target for the airplane. The time to turn to a direct heading toward the target is computed, based on aircraft speed and some 'standard' g-loading in a turn such as 3g. Let this time be T_r. The time of flight of a projectile to the target is computed (either from the on-going conventional prediction algorithm, from which it can be read out, or simply as an approximation based on present target position). Let this time be t_o.

T_r is computed approximately as:

$$T_r = \Delta H V/(ng) \quad ; \qquad (5.142)$$

where: $ng = V\omega_a$; and

ω_a = turn rate

where: V = target speed, ΔH = heading change required, ng = standard turn acceleration. This is compared with t_o.

If $T_r > t_o$, the fire control system continues to operate with conventional extrapolation-prediction.

If $T_r \leq t_o$, the fire control system predicts on the assumption that the aircraft will in fact turn to an attack path.

In the latter case prediction is made on the basis of:

a. A level turn to head directly at the ground target.

b. Entry into a straight-line dive passing through (extrapolated) the ground target.

c. Aircraft speed as measured by the computer and corrected for acceleration depending on dive angle.

The major advantage of this system is that there is no settling time in rate measurement after the target aircraft has completed its turn. Depending on how much the aircraft deviates from the 'standard turn' programmed in the computer, the system may even be highly effective during the turn to attack. (The effect of different turn rate is wiped out completely, of course, when the airplane has completed its turn.)

The geometry of an attack on a known point is shown in Figure 5-37. The target is at D, the defended point is at the origin of the coordinate system at C. The target has a heading angle H relative to the line of length R_o to it from the origin. The target turning radius is ρ, and a speed of V gives it a turning rate of:

$$\omega_a = V/\rho \quad . \qquad (5.143)$$

ρ is given by:

$$\rho = V^2/(ng) \quad . \qquad (5.144)$$

We want to know the target position and time at the instant it is heading directly at the origin. We define the desired position in terms of the radial distance R_p and the angle A between R_o and R_p. Beyond this point, prediction takes place on a straight-line connecting present target position and the defended point.

It turns out that an economical method of getting R_p, A and T_r is to compute them in that order. The method follows:

R_x is drawn from the defended point to the center of the airplane's radius of turn E. In the triangle BCE:

$$R_x^2 = R_p^2 + \rho^2 \qquad (5.145)$$

where: ρ is the radius of turn.

In the triangle CDE:

$$R_x^2 = R_o^2 + \rho^2 - 2 R_o \rho \sin H \qquad (5.146)$$

Hence:

$$R_p^2 = R_o^2 - 2\rho R_o \sin H \qquad (5.147)$$

and all the quantities on the right side of the equation are known.

From the same triangle:

$$R_x \sin (A + A_x) = \rho \qquad (5.148)$$

$$R_x \cos (A + A_x) = R_p \qquad (5.149)$$

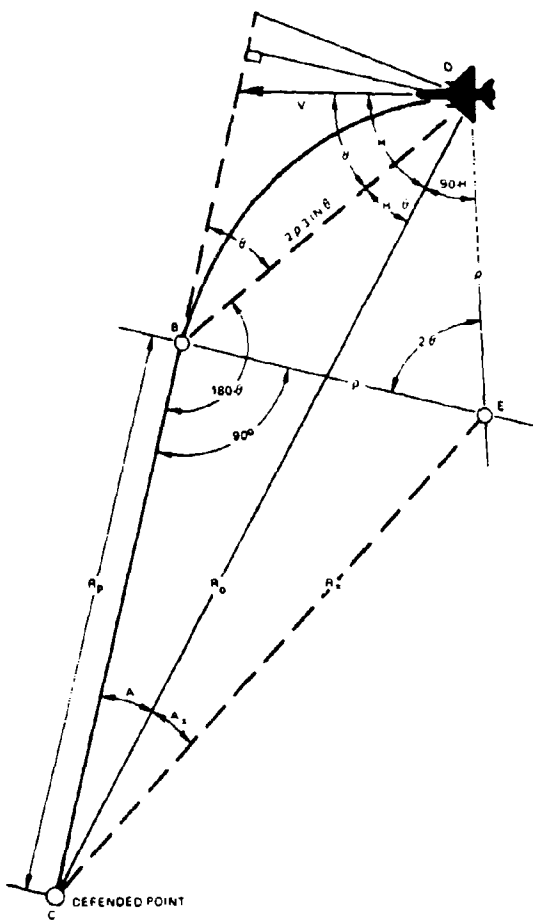

00878 538A

Figure 5-37. Geometric Drawing of Attack on Known Point

$$R_X \sin A_X = \rho \cos H \qquad (5.150)$$

$$R_X \cos A_X = R_O - \rho \sin H \qquad (5.151)$$

hence:

$$\tan (A + A_X) = \rho / R_p \qquad (5.152)$$

$$\tan A_X = (\rho \cos H)/(R_O - \rho \sin H) \qquad (5.153)$$

$$\tan A = [\tan (A + A_X) - \tan A_X] / [1 + \tan (A + A_X) \tan A_X] \qquad (5.154)$$

$$\tan A = \frac{\rho(R_O - \rho \sin H) - R_p \rho \cos H}{R_p(R_O - \rho \sin H) + \rho^2 \cos H} \qquad (5.155)$$

and again, having computed R_p, we know all quantities on the right.

With reference to the figure, the time to turn T_t is:

$$T_t = 2\theta \omega A \qquad (5.156)$$

But, from the figure:

$$2\theta = A + H \qquad (5.157)$$

Hence:

$$T_t = (A + H)(\rho/V) \qquad (5.158)$$

and again we know all quantities on the right.

Although the preceding relations can be programmed in a few minutes it is of some interest to determine the approximate form by expanding sin, cos H to terms in H^2 only. As a result, we obtain:

$$R_p = R_O - \rho H - (1/2)(\rho H)^2 / R_O \qquad (5.159)$$

and:

$$A = (1/2)\rho H^2 / R_O \qquad (5.160)$$

so that:

$$T_t = \left[\rho H + \frac{1}{2}\frac{(\rho H)^2}{R_O}\right] V \qquad (5.161)$$

To use (5.147), (5.155), (5.158), or their approximate forms in a computer operating in rectangular coordinates, they must be transformed to X, Y coordinates. This coordinate system is particularly well suited to setting in the X, Y displacement of the gun, relative to the defended point.

The algorithm is intended, by means of the decision function, not to go into action unless time to turn is less than or equal to the time of flight. Initially, however, part of the time of flight passes while the airplane is still turning. We therefore have the following two cases:

Case I: Where the time to turn remaining T_t is greater than 0. For this case the prediction algorithms are:

$$X_p = X_t\left(1 - \frac{L}{D_t}\right) \qquad (5.162)$$

$$Y_p = Y_t\left(1 - \frac{L}{D_t}\right) \qquad (5.163)$$

$$Z_p = Z_t\left(1 - \frac{L}{D_t}\right) \qquad (5.164)$$

$$D_t^2 = X_t^2 + Y_t^2 + Z_t^2 \qquad (5.165)$$

where: L is distance along the straight segment and:

$$L = V(a - T_r) + \frac{g}{2}\left(\frac{Z_t}{D_t}\right)(a - T_r)^2 \qquad (5.166)$$

where:

a = time of flight,

$$a = a(X_p, Y_p, Z_p) \qquad (5.167)$$

the second term being a 'constant energy' correction for the fact that the airplane is expected to accelerate in the dive. The updating corrections for smoothing lag in present position and velocity are not shown.

Case II: For $T_r \leq 0$:

$$X_p = X_o\left(1 - \frac{L}{D_o}\right) \qquad (5.168)$$

$$Y_p = Y_o\left(1 - \frac{L}{D_o}\right) \qquad (5.169)$$

$$Z_p = Z_o\left(1 - \frac{L}{D_o}\right) \qquad (5.170)$$

$$L = Va + \frac{g}{2}\left(\frac{Z_o}{D_o}\right)a^2 \qquad (5.171)$$

$$D_o^2 = X_o^2 + Y_o^2 + Z_o^2 \qquad (5.172)$$

On this leg, the computer uses the continuous measurement of target present position (X_o, Y_o, Z_o) and velocity V; and predicts exactly along the straight line between present position and the point target on the ground. Thus present position is always up to date, there is only one velocity measurement V and this affects only one coordinate; i.e., along the flight path.

A number of alternate forms for the preceding algorithms are possible, some of which may be better adapted to economical computation. However, the preceding algorithms allow the method to be demonstrated on the simulation.

To monitor the progress of the attack and determine when to abandon the above algorithm and revert to an extrapolation based on rates, the following decision process is suggested. The computer maintains an up-to-date measurement of target heading H with respect to the defended point on the ground. If the condition $R\ H < r_c$ exists, then the computer will predict on the assumption the attack will continue. If the condition $R\ H > r_c$ exists, then the computer will revert to a rate-extrapolation algorithm.

where: r_c is a constant

In addition, a lower limit can be placed on Z_p in the preceding algorithms; certainly $Z_p > 0$. Experience may indicate that dive bombing attacks always pull out so that minimum altitude is above M_o. In either case, the Z_p algorithm (5.170) can be modified as:

$$Z_p = Z_o\left(1 - \frac{L}{D_o}\right) : \text{if } Z_p > M \qquad (5.173)$$

or:

$$Z_p = M; \quad \text{if } Z_p \leq M \qquad (5.174)$$

A standard arc for pullup could be used, but since the aircraft is unloaded at that point and can pull up to 8g, it is not believed that such refinement would be justifiable.

In programming this algorithm for the simulation, it was found that an additional condition was necessary; namely the determination of whether the airplane could turn to an attack course at the specified acceleration without overshooting the target. This conditon requires that:

$$2\rho \sin H < R_o \qquad (5.175)$$

For the computer to get the target into (5.175) this prediction algorithm and out again, a number of inequalities must be routinely queried. A flow diagram showing the order found convenient for the simulation is shown as Figure 5-38.

It is considered that the most important finding of this portion of the study is not whether this algorithm, in its present form, is more effective than more conventional extrapolations; but rather the demonstration that it is possible with a digital computer to make it work at all. Feasibility having been demonstrated, further effort can substantially improve the efficiency of the computation, and the effectiveness of the prediction.

5.4.1.5 Stochastic Prediction

When the target aircraft or helicopter is doing terrain following or nape of the earth flying, its path will be related to the terrain contours. In Section 4.3 it was indicated that altitude changes under these circumstances might be described as a stochastic process. Although not investigated, the same conclusion might be reached with regard to course changes in the horizontal plane to go around obstacles.

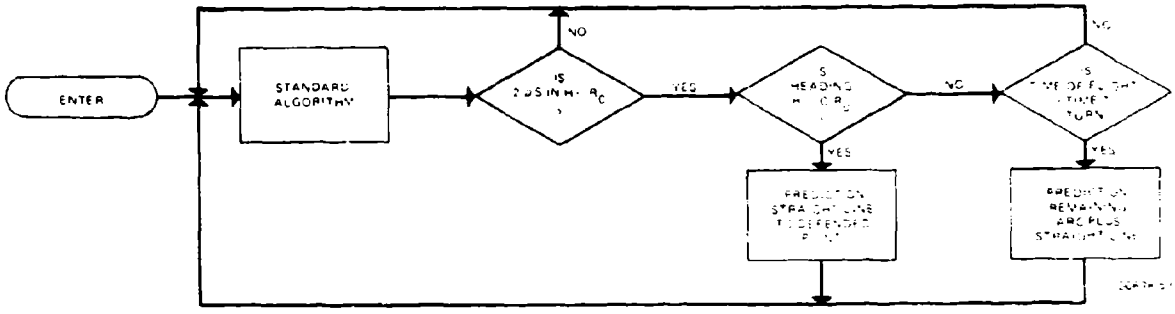

Figure 5-38. Flow Diagram of Decision Algorithm for Defense Against Attack of Known Point

It was also indicated that one might consider putting some information about local terrain into the computer, to introduce a deterministic element to the prediction. This will be discussed briefly later. The immediately following paragraphs consider the probabilistic aspects of prediction when the aircraft is contour chasing.

In Section 4.2 it was indicated that the power spectral density of vertical motion of the aircraft in terrain following might be approximated as:

$$\sigma_t^2 \frac{2}{\pi} \frac{T_1}{[1+(\omega T_1)^2][1+(\omega T_2)^2]} \qquad (5.176)$$

This is the power spectral density (PSD) of aircraft altitude about its mean,

where:

σ_t = standard deviation of terrain height variation from a mean

T_1 = L/V

L = characteristic length of terrain

V = target velocity

T_2 = a time constant aggregating the pilot plus aircraft response lag to terrain variations.

Since $T_2 << T_1$, the term containing T_2 in the above PSD can be set to zero to a first order approximation.

The autocovariance corresponding to the above PSD is:

$$R(\tau) = \sigma_t^2 e^{-|\tau/T_1|} \qquad (5.177)$$

The altitude prediction problem can now be described as follows: The airplane altitude as a function of time consists of a polynomial component plus a stochastic component. The fire control device tracks with an error which can be described in terms of the error PSD. The tracking error is correlated with the stochastic component of target motion, and the correlation can be estimated from the tracker transfer function.

The 'optimum' predictor can be determined for finite smoothing time, using the above assumptions and the Zadeh-Ragazzini method of solution, which yields the weighting function having the minimum average square error of prediction. Limited time does not permit the optimum solution to be derived in the general case. Therefore this discussion is limited to some estimates of the errors in special cases.

First, consider the error resulting from prediction with a simple two-point discrete predictor, based on the assumption that the polynomial content of target motion is a + bt. The prediction error resulting from the stochastic component of target motion, ignoring tracking noise, is:

$$Z_0\left[e^{sa} - 1 - (a\ T_S) + (a\ T_S)e^{-sT_S}\right] \qquad (5.178)$$

where: a = time of flight

T_S = smoothing time

$s = d/dt$

This expression has a mean square value for input frequency Ω of:

$$2(1+\beta)(1-\cos\omega a) + 2\beta(1+\beta)(1-\cos\omega T_S)$$

$$- 2\beta[1-\cos\omega(a+T_S)];$$

$$\beta = a\ T_S \qquad (5.179)$$

and after multiplying by the terrain PSD and integrating over Ω, we obtain the variance of prediction error as:

$$(\sigma_p/\sigma_t)^2 = 2(1+\beta)\left(1 - e^{-\alpha T_1}\right) + 2\beta(1+\beta)\left(1 - e^{-T_s/T_1}\right) - 2\beta\left|1 - e^{-(\alpha + T_s)/T_1}\right| \quad (5.180)$$

If the terrain PSD, as experienced by a 600-knot aircraft, has a break frequency at about 0.08 rad/sec, $T_1 = 12.5$ sec and $T_1 >> \alpha, T_s$ so that:

$$(\sigma_p/\sigma_t)^2 \sim (2\alpha/T_1)[1 + (\alpha/T_s)] \quad (5.181)$$

For $\sigma_t = 50$ meters, $\alpha = 3$ sec, $T_s = 1.5$ sec, we obtain $\sigma_p = 60$ meters.

For a 150-knot helicopter the same computaton yields $\sigma_p = 30$ meters.

These large errors will seriously degrade hit probability, especially since their autocorrelation characteristic time is essentially that determined by the terrain; namely, 12.5 sec for the 600-knot aircraft and 50 sec for the helicopter. We therefore consider what can be done to reduce them.

The simplest solution is to make no prediction in altitude at all. In this case:

$$(\sigma_p/\sigma_t)^2 = 2\left(1 - e^{-\alpha/T_1}\right) \quad (5.182)$$

or:

$$\sim 2\alpha/T_1$$

The variances are 34 meters and 17 meters respectively. This is a significant improvement.

If we assume that the mean flight path is level, and apply the Zadeh-Ragazzini method to obtain the best minimum variance prediction, we find for this case:

$$(\sigma_p/\sigma_t)^2 = 2\left(1 - e^{-\alpha/T_1}\right) - \frac{T_s}{T_s + 2T_1}\left(1 - e^{-\alpha/T_1}\right)^2 \quad (5.183)$$

or:

$$\sim 2\alpha/T_1$$

So, for the short smoothing and prediction times (compared with T_1), 'optimum' filtering is of no advantage. Without going through the tedious algebra to obtain the minimum variance assuming a basic polynomial $a + bt$, we may anticipate that its variance will be larger than those shown for the constant altitude predictor.

If we disable the altitude prediction for low altitude aircraft and in fact the aircraft has a mean vertical rate V_z, an additional bias of magnitude $V_z\alpha$ will be introduced. For $\alpha = 3$ sec, this systematic error will equal σ_p when $V_z = 11.3$ meters/sec for the aircraft (2.2 degree angle of climb or dive); or when $V_z = 5.7$ meters/sec for the helicopter (4.4 degree angle of climb or dive).

A suggested solution, therefore, is to use a threshold- (or gradient type) decision algorithm in the computer which uses the normal altitude prediction varying in amount from 0 to 1.0 depending on target altitude, measured rate of change of velocity, and possibly range. The algorithm can also include recognition of the fact that a diving aircraft will usually pull out of the dive before reaching ground level and make appropriate modification of the predicted altitude. Further analysis and computer simulation will provide a feasible algorithm.

In summary, it appears that the best altitude prediction to use against a terrain following aircraft may be no prediction at all; predicted altitude is assumed to be the same as present altitude. This should only be used when the aircraft is below some minimum altitude, the minimum itself being a function of target velocity.

5.4.1.5.1 Use of Digitized Terrain in the Computer

The target ignores the high frequency content of terrain. We may ask how many terrain points we need store in the computer to make a semideterministic prediction of a terrain-following aircraft. The PSD of terrain itself is down by a factor of more than 10^4, beyond about 1 cycle per nautical mile. By the sampling theorem, samples at $S = 1/(2f)$ of a function whose frequency spectrum does not extend beyond f will permit perfect reconstruction of the function. If the terrain is stored at intervals of 1/2 mile, or about 1000 meters, the portion of the PSD which affects aircraft flight should be adequately represented. About 40 points should provide an excellent representation in the AFAADS area of interest, and a smaller number would also probably be effective. In view of the large prediction errors expected by more conventional prediction schemes against terrain-following aircraft, the concept of using a few dozen stored digitized terrain points, together with an appropriate prediction algorithm, appears attractive. More extended analysis is required to determine its probable cost in computer capability and its effectiveness. The possibility of using this information to assist a tracking radar in resolving multipath images at low angles as discussed in Section 4.2, SENSORS, should also be investigated.

5.4.2 Filtering Algorithms

The target position data provided to the AFAADS computer by the tracker is contaminated by noise. The object of the filtering or 'smoothing' algorithms is to

recover the best possible estimate of the signal from the signal plus noise. Data smoothing and procedures for doing it are centuries old (Karl Friedrich Gauss used the 'least-squares' method in 1795).[30] Furthermore, the field, stimulated by the requirements of satellite and re-entry vehicle tracking, has been highly active in recent years. However, the AFAADS problem has several aspects which are more prominent than in other data smoothing applications. These are:

a. The desired smoothing time is so short that the autocorrelation time of the input noise may be comparable to, or of greater magnitude than, the smoothing time. Hence the assumption of white noise is unacceptable without careful scrutiny of its limitations.

b. Regenerative tracking recirculates the noise through the portion of the smoothing circuits associated with the tracking process.

c. The target path, unlike that of an orbiting satellite, is not analytic. Discontinuities in acceleration and high derivatives appear at the will of the aircraft pilot. Hence, data weighting functions with extended tails are undesirable.

d. The 'optimum' filter is not necessarily that which minimizes the variance of prediction error. This may be an acceptable working tool, but the important portion of the miss-distance probability density function is the portion comprised of small miss distances; whereas all large misses have equal, and zero, value.

In the following paragraphs, we discuss the interaction between noise autocorrelation and the filter at some length. The problem of recirculation of noise through the regenerative tracking unit requires analysis of the tracking loop to a greater level of detail than time permits in this contract. However, we indicate the method of approach and design criteria.

The concept we have developed with regard to variability in the target path follows from our discussion of flight trajectories, and is exemplified by the discussion of prediction algorithms. We argue that any flight path can be considered as a series of segments of varying length for each of which there is a preferred prediction option. We develop decision algorithms for activating the preferred prediction option against each segment type. In fact, we expect to find that only a few options are worth implementing, and that some path segment types are for all practical purposes unpredictable because of their short duration.

Our expected result, however, is excellent prediction against the most important and probable path segments, rather than a single prediction algorithm giving the best average (and probably very low) performance against all possible target paths.

Chang[12] has illustrated this point very neatly in the diagram reproduced as Figure 5-39a and b. A target is shown 'jinking' in the direction of the y-axis, and the results are shown for zero tracking noise. The predictor having minimum variance of prediction error is shown in 5-39a. It is never on target, although its mean-square error averaged over time is a minimum. The predictor shown in 5-39b is based on the polynominal prediction a + bt with finite memory; and although its average prediction variance is higher than that of the minimum variance predictor, when the target segment is straight, the error is zero.

This brings us back to the measure of effectiveness of a prediction algorithm. The subject has been clearly

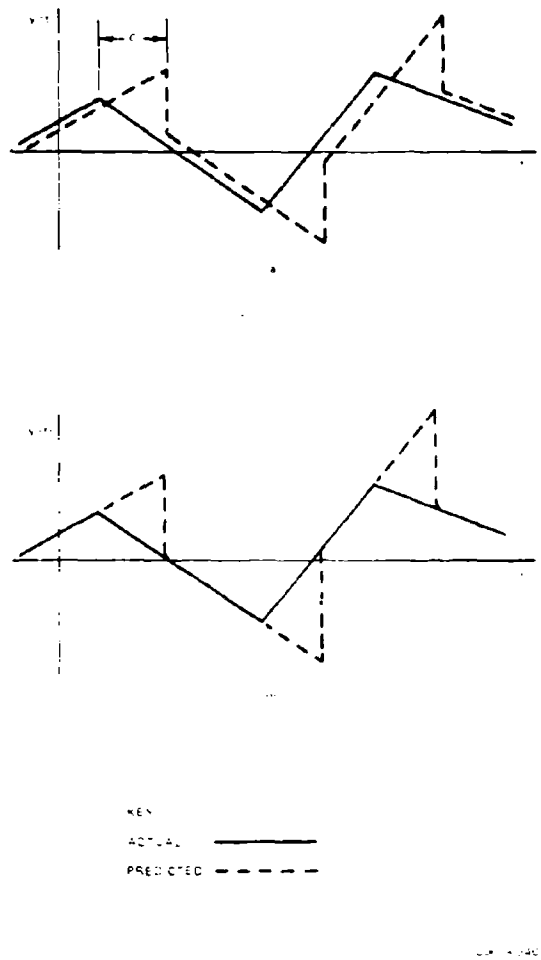

Figure 5-39. Comparison of a System with Least-Square Prediction (a) and a System with Errorless Constraint for a Number of Deterministic Signals (b)

discussed by Stibitz[31] and others. Our approach is the pragmatic one of: (1) basing each prediction mode on a set of target dynamics, (2) using minimum variance as a tool to proportion the filter, approximately, and (3) make simulator runs, with gun dispersion and aim wander included, to make final comparisons.

5.4.2.1 Filter Types

Depending on whether the AFAADS computer is digital or analog, the weighting functions to be applied to input data are expressed in discrete or continuous forms. There is no difference in principle; although implementation may be simpler with analog or digital computer, depending on the desired weighting function. Blackman[9] has described so well the correspondence of the two types and the ways of implementing each formulation in the algorithms of the other, that it is not felt necessary to carry through a parallel discussion of both modes of implementation in the following paragraphs. Since one of our objects has been the digital simulation and demonstration of some of our concepts, most of our development has been phrased in terms of digital data processing

The filter can be characterized by the memory length and the weighting function. In the case of digital processing, the filtering may be done recursively or nonrecursively.

Memory length may be finite and constant, finite but expanding with time, or unlimited, but with past inputs successively discounted.

The weighting functions are related to the criterion which is chosen for optimization.

Analytical procedures for developing nonlinear filters exist, and are progressively being extended in capability. Time has not permitted the determination of their applicability although they should be reviewed in future studies.

5.4.2.1.1 Finite Memory, Filters

For finite, constant smoothing time T, the weighting function that minimizes the variance of the signal measurement, when it is contaminated by stationary noise, is symmetrical about the midpoint of the smoothing interval. Depending on the form of the autocorrelation of the noise, the weighting function may have delta functions at the ends of the smoothing interval. Blackman[9] presents a complete analysis of this problem for both discrete and continuous smoothing, when the noise is of the Markov type, or band limited white noise. He also shows how to approximate the minimum variance weighting function closely with realizable physical circuit components in the case of analog smoothing. It is assumed that signal and noise are not correlated with each other.

The following material is based on Blackman's book,[9] to which the reader is referred for the detailed development. Emphasis in the present material is on the discrete case; with the continuous case included as the asymptote approached as the number of data points, within smoothing time T, becomes very large.

In the discussion, we use the following definitions:

By 'least squares' we mean a filter than minimizes the sum of the squares of the deviations of individually measured points from a fitted polynomial.

By 'optimum' we mean a filter that minimizes the variance in the coefficients of the polynomial.

The two definitions are identical and yield the same weighting functions, only when the successive data points are uncorrelated. For an extended discussion of this point see Morrison.[13] To realize the 'optimum' filter, it is necessary to know the autocorrelation function of the noise.

The simplest discrete velocity measuring algorithm is based on only two data points, and the simplest acceleration algorithm uses three. These cases are included in the following comparisons.

Tables V-2, V-3, and V-4 tabulate the weighting functions, variance reduction ratios, and asymptotical approximations to variance reduction for the 2-point, 3-point, least squares, and optimum filters for position, velocity, and acceleration. In these tables, the noise autocovariance is:

$$R(s) = \sigma_o^2 e^{-\lambda s} \qquad (5.184)$$

Smoothing time is T, and $a = \lambda T$.

These velocity and acceleration algorithms are compared in dimensionless form in Figures 5-40 and 5-41. The small differences across algorithms suggests that for small λT, a small number of points in discrete data processing will be satisfactory which is a desirable conclusion from the point of view of data storage capacity in the computer. This aspect is therefore examined in greater detail.

Writing the general n-point smoothing algorithms as:

$$\underline{x}(j) = \sum_{r=0}^{n} W_{0r}\, x(j-r) \qquad (5.185)$$

$$\dot{x}(j) = \sum_{r=0}^{n} W_{1r}\, x(j-r) \qquad (5.186)$$

$$\ddot{x}(j) = \sum_{r=0}^{n} W_{2r}\, x(j-r) \qquad (5.187)$$

where: $x(j-r)$ is the input data point at time $j-r$, and there are $n+1$ points in the fixed smoothing interval T spaced at constant intervals Δ, so that $T = n\Delta$

(Insert Equation 5.188)

Table V-2. Position Smoothing Algorithms

Algorithm	Weighting Function $W_1(s)$
2-Point	$[\delta(t) + \delta(t-T)]/2$
Least Squares	$1/T$
Optimum	$[\delta(t) + \delta(t-T) + (a/T)]/(2+a)$

Algorithm	Variance Reduction $(\sigma/\sigma_o)^2$
2-Point	$(1+e^{-a})/2$
Least Squares	$(2/a^2)(a-1+e^{-a})$
Optimum	$2/(2+a)$

Algorithm	Asymptotic Approximations to Variance Reduction	
	Small λT	Large λT
2-Point	$1-(\lambda T/2)$	$1/2$
Least Squares	$1-(\lambda T/3)$	$2/(\lambda T)$
Optimum	$1-(\lambda T/2)$	$2/(\lambda T)$

Note: $a = \lambda T$

00678-541

Letting $\rho = e^{-\lambda\Delta}$ for Markov noise, (5.188)

and $k = (1-\rho)/(1+\rho)$ (5.189)

the optimum position weighting sequence is:

$$W_{0r} = [(n+1) - (n-1)\rho]^{-1} \; ; \; r = 0, 1, \cdots, n \quad (5.190)$$

with variance reduction:

$$(\sigma/\sigma_o)^2 = \frac{(n+1) - 2\rho - (n+1)\rho^2 + 2\rho^{n+2}}{(n+1)^2(1-\rho)^2} \quad (5.191)$$

and the optimum velocity weighting sequence is:

$$W_{10} = -W_{1n} = \frac{3(1+k)[1+k(n-1)]}{T[(1+kn)(2+kn)+(1-k^2)]} \quad (5.192)$$

and:

$$W_{1r} = \frac{6k^2(n-2r)}{T[(1+kn)(2+kn)+(1-k^2)]} \; ;$$

$$r = 1, 2, \cdots, n-1 \quad (5.193)$$

The velocity variance reduction is:

$$(\sigma_v T/\sigma_o)^2 = \frac{12\,kn}{(1+kn)(2+kn)+(1-k^2)} \quad (5.194)$$

The variance reduction as a function of the number of points has been plotted in dimensionless form in

Table V-3. Velocity Smoothing Algorithms

Algorithm	Weighting Function $W_I(s)$
2-Point	$\frac{\delta(t) - \delta(t-T)}{T}$
Least Squares	$\frac{6}{T^3}(T - 2s)$
Optimum	$\frac{6\lambda^2(T - 2s) + 6(\lambda T + 2)\lvert\delta(t) - \delta(t-T)\rvert}{T(\lambda^2T^2 + 6\lambda T + 12)}$

Algorithm	Variance Reduction $(\sigma_I/\sigma_0)^2$
2-Point	$\frac{2}{T^2}(1 - e^{-a})$
Least Squares	$\frac{12}{T^2}\left[\frac{24 - 6a^2 + 2a^3 - e^{-a}(24 + 24a + 6a^2)}{a^4}\right]$
Optimum	$\frac{24}{T^2}\left[\frac{a}{a^2 + 6a + 12}\right]$

Algorithm	Asymptotic Approximations	
	Small λT	Large λT
2-Point	$\lambda^2\lvert(2/a) - 1\rvert \sim \frac{2\lambda}{T}$	$\lambda^2(2/a^2) \sim \frac{2}{T^2}$
Least Squares	$\lambda^2\lvert(12/5a) - 1\rvert \sim \frac{2.4\lambda}{T}$	$\lambda^2(24/a^3) \sim \frac{24}{\lambda T^3}$
Optimum	$\lambda^2\lvert(2/a) - 1\rvert \sim \frac{2\lambda}{T}$	$\lambda^2(24/a^3) \sim \frac{24}{\lambda T^3}$

NOTE:

T = smoothing time

Markov noise, autocorrelation $e^{-\lambda\tau}$; variance σ_0^2

$a = \lambda T$

00678-542

Table V-4. Acceleration Smoothing Algorithms

Algorithm	Weighting Function $W_2(s)$
3-Point	$\frac{4[\delta(t) - 2\delta(t - T/2) + \delta(t - T)]}{T^2}$
Least Squares	$\frac{60}{T^5}(T^2 - 6sT - 6s^2)$
2-Point Plus	$\frac{6}{T^2}[\delta(t) + \delta(t - T) - 2]$
Optimum	$\frac{30}{T^3}\frac{2(12 + 6a + a^2)[\delta(t) + \delta(t - T) - 2] + 2a^2(2 + a)[T^2 - 6sT - 6s^2]}{120 + 60a + 12a^2 + a^3}$

Algorithm	Variance Reduction $(\sigma_2/\sigma_0)^2$
3-Point	$\frac{16}{T^4}(6 - 8e^{-a/2} + 2e^{-a})$
Least Squares	$\frac{1440}{T^4 a}\left\{1 - \frac{5}{a}(1 + \frac{6}{a} + \frac{12}{a^2})[1 - \frac{6}{a} + \frac{12}{a^2} - (1 + \frac{6}{a} + \frac{12}{a^2})e^{-a}]\right\}$
2-Point Plus	$\frac{72}{T^4}(1 + \frac{2}{a})[(1 - \frac{2}{a}) + (1 + \frac{2}{a})e^{-a}]$
Optimum	$\frac{1440}{T^4}\frac{a(2 + a)}{(120 + 60a + 120a^2 + a^3)}$

Algorithm	Asymptotic Approximations	
	Small λT	Large λT
3-Point	$\lambda^4(\frac{32}{a^3}) \sim \frac{32\lambda}{T^3}$	$\lambda^4(\frac{96}{a^4}) \sim \frac{96}{T^4}$
Least Squares	$\lambda^4(\frac{240}{7a^3}) \sim \frac{34\lambda}{T^3}$	$\lambda^4(\frac{1440}{a^5}) \sim \frac{1440}{\lambda T^5}$
2-Point Plus	$\lambda^4(\frac{24}{a^3}) \sim \frac{24\lambda}{T^3}$	$\lambda^4(\frac{72}{a^4}) \sim \frac{72}{T^4}$
Optimum	$\lambda^4(\frac{24}{a^3}) \sim \frac{24\lambda}{T^3}$	$\lambda^4(\frac{1440}{a^5}) \sim \frac{1440}{\lambda T^5}$

00678-543

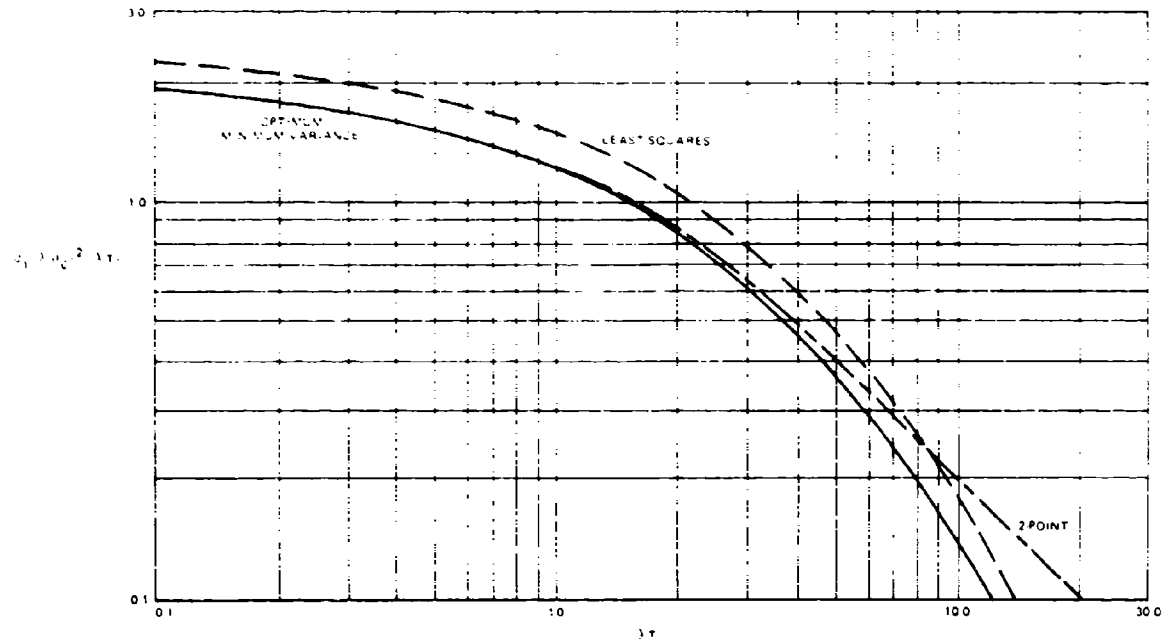

Figure 5-40. Comparison of Variance Reduction for Three Velocity-Smoothing Algorithms

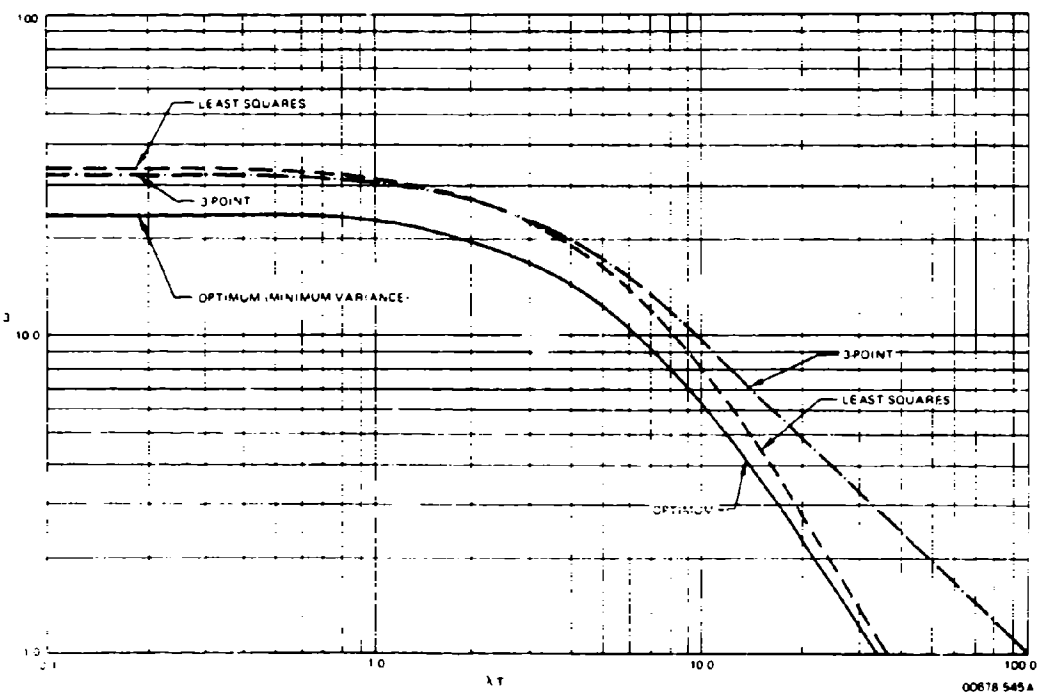

Figure 5-41 Comparison of Variance Reduction for Three Acceleration-Smoothing Algorithms

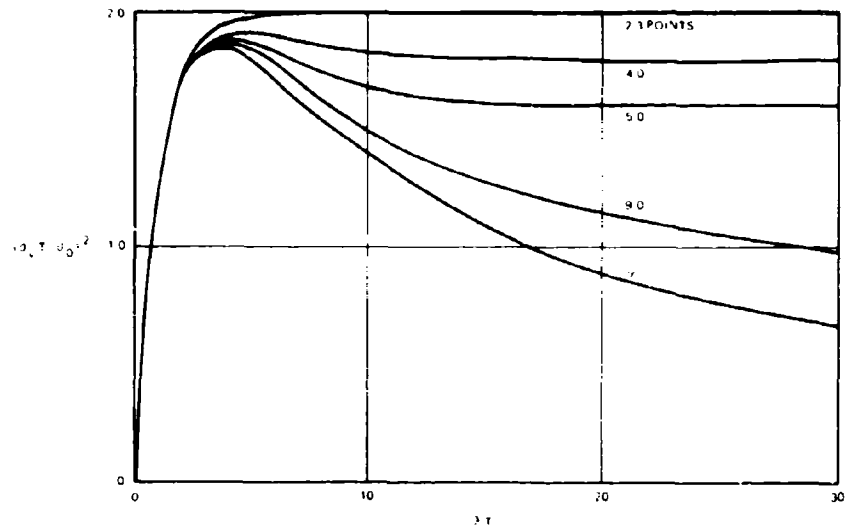

00678 546

Figure 5-42. Velocity Variance Reduction

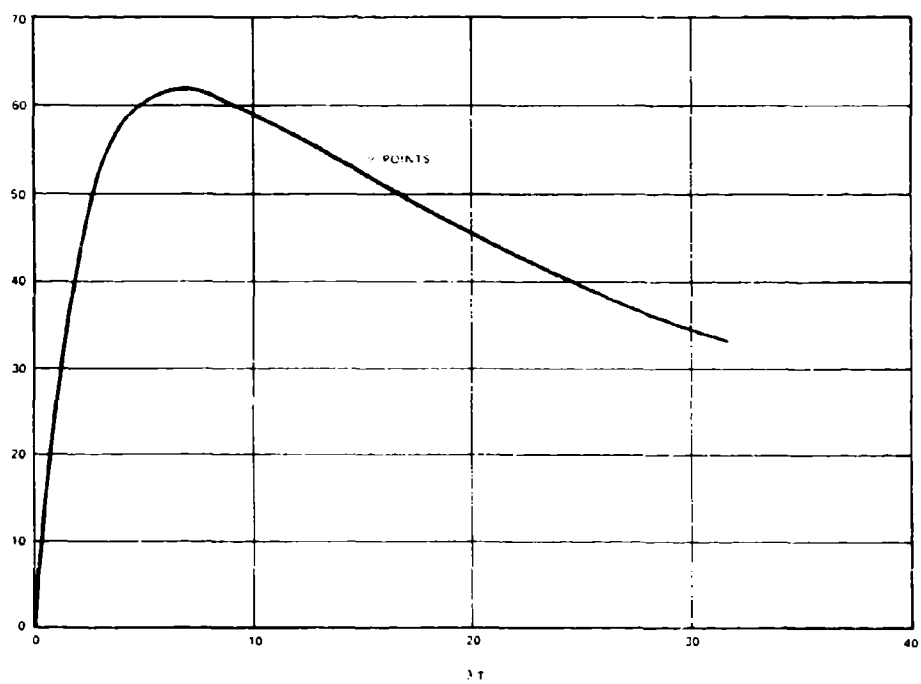

Figure 5-43. Acceleration Variation Reduction

Figure 5-42. The dimensionless ratios have been chosen differently from those of Figures 5-40 and 5-41 to emphasize that as $\lambda \longrightarrow 0$: variance $\longrightarrow 0$, and there is a 'worst' λ. One can obtain a small λ with sluggish sensor servos, but the penalties paid in lagging data have been discussed earlier.

The asymptotic curve of acceleration variance reduction has been replotted in similar form in Figure 5-43 for comparison of the effect of λ.

To be more specific with regard to AFAADS parameters, a value of $\lambda = 5.0\ sec^{-1}$ has been chosen, and velocity variance reduction has been plotted in Figure 5-44 versus smoothing time as a function of the number of data points. This value of λ, corresponds to a characteristic time of 0.20 seconds, and is considered to be about right for a high performance radar tracking loop.

We note from Figure 5-44, that for smoothing times of about 2 seconds, there is no justification for more than 9-point smoothing, and that a smaller number would probably be satisfactory.

If, as we believe is probable, the autocorrelation characteristic time with manual tracking is at least 0.5 second, or $\lambda = 2.0$, a 4-point smoother should be satisfactory.

Finally, in view of the small differences between the optimum and least squares weighting sequences, it would probably be satisfactory to use the latter, and they are listed below for reference.

$$W_{0r} = (n+1)^{-1} \tag{5.195}$$

$$W_{1r} = \frac{6(n-2r)}{T(n+1)(n+2)} \tag{5.196}$$

$$W_{2r} = \frac{60\,n[n(n-1) - 6nr + 6r^2]}{T^2[(n-1)(n+1)(n+2)(n+3)]} \tag{5.197}$$

5.4.2.1.2 Variance of Prediction

If the optimum weighting sequences are used, Blackman shows that the smoothed estimates of position, velocity and acceleration are not correlated with each other, so that if prediction is made as:

$$x_p = x + k_1 \dot{x} + k_2 \ddot{x} \tag{5.198}$$

where: $k_1 = \alpha + (T/2)$; $k_2 = [\alpha^2 + \alpha T + (T^2/6)]/2$ (5.199)

the variance of prediction error is, in terms of variances of position, velocity, and acceleration:

$$\sigma_p^2 = \sigma^2 + k_1^2 \sigma_1^2 + k_2^2 \sigma_2^2 \tag{5.200}$$

Figure 5-45 shows the variance ratio for position and velocity smoothing for a 3-sec time of flight as a function of smoothing time.

5.4.2.1.3 Expanding Memory

In its simplest form, a fixed memory system provides no output until one memory time has elapsed. We should prefer to have a less accurate output available almost immediately (3 data points, for example) with progressive improvement of the output until the full memory length is utilized. Since Blackman provides algorithms for this process, they will not be reproduced here. These algorithms represent the initial loading process of the filters in the system.

We might also consider allowing the memory to expand indefinitely, i.e., at each moment making the best estimate according to the totality of past data. However, in the absence of actual target data, we are inclined to give this type of algorithm a low priority for investigation, because of the low probability that any of the polynomial coefficients of the target signal will remain usefully stable for more than a few seconds.

5.4.2.1.4 Recursive Smoothing

The simplest form of discrete recursive smoothing of successive position measurements with no trend is:

$$\underline{x}(j) = a\,x(j) + (1-a)\,\underline{x}(j-1) \tag{5.201}$$

where:

$\underline{x}(j)$ = smoothed value of x at the j'th point

$x(j)$ = measured value of x at j

a = constant, $0 < a < 1.0$

$$\underline{x} = a\sum_{k=0}^{\infty} (1-a)^k\, x(t-k) \tag{5.202}$$

and is the digital equivalent of analog 'exponential smoothing,' for which the Laplace transform is:

$$\underline{x}(s) = x(s)/(1+sT) \tag{5.203}$$

Since only one value, the most recently computed x, must be stored between computations; the method is highly economical of computer storage.

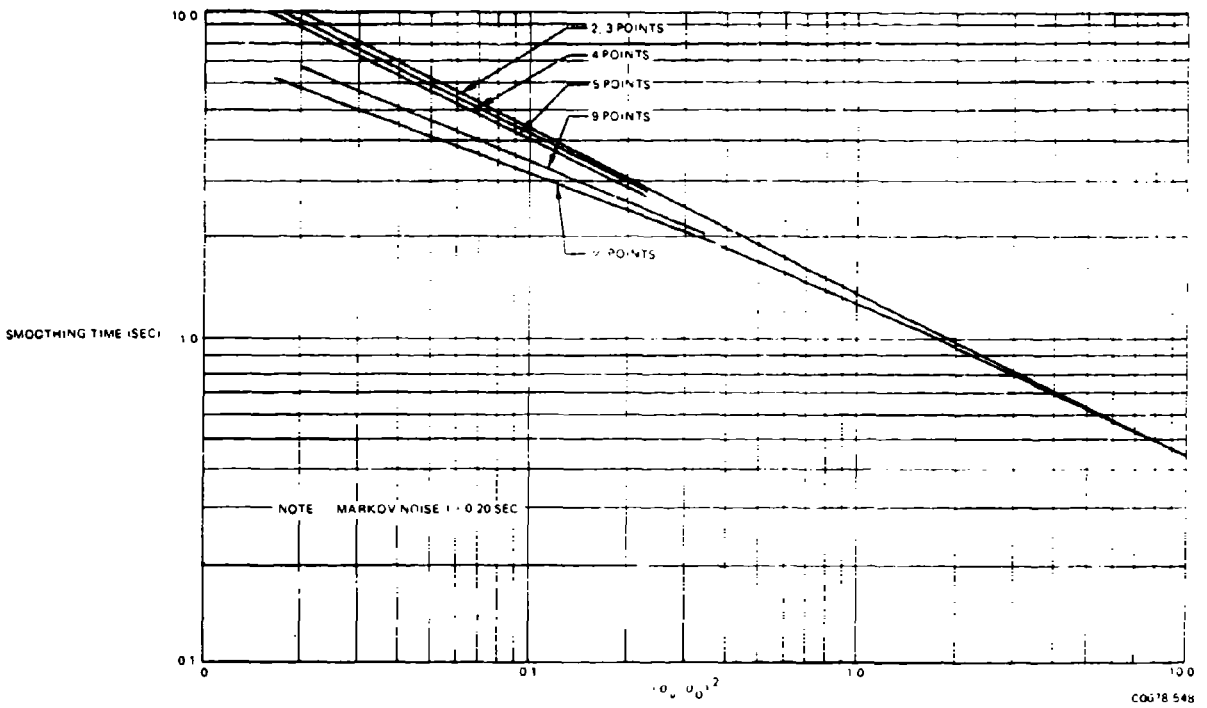

Figure 5-44. Effect of Number of Data Points on Variance Reduction for Velocity Smoothing

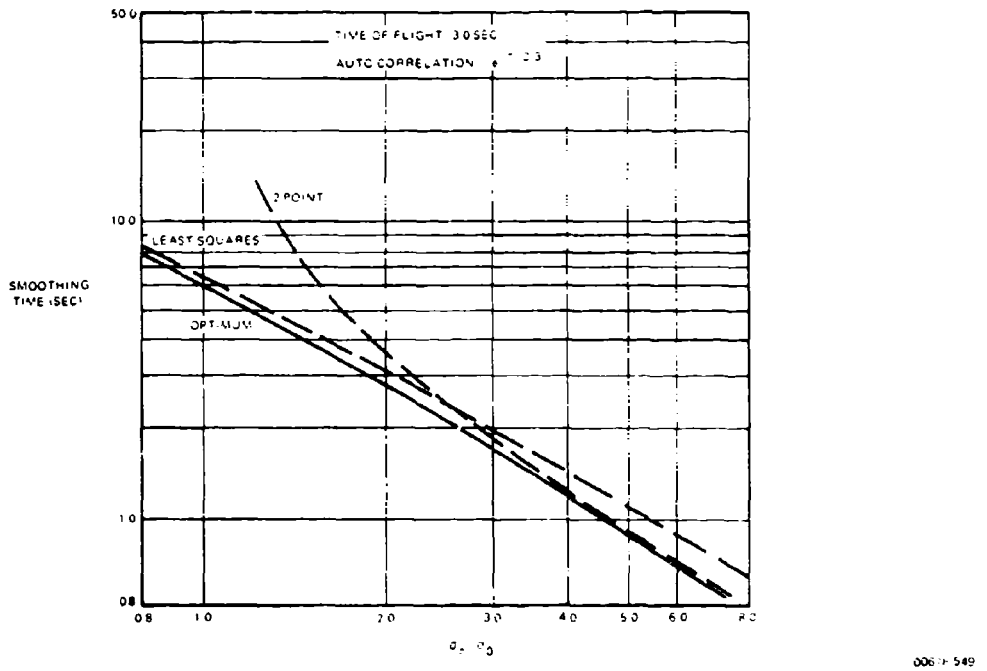

Figure 5-45. Prediction Variance as a Function of Smoothing Algorithm

When both position and velocity are desired, the algorithms can be written as:

$$x(j) = x_p(j) + a[x(j) - x_p(j)] \quad (5.204)$$

$$v(j) = v(j-1) + (b/T)[x(j) - x_p(j)] \quad (5.205)$$

where:

$$x_p(j+1) = x(j) + T\,v(j); \quad (5.206)$$

T is the sampling interval, and b is a constant.

The preceding set of algorithms[21], known as the 'alpha-beta tracker equations,' found a large market in the early days of track-while-scan radars when it was desired to maintain hundreds of tracks within limits of available computer capacity. The x_p estimate was used to assist in correlating new blips with past tracks; and in the case of a missed blip, the computation could proceed using x_p in place of x. The maximum prediction (if no blips were missed) was one unit.

An optimum value of b, considering settling time and variance reduction, was found to be $b = a^2/(2-a)$ for the radar application.[21]

Corresponding algorithms have been published for a third-order (alpha,beta,gama) tracker.[23]

In the past eight years, radar track-while-scan smoothing algorithms have become considerably more sophisticated as computer capabilities have improved. However, such systems rarely need to predict more than one data interval forward.

Recursive algorithms for least squares weighting have been developed by Blackman. These are more economical of computer usage that the equations given earlier, when the number of points used is very large. Since we indicate that about 10 data points can be a maximum for AFAADS, and only one track may be developed, this consideration is of lesser importance.

One of the advantages of a recursive algorithm, however, is that the weighting coefficients can be changed fairly easily as a function of other parameters. For example, in some TWS-radar algorithms it is found desirable to vary the weights with range, to account for changing radar accuracy; or with time, as a new track becomes well established.

In the case of AFAADS we have conjectured that tracking error in linear measure is not likely to vary widely over most of the AFAADS envelope. However, as time of flight increases, the prediction error will increase as velocity and acceleration variances are multiplied by time of flight squared and to the fourth power respectively. This suggests that smoothing time should increase with time of flight.

Varying smoothing time with time of flight is rather awkward for a fixed memory time algorithm, but relatively straightforward with a recursive algorithm. One still desires a short tail for the weighting sequence and efficient use of the data points within the effective smoothing time. Therefore the recursion should be based on a small number of stored data points of the immediate past.

The development of appropriate efficient algorithms, for recursive smoothing with effective smoothing time proportional to projectile time of flight, is a promising area for further study.

5.4.2.1.5 Interaction with Regeneration

The best weighting sequence for prediction, and the best weighting sequence for rapid settling and stable functioning of the regenerative tracking unit, are unlikely to be identical. Rather than compromise the prediction function, it may be preferable to generate two sets of rates; one for regeneration, and one for prediction. Tne exponential smoothing of the simplest recursive algorithm is probably an essential component (if not all) of the rate computation for regeneration. However, exponential smoothing makes inefficient use of available data for longer prediction intervals such as projectile time of flight. A proper analysis will determine the algorithms to provide regenerated information to the tracker guaranteeing stability and rapid settling, and to the predictor (operating on the output of the regenerated tracking loop) for a most accurate prediction within a specified effective memory time. Optimization of both functions might require separate filters.

5.5 BALLISTICS

The ballistic computation provides time of flight for the prediction algorithm, corrections for gravity drop (superelevation), drift, and, if necessary, the effect of wind on the trajectory of the projectile. The parameters defining the trajectory are the gun's quadrant elevation, muzzle velocity, and the structure of the atmosphere.

How accurately ballistics should be computed depends on other sources of prediction error, as well as on how well the parameters defining the trajectory are known.

These parameters may be discussed in two classes: depending on whether they would exist in a vacuum, or whether they depend on the projectile's interaction with the atmosphere. In the former case, the effect is realized through variations in the muzzle velocity of the gun. Figure 5-46 lists the parameters grouped according to the two classes.

Muzzle velocity variations will occur because of the following: variations in propellant characteristics

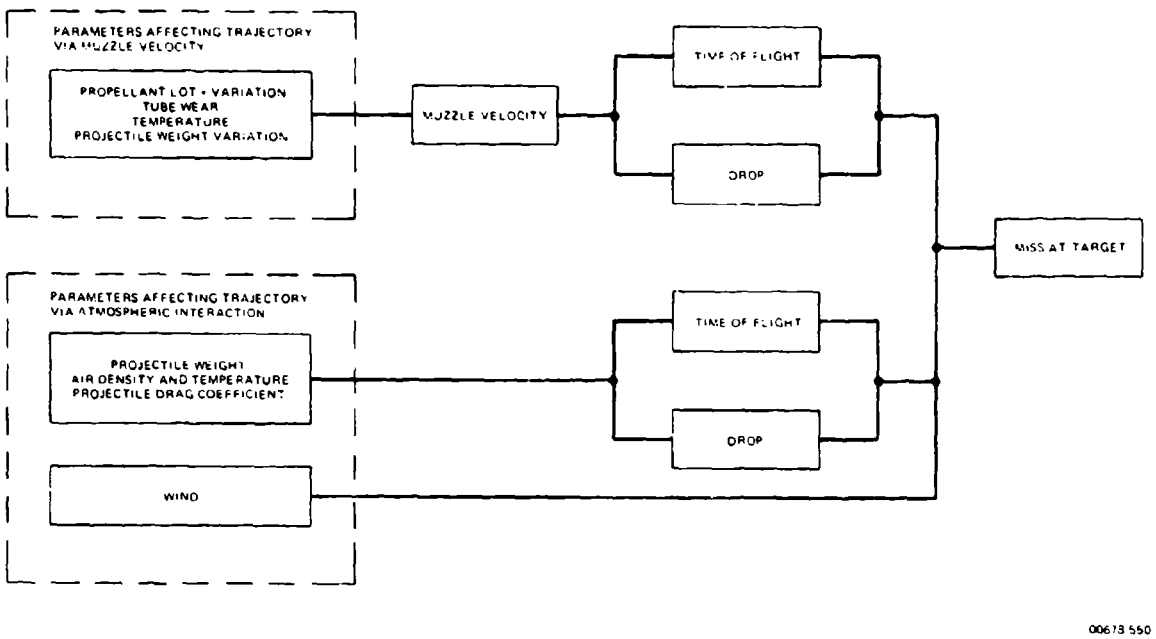

Figure 5-46. Ballistic Parameters Affecting Miss Distance

within and across lots, variations in propellant temperature and projectile weight, and as a function of tube wear. Some of these variations from the expected value will be systematic and vary slowly, if at all across rounds; while others will vary from round to round. In the case of the slowly changing parameters, such as tube wear or propellant lot, it is possible to eliminate them by measuring muzzle velocity by an on-mount device, and applying a correction based on the average over several rounds, as is done by Oerlikon.

The parameters, which affect the trajectory through the action of the atmosphere on the projectile, tend to be roughly proportional to the loss of velocity of the projectile, as caused by drag. Their effect is reduced over a given distance traveled, as time of flight is shortened by increasing muzzle velocity, and/or reducing projectile drag.

Since the state of the art in designing computing elements to match a given set of ballistics is well advanced, an in-depth analysis of the most efficient algorithms to use for AFAADS can be done with low risk at the appropriate point in the development cycle. The University of Michigan has developed second-order corrections to the Siacci-Kent-Hitchcock ballistic algorithms. These algorithms are easy to implement and may be adequate. At the limits of extreme precision, the Litton-developed TACFIRE System has implemented ballistic algorithms that are probably as precise as the ballistic tables derived from proving ground firings.

The emphasis in the following paragraphs is in relating the principal errors in input parameters to miss distances at the target. This relationship will provide a basis for estimating whether, for example, there should be a correction for wind, as well as what control should be held on muzzle velocity variation within lots. For this purpose, the simplest Siacci representation of the trajectory is considered adequate.

5.5.1 3/2 Law Ballistics

It was observed by Dr. T.E. Sterne about 25 years ago that, for a low drag projectile, the drag coefficient at supersonic velocities could be well represented as varying as the -1/2 power of velocity, so that the drag itself varied as the 3/2 power of velocity. For trajectories with relatively small gravity drop, the equations of motion can be integrated to yield the following first order approximations:

$$t_p = D\left[V_o - (K/2)DV_o^{1/2}\right] \qquad (5.207)$$

$$V^{1/2} = V_o^{1/2} - (K/2)D \qquad (5.208)$$

$$V_a = V_o - (K/2)V_o^{1/2}D \qquad (5.209)$$

$$V V_o = V_a^2 \qquad (5.210)$$

where:

V_o = muzzle velocity

V = projectile velocity at range D

t_p = time of flight to range D

V_a = average projectile velocity to range D

K = a coefficient in the deceleration expression:

$$dV/dt = -K V^{\alpha} \qquad (5.211)$$

and for the '3/2 law', $\alpha = 3/2$.

The University of Michigan has generalized this approach to include arbitrary values of α. The composition of the coefficient K can be seen by writing the deceleration relation in conventional form:

$$dV/dt = -C_d V^2 (\rho g/2)(A/W) \qquad (5.212)$$

where:

C_d = drag coefficient

ρ = air density

A = cross sectional area of the projectile

W = projectile weight

5.5.2 Projectile Gravity Drop

In a vacuum, projectile drop/Q, under the influence of gravity, is given by:

$$Q = (1/2)\, g t_p^2 \qquad (5.213)$$

where: t_p = time of flight. Kelly, et al. have shown that within the validity of the Siacci approximation, over a wide range of projectile drag laws:

$$Q = (1/2) g t_p^2 \, f(V/V_o) \qquad (5.214)$$

where: the value of $f(V/V_o)$ is very nearly the same for given ratio of remaining to muzzle velocity, V/V_o, in spite of changes in the drag function.

For the '3/2 law':

$$Q = (1/2)\, g t_p^2 [1 - (2/3)(V_o - V_a)/V_o] \qquad (5.215)$$

where:

V_a = average projectile velocity over t_p, and $V_a^2 = V_o V$

The preceding expression can also be written:

$$Q = (1/6)(g t_p^2)[1 + 2(V_a/V_o)] \qquad (5.216)$$

5.5.3 Effect of Parameter Variations

Differentiating the expressions for time of flight for constant range, we find that:

$$\partial t_p/\partial V_o = -(t_p/V_o)(V_o + V_a)/(2V_a) \qquad (5.217)$$

$$\partial t_p/\partial K = (t_p/K)(V_o - V_a)/V_a \qquad (5.218)$$

and from the expression for K:

$$\partial K/\rho = K/\rho \qquad (5.219)$$

$$\partial K/\partial w_p = -K/w_p \qquad (5.220)$$

Variations in projectile weight also affect muzzle velocity approximately as:

$$\partial V_o/\partial w_p = -(1/2) V_o/w_p \qquad (5.221)$$

If the time of flight of the projectile to the target differs from that used in the prediction by a small quantity Δ, the miss distance from this source will be, very closely:

$$M = V_t \sin \Omega_p \Delta \qquad (5.222)$$

where: Ω_p is the angle between the target path and the correct trajectory, and V_t is target velocity.

This expression has a maximum value at $\Omega_p = 90$ degrees, at which point:

$$\partial M/\partial t_p = V_t \qquad (5.223)$$

Combining the above expressions to obtain the miss resulting from muzzle velocity deviations:

$$\partial M/\partial V_o = (V_t t_p/V_o)(V_o + V_a)/(2V_a) \qquad (5.224)$$

For the Vigilante ballistic options presented earlier, and considering the worst case of maximum range, at which the projectile has almost dropped to sonic velocity, and assuming a target speed of 300 meters/second, this works out to about 2-3 meters of miss per meter/sec error in muzzle velocity. However, at 3-sec time of flight the ratio is from 0.38 to 0.45 meter of miss per meter/sec error in muzzle velocity.

Similar computations can be done on the effects of variation in air density and projectile drag coefficient,

but a larger percentage variation will be allowable, since the expression describing their effect on time of flight depends on the difference between muzzle velocity and average velocity rather than the sum. Variations in projectile weight affect both muzzle velocity and slowdown. A slightly underweight projectile emerges at a higher velocity, but slows down more rapidly.

Returning to the consideration of gravity drop, we find for the variation of Q with V_o:

$$\partial Q/\partial V_o = -g D^2 \left(V_o^2 + 2 V_o V_a + 3 V_a^2\right)/\left(6 V_o^2 V_a^3\right) \quad (5.225)$$

where: D is slant range.

For the four ballistic types described earlier for Vigilante, gravity drop at that range where the projectile approaches sonic velocity is about 100-200 meters, depending on the projectile. The change in drop per meter per second change in muzzle velocity is from 0.2 to 0.4 meter. This is a very small effect, compared with the effect on lead.

Furthermore, since the effect varies with the square of range, it will be completely negligible at short ranges.

5.5.4 Wind

For a horizontal trajectory, using the Siacci-Kent-Hitchcock method, we find the displacement of the projectile caused by a cross wind to be:

$$Y = w t_p (V_o - V_a)/V_o \quad (5.226)$$

where: w = cross wind velocity which, for the 3/2 drag law can be approximated as:

$$Y = w t_p^2 \left(2K V_o^{1/2}\right) \quad (5.227)$$

The expression for the effect of a range wind is not at compact, but it can be approximated as:

$$X = w t_p^2 \left(3K V_o^{1/2}\right) \quad (5.228)$$

The projectile displacement caused by wind increases as the square of time of flight. For a 3-sec time of flight, we find about 6-10 meters of projectile deviation per 10 knots of wind.

The Weather Bureau indicates an average wind velocity of 7-12 knots over the United States (Maxima range from over 200 knots on top of Mt. Washington to 45 knots in San Diego).

An error budget for AFAADS is suggested later. At this point we note that if we wish to hold the individual ballistic contributions of error to less than 3 meters for a 3-sec time of flight, against a 600-knot target, we need to hold muzzle velocity to 7 meters/second, and compute time of flight to within 0.01 sec. We also need to provide a wind correction.

5.6 HIT AND KILL PROBABILITY

In order to place the computations of kill probability in perspective, some of the limited available historical data on rounds per aircraft killed is summarized in Figures 5-47 and 5-48. We have already presented some overall summaries on numbers of aircraft lost to antiaircraft guns in an early section of this report. From Figure 5-47 we see that in World War I, the effectiveness of heavy antiaircraft guns improved by a factor of over five in four years, as the result of weapon and fire control improvements, and operational experience.

In World War II (Figure 5-48), British antiaircraft guns, both heavy and light, began with a high level of effectiveness against daylight attacks. When the Luftwaffe switched to night attacks, antiaircraft guns, using sound locators and searchlights, were relatively ineffective; but successively better models of radar improved the effectiveness of heavy antiaircraft (HAA) rapidly. By the end of the war, radar and fire control developments, and the proximity fuze for HAA projectiles had reduced the rounds per kill to a few hundred for both guns and automatic weapons. The U.S. Caliber 0.50 with no fire control and low probability of a kill given a hit, remained at a very high RPB level. German systems were improved mostly by increased muzzle velocity, and increased calibers. They did not utilize proximity fuzes, but, by the vast numbers of guns, they were able to hit U.S. aircraft above 20,000 feet with high frequency as shown in Figure 5-49. This figure represents the number of aircraft damaged, whereas Figures 5-47 and 5-48 are for the number of aircraft killed.

Considering that the results shown were obtained in combat with operational degradation of the systems which may be estimated as factors of from 5 to 10, one may conclude that a modern antiaircraft gun system should have a design objective of fewer than 10 rounds per kill on a nonevading target. The U.S. M5A3 version of the Kerrison predictor, with the Bofors 40-mm gun, reliably obtained 30 percent hits on sleeve targets in proving ground tests in 1945, and the instrumental (i.e., system exclusive of target evasion) objective of a new system should be at least as high.

The following material develops the methodology for computation of hit and kill probability. It has two objectives, (1) to provide a means for anticipating simulation results by using simplified forms of the resulting relationships, and (2) to develop the algorithms for computer simulation. In the latter case, we would like to have a means for using the simulation in a deterministic mode, as opposed to a Monte-Carlo mode. This object has not yet been fully realized because of the difficulty of accounting for aim wander

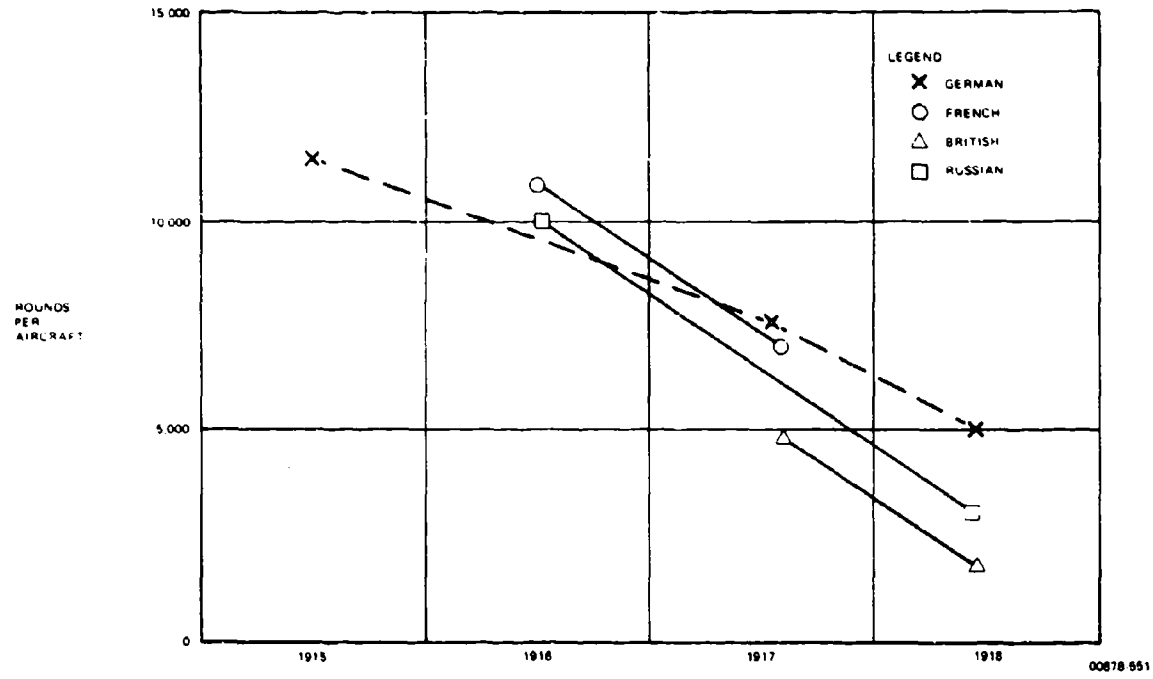

Figure 5-47. Heavy Antiaircraft Rounds Per Aircraft Kill from 1915 to 1918

and cross-correlations in closed form. For the present simulation, a compromise solution has been adopted: the point of aim of the gun is determined by a Monte-Carlo process; this is then combined with analytic expressions for kill probability as a function of miss distance, to obtain kill probability in simulation runs. The result is that the variation in results across replications is reduced, and a smaller number of replications are required to obtain significant differences.

The development begins with representations of the target and proceeds through single-shot probability to burst-kill probability.

5.6.1 Representation of the Target

Although it is probable that the target size (and especially its vulnerable area) will be small compared with the shot pattern throughout most of the AFAADS operational envelopes, there may be relatively large changes in the area presented to the pattern as determined by the target aspect (e.g., head on, almost directly overhead, etc.). This paper presents a target model which is consistent with the capabilities of the Ginsberg simulation. Furthermore, the target model is realistic, accounts for the size variations with target aspect, and avoids the assumption that the target size is necessarily small compared with the shot pattern.

We use the Von-Neumann/Carleton approximation of a 'diffuse' target. This states (for a circular target for simple exposition), that if a round passes the target at a distance u, v from the center of area, the probability that the target is hit is:

$$V = e^{-(u^2+v^2)/a^2} \tag{5.229}$$

Here a^2 is defined by:

$$\iint_{-\infty}^{\infty} e^{-(u^2+v^2)/a^2}\,du\,dv = \pi a^2 = A_t \tag{5.230}$$

where: A_t = the area of the target, normal to the projectile trajectories.

For a circular, normal distribution of the probability density function of bullets relative to the target with standard deviation σ, multiplying v by the power density function and integrating, the probability of a hit is:

$$a^2/(a^2+2\sigma^2) \tag{5.231}$$

If a target were a disc (flying saucer from directly above), the probability of a hit would be:

$$1 - e^{-a^2/(2\sigma^2)} \tag{5.232}$$

and the two expressions are to be identical for small $a^2/2\sigma^2$ and asymtotically correct for large $a^2/2\sigma^2$.

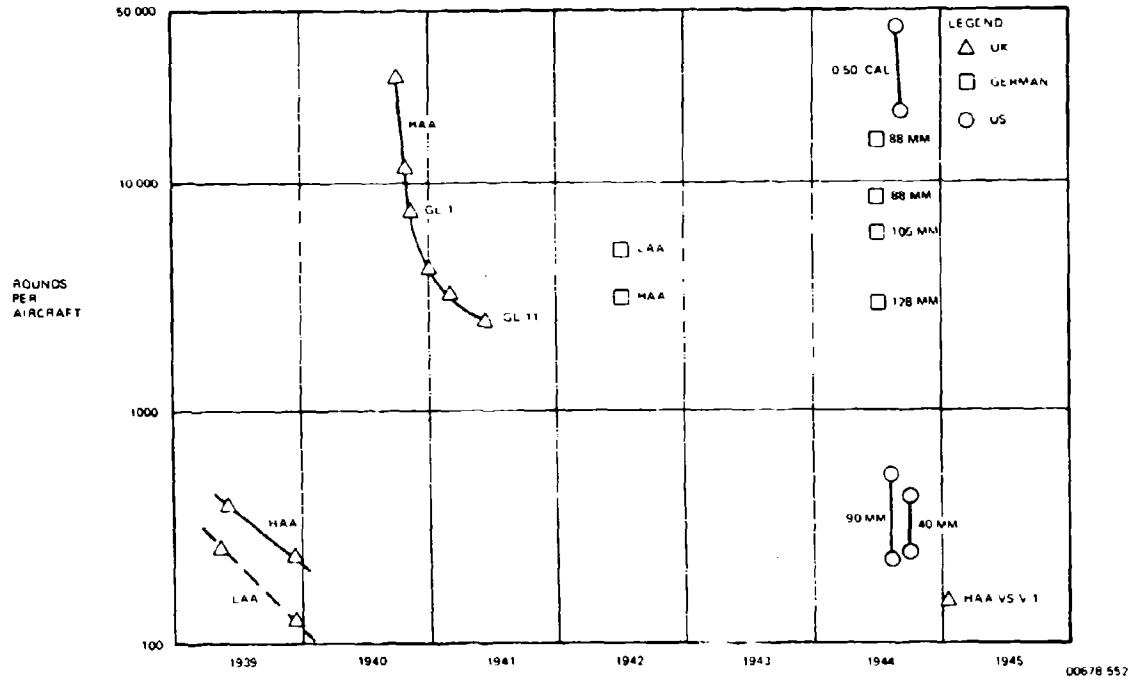

Figure 5-48. Heavy and Light Antiaircraft Rounds Per Aircraft Kill from 1939 to 1945

The probability that the target is killed, is obtained by multiplying the probability of a hit by the probability that a hit causes a kill, p(K H). When the presented area of the target is small compared with the shot pattern, the diffuse target approximation can be used by replacing target presented area A_t, by target vulnerable area A_v, where:

$$A_v = A_t p(K|H) \qquad (5.233)$$

Simply using A_v in the diffuse target representation instead of A_t may be close to the facts of vulnerability even when the target presented area is not small compared with the shot pattern, particularly since strikes on the extremities of the target (wing tips, fuselage remote from the crew station), are less likely to produce an immediate kill than strikes on the crew compartment, fuels cells, and armament bay.

Therefore, in the following development, the target is represented in terms of its vulnerable area only. If more detailed vulnerability data is provided by the vulnerability experts, the computation can be modified appropriately in a straightforward manner.

An earlier section of the report presented some estimates of p(K H) extrapolated from German WW II estimates. Because of the current European antiaircraft system development, a very conservative estimate (Figure 5-50) of p(K H) by Dr. Hans Brandli,[41] Director of Contraves, Zurich, is of considerable interest.

We represent the isoprobability contours of the fuselage by an ellipsoid with its long axis along the flight path. The projection of this ellipsoid is taken in a plane perpendicular to the direction of relative velocity of the projectile at the target, u axis horizontal, and the v axis in a vertical plane. Then for the fuselage:

$$V_f = e^{-(1/2)X' H_f X} \qquad (5.234)$$

where:

$$X' = [u \; v] \qquad (5.235)$$

$$H_f = \frac{2}{(1-r_f^2)^{1/2}} \begin{bmatrix} \frac{1}{a_f^2} & -\frac{r_f}{a_f b_f} \\ -\frac{r_f}{a_f b_f} & \frac{1}{b_f^2} \end{bmatrix} \qquad (5.236)$$

and

$$\iint_{-\infty}^{\infty} V_f \, dX = \pi a_f b_f = A_{vf} \qquad (5.237)$$

NOTE: $r_f = 1.0$ is a 'line' target. In integrating $V_f dX$, we have used the expression:

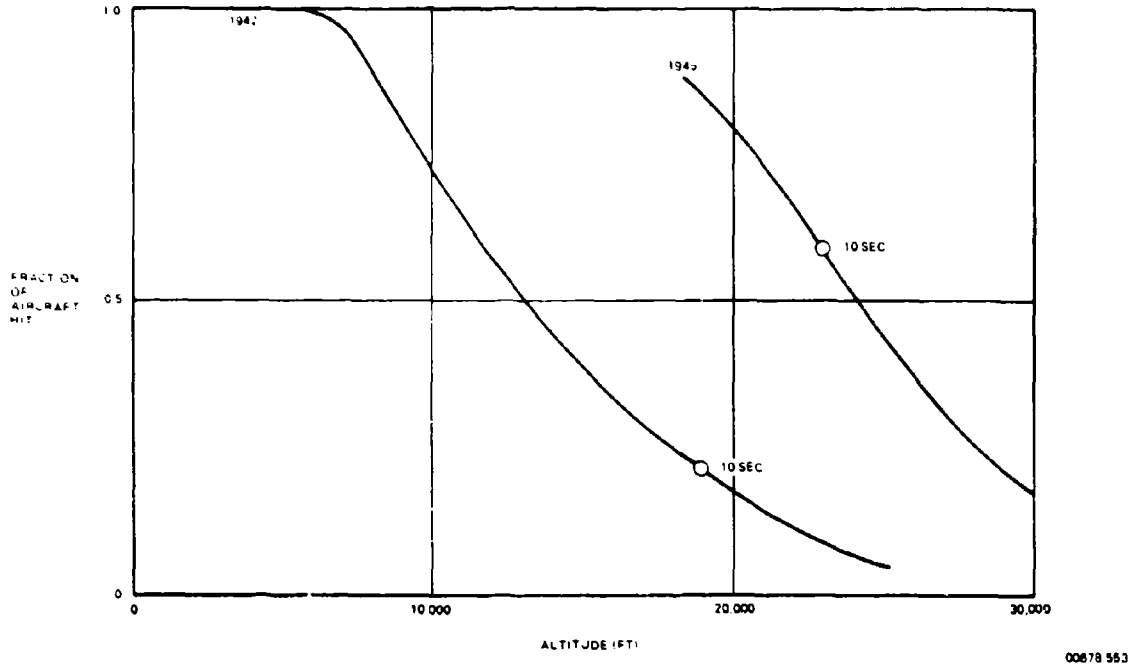

Figure 5-49. Eighth Air Force Aircraft Hit by Antiaircraft Versus Altitude

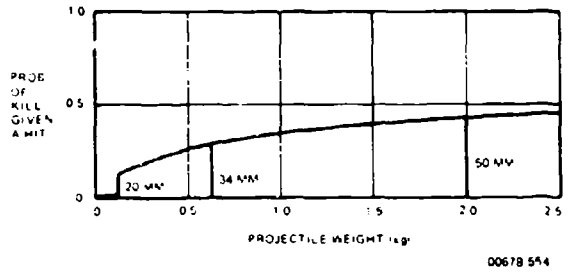

Figure 5-50. Probability that a Hit Destroys an Aircraft as a Function of Projectile Weight[41]

$$\iint_{-\infty}^{\infty} e^{-(1/2)X^T H X}\, dX = \frac{2\pi}{|H|^{1/2}} \qquad (5.238)$$

A_w is the projection of the fuselage vulnerable area in the plane perpendicular to the direction of approach of the bullets relative to the target, and r_c, a_c, h_c are obtained by coordinate transformations from the ellipsoid along the flight path.

A similar expression is obtained for the wing (which is a very 'thin' ellipsoid). To use this we need to know the bank angle of the aircraft, and this is obtainable from the information in the simulation when it is desired to introduce this improved representation. Then to take account of overlap, we have for the whole airplane:

$$V = V_f + V_w - V_f V_w \qquad (5.239)$$

$$V = e^{-(1/2)X^T H_f X} + e^{-(1/2)X^T H_w X} - e^{-(1/2)X^T [H_f + H_w] X} \qquad (5.240)$$

This is the desired result. The three terms are identical in form and go into the kill probability computation in the same way. The extension of the method to include multiply vulnerable targets is straightforward, tedious by hand, but could be easily done on the simulation.

5.6.2 Single-Shot Hit Probability

The arithmetic of computing hit probability becomes tedious even for single shot probability because the random round-to-round errors are not necessarily circularly distributed and the target may not be circular. The complexity increases when some components of error are constant during a burst, but randomly distributed across bursts, and are not drawn from a circular normal distribution. The notation presented by R. C.

Banash in SY-TN3-70[36] is a considerable assist and is applied and extended in the following discussion:

a. The coordinate system is assumed to be rectangular in a plane normal to the direction defined by the velocity of the projectile relative to the target. This plane contains the target center of gravity. The u axis is horizontal and the v axis is vertical.

b. The target is assumed to be diffuse, and is the projection of an ellipsoid (or two if wings are included) into the u, v plane.

Considering only one ellipsoid in the following (the extension to the fuselage plus wing, including correction for overlap is straightforward), the probability that a round passing at (u, v) kills the target is:

$$V = e^{-(1/2)X'HX} \qquad (5.241)$$

The distribution of trajectory intercepts with the u, v plane is defined by its characteristic function:

$$\chi(T) = e^{iM'T - (1/2)T'ST} \qquad (5.242)$$

where:

$T' = [T_1\ T_2]$; T_j are indices

$M' = [M_u\ M_v]$; M_j are means

$$S = \text{moment matrix} = \begin{bmatrix} \sigma_u^2 & \rho\sigma_u\sigma_v \\ \rho\sigma_u\sigma_v & \sigma_v^2 \end{bmatrix} \qquad (5.243)$$

The characteristic function and the probability density function f(X) are related by:

$$f(X) = (2\pi)^{-2} \iint_{-\infty}^{\infty} e^{-iT'X} \chi(T)\, dT \qquad (5.244)$$

$$\chi(T) = \iint_{-\infty}^{\infty} e^{iT'X} f(X)\, dX \qquad (5.245)$$

The single shot hit probability is:

$$P_{ss} = \iint_{-\infty}^{\infty} V(X) f(X)\, dX \qquad (5.246)$$

We make use of the integral:

$$\iint_{-\infty}^{\infty} e^{iR'Y - (1/2)Y'AY}\, dY$$

$$= \frac{2\pi}{|A|^{1/2}} e^{(1/2)R'A^{-1}R} \qquad (5.247)$$

substitute f(X) is terms of its characteristic function in P_{ss}, then:

$$P_{ss} = (2\pi)^{-2} \iint_{-\infty}^{\infty} e^{-(1/2)X'HX - iT'X} \chi(T)\, dT\, dX \qquad (5.248)$$

integrate over X and denote $J = H^{-1}$:

$$P_{ss} = \frac{|J|^{1/2}}{2\pi} \int_{-\infty}^{\infty} e^{-(1/2)T'JT} \chi(T)\, dT \qquad (5.249)$$

$$= \frac{|J|^{1/2}}{2\pi} \int_{-\infty}^{\infty} e^{iM'T - (1/2)T'[J+S]T}\, dT \qquad (5.250)$$

$$P_{ss} = \frac{|J|^{1/2}}{|J+S|^{1/2}} e^{-(1/2)M'[J+S]^{-1}M} \qquad (5.251)$$

This is the desired result.

As an example, the following conditions are assumed:

The target is assumed to be elliptical, the shot pattern is not centered on the target, and the random errors have an elliptical normal distribution with major axis differently inclined from the target's major axis;

Then:

$$J = H^{-1} = \frac{1}{2(1-r^2)^{1/2}} \begin{bmatrix} a^2 & rab \\ rab & b^2 \end{bmatrix} \qquad (5.252)$$

NOTE: r = 1.0 would represent a line target of zero depth.

and:

$$|J|^{1/2} = \frac{ab}{2} \qquad (5.253)$$

$$[J+S] = \begin{bmatrix} \dfrac{a^2}{2(1-r^2)^{1/2}} + \sigma_u^2 & \dfrac{rab}{2(1-r^2)^{1/2}} + \rho\sigma_u\sigma_v \\ \dfrac{rab}{2(1-r^2)^{1/2}} + \rho\sigma_u\sigma_v & \dfrac{b^2}{2(1-r^2)^{1/2}} + \sigma_v^2 \end{bmatrix} \qquad (5.254)$$

Rather than write out the complete expression for P_{ss}, we write the reduced form for small target area from the preceeding:

$$P_{ss} = \frac{A_V}{2\pi\sigma_u\sigma_v\sqrt{1-\rho^2}} e^{-\frac{1}{2}\left[\frac{M_u^2}{\sigma_u^2} - 2\rho\frac{M_uM_v}{\sigma_u\sigma_v} + \frac{M_v^2}{\sigma_v^2}\right]} \qquad (5.255)$$

which we could have written down by inspection initially. However, it checks the preceding algebra. When target size is not small, but $r = \rho = 0$, then:

$$p_{ss} = \frac{a\,b}{\left[(a^2 + 2\sigma_u^2)(b^2 + 2\sigma_v^2)\right]^{1/2}} e^{-\frac{M_u^2}{a^2 + 2\sigma_u^2} - \frac{M_v^2}{a^2 + 2\sigma_v^2}} \qquad (5.256)$$

Again this is a well known result. The principal advantage of the more general solution is that it allows r and ρ to be included.

5.6.3 Probability of at Least One Hit in a Burst

There are three categories of errors in the hit probability problem. They are: (1) errors which are random round to round, (2) errors which are deterministic, once the target path and fire control dynamics are fixed (for example, servo lags, linear predictor lags on a curved course, bore sight errors, etc.), and (3) errors which can be assumed constant during a burst, but are chosen from a random distribution across many bursts. For present purposes, we assume that the last class can be described as stationary time series (functions) with specified variance and autocovariance with time. This assumption can be relaxed on the simulator.

5.6.3.1 Aim Wander

Class (3) errors are commonly called 'aim wander' and this is a convenient term. In fact, they are not generated by a stationary process, and properly, both the variance and the autocovariance in time should be expressed as functions of time. We recognize this fact and allege that the precision sought for the present analysis allows a simpler description. However, the magnitude of this component could be so large for short smoothing times and especially with a quadratic component of prediction, that we feel it must be treated explicitly for burst times which approach the characteristic time (however defined) of the autocovariance function. For 2-second smoothing and a 1-second burst, the interaction is intimate.

As previously developed, the single shot hit probability p_{ss} is:

$$p_{ss} = p_0\, e^{-(1/2)\,M\,A^{-1}\,M} \qquad (5.257)$$

where:

p_0 is single shot hit probability with zero 'bias'

M is the bias matrix

A^{-1} is a 2 by 2 matrix describing the random round to round variances, correlations (uv) in the plane at a specified time, projected target vulnerability dimensions, and orientation.

The matrix M has two components:

$$M = \mu + m \qquad (5.258)$$

where:

μ defines the 'deterministic' components and,

m defines the components which are constant during a burst but random across bursts.

5.6.3.2 Burst Probabilities

Consider a burst with n rounds. For specified M, the probability that the target survives is:

$$\phi = n(1 - p_{ssj}) = e^{\sum_n \text{Log e}\,(1 - p_{ssj})}$$

$$= e^{-\sum_n p_{ssj} - (1/2)\sum_n p_{ssj}^2} \qquad (5.259)$$

and if all the single shot probabilities are the same:

$$\phi = e^{-n\,p_{ss}} \qquad (5.260)$$

$$\phi = \sum_{k=0}^{\infty} \frac{(-np_{ss})^k}{k!} \qquad (5.261)$$

The expected value of ϕ averaged over all m is:

$$\underline{\Phi} = \langle \varphi \rangle = \sum_{k=0}^{\infty} (-n)^k / k! \iint_{-\infty}^{\infty} (p_{ss})^k\, f(m)\, dm \qquad (5.262)$$

and since we have assumed that f(m) has an elliptically normal density function with zero mean,

$$f(m) = |B|^{1/2}/(2\pi)\, e^{-(1/2)m'Bm} \qquad (5.263)$$

Then substituting $M = \mu + m$ in the p_{ss} expression (5.257):

$$\varphi = \frac{|B|^{1/2}}{2\pi} \sum_k \frac{(-np_0)^k}{k!} \iint_{-\infty}^{\infty} e^{-(k/2)[\mu + m]' A^{-1} [\mu + m] - (1/2)m'Bm}\, dm \qquad (5.264)$$

Expanding the terms in the exponent inside the integral, we obtain:

$$(k/2)\left\{\mu' A^{-1}\mu + m' A^{-1}\mu + \mu' A^{-1} m + m' A^{-1} m\right\} + (1/2)m'Bm \qquad (5.265)$$

Now $A^{-1}m = m'A^{-1}$ since both are scalars and A is symmetric.

Denote $C = kA^{-1}$; $K = B + C$

Then:

$$\underline{\phi} = \frac{|B|^{1/2}}{2\pi} \sum_{k=0}^{\infty} \frac{(-np_o)^k}{k!} e^{-(1/2)\mu' C\mu} \iint_{-\infty}^{\infty} e^{-R'm - (1/2)m'Km}\, dm \tag{5.266}$$

where: $R' = \mu' C$; $R = C'\mu$

so that:

$$\underline{\phi} = \frac{|B|^{1/2}}{2\pi} \sum_{k=0}^{\infty} \frac{(-np_o)^k}{k!} \frac{2\pi}{|K|^{1/2}} e^{-\frac{1}{2}\mu' C\mu + \frac{1}{2} R' K^{-1} R} \tag{5.267}$$

Expanding the exponent we obtain:

$$-(1/2)\mu' C\mu + (1/2)\mu' CK^{-1}C'\mu \tag{5.268}$$

Now:

$$K = B + C \tag{5.269}$$

Postmultiply by K^{-1}

$$I = BK^{-1} + CK^{-1} \tag{5.270}$$

Postmultiply by C'

$$C' = BK^{-1}C' + CK^{-1}C' \tag{5.271}$$

C is a symmetric matrix, C = C'

hence the exponent reduces to:

$$-(1/2)\mu' B\,[B + C]^{-1} C'\mu \tag{5.272}$$

and finally:

$$\underline{\phi} = \sum_{k=0}^{\infty} \frac{|B|^{1/2}}{|B + C|^{1/2}} \frac{(-np_o)^k}{k!} e^{-1/2\,\mu' B\,[B+C]^{-1}C'\mu} \tag{5.273}$$

This is the desired result.

A simple special case of our general expression which has been much studied is the following:

a. The target is circular, and diffuse, with an effective radius a.

b. Round to round dispersion has a circular normal distribution with variance σ^2 in each coordinate.

c. Bias has a circular normal distribution with variance σ_r^2 in each coordinate, and a zero mean.

Although widely used, *this is a dangerous assumption* when the objective is to determine 'optimum dispersion.' If the distribution of 'bias' is a very narrow ellipse, the advantages of increased artificial dispersion by means of a circular normal distribution appear to vanish almost completely. We discuss this in the section on Artificial Dispersion.

Writing ϕ directly:

$$\underline{\phi} = \int_0^{\infty} e^{-np_o e^{-r^2/c}} e^{-r^2/(2\sigma_r^2)}\, d(r^2/2\sigma_r^2);\ c = a^2 + 2\sigma^2 \tag{5.274}$$

Expanding the exponential and integrating term by term:

$$\phi = \sum_{k=0}^{\infty} \frac{(-np_o)^k}{k!} \left[\frac{a^2 + 2\sigma^2}{a^2 + 2\sigma^2 + 2k\sigma_r^2}\right];\ p_o = \frac{a^2}{a^2 + 2\sigma_r^2} \tag{5.275}$$

For comparison we apply the general formula of the present paper and allow 'bias' to have, in addition, a component that is constant over all bursts. The matrices are:

$$kA^{-1} = C = \frac{2k}{a^2 + 2\sigma^2}\, I \tag{5.276}$$

$$B = \sigma_r^2\, I \tag{5.277}$$

$$B + C = 2\left[\frac{a^2 + 2\sigma^2 + 2k\sigma_r^2}{2\sigma_r^2(a^2 + 2\sigma^2)}\right] I \tag{5.278}$$

$$\frac{|B|^{1/2}}{|B + C|^{1/2}} = \frac{a^2 + 2\sigma^2}{a^2 + 2\sigma^2 + 2k\sigma_r^2} \tag{5.279}$$

$$B\,[B + C]^{-1} C = \frac{2k}{a^2 + 2\sigma^2 + 2k\sigma_r^2} \tag{5.280}$$

and finally:

$$\phi = \sum_{k=0}^{\infty} \frac{(-np_o)^k}{k!} \left[\frac{a^2 + 2\sigma^2}{a^2 + 2\sigma^2 + 2k\sigma_r^2}\right] e^{-\mu_r^2 \frac{2k}{a^2 + 2\sigma^2 + 2k\sigma_r^2}} \tag{5.281}$$

where:

$$\mu_r^2 = \mu_u^2 + \mu_v^2 \tag{5.282}$$

This series converges since for large k an individual term is:

$$\frac{(-np_0)^k}{(k+1)!}\, e^{-\mu_r^2/(2\sigma_r^2)} \qquad (5.283)$$

5.6.3.3 Resolution of Aim Wander into Components

By aim wander, we mean that component of error in aiming the gun which can be represented by a stochastic process, correlated in time, with a zero mean. It may arise from 'flight roughness' of the target trajectory, or correlation resulting from the processing of tracking noise in the smoothing and prediction elements of the computer.

An ingenious method for dividing aim wander into two components was developed by Dr. J. G. Tappert some years ago. It consists of resolving aim wander into two components, one of which can be included with the random round to round errors during a burst, and the other of which is considered to be constant during a single burst and randomly distributed across more than one burst. For a given autocorrelation function of aim wander, as the burst length increases the proportion of aim wander variance which is considered to be random round to round increases.

The method, although approximate, is both convenient to use and asymptotically correct for long and short characteristic times of the correlation functions.

The following development is different from that used by Tappert but the results are identical.

The method is described for a single coordinate. Let x(t) be the component of aim error which we call 'aim wander.' It is described by its autocovariance R(s), or alternately, but the power spectral density $\phi(\omega^2)$ which is the Fourier transform of the autocovariance function.

Assume that x(t) is passed through a filter which simply averages x(t) over the length of burst T_b, so that the filter output x(t) is:

$$x(t) = T_b^{-1} \int_0^{T_b} x(t-s)\, ds \qquad (5.284)$$

The transfer function of the filter is:

$$H_f(j\omega) = (1 - e^{-j\omega T_b})/(j\omega T_b) \qquad (5.285)$$

and the square of the absolute magnitude of the filter's transfer function is:

$$|H_f(j\omega)|^2 = 2(1 - \cos \omega T_b)/(\omega T_b)^2 \qquad (5.286)$$

Then the standard deviation of the average value of x(t) over burst time T_b is obtained from:

$$\sigma_m^2 = \int_0^\infty \phi(\omega^2)\, |H_f(j\omega)|^2\, d\omega \qquad (5.287)$$

and this portion of the variance of aim wander is treated as constant during a single burst and random across more than one burst. The residue is treated as random round to round.

If we confine our attention to relatively short segments of the target path, so that we need not deal explicitly with the inherent nonlinearities of prediction geometry, and still consider only one coordinate, we may estimate the interrelationships among smoothing time, burst length, and the prediction algorithm. The concept has certain elements of similarity with those described in the more general paper of Slook.[37]

Define:

$S(\omega^2)$ = power spectral density of target roughness of flight

$N(\omega^2)$ = power spectral density of tracking noise

$\phi(\omega^2)$ = power spectral density of aim wander

$H_p(j\omega)$ = transfer function of the smoothing and predicting element of the computer.

Then:

$$\phi(\omega^2) = N(\omega^2)|H_p(j\omega)|^2 + S(\omega^2)|1 - H_p(j\omega)|^2 \qquad (5.288)$$

The first term represents the error produced because the predictor treats the noise as target signal; the second term represents the error produced because the predictor cannot predict target motion perfectly. These expressions can be computed in a straightforward manner. For a simple example to show how the prediction process correlates noise, we consider only the noise component of the above relation and assume that sensor noise is white.

For a predictor we assume exponential smoothing in position, and double exponential smoothing in velocity; so that high frequency noise is filtered out. The transfer function is:

$$H_p(s) = [1 + s(t_p + 2T)]/(1 + sT)^2 \quad ; s = j\omega \qquad (5.289)$$

and: T = effective smoothing time, t_p = time of flight.

Note that T for this filter is not the same as T for a finite memory filter.

We could combine this expression directly with the transfer function of the averaging filter and obtain σ_m^2, but we first perform the intermediate operation of determining the autocorrelation of predictor output error; as a result of its operation on white noise. It is, normalized to unit variance:

$$\rho(\tau) = \left\{1 - \frac{\tau}{T}\left[\frac{(2T + t_p)^2 \cdot T^2}{(2T + t_p)^2 + T^2}\right]\right\} e^{-\tau/T} \qquad (5.290)$$

This expression is very close to:

$$\rho(\tau) = (1 - \frac{\tau}{T})\, e^{-\tau/T} \qquad (5.291)$$

and we will not be far wrong if we approximate it as:

$$\rho(\tau) \cong e^{-2\tau/T} \qquad (5.292)$$

We infer the interesting conclusion that when we include the differentiating function in the filter, the characteristic time of the output error, expressed as an approximately equivalent Markov process, is only half the effective smoothing time of the filter.

If we put Markov noise with variance σ^2, and characteristic time T_m through the averaging filter, we find that:

$$\sigma_m^2/\sigma^2 = 2(\lambda - 1 + e^{-\lambda})/\lambda^2 \quad ; \lambda = T_b/T_m \qquad (5.293)$$

and this can be approximated for small λ as:

$$\sigma_m^2/\sigma^2 \cong e^{-\lambda/3} \qquad (5.294)$$

Our final approximation for the fraction of aim wander variance that is to be considered constant during a single burst and random across more than one burst is:

$$\sigma_m^2/\sigma_a^2 \cong e^{-(2/3)(T_b/T_s)} \qquad (5.295)$$

We conclude, subject to the limits of the various approximations made previously that if the characteristic time of correlation of sensor noise is small compared with smoothing time, and burst length is roughly equal to smoothing time, all of the aim wander component caused by tracking noise can be considered random round to round. These relationships are characteristic of a major set of our simulator runs, and the above argument probably explains why we found no advantage in artificial dispersion for these runs, in the absence of target evasion.

On the other hand, if the characteristic time of noise autocovariance is long relative to smoothing time, as it may be with manual tracking; or target flight roughness is considered, most of the resulting component of aim wander should be considered constant over a burst as shown in Tappert's analysis.

We note one additional characteristic of aim wander. The miss distance is the rms value of the miss distances in u and v. If we assume as a limiting case that the separate components are exponentially correlated in time but have zero cross correlation, we can compute the autocorrelation function of the radial miss. If both components are normally distributed with a zero mean, and the same variance σ^2, and the same autocorrelation $\rho(s)$; then from results appearing in the literature,[38] we find that the normalized autocorrelation of r is (all terms normalized to unit variance):

$$R(s) = \frac{F(s) \cdot (\underline{r})^2}{F(o) \cdot (\underline{r})^2} \qquad (5.296)$$

where:

$$F(s) = (1 + \rho)\, E[(4\rho)/(1 + \rho)^2] \quad : \text{E is the complete elliptic function of the second kind}$$

$$F(o) = 2.0$$

$$\underline{r}^2 = \pi/2 \qquad (5.297)$$

and to within 10 percent:

$$R(s) = [\rho(s)]^2 \qquad (5.298)$$

The time correlation of radial error is thus substantially less than the time correlation of the component errors for the preceding assumptions.

5.7 ARTIFICIAL DISPERSION

By artificial dispersion we mean the deliberate increase of the round to round deviation of individual projectile trajectories from the trajectories computed by the fire control system. The effect could also be called pattern fire, since it builds up over time a pattern of shots about the expected target position like that of a shotgun.

With the Gatling Gun an artificial dispersion pattern can be developed by canting individual barrels relative to the axis of rotation. The distribution function of the pattern depends on the inherent dispersion of individual barrels as well as on the amount of cant. It may be desirable to cant only every other barrel to develop a uniform coverage pattern.

An artificial dispersion pattern can also be developed by 'dithering' the gun servos. How effective this may be depends on the attainable frequency-amplitude relationship. One would like several cycles of dither within

a given burst, and the burst length may be a second or less.

An important consideration is how the desired artificial dispersion, if any, should vary with range. It would indeed be fortuitous if the constant angular dispersion produced by barrel canting were optimum for all ranges. Dithering does not have the disadvantage of constant angular value, and its amplitude may be controlled by the computer. The problem is one of mechanical realization.

In the following sections we consider first the use of artificial dispersion to maximize single-shot probability against a maneuvering target, and then consider the more general case of burst probability.

5.7.1 Polynomial Prediction Versus Noise and Artificial Dispersion

As noted in Section 5.6, artificial dispersion is more likely to be helpful in compensating for target maneuvers than for aim wander generated by tracking noise correlated in the filtering unit, since the latter can be kept low by proper design. We therefore consider briefly the interaction among quadratic prediction, tracking noise, and artificial dispersion, when the target generates a constant acceleration. This analysis provides a basis for anticipating results likely to be obtained on the simulation. To facilitate slide-rule computations, the simplest two- and three-point predictors are used. It was shown earlier that these predictors provide results consistent with the more sophisticated predictors.

Algorithms are given for one coordinate. In computing kill probability it is first assumed that the same prediction function is used in all coordinates; then the consequences of using acceleration prediction in one coordinate only are examined. Errors in computing time of flight are not included.

Considering a single coordinate, the target motion is:

$$x = A + Bt + 1/2\,Ct^2 \tag{5.299}$$

The simplest prediction algorithms are used, namely:

a. Linear Prediction:

$$x(t + a) = x(t)(1 + \beta) - x(t - T)\beta \tag{5.300}$$

b. Quadratic Prediction:

$$x(t + a) = x(t)(1 + 3\beta + 2\beta^2) - x\left(t - \frac{T}{2}\right)(4\beta + 4\beta^2) + x(t - T)(2\beta^2 + \beta) \tag{5.301}$$

where: $\beta = a/T$

T = smoothing time, or memory

a = time of flight.

If the target is accelerating, the bias of the linear predictor (steady state, constant acceleration) is:

$$Ca^2/2\,(1 + \beta)/\beta \tag{5.302}$$

Assume that position measurements are contaminated by tracking errors which are defined by zero mean, variance σ_o^2, and autocorrelation zero over T/2. Then the prediction error of the quadratic algorithm, against a constant acceleration target, has a zero mean and a variance σ_p^2 given by:

$$\left(\sigma_p/\sigma_o\right)^2 = 1 + 6\beta + 30\beta^2 + 48\beta^3 + 24\beta^4 \tag{5.303}$$

and the linear algorithm yields a variance of:

$$\left(\sigma_p/\sigma_o\right)^2 = 1 + 2\beta + 2\beta^2 \tag{5.304}$$

with a mean (lag, bias):

$$b = Ca^2/2\,(1 + \beta)/\beta \tag{5.305}$$

The variance ratios $(\sigma_p/\sigma_o)^2$ are plotted in Figure 5-51.

5.7.2 Kill Probability

We assume that the autocovariance of filtered tracking error has a sufficiently short characteristic time that we can obtain some understanding of the relationships among noise, prediction algorithm, and target acceleration can be achieved by examining single-shot probability alone. This is most likely to be acceptable when the single-shot probability is small. In a later section we consider burst kill probability in a more general way. On the simulation, aim wander, resulting from filtering of tracking error as well as target maneuvers, is considered explicitly. Then single shot probability can be assumed to be represented as:

$$P_{ss} = \frac{a^2}{a^2 + 2\sigma^2}\, e^{-b^2/(a^2 + 2\sigma^2)} \tag{5.306}$$

where: πa^2 = target vulnerable area. σ^2 = random round to round variance

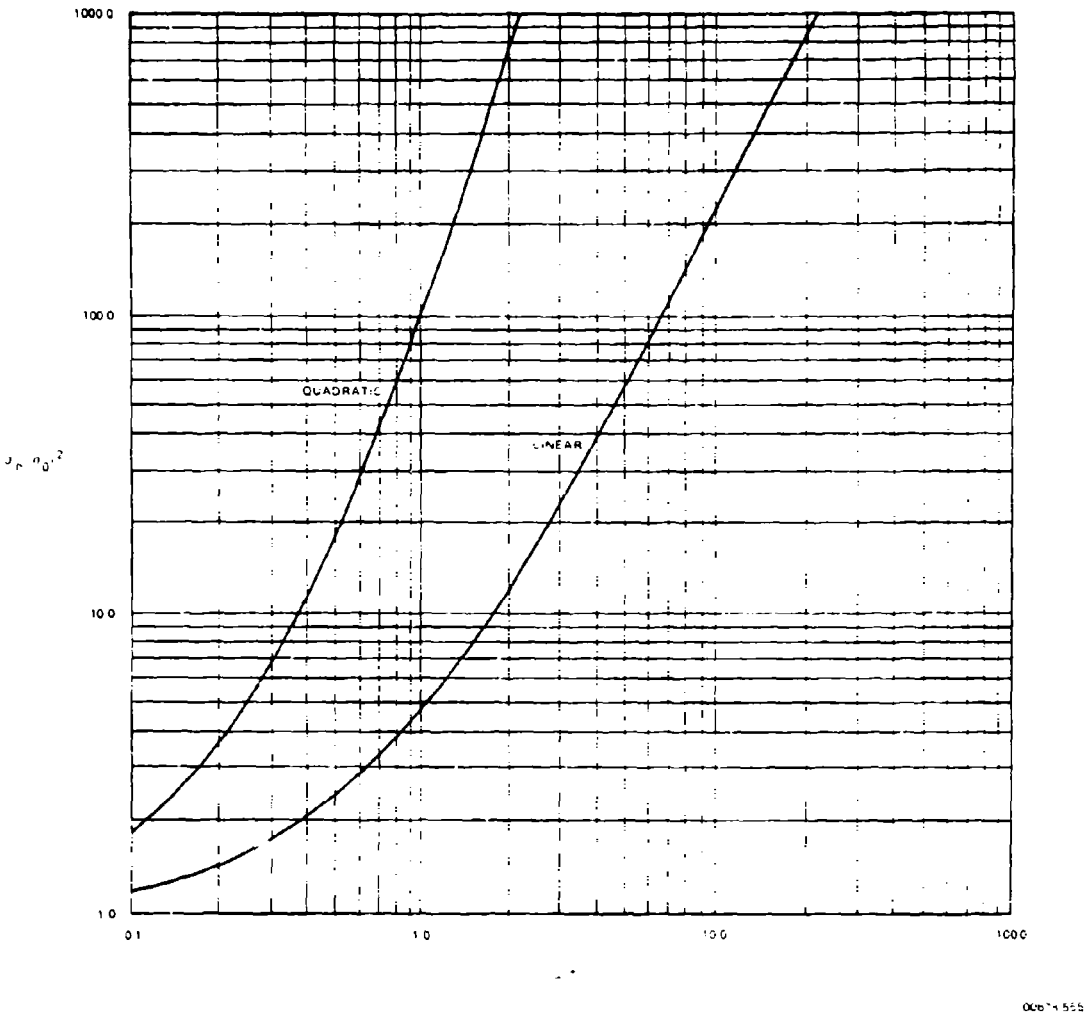

Figure 5-51. Noise Amplification in Quadratic and Linear Prediction

Assume in addition that:

$$\sigma^2 = \sigma_p^2 + \sigma_c^2 \tag{5.307}$$

where σ_c^2 is the variance of all other sources of random round to round error (including, for example, gun dispersion), and for simplicity assume:

$$a^2 + 2\sigma_c^2 \ll 2\sigma_o^2 \tag{5.308}$$

Again, this assumption can be removed without difficulty when desired, at some expense in algebra.

5.7.3 Optimum Dispersion

In the presence of known bias, single-shot probability may be improved by providing artificial dispersion. The optimum incremental dispersion is readily determined to be that value σ_a^2 which makes:

$$a^2 + 2\sigma^2 + 2\sigma_a^2 = b^2 \tag{5.309}$$

and so incremental artificial dispersion helps p_{ss} when:

$$b^2 > a^2 + 2\sigma^2 \tag{5.310}$$

or, for our simplified case, when:

$$b^2 > 2\sigma_p^2 \tag{5.311}$$

To further simplify notation, we designate:

$$P_{sso} = a^2/\left(2\sigma_o^2\right) \tag{5.312}$$

which is the single-shot hit probability with zero bias, and prediction variance equal to tracking variance.

5.7.4 Criteria and Boundaries

Define:

$$M_T = \tfrac{1}{2}CT^2 \tag{5.313}$$

Then in the (M_T, β) plane, regions can be developed showing where linear or quadratic prediction are preferred, and also the effect of incremental artificial dispersion. Taking these in order, comparing quadratic prediction with linear prediction without artificial dispersion, the decision boundary is defined by:

$$(P_{ss})_{linear} = (P_{ss})_{quadratic} \tag{5.314}$$

which, after some manipulation of the P_{ss} expressions, is determined to be:

$$\left(M_T/\sigma_o\right)^2 = 2\,\frac{(1 + 2\beta + 2\beta^2)}{\beta^2(1+\beta)^2} \times \log_e\left[\frac{1 + 6\beta + 3\beta^2 + 48\beta^3 + 24\beta^4}{1 + 2\beta + 2\beta^2}\right] \tag{5.315}$$

For small β: $\left(M_T/\sigma_o\right)^2 \cong 8/\beta$ (5.316)

For large β: $\left(M_T/\sigma_o\right)^2 \cong (4/\beta)^2(\log_e 12\beta^2)$ (5.317)

Now consider when incremental artificial dispersion is desirable with linear prediction and an accelerating target. The boundary is readily determined to be:

$$\left(M_T/\sigma_o\right)^2 = 2(1 + 2\beta + 2\beta^2)/[\beta^2(1+\beta)^2] \tag{5.318}$$

For small β: $\left(M_T/\sigma_o\right)^2 = 2/\beta^2$ (5.319)

For large β: $\left(M_T/\sigma_o\right)^2 = 4/\beta^2$ (5.320)

Artificial dispersion, when used, improves P_{ss} in a region where quadratic prediction is preferable to linear prediction without artificial dispersion. In fact, artificial dispersion extends the region in which linear prediction is preferred. We therefore determine the boundary between linear prediction with the best artificial dispersion and quadratic prediction. Single-shot probability with optimum artificial dispersion is readily determined to be:

$$P_{ss}\,P_{sso} = e^{-1}2\left(\sigma_o/M_T\right)^2[\beta^2(1+\beta)^2] \tag{5.321}$$

Setting this expression equal to P_{ss} for the quadratic prediction:

$$\left(M_T/\sigma_o\right)^2 = \frac{2e^{-1}\,[1 + 6\beta + 30\beta^2 + 48\beta^3 + 24\beta^4]}{[\beta^2(1+\beta)^2]} \tag{5.322}$$

and;

For small β: $\left(M_T/\sigma_o\right)^2 = 2e^{-1}/\beta^2$ (5.323)

For large β: $\left(M_T/\sigma_o\right)^2 = 48e^{-1}$ (5.324)

5.7.5 Partial Quadratic Prediction

As previously noted, when the target acceleration is not high, a higher hit probability is obtained with linear prediction and artificially increased dispersion than with quadratic prediction. This is because the quadratic prediction amplifies the tracking noise greatly, even though it eliminates the bias. An obvious compromise is to use only a portion of the quadratic prediction term. This has the dual advantage of reducing bias and increasing dispersion, and if these are optimally balanced, one would expect a better hit probability than shown by the methods of the prior paragraphs.

We write the quadratic algorithm in modified form as:

$$x(t + a) = x(t) + \beta[x(t) - x(t - T)] + 2\lambda\beta(1+\beta) \times [x(t) - 2x\left(t - \frac{T}{2}\right) + x(t - T)] \tag{5.325}$$

Then:

$$\left(\sigma_p/\sigma_o\right)^2 = 1 + \beta(2 + 4\lambda) + \beta^2(2 + 4\lambda + 24\lambda^2) + 48\lambda^2\beta^3 + 24\lambda^2\beta^4 \tag{5.326}$$

and the bias is:

$$\tfrac{1}{2}CT^2\beta(1+\beta)(1-\lambda) \tag{5.327}$$

Set. $f(\lambda) = \left(\sigma_p/\sigma_o\right)^2$ (5.328)

$g(\lambda) = [\beta(1+\beta)(1-\lambda)]^2$ (5.329)

Then: $P_{sso}/P_{ss} = f\exp\left[\dfrac{M_T^2 g}{2f}\right]$ (5.330)

which has a minimum when:

$$2/M_T^2 = (g/f) - [(dg/d\lambda)/(df/d\lambda)] \tag{5.331}$$

It is possible for the optimum λ to be negative, for low target accelerations. This is because the algorithm is a three-point predictor; and in fact, for zero target

acceleration, a three-point minimum variance predictor reduces the effect of noise best when:

$$\lambda = -[1 2\beta(1+\beta)]^{-1} \qquad (5.332)$$

The algebra becomes increasingly tedious, and the expressions will not be written out here. For computation it is most convenient to choose λ,β and solve for M_T and p_{sso}/p_{ss}. The expressions are relatively simple for $\lambda = 0$. They are:

$$M_T^2 = \frac{4(1+2\beta+2\beta^2)}{\beta(1+\beta)(1+2\beta)^2} \qquad (5.333)$$

$$P_{sso}/P_{ss} = (1+2\beta+2\beta^2)\, e^{\frac{2\beta(1+\beta)}{(1+2\beta)^2}} \qquad (5.334)$$

The comparative effectiveness and regions of preferred use of the preceding prediction modes, as well as this interrelationship with dispersion, have been developed in the following figures:

Figure 5-52 shows the contours of the constant hit probability in the M_T,β plane; for simple linear, two-point prediction. Hit probability drops off very rapidly as the acceleration-produced component of target displacement approaches and exceeds the standard deviation of tracking error.

Figure 5-53 shows how optimum incremental dispersion expands the region within which hit probability does not drop below some specified value (such as the 0.01 contour). The effect is greatest for the low probability contours.

Figure 5-54 compares the linear with the quadratic prediction and shows the regions within which each is preferable. There is still a reduction in hit probability with target acceleration, within the linear prediction region, but the reduction in probability is arrested when the quadratic region is entered.

Figure 5-55 shows the preferred regions for linear, linear with increased dispersion, and quadratic prediction. The intermediate region is somewhat improved by using linear plus dispersion rather than quadratic.

Figure 5-56 shows the contours of the constant-hit probability, when the optimum partial quadratic algorithm is used. Below the $\gamma = 0$ contour only a very small improvement results, since the improvement represents, essentially, a smoothing of present position. Above the $\gamma = 0$ contour substantial improvement is indicated. The degree of improvement is easier to see in Figure 5-57, where the constant-hit probability contours are overlaid for the simple linear predictor and the optimum partial quadratic predictor. For example, when $\alpha/T = 2.0$ and the target acceleration produced displacement in T is twice the standard deviation of tracking error, the partial quadratic yields ten times the hit probability of the linear predictor.

In the foregoing figures, the effect of smoothing time T is submerged in the parametric representation. In fact, straight lines of constant slope T^3 represent constant smoothing time. The effect is made visible in Figure 5-58 for linear prediction and Figure 5-59 for the partial quadratic prediction. It is interesting to note, that in Figure 5-59, there is a region where the predictor performance appears relatively insensitive to smoothing time. This is further illuminated in Figure 5-60 which shows the effect of smoothing time on linear versus full quadratic predictor.

5.7.6 Comparison of Prediction Modes

As a specific example comparing prediction modes, first consider the threshold target acceleration, above which we obtain improvement from the quadratic prediction. The following are assumed: two values of σ_{ss}, 10 meters and 1 meter respectively, a time of flight = 3 seconds, and a smoothing time of T = 3 seconds. For the 10-meter tracking, there is no point in correcting for target accelerations less than 0.2g. For the more precise tracking, the boundary is 0.02g. Now consider the single-shot hit probability against a 1 meter target. Various cases of interest are summarized in Table V-5.

With poor tracking (10 meter), the optimum partial-quadratic prediction allows shooting at a 0.5g target with a degradation in hit probability of a factor of 6 compared with a factor of 17 for complete quadratic prediction, thereby resulting in 17,200 rounds per aircraft. With good (1 meter) tracking, a degradation of a factor of 17 is realized (since hit probability was originally so high), but rounds per aircraft against the accelerated target is 500. There is no point in shooting at the accelerated target at all without some form of quadratic prediction.

The above figures should be accepted with reservations, of course, since they are based on the assumption of no round to round correlation resulting from filtered tracking noise.

As a result of the preceding exercise, which was conducted early in the study, it was apparent that acceleration prediction at best was not likely to be very good if done in all three coordinates, because of the associated amplification of tracking noise. It was therefore decided to use the acceleration measurement for prediction in only one coordinate; with that coordinate to be in a horizontal plane perpendicular to the flight path, to correct for horizontal turns of the target. It was also decided to correct for target acceleration in a climb, or deceleration in a dive, by assuming 'constant total energy'; i.e., estimating vertical acceleration as -g sin θ; where θ = angle of climb. The latter correction is computed from the velocity measurements directly, and therefore does not introduce additional noise amplification.

Noting (from Figure 5-57 for example) that the

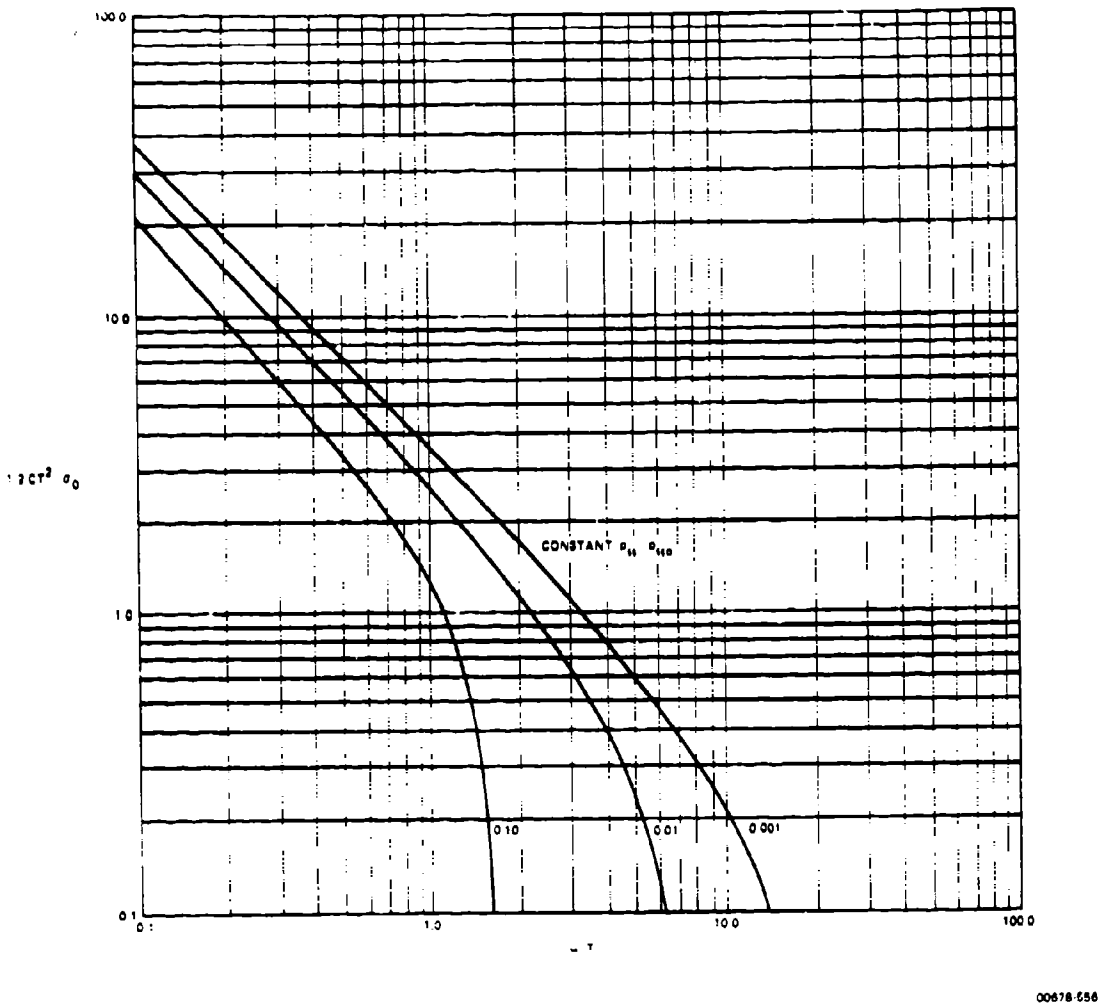

Figure 5-52. Contours of Constant-Hit Probability with Linear Prediction

most rapid degradation of kill probability is with the increasing time of flight for all prediction modes, and that this degradation can be arrested by increasing smoothing time with time of flight, it was also concluded that the smoothing functions should smooth the input data more heavily at the longer times of flight. As noted in the section on filtering, this is more easily done in a recursive algorithm than with a fixed memory filter. Therefore, future effort should be concentrated on appropriate recursive algorithms with weighting varying with time of flight (and possibly other parameters determined to be significant in further study).

5.7.7 Interaction of Optimum Dispersion with Acceleration Prediction Mode in Only One Coordinate

If the target accelerates in only one coordinate, for example in the direction of the v axis in the (u, v) plane, then the single shot probability is:

$$P_{ss} = \frac{a^2}{\left[\left(a^2 + 2\sigma_u^2\right)\left(a^2 + 2\sigma_v^2\right)\right]^{1/2}} \times e^{-b_v^2/\left(a^2 + 2\sigma_v^2\right)} \qquad (5.335)$$

and this reduces to our previous equation if we use the same prediction mode in both coordinates, and a circular dispersion pattern. If, however, we are clever

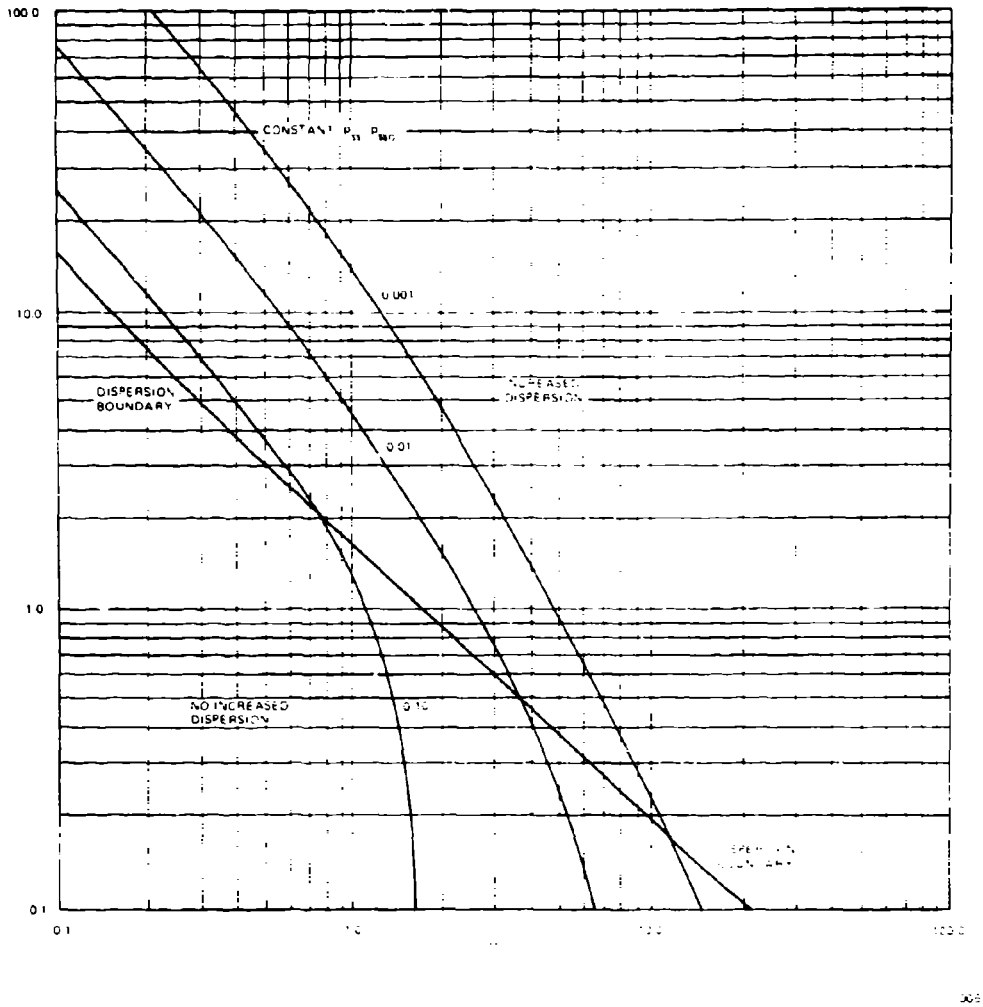

Figure 5-53. Region for Employing Increased Dispersion

enough to introduce artificial dispersion only in the direction of acceleration, the optimum dispersion (when required) in the v direction is:

$$\left(a^2 + 2\sigma^2 + 2\sigma_a^2\right)_v = b_v^2/2 \qquad (5.336)$$

and the kill probability with optimum dispersion is, using the same assumptions as before:

$$P_{ss}/P_{sso} = e^{-1}\left(\sigma_o/M_T\right)^2/[\beta^2(1+\beta)^2] \qquad (5.337)$$

Comparing this with the previously obtained expression, we see that we have doubled the kill probability over the case where we apply artificial dispersion with linear prediction in two dimensions.

Next, comparing kill probability with linear prediction in one coordinate and quadratic prediction in the direction the target is accelerating with quadratic prediction in both coordinates, we obtain the comparative kill probabilities as a function of $\alpha \cdot T$ as shown in Figure 5-61.

At a time of flight equal to smoothing time, kill probability is increased by a factor of five; if quadratic prediction is made only in the coordinate in which the target is accelerating. For a time of flight twice that of smoothing time, an improvement factor of ten is realized.

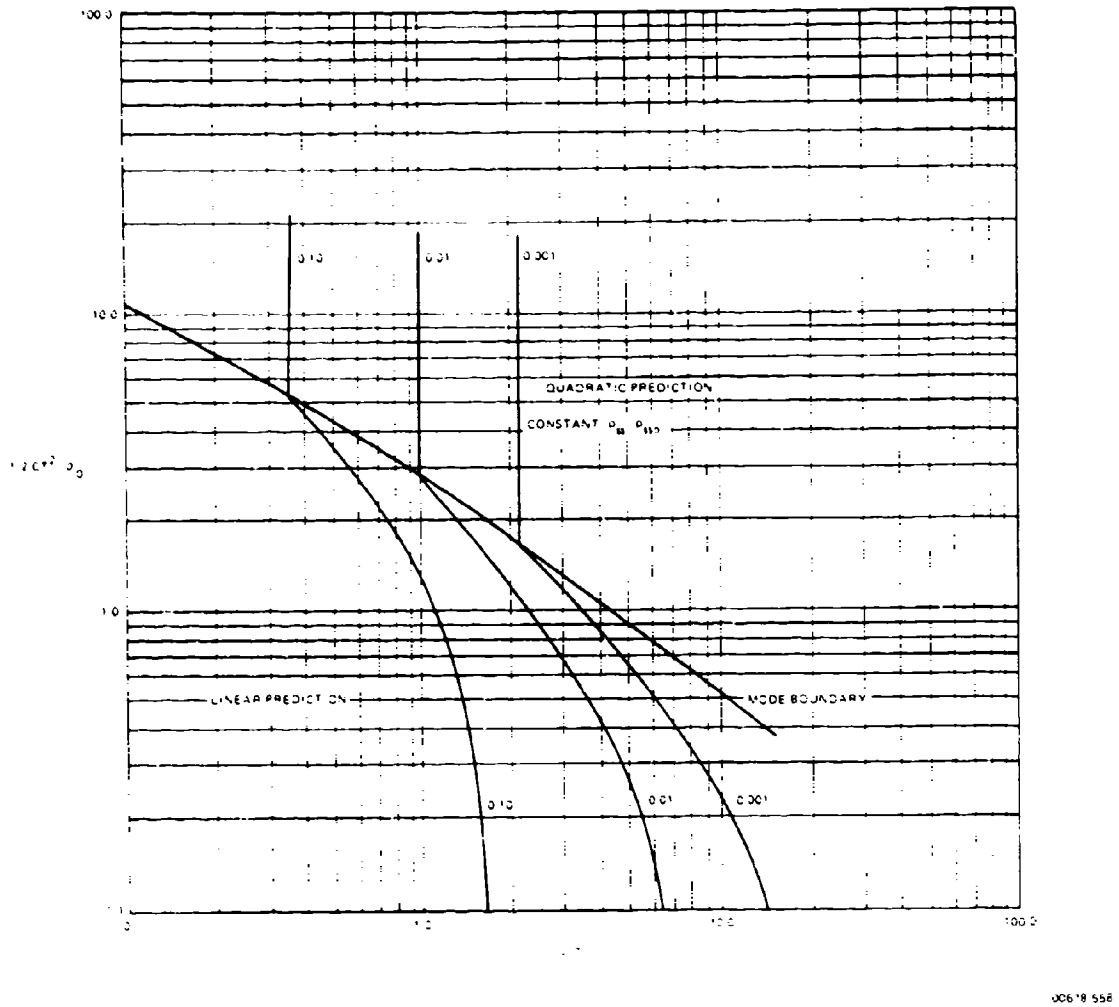

Figure 5-54. Linear Versus Quadratic Prediction Modes

5.7.8 Conclusions

We expect the findings obtained above to be valid for other weighting functions than the simple 2- and 3-point predictors considered here, but with higher probabilities in all cases, resulting from better smoothing of the noise. If turning targets are to be considered, the acceleration prediction should be only in one coordinate. The amount of quadratic prediction made (full or part correction) should be a compromise between systematic error, caused by incomplete prediction, and noise amplification in the acceleration measurement. Further analysis against realistic target paths should preferably be done on the simulation.

5.7.9 Artificial Dispersion When Target Acceleration is Not Measured

The previous section considered the case where target acceleration was constant for a sufficiently long time for the computer to measure the acceleration and predict, and for the projectiles to reach the target. An alternate possibility is that the target weaves, jinks, etc., so that a short burst will have a systematic error of center of aim. However, the error of aim point can be considered randomly distributed across bursts. This assumption also applies when the cause of aim error is slowly varying, i.e., 'aim wander'.

If we assume that the probability density function of point of aim is normally distributed in one or two dimensions, with zero mean, we will tend to prefer

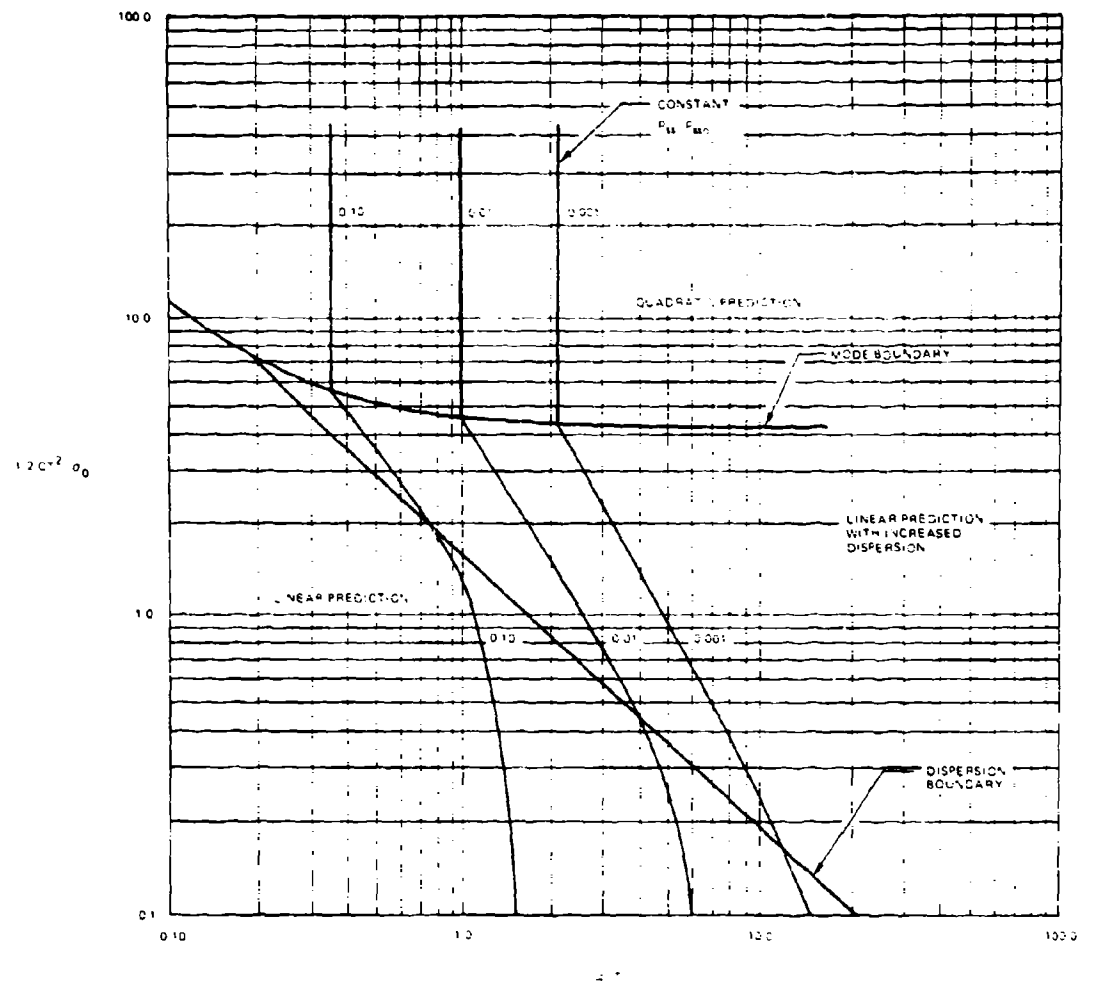

Figure 5-55. Optimum Prediction Modes

smaller artificial dispersion than if bias were constant across bursts, so as not to prejudice the effectiveness of the bursts fired when aim error is small. In fact, for one round we would always fire at the most probable target position, with zero dispersion, if possible.

The relationships for obtaining optimum dispersion in the general case are summarized in the following paragraphs.

First consider the case where both aim error and dispersion have circular normal distributions, with variance σ_r^2 and σ^2 respectively.

The basic expressions are well known:

$$p_{ss} = \frac{a^2}{a^2 + 2\sigma^2} e^{-\frac{r^2}{a^2 + 2\sigma^2}} = \text{single shot hit probability} \quad (5.338)$$

$$p_2 = \int_0^\infty e^{-Ae^{-By}} e^{-y}\, dy = \text{average target survival probability} \quad (5.339)$$

$$A = \frac{\pi a^2}{a^2 + 2\sigma^2}; \pi a^2 = \text{target area}; \sigma^2 = \text{random round to round variance} \quad (5.340)$$

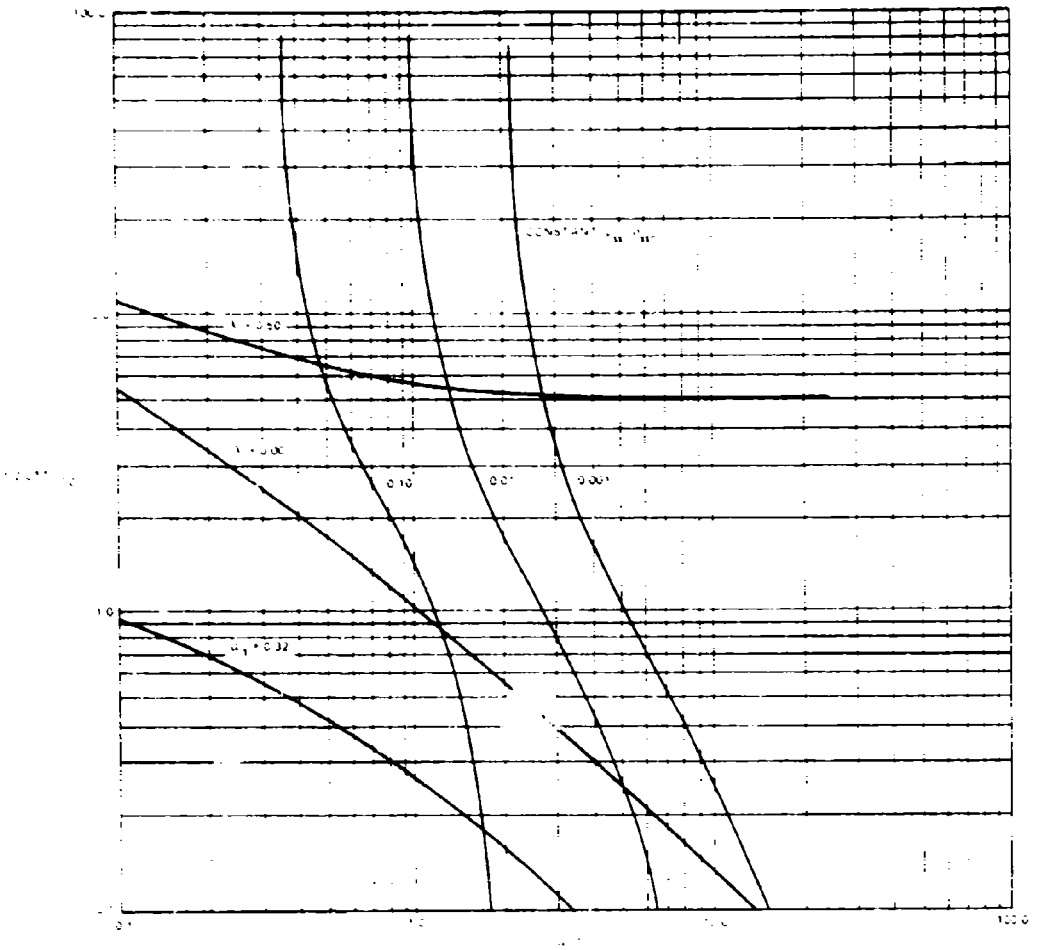

Figure 5-56. Partial Quadratic Prediction

$$B = \frac{2\sigma_r^2}{a^2 + 2\sigma^2} \quad ; \quad \sigma_r^2 = \text{variance of aim error across bursts} \qquad (5.341)$$

then:

$$\varphi_2 = \frac{1}{B} A^{\frac{1}{B}} \int_0^A e^{-y} y^{\frac{1}{B}-1} dy \qquad (5.342)$$

If the bias is distributed in one dimension only:

$$\varphi_1 = 2(\pi)^{-1/2} \int_0^\infty e^{-Ae^{-By^2}} e^{-y^2} dy \qquad (5.343)$$

and, unfortunately, this has not been related to a tabulated function.

The integrals can be expressed as series.

$$\varphi_2 = \sum_{j=0}^{\infty} \frac{(-A)^j}{j!(1+Bj)} \qquad (5.344)$$

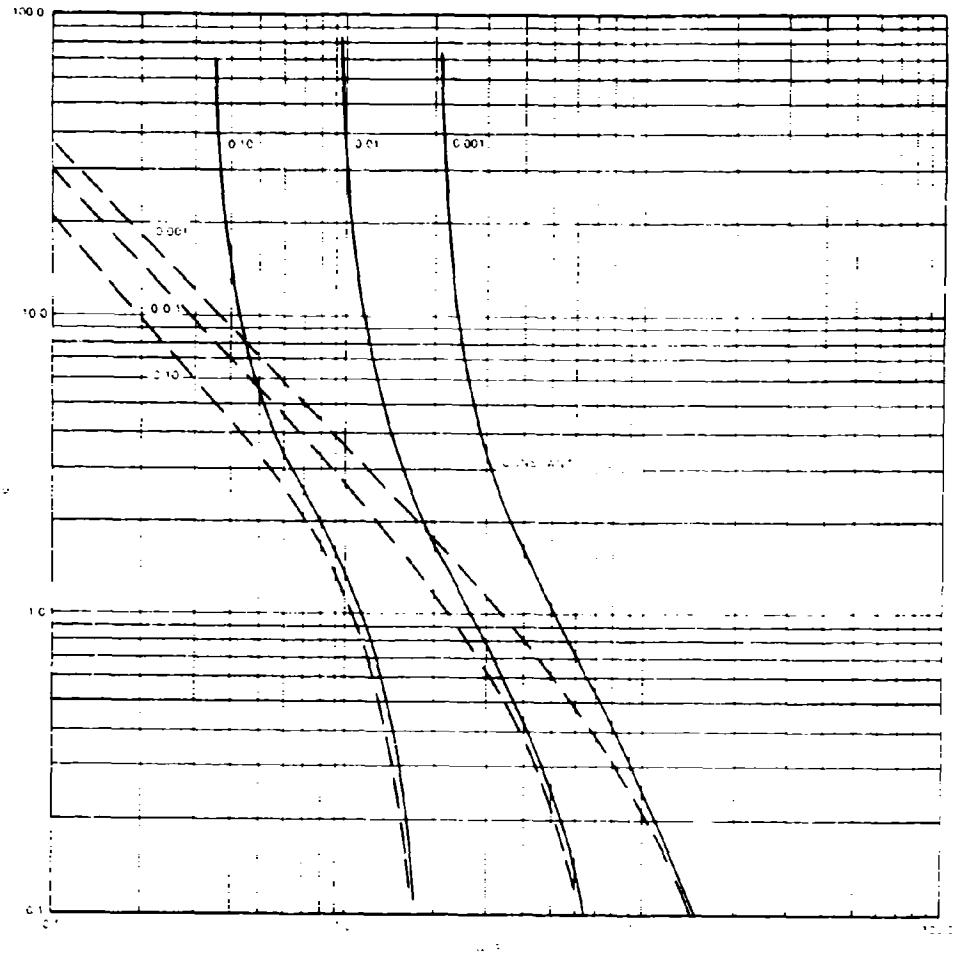

Figure 5-57. Linear Prediction Versus 'Best' 3-Point Predictor

$$\phi_1 = \sum_{j=0}^{\infty} \frac{(-A)^j}{j!(1 + Bj)^{1/2}} \qquad (5.345)$$

To obtain the optimum dispersion we set:

$$\partial \phi / \partial \sigma = 0 \qquad (5.346)$$

We can do this easily without extensive computations, only when A is small, and remains small within the region of optimization. This is true if na^2/σ_r^2 is small.

For this region we obtain the following results:

For bias and dispersion both having circular, normal distributions:

a. Optimum dispersion.

$$2\hat{\sigma}^2 \approx (na^2\sigma_r^2 2)^{1/2} - a^2 \qquad (5.347)$$

b. Kill probability.

$$\hat{p}_k \approx na^2/2\sigma_r^2 \qquad (5.348)$$

For circular normal distribution of dispersion, but bias normally distributed in one coordinate only:

a. Optimum dispersion.

$$2\hat{\sigma}^2 \approx (3na^2 2^3)^{2/3} - a^2 \qquad (5.349)$$

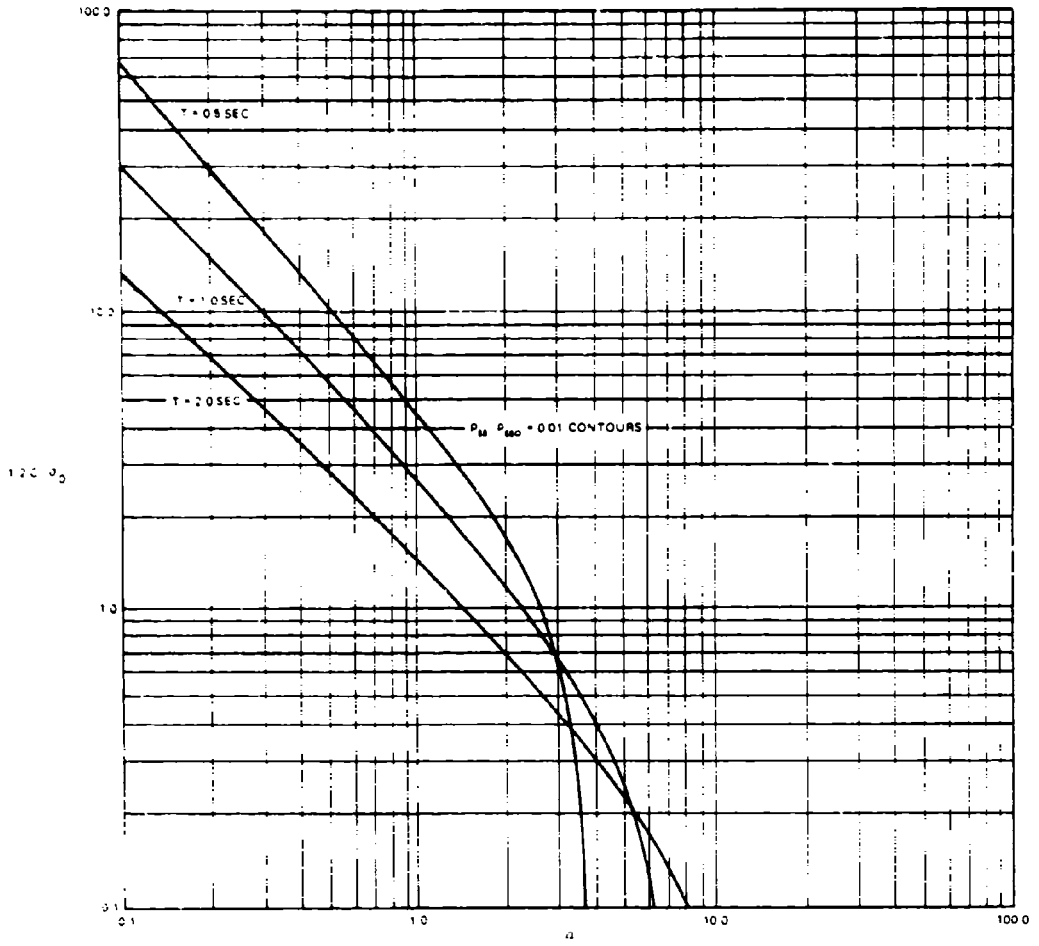

00678 562 A

Figure 5-58. Probability Contours Versus Time of Flight using Linear Prediction

b. Kill probability.

$$\bar{P}_K \sim \left[(2)^{1/2}\, n a^2\, 6\sigma_r^2\right]^{1/2} \qquad (5.350)$$

Note that to this order of approximation, when bias is distributed in one coordinate only, the optimum dispersion depends only on the number of rounds and the target size. This will be the normal case for a passing target. In addition, the optimum dispersion in meters is independent of range, and so cannot be achieved by constant angular dispersion at the gun. Assuming that the preceding algebra is correct, this is another reason for expecting the optimum circular dispersion pattern as derived on the simulation to be very small, even against maneuvering targets.

If dispersion can be varied in one dimension only, and that in the direction of the one dimensional bias distribution, the optimum dispersion is given by:

$$2\sigma_v^2 \sim \frac{1}{2}\left[\frac{2na^2\sigma_r^2}{(a^2 + 2\sigma_v^2)^{1/2}}\right]^{2/3} - a^2; \qquad (5.351)$$

σ_v is dispersion in the direction of bias.

and this does indeed increase with σ_r.

Comparing these three cases and noting that if σ_r results from a random target acceleration, it is therefore proportional to time of flight squared, we find that in the first case, artificial dispersion in meters should increase with range, corresponding roughly to constant angular dispersion. In the second case it

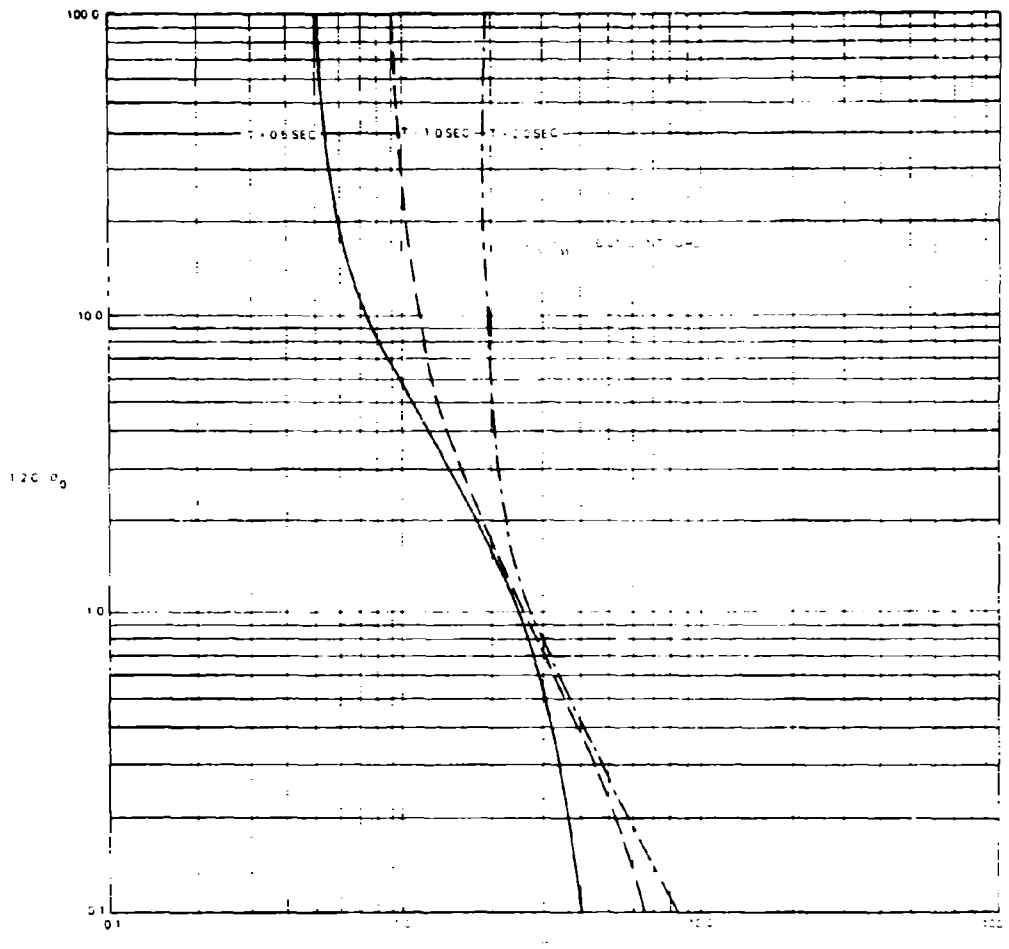

Figure 5-59. Probability Contours Versus Time of Flight using Optional Partial-Quadratic Prediction

should be constant with range, corresponding to angular dispersion decreasing with increasing range. In the third case it should increase more rapidly than range, but should be very small for close ranges.

The conclusion from the preceding considerations is that if constant angular dispersion is useful, it should show the greatest value against incoming targets maneuvering in two dimensions. We expect it to be of lesser value against crossing targets, even when they are jinking. It is hoped that time will permit the experimental investigation of these conclusions on the simulation.

5.7.10 Power Required for Dither

If:

I = inertia of the gun + moving parts in azimuth.

A = peak amplitude of dither.

ω = frequency of dither

θ = dither amplitude as a function of time.

Then: $\theta = A e^{j\omega t}$ (5.352)

The torque required to dither the inertia (ignoring friction) is:

$$T = I\ddot{\theta} \quad (5.353)$$

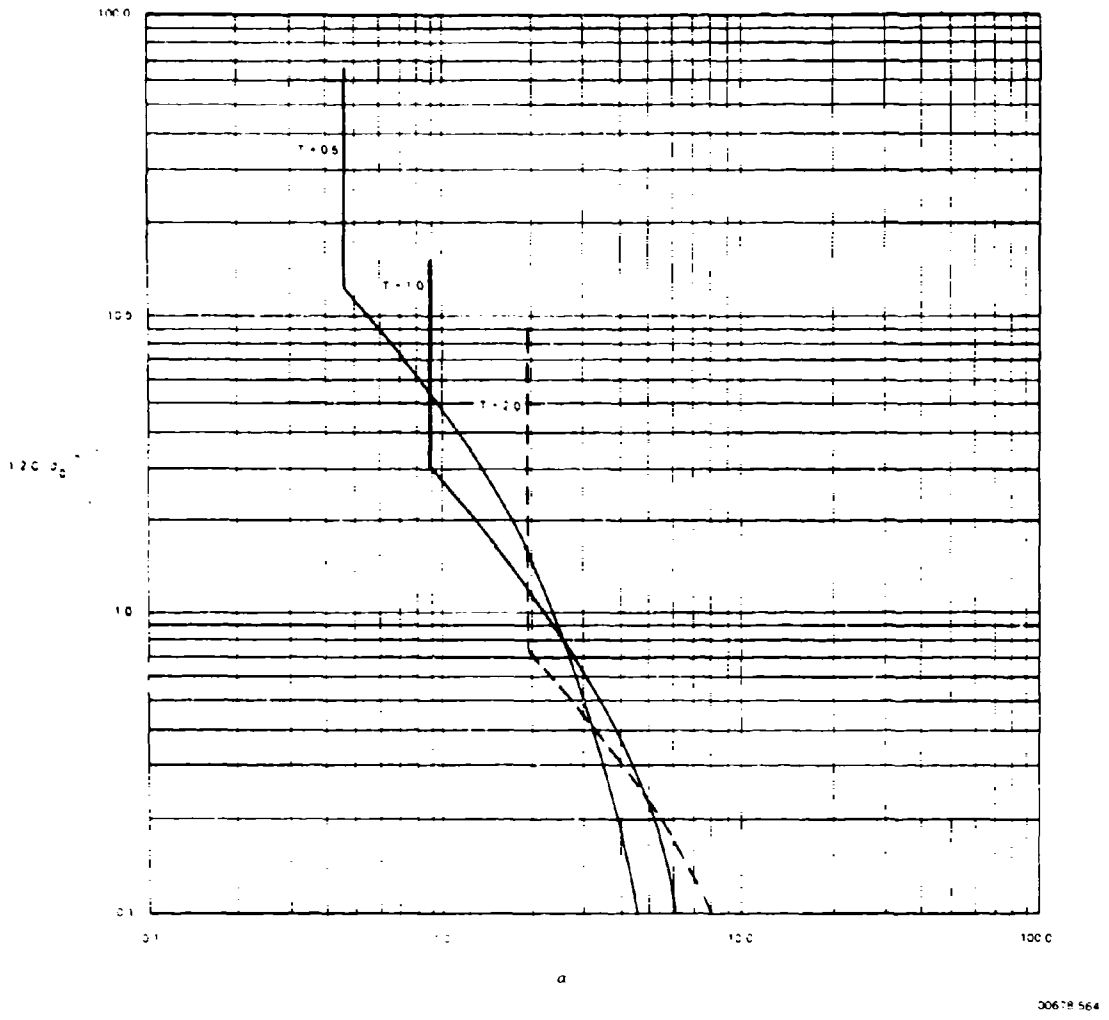

Figure 5-60. Probability Contours Versus Time of Flight using Linear and Quadratic Prediction

And the power required is:

$$P = I\ddot{\theta}\dot{\theta} \qquad (5.354)$$

For Vigilante in azimuth:

$$I = 6300 \text{ inch-lb-sec}^2$$

Writing $\omega = 2\pi f$, where f is frequency in Hz, peak power required to dither is:

$$P_{max} = IA^2\omega^3 = IA^2(2\pi f)^3 \qquad (5.355)$$

Letting θ_m = peak mil amplitude of dither in mils, and inserting the numerical constants:

$$P_{max} = \left(\frac{\theta_m}{1000}\right)^2 \left(\frac{6300}{(12)(550)}\right)(2\pi)^3 f^3 \qquad (5.356)$$

$$= \theta_m^2 f^3\, 2.5 \times 10^{-4} \text{ HP} \qquad (5.357)$$

A 5 mil dither at 3 Hz would require about 0.2 HP peak power. This seems feasible from the point of view of power, but needs to be carefully studied with regard to reactions on the mount, interference with the stabilization loops, gunner annoyance, gear wear, noise, and the general impression given an observer that something is wrong with the system.

Dither might be explored experimentally with the existing Vigilante by putting the gun servos out of adjustment, to see what it looks and sounds like in real life.

Table V-5. Expected Number of Hits with 100 Rounds

Target acceleration	0g		0.5g	
Tracking σ_0	10 Meters	1 Meter	10 Meters	1 Meter
Linear prediction	0.035	3.5	0.0000	0.0000
Quadratic prediction	0.002	0.2	0.002	0.20
Optimum part-quadratic	0.035	3.5	0.0058	0.20

00678-565

5.8 DYNAMIC CALIBRATION OF THE AFAADS SYSTEM

Anyone who has used fire control systems in the field is well aware of the problems involved in keeping them in good adjustment. In this respect digital components may have an advantage over analog components. For example, the digital components either work properly or not at all, whereas an analog component can be badly out of adjustment and still operate after a fashion. In reviewing the literature on fire control system experimentation for this contract it was noted that an important set of experimental firings produced questionable results because 'the exact cause for this apparent bias in the radar data is not known.' It is the personal opinion of this writer that there is an energetic group of technicians, who could be called 'The Adjusters' and who are always represented in any complex technological field operation. 'The Adjusters' use their skills to adjust radars so that they track smoothly, but with serious lag, analog computers so that they pass standard check point problems, but fail on operational courses, and air to ground rocket safety devices so that the warheads will never arm accidentally in flight, or intentionally when they hit the target. Probably the greatest coup of the 'Adjusters' resulted from their participation in the Navy pre-World War II torpedo development program.

A year after the SCR-584 was introduced to combat in the European theatre the Army found it necessary to send a special task force from the United States to deactivate the field fixes the 'Adjusters' had put on the sets in operation.

Boresighting and calibrating a complex fire control system is a difficult task in itself, aside from the enthusiastic assistance of maladjusting personnel. Maladjustment is the principal reason for using large artificial dispersion in AFAADS. If a simple, reliable method of field calibration can be provided that will allow daily calibration, much of the normal operational degradation may be avoided and a very high equipment effectiveness will be realized.

The following paragraphs suggest an approach to dynamic calibration. Its detailed implementation requires further study in conjunction with specific designs as AFAADS goes forward.

The basic idea is similar to that employed by Col. Kerrison in field adjustments of his Kerrison predictor for the 40-mm Bofors gun. That application was as follows: the predictor used a simple rate times time of flight solution. Gun superelevation was set in as a fixed value for a specific range. The time of flight corresponding to that range was set into the predictor as a constant value, and constant azimuth rate (arbitrary) was set into the predictor aided tracking control. The predictor traversed at the preset constant rate; and if the system was in proper adjustment, the guns led the line of sight by an amount equal to rate times time of flight. The gun was then fired, and the commander observed the trajectory (tracer) through the tracking telescope. If all was well, the tracer would enter the field of the moving telescope from above and pass diagonally down through the intersection of the vertical and horizontal cross hairs. Crossings of the horizontal cross hair in advance or behind of the vertical cross hair indicated faulty prediction and/or gun servo functioning. A small tolerance in adjustment was allowable because of ballistic dispersion. The method allowed systematic errors to be recognized quickly and simply, so that corrective action could be taken at once.

The same idea can be applied to AFAADS. If a rectangular coordinate system is used, constant X, Y, Z rates may be injected into the system so that the tracker points at the corresponding present position through the regenerative unit and the gun fires at the appropriate predicted position. The gun commander, watching through the visual sight, should see the tracers cross the intersection of the cross hairs, within the tolerance of whatever artificial dispersion is set. If

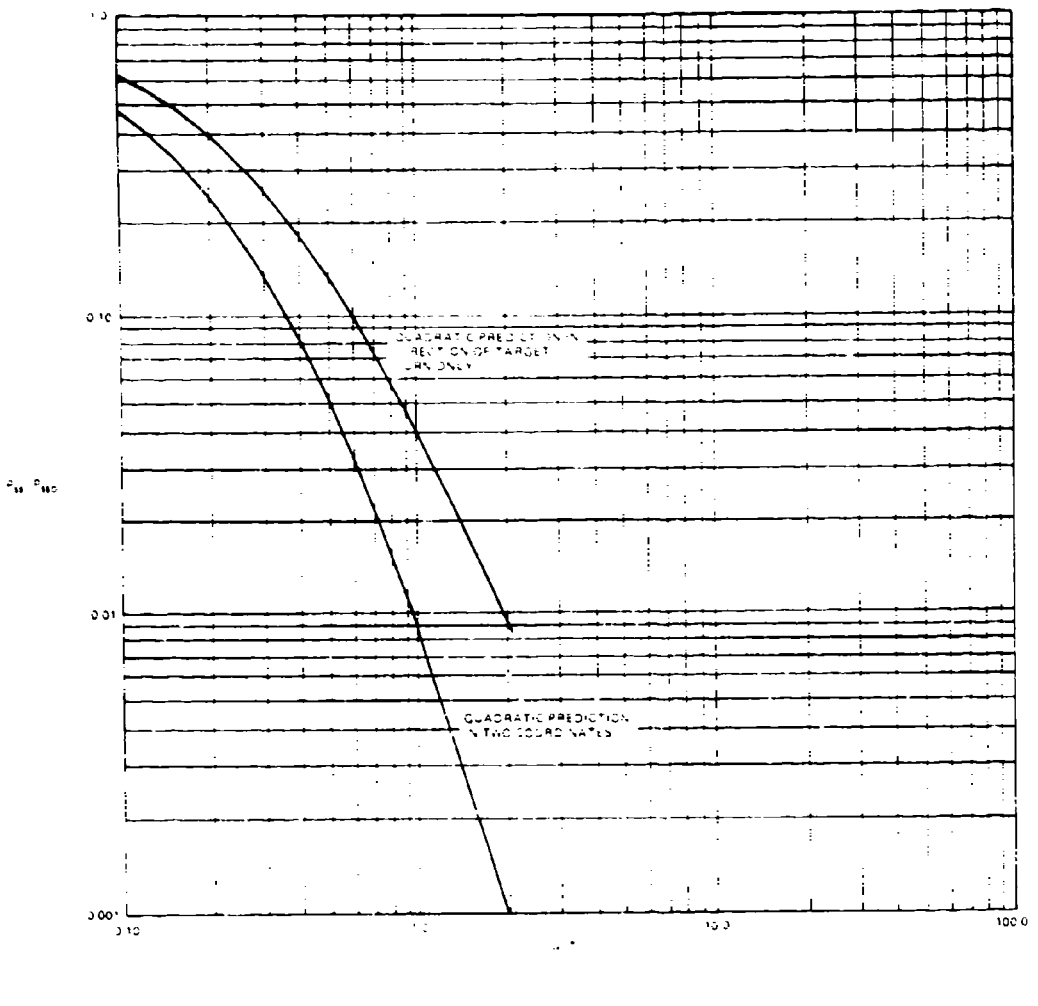

Figure 5-61. Comparison of Quadratic Prediction in One Versus Two Coordinates

artificial dispersion is set at a constant milvalue, the tracer pattern should form a symmetrical group within an appropriate milring in the sight. If the group is not symmetrical about the intersection of the cross hairs, the system is out of adjustment. He will not see a circular group, of course, but rather a pattern crossing his sight diagonally from above with an angular width equal to dispersion. See Figure 5-62.

This procedure does not test the sensor adjustment. To test the sensor and all of the servos in the system, including the gun servos, the ballistic element is set to a mode in which it outputs zero time of flight, superelevation, and other ballistic corrections. A real target is then tracked. The gun commander looks through a sight fastened to the gun tube. He will see the target remaining on the cross hairs of this sight if the system, with the possible exception of the ballistic unit, is in proper adjustment. For this test any passing aircraft, including friendly aircraft, will serve. The combination of the two tests thus tests the complete system dynamically.

5.9 MOUNT OSCILLATION AND VIBRATION ISOLATION

In this section we discuss the problems of firing while the AFAADS mount is in motion, as well as the problems of shock and vibration of the mount, caused by the gun firing, which are communicated to the human operator.

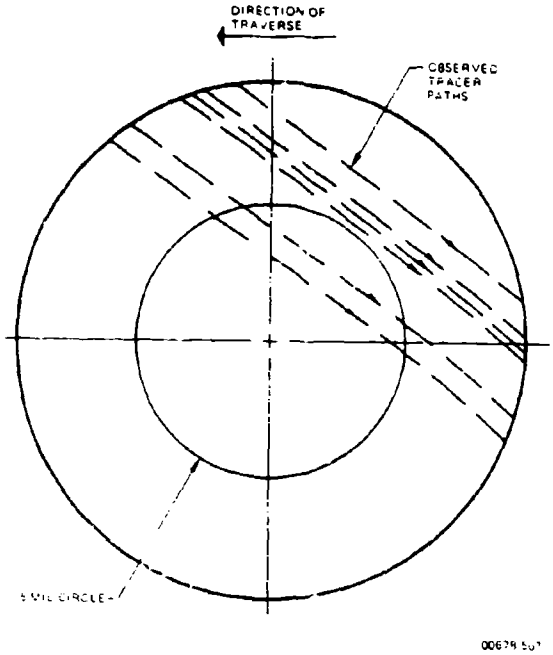

Figure 5-62. View Through Sight Showing Out-of-Adjustment Condition of System

5.9.1 Fire on the Move

It is desired that AFAADS have the (secondary) capability of engaging an aircraft target, while the AFAADS vehicle is in motion on a paved road. This section develops some tentative spectra for vehicle motions and their implications on tracking requirements.

The approach is: (1) to establish power spectral densities (PSD) of road unevenness, (2) determine transfer functions of the vehicle and its suspension, (3) determine the power spectral density of resulting angular deflection at the sight head. This final PSD can be compared with the man's ability to track, and/or used as a design objective for sight stabilization.

5.9.1.2 Ground Roughness

Many measurements have been made of the power spectral densities of terrain, varying from very smooth concrete runways to very rough cross country terrain. Bekker[36] has presented extensive summaries of these findings. For present purposes, it seems adequate to summarize these measurements as follows:

a. The power spectral density can be approximated as:

$$\Phi(\Omega) = \sigma^2 \frac{2}{\pi\Omega_0} \frac{1}{1 + (\Omega/\Omega_0)^2} \tag{5.358}$$

$$\frac{2}{\pi} \int_0^\infty \frac{d\Omega/\Omega_0}{1 + (\Omega/\Omega_0)^2} = 1.0$$

where Ω = cycles per foot and σ is expressed in feet.

Cornell[37], using the same data for very rough terrain, prefers to square the denominator of the above expression, with appropriate change in the coefficients. But for smooth terrain such as paved roads, the preceding expression seems to give a better fit.

b. The break frequency Ω_0 tends to fall between 3×10^{-3} and 10^{-2} cycles/foot (100-300 ft/cycle) on Bekker's chart.

c. The principal difference across terrain samples is in the value of σ. The zero frequency intercept:

$$\Phi(0) = \sigma^2 \frac{2}{\pi\Omega_0} \tag{5.359}$$

can vary over seven orders of magnitude (10^7), from concrete roads to rough terrain. This, of course, is not surprising. What is surprising is the relative invariance of the first-break frequency in measurements made for application to ground vehicles, and the identical shape of the PSDs over wide variations of terrain types (except, of course for the microstructure).

d. The principal difference between the Cornell approximation and the one used here appears to be at cycles shorter than 10 feet. This would be important for a jeep, but would be averaged by the AFAADS suspension. Hence, present findings can be extended, to some degree, to off-road motion.

In Figure 5-63, three terrain power spectral densities from Pradko[38] are shown. These are for cross country motion. Curve VI is for the Perryman Cross Country course at Aberdeen, and XII and XIII represent two samples of 'Cross Country Severe Roughness' at Fort Knox. Note that the break frequency appears to lie at about 10^{-2} cycles per foot. Comparing these with Bekker's curves for roads, we again confirm that the break frequencies are about the same. However, the zero intercept is about 10^{-2} ft^2/cycle/ft for cross country, whereas it is about 10^{-5} for roads.

We note a discrepancy across PSD measurements for ground vehicles and for terrain following aircraft. The PSDs for both should be consistent. If they were, the break frequencies for ground vehicles would be about

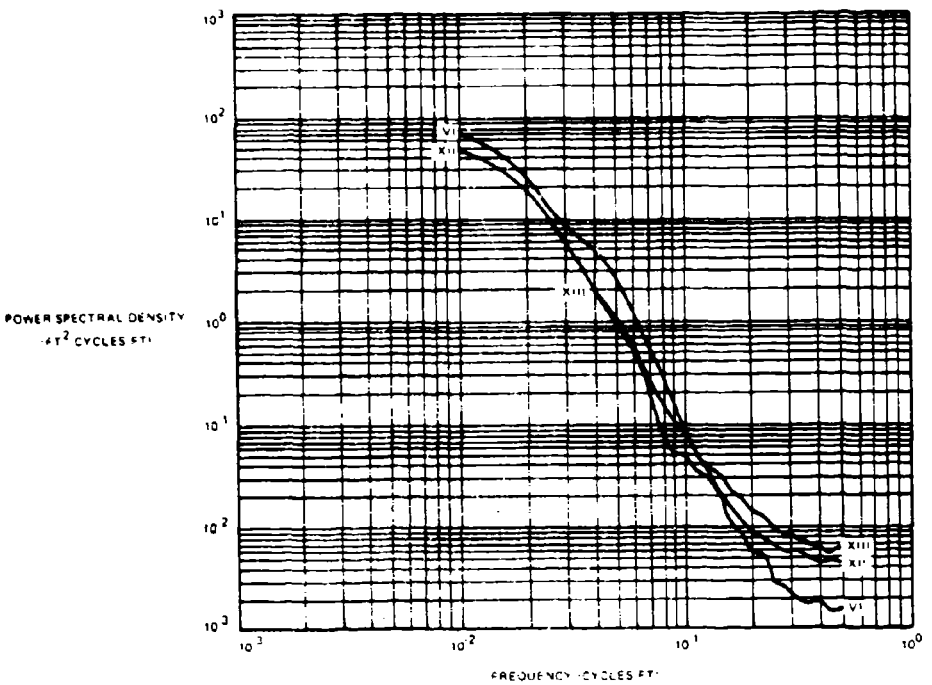

Figure 5-63. Power Spectral Density of Various Terrains

two orders of magnitude smaller. This is an area of terrain analysis that requires further study.

5.9.1.3 Vehicle Suspension

The simplest model of the vehicle and its suspension system is assumed. For simplicity we call the 'vehicle' all those elements which are supported by the suspension. A tracked or many-wheeled vehicle is implied. The weight of the vehicle W is supported by n springs, each having a spring rate of k, K = nk. The vehicle mass m = W/g. Ignoring damping and summing vertical forces, with y = vehicle, c.g., position in inertial space, relative to a fixed reference; and y_t = ground height from the same reference on flat ground then:

$$K(y - y_t) = W - m\ddot{y} \qquad (5.360)$$

The steady state spring deflection is:

$$Y_{ss} = W/k \qquad (5.361)$$

The natural frequency of the vertical oscillation is:

$$\omega_{nv}^2 = K/m = g/y_{ss} \qquad (5.362)$$

If the suspension deflects one foot under the weight of the vehicle then:

ω_{n_v} = 5.7 rad/sec = 0.9 cycles/sec

As will be shown, this is about right for at least one existing vehicle.

If a vertical sine wave excitation were applied uniformly across the base of the vehicle, the mean square amplitude of the vehicle motion would be:

$$\left|\frac{y}{y_i}\right|^2 = \left[\frac{1}{1-\left(\frac{\omega}{\omega_n}\right)^2}\right]^2 \qquad (5.363)$$

In real life, the suspension incorporates dampers. However, dampers reduce the ability of a spring suspension to perform vibration isolation at high frequencies, and to the degree that the suspension is supposed to achieve this end, damping should be kept as small as possible, consistent with reducing the amplification of motion at the resonant frequency.

Now consider the same simple model in pitch. Representing the vehicle approximately as a block L long and H high, its moment of inertia is:

$$I = m(L^2 + H^2)/12 \qquad (5.364)$$

Further assuming that the suspension can be represented as a spring force uniformly distributed along L at k (lb/ft/deflection/ft), the restoring torque for a rotation θ is:

$$T = 2\int_0^{L/2} k\,x^2\,\theta\,dx = k\frac{L^3\theta}{12}; \qquad (5.365)$$

$$\int_0^L k\,dx = kL \equiv K$$

and so the natural frequency in pitch is:

$$\omega_{np}^2 = \frac{k}{m\left(1+\frac{H^2}{L^2}\right)} = \frac{\omega_{nv}^2}{\left(1+\frac{H^2}{L^2}\right)} \qquad (5.366)$$

which we therefore expect to be less than the natural frequency of vertical motion.

If the vehicle is W wide, the same method gives a natural frequency in roll of:

$$\omega_{nr}^2 = 3\omega_{nv}^2\left(\frac{W^2}{W^2+H^2}\right) \qquad (5.367)$$

again, probably higher than that in vertical motion.

The U.S. Army Tank and Automotive Command did a very careful computer simulation of the M-56 vehicle and its suspension system. Assuming that the vehicle rested on a flat platform, which was oscillated vertically and then in pitch, the response curves were obtained as shown in Figure 5-64. These agree with the predictions of our simple model.

5.9.1.4 Combining the Problem Elements

The terrain PSD contains all frequencies to varying degrees. They are transformed from cycles per foot to cycles per second by the vehicle motion. In addition, the vehicle averages the very short wavelength components because of its own length. The averaging effect of vehicle length can be approximated by the transfer function whose mean square magnitude is:

$$\left|\frac{L\theta}{A}\right|^2 \cong \frac{36\mu^2}{4+\mu^4} \quad ;\mu = \frac{L\Omega}{2} \qquad (5.368)$$

This function is independent of speed: it represents the mean square value of pitch if the vehicle is simply placed at random at any point on the terrain.

In Figure 5-65 the preceding function, expressing the effect of vehicle length, is shown for an arbitrary 10-ft long vehicle.

In Figure 5-66 the terrain function, approximated by straight lines on log-log paper and the vehicle response of Figure 5-65, are multiplied together and plotted; using appropriate scales to convert to cycles per second for vehicle speeds of 20 and 5 mph. The slower speed is more likely, and the overlap with the dynamic response peak of Figure 5-64 at this speed is marginal. But at 20 mph there is complete overlap.

Note that if the terrain break frequency in fact has a lower value, the horizontal portion of the response curve in Figure 5-66 will extend to lower frequencies. Noting, however, that the upper cutoff is at about 1 Hz, and remembering that the man is at best a 1 Hz servo, we may conclude that he will not track well without sight stabilization while the vehicle is in motion.

Integrating over the terrain PSD and the vehicle length averaging function but excluding the vehicle dynamics, we obtain a mean square pitching motion of:

$$\sigma_\theta^2 = (\sigma^2\Omega_0 L)^9(2+\mu-2\mu^{1/2})(4+\mu^2) \qquad (5.369)$$

where:

$$\mu = (L\Omega_0/2)^2 \qquad (5.370)$$

The quantity $\sigma^2\Omega_0$ is the same 'terrain roughness parameter' used in the study of contour flying, and should be identical. Differences are probably accounted for by the difference in length of record, and the fact that in computing PSD for ground vehicles, records have been too short to represent the very long wavelengths accurately.

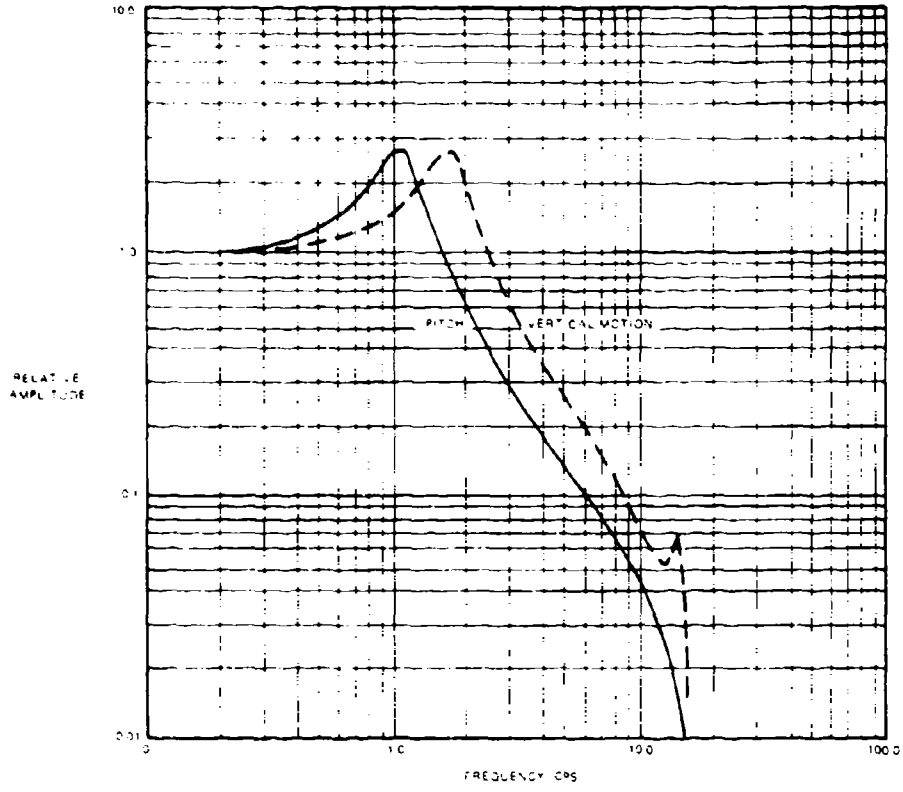

006 78 569

Figure 5-64. Computer Simulation of the M-56 Vehicle Suspension System

For a 10-ft long vehicle

$$\sigma_\theta^2 \sim 70\,\Phi(0)\ \text{mil}^2 \qquad (5.371)$$

so that on a good road, the pitching motion, including vehicle dynamics, should be only a few mils. Off road, of course, it can be many degrees. Since

$$\sigma_\theta^2 \sim \Omega_0^{-1} \qquad (5.372)$$

Reducing the break frequency will increase the mean square pitch, but the increase will occur at very low frequencies.

The principal observation is that at vehicle speeds of 5 mph and above, the PSD has significant power at the maximum frequencies that the man can track effectively. This strengthens the argument for a stabilized sight.

5.9.2 Effect of Firing the Gun

Some simulator results on Vigilante firing, communicated to us by Frankford Arsenal, indicates that for Vigilante 'A' (Mount and Carriage), at a gun rate of 3000 rpm, the mount responds with a vertical motion (bounce) of about 13 Hz and a double amplitude of 1/4 in. The angular response is at about 9 Hz with 9-mil double amplitude. In the case of Vigilante 'B' (Mount and Chassis), angular motion is excited at about 2 Hz with a double amplitude in side firing, with the suspension unlocked, of 42 mils.

The latter frequency is consistent with our prior

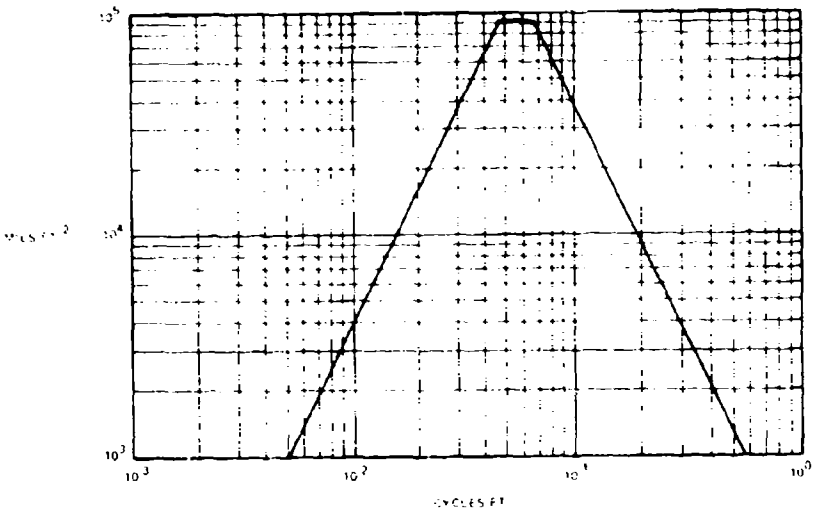

Figure 5-65. Vehicle Pitch Response

estimates of the natural frequency associated with the suspension. Clearly this frequency and amplitude will be extremely difficult for the human operator to cope with in fire on the move without a stabilized sight. Furthermore it appears to be far more of a problem than the pitching of the vehicle from movement when the gun is not firing.

In the case of Vigilante 'A' the angular motion is also beyond the capability of the operator to track out.

The fundamental frequency of the gun at 3000 rpm, or 50 Hz, will also be present to some degree, but is less likely to excite component resonances.

5.9.3 Effect of Vibration on the Human Operator

The interaction between the type of manipulator which the human operator performs the tracking function, and the effects of vibration, has been discussed in Section 4.3. In this section it was indicated that force controllers have been determined to be less adversely affected by vibration than displacement controllers. In the following paragraphs the effect of vibration on the operator is reviewed in greater detail, particularly with regard to visual problems.

The vibration of the mount, while partially dampled when transmitted to human occupants, does produce marked spatial displacement of the eye.

An outline of Coermann's model[51] and results will serve to describe the vibrational effects upon, and the mechanical impedance of the human body. His model consists of a single mass m, one spring with elasticity k and one damper with the damping constant c. Instead of using the complex equations which describe the motion of the mass, depending as it does in this system upon the seat, he obtains a good insight into the dynamic properties of the system by a theory of mechanical impedance. In studies utilizing this mechanical impedance paradigm, Coermann's data disclosed that in the sitting erect posture, man's body has the highest impedance peak, the highest natural frequency, and the lowest damping factor. Parameters for one subject, for example, show the first resonant frequency at 6.3 cps; and a damping factor equal to 0.57. While phase angle was not given, Coermann states that generally the motion of the mass is out of phase with the seat.

These data are corroborated by Goldman and von Gierke (1960), and Dieckmann (1957). Moreoever, Dieckmann's studies demonstrated a resonant peak for the human head at 5.5 cps.

An effect of vibration is that visual acuity suffers. Studies by Lange and Coermann[52] established that decrement of visual acuity of seated subjects under vertical sinusoidal vibration is dependent on the mechano-dynamic response of the human body. Generally, at frequencies below 12 cps, physiological stresses are

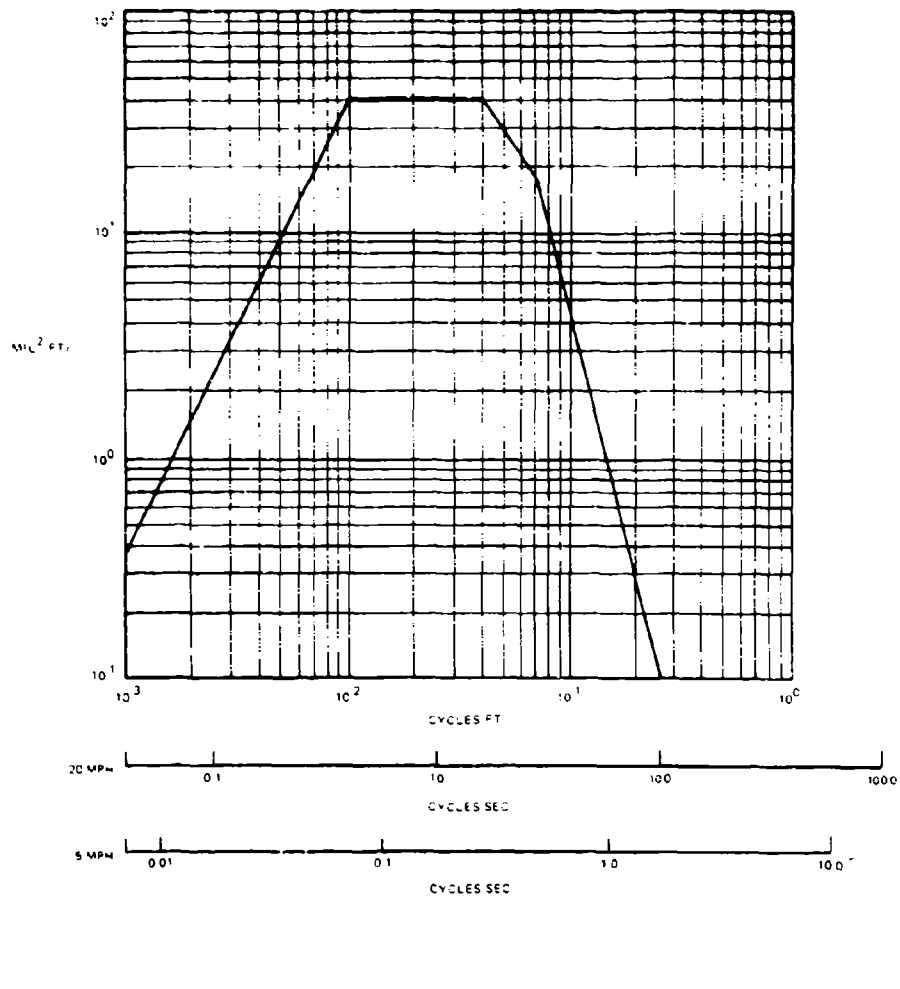

00678 571

Figure 5-66. Vehicle Response as a Function of Terrain and Vehicle Speed

produced which impair human body functions, while at frequencies above 12 cps, retinal image shift cannot be analyzed by the brain because it is above the critical flicker frequency. Physiologically, parallel insulated nerve-fiber chains could translate these frequencies to the cerebral cortex (occiput). However, temporal summation at the synapse is hindered by the extremely brief stimulation of the nauronal soma. These impinging discharges do not last, at some synapses, at a peak value beyond the refractory period of the axon.

More specifically, data normalized to a one-g shake table peak acceleration shows the first substantial visual acuity decrement peak at 5 cps, with the smallest standard deviation σ of all tests.[43] The next decrement peak appears at 7 cps, again accompanied by a low σ.

Experiments to determine the effect of vibration on operator performance with imaging sights, indicate again that the effect of vibration can be interpreted in terms of reduction in visual acuity.[39] The effects can therefore be expected to be most serious in those tracking regimes where the operator is able, in the absence of vibration, to track to fractional mil accuracy.

With regard to the control manipulator, vibration plays as great a role toward error contribution as it does at the sight-eye interface. A handle secured firmly to the mount and vibrating at the same frequency and amplitude could (and is some cases does) contribute error (noise) even before it is gripped by the human.

Man's unsupported arm and shoulder system, on the

other hand, is resonate at approximately 4 cps when the energy is transmitted via hips thorax-abdomen, and upper torso (Dieckman[49]). With the arm and hand resting on a semi-rigid support, it is likely that they will vibrate at frequencies closer to those which are impressed, but with phase-dissonance. In this instance, the vibrations of man *and* the control should be damped; or less acceptably, matched with respect to frequency, phase, and amplitude.

Isolation of the operator and the sight from very high frequency vibration can be achieved by conventional soft mounts. Figure 5-67 shows the Nord Vosper mount for installation on a motor torpedo boat.[53] Both the sight (which is gyro stabilized) and the operator, are isolated from the hull by shock mountings.

The natural frequency of a shock mount ...

$$f_n = 3.2/y_s^{1/2} \qquad (5.373)$$

where: y_s = static deflection in inches.

Significant vibration isolation is not achieved below about 3 f_n. A static deflection of 1/4 inch would only isolate the sight from vibration above abo it 20 Hz.

5.9.4 Conclusions

The preceding findings may be interpreted in terms of the requirements for sight stabilization, and isolation of the operator in a tracking mode from vibration.

Disturbances of sufficient magnitude to create tracking problems were described covering the range of frequencies from very low frequencies (fractions of a Hz) to as high as 50 Hz. At the very low end (under 0.2 Hz) even the human operator can cope with them.

Since the human operator begins to degrade badly at about 1 Hz, a stabilized sight is required to isolate the sight motion from frequencies above about 0.5 Hz. Even when the load on the stabilization servos is light, consisting of a mirror or prism, it may be difficult to achieve mechanical stabilization above 5-8 Hz. A dual servo system may be considered,[51] in which the sight pedestal is approximately stabilized by a low-bandpass servo of moderate power, and the sight line is stabilized by a very high performance servo positioning a mirror or prism. Ingenious approaches to reducing the inertia of moving parts have been developed, such as the Dynasciences fluid prism used in the XM76 stabilized sight.[52] If tracking is done by an imaging system, open loop electronic stabilization of the image may be considered. Published analyses indicate that stabilization of this type can be achieved with available gyros up to 200-300 Hz.[50]

In any case, the operator and the sight should be isolated from very high frequency vibration such as that caused by the vehicle engine, power motors, etc.,

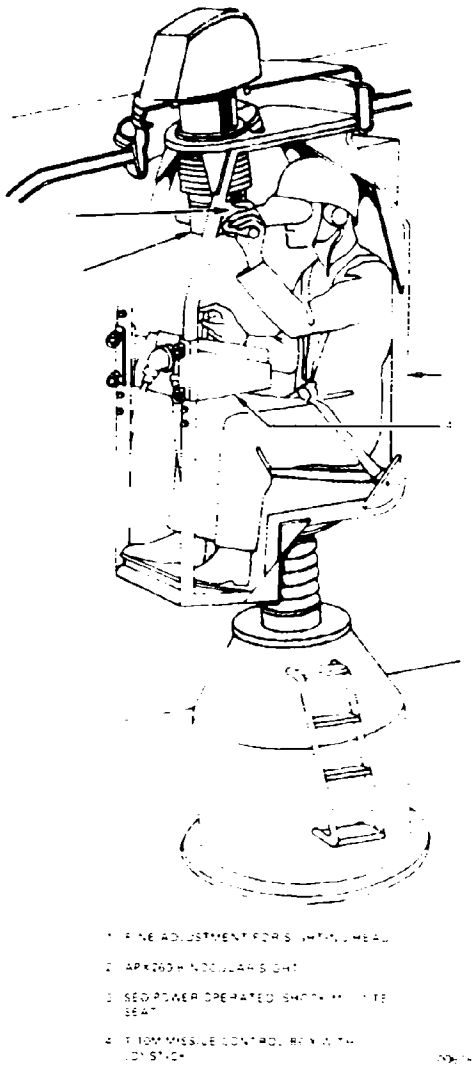

Figure 5-67 The Nord Vosper Specially Designed Aiming Turret

and the 50 Hz fundamental frequency of the gun at maximum firing rate, by conventional shock mounting.

A practical system, within the cost constraints of AFAADS, may have to accept some degradation in manual tracking accuracy from vibration inputs at about 10 Hz while the gun is firing. Field firings of the Vigilante mount are now underway to obtain actual measurements of gun-induced vibration at critical locations on the mount, and with these available, the requirements on sight stabilization and vibration isolation can be more precisely defined. The very large body of information now available on stabilized sights in helicopters also need to be reviewed with AFAADS objectives in mind.

5.10 GROUND FIRE ROLE FOR AFAADS

It is desired that AFAADS be capable of engaging ground targets out to 4000 meters, as a secondary mission. This role may be discussed in terms of target acquisition and tracking, ballistic computation, dispersion, and terminal effectiveness.

Since the gun is a flat trajectory weapon, target acquisition will be limited by the probability that a clear line of sight exists to the target. As many terrain studies have shown, the probability of seeing a target on the ground 4000 meters from a ground mount without intervening terrain obstruction is very small, even when the gun position has been carefully chosen to maximize its coverage against ground targets. Occasionally AFAADS may be called upon to deliver indirect fire but antiaircraft performance should in no way be prejudiced for this low-effectiveness mode.

The maximum range for target acquisition at night by an infrared or other imaging sight is not considered to exceed about 1000 meters in the immediate future,[54] and 4000 meters may not be achieved within the next decade.

Assuming, however, that by day targets may be acquired occasionally at 4000 meters, the accuracy to which ballistics need to be computed is strongly influenced by the mininum dispersion which can be achieved with the gun. Two and one-half mils at 4000 meters correspond to 10 meters in dispersion, on a vertical plane, at the target. Because of the flat trajectory, there is much greater dispersion in the range pattern of ground impacts against a horizontal target.

Pfeilsticker[55] has indicated that against a 'standard' 7-1/2 by 7-1/2 ft tank target, a dispersion of 10 meters would degrade performance, for a burst of 60 rounds, unless the systematic error during the burst was considerably in excess of 10 meters. Systematic error is always bad, of course, but its effect can be reduced by optimum dispersion.

Since we propose that AFAADS include corrections for wind, muzzle velocity, and other ballistic parameters, and since ground to ground firing would be done with the assitance of the laser range finder, we would expect that the principal contribution of the ballistic solution to systematic error in miss distance in ground to ground fire, would be in the computation of superelevation. There should be no problem in holding this error to less than a mil in the ground to ground mode at 4000 meters.

It seems likely therefore, that the accuracy of ballistic computation for the surface to air role will satisfy the ground to ground role, provided that the maximum range of the computation extends at least to 4000 meters.

The limiting influence on the hit probability against a small target at 4000 meters would then be the gun dispersion. If artifical dispersion is put in by dither which is easy to remove, the residue can be reduced to perhaps 1 mil. If dispersion is put in by mechanical adjustment, it can be reduced, provided that the air threat no longer exists.

It is doubtful, however, that AFAADS would be required to engage small targets, such as vehicles, at 4000 meters often enough to make a high-hit probability on these rare occasions a reason for special design provisions. A better way of engaging such targets is suggested later.

With regard to terminal effectiveness, the high-velocity 37mm round can have very good armor penetrating capability with AP ammunition. Other ammunition options, possibly including squash head projectiles should be investigated. The HE round, developed for AA fire, should be effective against personnel and unarmored and lightly armored vehicles. However, the provision of a mix of ammunition types with selective option needs to be considered in terms of the effect on the gun loading and belting. In view of the limited on-mount ammunition storage capability of any high rate of fire weapon, it would probably be undesirable, from an overall mission viewpoint, to load anything but HE ammunition unless the antiaircraft role is completely inactive because of the complete absence of enemy aircraft.

The possible tactics for the employment of AFAADS in a ground to ground role need to be developed.[56] The current two options (3000 rpm or 120 rpm with fixed burst size of 48 rounds) may not provide sufficient flexibility. A wider range of burst sizes, such as those provided for the 20mm Vulcan weapon, would probably oe preferred. For example, a very small burst option of six rounds or even single shot fire could satisfy certain circumstances that do not require a large expenditure of rounds. With its fire on the move capability, AFAADS, while accompanying a column, could provide effective suppressive fire, but the limited on-board supply of ammunition would make this most effective if fire could be maintained for longer time periods with shorter bursts.

The development of ground-based laser target designators for accurate weapons delivered by aircraft, helicopters, or remotely from launchers at the rear suggests that a laser designator should be considered for AFAADS, so that it could obtain effective support when threatened by enemy armor. Although early laser range finders for use against ground targets operated typically at 0.2 pulses per second, the antiaircraft application will require about 10 pulses per second. This is consistent with the requirement of a target designator for which the PPS requirement is set by the sensor and control characteristics. It may be feasible therefore, to combine the ranging and target designation features in the AFAADS laser.

To engage ground targets out to 4000 meters, magnification in the sight optics is probably required.

In general, however, no serious additional difficulties are expected to be imposed on the AFAADS design by the requirement to engage ground targets.

5.11 RELIABILITY

System reliability as well as the reliability of its components are inputs to the overall evaluation of system effectiveness and life cycle cost. In the case of effectiveness, reliability affects both the probability that the system will be in an operable condition when required to engage an enemy, and the probability that it will function properly during the engagement. In the case of life cycle costing, reliability affects the maintenance and spares requirements.

At this stage in AFAADS system definition, a detailed numerical evaluation of the elements of the effectiveness matrices would not be justified, since the specific components to be eventually utilized are too ill-defined to allow good estimates of probable reliability. This section is therefore confined to outlining the elements to be considered in the reliability evaluation as the program goes forward.

Reliability is often included in the effectiveness computation by the symbology developed by the Weapon Systems Effectiveness Advisory Committee (WSEIAC),[59] in the 'availability' and 'dependability' matrices of the expression:

$$E = A' [D] [C] \qquad (5.374)$$

The elements of reliability are defined as follows:

a. *System Effectiveness* is 'a measure of the extent to which a system may be expected to achieve a set of specific mission requirements and is a function of availability, dependability and capability.'

b. *Availability* is 'a measure of the system condition at the start of a mission and is a function of the relationships among hardware, personnel and procedures.'

c. *Dependability* is 'a measure of the system at one or more points during the mission, given the system condition at the start of the mission.'

d. *Capability* is 'a measure of the ability of a system to achieve the mission objectives, given its state during the mission.'

The elements: E A D C of Equation (5.374), are defined as follows:

where:

E = the effectiveness vector

A = the availability vector

D = the dependability matrix

C = the capability matrix

e_k = the value of the k th figure of merit.

a_i = probability the system is in state i at the beginning of a mission. A mission might be defined as beginning with the appearance of an enemy aircraft in the surveillance volume of AFAADS.

d_{ij} = probability that the effective state of the system during the mission is j, given that it began the mission in state i.

c_{jk} = value of the k th figure of merit, given that the system is in state j.

State transition probabilities can be estimated from the reliability estimates of the components defining each state. The distribution of maintenance times has repeatedly been demonstrated to be log-normal, which calls for computer simulation to solve the problem. However, if as a first approximation all distributions are assumed to be Poisson, analytic solutions are possible.

As a very simple example of the availability computation under this assumption, consider availability if AFAADS is either operational or non-operational. Let the failure rate λ be random with time, and the repair rate (inverse of the mean time to repair) be μ. Then the system availability A at an arbitrarily chosen point in time is:

$$A = \mu / (\lambda + \mu) \qquad (5.375)$$

or equivalently:

$$A = MTTR / (MTBF + MTTR) \qquad (5.376)$$

where

MTBF = Mean time between malfunctions

MTTR = Mean time to restore to operating condition

The availability, dependability, and effectiveness matrices (including a distribution function for the engagement of targets) can all be combined in a simulation. However, the fact that the time occupied in engaging targets will be very small, compared with total time during which the system is active in modes ranging from shutdown to simple surveillance, suggests that no loss in realism will be incurred by computing the availability, dependability, and effectiveness matrices separately, and then multiplying them out.

If, to a first approximation, state transitions in the availability computation can be represented as a Markov process, then

$$dA/dt = [B]\,A \qquad (5.377)$$

where B is the matrix of state transition probabilities. We are usually interested in the steady state values when $dA/dt = 0$, and these are obtained by solving:

$$[B]\,A = 0, \text{ subject to } \sum_i a_i = 1.0 \qquad (5.378)$$

The system states prior to target engagement, can be categorized as follows:[57]

a. System fully operational.

b. System able to engage targets in degraded mode.

c. System inoperative, waiting for spares.

d. System inoperative, under repair.

e. System down for preventive maintenance.

Each of these categories can be further subdivided. For example, since AFAADS will be able to operate in a number of degraded modes (in fair weather without radar tracking, with range estimation, or with all fire control computations inoperative but with estimated leads), a complete effectiveness computation would include the detailed specification of the availability matrix, in terms of the probability that each mode of operation is available, when AFAADS is called upon to engage a target.

Since the availability computation includes both failure rates and repair rates, one needs to make estimates of the kinds of maintenance that can be performed at various organizational levels, what components are repaired, and what components are discarded and replaced, etc. This is required in order to determine the probabilities that the system will be operational or down in each of its possible modes. The techniques for doing this are all well known and can be applied as concept definition proceed.

The life cycle cost implications of maintainability and reliability are important in making design tradeoffs. For example; for some of the older radars, maintenance cost *per year* equalled the procurement cost of the equipment.[61] Since the mean time between failure was only about 250 hours, and the mean time to repair was about 5 hours, an availability value of 0.98 was yielded.

However, in the case of a radar (AN/TPS-39(V)) designed for high reliability, a mean time between failure of 6000 hours was achieved.[61] This set is admittedly simpler than a precise tracking radar, however, the MTTF is notable. It resulted from early attention to possible reliability problems, and the allocation of 3 percent of the program cost specifically to improve reliability.

Available reliability information on radars needs to be reinterpreted in view of the environment created by vehicle movement on rough roads, and the shock and vibration caused by gunfire.

It is possible that the relatively small physical dimensions of K-band radars will aid in obtaining high operational reliability of the mechanical components.

The effectiveness evaluation is expected to show a considerable payoff to AFAADS by the use of on-carriage radar. Aside from questions of cost-effectiveness, the system will be satisfactory in the field only if it imposes a minimum maintenance burden on the already excessive maintenance effort of a modern field Army. This objective can be achieved only by high intrinsic reliability.

Reliability information on laser range finders is not yet available, although some of the factors to be considered have been indicated in the literature.[58]

The reliability of field-qualified digital computers has become so high that this type of computer is expected to be a low failure rate item. However, this is not necessarily true of the analog equipment which couples the computer outputs to the gun.

Since engagements are short, the entries in the 'dependability' matrix would be expected to be close to unity. The principal factor, causing an abort during an engagement, would probably be a gun malfunction. Since this would ordinarily require a relatively short time to clear, the gun would be ready almost at once for the next engagement. The stoppage rate for the Vulcan 20mm has been indicated to be only one in 25,000 rounds.

Because the capability matrix involves measures of effectiveness of the system, it would more properly be discussed under system effectiveness. However, it may be noted here that the method allows several figures of merit or measures of effectiveness to be carried through simultaneously. For example, one might be interested in both the probability that the target aircraft is destroyed before it can drop its bombs, and the probability that the target aircraft receives damage that will prevent its return to base or cause it to go down for extended repairs. If judgments can be made as to the relative values of these possible events on an overall combat effectiveness basis, the effectiveness matrix can be multiplied by the military value matrix to obtain an overall effectiveness number.

The figures of merit can be extended to describe individually the effectiveness of the system under each of a number of operational conditions, such as day, night, bad weather, whether the enemy uses ECM, the category of the enemy flight path, etc. Again using judgment supported by analysis, if the relative probabilities of the operational parameters are estimated, the expected effectiveness of the overall system can be

computed. Such an average should, however, be undertaken with caution, since the relative probabilities of some of these states are under the control of the enemy. If antiaircraft effectiveness by day is very high, the enemy can be expected to shift the weight of his attacks to night, for example. It is probably better to list the system effectiveness for each set of environmental and operational parameters, and make judgmental decisions at that point.

5.12 FIRING DOCTRINE

With the T250 37mm Gatling Gun in its present configuration, the gunner has only two options with regard to rate of fire (3000 rpm and 120 rpm), and apparently only one option as to burst size (48 rounds). At the 3000 rpm rate of fire his ammunition load will be expended in three one-second bursts, after which the mount must be reloaded. At the low rate of 120 rpm, a 'burst' of 48 rounds would extend over 24 seconds. As noted earlier, considerably more flexibility in choosing the number of rounds per burst has been provided for the 20 mm Vulcan Gatling Gun. There is no reason to suppose that this cannot be done with Vigilante, if determined to be desirable.

To minimize lost time while the operator is deciding what option to use, however, the number of options should be kept as small as is consistent with the best use of the weapon.

In addition, the operator must be provided with some indication of when to fire. A perennial problem with high rate of fire antiaircraft weapons has been the tendency of the gunner to open fire too soon and exhaust his ammunition before the target comes within the effective range of the gun. A less obvious problem is that of firing before the tracking has been 'smooth' for long enough to allow the computer to generate a good prediction.

How much information can be provided the gunner for guidance in when to fire depends on whether he is actually tracking the target, or whether he is monitoring the system while tracking is automatic via radar or other sensor. In the former case he should be distracted as little as possible from his tracking function.

A minimum 'open fire' indicator could be a symbol projected on the sight reticle which indicated that: (1) the target was within effective range, and (2) sensors were locked on. In the case of visual tracking, the only sensor involved would be the ranging device. The sensor lock-on might be indicated by the appearance of a cross; the in-range indication might be by a circle enclosing the cross.

To indicate the state of the lead solution, the size of the circle might be made proportional to the *measured* target acceleration. This would be very large before the computer settled, since the measurement would contain transient errors.

Even with smooth tracking, a large circle would indicate evasive action by the target, reducing the likelihood of a hit. The pulsing of circle size as a function of the tracking noise would be a sensitive measure of how smoothly tracking was being accomplished.

Alternately, the target size might be made proportional to measured target velocity. Again, pulsing circle size would indicate tracking roughness, and a slow change in size would indicate target acceleration.

Cease fire should probably be a positive indication, when the target passes out of range, such as a large X displayed across the indicator, rather than the simple vanishing of the indicator.

What should be displayed, where in the sight field the indication should appear, and in general, the human factors aspects of the process would need to be worked out and tested in the laboratory.

Mr. S. Olson has suggested that the computer might be considered as a means for recommending or automatically selecting firing points, rate of fire, and burst duration. This possibility needs to be analyzed to a greater depth than is possible here. Since target speed, range, and heading with respect to the gun are closely related to the length of time the target is likely to remain within the field of fire, they may be used in a firing doctrine algorithm. Against a passing target, it is probably desirable, and could be confirmed by simulation runs, to fire all available rounds before the target reaches the path midpoint. At the same time, to conserve ammunition for use against other targets which may be involved in the same attack, burst spacing sufficient to identify possible kills between bursts would be desirable.

The presence of 'aim wander' makes the concentration of fire in three spaced bursts less efficient, all other factors being equal, than the same number of rounds equally spaced over the same total interval. This is particularly true against terrain following aircraft; where the slow deviations of aim error, caused by the contour following of the target, will be of substantial magnitude.

These considerations suggest that the rate of fire options of the gun need to be considered in more detail with the aid of the simulation.

For an incoming target aircraft preparing for, or engaged in an attack on a ground target, additional considerations are involved. Considering dive or glide bombing, to be specific, the accuracy of bomb delivery increases as the release range decreases. The higher the accuracy, the fewer aircraft sorties need to be laid on in order to destroy the ground target (if the aircraft survives). If the antiaircraft gun opens at a long range it has a lower probability of killing the target with limited ammunition than if it holds fire to a shorter

range. The airplane counters this by releasing its bombs at longer range. This is a rather straightforward problem in game theory. Time has prevented a solution from being presented here. It is conjectured that the 'game' solution will be for the attacking aircraft to choose its drop range from a probability distribution (normal pilot to pilot variation in performance may be roughly equivalent), while the gun distributes its fire over a range interval. The solution will depend on the relative values assumed for the aircraft and the target it is attacking.

The realism of a solution obtained by game theory may be slight; but the insight gained in considering this interaction between firing doctrine for the gun and the ability of the aircraft to destroy the ground target in conjunction with its own survival probability, will be important in understanding what firing doctrine to recommend.

Basic to the recommendation of a firing doctrine is a knowledge of the probable system effectiveness against various target types, paths, and in various operational modes. This knowledge can be obtained from more extensive simulation runs than have been possible within the duration of the present contract.

5.13 SIMULATION RESULTS

This section presents the results of simulation runs to compare the effects of prediction modes, tracking errors, ballistics, lags in the sensors and gun, dispersion, target paths, and maneuvers on system effectiveness. A number of sensitivity runs were made to determine the effect of changes in input parameters on system effectiveness. Runs were also made to test and demonstrate the functioning of the decision algorithms for switching prediction modes, and to determine the effects of varying the decision thresholds.

The design of the simulation is described in Volume II. The AFAADS system was described to a level of detail which was considered to offer the best balance, within the scope of the present contract, between simulation complexity and the obtaining of useful results regarding the most important system parameters.

The modular construction of the simulation program allows progressive increments of realism to be added in the future without complete reprogramming. As a consequence of this modular construction, it was found to be possible, even within the course of the present contract, to add capability and define elements of the system to greater detail when these were found to be of particular interest.

The simulation can be run in a deterministic mode to determine the miss distances resulting from servo lags and target maneuvers; or in a Monte-Carlo mode to account properly for noise autocorrelation and geometric cross-correlations of tracking errors. Some results obtained in the deterministic mode are presented first, and then the Monte-Carlo mode is discussed in greater detail, and the results obtained with it are presented.

5.13.1 No-Noise Runs to Determine Systematic Errors Caused by Target Maneuver

Initial exploratory runs were made to compare the systematic errors resulting from target maneuvers with five different prediction algorithms. Tracking noise and dispersion were set at zero so that systematic error could be observed directly.

The horizontal projection of the target path (Path No. 1), with time marks and a plot of altitude versus time, are shown in Figure 5-68.

The aircraft approaches a target on the ground at low altitude and about 450 knots. On sighting the target it pulls up in a climbing turn, losing some velocity in the climb. The aircraft, while still turning, levels out at about 1500 meters, and then makes a sharp diving turn which puts it on a straight line attack pass at the target. It accelerates in the dive, releases its weapons, and then makes a very high g-pullup and turn, and departs.

Total path length is about 100 seconds. Very little of the curved flight segments are at a constant turn rate, so as not to bias the answer in favor of a quadratic predictor.

The gun is on the vertical axis, 1500 meters from the ground target.

The system elements that were simulated include the following:

a. Tracking error was taken as zero.

b. Rates and accelerations were measured by 2- and 3-point algorithms with an 0.2[illegible] second base.

c. Prediction modes were:

(1) *Rate by time.* Azimuth, elevation, and range were simply computed by multiplying rate of change by time of flight and adding to present position.

(2) *Linear.* A constant velocity extrapolation from present position.

(3) *Linear plus energy.* Acceleration along the flight path was computed from exchange of potential for kinetic energy and vice versa. This along-flight path correction was added to the basic linear prediction.

(4) *Quadratic.* This was based on the assumption of a constant turn rate, hence it is 'quadratic' in one dimension only, in order to minimize

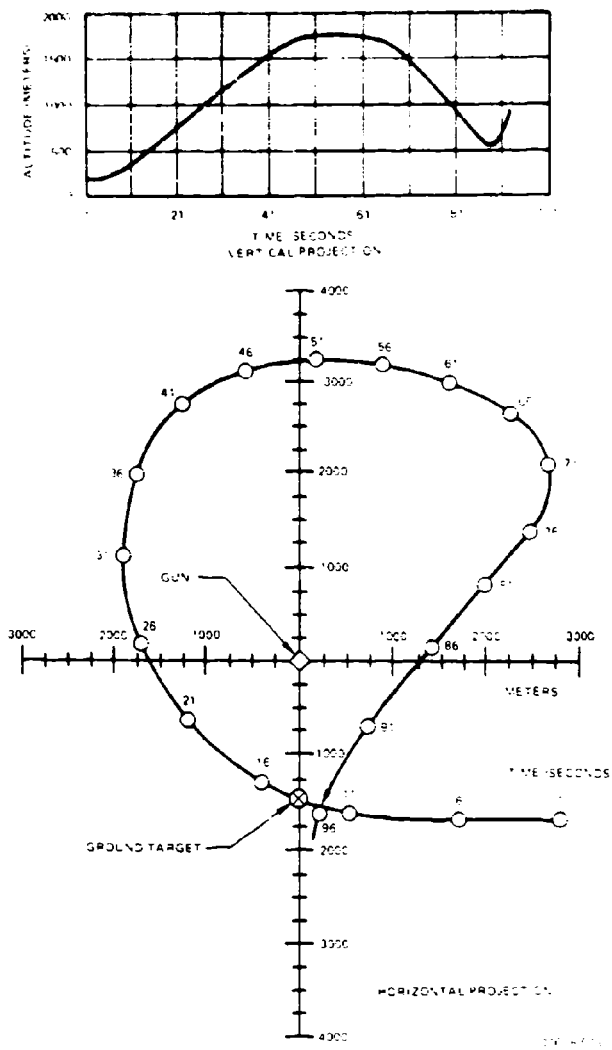

Figure 5-68. Simulation Flight – Path No. 1

the degradation from tracking noise when the latter is included.

(5) *Quadratic plus energy.*

In accordance with the objective of emphasizing those functions most likely to affect system performance and postponing the introduction of those which would have a secondary effect but would increase running time and complexity of the simulation, only time of flight was generated in the simulator, but not superelevation. Three sets of ballistics were used, and these are shown in terms of time of flight (Figure 5-69) and remaining velocity (Figure 5-70). The most recent ballistic information received from Frankford Arsenal, indicates the possibility of providing Vigilante ballistics with 3600 fps muzzle velocity but with a better ballistic coefficient than shown here as Ballistics 3, the net effect being so close to Ballistics 3, that no changes were made in '3' for the simulation runs.

The simulation was also instructed to 'cease fire' when projectiles dropped to sonic velocity, so that the simple power-law approximation to deceleration could be used for time of flight.

The rms miss distances (in meters) are compared with Ballistics 1 for the various prediction modes in Figure 5-71. The following conclusions are drawn:

a. The rate by time solution is unacceptable.

b. Linear prediction is relatively poor over the whole course, except for the straight line dive where it is impaired by the target acceleration along the flight path.

c. Linear prediction plus energy is excellent on the straight line dive.

d. Quadratic plus energy is excellent over much of the curved pattern as well as the straight line dive.

A comparison of ballistics generates similarly shaped curves, but with a moderate reduction in systematic error as the ballistics are improved. The principal effect is that, with Ballistics 3, the range at which shell velocity drops to sonic velocity includes the whole course. There is in fact a 5-second interval from 51-56 seconds where the systematic error with the quadratic algorithm drops to under 5 meters.

Figure 5-71 shows systematic error in meters. If the same plot were reproduced in mils, it would be found that the linear-prediction systematic error, after the 6-second time point, has a minimum value during the diving segment of about 5 mils.

As a quick summary of the results obtained in these runs, the total time, that the error was less than 15 meters for each option, was summed and is presented in Table V-6.

The flight path is not a difficult one in terms of target accelerations. However, it is considered to be a realistic one. It was concluded at this point, therefore, that the rate-times-time prediction option should be dropped from further consideration, and the other four prediction options retained.

5.13.2 Simulation with Tracking Noise

No simple analytic solution was found to the problem of accounting for the autocorrelation in time of aim wander error produced by correlated tracking errors, additionally correlated by the smoothing operation, or for the cross correlations among coordinates introduced by the geometry of the prediction problem. Such a solution would have allowed the simulation to be run in a deterministic mode.

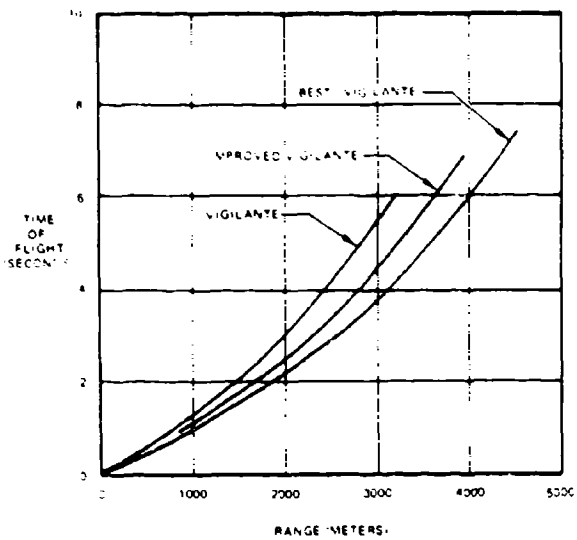

30678 574

Figure 5-69. Time of Flight Ballistics Used on Simulation

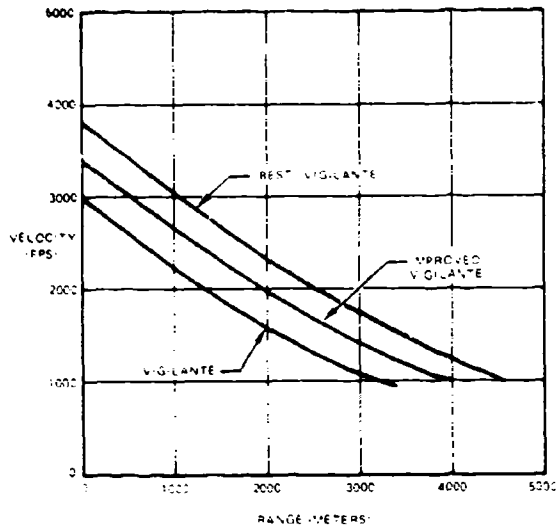

30678 575

Figure 5-70. Remaining Velocity Ballistics Used on Simulation

It was therefore decided to use a Monte Carlo mode, in which tracking errors were generated with variance and autocorrelation, appropriate to the sampling interval. The probability density function of the generated sequence has zero mean. To simulate *radar* tracking, the variance in (meters)^2 at the target was held constant over each set of runs in accordance with the findings of Section 4.2. The servomechanism lag of the sensor and gun were introduced explicitly as functions of angular rates and accelerations. Considering the uncertainties in how to represent *manual* tracking errors as a function of range, angular velocity etc., the same model with appropriate variances, autocorrelations, and lag coefficients might be assumed to represent the man. However, the man in the tracking function was also explicitly simulated by a program used in a separate series of runs. The explicit simulation of the man assumed, in agreement with some of the findings reported in Section 4.3, that the noise component of the man's tracking error increases with the amount of lag in his response, in addition to having a constant base component.

For all runs, miss distances were obtained as a function of time. These miss distances were then converted by the computer to single-shot kill probabilities, and probabilities of kill in bursts of a specified duration and number of rounds. Averages were taken over a number of replications with different tracking noise samples. A summary of the statistics was printed out by the computer.

In the case of the single-shot probability, the computed values were summed over each course and multiplied by the interval between samples to obtain a measure designated 'kill-seconds.'

The significance of these three measures is as follows:

The distribution of miss distances is self explanatory. It is not affected by dispersion or vulnerability, and shows at once how often the projectile passed within specified distances of the target.

The kill-seconds computed over the course is essentially a weighted average of the miss distances; weighted in the same way as the probability of kill function. It has the physical significance that if a gun fired at a constant rate over the flight path, the kill-seconds could be multiplied by rate of fire, and the target survival probability for that run obtained as:

$$p = \exp\left[-(\text{rate of fire}) \times (\text{kill-sec})\right] \quad (5.379)$$

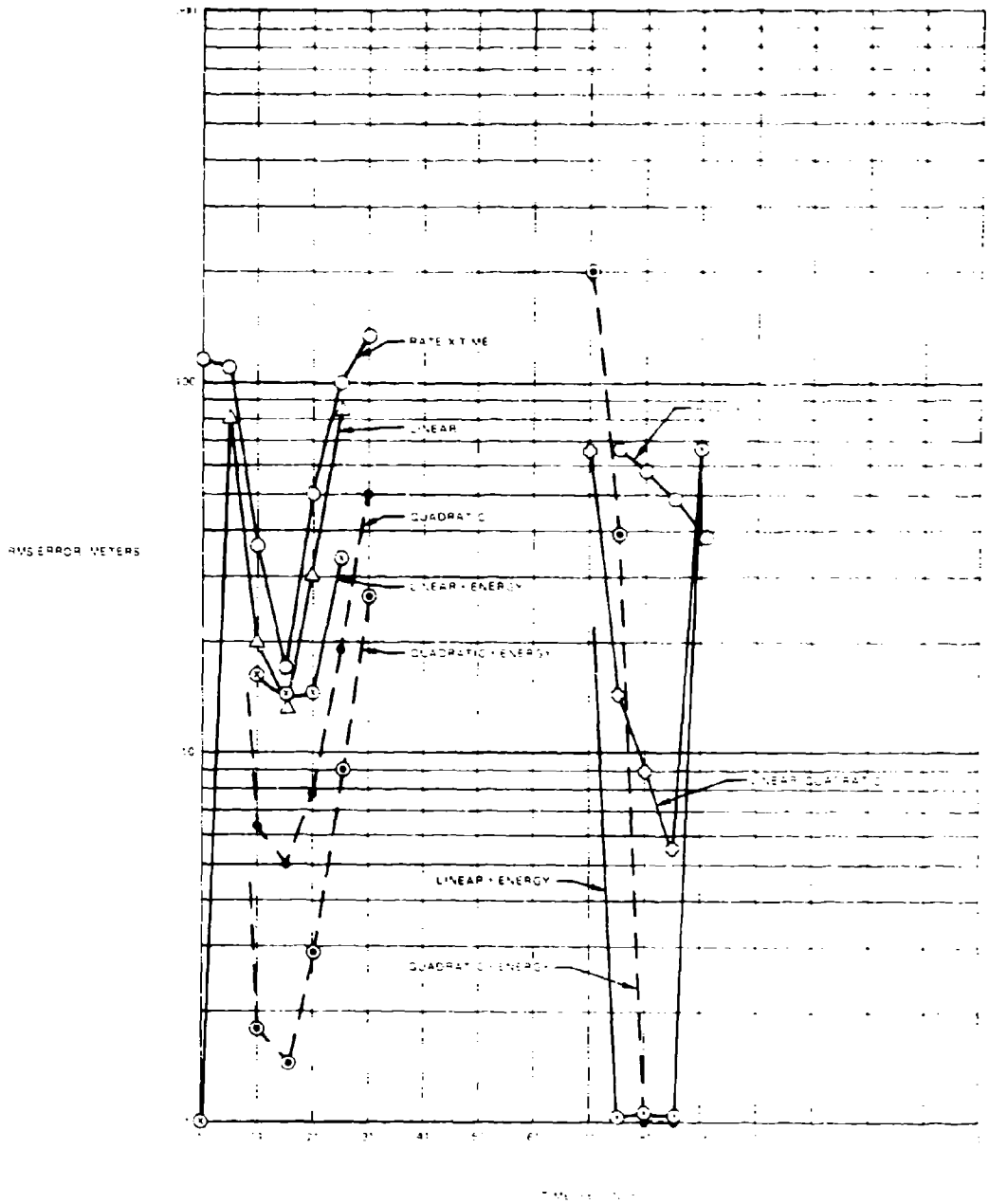

Figure 5-71 Comparison of Prediction Modes of Vigilante Ballistics No 1

Table V-6. Summary of the Time the Systematic Error was Less than 15 Meters

Prediction Mode	Ballistics No. 1 (sec)	Ballistics No. 2 (sec)	Ballistics No. 3 (sec)
Rate x Time	0		
Linear	14	22	24
Linear + Energy	24		
Quadratic	28		48
Quadratic + Energy	32		

NOTE: Symbol ( ) means no runs were made for that case.

00678-577

To average over replications, this value should be averaged over the distribution of (kill-sec) obtained in the replications. This takes account of aim-wander properly.

The number of possible bursts with kills above some specified index is intended to include the effect of aim wander in specific bursts. It represents the number of opportunities to get burst kill probabilities above the specified levels.

Since at this stage we are interested in narrowing down system options (prediction, smoothing, ballistics . . .) we have not included firing doctrine. The course with the most opportunities to fire bursts with high kill probabilities should be the best for that length of burst when combined with a firing doctrine. Similar conclusions can be drawn from kill-seconds in the case of continuous fire.

A flow diagram of how to get from the present measures to system recommendations, including firing doctrine and system effectiveness, is shown in Figure 5-72.

The algorithms for computing kill-seconds and probability of target kill with a burst are developed below. Of the two approximations shown, the first assumes a circular target and circular normal dispersion pattern. The second approximation assumes an ellipsoidal target, and ellipsoidal dispersion pattern. It is relatively easy to introduce the second approximation (and further improvements beyond it) into the simulation, but with limited time it was decided that the first approximation would be satisfactory to reveal the effects of parametric variations of interest at this stage of system definition.

The first approximation includes the following:

Assumptions:

Circular target

Circular normal shot pattern

Notation:

a = target vulnerable radius (meters).

A = target vulnerable area, $= \pi a^2$, (meters)^2.

D = slant range in meters/1000.

σ = standard deviation of dispersion pattern (mils).

R_m = miss distance (closest approach) from simulation (meters). (This is for the trajectory without dispersion, and is computed at intervals Δ.)

T_s = duration of fire.

m = number of simulation points in T_s.

p_{ss} = single shot probability.

where:

$$p_{ss} = \frac{a^2}{a^2 + 2(\sigma D)^2} e^{-\frac{R_m^2}{a^2 + 2(\sigma D)^2}} \quad (5.380)$$

Then the average p_{ss} over m points $= \bar{p}_{ss} = \frac{1}{m} \sum_m p_{ss}$ (5.381)

Let:

n = number of shots in T_s (assumed uniformly spaced).

E = expected number of killing hits in burst.

ϕ = probability target survives.

K = probability target is killed by a burst of n shots of duration T_s.

Then:

$$E = n \bar{p}_{ss} \quad (5.382)$$

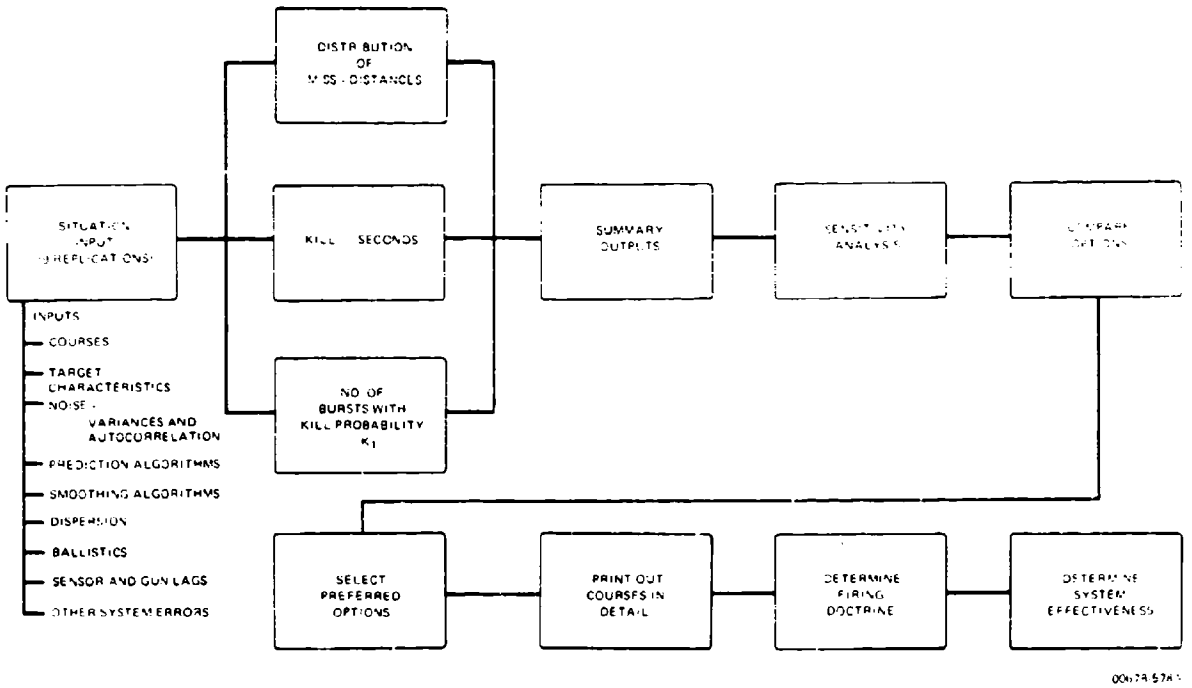

Figure 5-72. Flow Diagram Depicting Use of Simulation to Optimize System

$$\phi = e^{-E} \tag{5.383}$$

$$K = 1 - \phi \tag{5.384}$$

and finally kill seconds is computed as:

$$KS = \Delta \sum p_{ss} \tag{5.385}$$

The summation is over the whole flight path. Both the average of KS and its standard deviation are computed over the set of replications.

The second approximation (for future use) includes:

Assumptions:

Ellipsoidal target

Ellipsoidal shot pattern

This is an improvement because the head-on area of a target is 10 percent or less of the side on area. We ignore the wings in this approximation because they are less vulnerable to 37mm fire than the fuselage. Muzzle velocity dispersion is approximated by the spreading of the shot pattern along the direction of flight.

It is necessary to resolve the miss distance of closest approach into components along, and perpendicular to, the flight direction as projected on a plane, perpendicular to the trajectory and containing the point of closest approach.

In this plane, take axes u, v; where v is perpendicular to flight direction. R_m resolves into components U, V.

The target velocity vector makes an angle with this plane.

The target ellipsoid has dimensions S_L, S_H.

Projected into the U, V plane, the ellipsoid has dimensions (max and min radii):

$$a_v = S_H \tag{5.386}$$

$$a_u = (1/2)\left[S_H^2 + (S_L^2 - S_H^2)\cos^2 \varphi\right]^{1/2} \tag{5.387}$$

$$\sigma_v^2 = \sigma^2 \tag{5.388}$$

The components of gun-ammo dispersion are (in mils):

$$\sigma_u^2 = \sigma^2 + \sigma_M^2 \cos^2 \varphi \tag{5.389}$$

Let:

σ = constant for all points

v = target velocity

v_0 = muzzle velocity

v_m = a parameter with dimensions of velocity, constant over the course

then:

$$\sigma_M = \left(v_m v / v_0^2\right) \tag{5.390}$$

Since σ_w is an approximation to the combined effects of all random noise sources affecting dispersion in the direction of flight, it will be a constant for each course at this level of approximation.

The expression for p_{ss} is now:

$$p_{ss} = \frac{a_u a_v}{\left\{\left[a_u^2+2(\sigma_u D)^2\right]\left[a_v^2+2(\sigma_v D)^2\right]\right\}^{1/2}} e^{-\frac{u^2}{a_u^2+2(\sigma_u D)^2}-\frac{v^2}{a_v^2+2(\sigma_v D)^2}} \tag{5.391}$$

The statistical summaries with this approximation would be identical with those used for the first-order approximation.

A typical summary print out from the computer is shown in Figure 5-73. The same statistics are also printed out for each replication.

5.13.3 Simulator Results on Pass Path (Path No. 2)

This is the simplest path from the point of view of prediction, since the target is unaccelerated. However, the target speed and path position were taken as those specified by the Army to stress the system most severely with regard to angular velocities and accelerations.

Inputs were intended to be characteristic of radar tracking. They are as follows:

a. Standard deviation.

azimuth: 5 meters
elevation: 0.6 meter
range: 5 meters
noise autocorrelation time: 0.2 sec

b. Target vulnerable radius: 1 meter.

c. Target speed: 310 meters/sec.

d. Target altitude: 250 meters.

e. Target minimum horizontal range: 200 meters.

Three sets of ballistics were used:

a. Present Vigilante (No. 1)

b. Improved Vigilante (No. 2)

c. 'Best' Vigilante (No. 3).

Three smoothing times were used: 0.4, 1.8, and 3.6 seconds. Smoothing was accomplished by least squares weighting in position, rate, and (where used) acceleration for the target turn prediction mode.

Although gun dispersion was normally 4 mils, a sensitivity run was made varying dispersion.

A sensitivity run was also made with all input errors multiplied by 0.4 (as estimated to be possible with a frequency diverse radar).

Runs were also made with gun and sensor lag, and with both corrected by a regeneration algorithm. Lag coefficients were:

a. Sensor: $K_v = 500\ sec^{-1}$, $K_a = 90\ sec^{-2}$.

b. Gun $K_v = 250\ sec^{-1}$, $K_a = 50\ sec^{-2}$.

The three measures (kill-seconds, number of samples within 2 meters, and number of bursts with K GRK8 0.20) are compared for combinations of ballistics and smoothing times in Tables V-7, V-8, and V-9.

On this course, which passes very close to the gun, most of the effectiveness is gained at fractional-second times of flight. With the longer smoothing times, the

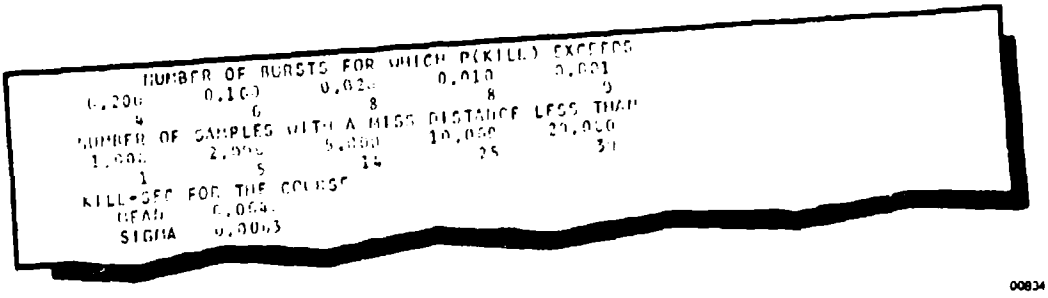

Figure 5-73 Typical Summary Print Out

Table V-7. Comparison of Smoothing Times and Ballistics by 'Kill-Seconds' Measure

	Ballistics		
Smoothing	1	2	3
0.4 sec	0.2473 (0.0872)*	0.2729 (0.0885)	0.2946 (0.0891)
1.8 sec	0.2866 (0.0555)	0.3031 (0.0579)	0.3113 (0.0608)
3.6 sec	0.4363 (0.1989)	0.4390 (0.1967)	0.4380 (0.1943)
No tracking noise; gun dispersion only	0.8632 (0)		0.8612 (0)

*The numbers in parentheses are the standard deviations of the kill-second average across nine replications.

00678-579

Table V-8. Comparison of Smoothing Times and Ballistics by 'Number of Samples Within 2 Meters' Measure

	Ballistics		
Smoothing	1	2	3
0.4 sec	10	12	14
1.8 sec	19	22	24
3.6 sec	36	40	40
No tracking error	--		135

00678-580

noise is fairly well smoothed, so that only a small improvement results from improving the ballistics. This is also to be expected since there are no target maneuvers. When prediction is excellent, there is no payoff in shortening the time of flight.

The distribution of miss distances for present Vigilante ballistics is shown as a function of smoothing time in Figure 5-74. To interpret these curves it is interesting to look at the variance in the position derivatives expected from the one-coordinate curves presented earlier in this report.

Smoothing was done by least squares, finite memory, which, as was shown in Section 5.4 is close to optimum for this case. For a noise autocorrelation of 0.20 sec, Table V-10 shows the variance ratios for optimum smoothing in each derivative for the three smoothing times used on the simulation; i.e., $(\sigma_y/\sigma_z)^2$, where σ_z^2 is the variance of input noise and σ_y^2 is the variance in the measured derivative.

The short times of flight on this path and the relatively large position errors assumed depress the effect

Table V-9. Comparison of Smoothing Times and Ballistics by 'Number of Bursts with K > 0.20' Measure

	Ballistics		
Smoothing	1	2	3
0.4 sec	9	11	11
1.8 sec	12	13	13
3.6 sec	16	16	16
No tracking error			18

00678-581

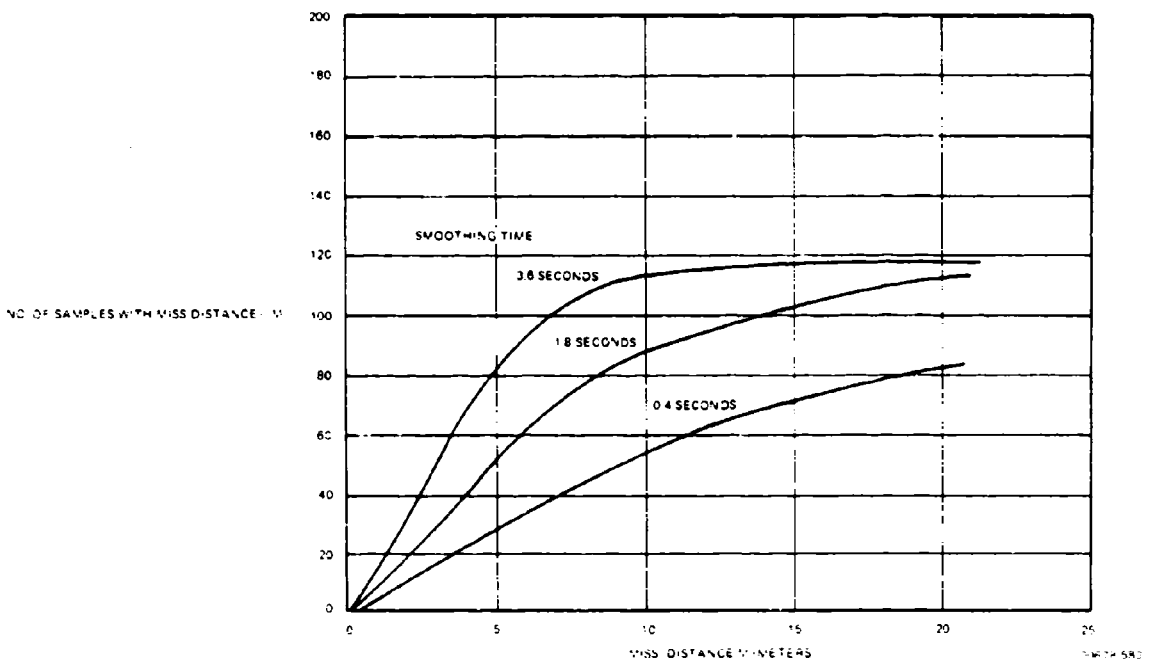

Figure 5-74. Effect of Smoothing Time on Distribution of Miss Distances for Ballistics No. 1

of variance in velocity in the case of the shortest smoothing time shown in Table V-10.

The effect of varying gun dispersion was determined for Smoothing No. 2 (1.8 sec) and for present Vigilante ballistics. Trial runs with Smoothing No. 2 and the 9 replications indicated that the effect was fully shown by 2 replications, hence this number was used. Table V-11 shows the results. Both the kill-second and burst measures degrade smoothly as dispersion is increased from 2 mils. An optimum might have been found for still smaller dispersions, but it was felt that it would be difficult to hold the random round to round errors, in the complete AFAADS system, to less than 2 mils rms.

All of the runs to this point assumed that there is no lag introduced by the sensor or gun servomechanisms. Since this course is intended to stress the angular following ability of the system most severely, the lags were introduced according to the K_v, K_a algorithms, and then the approximate regeneration algorithm described earlier was applied. The results, shown in Table V-12, present a comparison between the lag and the no-lag case. These runs were with Ballistics 3 and 1.8 second smoothing. For the K values assumed, lag

Table V-10. Variance Ratios for Optimum Smoothing of Position, Velocity, and Acceleration

Quantity Smoothed	Smoothing Time		
	0.4 sec	1.8 sec	3.6 sec
Position	0.50	0.18	0.10
Velocity	10.8	0.44	0.092
Acceleration	1520.0	5.8	0.26

100678-582

Table V-11. Effect of Dispersion Based on 2 Replications, Smoothing No. 2 (1.8 sec) and Ballistics No. 1

σ (mils)	Kill-Sec	Number of Samples < 2 Meters*	Number of Bursts with K > 0.20
2	0.4985	20	19
3	0.3693	20	17
4	0.2893	20	12
5	0.2334	20	10
6	0.1922	20	11
8	0.1364	20	-
10	0.1011	20	-
15	0.0550	20	4

*These entries independent of gun dispersion.

100678-584

degraded the kill-second and miss distance measures badly, but not the index of number of 1-second bursts with K > 0.20. The reason is probably that the interval, over which lag error is large, occupies only 1-2 seconds near the midpoint of the course. Since the K index is rounded to integers, fine detail is lost. The regeneration algorithm recovered almost all of the lost effectiveness; in fact K rounded to one integer higher than without lag. If it were not for the advantages of regenerative tracking in maintaining track when the target is obscured, one might argue from the preceding results that with radar tracking, tight servos of the best design would obviate the need for regeneration.

As we show in later runs, the man with K, no better than about 10 sec^3 is another matter, and cannot be expected to function satisfactorily without regenerative aids.

There is no expected advantage in using quadratic prediction against an unaccelerated target, but it is of some interest to determine how badly the additional noise amplification would affect the system performance if quadratic prediction were used continuously.

Table V-12 Effect of Lag and Regeneration Based on 9 Replications, Smoothing No. 2 (1.8 sec) and Ballistics No. 3

	Kill-Sec	Number of Samples < 2 Meters	Number of Bursts with K > 0.20
No lag	0.3113 (0.0608)*	24	13
With lag	0.1849 (0.0351)	15	12
With lag and regeneration	0.2769 (0.0507)	21	14

* The numbers in parentheses are the standard deviations of the kill-second average across seven replications

00628-585

Table V-13 compares both the linear and the quadratic predictions on this straight line course. Performance degradation is significant, but not excessive, again, probably because of the relatively short times of flight associated with the most important segment of the course.

Finally, to observe the effects of reduction of tracking noise, the shortest smoothing time of 0.4 seconds was run with two sets of ballistics and with each of the input noise standard deviations multiplied by 0.40. This reduction by a factor of 2.5 was considered possibly attainable with a frequency diverse radar.

As shown in Table V-14, a very large improvement in the effectiveness results was achieved by all measures used. In fact, with this accuracy of tracking, the 0.40-second smoothing was as good as the 3.6-second smoothing with the larger errors. The payoff from improved tracking can thus be taken in high kill probability when the system has settled, or in quicker settling and increased firing time.

5.13.4 Simulator Results on Attack Path (Path No. 3)

Path No. 3 consists of a pop-up from 200 meters to 1700 meters, a turn, an accelerated dive at a ground target, and a pullout. The horizontal projection of the course is shown in Figure 5-75. The altitude as a function of time is shown in Figure 5-76. The path was constructed from the pop-up maneuver combined with the attack segment of Path No. 1. Target speed varied from a maximum of 234 meters/sec in the run-up, to a minimum of 150 meters/sec as the airplane lost velocity in the climb. (See Figure 5-77.) The airplane gained about 50 meters in the dive.

5.13.4.1 Comparison of Prediction Algorithms and Ballistics

The prediction algorithms compared were:

a. Linear.

b. Linear and Energy Correction.

c. Quadratic (horizontal turn).

d. Quadratic plus energy correction.

e. Defense against attack on a known point.

Since prior runs had shown Ballistics No. 2 to be always intermediate between No. 1 and No. 3 (the 'present' and the 'best' Vigilante ballistics respectively), only these two sets were retained. These runs were made with Smoothing No. 2 (1.6 sec). Table V-15 shows results for 9 replications of each case. The energy correction improved each algorithm with which it was used. It is incorporated in the defense of a known point algorithm as well. The most effective

Table V-13. Comparison of Linear and Quadratic Prediction Based on: 9 Replications and Smoothing No. 2 (1.8 sec)

Prediction Mode		Kill-Sec	Number of Samples < 2 Meters	Number of Bursts with K >= 0.20
Ballistics No. 1	Linear	0.2866 (0.0555)*	19	12
	Quadratic	0.2450 (0.0492)	12	10
Ballistics No. 3	Linear	0.3113 (0.0608)	24	13
	Quadratic	0.2800 (0.0593)	16	11

*The numbers in parentheses are the standard deviations of the kill-second average across nine replications.

0067S-586

Table V-14. Effect of Improved Tracking Based on: Smoothing No. 1 (1.8 sec) and a Gun Dispersion of 4 mils

Ballistics	Standard Deviation of Tracking Errors (Meters)			Kill-Sec	Number of Samples < 2 Meters	Number of Bursts with K >= 0.20
	Azimuth	Elevation	Range			
1	5	0.6	5	0.2473 (0.0872)*	10	9
	2	0.24	2	[illegible]342 [illegible]29)	29	15
3	5	0.6	2	[illegible]46 [illegible]891)	14	13
	2	0.24	2	0.5893 (0.0824)	15	15

*The numbers in parentheses are the standard deviations of the kill-second average across nine replications.

0067S-587

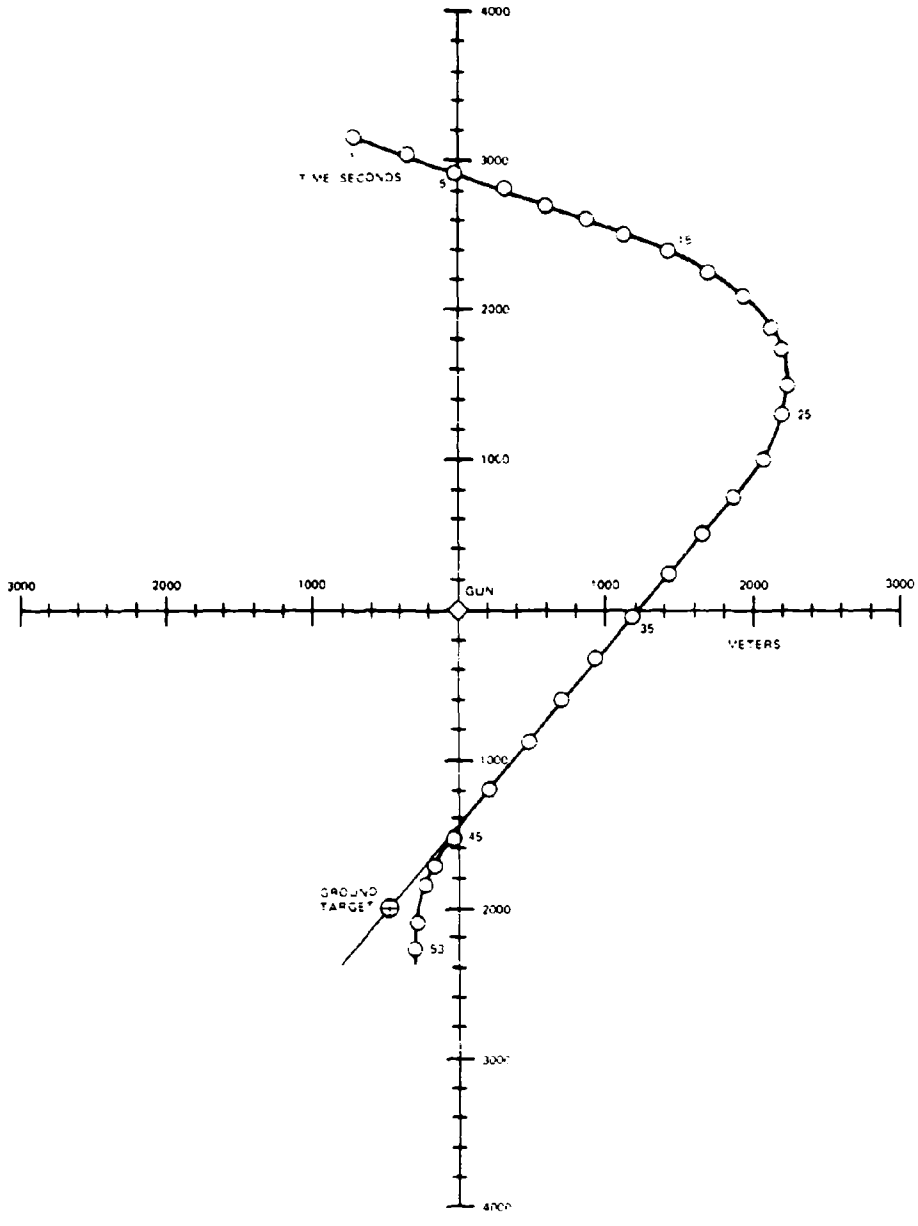

Figure 5-75. Horizontal Projection of Simulation Flight Path No. 3

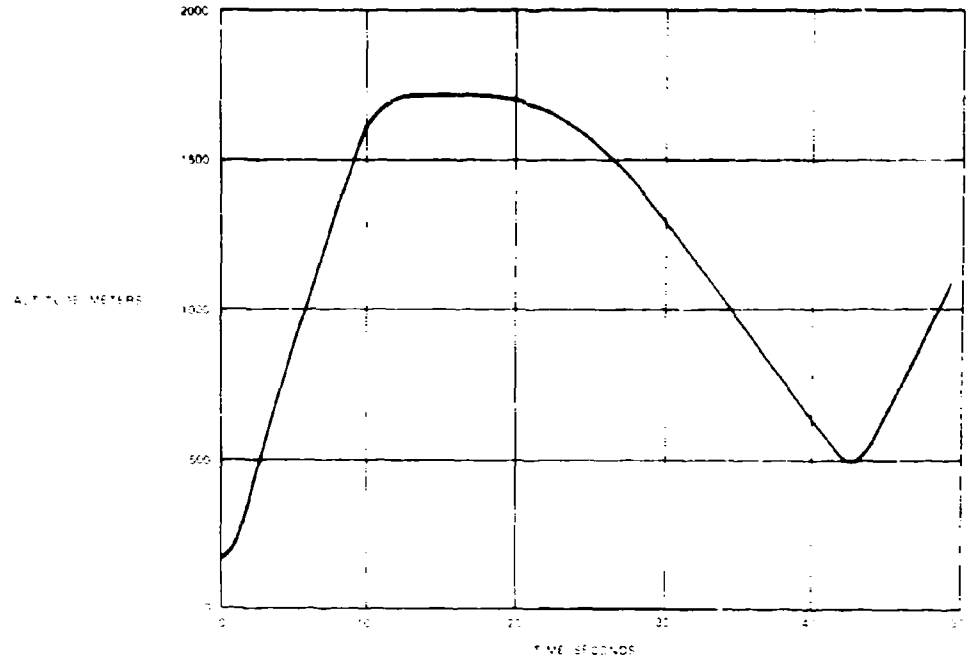

Figure 5-76. Altitude versus Time Projection of Simulation Flight Path No. 3

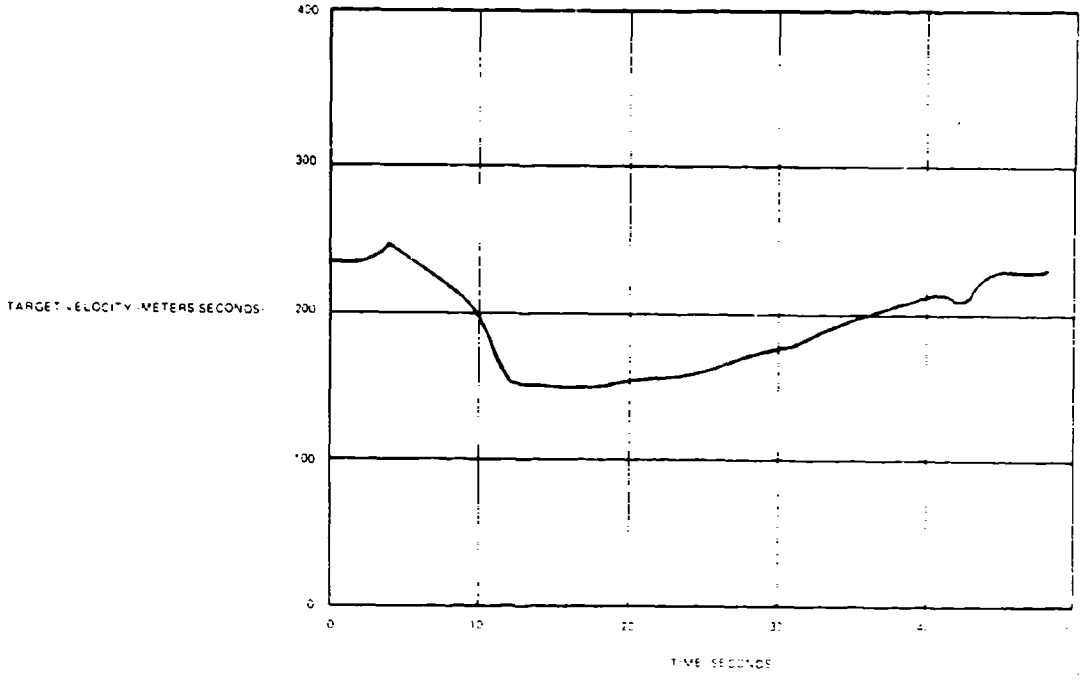

Figure 5-77. Target Velocity along Flight Path versus Time for Simulation Flight Path No. 3

Table V-15. Comparison of Prediction Algorithms and Ballistics Based on: 9 Replications, Path No. 3, and Smoothing No. 2

Measure	Ballistics	Linear	Linear Plus Energy	Quadratic	Quadratic Plus Energy	Defended Point
Kill-Seconds	"Present" (No. 1)	0.0665	0.1149	0.0282	0.0506	0.1349
	"Improved" (No. 3)	0.0947	0.1305	0.0534	0.0747	0.1457
Number of Bursts with K > 0.20	"Present" (No. 1)	6	10	2	4	11
	"Improved" (No. 3)	8	10	5	6	11
Number of Samples Within 2 Meters	"Present" (No. 1)	2	12	1	2	16
	"Improved" (No. 3)	4	14	1	3	18

NOTE: Gun Dispersion = 4 mils, σ_R = 5 meters, σ_A = 5 meters, σ_E = 0.6 meters.

00678-591

algorithm is that for the defense of a known point, and the next best is the linear plus energy correction. With the two best prediction algorithms, there is no difference between the two sets of ballistics in terms of the number of bursts above K = 0.20; but the more sensitive measures of kill-seconds and miss distance show a significant advantage to the better ballistics. The distribution of miss distances is compared in Figure 5-78.

5.13.4.2 Determination of Optimum Dispersion

By running a series of 2-replication sets, we find an optimum gun dispersion of 2-3 mils as shown in Figures 5-79 through 5-82. Note that this is revealed by the burst measure, and not by the kill-seconds index. The burst measure was introduced for precisely this reason. The kill-second index shows the expected number of killing hits, without regard for whether some targets get more than their share, while the burst measure shows the probability that each target will receive at least one killing hit.

5.13.4.3 Effect of Tracking Noise Variance

Input noise variances were then varied individually to determine the sensitivity of the system to each input coordinate. Table V-16 shows the values used, and the effectiveness indices. The system is far more sensitive to azimuth and elevation errors than to range errors. A brief analysis of the lead equations indicates that the variation of miss distance with range error is roughly proportional to the ratio of target speed to average projectile velocity, and, hence, always less than unity. The variation of miss distance with azimuth or elevation error is roughly proportional to the ratio of time of flight to smoothing time; with a multiplying coefficient such that the factor can exceed unity. Figures 5-83 and 5-84 show the results of varying range sigma and elevation sigma separately.

5.13.4.4 Interaction Between Tracking Noise and Smoothing Time

The advantages of accurate tracking and the interaction with the smoothing time obtained on the pass path were reconfirmed by runs on this course, the results of which are shown in Table V-17.

5.13.4.5 Effects of Servomechanism Lag and Regeneration

The angular rates and accelerations on this flight path are not as severe as on the pass path. A rerun of the lag and regeneration modes indicate lag to have a

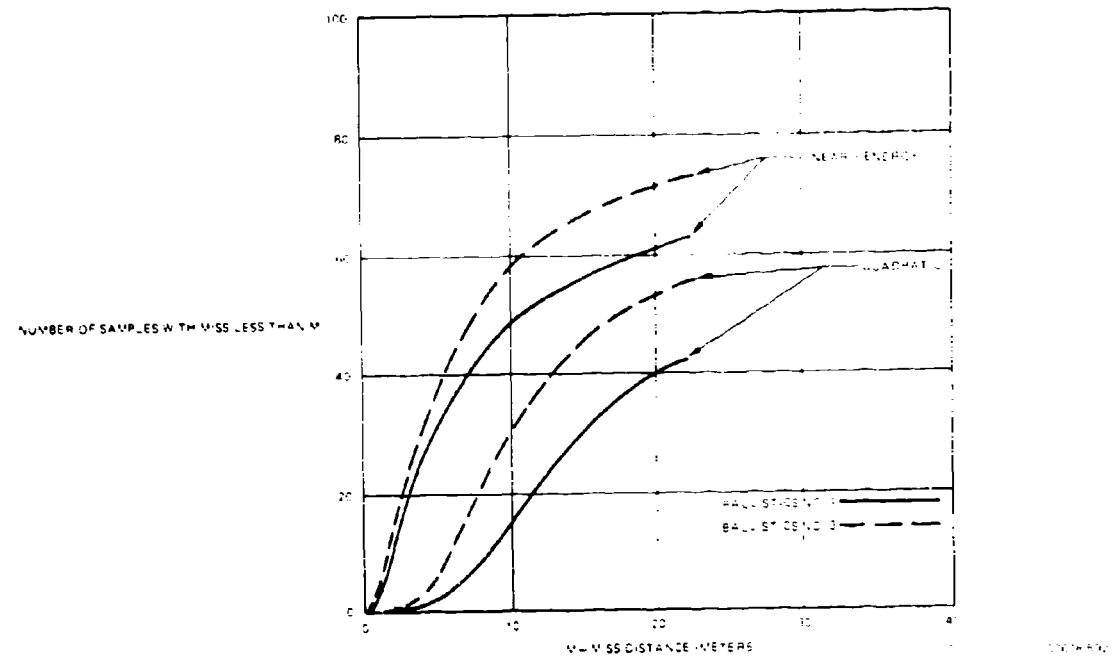

Figure 5-78. Distribution of Miss Distances for Path No. 3

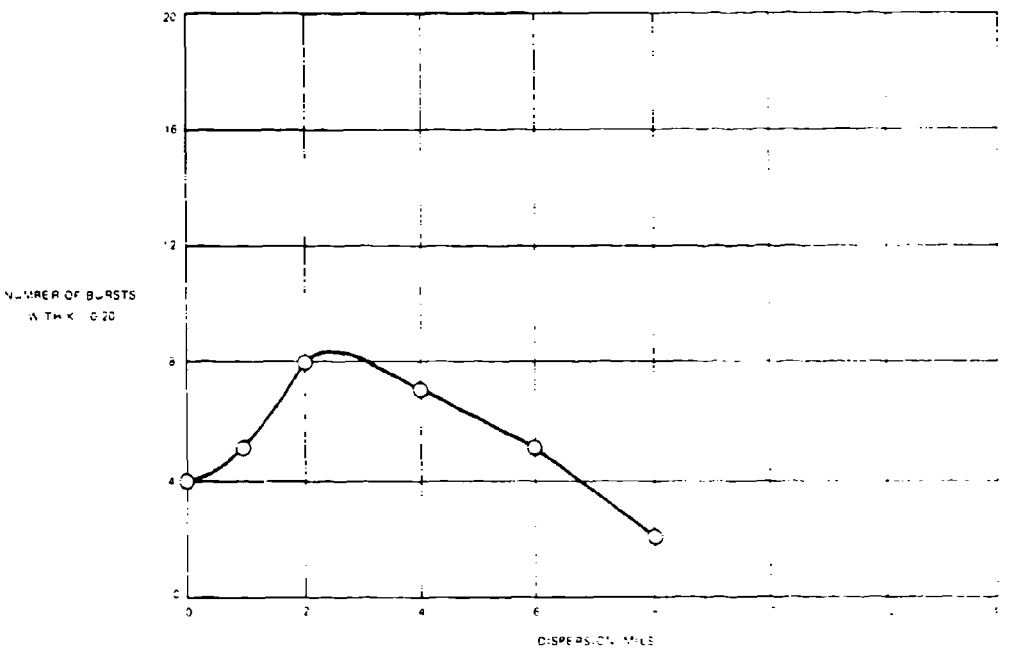

Figure 5-79. Effect of Dispersion on Number of Bursts with K < 0.20 Measure with Quadratic plus Energy Prediction and Based on: 2 Replications, Smoothing No. 2 and Ballistics No. 3

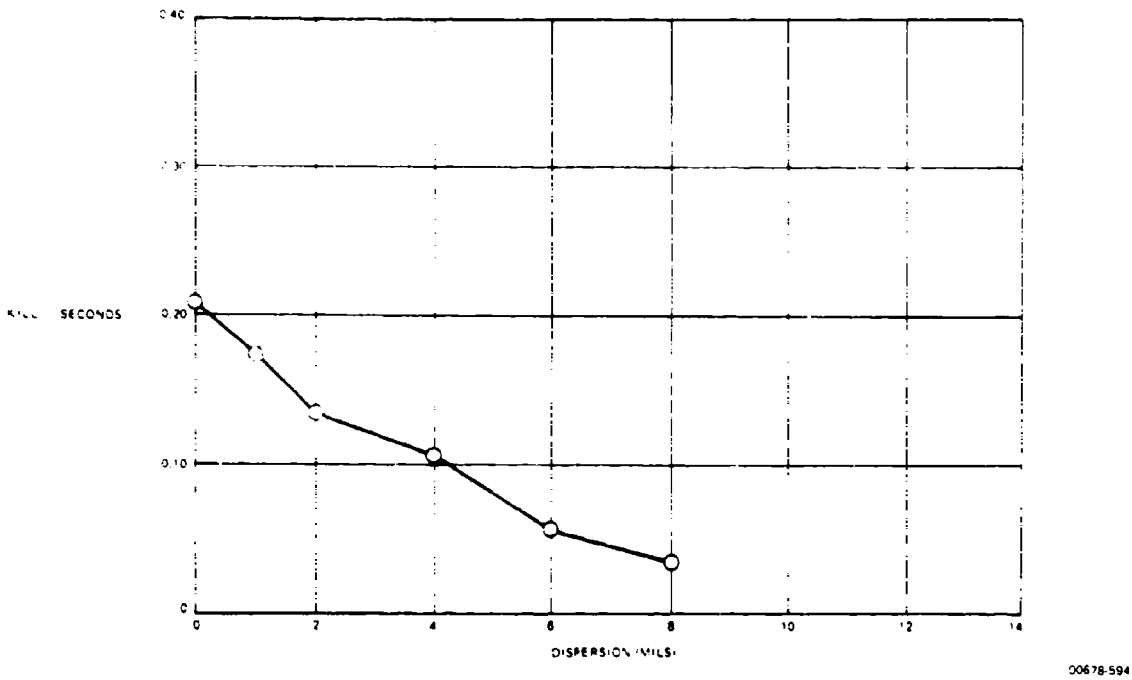

Figure 5-80. Effect of Dispersion on Kill-Sec Measure with Quadratic plus Energy Prediction and Based on 2 Replications, Smoothing No. 2, and Ballistic No. 3

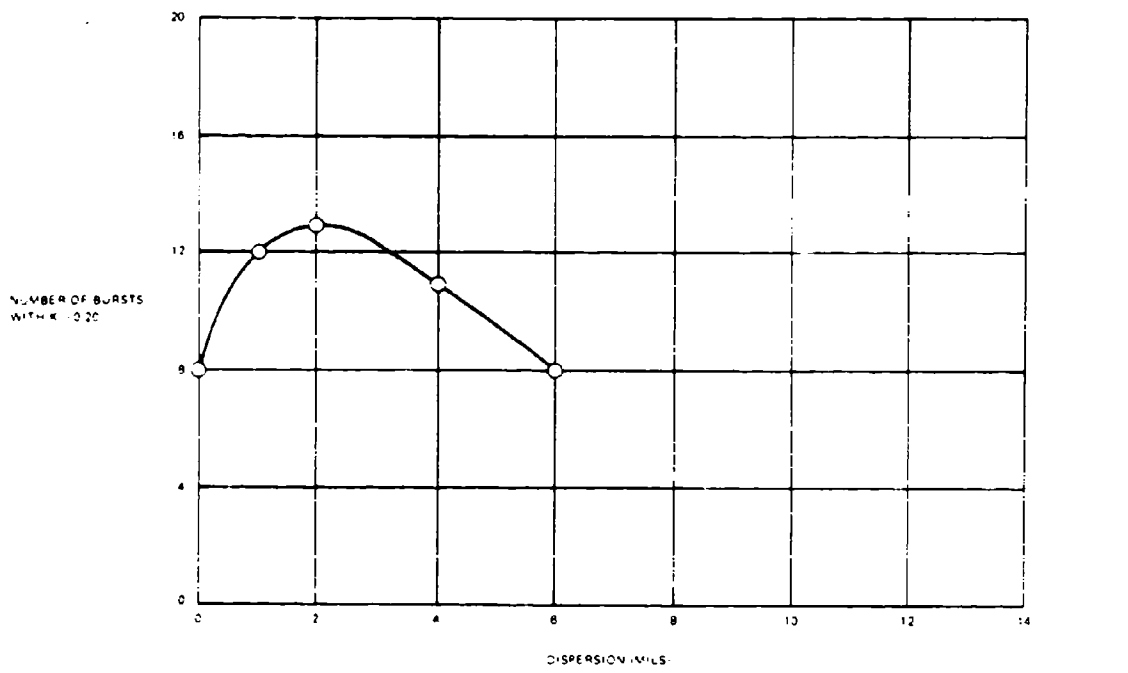

Figure 5-81. Effect of Dispersion on Number of Bursts with K < 0.20 Measure with Linear plus Energy Prediction and Based on 2 Replications, Smoothing No. 2 and Ballistics No. 3

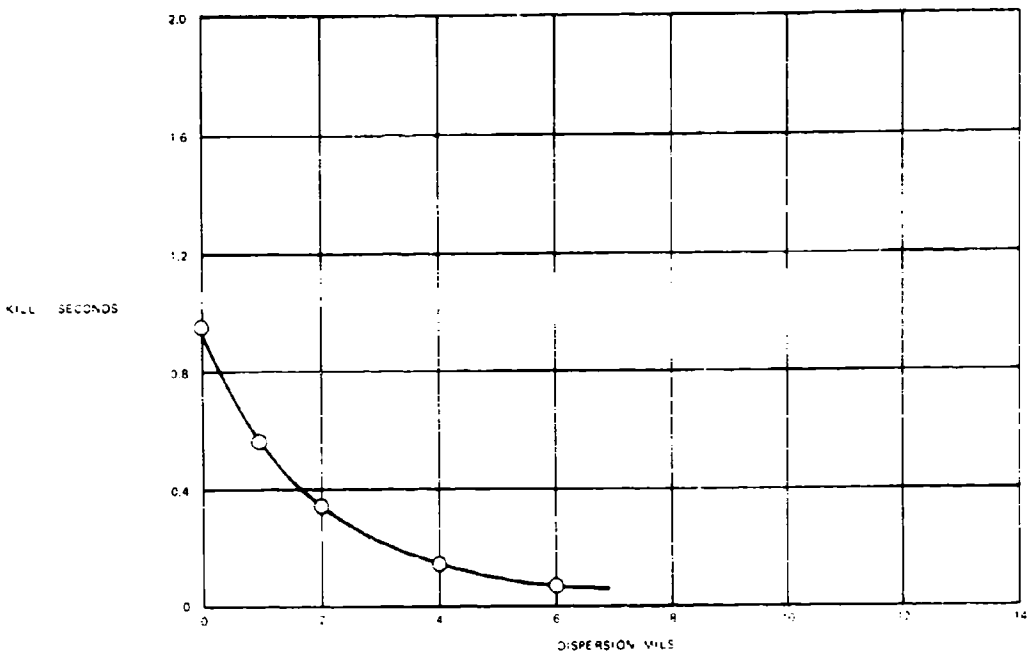

Figure 5-82. Effect of Dispersion on Kill-Sec Measure with Linear plus Energy Prediction and Based on: 2 Replications, Smoothing No. 2, and Ballistics No. 3

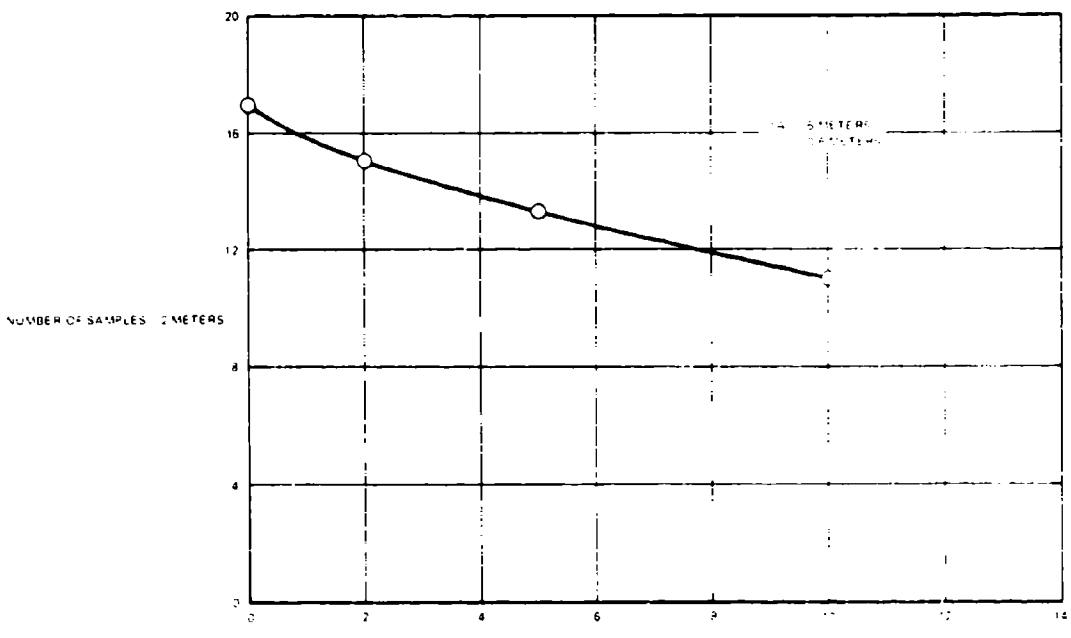

Figure 5-83. Effect of Varying Range Noise Variance

Table V-16. Effect of Noise Variance Using Linear plus Energy Prediction Based on: 2 Replications Each, Smoothing No. 2 and Ballistics No. 3

σ_R	σ_A	σ_e	Kill-Sec	K >0.20	S< 2 Meters
5.0	5.0	0.6	0.1433	11	15
2.0	2.0	0.24	0.1866	12	40
10.0	5.0	0.6	0.1392	11	12
2.0	5.0	0.6	0.1455	11	16
0.0	5.0	0.6	0.1468	11	17
2.0	10.0	10.0	0.0521	4	2
2.0	5.0	5.0	0.1103	9	5
2.0	5.0	0.0	0.1463	11	17
2.0	0.0	0.6	0.1985	13	61

00678-597

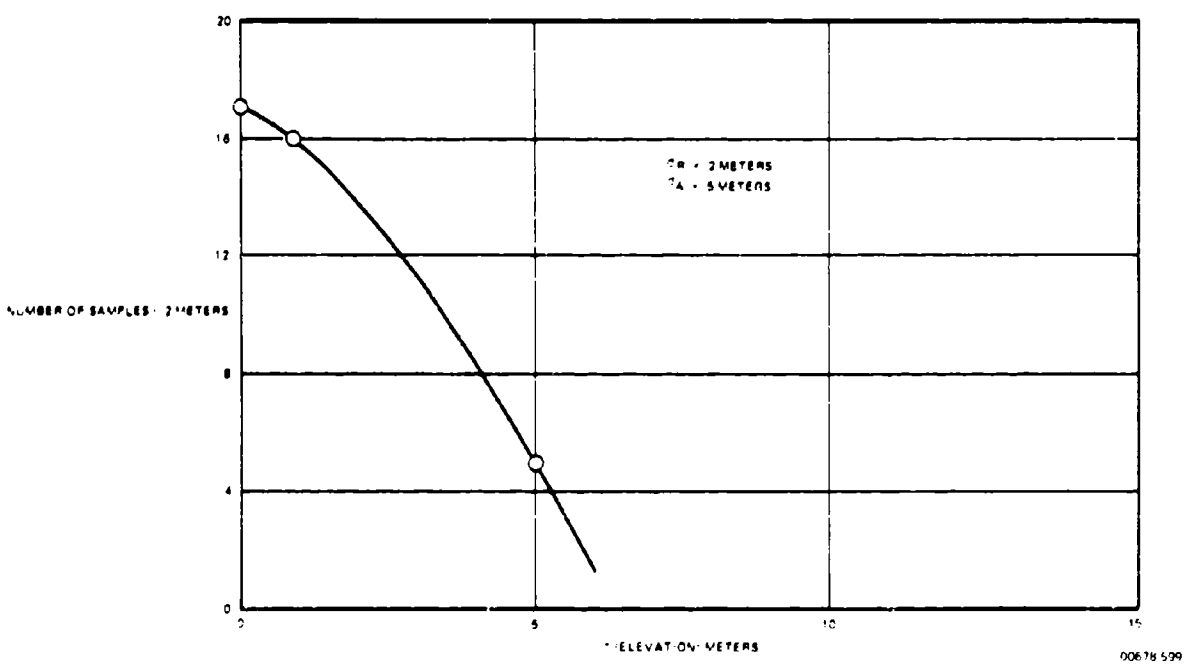

Figure 5-84. Effect of Varying Elevation Noise Variance

Table V-17. Comparison of Smoothing Times plus Noise Using Linear plus Energy Prediction and Based on 9 Replications, Ballistics No. 3 and Path No. 3

	Kill-Sec	K > 0.20	S < 2 Meters	Standard Deviations of Tracking Error		
				σ_R	σ_A	σ_c
Smoothing 1	0.1435	12	16	2	2	0.24
Smoothing 2	0.1810	12	34	2	2	0.24
Smoothing 2	0.1305	10	14	5	5	0.6

00678-5101

negligible effect for the K values used. However, regeneration is effective in eliminating most of the small adverse effects noted. Results are shown in Table V-18.

5.13.4.5 Effect of Switching Algorithm Threshold

This target path does not have a steady-turn segment of sufficient duration to offer the quadratic prediction algorithm an opportunity to perform. However, an investigation was made in which the threshold for switching from linear to quadratic was smoothly varied from zero to very large rates of turn. Effectiveness was shown to have a smooth increase as the threshold was raised until full linear operation was obtained.

5.13.4.7 A Microscopic View of Details of Path No. 3

For Path No. 3, Ballistic No. 3, Smoothing No. 2, and the Linear plus Energy Prediction, a print-out of interesting indicators was made at 0.20 second intervals.

With the exception of very short path segments, during the climb, and the level straight segment (prior to turn at the top of the pop-up), miss distances exceeded 20 meters. Some were as large as several hundred meters, until the target enters the straight-line accelerated dive. Since the print-out was for the linear plus energy mode, the algorithm was not able to cope with the turn at the top of the pop-up. The print-out showed a one second opportunity to get a burst kill with a probability of 0.30 in the climb.

Effectiveness of the system did not become significant until the diving segment.

With two exceptions, a one-second burst fired anywhere from 28 to 40 seconds would have a better than a 0.30 chance of killing the target.

5.13.4.8 Effect of Dispersion on Single-Shot Probability

We can view the effects of dispersion through this microscope by plotting single-shot kill probability versus time. This is done in Figure 5-85 for the segment from 28 to 41 seconds. Note that on this run, 2-mils dispersion shows single-shot kill probabilities as high as 0.07; whereas the highest with 4-mils dispersion is only 0.02. However, the larger dispersion smooths out the wide fluctuations in the single-shot kill probability, thereby reducing the peaks, but raising the valleys. This is what one would expect. If we showed 1- or 0-mils dispersion the peaks would be still higher and the valleys lower and wider.

Optimum dispersion is that dispersion that strikes the best balance between the fluctuations in p_{ss} and its mean level. Since we don't know miss distance when a burst is fired, dispersion mitigates the effect of possible transient large errors during the burst.

Table V-18. Comparison of Effect of Lags Using Linear plus Energy Prediction and Based on: 9 Replications, Ballistics No. 3 and Smoothing No. 2

No Lag	0.1305	10	14
Sensor Lag	0.1298	10	14
Sensor and Gun Lag	0.1259	10	12
Sensor and Gun Lag plus Regeneration	0.1295	10	13

00678-5102

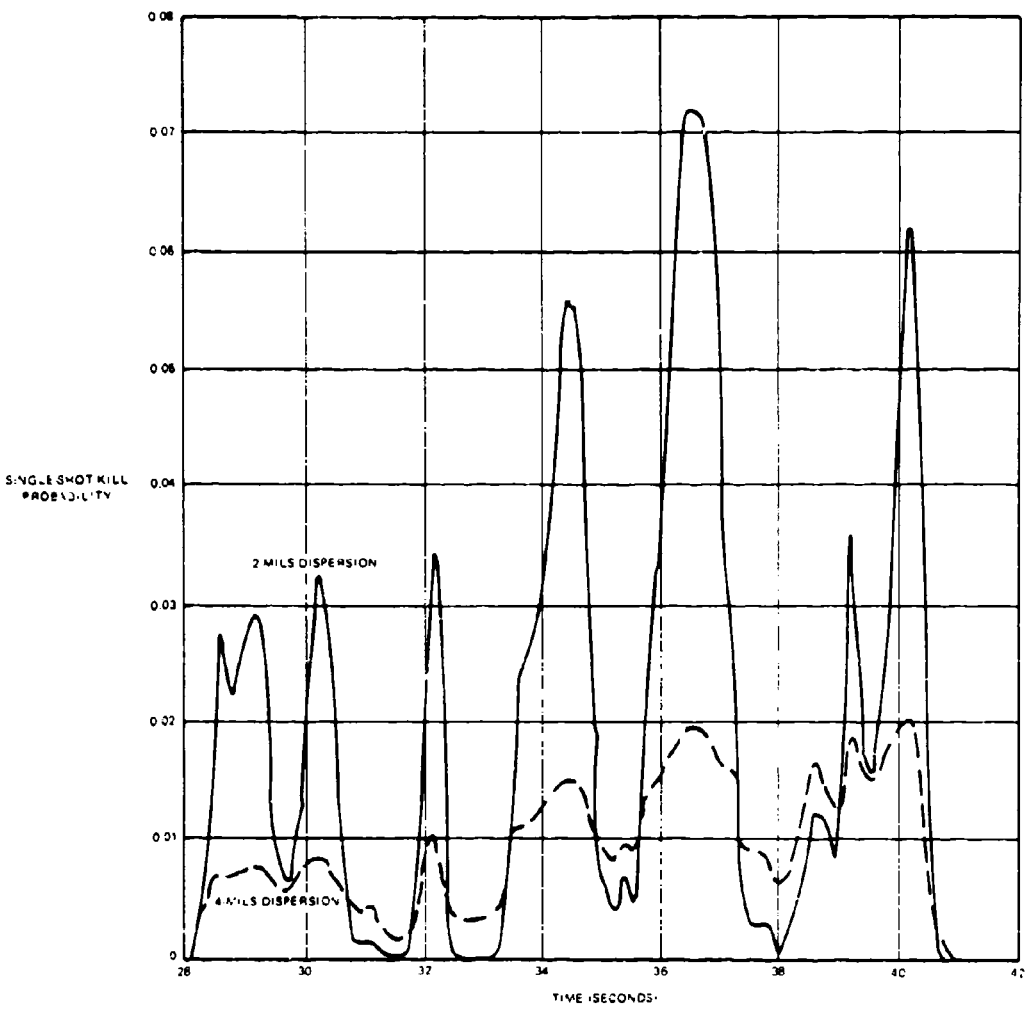

00678-5103

Figure 5-85. Effect of Dispersion on Path No. 3 Based on the Single-Shot Kill Probability Versus Time

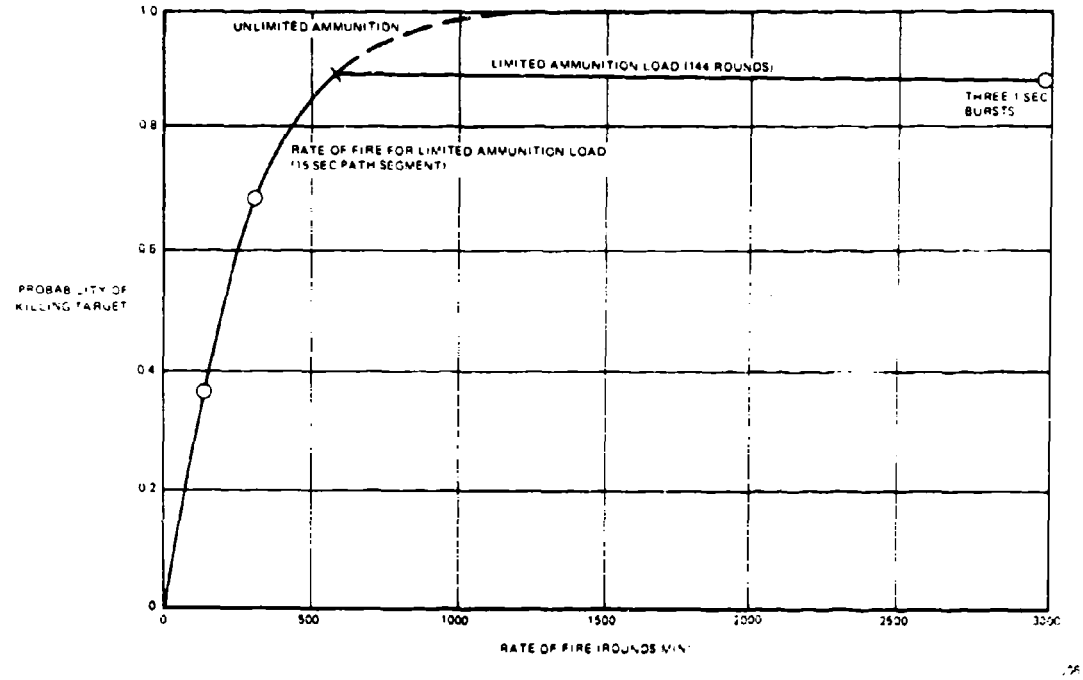

Figure 5-86. Effect of Rate of Fire and Ammunition Load

The fluctuations in the single-shot kill probability are the result of tracking noise, initially correlated at input and further correlated by the smoothing functions.

5.13.4.9 Effect of Varying Rate of Fire

We can rework the computation of kill probability as printed out over the path in various ways. First, suppose that the gun fires 3 bursts of 48 rounds each at the beginning, midpoint, and toward the end of the dive. The bursts are arbitrarily located at 29.2-30.2 sec, 32.2-33.2 sec, and 35.2-36.2 sec. The probability that the target survives all three is 0.11; the probability that it is killed is 0.89.

Next suppose that the gun fires at a low, constant rate throughout the dive. The interval over which p_{ss} is greater than zero is about 15 seconds. Figure 5-86 shows how the probability of killing the target increases with rate of fire. At about 600 rpm, the gun uses up its 148-round load, and has attained a kill probability very close to that obtained by the three 1-second burst at 3000 rpm. In fact, the probability is slightly higher, because one of the three bursts fell in a low probability interval.

Figure 5-87 compares the way that target survival probability decreases versus the three bursts and the continuous rate of fire at 600 rpm. The low rate of fire produces a steady reduction of survival probability whereas the bursts reduce it in three steps, one of which is very small.

Although there is no strong argument for 3000 rpm versus 600 rpm on this path segment, it is clear that what determines effectiveness for a given ammunition load is the ability to fire all of the ammunition while the target is on a predictable leg, and not to waste ammunition when it is not. The 3000 rpm option is valuable if one has only 3 seconds of good shooting time, and can identify those 3 seconds, as opposed to the total time the target is within range. It is probable, however, that Vigilante would benefit from a 1200 rpm option.

5.13.4.10 The Effect of Boresight Errors

In our simulation runs we included the effect of target maneuvers as a cause of large slowly-varying 'systematic' errors, and the effect of 'aim wander' generated by correlated noise with zero mean, further correlated by the filter. We have also included systematic errors resulting from servo lags, by expressing these as a function of rates and accelerations. We feel that this fairly well covers the wander of the point of aim caused by sources that are difficult to design out of the system.

In the field, errors will appear because the system is not properly calibrated and boresighted. In Section 5.8 we proposed a method of dynamic calibration to get

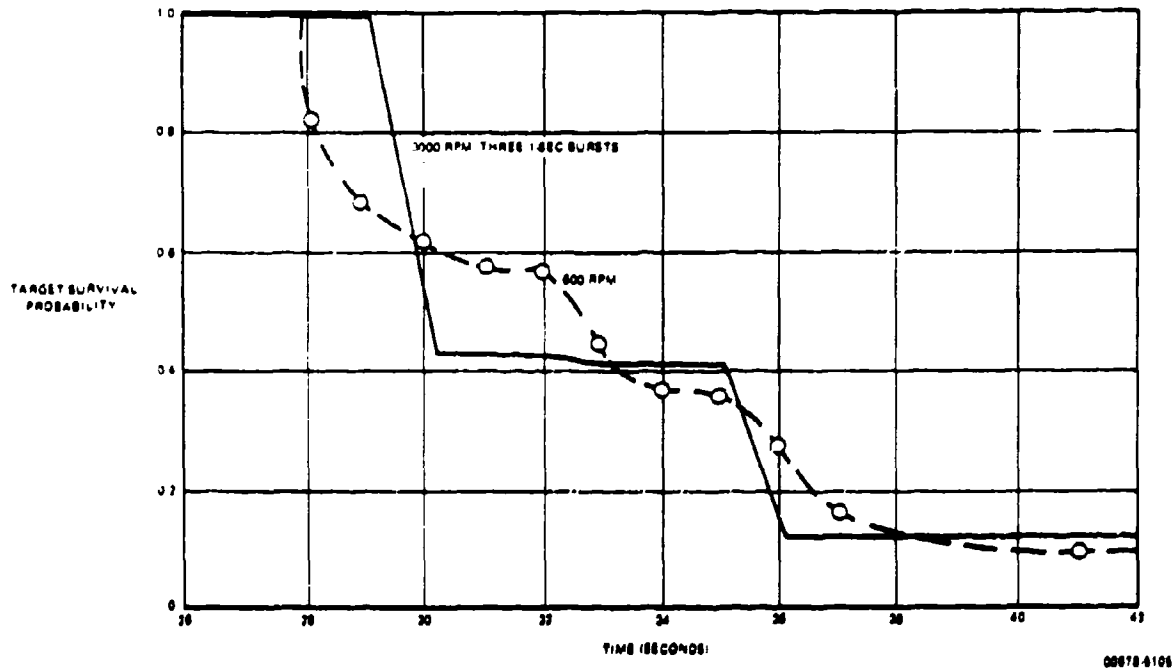

Figure 5-87. Effect of Rate of Fire on Target Survivability as a Function of Time

rid of these errors. However, to see what happens when there is a constant angular misalignment error in the system, we applied a constant angular error to azimuth input and observed the results with the simulator.

Boresight error was varied from zero to 8 mils in steps of 2 mils. The flight path was Path No. 3, with linear plus energy prediction. Also included are the 5.0 meter azimuth, the 0.6-meter elevation and the 5.0-meter range standard deviations of input error and 4-mils dispersion.

Results of two replications are shown in Figure 5-88 through 5-90. All boresight error is bad, but on this course with this set of parameters, we could accept perhaps 2 mils of boresight error without serious degradation.

The inverse statement is probably true; i.e., the amount of dispersion one uses should increase with the expected misalignment of the system. This degrades the antiaircraft system. Dynamic calibration should be preferred.

Looking at the distribution of miss distances, it is interesting to note that we apparently chose the boresight error in a direction to cancel a target maneuver error over a very short path segment. This would explain the waves in the curves for the 2- and 4-mil error cases.

5.13.5 Simulator Results on Climbing Turn

The climbing turn segment of Path No. 1 was used to compare linear plus energy versus quadratic plus energy options. The larger radar errors were used as inputs, gun dispersion was 2 mils and smoothing was 1.6 sec. As shown in Table V-19, the quadratic mode was effective whereas the linear mode had zero effectiveness. The distribution of miss distances is shown in Figure 5-91. Although the linear mode never came within 10 meters of the target, the quadratic mode had almost 20 samples within 5 meters.

On this path, the target was turning at about 0.05 radians per second. As the acceleration theshold (which is currently programmed in terms of rate of turn) was increased from zero, the efficiency of the prediction collapsed abruptly when the threshold excluded the target turn rate. The decay is not a perfect step because of noise which also triggers the algorithm. However, for low thresholds (up to 0.02), noise never knocked the system back into the linear mode (or at least so rarely that the effect on performance was negligible).

The threshold operation thus functions properly on this path segment. It can be set low and non-zero to keep the quadratic mode from being invoked on non-turning paths by noise; and still capture targets where turn rate is large enough to cause linear prediction to fail.

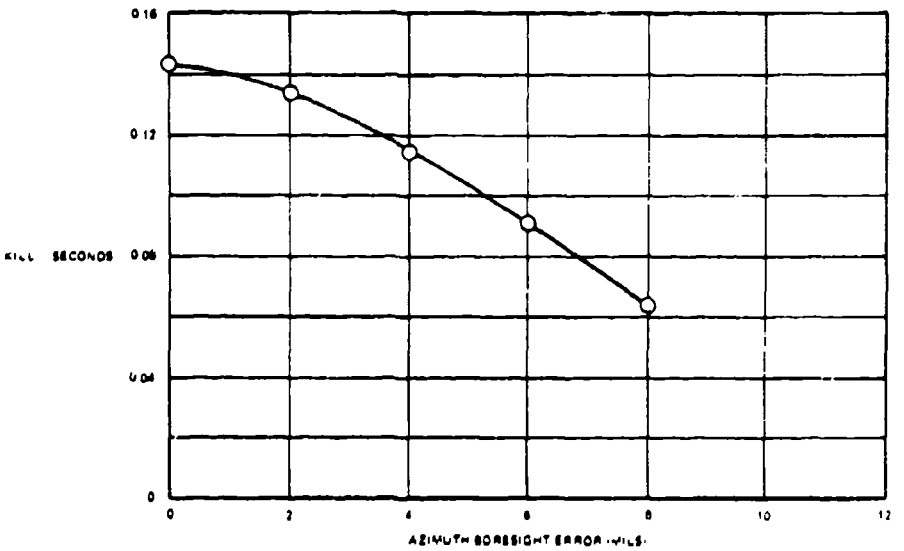

Figure 5-88. Effect of Azimuth Boresight Error on Kill-Sec Measure with Linear plus Energy Prediction and Based on: 2 Replications, Smoothing No. 2 and Ballistics No. 3

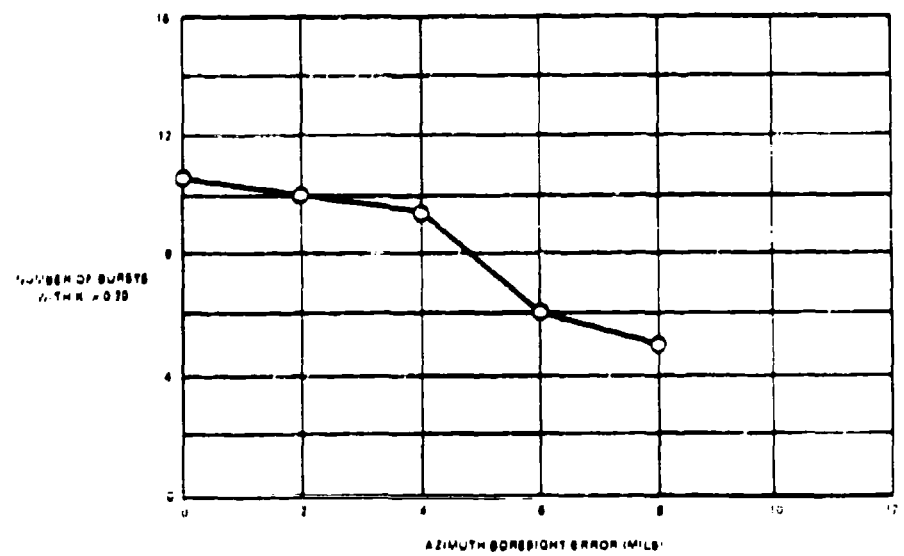

Figure 5-89. Effect of Azimuth Boresight Error on Number of Bursts with K < 0.20 Measure with Linear plus Energy Prediction and Based on: 2 Replications, Smoothing No. 2 and Ballistics No. 3

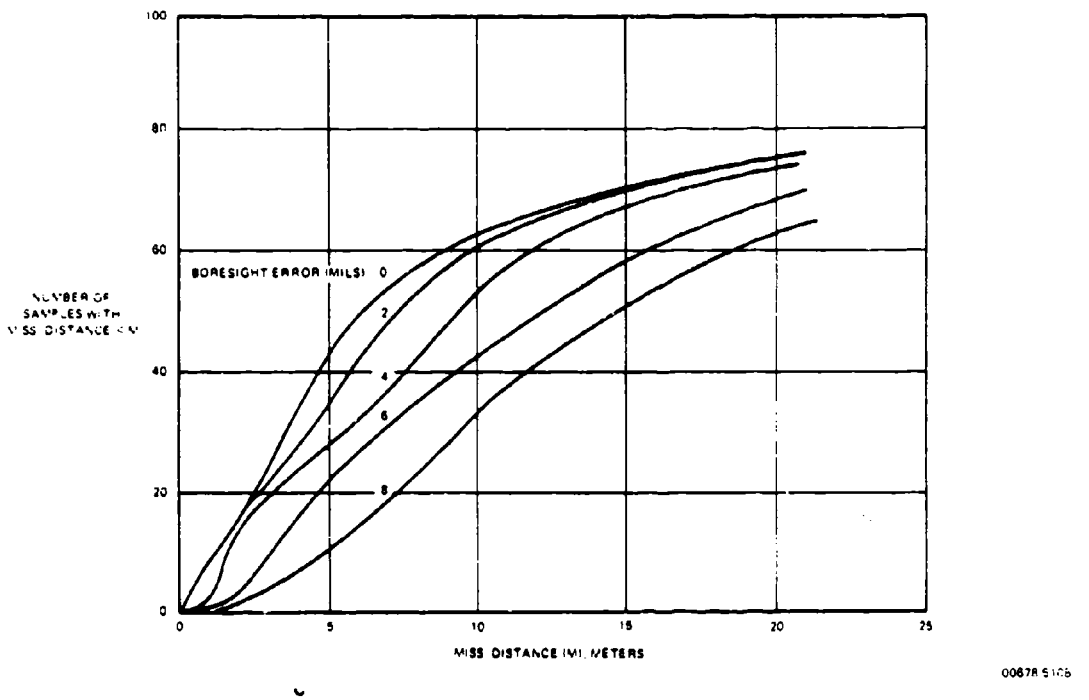

Figure 5-90. Distribution of Miss Distances as a Function of Boresight Error

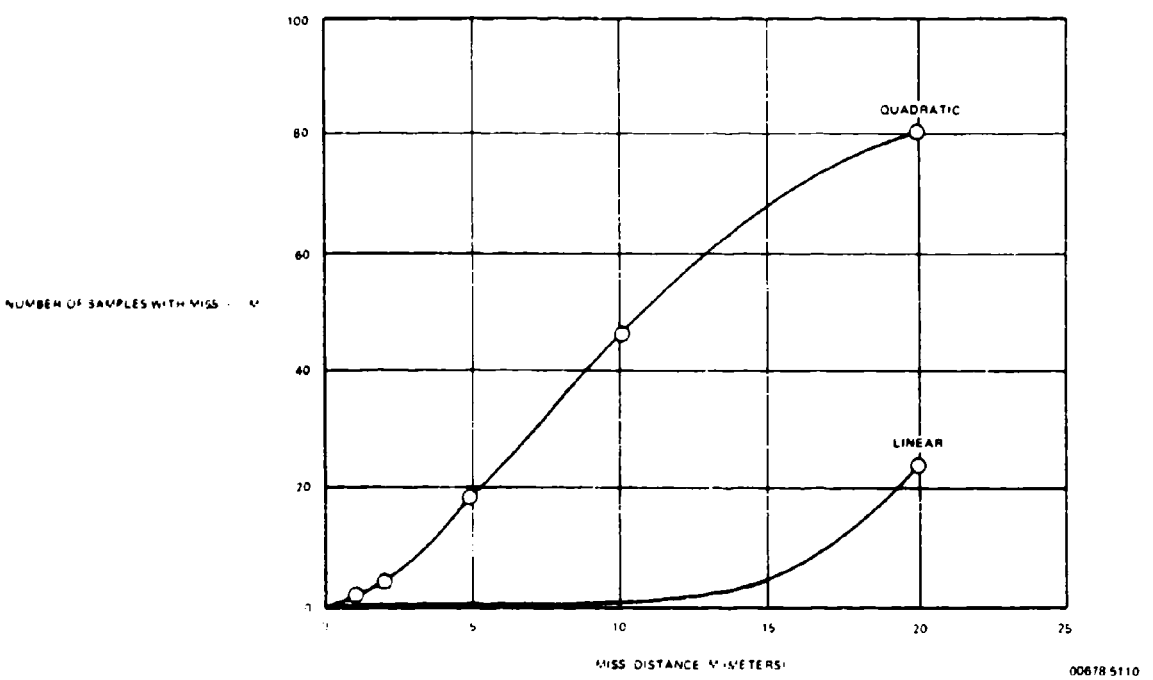

Figure 5-91. Distribution of Miss Distances on a Climbing Turn

5.13.6 Simulator Results Against Jinking Target

Four aircraft paths were used to investigate the effectiveness of candidate prediction modes against aircraft employing a jinking maneuver. Each path was composed of a mixture of two maneuver types, with the same representative of a maneuver type being used on each of its occurances. Three maneuver types were employed:

a. Straight flight.

b. 0.5g jinking

c. 2 - 3g jinking.

Tables V-20 and V-21 present the exact course content used for the 0.5g, and for the 2 - 3g jinking maneuvers respectively.

The four pathes used were:

a. Path 4 - This path started with a straight line-segment of duration equal to the smoothing time being used. The straight segment was followed by the 2-3g jinking and the 0.5g jinking maneuver. The jinking is around a basic fly-by course which passes the gun at a distance of 500 meters. The aircraft maintains a constant altitude of 250 meters. The variation of the Y coordinate of path 4 with time is shown in Figure 5-92.

b. Path 4a - Path 4a is an exact copy of Path 4 except that the basic fly-by course has been moved out to 1500 meters.

c. Path 5 - This path starts with a straight-line segment of duration equal to the smoothing time being used. The straight-line segment is followed by the 2-3g maneuver, and another straight-line segment starting at 'cross over' and lasting for 10 seconds. Fly-by is at 500 meters and a constant altitude of 250 meters is maintained.

d. Path 5a - This path starts with a straight line-segment of 10-second duration. The line ends at 'cross over;' which is at a distance of 500 meters from the gun. At that point 10 seconds of 2-3g jinking occurs while constant altitude of 250 meters is maintained.

The simulation runs were made comparing the linear plus energy prediction with the quadratic plus energy prediction. There is no advantage to the energy add-on against this path, however it was left in because (1) it introduces no noise amplification (2) it is desired for flight paths where the altitude changes, and (3) it is not expected to influence these results and comparisons. Smoothing No. 2 (1.6 second) and Ballistics No. 3 were used with a 4-mil gun dispersion.

The results are shown in Tables V-22 through V-24. When the jinking maneuver is performed close to the

Table V-19. Comparison of Prediction Algorithms on a Climbing Turn

	Kill-Sec	K >0.20	M< 2.0 Meters
Linear + Energy	0.0020	0	0
Quadratic + Energy	0.086	8	4

00678-5109

Table V-20. Course Content of the 0.5g Jinking Maneuver

Segment	Type	Direction	Turn (degrees)	Radial Acceleration (g)
1	circle	right	2.0	0.5
2	circle	left	3.0	0.5
3	circle	right	4.0	0.5
4	circle	left	6.0	0.5
5	circle	right	3.0	0.5

00678-5111

Table V-21. Course Content of the 2 - 3g Jinking Maneuver

Segment	Type	Direction	Turn (degrees)	Radial Acceleration (g)
1	circle	right	5.0	2.0
2	circle	left	8.0	2.5
3	circle	right	10.14	3.0
4	circle	left	9.0	2.0
5	circle	left	8.0	2.5
6	circle	right	9.79	2.5

00678-5112

Table V-22. Comparison of Prediction Modes on Jinking Path by 'Kill-Sec' Measure

Prediction Mode	Path Segment (sec) 0-20	0-10	10-20	
Linear + Energy	0.1131	0.0396	0.0646	Path 4
Quadratic + Energy	0.1870	0.0748	0.0743	
Linear + Energy	0.0576			Path 4a
Quadratic + Energy	0.0487			

00678-5114

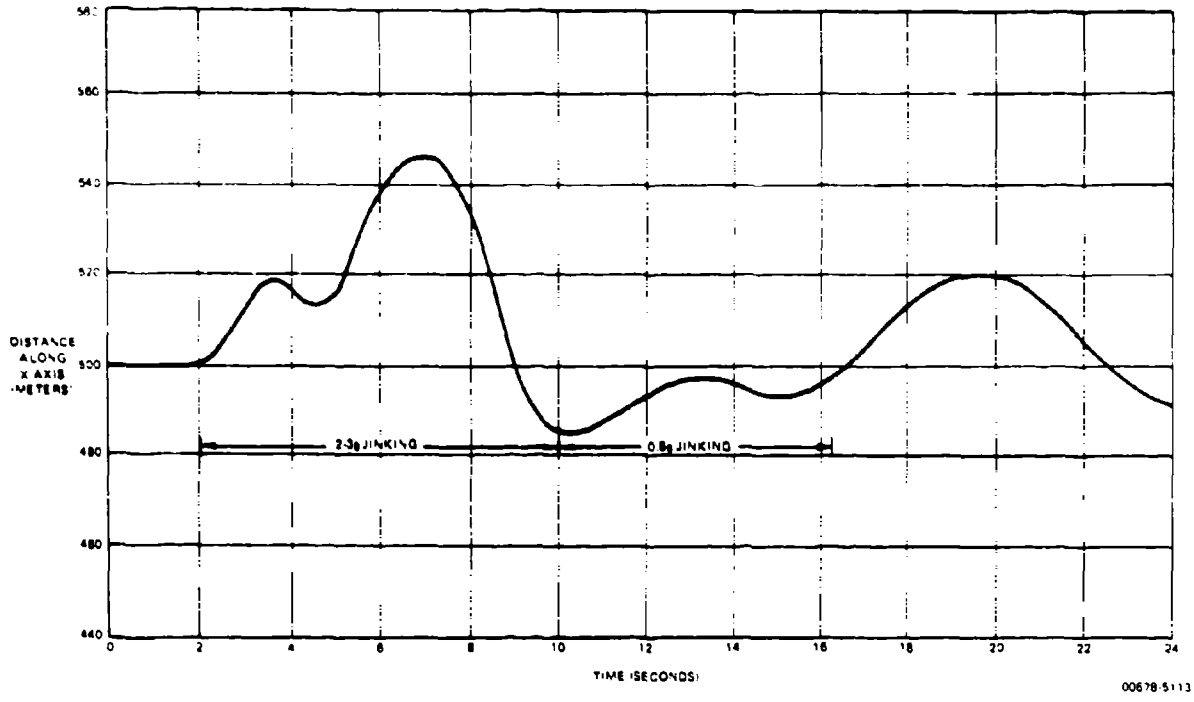

Figure 5-92. Deviation with Time on Jinking Path Normal to Mean Flight Path

gun, the quadratic prediction is preferred. It probably performs better than the linear prediction because the time of the turns extends beyond that of the smoothing time plus time of flight. As a result the quadratic is occasionally able to make an excellent prediction. When the path is moved out, this is no longer true, and the quadratic degrades faster than the linear.

This finding emphasizes our earlier expectation that the usefulness of the quadratic prediction would depend on the duration of steady turns. Experimental data on a large set of real attack paths would be very helpful in this regard. Since we do show the quadratic mode to be superior against close-in jinking targets, and almost as good as the linear mode against jinking farther out, we immediately come to the question of whether the decision algorithm can function quickly enough to revert to a linear mode effectively if the target jinks before an attack, then straightens out for the attack.

We therefore investigated paths composed of jinking and straight-line segments. Table V-25 shows results for the two prediction algorithms without mode switching. Only moderate differences were observed.

For the jinking course followed by the line segment, we allowed the prediction-mode switch to operate, but varied its threshold systematically. Results are shown in Table V-26 and plotted in Figures 5-93 and 5-94. With the proper threshold setting, we obtain results, for the two modes with switching, which are better than either prediction mode by itself. The quadratic mode is used only when the measured rate of turn exceeds the threshold. If the threshold is set too low, the system will be held in the quadratic mode by tracking noise; if it is too high, the target turn rate will never exceed it. The figures show that the threshold can be set high enough so that it will not be vulnerable to tracking noise and still function effectively against turning targets, yet revert to linear prediction when the turn rate is very small or zero.

This is the desired mode of operation, and the simulation has demonstrated the feasibility of the automatic prediction mode switching.

5.13.7 Simulation of Manual Tracking

A first approximation to the system performance with manual tracking might be obtained by estimating standard deviations for manual tracking in azimuth and elevation, and using the 'radar' mode with these inputs. As discussed in Section 4.3 of this report, there are both theoretical and experimental reasons for believing that the error in manual tracking will tend to vary with range in such a way as to make its linear value essentially constant over the AFAADS range of interest.

This would ignore the problem that the man has in

Table V-23. Comparison of Prediction Modes on Jinking Path by 'Number of Bursts with K > 0.20' Measure

Prediction Mode	Path Segment (sec) 0-20	0-10	10-20	
Linear + Energy	7	4	4	Path 4
Quadratic + Energy	9	4	5	
Linear + Energy	6	-	-	Path 4a
Quadratic + Energy	4	-	-	

00678-5115

Table V-24. Comparison of Prediction Modes on Jinking Path by 'Number of Samples with Miss <5 Meters' Measure

Prediction Mode	Path Segment (sec) 0-20	0-10	10-20	
Linear + Energy	19	6	14	Path 4
Quadratic + Energy	23	9	14	
Linear + Energy	15	-	-	Path 4a
Quadratic + Energy	12	-	-	

00678-5116

Table V-25. Comparison of Prediction Modes on Jinking Path Plus Straight-Line Segments

Prediction Mode	Kill-Sec	Number of Bursts with K >0.20	Number of Samples with Miss <5 Meters	
Linear + Energy	0.1554	9	26	Path 5
Quadratic + Energy	0.1671	9	24	
Linear + Energy	0.2906	11	36	Path 5a
Quadratic + Energy	0.2477	10	29	

00678-5117

coping with angular accelerations, and the lag he produces as a result.

A manual tracking algorithm was therefore developed on the following assumptions:

a. The man's lag can be represented by K_v, K_a of appropriate values. Section 4.3 indicated that these should be very low compared with those attainable with a servomechanism.

Table V-26. Effect of Threshold Setting on Jinking Path Plus Straight-Line Segment

Threshold (Rad/Sec)	Kill-Sec	Number of Bursts with K>0.20	Number of Samples with Miss <5 Meters
0.0	0.1671	9	24
0.02	0.1658	9	23
0.03	0.1723	9	25
0.04	0.1879	10	28
0.05	0.1980	11	30
0.06	0.1979	11	30
0.07	0.2059	12	32
0.08	0.1865	11	29
0.10	0.1505	9	25
0.11	0.1515	9	26
0.15	0.1554	9	26
0.20	0.1554	9	26

00678-5118

b. The larger the lag (and the error as seen through the sight), the more the man's 'noise' component increases. The random component of the man's error is therefore computed from:

$$E_m = \eta(C_0 + \mu L) \qquad (5.392)$$

where c_0 is a constant value in meters, L is lag converted to meters at the target range, η is a random number chosen from a normal distribution with unit variance, and μ is taken as 0.25.

c. Autocorrelation of the Markov type is then introduced by operating on successive E_m samples, as in the radar case with appropriate autocorrelation time for the man.

Table V-27 shows the parameters used for the simulation runs. A radar run is included for comparison. The parameters have the following basis:

For rate tracking it is assumed that the transfer function of man plus control is:

$$Y = (K_v/s)e^{-sT_m} \qquad (5.393)$$

where K_v = 5.0 /sec and T_m = 0.20 sec. This is based on the findings of Section 4.3. To get the lag coefficients expand:

$$\theta_0 \theta_1 = 1 - Y^{-1} + Y^{-2} \ldots \qquad (5.394)$$

as a series in s. To this level of approximation, the coefficient of s^2 turns out to be zero.

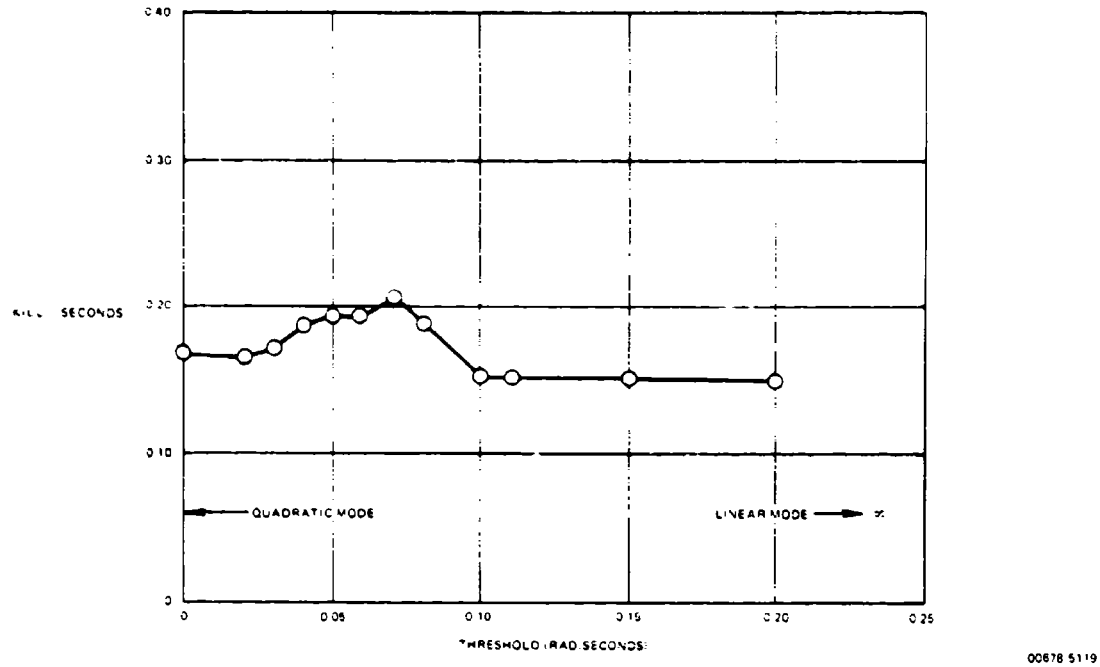

Figure 5-93. Effect of Threshold Setting in Automatic Prediction Selection Algorithm for 'Kill-Sec' Measure

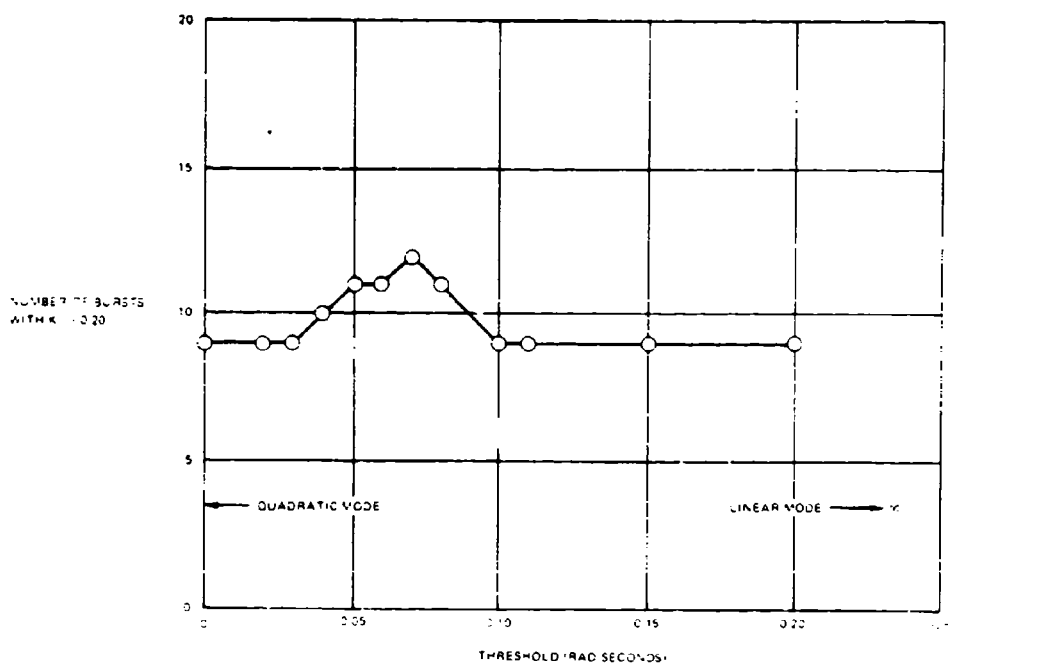

Figure 5-94. Effect of Threshold Setting in Automatic Prediction Selection Algorithm for Number of Bursts with K > 0.20' Measure

Table V-27. Simulation Parameters for Manual-Tracking Mode

	Rate	Rate-Aided	Regenerative-Aid	Radar
K_v	5.0 sec^{-1}	10.0 sec^{-2}	10 sec^{-2}	500 sec^{-1}
K_a	Very Large	10.0 sec^{-2}	10 sec^{-2}	90 sec^{-1}
Autocorrelation τ	1.0 sec	0.5 sec	0.5 sec	1.0 sec
Random Components of Lag, μ	0.25	0.25	0.25	0.0
σ_A (Meters)	5.0	2.5	1.0	5.0
σ_e (Meters)	0.6	0.3	0.2	0.6
σ_R (Meters)	2.0	2.0	2.0	2.0
Gun Dispersion (Mils)	4.0	4.0	4.0	4.0
	-	8.0		
	-	10.0	-	
	-	12.0		

00678-5121

For rate aided tracking, the K_i noted in Section 4.3 are used.

For regenerative tracking, it is assumed that the operator only needs to supply the deficit between the actual target rates and accelerations, and those regenerated from the smoothed, measured velocities on the assumption of unaccelerated start target flight. It was assumed that he would respond with the same K values as for aided tracking, but that his task was now so much simpler that he could reduce the random noise content of his error and take advantage of magnification in his optics to attempt to track a point on the target, such as the intersection of wing and fuselage. The proportional increment of random error, resulting from his perception of residual lag, was retained.

We thus account for operator lag, random noise, and the increase of random noise with lag. These conjectures need to be tested against a reasonable body of real tracking data. Tracking data with the present Vigilante fire control system, which has a regenerative mode, would be of particular interest, especially if taken with and without the regenerative aid operating.

Results obtained with the present assumptions are shown in Table V-28 for Path No.3. Rate-aided tracking is superior to rate tracking because of the more favorable K values used; but both are unacceptable, when compared with the radar. Under the optimistic assumptions made regarding tracking precision with regenerative aid, the man does better in this mode than the radar.

Table V-28. Comparative Effectiveness of the Various Tracking Modes

	Gun Dispersion (mils)	Kill-Sec	K = 0.20	M = 2 Meters
Manual				
Rate	4	0.0028	0	0
Rate-Aided	4	0.0159	0	0
	6	0.0179	0	0
Regenerative-Aid	4	0.1781	12	36
Radar	4	0.1433	11	15

00678-5122

To determine how much rate-aided tracking might be improved by increasing gun dispersion, runs were made with this as a variable. The results are plotted in Figures 5-95 and 5-96. The optimum dispersion is about 7 mils, but effectiveness is still very low.

The results are, of course, specific to this target path. The poor performance of the man results from his lags on this crossing course. For very low target angular velocities and accelerations the model would show good effectiveness for manual tracking even without regeneration. However it is believed that there is sufficient doubt regarding the man's ability to track difficult and changing rates to exclude nonregenerative manual tracking from further consideration for AFAADS except in a back-up mode, as a degraded mode of operation.

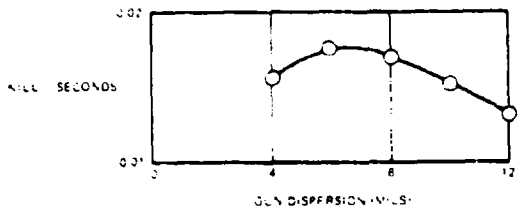

Figure 5-95. Effect of Gun Dispersion on Effectiveness of Rate-Aided Manual Tracking for the 'Kill-Sec' Measurement

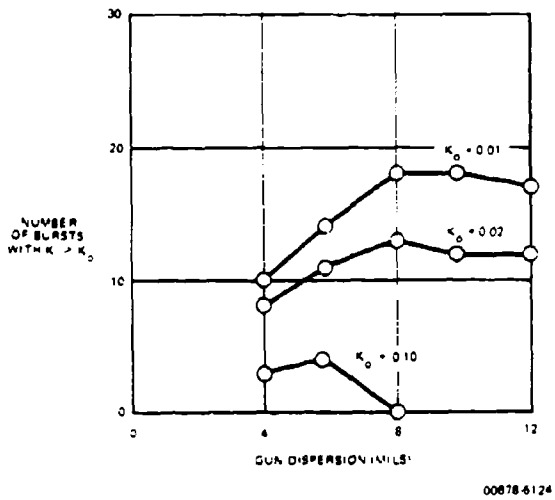

Figure 5-96. Effect of Gun Dispersion on Effectiveness of Rate-Aided Manual Tracking for the 'Number of Bursts with K > K_0' Measure

5.13.8 Conclusions

The following conclusions are drawn from the simulation runs.

If only one prediction mode could be chosen, it should be linear prediction with the energy correction for target acceleration under gravity in a dive or climb.

Reasonable and likely target path segments have been identified where quadratic prediction plus the energy correction is the preferred algorithm. The quadratic prediction corrects solely for turns in a horizontal plane and is applied only perpendicular to the flight direction.

The switching algorithm, for automatically choosing between linear and quadratic modes, can be made to function satisfactorily so that the best performance of each mode can be realized. More study of the decision criteria is desirable.

The algorithm for defense of a known point works extremely well on the path type for which it was intended. The several-threshold decision algorithms, for switching this algorithm in at the right time and then reverting to normal prediction when it is not needed, were demonstrated to be feasible and efficient. This is an entirely new type of prediction mode and warrants high priority for future attention.

There is a substantial payoff in high muzzle velocity and low projectile drag. Further gains are likely beyond the values tested in these simulations.

Excellent performance is expected with single-frequency radar and 1.6-second smoothing. A frequency-diverse radar should permit even higher performance, and the payoff can be taken either in effectiveness or in smoothing times as short as 0.6 seconds.

The optimum angular dispersion with radar tracking, or manual tracking with regenerative aid, is no more than about 2-3 mils.

Boresight errors and systematic errors in the solution (instrumental errors) should be held to no more than 1 mil.

Manual tracking without regenerative aiding is unlikely to be even marginally adequate. The potential of manual tracking with regenerative aiding is excellent if it can be realized.

The step thresholds on the decision algorithms worked satisfactorily. Whether a gradiant threshold, indicated to be possibly preferable in Section 5.4, would provide further improvement remains to be determined by possible future simulation runs.

It was not possible to simulate terrain-following aircraft because of limited time. Terrain following may approximate, in a vertical plane, the jinking runs that were made in a horizontal plane; but explicit simulation would permit better judgements as to system performance.

5.14 SYSTEM EFFECTIVENESS

In the preceding sections of the report we have developed a basis for comparing system effectiveness under a wide range and variety of configuration options. A logical way of making overall comparisons, if time permitted, would be by the WESIAC relationship and with the procedures as outlined in the following paragraphs.

The expression for effectiveness is:

$$E = A\,D\,C \qquad (5.395)$$

where, as described earlier, the availability matrix A estimates the probability that the system will be operational in each of its possible operational modes when the engagement begins, D represents the probability of

changing from one mode to another during the engagement, and C contains (as elements) the effectiveness of the system in each mode against each of the tactical and environmental situations for which it is desired to obtain an effectiveness measure.

Environmental states might be categorized as: day, clear; night, clear; heavy rain or fog; enemy using countermeasures or no countermeasures; etc. Tactical states might include high passing target, terrain-following passing target, attack path, etc. For each of these states, the matrices could be multiplied out and the desired measures of effectiveness obtained.

For the present, it is necessary to limit the discussion of system effectiveness to less-detailed comparisons. We discuss briefly some of the implications of the target acquisition process on system configuration, and then the relative ranking of some of the alternative elements with regard to sensors and prediction algorithms.

5.14.1 Detection and Acquisition of Fast Targets on Low-Pass Flight Paths

The time and range relationships in target detection and acquisition require analysis in greater depth than was possible in the present study. However, from the brief survey of target paths, and the man's ability to detect aircraft (as reported earlier), some preliminary conclusions can be drawn.

Consider a 'worst case' of a 600-knot target on a passing course with short mid-range, and a rather difficult terrain mask of 6 degrees. At this speed, the airplane has a minimum altitude above ground in terrain following (as estimated in Section 3.4) of about 150 meters. The boundaries, within which the aircraft is exposed in terms of altitude and distance along flight path, are shown in Figure 5-97.

For visual target detection and manual tracking assume that the man can do as well against this 600-knot target as it was indicated he was able to do against a slower F-86 type under extremely clear atmospheric conditions; i.e., a 50 percent probability of detection by 3000 meters range and an 80 percent by 1500 meters. This also assumes that by RAID or some similar aid he is able to narrow his field of search to under 45 degrees. Once the target has been detected, we assume: (1) that the man requires 3 seconds to acquire it and begin tracking, including activating the ranging device, (2) that the computer requires 2 seconds to settle, and (3) that time of flight is 1 second. Time of flight variation with range has not been considered in detail.

The resulting contours are shown in Figure 5-97.

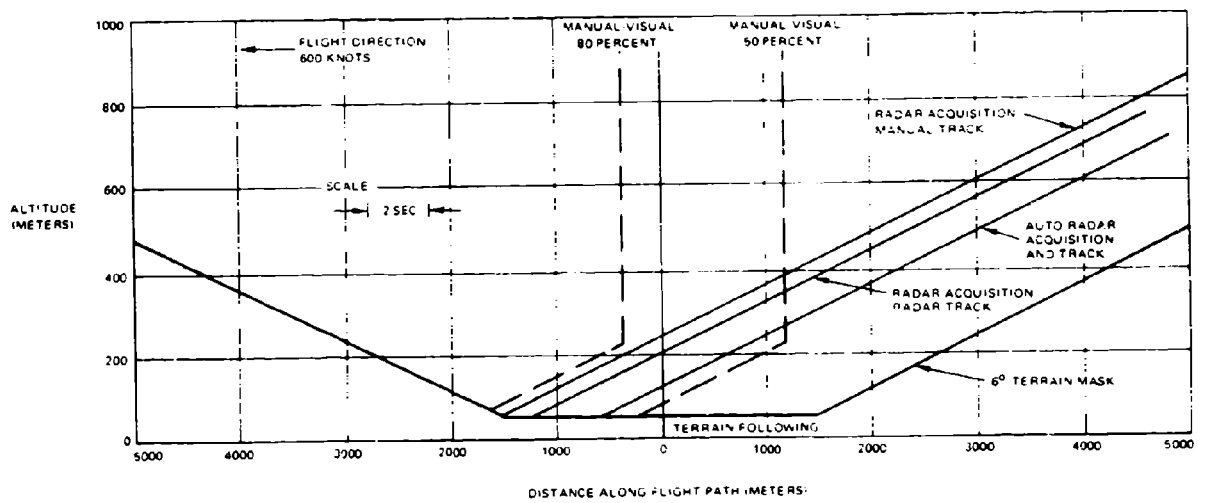

Figure 5-97. Effect of Target Acquisition Mode on Firing Envelope

Regardless of altitude, the man has less than an 80 percent chance of getting the projectiles to the target before midpoint. However, even against the terrain-following mode he has about an even chance of getting in 2-3 seconds of fire.

For radar acquisition we assume a 30 rpm antenna rate with 3 blips required for detection. Given detection, we assume that the man can be put on target by automatic target designation in 3 seconds, or that a tracking radar can be put on in 2 seconds. Three additional seconds are again required by the computer and time of flight. These contours are also shown.

Finally, we assume automatic target detection and tracker put-on, on the basis of 2 blips. This mode would have to be investigated for false-alarm rate. It could save 1 scan and 2 seconds. Its contour is also shown in the figure.

For very low altitude targets under 300 meters, the radar acquisition mode is hindered by the 30 rpm antenna rotation rate, and the requirement that blips be confirmed.

Since we have given the man the benefit of RAID warning, the same advantage could be given the radar by putting it in a sector scan mode. If it scanned only a 90-degree sector, the whole process might be shortened sufficiently to allow the first projectiles against the terrain following aircraft to reach it at midpoint.

The 2-second settling time of the computer can be further shortened if smoothing time is made a function of time of flight. But for this 'worst case' it seems difficult to achieve more than 6 seconds of effective fire. This is an argument for retaining the 3000 round per minute capability of Vigilante.

The above crude estimates suggest that the man's performance in target detection is marginal under the best conditions. Radar target detection, however, will provide satisfactory performance under all conditions of light and weather. Any aids that can be given the man to reduce his field of search will assist the radar as well, and thereby shorten its time to detect.

So few seconds are available, however, for the whole process of detection, acquisition, tracking, computing, and firing, that it is clear that all data transfer must be automatic.

Identification was not considered above. If visual identification is required, system effectiveness against the target considered will degrade badly.

We conclude tentatively from the above brief survey that:

a. The man's ability to detect and acquire fast, low targets is likely to be marginal under the best of conditions.

b. The detection and acquisition process should be automated to the maximum degree possible.

c. The 3000 rounds per minute firing rate of Vigilante should be retained. However, consideration of less transitory attack paths suggests the desirability of an alternate lower rate to be used at the discretion of the gunner (or the computer).

5.14.1.2 Radar Multipath Error

In Section 4.2 it was indicated that the principal radar multipath problem is in elevation. While the error is maximum when the elevation angle is 0.8 times the half-power beam width, it is negligible at 4 times this elevation. If the terrain-following target (as described previously) is flying at 150 meters above ground level and if the radar beam width is 1 degree, then the target elevation is above 0.8 degree for all ranges within 11,000 meters, and above 3.2 degrees for all ranges within about 3000 meters. Local terrain contours will influence multipath, but the above considerations suggest that multipath may not be as difficult a problem for AFAADS as originally thought. Within reasonable reflector diameters, the beam width may be further reduced; if K_a-band radar is determined to be feasible for this application.

The possible utility of the computer in inhibiting the radar from tracking 'underground' targets also may be of some value.

5.14.2 Detection and Acquisition of Targets on Attack Paths

A target making a dive or glide bomb attack with conventional iron bombs is expected to be easier to acquire than a high-speed passing target. This is because the aircraft must: (1) acquire its target on the ground, (2) then go into an attack pass, (3) maintain steady flight for 5-10 seconds while its computer settles, and (4) then breakaway. The more the aircraft compresses the time for these maneuvers in order to reduce exposure time, the poorer its effectiveness is likely to be in terms of bombing accuracy. It can reduce its vulnerability by releasing its munitions at substantial stand-off ranges, but at higher altitudes it should be detected more easily. The engagement then becomes a trade-off between the effectiveness of AFAADS at the outer limits of its effectiveness envelope, and the accuracy of bombing from those ranges. In the case of air to surface guided weapons, there is a further trade-off on the part of the attacker between the high cost of long-range standoff weapons, and the greater exposure of the aircraft when releasing short standoff weapons. The whole subject of interaction between offense and defense can be explored with facility on the present simulation, but time has not permitted this to be done in this present contract.

In formulating realistic paths for the simulation, however, it was found difficult to set up realistic attack paths in which the target exposure was only a few seconds. For a given ammunition load on the mount, and a given exposure time during which it is not possible to identify 'optimum' firing points, the best chance of killing the aircraft is secured by firing the available rounds over a long rather than a short period of time, in order to minimize the chances of missing with all rounds. Although the subject requires further analysis, it appears that the Vigilante would benefit from an alternate rate of fire option of about 1200 rounds per minute, in addition to the 3000 rpm option. An increase in the ammunition load carried on mount above 144 rounds also appears advantageous, but this judgement needs to be supported by simulation and analysis.

5.14.3 Comparison of Prediction, Ballistics, and Tracking Options

In this section we summarize the gain factors associated with the options compared on the simulator, by type of target path. The basis for comparison is the kill-second index. This is considered to represent a measure of the effectiveness which we have at our disposal to utilize in terms of firing doctrine. The burst index would be preferable except for the fact that our choice of 0.20 as the highest value in the print-out reduces its sensitivity. Had we chosen readouts for number of bursts with kill probability greater than 0.50 and 0.80 for example, this index would have shown the same discriminating ability as the kill-second index. However, we use the burst index for comparing the effect of dispersion.

In each case we compare the kill-second index for an option against the index value for a standard configuration. The standard is identified for each path type.

Pass Course

Reference: Linear prediction, Ballistics No. 1, 1.8-sec smoothing, and 4 mil gun dispersion.

Option	Index Ratio
Eliminate gun and sensor lags	1.7
Use Ballistics No.3	1.1
Use 0.4 sec smoothing	0.9
Use 3.6 sec smoothing	1.5
Reduce tracking errors to 0.4 of standard values	2.2
Reduce gun dispersion to 2 mils	1.1

On this course the major payoff options are: eliminating gun and sensor lags, improving tracking, and (since the target is not maneuvering) increasing smoothing time.

Attack Path

Reference: Linear + energy prediction, Ballistics No. 3, 1.8-sec smoothing, and 4-mil gun dispersion.

Option	Index Ratio
Eliminate gun and sensor lags	1.1
Use Ballistics No.1	0.9
Use linear prediction	0.7
Use quadratic prediction	0.4
Use quadratic plus energy prediction	0.6
Use defended point prediction mode	1.1
Use 0.4 sec smoothing	0.8
Reduce tracking errors to 0.4 of standard values	1.4
Reduce gun dispersion to 2 mils	1.2
Increase boresight error from 0 to 4 mils	0.8

In all simulation runs, the value of improving the ballistics diminished as prediction improved. While on the attack path and in the simple linear prediction mode, going from Ballistics No. 1 to Ballistics No. 3 yielded a gain factor of 1.4; as compared with 1.1 for the superior linear plus energy algorithm.

On the above path, the higher gain-factor options are: improving tracking accuracy, using optimum gun dispersion, and minor improvements resulting from the defended point mode, and eliminating servomechanism lags. The major gain was achieved in the original selection of linear plus energy prediction as the reference case. This selection provided a gain of 1.4 over simple linear prediction.

The penalty in allowing a 4-mil boresight error should be noted.

Climbing Turn Path

There was only one comparison on this path segment. The index ratio for quadratic plus energy prediction, compared with linear plus energy, was 43.0. This interesting result is sufficient to retain quadratic plus energy on the basis of this single path segment.

Jinking Path (all jinks, mixed)

Comparing quadratic plus energy against linear plus energy, the index ratio was 1.7 for a close-in path and 0.9 for a farther out path. Quadratic prediction again seems to have a place in the concept.

Jinking Path plus Line Segment (Close in)

For a path on which the target jinked then settled to a straight line segment, the index ratio for quadratic plus energy (compared to the linear plus energy predic-

tion mode) was 1.1. When the decision option was allowed to function so that the computer automatically switched to whichever mode it preferred based on its measurement of target turn rate, the index rose to 1.3. This supports the inclusion of the switching algorithm.

Manual Tracking on Attack Path

All of the comparisons were run with linear plus energy prediction, 1.8 seconds smoothing, and Ballistics No. 3. The basis for comparison was radar tracking of the same course. On this basis the index ratio, for the man with simulated rate tracking, was 0.02. For the man with rate-aided tracking and dispersion adjusted to optimum angular value, the index ratio was 0.12; and for the man with regenerative tracking and noise considered to be appropriate to tracking with optical magnification, the index ratio was 1.2.

We feel that the simulation of the man's performance in the rate and rate-aided modes was realistic, and that in the regenerative mode probably optimistic. We conclude that the man should not track unless he has regenerative aiding, and that manual tracking (even with regenerative aiding) should preferably be a back-up rather than a prime mode of operation.

The relative weighting of the path segment types compared on the simulator is a matter of judgement. Each of the options is associated with a cost and is discussed on this basis in Section 6. At this point, however, we order the options tested on the simulator into three classes: low, medium, and high cost, and within each class is what appears to be a reasonable order of priority.

a. Relatively low-cost options
   (1) Energy correction for linear prediction.
   (2) Improved ballistics.
   (3) Minimal sensor and gun lags.
   (4) Boresight errors under 1 mil.
   (5) Smoothing time proportional to projectile time of flight.
   (6) Variable dispersion by dither.

b. Medium-cost options
   (1) Regenerative tracking.
   (2) Quadratic mode with automatic decision algorithm.

c. High-cost options
   (1) Reduced radar tracking error (frequency diversity).
   (2) Automatic optical tracking mode (TV or imaging IR).
   (3) Defended point algorithm in prediction.

5.14.4 System Error Budget

A review of the distribution of miss distances obtained on the simulation reveals a remarkable number of samples within 2 meters. This is in spite of target maneuvers and tracking noise including a 5-meter standard deviation in azimuth. With the exception of sensor and gun servo lags, we did not include estimates of errors developed within the computer (instrumental error); other than those associated with the smoothing of target position, velocity, and rate of turn. Neither did we include muzzle-velocity systematic error or round to round dispersion explicitly except to the degree their effects can be inferred from the effects of changing gun dispersion and boresight error. There is, of course, no problem in adding these effects to the simulation. Their exclusion at this time was the result of limitations on resources within the present contract.

It is reasonable, however, to require that the fire control solution introduce no errors that will degrade system performance below the level resulting from target maneuvers and tracking accuracy. Since we believe that the occasional straight-line segment, which appears in most attack paths, and non-jinking level passing targets is a prime opportunity for AFAADS, we feel that system effectiveness should not be impaired by instrumental errors during these opportunities. The result will be either very high kill rates, or the denying to the enemy the attack paths which are most effective for him, thereby requiring expenditures on his part for costly fire control equipment and/or air to surface missiles. Both objectives are worth seeking.

On this basis, we assume tentatively that the instrumental error budget should be laid out so that on a set of standard, difficult pass courses with no target acceleration, the overall AFAADS instrumental errors, expressed in standard deviations exclusive of tracking errors and their effects, should be less than 2 meters out to 2000 meters slant range, and less than 2 mils beyond that range. The systematic error should be less than half these values. A reasonable set of courses might begin with the design point course furnished by the Army for this study (Path 2), with two of three courses otherwise identical, but moved out progressively to 1000 and 2000 meters minimum horizontal range.

It is suggested that the instrumental errors suggested above should be held out to the range at which projectile velocity drops to 1.10 times the speed of sound (standard conditions). With the improved ballistics this will be about 5000 meters.

More simulation runs are needed to explore system effectiveness on the fringes of the effective defense envelope in depth. In reviewing the history of U.S. dive bombing in Korea, laying out reasonable attack

paths for the simulator, and considering the implications of air to surface guided munitions, it appeared to us that the original 3000-meter maximum effective range suggested by the Army was too short from both a tactical effectiveness point of view, and from the limitation it would impose on the potential effective range of AFAADS with improved 37mm ballistics. It did, however, represent a reasonable maximum for the original, rather inefficient, Vigilante ballistics.

Interpreting the tentative instrumental errors in terms of the ballistic solution, some rough computations (based on the formulas in Section 5.5) indicate that for a target speed of 300 meters/second, the time of flight should be computed to within 0.005 sec, and that the allowable systematic error in muzzle velocity is 1.5 meters/second, with a round to round dispersion in muzzle velocity of about 3 meters/second.

Since errors in time of flight and muzzle velocity have their principal effect along the direction of flight, and the radar and probably the man tend to develop tracking errors proportional to target dimensions and thus along the direction of flight, the above estimates may be too stringent by a factor of perhaps 2.0. This subject deserves further analysis in depth on the simulation.

We conclude that:

a. AFAADS instrumental errors (exclusive of those caused by tracking errors and target maneuvers) should be held to within a standard deviation, about their mean, of 2 meters out to 2000 meters slant range, and 2 mils beyond that.

b. AFAADS systematic errors should not show a mean value exceeding one half the standard deviation given above.

c. The allowable systematic error in muzzle velocity on this basis is about 1.5 meters/second, with a standard round to round deviation of about 3 meters/second.

d. Time of flight should be computed to within 0.005 seconds.

e. Further analysis is required to determine the interaction among instrumental errors, ballistic errors, system performance, and system cost.

f. Automatic muzzle-velocity measurement and correction, as developed by Oerlikon, is worth considering. 5.14.5 Degraded Modes of Operation

The system should retain some capability of delivering defensive fire as long as the gun can fire and the mount can be aimed. We therefore consider degraded modes of operation, beginning with this ultimate degradation and working up to full functioning. 5.14.5.1 The Ultimate Degradation

All systems are down except for the power controls associated with manual tracking, the man, and the gun. The gunner uses the 'fly-through' method of lead estimation. He estimates target speed, and holds the target on a speed ring in his optical sight so that the target heading is always toward the center of the sight (intersection of crosshairs). In effect, he holds a constant angular lead, and in about the right slant plane. Since required lead on a pass course starts small, increases to a maximum and then decreases again, this procedure should create at least one and possibly two positions on the course at which the lead is correct. The gun is fired at a low but steady rate.

The angular lead required is approximately:

$$\Delta_r = (V / v_a) \sin \Omega_0 \qquad (5.396)$$

The lead held is:

$$\Delta_L = \text{constant} \qquad (5.397)$$

The error in lead is:

$$\Gamma = \Delta_L - \Delta_r \qquad (5.398)$$

The angle subtended by the target fuselage along the flight path is:

$$\Upsilon = L_t \sin \Omega_0 / D_0 \qquad (5.399)$$

From the preceding relations, compute the rate of change of lead error at the time lead error is zero, and divide this into target size to determine how long the lead is within the target dimension. Assuming that the guessed lead causes this to happen at about $\Omega_0 = 60$ degrees (the result is not very sensitive to Ω_0 as long as it is under 90 degrees),

then:

$$t_h = (2 v_a / V)(L_t / V) \qquad (5.400)$$

where

V = target speed

L_t = target length

v_a = average projectile speed

t_h = length of time lead is correct

If:

L_t = 2 meters (vulnerable length)

V = 300 meters/sec

v_a = 800 meters/sec

then:

t_h = 0.035 sec

Now assume dispersion perpendicular to the flight path of 4 mils at 1000 meters (4 meters). The probability that a round is on target vertically, for a 2-meter vertical target vulnerable dimension is:

p_v = 0.10

Hence the kill-seconds for this mode is:

KS = 0.0035

It's interesting to note that this is about the result we got on the simulation of the attack path with manual tracking using rate control, and a sophisticated prediction scheme. A pessimistic judgement at this point might be that if you have a man tracking with a rate control, there is no point in providing a good fire control system; and conversely, if you have a good fire control system, manual tracking should be avoided.

To ensure that there are some rounds in the air when fly-through occurs in the constant-lead degraded mode, the gun will have to fire at a reduced rate. At 1200 rpm with the present Vigilante ammunition load, it could fire from 7-10 seconds which would be about right. The probability of killing the target in this mode would then be:

PK = 0.07

5.14.5.2 Range Information Denied

If the system is all operative except for the range finder, which is either down for repair or countermeasured, it would be necessary to operate on estimated-range information. It is suggested that the regenerative mode include an algorithm for regenerating range from angular velocities and occasional intermittent range estimates. Algorithms for doing this were described in Section 5.3. The simulation runs indicated that solution accuracy was less affected by range errors than by angular errors. Additional runs with the range regeneration algorithm would determine the feasibility and performance of this mode. Against on-board jamming, the cost of getting position data by triangulating across several AFAADS fire units should be investigated.

5.14.5.3 Tracking Sensor Inoperative

The optical sight, although it may embody an imaging device with automatic tracking mode, should have backup modes of operation so that it can be used as:

a. A fixed sight with estimated lead as noted earlier.

b. A visual tracking sight with stabilization and regeneration for manual control.

c. A visual tracking sight for manual control with stabilization and conventional-aided tracking (with position components) in case the regenerative mode becomes inoperative.

5.14.5.4 Surveillance Sensor Inoperative

The tracking sensor should have a limited search capability. The man is the final fall-back mode.

5.14.5.5 Degradation by Weather

A careful statistical study needs to be done on the probability that an AFAADS configuration without radar would be limited to varying degrees by cloud cover, haze, fog, rain, etc. The brief survey made for this report indicates the possibility of frequent and serious limitations.

SECTION 6
RECOMMENDED CONFIGURATIONS

In the body of this report we have attempted to identify a large number of design options with regard to system elements and system configurations on the basis of potential improvement in system capability and performance. We have also attempted to include in this selection as many concepts as possible that had potential, were realizable within the state of the art, and were new, in that they had not previously been implemented in antiaircraft predicted fire systems. Which concepts should be considered for an early system and which should be considered for the future depend on time, money, and requirements.

In this section we attempt to consider the design options in configuring a system in terms of potential advantage in performance and cost. At this point a considerable degree of judgement is used, partly because there was not time to analyze all items subject to analysis and partly because some options will always be beyond analysis. The reader will have his own ideas. We attempt here to give him enough supporting background to assist him in forming his own judgements.

We feel that the development of AFAADS should be time-phased with progressive improvement. The design should be modular, so that as improvements in sensors computers, and guns and ammunition become available, the system can be upgraded without a complete redesign.

As a caveat in this regard, it may be noted that it is one of the unfortunate facts of development that brassboard experimental models tend to become standardized, contrary to plan, whenever they demonstrate significant improvement over existing equipment, or because the demonstrated improvement reduces the pressure on further expenditures for development. Brassboard items are essential to orderly development, but they should be conceived with the foresight that if they are pulled out of the program and standardized, the planned future growth is consistent with their interim implementation.

6.1 OPTIONS FOR CONSIDERATION IN SYSTEM CONFIGURATION

The various design and algorithmic options discussed in the body of the report have been assembled in Table VI-1, and an attempt has been made to categorize them according to payoff (high or medium) and cost (low, medium, or high). These categorizations are highly subjective at this stage. There has been no attempt to rank options in order of importance within groups.

The cost categorization is particularly vulnerable to criticism at this stage since the life cycle costs must include developmental costs, maintenance, and operation as well as procurement. An item with a high procurement cost may prove more cost effective if it exists and requires minor development cost. Conversely, a high maintenance cost item may be undesirable in spite of a low procurement cost.

For developmental items, in view of current prospects for a drastically reduced military budget, considerable weight should be given to those developments which have an essential place in the civilian economy. Lasers and digital computers are typical. Industrial funding of digital computer R&D in particular will ensure the continued and accelerated growth of this field of technology regardless of military funding. Gun and ammunition development, on the other hand, is not likely to be done except with military funding.

The entries in Table VI-1 are discussed in the following subsections.

6.1.1 Relatively Low Cost, High Payoff Items

Improved ballistics. The analysis and simulation runs showed a significantly increased effectiveness as muzzle velocity was increased, and projectile slowdown reduced: the better the prediction the smaller the improvement. However, short time of flight is always insurance against unforeseen contingencies.

1200 round per minute gun rate option. The present Vigilante apparently has only two options: 3000 rpm and 120 rpm. The former exhausts the on-board ammunition load in three 1-second bursts (or with special loading four bursts), and the three bursts could easily be fired at unfavorable points on the course. The 120 rpm mode is too low for antiaircraft fire except possibly against passing helicopters or light planes. The 1200 rpm is a reasonable alternate option, *in addition to* the other two modes.

Laser range finder. This is essential on a mount without radar ranging. It provides backup in case of radar range jamming.

Linear plus energy correction prediction mode. This really needs to be validated against real aircraft attack paths although it showed excellent performance on the simulator. It can be included in any prediction solution, whether analog or digital.

Low altitude, altitude prediction cutout. This is for use against terrain-following aircraft to reduce the amplification of altitude prediction errors by the random-like vertical motion of the aircraft. It was suggested by analysis and has not yet been validated on the simulator. It should also be helpful when the radar

Table VI-1. Options for System Components and Functions

Cost \ Payoff	High	Moderate
Relatively Low	Improved ballistics 1200 rounds/minute gun rate option Laser range finder Linear + energy correction prediction mode Low altitude, altitude prediction cutout Open and cease fire indicator Increased on-mount ammunition load	Increase HE content in projectile Better RAID data 3X optics Adjustable dispersion Present position smoothing Ammunition status indicator
Moderate	Regenerative tracking Digital computer Quadratic prediction option Automatic prediction option selection Automatic system checkout Stabilized sight Dynamic system calibration Infrared search sensor Automatic imaging tracker On-mount cooperative IFF Automatic muzzle velocity measurement and computer adjustment Night sight for ground to ground fire Laser target designator for support fire ground to ground	2-man mount (commander and gunner) Automated firing doctrine IR hot spot tracker Dithered dispersion Doppler range rates Range estimate regenerative mode Combat record storage of enemy target paths
Relatively High	Surveillance radar (freq diverse) Tracking radar (K-band, freq diverse) Computer processing to reduce multipath effect On-mount noncooperative IFF Hypervelocity projectiles	Defended point prediction option Gearless gun and sensor servo drives Digitized terrain storage to aid prediction against contour chasing aircraft and possibly help reduce multipath errors in radar Cross-mount triangulation on aircraft with on-board ECM jammers Integrated forward area air defense information net Radar projectile tracking Fully stabilized system including gun for fire on the move

00678-601

is having multipath trouble at low elevations if manual tracking is not possible because of darkness or weather.

Increased on-mount ammunition load. This interacts with rate of fire. It may not be needed with the 1200 rpm option, but should be considered especially if only the 3000 rpm option is available for antiaircraft fire.

Open and cease-fire indicator. This is required to ensure that the gunner fires only when the target is within range, and a good solution is being generated by the computer.

6.1.2 Relatively Low Cost, Moderate Payoff Items

Increased HE content in projectile. There is a trade-off among muzzle velocity, projectile ballistic coefficient, and HE content of the projectile. To select the best combination of these characteristics in the context of overall system performance, target vulnerability data will be required from the Ballistic Research Laboratories.

Better RAID data. The ability of man to detect targets with his unaided eye appears to be critically dependent on his field of search. RAID-type data can reduce the search field. It can also allow sector scan with an on-mount acquisition sensor and shorten acquisition time.

3X optics. Magnification is required in the optics for ground to ground fire. It will pay off in aircraft tracking when the man has effective regenerative tracking to simplify his task. With conventional rate or rate-aided manual tracking there is no payoff.

Adjustable dispersion. This allows gun dispersion to be set to whatever value is determined to be the best compromise after the system is in the field and experimental data on its performance is obtained.

Present position smoothing. At short times of flight, with good data smoothing, the error in present position is almost as important as the error in measured velocity. It is easy to accomplish with a digital computer.

Ammunition status indicator. This is a low priority item but would help to inhibit the gunner from emptying his ammunition drum before the target came within effective range.

6.1.3 Moderate Cost, High Payoff Items

Regenerative tracking. Although the servo loops of a sensor system incorporating automatic tracking might be made tight enough to perform satisfactorily if the target is not obscured, regenerative tracking is required if the man is in the tracking loop. With only conventional rate or rate-aided manual tracking, the potential of a good fire control system is unlikely to be realized. The regenerative algorithms also allow tracking when the target is obscured, or when the laser misses a few blips, and can be used to assist and eliminate the lags in the sensor and gun servo loops.

Digital computer. The digital computer allows greatly increased reliability, accuracy, conservation of space and weight, and is obtainable at reasonable cost. Maintenance costs should be very low compared with an analog computer. Continued rapid growth of the state of the art will permit expanded capability by simple replacement. The digital computer makes feasible the use of alternate prediction algorithms without incurring added settling times, automatic mode selection, and automated firing doctrine, as well as automatic system checkout.

Quadratic prediction option. When called up by the computer, this will allow improved effectiveness against turning and some jinking targets. The digital computer allows several prediction modes to be maintained current, so that there is no additional settling time in transmitting orders from one mode or another to the gun.

Automatic prediction option selection. This is easily done by the computer. There can be a manual override.

Automatic system checkout. This is standard practice with digital computers.

Dynamic system calibration. As described in Section 5.8, this is a method of using an internally generated course to check the boresighting and computational dynamics of the system on a firing course. An additional check of the sensors is made by tracking any passing target with zero time of flight set in the computer. Automatic confirmation of system function might be done by a small sensor on the gun receiving laser reflected pulses from the target.

Infrared search sensor. This is to assist man in acquiring targets at night, but only in fair weather. A radar is preferable.

Automatic imaging tracker. It remains to be seen whether regenerative tracking will allow the man to provide precision angular data. There are many types of imaging trackers in existence, ranging from TV trackers to IR imaging trackers. The contrast-seekers developed for air to ground homing missiles have a frequency response with bandpass several times that of the man. They may provide more accurate tracking than hot-spot IR trackers, for example. Their capabilities and costs need to be evaluated in depth.

On-mount cooperative IFF. AFAADS will have greatly reduced effectiveness if firing must wait on visual target identification. Conventional IFF may be helpful. The problem may be solved when the Army has its planned Army-wide vehicle location and position determination and reporting system in operation.

Automatic muzzle velocity measurement and computer

adjustment. Oerlikon has a system of this type operational. Whether the Oerlikon system could be adapted to the Gatling gun is not known. Its value depends on quality control of ammunition and empirical estimates of the effects of gun tube wear, powder temperature, etc., on muzzle velocity. Somewhat similar information might be obtained from the dynamic calibration scheme suggested above, but not as precisely or reliably.

Night sight for ground to ground fire. This will be standard Army equipment when AFAADS is built.

Laser target designator for support fire, ground to ground. This capability will greatly augment AFAADS ability to provide support fire. If the laser range finder can do double-duty, the capability may be realized economically.

6.1.4 Moderate Cost, Moderate Payoff Items

Two-man mount. The self-propelled version of AFAADS will certainly carry two and possibly three men. This allows one man to conduct the surveillance and target detection function continuously, while the gunner disposes of targets already acquired.

Automated firing doctrine. Further analysis is required. It may be that the computer can provide a greater assist in indicating when to fire than the earlier mentioned fire indicator which based its indication solely on range, sensor lockon, and computer settling.

IR hot spot tracker. This should be the least expensive of the automatic trackers. Its possible accuracy has not been evaluated in this study. It is limited to fair weather, but gives a night capability.

Dithered dispersion. Computer simulation indicates that with good tracking and prediction, the optimum dispersion (angular) will be only 2 or 3 mils. If the system must function in a degraded mode, it might be desirable to have a quick means of increasing dispersion. This seems feasible with dither. Variation of optimum dispersion with range and other parameters needs to be further evaluated and, if profitable, might be implemented by dither.

Doppler range rates. The simulation indicated that under normal operating conditions the solution is not as sensitive to range errors (and range rate errors) as to angular errors. Further analysis of regeneration may indicate advantages to be derived from precise range rate. With such rates, a very good solution for time of flight can be obtained without using angular information.

Range estimate regeneration mode. It is desired to preserve as much capability as possible even when range information is lost. This is a 'range-keeping' algorithm which allows range to be generated continuously, based on range readings or estimates set in intermittently.

Combat record storage of enemy target paths. If enemy attack paths are recorded in combat they can be periodically analyzed and advantage taken of the flexibility of the digital computer to adjust the prediction modes and decision algorithms to best counter enemy tactics.

6.1.5 Relatively High Cost, High Payoff Items

Surveillance radar (frequency diverse). This fills the greatest need of AFAADS under all operating conditions: early detection and position determination of targets. Even under good weather, daytime conditions, the man without aids is not likely to detect targets at sufficient ranges to realize the full potential of AFAADS. Frequency diversity is a protection against ECM.

Tracking radar (K-band, frequency diverse). This radar satisfies the requirement for accurate tracking under all environmental conditions. K-band (preferably K_a) allows a pencil beam with reasonable size dish. Frequency diversification is a protection against ECM, reduces errors arising in glint, and may reduce multipath errors.

Computer processing to reduce multipath effect. There are some indications that the computer can be used to assist the radar in separating the real target from its multipath image.

On-mount noncooperative IFF. The potential, feasibility, and complexity of implementation have not been assessed. The concept is to use pattern identification techniques based on computer analysis of the radar signal, or the laser return from the target.

6.1.6 Relatively High Cost, Moderate Payoff Items

Defended point prediction option. This is a new prediction scheme. It worked well on the simulation. It may be expensive in computer capacity and that aspect needs to be analyzed. It should be tested against real target attack paths. Its effectiveness and value may increase as free-maneuver bombsights come into use by an enemy.

Gearless gun and sensor servo drives. These need to be investigated for cost, performance, and possible application to AFAADS. They may allow higher servo performance with reduced wear and make dithering dispersion more attractive.

Digitized terrain storage. This can aid prediction against terrain-following aircraft, and may help reduce radar multipath errors. It has not been possible to evaluate its potential and cost in depth in this report.

Cross mount triangulation on aircraft with on-board ECM jammers. If range information is denied by an aircraft carrying an on-board jammer, range could be obtained by exchanging angular information across AFAADS mounts and triangulating.

Integrated forward area air defense information net.

This is expected to be the natural direction of growth of the Army's air defense regardless of AFAADS. However AFAADS will benefit from the improved information on enemy targets.

Radar projectile tracking. This could be used in dynamic system calibration, as well as constituting a method for measuring muzzle velocity.

Fully stabilized system including the fun for fire on the move. Although feasible, the payoff is expected to be low with relation to the cost. Sight stabilization alone is considered adequate and preferable.

6.2 COST CONSIDERATIONS

Cost enters the AFAADS concept formulation problem in two ways. The complete life cycle cost of the AFAADS system determines, in conjunction with its effectiveness in a tactical context, how successfully AFAADS can compete for funds against other possible allocations of the Army's always limited budget. This determination involves many factors beyond those susceptible to resolution by analysis.

Cost also enters concept formulation in the choices among alternate ways of solving the problem; in this more limited context it is the system designer's tool.

For present purposes we need to consider both ways of using cost estimates, but our principal interest is in the cost implications of design options. We cannot, within the scope of the present contract, attempt to estimate the level of life cycle cost at which AFAADS and missile systems become competitive, for example, although the work done in the present effort will certainly assist in such a resolution.

Total life cycle system costs, however, reflect down into the design option comparison, as will be shown. Fortunately, the effect of uncertainty in life cycle cost is greatly reduced in its implications on design option comparisons; so that at this stage in concept formulation, one need not detail all elements of life cycle cost. In this section the object is to develop a systematic basis for making cost-effectiveness trades as the AFAADS program goes forward. The cost estimates should be considered as illustrative, rather than definitive at this time.

6.2 1 Life Cycle Costs

We begin by making a base-point estimate of life cycle costs of AFAADS assuming that AFAADS would be integrated into the Army's air defense in a roughly similar way to that in which Vulcan and Chaparral are incorporated.

Costs are considered in three major categories; RDT&E, Acquisition and Activiation, and Annual Operating Costs. A more detailed subdivision is indicated in Figure 6-1.

Antiaircraft guns, historically, have a long service life. The Army still uses the World War II quad-0.50 and 40mm Duster. We therefore assume a 10-year life for AFAADS. This assumption means that procurement costs will be amortized over 10 years, and are likely to be dominated by operating costs, which include personnel and maintenance.

We also assume procurement of enough AFAADS fire units to equip one field army (12 divisions) with about 576 AFAADS fire units. This means that RDT&E costs will be spread over 576 fire units.

If:

N = number of AFAADS fire units procured.

S = a service life of 10 years.

C_a = acquisition and activation cost on a per fire unit basis.

C_o = annual operating costs on a per unit basis.

C_d = development costs.

L_T = total life cycle cost of a single fire unit.

then: $L_T = (C_d/N) + C_a + C_o T$ (6.1)

We now estimate the life cycle cost of an Air Defense Arillery Battalion which can be attributed to AFAADS. It is assumed that the battalion may contain both AFAADS and a missile system such as Chaparral, and that battalion costs and personnel are allocated equally between the two systems. Two estimates are made: (1) a high estimate for a self-propelled battalion, with a rather sophisticated AFAADS, and (2) a battalion using towed-AFAADS and a possibly reduced fire unit capability.

A rough estimate of AFAADS fire-unit costs bounds is obtained by comparison with similar systems on the basis of very limited available data. The systems compared are: the obsolescent Skysweeper, Vulcan, and the current Oerlikon system.

Skysweeper, a 75mm antiaircraft gun system with on-carriage radar and fire con' ol system cost about 313,000 dollars in a towed configuration abou: 15 years ago. This is equivalent to about 500,000 dollars in 1970 dollars.

Vulcan is believed to cost about 280,000 dollars in a self-propelled version. The current, modern Oerlikon system with both surveillance and tracking radars, twin 30mm guns, and a self-propelled tracked mount is believed to cost from 800,000 to 1,000,000 dollars each; of which about half is believed to represent radars, computer, operator displays and other fire control accessories and components.

Arranging this limited, unofficial and unverified cost information in tabular form, we obtain the values shown in Table VI-2. It should also be noted that the cost of system elements are also estimates.

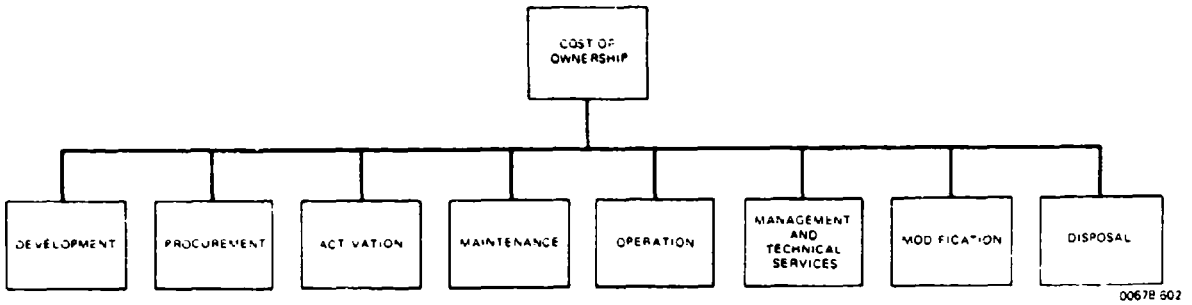

Figure 6-1. Factors Contributing to Total Cost of Ownership

Table VI-2. Very Rough Fire-Unit Procurement Cost Estimates of Air Defense Gun Systems

	Weapon System					
	Skysweeper	Vulcan	Vulcan	Oerlikon	AFAADS	AFAADS
Mobility	Towed	Towed	Self-Propelled	Self-Propelled	Towed	Self-Propelled
Gross Weight (lb)	20,000	3000	26,000		20,000	40,000
Cost (1970 dollars)						
Gun	–	18,000	18,000	–	30,000	30,000
Gun, Mount, and Servos	–	120,000	120,000	300,000	175,000	175,000
Vehicle	–	–	100,000	200,000	–	150,000
Radars, fire control, communication and other electronics and displays	60,000	60,000	60,000	400,000	150,000	400,000
Cost per fire unit, not including cost of tow vehicle for towed configurations	$500,000	$180,000	$280,000	$900,000	$325,000	$725,000

00678-603

The AFAADS fire unit costs have next been expended into total life cycle costs for the AFAADS slice of a hypothesized ADA Battalion.

Development costs are not shown explicitly at this time. The battalion is assumed to include 32 AFAADS fire units, and from 400 to 450 personnel. Results are shown in Table VI-3.

We observe that more than doubling the estimated cost of an AFAADS fire unit only results in a 27 percent increase in life cycle cost. Two conclusions follow at once. The first is that the cost to operate any complex military system in the field is so high that dollars spent for high effectiveness in a combat environment will be well spent. We show later how to assess this trade explicitly. The second conclusion is that manpower and maintenance are likely to be the principal contributors to life cycle cost. Hence, a significant fraction of the development effort should be devoted to obtaining: high reliability, low-maintenance features, and to the reduction in the numbers of required support personnel.

In this context we consider the costs associated with the possible inclusion of radars in the AFAADS system.

Table VI-3. Estimated Life Cycle Costs of 32 AFAADS Fire Units

Cost		Low Estimate	High Estimate
Acquisition and Activation Costs			
AFAADS fire units plus spares		$10 x 10^6	$24 x 10^6
Other battalion equips plus spares		6 x 106	8 x 106
Other activation costs, training, etc.		4 x 106	4 x 106
	Total	$20 x 106	$36 x 106
Annual Operating Costs			
Personnel (at $7500/year/man)		$3 x 106	$3.4 x 106
Maintenance		3 x 106	3.4 x 106
POL, Ammo, etc.		1 x 106	1 x 106
	Total	$7 x 106	$7.8 x 106
Annual Life Cycle Cost for 10-year life		$90 x 106	$114 x 106

00678-699

6.2.1.1 Radar Cost Estimates

Acquiring a radar is like acquiring a wife, the initial cost is small compared with the upkeep. We therefore review some of the limited data available in the open literature on the cost of radar ownership.[1]

The published cost-estimating relationships were obtained from an in-depth analysis of ten items including: Navy radar, sonar, and communications equipment. Since there were only four radars included, only limited extrapolation can be done. The examples serve two purposes: they provide good insight into the cost buildup of radar equipment in service in the Navy, and the methodology serves as a model for future Army analyses. This may already have been done by ECOM, but results are not available at the time of publication.

Table VI-4 shows mean time malfunction data and mean time to repair for the four radars. The resulting availability values range from 0.95 to 0.99. If these values cannot be raised for AFAADS, the radar or radars will probably constitute the principal reasons for system downtime. Table VI-5 compares cost categories on an annualized basis. The high maintenance costs relative to procurement costs should be noted. To keep AFAADS operating costs down, particular attention must be given to the design for high reliability and maintainability of any radars incorporated in the system.

The cost estimating relationships are given below. The listed 'coefficient of determination' represents the fraction of cost that is explained by the CER formulas.

The frequency range covered by these formulas does not extend down into the K-band (16,000-35,000 MHz). If, however, the CER for procurement cost were valid down to the K-band, it would indicate, for constant peak power output and number of active element groups (AEGs), that a K_u-band radar would cost about one-half as much as an X-band radar.

The importance of shock mounting and vibration isolation on maintenance cost, as indicated by the first CER for maintenance cost, is important in the AFAADS context because of the shocks to which the radar will be exposed while the vehicle is moving, and/or the gun is firing.

The importance of equipment reliability, and expressed in large mean time between malfunctions and rapid repair, as expressed by small mean time to repair is emphasized for the CER for total annualized cost of ownership, which indicates that for the three classes of equipment these factors dominate all other cost sources to the degree that together with the percent of utilization, they can be used to explain 93 percent of the cost of ownership.

Table VI-4. Cost of Ownship and Operational Measures

Equipment	Utilization	MTBM (Hours)	MART (Hours)	Intrinsic Availability	Annual Cost of Ownership in Thousands of Dollars for One Equipment
Radar A	66.0	236	2.1	0.99	37.1
Radar B	42.8	94	4.3	0.96	67.9*
Radar C	45.9	130	3.8	0.97	55.5
Radar D	44.7	118	5.6	0.95	79.2

Notes: Projected equipment life is ten years.

MTBM = Mean time between malfunctions.

MART = Mean active-repair time.

*Cost includes special support equipment.

00678-605

Table VI-5. Breakdown of Cost of Ownership

Equipment	Annual Cost in Thousands of Dollars for One Equipment							
	Develop	Procure	Installation	Maintain	Operate	Man and Technician	Modify	Disposal
Radar A	0.04	1.52	1.53	3.68	29.32	0.15	0.02	0.83
Radar B	1.25	16.74	7.84	17.03	19.02	0.96	0.29	4.76
Radar C	*	17.28	6.77	7.29	20.40	0.39	0.51	2.82
Radar D	3.57	19.37	9.69	19.35	19.87	1.43	0.07	5.85

*Unknown or not identifiable as a separate charge to the Government.

00678-606

Radar Cost Estimating Relationships (CER)

a. Procurement Cost (Dollars) per Unit

$\text{Log}_e(\text{Cost}) =$ 11.4509 + 0.0041436 (Number of AEGs) - 0.000282 (Highest Frequency) + 0.000124 (Peak Power Output)

Limits on Variables:

Number of AEGs: (Active Element Groups)	41 to 1643 tubes and transistors
Highest Frequency:	224 to 9405 MHz
Peak Power Output:	250 to 20,000 kw
Coefficient of Determination:	0.99
Range of Estimates:	82 percent to 138 percent

b. Maintenance Cost (Dollars) per 1000 Calendar Hours per Unit (CER-1)

$\text{Log}_e(\text{Cost}) =$ 5.654 + 1.121 (Indicator) - 1.449 (Vibration Isolation) + 0.00312 (Number of AEGs)

Limits on Variables:

Type of Indicators:	0 = No meters or CRTs 1 = Meters only 2 = CRTs
Vibration Isolation:	0 = No shock mounts 1 = Some form of shock mounts
Number of AEGs:	Transistors or tubes 76 to 483
Coefficient of Determination:	0.96
Range of Estimates:	85 percent to 120 percent

c. Maintenance Cost (Dollars) per 1000 Calendar Hours per Unit (CER-2)

$\text{Log}_e(\text{Cost}) =$ 7.00 - 0.000210 (Highest Frequency) + 0.0000623 (Peak Power) + 0.128 (Number of Displays)

Limits on Variables:

Peak Output Power:	250 to 20,000 kw
Highest Frequency:	224 to 5825 MHz
Number of Display Units:	0 or 1
Coefficient of Determination:	0.74
Range of Estimates:	71 percent to 175 percent

d. Total Annual Cost of Ownership of Radar, Sonar, or Communications, per Unit for 1 Year, Based on a 10-Year Projected Life

$\text{Log}_e(\text{Cost}) =$ 1.876 + 146.5 $(\text{MTBM})^{-1}$ + 0.0145 (Percent Use per Year) + 0.0924 (MTTR)

Cost is expressed in thousands of dollars

Limits on Variables:

MTBM:	94 to 2014 hours
Utilization Rate:	27 to 66 percent
MTTR:	2.1 to 5.9 hours

NOTE: One equipment operator assumed. Coefficient of Determination: 0.93

Range of Estimates: 127 percent

e. *Cost of Operation, All Equipment, per Unit*

Cost = (Estimated operating hours per year) x (number of operators) x (hourly rate for labor class)

f. *Disposal Cost, All Equipments, per Unit*

Cost = 0.8 (Installation Labor Cost) - 0.1 (Procurement Cost)

6.3 COST-EFFECTIVENESS COMPARISONS

In judging the effectiveness of AFAADS against its cost, the most important consideration is beyond the scope of this report. That is the question of whether air defense, by air defense artillery, will be required at all. In Korea and Vietnam, the U.S. Air Force was able to deny the air over the battlefield to the small enemy air forces so that there was no job for U.S. air defense artillery.

Against an enemy with significant airpower and resources to replace lost aircraft, this fortunate situation will be difficult to achieve.

The Luftwaffe was able to maintain significant air effort against Allied ground forces for the duration of WWII in spite of heavy losses inflicted by massive Allied air power, and Allied antiaircraft guns filled a critical need throughout the war.

The land battle in a future conflict is not likely to wait out the acquisition of complete air superiority. The defense of the ground forces in-depth against enemy air during the initial and interim period will require the best possible ground-based air defense.

In Korea, Vietnam, and the Middle East, the Soviet Union has demonstrated that an effective means of supporting a technologically retarded country against a modern air force is by the provision of surface to air weapons. This is a possible consideration in U.S. support of small nations of the Free World.

A second important consideration in judging AFAADS configuration options is the frequency with which AFAADS will be required to operate at night and during unfavorable weather. The frequency of rain, cloud cover, haze, fog, etc., in the probable theatres of operation can be determined by analysis, but the technological capability of a potential enemy to conduct tactical air operations effectively under such conditions is a matter of intelligence estimates and forecasts. It is clear, nevertheless, that the thrust of modern military technology is to achieve the capability of conducting military operations 24 hours a day

regardless of weather, and tactical air operations in Vietnam have accelerated this development.

The question of effectiveness measures for the AFAADS system is not easily resolved. At a high level, the effectiveness of AFAADS is judged in terms of its contribution to overall force effectiveness, which includes friendly units saved from air attack and the cost to an enemy in terms of lost and damaged aircraft. An evaluation at that level would require a fairly elaborate 'war game' type of simulation.

The method of comparison used in the following paragraphs is more restricted. We compare an index of effectiveness against the system life cycle cost to determine a threshold criterion for a justifiable increment in cost in terms of the increment in effectiveness which it produces. As will be seen, the rough estimates of life cycle cost previously obtained are accurate enough for such a threshold criterion.

The question of an effectiveness index cannot be answered uniquely. The probability of killing a target on a specific course is too limited. Average probability of kill over a wide variety of courses would be better, but the statistics are not available. We use the kill-seconds index previously used on the simulation as a convenient screening device on the grounds that it represents a capability of the potential of which can be utilized by a suitable firing doctrine.

For a given budget expenditure B, we are able to buy B/C AFAADS fire units, where C is the life cycle cost per unit. The effectiveness of the buy is EB/C, where E is the effectiveness measure. If B is constant, we wish to maximize E/C.

One might object that a specific number of AFAADS units would be required. A possible answer is that targets of varying value are defended by AFAADS, and a change in the number of AFAADS units results in the targets of least value being undefended, so that the variation of AIDA defense effectiveness with numbers of AFAADS is a smoothly varying rather than a step function.

Then, using the chosen index of effectiveness, E, and the life cycle cost on a per-fire unit basis, C, we wish to obtain the maximum value of E/C.

Comparing two options, of different effectiveness and cost, we prefer the second compared with the first, if

$$E_2/C_2 > E_1/C_1 \qquad (6.2)$$

or, equivalently, if

$$E_2/E_1 > C_2/C_1 \qquad (6.3)$$

Write

$$C_2 = C_1 + \Delta C \qquad (6.4)$$

where: ΔC is the incremental cost of adding a component.

Then the addition is cost-effective if its cost increment ΔC is:

$$\Delta C < C_1 [(E_2/E_1)-1] \qquad (6.5)$$

From Table VI-3 in Section 6.2.1 the life cycle cost of a single fire unit over 10 years operational life is from 2.8 dollars to 3.5 dollars x 10^6. From the above expression, an option generating a 10 percent improvement in effectiveness is worth incorporating, if its contribution to the life cycle cost per fire unit, is less than 280,000 dollars to 350,000 dollars.

We can see at once that the initial estimate of life cycle cost provides us with a valuable reference point, and that rather large uncertainties in the elements of the life cycle cost estimate will not significantly change the position of the cost boundary that we draw between cost-effective and non cost-effective options of configuration elements.

If the 300,000 dollar threshold appears large, consider the possibility of a 40,000 dollar radar that costs 40,000 dollars a year to maintain. On a 10-year basis it would add at least 440,000 dollars to the system life cycle cost and so would be excluded unless the effectiveness index showed that it improved system effectiveness more than about 15 percent. For so large a cost increment, the costs would have to be done more carefully.

As another example, consider the development of improved ammunition. The simulation results showed that ammunition with improved ballistics improved system performance by factors of from 1.1 to 1.4. In production the improved ammunition would cost about the same as present ammunition, and operating costs would not be affected since it is presumed that there is not a large stockpile of present ammunition to be written off. The improvement factor of 1.1, or 10 percent on each of the assumed buy of 570 fire units, would make the improvement desirable if the research and development program could be accomplished for less than 570 x 300,000 dollars, or 170 dollars x 10^6. The job can certainly be done for a fraction of the amount indicated. It is clear, therefore, that the development of improved ammunition is cost-effective.

We now consider some of the more important options listed in Section 6.1 from a judgmental and a cost-effectiveness point of view.

6.3.1 Stabilised Sight

A major advantage of a stabilized line of sight is that, within the limits of the stabilization loop, the sight is free of disturbances caused by normal gun

motion, shock, and vibration produced by firing, mount flexure caused by firing, and vehicle pitch and roll when in motion.

As a basic design principle it was recommended that the sight pedestal, even though it may be mounted on the gun's lower carriage for design convenience, should be back-driven so that within the limits of gear backlash, shaft resilience, etc., the gun motion would not affect the sight motion. Since mechanical drives are imperfect, we would expect a small residue in the gun's motion to appear at the sight pedestal even when the gun is not firing and the vehicle is not moving. Stabilization should effectively eliminate this residue.

On a 10-year life cycle basis, we would not expect the stabilized sight to contribute a cost increment, including maintenance, of over 150,000 dollars. It will thus be cost effective if it adds only 5 percent to overall system effectiveness, as compared with an unstabilized sight. A judgment at this point is that a stabilized sight will be cost-effective.

6.3.2 Regenerative Tracking

Regenerative tracking is considered to provide a gain factor of about 10 percent when associated with automatic tracking sensors under unimpeded tracking conditions. The gun servos can be up-graded so that they do not need the regenerative assist, however the design of both servo loops is considered to be less stringent when regeneration is employed, so that there is a trade-off between servomechanism design and the use of regeneration in this mode of operation. Regeneration may also reduce the solution rate requirement on a digital computer.

Regeneration is essential to maintain high performance even with automatic sensor tracking when the target is occasionally obscured by terrain obstacles, or when the sensor, as is expected with early laser range finders, occasionally misses a blip.

If manual tracking is a primary mode, there is no point at all in attempting to provide an accurate solution of the prediction problem, *unless the man is given a regeneration aiding*. Since the man will always represent a primary back-up mode of tracking, and may have to take over from the radar where multipath degrades elevation tracking, it is concluded that the relatively minor cost increment associated with regenerative tracking is far outweighed by the gain in effectiveness under all modes of operation.

6.3.3 Surveillance Radar

We have no confidence in the ability of the man to detect and acquire targets at ranges that will allow the full potential of the Vigilante weapon to be realized even in clear, daylight operation. The problem passes completely beyond the capability of the man to solve, when the attacking aircraft uses even relatively simple stand-off air to surface guided munitions. Since the gain factor is at least 2.0 in clear, daylight operation, and infinite at night, or in bad weather, a surveillance radar is considered to be cost-effective.

Unless the radar is designed from the beginning for high reliability, low maintenance, and operation in the difficult shock and vibration environment of on-carriage mounting, the maintenance costs are likely to exceed procurement costs by a factor of 10. A design object should be set on life cycle costs, to hold 10-year maintenance costs down to no more than 3-times procurement costs.

6.3.4 Tracking Radar

There appears to be no alternative to radar for the tracking function under all weather conditions. Even when the man can track visually, we feel that the question of whether he can outperform a frequency diverse radar, even with regenerative tracking, remains to be answered. Although we emphasize the absolute need for regenerative tracking for the man either in a primary or back-up mode, we feel that both radar tracking and automatic tracking in fair weather with imaging devices cannot be removed from consideration. And to repeat, radar tracking is essential for all weather operations.

Foreign developments in tracking radars now extend down to the K_a-band. A very compact and mount-compatible set should be possible at this frequency. However, the development costs would have to be amortized over the AFAADS program if a set were developed solely for AFAADS. The same requirements on design for high reliability and low maintenance costs indicated for the surveillance radar should be imposed from the beginning of the program. As the only method of conducting effective fire in bad weather, it is our judgment that detailed cost and effectiveness analysis would indicate development and utilization of a tracking radar for AFAADS to be cost effective, even if bad weather required its use against only 20 percent of the targets exposed to AFAADS. The important cost here is the cost increment between a night/fair weather system such as an imaging tracker and the radar. We believe also that analysis will indicate a performance differential in favor of the radar over an IR hot-spot tracker sufficient to justify its cost in a night/fair weather comparison; but this conjecture needs to be resolved by analysis.

6.3.5 Computer

This study has by direction been concerned more with the mathematical aspects of the system rather than the techniques that will be utilized for its mechanization. It was, however, specifically desired that the study consider the effects of sensor and processing data rates on overall system accuracy.

For this reason, and because in our study of prediction algorithms we indicated the desirability of performing some apparently intricate operations within the computer in maintaining several prediction modes in parallel, automatically switching from one to the other, etc., this section discusses in some detail some of the aspects of computer operation. Unfortunately time has not permitted a complete computer sizing and costing study in the present contract.

We begin by noting that although a good solution to the simplest, single algorithm prediction problem could be obtained with an analog computer, growth in analog state of the art is limited, accuracy is less than that of a digital computer, and although we have not carried out an appropriate life cycle cost comparison we believe that whatever the level of solution complexity a digital solution can be developed to provide higher performance at lower cost. This statement, of course, needs to be verified by comparative analyses in depth if the analog is felt to be desirable, possibly because of the existence of applicable components.

Our simulation runs, however, have indicated that a rather substantial payoff in performance exists if the computer can maintain several prediction modes in a current state simultaneously, and switch the appropriate mode to the gun based on suitable decision algorithms. It is believed that this capability is attainable by relatively small modular increments to a digital computer, whereas it would be more costly to implement with an analog.

Moreover, as noted earlier, a major argument for the digital implementation of as much of the fire control system as possible is the continued and explosive growth of the state of the art in digital computers. Not only are size, weight, power requirements, and cost to do a given job shrinking rapidly; but reliability is already very high, and automatic diagnostic circuits reduce mean time to repair to a few minutes. For an AFAADS digital computer, a mean time between failure of over 5000 hours and a mean time to repair of less than 10 minutes are consistent with current state of the art. This capability would have a healthy effect on life cycle cost.

With regard to word size in the computer in Section 5.14.4 an overall system instrumental error of less than 2 mils or 2 meters (the larger value controlling) was suggested as an objective. This would be easily met with an 18-bit word, and fewer bits might be acceptable.

In the discussion of the effect of number of samples on the data smoothing function, it was indicated that an upper limit to the useful input data rate was set by the autocorrelation in time of sensor errors. A frequency diverse tracking radar would make the best use of a high input data rate, but even in this case there seems to be little advantage in an input rate of higher than 10 data points per second, while a value as low as five may be satisfactory. With up to four coordinate inputs (including range rate from a doppler radar), the input data rate would be only 720 bits per second. Some consideration needs to be given to the possibility of non-simultaneity in samples in the separate coordinates which would introduce small errors because of high rates of change in the separate coordinates.

The object of coordinate transformation is to do smoothing in parameters which vary relatively slowly. If, as is considered preferable, a basic rectangular coordinate system is used, the requirement on data rate lessens once X, Y, and Z have been computed. It rises again when the conversion back to gun orders is required.

For the linear prediction mode, with smoothing in position and velocity, six functions are subjected to data weighting operations. If done non-recursively with a maximum of 10 points for each function, 60 data points would be held in memory. For the quadratic mode, a maximum of 80 data points would be held (Z is not used). This moderate number could be reduced by a factor of 2 to 4 by the use of recursive smoothing.

The possibility that regenerative tracking would work best with a different set of weights would lead to a larger number of data points at this stage. On the other hand, the most likely mode to stabilize the regenerative loop is simple exponential weighting which has very small memory requirements.

A data rate of 10/second is believed to be satisfactory for regenerative tracking, but this needs to be validated by analysis and simulation.

The prediction triangle is solved iteratively, from the smoothed positions, derivatives, and the ballistics. The algorithm developed for the simulation (using a unique convergence method) obtained a solution to within 0.001-sec time of flight on an average number of five iterations, and never exceeded about 10. Solutions of the prediction triangle were within 0.5 meter.

The solution rate of the prediction problem, however, must be considered in terms of the required data rate to be applied to the gun. If the digital to analog conversion is visualized in its simplest form as transmitted via a zero-order hold, the associated lag error caused by angular velocity is equal to the angular velocity multiplied by half the interval between samples. For the most difficult course considered this suggests a data rate to the gun of about 50 data points per second. This may be relieved by using regeneration in a feed-forward mode since the derivatives of gun motion can be computed by methods given in the body of the report.

If five iterations are required for each data point, the output rate of 50 per second would require 250 trial

solutions per second. The five iterations can probably be reduced by reducing the time of flight solution to an incremental one working from each previously obtained time of flight, and possibly taking advantage of the rate of change of time-of-flight algorithm given earlier in this report. This is only one of many program design trades that can be applied to balance algorithms against memory against computer speed.

If the quadratic prediction algorithm is carried in parallel with the linear algorithm there are two possibilities for implementation. One is to continuously compute gun orders by both algorithms and switch in accordance with the decision algorithm. A more economical method is to carry only the acceleration and target rate of turn computations, and switch them into the prediction triangle solution when the quadratic option is called for. If the prediction triangle is being solved at a rate of from 50 to 250 times per second, the lag involved in the latter, and more economical procedure would be negligible.

The defended point algorithm is somewhat more complex. The several decision algorithms are carried continuously, but the prediction relations need not be solved until the algorithm is called up. The computation of decision measures and their comparison against thresholds can be satisfactorily done without iteration at a rate of 10 per second. Once in use, the number of solutions of the prediction problem per second would, as in the case of the simpler algorithms, depend on the data rates required by the gun servos.

The data rates indicated above are relatively trivial in the present state of the art of military computer technology. A typical central computer for a modern fighter aircraft has an input/output rate of 10^7-bits/second, and a computational speed of 10^5 multiplications per second.

Our judgment at this point is that a digital solution will cost less to implement than an analog solution (except for possibly the simplest, approximate, rate x time solutions), and that its maintenance costs will be negligible by comparison.

If we estimate annual maintenance cost of an analog solution optimistically at one-third the procurement cost, and annual maintenance cost of the digital solution at one-tenth procurement cost, a digital solution having twice the procurement cost of an analog will have the same life cycle cost. In fact, we expect the procurement cost to be less, and the system effectiveness to be higher by a factor of at least 2.0.

We therefore believe that further analysis will show a digital computer solution to be cost-effective.

Since the present discussion contains more judgment than analysis, we prefer to terminate it at this point having indicated a general method of approach to the problem of cost-effectiveness trade-offs in component selection as the AFAADS program goes forward. We conclude by reverting to an illustrative example of how overall systems cost-effectiveness comparisons may be done. This is contained in the following and final section of this report.

6.4 SYSTEM CONFIGURATION

In Section 6.1 about 40 design options were offered for consideration in system configuration. A basis for selecting options was provided in Sections 6.2 and 6.3 in terms of cost-effectiveness. To place these in a more coherent perspective, three tentative system configurations are described in the following paragraphs. Although it is believed that the components shown can be justified by a thorough analysis of effectiveness and cost, this section should be considered simply as an outline of how alternate configurations may be compared on an overall basis.

The three systems considered are: (1) a day, fair-weather system, (2) a day or night, fair-weather system, and (3) an all-weather system. Their elements are listed in Table VI-6. Life cycle costs have not been worked out in detail, but to make the illustration concrete, guessed life cycle costs are listed. It is assumed that the life cycle costs of a single fire unit over a 10-year period, exclusive of costs of the fire control system, but including a proportional allocation of overall battalion costs, is 2.3 dollars x 10^6. To this basic cost, an increment is added which increases with the complexity of the fire control system.

Effectiveness is arbitrarily estimated against a base of 1.0 for the all-weather system. It is assumed that weather would prevent the fair-weather system from functioning 20 percent of the time. The fraction of enemy attacks taking place at night, regardless of weather, is assumed to be 50 percent. Tracking with the K-band radar is assumed to generate at least a 10 percent higher effectiveness than tracking with any of the non-radar modes. The day/fair weather minimal system is further degraded 50 percent because of its lack of surveillance radar. Figure 6-2 shows comparative costs and effectiveness of the three configurations. As shown by the lines drawn from the origin, the all-weather system in this illustration is preferred from a cost-effectiveness point of view.

The comparison is, it must again be emphasized, not significant in the results shown but as a method for comparing more carefully done system configuration cost and effectiveness analysis.

Table VI-6. Hypothetical Comparison of Configurations Having Various Capabilities (Sheet 1 of 2)

Function	Capability		
	Day/Fair Weather	Day/Night Fair Weather	All Weather
Surveillance and Detection	Visual + RAID	Radar or IR	Radar
Angular Tracking	Visual with Regenerative Tracking and 3 x Magnification	Imaging Sight with Regenerative Tracking and Automatic Tracking Mode, Visual Back-up	K-band Radar Imaging Sight Back-up mode Visual, Second Back-up Mode Cross-mount Triangulation vs On-Board Jamming
Ranging	Laser or radar with Regenerative Assistance for Estimated, Intermittent Range Back-up Mode	Laser or Radar with Regenerative Assistance for Estimated, Intermittent Range Back-up Mode	Radar, Laser Back-up with Regenerative Assistance for Estimated, Intermittent Range Back-up Mode
Line of Sight Stabilization	Yes	Yes	Yes
Prediction Algorithms	Linear + Energy Quadratic + Energy Altitude Prediction Cut-Out Automatic Option Selection Digital Computer with Automatic System Checkout	Linear + Energy Quadratic + Energy Altitude Prediction Cut-Out Automatic Option Selection Digital Computer with Automatic System Checkout	Linear + Energy Quadratic + Energy Altitude Prediction Cut-Out Automatic Option Selection Digital Computer with Automatic System Checkout
Weapon and Ammo Characteristics	Maximum Muzzle Velocity Minimum Projectile Drag High HE Content 120, 1200, 3000 rpm Options Adjustable or Variable Dispersion	Same as Day/Fair Weather	Same as Day/Fair Weather
Firing Doctrine Aids	Indicator Target In Range, Sensors on, Quality Of Solution	Same as Day/Fair Weather	Automatic Firing Doctrine
Ballistics	Wind Correction Automatic Muzzle Velocity Measurement and Correction	Same as Day/Fair Weather	Same as Day/Fair Weather
Dynamic Calibration	Yes	Yes	Yes

00678-607 (1 of 2)

Table VI-6. Hypothetical Comparison of Configurations Having Various Capabilities (Sheet 2 of 2)

Function	Capability		
	Day Fair Weather	Day/Night Fair Weather	All Weather
10-Year Life Cycle Incremental Cost of Fire Control per Fire Unit Including RDT&E Procurement and Maintenance	$600,000	$1,200,000	$1,800,000
10-Year Life Cycle Cost Per Complete Fire Unit Including Allocated Share of Battalion Costs	$2,900,000	$3,500,000	$4,100,000
Comparative Effectiveness Assuming 50 percent Night Attacks and 20 percent Bad Weather	0.1	0.7	1.0

00678-607 (2 of 2)

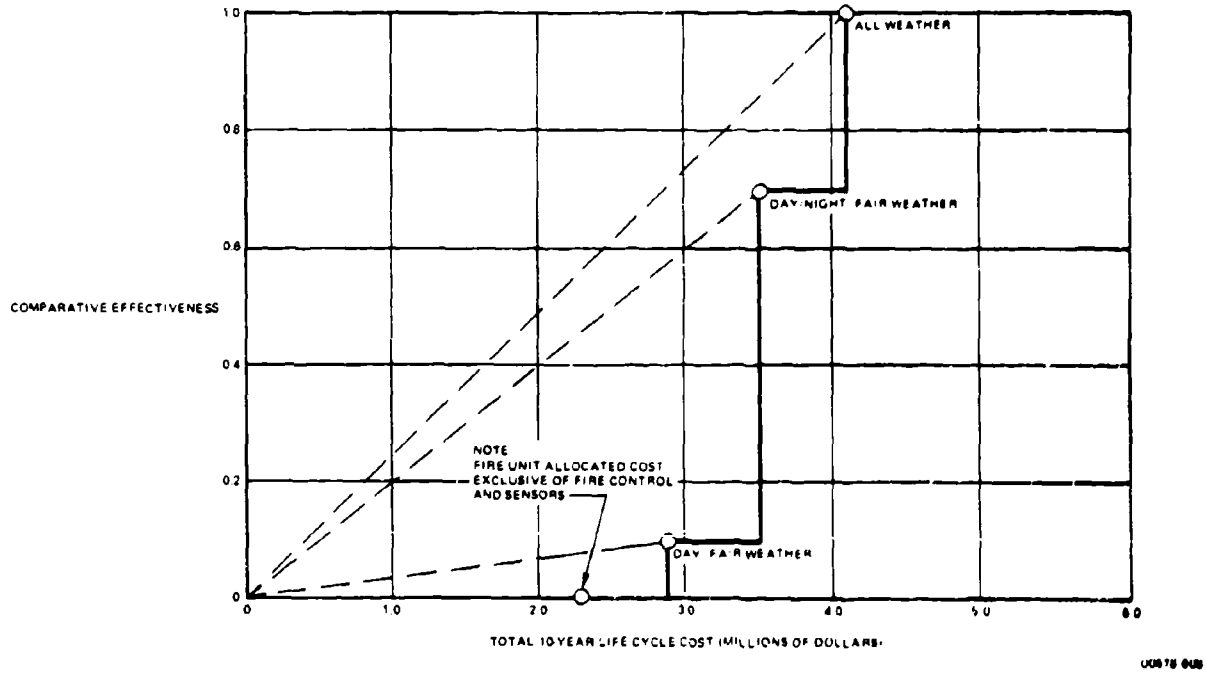

Figure 6-2. Comparison of Overall System Cost and Effectiveness

SECTION 7
RECOMMENDED PROGRAMS

It was desired that the study pinpoint areas in which improvements in the state of the art over that predicted for the postulated time period would result in significant improvement in the overall performance of the fire control system. It was also desired that the study list basic data that are required for adequately conducting studies of the present type and are not currently available. These topics are addressed in the present section. In addition we list areas for further analysis which are important to predicted-fire, air defense system concept definition, for which limited time has prevented adequate in-depth exploration in the present study.

7.1 AREAS FOR EXPLORATORY AND ADVANCED DEVELOPMENT EFFORT

The following paragraphs describe various areas that merit further exploratory and advanced-development efforts.

7.1.1 Radars

Increased effort should be devoted to frequency diversity, polarization diversity, and computer processing of radar data to improve countermeasures immunity, reduce multipath errors, and increase tracking accuracy by broadening the glint spectrum. This will improve the effectiveness of both surveillance and tracking radars.

Development should be initiated on a K-band tracking radar, preferably K_a-band, utilizing the above improvements.

Radar development should incorporate special funding from the beginning of the program to obtain very high reliability and low maintainability requirements in the difficult shock and vibration environment of the AFAADS on-carriage mount.

7.1.2 Target Identification by Noncooperative Means

All air defense systems will benefit from a fast, reliable method of identifying aerial targets without the use of conventional IFF interrogators and responders. Digital computer analysis of the reflected radar pulse, by Fast Fourier Transform or more sophisticated means, or analysis of the reflected laser pulses by holographic or other means may be eventually feasible. Exploratory development programs in this area should be expanded and augmented.

7.1.3 Human Operator Performance in the Tracking Function

Existing data on the performance of the human operator in tracking aircraft targets should be collected and analyzed in a systematic way to reveal the interaction among target flight-path characteristics, control dynamics, and human performance. The existing Vigilante mount, which incorporates regenerative tracking, should be used to collect additional data on this mode. Laboratory experiments incorporating a human operator, antiaircraft type forcing function, and appropriately varied control dynamics including regenerative modes, should be used to define the desired dynamics of an operational system; and the system thus defined should be brassboarded and tested in the field.

7.1.4 Imaging Trackers

The tracking accuracy obtainable with imaging trackers, both in the visible and infrared regions, in an automatic tracking mode against aircraft targets should be investigated. Performance of existing trackers, of which a variety exists, should be collected and analyzed. Of particular interest are the 'contrast seekers' developed for air to ground missiles. Experimental brassboards of the most promising trackers should be assembled and tested against actual aircraft targets. This program should be run in parallel with the program for improvement of human performance by regenerative aids. Automatic-imaging trackers should be able to track whenever the man can track, as well as at night or in clear weather when the man cannot track without aids. Designing an automatic-tracking mode into imaging trackers will avoid possible performance degradation as a result of using the man to track the image. It is noted that existing contrast seekers have been operated experimentally with 4-Hz servo bandwidths.[1] The possibility of extending tracking range by laser illumination should be investigated.

7.1.5 Lasers

The normal development of lasers is expected to provide satisfactory range and beamwidth when required for AFAADS. A more efficient way of providing the required capability, preferable to the brute force method of increasing power, is to increase the sensitivity of the detector. Better detectors will allow lasers to operate at lower power, with longer life, greater reliability, and lower maintenance costs. Effort to improve detector sensitivity should be increased.[1]

Lasers should also be considered in conjunction with the imaging trackers, described earlier, as a means for extending range and spectrum of operating conditions beyond that attainable with passive imaging alone.

7.1.6 Digital Computer

This study has indicated significant potential advantages in the use of a fire control system having several

optional prediction algorithms, with automatic computer selection of option, and automatic switching among options even while an engagement is in process. It is believed this flexibility can be attained at acceptable cost, within reasonable size only by a digital computer. The life cycle cost of digital solutions, moreover, is believed to be lower, by a large factor than the equivalent capability in an analog.

The maximum payoff from use of a digital computer will be realized, however, only if digitalization is used throughout the AFAADS system to the maximum degree possible.

On a broader basis, even more economy will be realized if a program is laid out for the systematic introduction of digital computation into all of the Army's gun fire control systems. Initiation of such a program would require more detailed justification than can be offered here, but the impressive continued reduction in weight, cost, and power requirements of digital computers and their very great increase in reliability suggests that such justification would be easy.

At the same time the Army does not want to load its logistic, training, and maintenance systems with support requirements for a number of different special purpose computers. An appropriate family of small computers, adjustable to fit specific needs by modular additions, would seem both feasible and economical. With reasonable foresight, the modules could easily be replaced when appropriate as each new generation of computer technology allows an increase in system capability at further reduced cost.

It is believed that the Army already has a program of this type, but it is not known whether computers for fire control systems of predicted fire weapons are included in the plan. Clearly, they should be a part of the overall program.

7.1.7 Weapon

Effort should be continued to increase muzzle velocity and reduce projectile drag. Continued payoff beyond the limits considered in the present study is indicated. The interaction with projectile payload and terminal effectiveness should be considered. Increased muzzle velocity will introduce considerations of tube life and barrel heating. Hyper-velocity projectiles, perhaps fin stabilized, should be considered with regard to compatibility with the gun loading mechanism, and in terms of overall system effectiveness.

7.2 DATA COLLECTION PROGRAMS

The 'data bank' on the observed performance of predicted-fire weapons is widely scattered, uncorrelated, and suffers rapid attrition with time as agencies are dissolved, relocated, or have their files purged.

7.2.1 Combat Data

A great deal can be learned from combat data as the British demonstrated in World War II, but although the Army has an excellent program to collect, analyze, systematize, and apply vulnerability data from Vietnam, as a result of long continued efforts by the Ballistic Research Laboratories, a comparable program to evaluate the overall effectiveness of enemy antiaircraft predicted fire weapons to obtain objective estimates of the effects of range, speed, altitude, and tactics on weapon performance under combat conditions apparently does not exist. A program of analysis of combat data from Vietnam could yield:

a. The paths flown by our aircraft in attacking both undefended targets and defended targets for each of a wide variety of munitions. These paths would be of inestimable value as inputs to simulations of proposed predicted-fire systems.

b. The combat effectiveness of enemy predicted-fire systems. Since some information on the type of fire control used by the enemy is probably available, this could be used for check-point runs on simulations to improve their validity. A program of this type should be instituted and maintained, even if at times it drops to a fractional man level.

7.2.2 Proving Ground Tests

The Army has been testing predicted-fire systems at proving grounds and test ranges since 1921. There has been no sustained effort to correlate this information across tests to establish a reference basis for the evaluation of new systems. Of more critical concern, there has apparently been no consistent program to feed the results of each test program back into the development program to guide the allocation of funds to the areas most critically requiring improvement.

The present Vulcan and Vigilante programs could serve as models for continued effort of this sort, and the effort should be maintained even at a minimal level after their completion.

7.2.3 Noncombat Information on Target Attack Paths

The JCS experiments, Air Force experiments at Eglin Field, CDCEC experiments, and many others have generated a large body of information of aircraft and helicopter target paths under simulated combat conditions. This information should be collected, abstracted, summarized, and put into a form in which it could be used by the designer of air defense weapons. At present it is widely dispersed.

7.3 RECOMMENDED AREAS FOR CONTINUATION OF THE PRESENT STUDY

The following areas of effort are recommended for consideration, and review in conjunction with the Army's needs, as direct continuation of the effort

reported in this report. The effort is categorized in the subareas of: (1) simulation improvement, (2) data acquisition and analysis, and (3) air defense system analysis and evaluation.

7.3.1 Simulation Improvement and Additional Simulation Studies

a. *Improvement of Target Model.* Because of limitations on time, the simulation runs described in the present report were run with a circular vulnerable area representing the target. All of the computational elements exist in the present simulation to allow the target to be represented by a fuselage ellipsoid and a thin flat plate wing, with proper angle of bank. Only a small modification to the target vulnerability program module is required. It is also possible to separately count hits on the target and kills to provide estimates of both damage and destruction.

b. *Improvement of Gun Dispersion Pattern.* Because of limitations on time, a circular dispersion pattern was used in the runs described in this report. A relatively simple modification of the appropriate program modules will allow dispersion resulting from muzzle velocity dispersion to be introduced properly, and to examine the effect of noncircular gun dispersion. This will allow the value of noncircular dispersion, and dispersion automatically varied with range, and other parameters by means of gun dither to be assessed.

c. *Improvement of Tracking Noise Simulation.* If better information can be obtained on the way that the standard deviation and power spectral density of glint vary with target angular velocity and aspect, these can be incorporated. The width of the glint spectrum is expected to increase with increased target angular velocity.

d. *Study of Terrain Following Aircraft.* Time did not permit aircraft and helicopters flying nape of the earth paths to be studied on the simulation. This can be done in two ways: (1) by generating appropriate paths consistent with the analyses contained in this report, and (2) using actual paths recorded in the field with real aircraft and helicopters.

e. *Increased Detail in Representation of Regenerative Tracking and Servo Loops of Sensors and Gun.* In the simulation runs made for the present study, servomechanism performance was included in terms of lag as a function of the appropriate derivatives. Regeneration was approximated in a semirealistic set of approximations. A rather careful study including both analysis and simulation needs to be done at the next level of detail of system representation to determine and optimize the circuit parameters and time constants particularly in the case of regeneration. This overlaps with the further study of weighting functions for data smoothing.

f. *Study of Recursive Smoothing Algorithms.* The present study indicated that the smoothing functions applied to measurements of target position and derivatives should vary with time of flight, and possibly with other parameters. It also indicated that finite memory smoothing was likely to create compatibility problems if the resulting rates were used for regeneration, particularly with regard to quick settling. Recursive smoothing needs to be investigated, with the possibility that two sets of smoothed derivatives should be generated, one for regeneration and one for prediction. This topic requires both analysis and simulator verification.

g. *Interrupted Tracking.* The simulation now incorporates the capability to periodically interrupt tracking inputs and continue prediction based on regenerated velocities. Time did not permit this capability to be exercised in the present contract. The divergence of the solution with time under this mode should be investigated.

h. *Operation in Degraded Modes* The simulation now incorporates the capability of switching on command among the prediction algorithms in its repertoire during an engagement (as well as automatic switching in response to decision algorithms). This can be used to study system performance in degraded modes, as when range information is suddenly denied. Algorithms for regenerating range based on intermittent and/or estimated ranges are presented in this report and they can be validated on the simulation.

i. *Development of Firing Doctrine and Algorithms for Its Automation.* Firing doctrine was treated only lightly in the present study because of limitations of time. It needs to be analyzed in some detail particularly with regard for its implications on the ammunition load that should be carried on the mount. In addition, the feasibility of, and appropriate algorithms for automated firing doctrine, as suggested by Mr. S. Olson should be explored by analysis and simulator verification.

7.3.2 Data Acquisition and Analysis

a. *Flight Path Data.* The simulation can easily be exercised against target paths recorded by tracking real aircraft. A large body of this data exists at various agencies. This should be reviewed and evaluated (1) to check the assumptions about flight paths made in generating the simulator courses in the present study, and (2) to select appropriate real flight paths against which to test the candidate prediction algorithms developed in the present study. Use of such real data would be

a convincing argument that the algorithms and the decision thresholds proposed in this report will work in real life. Although every effort was made to use 'plausible' target paths in the present study, it is considered that the value of the overall effort would be greatly enhanced by tests on the simulation against real flight paths.

b. *Analysis of Real Tracking Data (Manual, IR, and Radar).* To obtain inputs representing manual and radar tracking errors for the simulation, the present study attempted to make realistic estimates based on available information regarding error magnitude, autocorrelation, lags, etc., and the way that these attributes varied with range, angular velocity, etc. The result is an analytical structure (or logical basis) for processing real tracking data and expressing its characteristics in terms of a small number of parameters so that it can be used in future simulator runs, or analytical computations. It would be desirable to process a representative body of real data with this objective. In addition, the unprocessed data could be run on the simulation as recorded, as another increment of realism. The characteristics of IR and automatic optical trackers should also be reviewed to determine how best to simulate them.

c. *Analysis of Detection and Acquisition Ranges and Times.* Only a cursory review could be made of the existing experimental data on the ranges at which targets can be detected, acquired, and identified visually, or by sensor, as a function of target type, speed, range, weather, etc. Since the provision of a surveillance sensor on AFAADS is critically dependent on this operation, it requires a more comprehensive study.

7.3.3 Air Defense System Analysis and Evaluation

a. *Expanded Scope of Armament Characteristics.* The present study was concentrated on the 37mm Gatling Gun. Since all of the analytical methodology and simulation characteristics are completely general with regard to weapon characteristics, the effects of varying caliber, muzzle velocity, and ballistics over a much wider range would be worth investigating. Gun, ammunition, and target vulnerability inputs would be required from the Army. A particularly interesting topic would be the evaluation of a gun firing projectiles, possibly subcaliber, at muzzle velocities in excess of 5000 ft/sec. The methodology developed is also applicable to the evaluation of small caliber, low cost, 'proliferation' type antiaircraft weapons down to the man-portable size.

b. *Analysis of Real Shock and Vibration Data.* This kind of data is now being collected by the Army on the Vigilante in field experiments. The analysis of the present report needs to be reviewed and reinterpreted in terms of this experimental data.

c. *Evaluation of New Proposed Systems, or Upgrading of Present Systems.* The Army will probably prefer to do this kind of evaluation in-house because of the proprietary information involved. However, additional supporting parametric studies in particular areas of interest, and modifications of the present simulation to match proposed systems or system improvements can be provided.

d. *Use of Digitized Terrain Data in Computer.* The present study indicated that terrain, as it affects terrain-following aircraft might be represented in the computer by a relatively small number of points. This possibility deserves further study, both with regard to its use in a prediction algorithm, and with regard to its use in assisting the radar in coping with multipath problems.

BIBLIOGRAPHY/REFERENCE LIST

Section 1

1. Los Angeles Herald-Examiner, Friday August 28, 1970, p. A-4
2. Koch, Horst-Adelbert, *Flak; Die Geschichte der Deutschen Flakartillerie und der Einsatz der Luftwaffenhelfer*, Podzun Verlag, Bad Nauheim, 1965
3. Futrell, R.F., *The United States Air Force in Korea, 1950 - 1953*, Duell, Sloan and Pearce, New York, 1961
4. Frederick Pile, General Sir, *Ack Ack*, Harrap, London, 1949
5. Reinburg, J.H., *Air-to-Air Combat in World War II: A Quantitative History*, IDA Research Paper p. 345, November 1966, AD 659 043
6. Ashkerov, V.P., *Antiaircraft Missile Troops and Antiaircraft Artillery*, Moscow 1968, Technical Translation, U.S. Army Foreign Science and Technology Center, AD 696 188
7. USAF Historical Division, *USAF Tactical Operations in WWII and Korea*, 1962, AD 480 470
8. *Air Defense, an Historical Analysis*, US Army Air Defense School, June 1965

Section 2

1. Nathanson, F.E., *Radar Design Principles*, McGraw Hill, 1969, p. 183
2. Aircraft Sketches from H. Clark, *Military Aircraft*, Air Trails Military Aircraft, 1970

Section 3

1. *US Army Air Defense Artillery Employment*, FM 44-1, July 1967
2. *Air Defense Artillery Employment*, Chaparral/Vulcan, FM 44-3, April 1968
3. *Air Defense Artillery Employment*, Automatic Weapons, FM 44-2, Nov 1968

Section 4

1. Bertoni, E.A., *Clear Lines-of-Sight from Aircraft*, 1967
2. McCabe, J.T., *Estimating Mean Cloud and Climatological Probability of Cloud-Free Lines-of-Sight*, Technical Report 186, 1965, Environmental Technical Applications Center, USAF
3. Lund, I.A., *Estimating the Probability of Clear Lines-of-Sight from Sunshine and Cloud Cover Observations*, Journal of Applied Meteorology, 1965, 4:714-722
4. Fischer, A.D., Brigadier General, *Are Light and Medium Calibre Automatic Guns the Weapons of Modern War?*, Interavia, November 1967, p. 1652
5. London, M.P., *Tactical Air Superiority*, Space/Aeronautics, March 1968, pp 62-71
6. Miller, B., *Tactical Laser Use Advancing* - Part I, Aviation Week and Space Technology, January 19, 1970, pp 54-65
7. Gatland, K., *Directory of Air-Launched Guided Missiles*, Flying Review, November 1969, pp 45-51
8. Energy-Maneuverability (U) Vol. I (Elgin) APGC-TR-66-4, AD 372 287 Secret NF Report
9. Energy-Maneuverability Theory (U) APGC-TDR-64-35, ATL-TDR-64-28 AD 351 079, Secret Report
10. CH-47 Helicopter Man-Machine-Environment Compatibility Experiment, US Army Combat Developments Command Experimentation Command, Fort Ord, Calif., 27 September, 1968
11. *The Dassault Milan*, Interavia 11/1969, pp 1808-1810
12. *Air Defense Artillery Employment*, Chaparral/Vulcan, Dept of the Army Field Manual, FM 44-3, April 1968
13. Pfeilsticker, R.C., and Glynn, J.C., *Fire Control for UH-1B Helicopter*, Armament Subsystem XM3, Frankford Arsenal, US Army, Report M64-2-1, July 1963, AD 417 908
14. Flattner, C.M., *Navy Phasing A-7E's into Operation*, Aviation Week and Space Technology, 16 February 1970, pp 38-43
15. *The Strategic Balance*, Institute for Strategic Studies
16. Futrell, R.F., *The US Air Force in Korea, 1950-53*, Duell, Sloane, and Pierce, New York 1961
17. Austin, W.H. Jr., *A Summary of Some Recent Developments in the Description of Atmospheric Turbulence Used for Aircraft Structural Design*, Systems Engineering Group, Research and Technology Division, Air Force Systems Command, Wright-Patterson Air Force Base, Ohio, Technical Report SEG-TR-66-45, August 1966

18. Pritchard, F.E., Easterbrook, C.C., and McVehill, G.E., Cornell Aeronautical Laboratory, Inc., *Spectral and Exceedance Probability Models of Atmospheric Turbulence for use in Aircraft Design and Operation*, Air Force Flight Dynamics Laboratory Technical Report AFFDL-TR-65-122, R&T Division, AFSC, Wright-Patterson Air Force Base, Ohio, November 1965

19. Lappe, U.O., *Low Altitude Turbulence Model for Estimating Gust Loads on Aircraft*, Journal of Aircraft, January-February 1966, Vol. 3, No. 1, pp 41-47

20. Gault, J.D., and Gunter, D.E., Jr., *Atmospheric Turbulence Considerations for Future Aircraft Designed to Operate at Low Altitudes*, Journal of Aircraft, November-December 1968, Vol. 5, No. 6, pp 574-577

21. Chalk, C.R., *Simulator Investigation of the Effects of I_x and True Speed on Longitudinal Handling Qualities*, Journal of Aircraft, Vol. 1, No. 6, November-December 1964, pp 335-344

22. Stapleford, R.L., and Ashkenas, I.L., *Effects of Manual Altitude Control and Other Factors on Short-Period Handling Quality Requirements*, Journal of Aircraft, Vol. 5, No. 1, January-February 1968, pp 41-48

23. Harries, G., Dr., *Roughness of Flight of Aircraft and Towed Targets*, Contained in BRL Report No 932, 1955

24. Barnett, P.Q., and Dunne, J.J., Dr., *A Study of Prediction Errors, AAFCS I-III*, Contained in BRL Report No 932, 1955

25. Clay, L.I., Marshall, R.J., and Braun, J.F., Jr., *Continued Study of Random Altitude Deviations of General Aviation Aircraft During Cruise*, Technology Incorporated, Dayton, Final Report FA-65-WA-1163, January 1967, AD 652 615

26. McCudden, J.T.B., Major, *Flying Fury, Five Years in the Royal Flying Corps*, Ace Publishing Co., 1968, p 35

27. *Low Altitude Penetration Parameters Study*, Operational Analysis Section, LTV-Vought Aeronautics Division, Part I (1 April 1965, AD 476703) Part II, 8 March 1965, AD 476 704

28. Schwartz, I., *Toward the Optimization of a Terrain Following Flight Control System*, Proceedings of the IAS Symposium on Vehicle Systems Optimization, November 28-29, 1961, IAS Pub., New York

29. Hayre, H.S., and Moore, R.K., *Theoretical Scattering Coefficient for Near Vertical Incidence from Contour Maps*, Journal of Research, National Bureau of Standards, Vol 69D, No 9, September-October 1961, pp 427-432

30. Erickson, R.A., *Empirically Determined Effects of Gross Terrain Features Upon Ground Visibility from Low-Flying Aircraft*, US Naval Ordnance Test Station, NAVWEPS Report 7779, AD 267 174

31. *Advanced Concepts for Terrain Avoidance*, Summary Report, Cornell Aeronautical Laboratory, Report IH-1224-P-4, November 1958, AD-304 004 (cited in Ref. 3)

32. Stapleford, R.L., and Ashkenas, I.L., *Effects of Manual Altitude Control and Other Factors on Short-Period Handling Quality Requirements*, Journal of Aircraft, Vol. 5, No. 1, January-February 1968, pp 41-48

33. Bekker, M.G., *Introduction to Terrain-Vehicle Systems*, U. of Mich. Press, 1969

34. Buchheim, R.W., *Space Handbook*, the Rand Corporation, 1958

35. Weiss, Herbert K., *The Evasive Airplane*, Memo to President, Antiaircraft Artillery Board, Camp Davis, North Carolina, 28 February, 1945

36. Stein, A., *Terrain Mask Angles*, paper presented at Joint Session of AAAS and Geological Society of America, Chicago, December 1959

37. Wood, W.F., *The Relationship of Mask Angles to Terrain Geometry and its Applicability to Military Problems*, (Project CATVAR) Cornell Aero Laboratory, Report VT-1810-G-2, December 1963

38. Curran, L., *Reduction of Radar Tracking Errors with Frequency Agility*, IEEE Trans. on AES, May 1968, AES-4, No. 3, pp 410-416

39. Hatcher, J.L., and Cash, C., *Polarization Agility for Radar Glint Reduction*, paper presented at the IEEE Region 3 Convention, Huntsville, Ala., November 19-21, 1969, AD 700 138

40. *Low Angle Tracking Technique Study*, RCA/Defense Electronic Products, Moorestown, N.J., December 31, 1969, Final Report prepared for Office of Naval Research, AD 865, 560

41. Barton, D.K., *Radar Systems Analysis*, Prentice Hall, 1964

42. Barton, D.K., and Ward, H.R., *Handbook of Radar Measurement*, Prentice Hall, 1969

43. Berkowitz, R.S., *Modern Radar*, Wiley, 1965

44. Nathanson, F.E., *Radar Design Principles*, McGraw-Hill, 1969

45. Povejsil, D.J., Raven, R.S., and Waterman, P., *Airborne Radar*, Boston Technical Publishers, 1965

46. Schleisinger, R.J., *Principles of Electronic Warfare*, Prentice Hall, 1961

47. Friedman, H.J., *Jamming Susceptibility*, IEEE Trans on AES, AES-4, No. 4, July 1968, pp 515-528

48. Barton, D.K., *Radar System Performance Charts*, IEEE Trans on Military Electronics, MIL-9, Nos 3 and 4, July/October 1965, pp 255-263

49. Vakin, S.A., *Principles of Jamming and Electronic Reconnaissance*, Foreign Technology Division, WP-AFB, 23 May 1969, AD 692 643 (This translation has been released for unrestricted distribution)

50. Cunada, A.H., *Infrared, Its Military and Peacetime Uses*, General Electric Data Folder No. 87516, 1947 (contains much historical data)

51. Laufer, A.R. (Editor), *Special Issue on Infrared Physics and Technology*, Proc of the IRE, September 1959

52. *Applied Optics*, Special Issue of Proc of the IEEE, October 1966

53. Miller, N., *Tactical Laser Use Advancing*, Av Week and Space Tech, 26 January 1970, pp 51-59

54. Miller, N., *Infrared Fire Control Tests Start*, Av Week and Space Tech, 11 May 1970, pp 53-55

55. Leary, F., *Finding the Enemy*, Space/Aeronautics, April 1967, pp 92-104

56. Machol, R.E. (editor), *System Engineering Handbook*, McGraw-Hill, 1965, Freedman, J., Chapter 14, Adar, R., and Mundie, J.C., Chapter 15, Infrared

57. Wolfe, W.L. (editor), *Handbook of Military Infrared Technology*, 1965, US Govt Printing Office

58. Jamieson, J.A., et al., *Infrared Physics and Engineering*, McGraw-Hill, 1963

59. King, D.D., *Long Waves of Short Perspectives on the Millimeter Region*, IEEE Spectrum, May 1965, pp 84-88

60. Horan, J.J., *Spacecraft Infrared Imaging*, IEEE Spectrum, Part I, June 1968, pp 71-78, Part II, July 1968, pp 66-74

61. Goodman, J.W., *Some Effects of Target-Induced Scintillation on Optical Radar Performance*, Proc of IEEE, Vol 53, No 11, November 1965, pp 1688-1700

62. Weibel, G.F., and Dressel, H.O., *Propagation Studies in Millimeter-Wave Link Systems*, Proc of IEEE, Vol 55, No 4, pp 469-513

63. Pannenen, R.A., *Progress in Ionized-Argon Lasers*, IEEE Spectrum June 1966, pp 88-99

64. Burns, F.P., *High Power Lasers, Their Performance, Limitations, and Future*, IEEE Spectrum March 1967, pp 119-120

65. Moreau, R., *Systeme de Pointage Automatique pour Telemetre aLaser*, paper presented at AGARD meeting on optical-electronic techniques, Oslo, 29 September-3 October 1969, N70-13830

66. Rue, A.K., and Fisk, J.W., *Laser Ranging Capability as Affected by System Pointing Error*, IEEE Trans on AES, Vol. AES-4, No. 3, May 1968, pp 360-368

67. Rue, A.K., *Stabilization of Precision Electro-Optical Pointing and Tracking Systems*, IEEE Trans on AES, Vol AES-5, No. 5, September 1969, pp 803-819

68. Pay, R., *Army Developing Fog-Piercing Millimeter-Wave Imaging Unit*, Advanced Electronics, Missiles and Rockets, 25 April 1966, pp 34-36

69. Kelley, C.R., *Manual and Automatic Control*, Wiley, New York, 1968

70. Sinaiko, H.W. (editor), *Selected Papers on Human Factors in the Design and Use of Control Systems*, Dover Publications, New York, 1961

71. Sheridan, T.B., *The Human Operator in Control Instrumentation in Progress in Control Engineering*, Vol. 1, Ed. R.H. Macmillan, et al, Academic Press, New York

72. Hicks, S.A., Literature Review, *Tracking Control Mechanisms and Displays (Light Antiaircraft System Oriented)*, US Army Technical Memo 9-57, Human Engineering Laboratories, Aberdeen Proving Ground, Maryland, December 1957

73. McRuer, D.T., and Krendel, E.S., *Dynamic Response of Human Operators*, Wright Air Development Center, Technical Report 56-524, AD-110 693, October 1957

74. Weasko, R.J., McRuer, D.T., and Magdaleno, R.E., *Human Pilot Dynamic Response in Single-Loop Systems with Compensatory and Pursuit Displays*, Technical Report AFFDL-TR-66-137, Wright-Patterson Air Force Base, December 1966

75. McRuer, D.T., and Krendel, E.S., *Human Pilot Dynamics in Compensatory Systems*, AFFDL-TR-65-15, July 1965, AD-470 337

76. McRuer, D.T., et al, *New Approaches to Human-Pilot/Vehicle Dynamic Analysis*, AFFDL-TR-67-150, AD-667 849

77. McRuer, D.T., Graham, D., and Krendal, E.S., *Manual Control of Single Loop Systems*, Journal of the Franklin Institute, Part I, Vol 283, No 1, January 1967, pp 1-29 Part II, Vol 283, No 2, February 1967, pp 145-168

78. Walston, C.E., and Warren, C.E., *A Mathematical Analysis of the Human Operator in a Closed-Loop*

Control System, Air Force Personnel and Training Research Center, Lackland Air Force Base, Texas, AFPTRC-TR-54-96, 25 January 1954

79. Elkind, J.I., *Characteristics of Simple Manual Control Systems*, MIT Lincoln Laboratory Technical Report No. 111, 6 April 1956, Lexington, Mass., AD-94 646

80. Matheny, W.G., and Norman, D.A., *The Effect Versus Time Constant in Tracking Behavior*, NAVTRADEVCEN Technical Report 67-C-0034-3, August 1968, AD-675 806

81. Hall, I.A.M., *Effects of the Controlled Element on the Human Pilot*, ADC Technical Report 57-509, Wright Air Development Center, August 1958, AD-130 979

82. *Bibliography of Human Engineering Reports on Tracking*, NAVORD Report 5272, April 1956, NOTS, China Lake, AD-111 459

83. McRuer, D.T., and Krendal, B.S., *The Human Operator as a Servo System Element*, Journal of the Franklin Institute, Vol. 267, No. 5, May, and No. 6, June 1959

84. *Second Annual NASA University Conference on Manual Control*, 28 February-2 March 1966, NASA SP-128

85. Pew, R.W., et al., *Summary of Sine-Wave Tracking Studies*, reported in Reference 16

86. Todosiev, E.P., et al., *Human Performance in Single and Two Axis Tracking Systems*, reported in Reference 16

87. Levinson, W.H., *Two-Dimensional Manual Control Systems*, reported in Reference 16

88. Seidenstein, S., and Birmingham, H.P., *The Relation of Electronic and Optical Display Gain to System Performance*, IRE Trans on Human Factors in Electronics, March 1960, pp 30-32

89. McRuer, D.T., and Graham, D., *Pilot-Vehicle Control System Analysis*, Progress in Astronautics and Aeronautics, Vol. 13, Academic Press, New York, 1964, pp 603-621

90. Elkind, J.I., *A Survey of the Development of Models for the Human Controller*, Ibid, pp 623-643

91. Rosenberg, B.L., and Segal, R., *Dynamic Response of the Human Operator in Tactical Fire Control Situations: A Time Domain Matrix Approach to Modelling the Target-Tracking Behavior of the Antiaircraft Gunner*, Franklin Institute Research Laboratories, Final Report on US Army Contract No. DA-AA-25-67-C0612, April 1969

92. Magdaleno, R.E., et al., *Effects of Manipulator Restraints on Human Operator Performance*, Technical Report AFFDL-TR-66-72, December 1966, AD 646 653

93. McRuer, D.T., et al, *Human Pilot Dynamics with Various Manipulators*, Technical Report AFFDL-TR-66-138, December 1966, AD 645 189

94. Fisher, J.D., *Extension of Human Describing Function Models to Step Plus Random Appearing Inputs*, Thesis, Air Force Institute of Technology, May 1969, AD 699 571

95. Weiss, Herbert K., *Recommended Tracking Ratios for T-36 Director*, Memo to President, Antiaircraft Artillery Board, Camp Davis, North Carolina, September 1943

96. Weiss, Herbert K., *Aided Tracking for Ranging Devices*, Memo to President, Antiaircraft Artillery Board, Camp Davis, North Carolina, April 1945

97. Weiss, Herbert K., *Analysis of Tracking Error*, Report No. 649, Ballistic Research Laboratories, Aberdeen Proving Ground, Maryland, 11 September 1947, AD-481 853L

98. Weiss, Herbert K., *Desirable Characteristics for Director Trackers*, Memo to President, Antiaircraft Artillery Board, Camp Davis, North Carolina, 30 July 1944

99. Weiss, Herbert K., *Improvement of Tracking with Disturbed Reticle Sights*, Memo to President, Antiaircraft Artillery Board, Camp Davis, North Carolina, May 1945

100. Weiss, Herbert K., *Tracking Records on M5 Directors*, Memo to President, Antiaircraft Artillery Board, Camp Davis, North Carolina, 10 October 1945

101. Weiss, Herbert K., *Types of Tracking Devices*, Memo to President, Antiaircraft Artillery Board, Camp Davis, North Carolina, April 1944

102. *Report of the Model Evaluation Panel of the Working Group on Effectiveness Measures for Optically Directed Air Defense Weapons*, Dept of the Air Force, 1 May 1967, AD 670 252

103. Poulton, E.C., *Bias in Experimental Comparisons between Equipments due to the Order of Testing*, IEEE Trans. on Man Machine Systems, Vol. MMS-10, No. 4, December 1969, pp 332-344 (Part II)

104. Levison, W.H., et al, *A Model for Human Controller Remnant*, Ibid, (Part I), pp 101-107

105. Jex, H.R., and Magdaleno, R.E., *Corroborative Data on Normalization of Human Remnant*, Ibid, Part I, pp 137-139

106. Crossman, E.R.F.W., et al, *Application of Gabor's*

Elementary-Signal Theorem to Estimation of Non-stationary Human Spectral Response, Ibid, Part I, pp 118-123

107. Young, L.R., *On Adaptive Manual Control*, Ibid, Part II, pp 292-331

108. McRuer, D.T., and Weir, D.H., *Theory of Manual Vehicular Control*, Ibid, Part II, pp 257-291

109. Beare, A.C., and Kahn, A., *Describing Functions for Compensatory Tracking of Sine Waves Plus Noise*, Third Annual NASA University Conference on Manual Control, 1-3 March 1967, NASA SP-144, pp 121-135

110. Weisz, A.Z., et al, *An Evaluation of Three Types of Hand Controllers Under Random Vertical Vibration*, Second Annual NASA University Conference on Manual Control, NASA SP-128, pp 269-278

111. Frost, G.G., *A Comparison between Tracking with 'Optimum' Dynamics and Tracking with a Simple Velocity Control*, AMRL-TDR-62-150, AD 402 843

112. Kurke, M.I., and McCain, C.N., Jr., *Low Power Optical Systems and Aerial Target Detection*, Human Engineering Laboratories, Aberdeen Proving Ground, US Army, Tech Memo 5-57, June 1957

113. Baty, D.L., *Effects of Display Gain on Human Operator Information Processing Rate in a Rate Control Task*, IEEE Transactions on Man-Machine Systems, December 1969, MMS-10, No. 4, Part I, pp 123-131

114. Walston, C.E., and Warren, C.A., *A Mathematical Analysis of the Human Operator in a Closed-Loop Control System*, AFPTRC-TR-54-96, 25 January, 1954

115. Kahn, A., and Mazine, M., *Human Tracking Performance, I. Tracking Ability as a Function of System Noise, Scope Sensitivity and Forcing Function*, Westinghouse Electric Corp., Report 57-103-6-116-A-1, March 1957, reported in *Airborne Radar*, G. Merrill, editor, Boston Technical Publishers, 1965, pp 649-650

116. Hicks, S.A., *Literature Review: Tracking Control Mechanisms and Displays (Light Antiaircraft System Oriented)*, Human Engineering Laboratories, Aberdeen Proving Ground, Technical Memorandum 9-57, December 1957

117. Murray, E.A., *Accuracy of Tracking Airborne Targets*, Ballistic Research Laboratories, Technical Note No. 1587, October 1965

118. Wokoun, W., *Detection of Random Low-Altitude Jet Aircraft by Ground Observers*, US Army Human Engineering Laboratories, Tech Memo 7-60, June 1960

119. Wright, A.D., *Factors Influencing the Visual Detection and Recognition of Low-Altitude Aircraft*, HumRRO Paper 20-67, May 1967, AD 654 125

120. Bowen, J.H., and Chernikoff, R., *The Relationships between Magnification and Course Frequency in Compensatory Aided Tracking*, Naval Research Laboratory, Washington, D.C., NRL Report 4913, 16 April 1957, AD 129 691

121. Chernikoff, R., et al, *A Comparison of Zero-Order and Fourth-Order Compensatory Systems as a Function of Course Frequency*, Naval Research Lab., NRL Report 5262, 26 January 1959, AD 211 680

122. Chinn, G.M., *The Machine Gun*, US Govt. Printing Office, 1951

123. Weyl, A.R., *Fighter Armament, Part I, Important Lessons from the Past*, FLIGHT, 24 August 1950, pp 215-219. *Part II, German Equipment in the Second World War: Inefficient Intelligence*, FLIGHT, 21 September 1950, pp 338-340. *Part III, Guns v. Rockets*, FLIGHT, 5 October 1950, pp 379-381, 388. *Part IV, Ammunition and Elementary Ballistics: Vulnerability of Structures*, FLIGHT, 23 November 1950, pp 459-461. *Part V, Lessons from the Luftwaffe*, FLIGHT, 7 December 1950, pp 535-537. *Part VI, Gun Design and Installation*, FLIGHT, 4 January 1951, pp 6-8. *Part VII, Simple Rocket versus Guided Missile - and Some General Conclusions*, FLIGHT, 25 January 1951, pp 108-110

124. Weiss, Herbert K., *Analysis of World War II Air Combat Records*, Report No. 727, Ballistic Research Laboratories, Aberdeen Proving Ground, Maryland, July 1950

Section 5

1. *The Oerlikon-Contraves 35 mm AA Tank*, International Defense Review, Vol. 3, No. 1, March 1970, pp 72-74

2. *The Matador 30 ZLA Low-Level Antiaircraft System*, Ibid III, 1969, pp 262-264

3. *Engineering Design Handbook, Fire Control Series, Section 1, Fire Control Systems - General*, AMC Pamphlet, AMCP 706-327, January 1968, pp 4-137

4. Ewing, W.B., *Stabilization of Ship Antennas*, Chapter 4 in *Radar Scanners and Radomes*, MIT Radiation Laboratory Series, Vol. 25, 1948, Dover Reprint

5. Weiss, Herbert K., *Fire Control Device for Determining Slant Plane*, Report No. 824, Ballistic

Research Laboratories, Aberdeen Proving Ground, Maryland, September 1953

6. Kuhlenkamp, A., *Die Flak Kommandogerate*, Zeitschrift des Vereines Deutscher Ingenieure, 11 July 1942, Bd 86, Nr 27-28, p. 429

7. *Jane's Weapons Systems*, 1969-70, McGraw-Hill

8. Weiss, Herbert K., *Regenerative Tracking, A Study of Theories and Methods*, Memo to President, Antiaircraft Artillery Board, Camp Davis, North Carolina, 17 March 1943

9. Blackman, R.B., *Data Smoothing and Prediction*, Addison-Wesley Publishing Co., Inc., 1965

10. Krut'ko, P.D., *Statistical Dynamics of Sampled Data Systems*, Elsevier, 1969

11. Barton, D.K., and Ward, H.R., *Handbook of Radar Measurement*, Prentice-Hall, 1969

12. Chang, S.S.L., *Synthesis of Optimum Control Systems*, McGraw-Hill, 1961

13. Morrison, N., *Introduction to Sequential Smoothing and Prediction*, McGraw-Hill, 1969

14. Solodovnikov, V.V., *Introduction to the Statistical Dynamics of Automatic Control Systems*, Dover, 1960

15. Barton, D.K., and Ward, H.R., *Handbook of Radar Measurement*, Prentice-Hall, 1969

16. Zadeh, L.A., and Ragazzini, J.R., *An Extension of Wiener's Theory of Prediction*, Journal of Applied Physics, Vol 21, No 7, pp 645-655, July 1950

17. Brown, R.G., *Smoothing, Forecasting and Prediction of Discrete Time Series*, Prentice-Hall, 1963

18. Bucy, R.S., and Joseph, P.D., *Filtering for Stochastic Processes with Applications to Guidance*, Interscience, Wiley, 1968

19. Bryson, A.E., and Ho, Y.C., *Applied Optimal Control*, Blaisdell, 1969

20. Barbesrac, J. de, et Caumon, P.G., *Lissage Auto-Adaptatif Sur Les Informations Fournies pas un Radar de Poursuite*, AGARD Conference Proceedings, No. 47, Techniques for Data Handling in Tactical Systems, November 1968, pp 105-118, AD 699 488

21. Benedict, T.R., and Bordner, G.W., *Synthesis of an Optimal Set of Radar Track-While-Scan Smoothing Equations*, IRE Transactions on Automatic Control, Vol. AC-7, No. 4, July 1962, pp 27-32

22. Shaw, L.G., *Dual-Mode Filtering of Polynomial Signals in Noise*, IEEE Trans. on Automatic Control, Vol AC-8, No. 2, April 1963, pp 136-141

23. Simpson, H.R., *Performance Measures and Optimization Condition for a Third-Order Sample-Data Tracker*, IEEE Trans. on Automatic Control, Vol. AC-8, No. 2, April 1963, pp 182-183

24. Singer, R.A., *Estimating Optimal Tracking Filter Performance for Manned Maneuvering Targets*, IEEE Trans. on Aerospace and Electronic Systems, Vol. AES-6, No. 4, July 1970, pp 473-483

25. Weiss, Herbert K., *Prediction of Multiple Time Series*, BRL Report No. 869, Aberdeen Proving Ground, June 1953

26. Levine, N., *A New Technique for Increasing the Flexibility of Recursive Least Squares Data Smoothing*, Bell System Technical Journal, May 1961, pp 821-840

27. Grenander, U., *A Tactical Study of Evasive Manoeuvres*, FOA-P Report A 126, March 1963, Research Institute of National Defense, Stockholm 80

28. Bresson, M., *Problems of Pursuit and Evasion*, Technical Report No. 41, SACLANT ASW Research Centre, Viale San Bartolomeo 92, La Spezia, Italy, 1 June 1966, AD-487 149

29. Yovits, M.C., and Jackson, J.L., *Linear Filter Optimization with Game Theory Considerations*, I.R.E., 1955

30. Sorenson, H.W., *Least-squares estimation: from Gauss to Kalman*, IEEE Spectrum, July 1970, pp 63-68

31. Stibitz, G.R., *Programmed Dispersion*, Proceedings of the Second Fire Control Conference, US Army, March 1955

32. McShane, E.J., Kelley, J.L., and Reno, F.V., *Exterior Ballistics*, University of Denver Press, 1953

33. Bliss, G.A., *Mathematics for Exterior Ballistics*, Wiley, 1944

34. Moulton, F.R., *Methods in Exterior Ballistics*, Dover, 1962 (reprint of 1926 edition)

35. Nielsen, K.L., and Heyda, J.E., *The Mathematical Theory of Airborne Fire Control*, NavOrd Report 1493, 1951, Supt of Documents, Washington, D.C.

36. Banash, R.C., *Notes on the University of Michigan Analytic Gun Model*, Internal Note SY-TN3-70, Systems Analysis Directorate, US Army Weapons Command, Rock Island, Ill., April 1970

37. Slook, T.H., *Error Analysis for Control Systems*, Internal Working Paper, Frankford Arsenal

38. Middleton, D., *Introduction to Statistical Communication Theory*, McGraw-Hill, 1960, p. 1076

39.

Cunningham, L.B.C., and Hynd, W.R.B., *Random Processes in Problems of Air Warfare*, Supplement to the Journal of the Royal Statistical Society, 8 (1946) No. 1, pp 62-85

40. Brandli, H., *Theorie des Mehrfach-Schusses*, Verlag Birkhauser A.G., Basel, 1960

41. Brandli, H., *Waffe und Wirkung bei der Fliegerabwehr*, Birkhauser Verlag, *Basel*, 1956

42. Brandli, H., *Treffwahrscheinlichkeit und Abschusswahfscheinlichkeit bein Schieszen mit Automatgeschutzen*, Flugwehr und Technik, June 1965, pp 132-135, July 1965, pp 161-170

43. Bekker, M.G., *Introduction to Terrain-Vehicle Systems*, U. of Mich. Press, Ann Arbor, Mich., 1969

44. Schuring, D., and Belsdorf, M.R., *Analysis and Simulation of Dynamical Vehicle-Terrain Interaction*, Cornell Aeronautical Laboratory, Inc., Tech. Memo CAL VJ-2330-G-56, May 1969, AD 690 841

45. Pradko, F., *Theory of Human Vibration Response and its Application to Vehicle Design*, US Army Tank and Automotive Command, paper presented at the Man-Mobility-Survivability Forum, 11-12 April 1967, Indianapolis

NOTE: Pradko cites the following references which have not been reviewed for this report, but are included for the assistance of future researchers.

a. Wilcox, H.A., 'Implications of Current Scientific Research for Future Mobility', papers presented at the 1964 Mobility Forum, Allison Division, General Motors Corporation, Indianapolis, Indiana

b. Van Deusen, B.D., 'A Study of the Vehicle Ride Dynamics Aspect of Ground Mobility', Vol. 1, March, 1965

c. Heal, S.F., 'Suspension Analysis', Dynamic Simulations Laboratory, Research Division, U.S. Army Tank-Automotive Center, April 1961

d. Bussman, Dr. D.R., 'Vibrations of a Multi-Wheeled Vehicle', The Ohio State University, Technical Report, August 1964

e. Smith, R.E., 'Vehicle Random Terrain Response', Food Machinery Corporation, San Jose, California, September 1963

f. McKenzie, R.D., Howell, W.M., Skaar, D.E., and Butterworth, A.V., 'Evaluation of Counterinsurgency Mobility in Relation to Environment', GM Defense Research Laboratories, June 1966

g. Heal, S.F., and Cicillini, C., 'Micro Terrain Profiles', Report No. RRC-9, US Army Tank-Automotive Center, 14 August 1964

h. Bogdanoff, J.L., Kozin, F., and Cote, J., 'Atlas of Off-Road Ground Roughness PSD's and Report on Data Acquisition Technique', US Army Tank-Automotive Center, September 1966

i. Sattinger, I.J., and Smith, D.F., 'Computer Simulation of Vehicle Motion in Three Dimensions'

j. Pradko, F., Orr, T.R., and Lee, R.A., 'Human Vibration Analysis', 1965, Society of Automotive Engineers, 650426

k. Pradko, F., Kaluza, V., and Lee, R.A., 'Theory of Human Vibration Response', 1966, American Society of Mechanical Engineers, 66-WA/BHF-15

l. Pradko, F., and Lee, R.A., 'Vibration Comfort Criteria', 1966, Society of Automotive Engineers, 660139

m. Liston, R., 'Correlation Between Predicted and Actual Off-Road Vehicle Performance', January 1967, US Army Tank-Automotive Center, Warren, Michigan

46. Kinney, J.A.S., et al., *The Effect of Vibration on Performance with Electro-optical Aids to Night Vision*, US Naval Submarine Medical Center, Groton, Conn., Report No. 589, 18 July 1969, AD 700 241

47. *Human Factors*, Special Vibration Issue, Vol. 4, No. 5, October 1962, Pergamon Press

48. Coermann, R.R., *The Mechanical Impedance of the Human Body in Sitting and Standing Position at Low Frequencies*, loc cit supra, pp 227-254

49. Clark, W.S., et al, *Deformation of the Human Body due to Uni-directional Forced Sinusoidal Vibration*, loc sit supra, pp 255-274

50. Lange, K.O., et al, *Visual Acuity under Vibration*, loc sit supra, pp 291-300

51. Parks, D.L., *Defining Human Reaction to Whole-Body Vibration*, loc sit supra, pp 305-314

52. Coermann, R.R., et al, *Human Performance under Vibrational Stress*, loc sit supra, pp 315-324

53. Hornick, R.J., *Problems in Vibration Research*, loc sit supra, pp 325-330

54. Weisz, A.Z., et al, *An Evaluation of Three Types of Hand Controllers under Random Vertical Vibration*, Second Annual NASA-University Conference on Manual Control, 1966, NASA SP-128, pp 269-278

55. Goldman and von Gierke (1960), *The Effects of*

Shock and Vibration on Man, Lecture and Review Series No. 60-3, US Naval Medical Research Institute, Bethesda, Md.

56. Dieckmann (1957), Einfluss vertikaler mechanischer Schwingungen auf den menschen, *Int. Z. Augew. Physiol.*, 16,519 (Transl.: Damon and Stoudt, *Human Engineering Guide to Equipment Design*, 1963, McGraw-Hill, New York)

57. Dubbury, J., *Open Loop TV Image Stabilization*, IEEE Transactions on Aerospace and Electronic Systems, Vol. AES-6, No. 3, May 1970, pp 344-358

58. Barnard, T.W., et al., *Digital Laser Ranging and Tracking Using a Compound Axis Servomechanism*, Applied Optics, April 1966, Vol. 5, No. 4, pp 497-505

59. *XM76 Anti-Oscillation Sighting System*, Janes Weapons Systems, 1969-1970, p. 542, McGraw-Hill

60. Gladwin, S.W., *Missile Armament for the FPB*, US Naval Institute Proceedings, March 1970, pp 111-113

61. Milton, A.F., et al, *Detection Considerations for Laser Systems in the Near Infra Red: Prognosis for an Improved Technology*, Institute for Defense Analysis, Research Paper, P-581, AD 707 317

62. Pfeilsticker, R., et al, *Hit Probability on a Tank Type Target*, Frankford Arsenal Memo Report, M66-18-1, March 1966, AD 630 919

63. Shaddy, M.G., Major, *Alfa 38*, Army Magazine, June 1961, pp 35-37

64. Ebenfelt, et al, *Effectiveness Model of an Antiaircraft Fire Control System*, Proceedings 1970 Annual Symposium on Reliability, IEE Catalog No. 70 C 2-R, pp 68-74

65. Caldwell, et al, *An Introduction to Laser Reliability*, Proceedings of the 1969 Symposium on Reliability, IEEE Catalog No. 69-C-8-R, pp 482-489

66. *WSEIAC Reports*, AFSC-TR-65 -1,2,3,4,5,6, January 1965, US Air Force Systems Command

67. Coppola, A., et al, *RADC Case Histories in R&M Demonstration*, Proceedings 1966 Annual Symposium on Reliability, IEEE Catalog No. 7C 26, pp 395-408

68. Stokes, R.G., et al, *Some Life-Cycle Cost Estimates for Electronic Equipments, Methods and Results*, Proceedings 1968 Symposium on Reliability, IEEE Catalog No. 68C 33 R, pp 169-173

Section 6

1. Stokes, R.G. and Stehle, F.N.,*Some Life-Cycle Cost Estimates for Electronic Equipments: Methods and Results*, Proceedings of the 1968 Annual Symposium on Reliability, IEEE Catalog Number 68C 33-R, pp 169-183

Section 7

1. Milton, A.F. and Schnitzler, A.D., *Detection Considerations for Laser Systems in the Near Infrared: Prognosis for an Improved Technology*, Research Paper P-581, Institute for Defense Analysis, April 1970, AD 707 317

2. Durlach, N.I., *Influence of the Earth's Surface on Radar*, MIT Lincoln Laboratories, Tech Report 373, 18 January 1965, AD 627 635

3. Norman, L.W., *Final Report, Target Contrast Tracker*, Honeywell Inc., 23 September 1965, AD 813 074

APPENDIX A
DERIVATIVES OF TARGET MOTION IN POLAR COORDINATES

The derivatives of target azimuth, elevation angle, and range are frequently referred to in the text as well as used in computations. They are summarized here for convenient reference. The expressions are taken almost without change from Barton, in whose book the functions will be found plotted. They are all for constant target velocity.

Notation is the same as that used in the present report.

A.1.1 AZIMUTH

The derivatives are functions of the parameter λ, and the angle α where:

$$\lambda = v_h / R_m \qquad \text{(A.1)}$$

and:

v_h = horizontal component of target velocity

R_m = minimum horizontal range

Table A-I lists the derivatives of the azimuth angle.

A.1.2 ELEVATION

An additional parameter X is introduced:

$$X = H / R_m \; ; \; H = \text{target altitude} \qquad \text{(A.2)}$$

The expressions are for a target flying level. Table A-II lists the derivatives of an elevation angle.

The maximum values of the derivatives occur when $X \sim 1.0$, for a given value of λ. More precisely for $\dot{e}$, while holding λ, α constant and varying X; maximum $\dot{e}$ is attained when $\sin \alpha = X^{-1}$. Next, maximizing over α, the absolute maximum of e is found to be:

$$\dot{e}_{max} (\lambda = \text{constant}) = 0.25 \lambda \qquad \text{(A.3)}$$

where: $e = 45$ degrees

$\alpha = 45$ degrees, 135 degrees

$X = \sqrt{2}$

also $e_m = 54.7$ degrees, where $\tan e_m = X$ (A.4)

For a target diving at $-\theta$:

$$\dot{e} = \frac{\lambda}{1 + X^2 \sin^2 \alpha} (\sin \theta + \cos \theta \times \cos \alpha \sin^2 \alpha) \qquad \text{(A.5)}$$

The derivatives of slant range are presented in Table A-III.

Table A-I. Derivatives of Azimuth Angle

Quantity	Functional Expression	Maximum Value (radians, sec)	Angle at Which Max. Value is Attained (degrees)
$\dot{\alpha}$	$\lambda \sin^2 \alpha$	λ	90
$\ddot{\alpha}$	$2\lambda^2 \sin^3 \alpha \cos \alpha$	$\pm \frac{3\sqrt{3}\,\lambda^2}{8} = \pm 0.65\lambda^2$	60, 120
$\dddot{\alpha}$	$2\lambda^3 \sin^4 \alpha (4 \cos^2 \alpha - 1)$	$-2\lambda^3$	90
$\ddddot{\alpha}$	$24\lambda^4 \sin^5 \alpha \cos \alpha \cos 2\alpha$	$\mp 4.5\lambda^4$	72, 108

00678-B01

Table A-II. Derivatives of Elevation Angle

Quantity	Functional Expression	Maximum Value	Azimuth α at Maximum Value (degrees)
$\dot{e}$	$\lambda X \frac{\sin^2 \alpha \cos \alpha}{1 + X^2 \sin^2 \alpha}$	$\pm 0.38\lambda X$	55, 125 ($X \ll 1$)
		$\pm 0.24\lambda$	48, 132 ($X = 1$)
		$\pm \lambda / X$	0, 180 ($X \gg 1$)
$\ddot{e}$	$\lambda^2 X \sin^3 \alpha \frac{(2 - 3\sin^2 \alpha - X^2 \sin^4 \alpha)}{(1 + X^2 \sin^2 \alpha)^2}$	$-\lambda^2 X$	50 ($X \ll 1$)
		$-0.5\lambda^2$	90 ($X = 1$)
		$-\lambda^2 / X$	90 ($X \gg 1$)
$\dddot{e}$	$\lambda^3 X \sin^4 \alpha \cos \alpha \frac{[6 - 15\sin^2 \alpha - X^2 \sin^2 \alpha (2 + 10\sin^2 \alpha + 3X^2 \sin^4 \alpha)]}{(1 + X^2 \sin^2 \alpha)^3}$	$\mp 1.96\lambda^3 X$	70, 110 ($X \ll 1$)
		$\mp 0.71\lambda^3$	67, 113 ($X = 1$)
		$\mp 0.85\lambda^3 / X$	63, 117 ($X \gg 1$)

00678-B02

Table A-III. Derivatives of Slant Range

Quantity	Functional Expression	Maximum Value	Angle at Which Max. or Min. Occurs
$\dot{D}$	$-v \cos \Omega$	$\pm v$	0, 180 degrees
$\ddot{D}$	$v^2 \sin^3 \Omega / D_m$	v^2 / D_m	90 degrees
$\dddot{D}$	$3v^3 \frac{\sin^4 \Omega \cos \Omega}{D_m^2}$	$\pm 0.86 \frac{v^3}{D_m^2}$	$\tan^{-1} = 2.0$
$\ddddot{D}$	$\frac{3v^4 (4\cos^3 \Omega - 1)\sin^5 \Omega}{D_m^3}$	$3 \frac{v^4}{D_m^3}$	90 degrees

00678-B03